# Structural, electrochemical and optical properties of new cobalt porphyrin, tin and photochromic mercury complexes containing the dithizonato ligand

*A dissertation submitted in accordance with the requirements of the degree*

**Philosophiae Doctor**

*in the*

**Department of Chemistry**

**Faculty of Natural and Agricultural Sciences**

*at the*

**University of the Free State**

*by*

**Karel Grobler von Eschwege**

*Supervisor*

**Prof. J.C. Swarts**

January 2006

*Both riches and honour come of the Almighty,*
*and He reignest over all; and in His hand is power and might;*
*and in His hand it is to make great, and to give strength unto all.*

~ ***Chronicles***

# ACKNOWLEDGEMENTS

*My further gratitude hereby expressed to:*

***Prof. J. C. Swarts,***

*for being an enthusiastic research supervisor and facilitator,*

***Dr. J. Conradie,***

*for her quantum computational expertise and comprehensive assistance at all hours,*

***Prof. S. S. Basson***

*for useful discussions with regard to cobalt chemistry,*

***Prof. M. Aquino***

*for X-ray data-collections,*

***the Chemistry Department at the University of the Free State***

*for available facilities, and*

***the National Research Foundation***

*for financial support.*

# Contents

# ABBREVIATIONS

**The following abbreviations are used in the text of this dissertation:**

| | |
|---|---|
| 2H($Na_4$TCP) | tetra(sodium 4-carboxyphenyl)porphyrin |
| 2H($Na_4$TPPS) | *meso*- tetra(sodium 4-sulfophenyl)porphyrin |
| 2HOEC | octaethylcorrole |
| 2HOEP | octaethylporphyrin |
| 2HTPP | *meso*-tetraphenylporphyrin |
| ADF | Amsterdam density functional |
| B3LYP | B3 Becke 3-parameter exchange and Lee-Yang-Parr correlation |
| Bu | butyl |
| $Bu_4$NHDz | *tetra*-butylammonium dithizonato |
| CD | compact disc |
| CEP-31G | Stevens/Barch/Krauss effective core potential triple-split basis set |
| $Co(HDz)_3$ | *tris*-dithizonatocobalt(III) |
| CV | cyclic voltammetry |
| DBU | diazabicyclo[5.4.0] undec-7-ene |
| DCM | dichloromethane |
| DDz | dehydrodithizone |
| DFT | density functional theory |
| DMF | dimethylformamide |
| DMSO | dimethylsulfoxide |
| DVD | digital versatile disc |
| EDTA | ethylenediaminetetraacetic acid |
| Fc | ferrocenyl |
| G03 | Gaussian program package version 0.3 |
| $H_2$Dz | dithizone |
| HOMO | highest occupied molecular orbital |
| KHDz | potassium dithizonate |
| LSV | linear sweep voltammetry |
| LUMO | lowest unoccupied molecular orbital |
| Me | methyl |
| $Me_3$SnHDz | dithizonatotrimethyltin(IV) |
| NMR | nuclear magnetic resonance |
| OAc | acetate |
| OMe | methoxy |
| PECH | polyepichlorohydrin |
| Ph | phenyl |
| PhHg(S-Me)Dz | S-methyldithizonatophenylmercury(II) |
| PhHgHDz | dithizonatophenylmercury(II) |
| PSI | polysuccinimide |
| PW91 | Perdew-Wang (1991) exchange and correlation functional |
| SW | Oster Young square wave voltammetry |
| TBAP | tetrabutylammonium hexafluorophosphate |
| TDDFT | time dependant density functional theory |
| TZP | triple $\zeta$ plus polarization |
| UV/vis | ultra-violet and visible |
| ZORA | zero order regular approximation |

# STRUCTURES

**The following structures relate to experimental work done and reported in this study:**

**16**

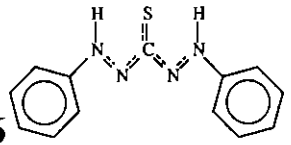

**17**

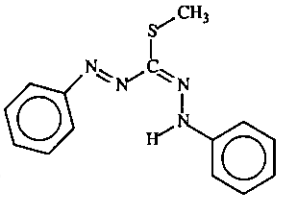

**18**

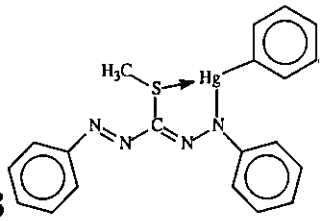

**19**

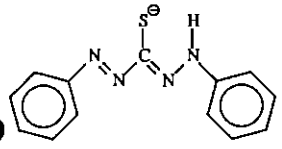

**20**

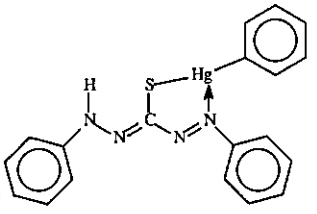

**21**

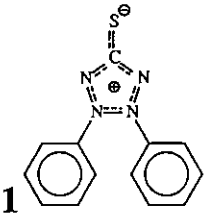

**22**

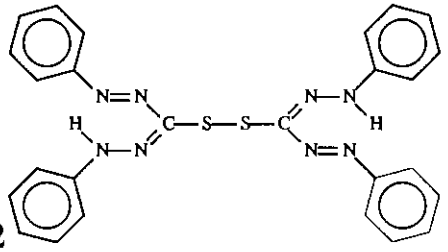

**23**

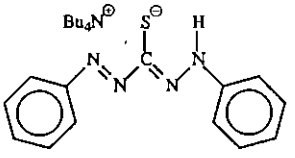

**24**

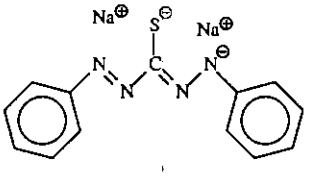

**25**

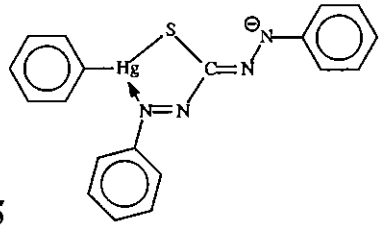

**26**

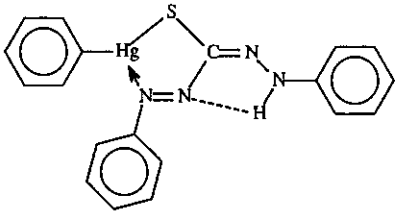

**27**

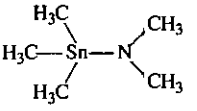

**28**

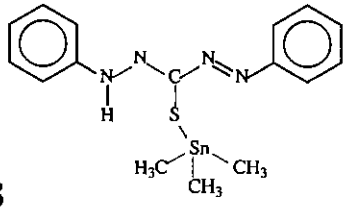

**29**

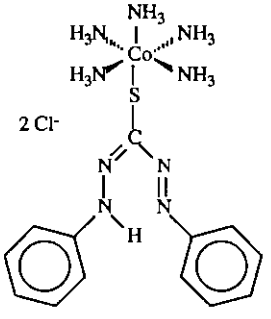

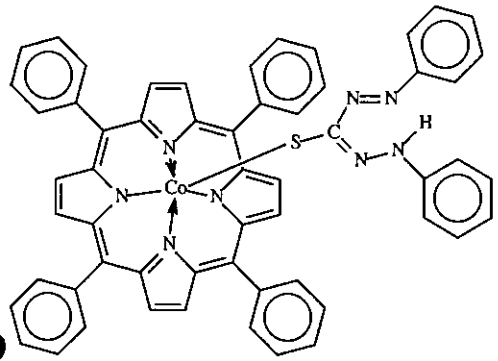

30

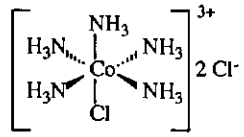

31

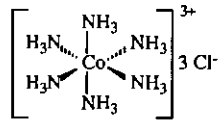

32

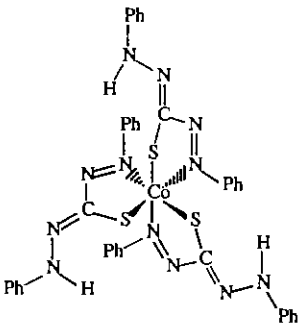

33

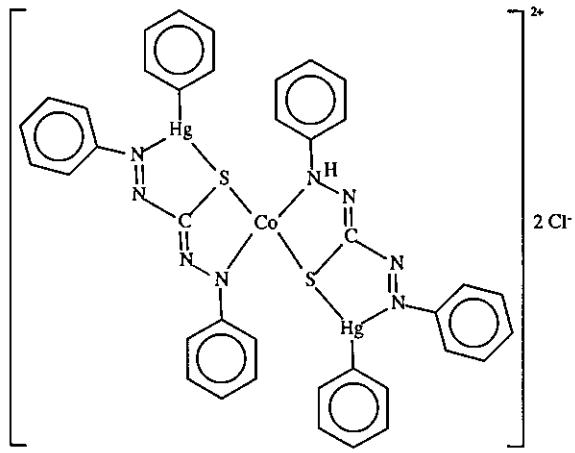

34

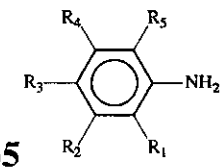

35

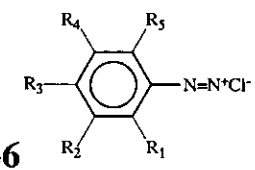

36

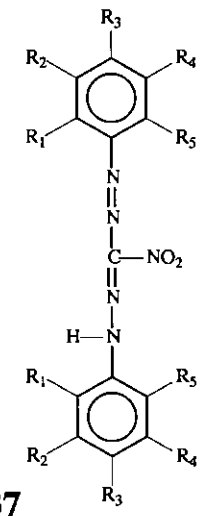

37

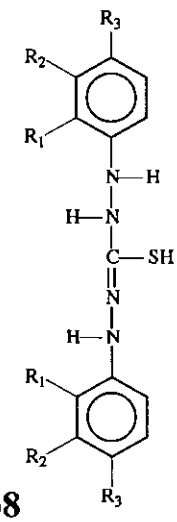

38

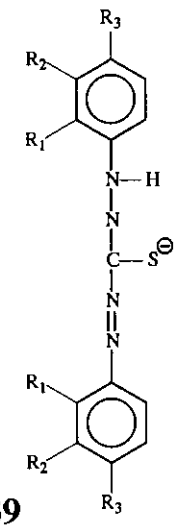

39

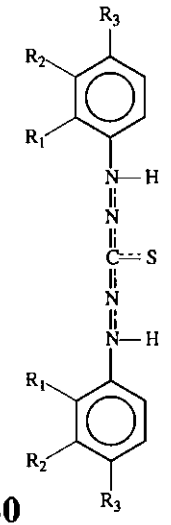

40

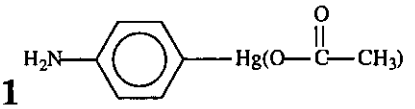

41

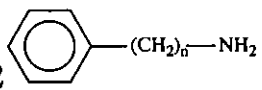

42

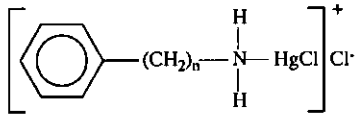

43

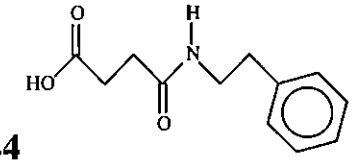

44

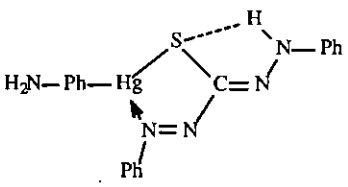

45

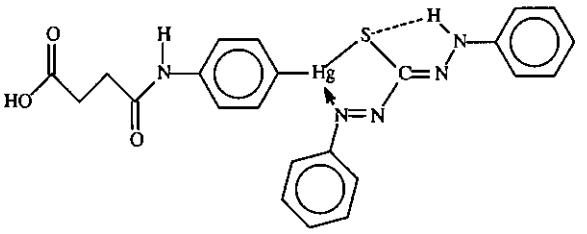

46

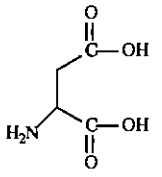

47

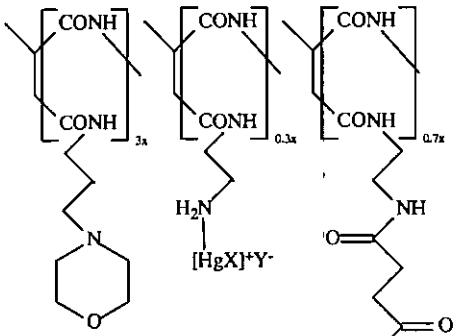

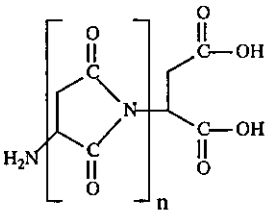

48

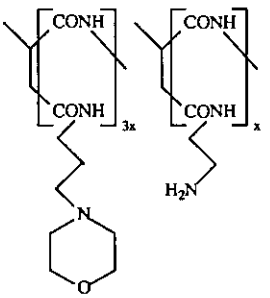

49

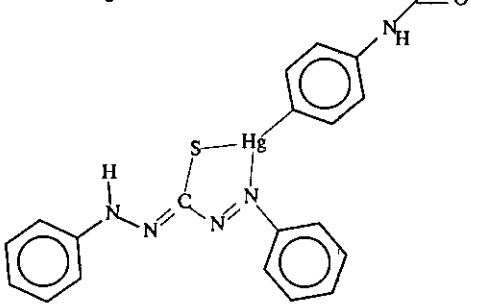

50

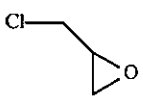


51

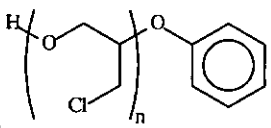


52

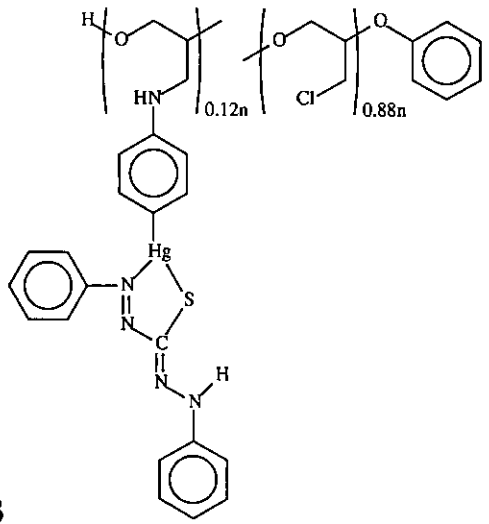


53

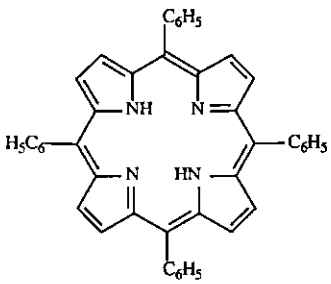


54

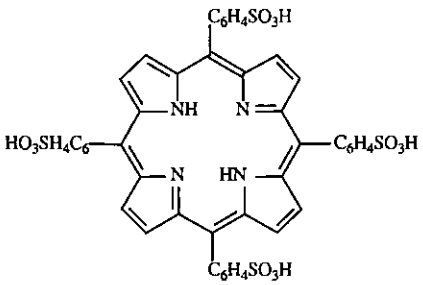


55

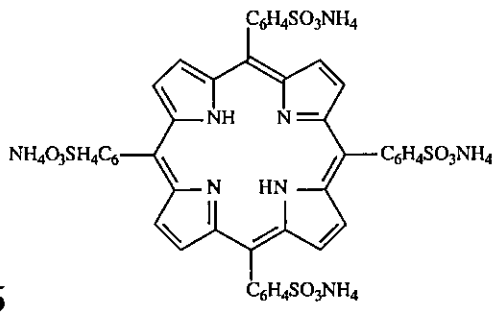


56

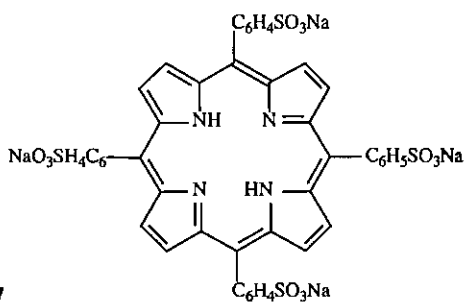


57

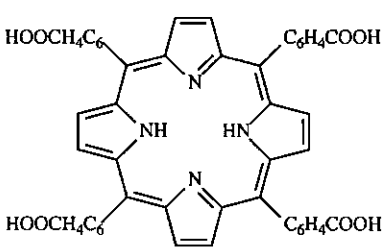


58

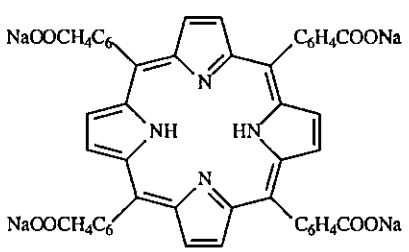


59

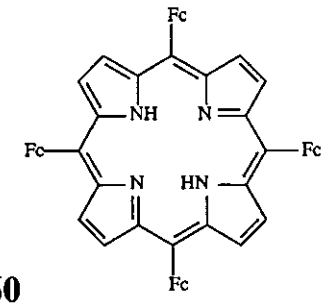


60

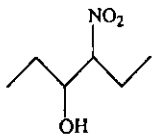


61

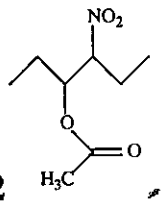


62

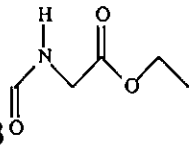


63

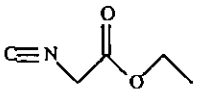


64

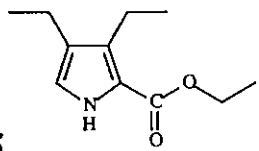


65

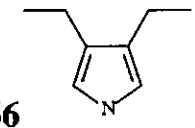


66

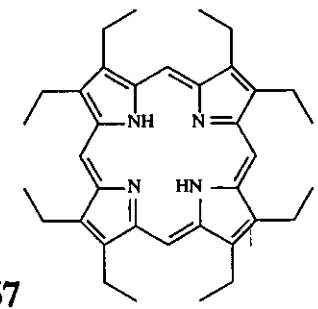


67

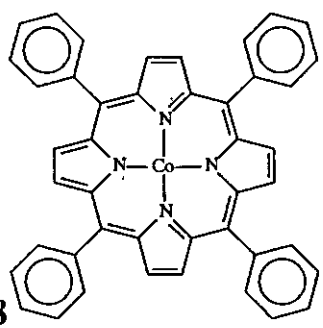


68

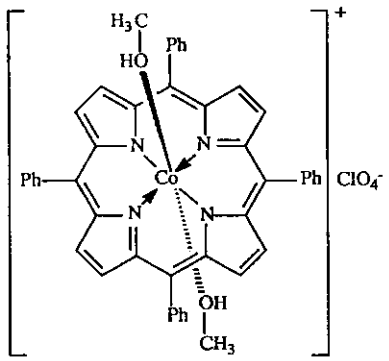


74

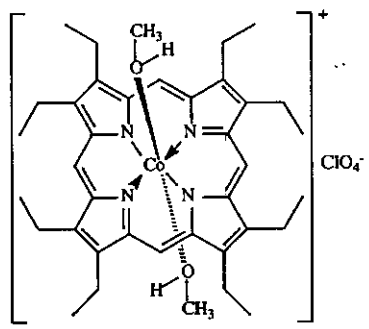


77

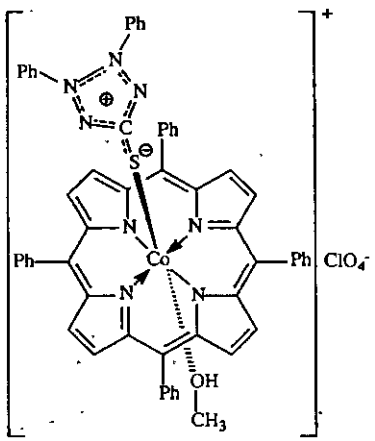


78

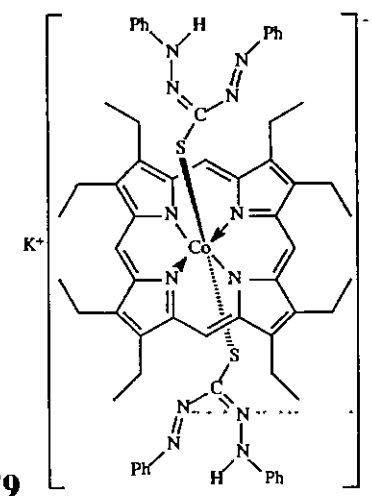


79

# 1. Introduction

The intensely coloured compound, dithizone (1,5-diphenylthiocarbazone, $(PhNHN)_2CS$, $H_2Dz$), has extensive applications as dithizonato metal complexes in analytical chemistry, especially in the spectrophotometric analyses of heavy metals.[1-3] Dithizone also has very promising applications in the fields of material science and nanotechnology, wherein the pronounced photochromicity (this term implies a colour change under the influence of light) exhibited by some metal dithizonato complexes (Figure 1) might be employed in exotic textiles,[4] graphic display systems, or as a means of data storage.[5,6] The relevance of the present dithizone study lies in the latter field.

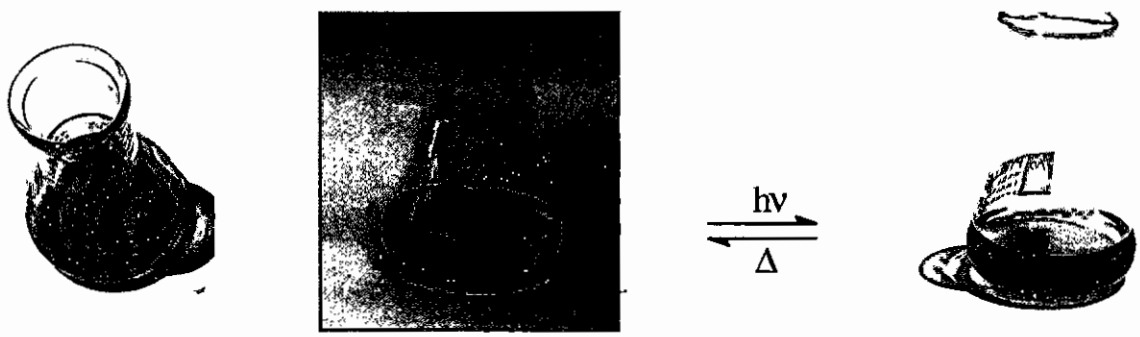


**Figure 1** Dithizone, dissolved in dichloromethane (left). Photochromic dithizonatophenylmercury(II), dissolved in dichloromethane, converts from yellow (center) to blue (right) upon light irradiation.

Whereas data storing until recently has mostly been done on ferromagnetic materials, developments are lately much more in favour of optical devices. In the case of CD's and DVD's, data is stored in patterned series of pits or holes that are burned into reflective surfaces by lasers. The ultimate, however, would be to store one bit of data on one single "switchable" molecule, where the different colours and/or other properties of two alternate molecular states could be "read".

Solutions of mercury dithizonato complexes in organic solvents of low polarity change colour from orange to blue (Figure 1) under blue-green light irradiation. This reversible photochromic reaction consists of

**a)** a photo-induced isomerisation forward reaction that generates the blue colour, followed by

**b)** a spontaneous radiationless thermal back-reaction to generate the orange form.[7,8]

It is this photochromic reaction of dithizonatophenylmercury(II) that brought about the objective of the research project at hand, namely to attempt the synthesis / construction of an optical molecular switch. The objective is that a suitable dithizonatophenylmercury(II) complex has to

be locked selectively under one set of conditions in one colour isomer, e.g. the blue isomeric form. When another set of conditions is applied, the complex should change its colour back to the orange isomeric form. Both colour changes must be effected fast, reversibly and repeatedly, by application of the appropriate light energy, without incurring molecular degradation.

To lock a photochromic molecule in a specific colour state, one needs a molecular device that will inhibit any spontaneous molecular structural changes in it once the desired colour or isomeric form has been generated. Many molecular species may be considered to attempt the trapping of a photochromic species in a specifically coloured isomeric form. These could include polymeric devices or porphyrins. Cobalt porphyrin was selected as one of a series of possible suitable molecular species whereby dithizonatophenylmercury(II) might be locked in the blue or "on"-state.

Metalloporphyrins are well known for being involved in reversible electron transfer reactions that involve their axial coordination sites. These include the following naturally occurring porphyrins:

- hemoglobin, where the iron porphyrin molecular fragment carries oxygen to the cells,
- cytochrome *b*, where the iron porphyrin is axially N-coordinated by imidazole on the one side and a methionyl side chain (S-coordination) on the other side,
- cyanocobalamin, also known as vitamin B12,
- and the green magnesium-centered chlorophyll molecule in plants.

All of the above naturally occurring porphyrin derivatives are involved in some reversible reactions that involve the metal center, whether by the mere flow of electrons and/or by the forming or breaking of chemical bonds.[9]

The complicating factor in understanding axial binding in metalloporphyrins is the relatively facile axial ligand exchange that occurs in most cases. This is, however, a much required property from an optical molecular switch point of view, as is also the light sensitivity of metalloporphyrins. Photo-induced axial bond homolysis in the case of cobalt porphyrin has been illustrated by Trommel and Marzilli,[10,11] an aspect foreseen to be imperative for the switching-off mechanism in an optical molecular switch.

To develop a first ever optical molecular switch based on dithizone requires a research program that includes basic research on several molecular species. Once combined into one unit, the molecular fragments will form the total optical device. The last stage of development will involve applied research on the final product to make it commercially viable.

To launch the research program, the following goals were set for this particular study:

1. An investigation into appropriate pathways for the axial coordination of dithizone to cobalt porphyrin, utilizing dehydrodithizone (DDz), potassium dithizonato ($K^+HDz^-$), *tetra*-butyl-ammonium dithizonato ($Bu_4N^+HDz^-$), and dithizonatotrimethyltin(IV) ($Me_3SnHDz$). The reactions of different cobalt amine and aqua complexes with dithizone will also be explored.
2. The anchoring of $H_2N$- and HOOC- functionalised dithizonatophenylmercury(II) derivatives onto a suitably functionalised hydrophilic polymer and a suitably functionalised lypophilic polymer. This will allow testing of the photochromic properties of the polymer bound dithizonatophenylmercury(II) devices in aqueous and non-aqueous media.
3. Single crystal X-ray structure elucidation of selected compounds to supplement UV/visible spectroscopy as the ideal tool for qualitative characterization of all the intensely coloured compounds investigated in this study.
4. A quantum computational investigation into the structure of S-methyldithizonatophenyl-mercury(II). The validity of results are first established by comparing computational data from the parent dithizone and dithizonatophenylmercury(II) compounds to experimentally obtained data.

   This system will serve as a model for the coordination of dithizonatophenylmercury(II) to a cobalt porphyrin, wherein cobalt porphyrin will be bound to the same binding site the methyl group is bound to in S-methyldithizonatophenylmercury(II).
5. A comparative electrochemical investigation into the redox properties of the following phenyl ring halide-substituted dithizone series: *para*-Cl-, *para*-F-, *meta*-F- and *ortho*-F-dithizone. The aim is to determine the required conditions by which the most stable dithizonato systems can still be oxidatively destroyed or altered.
6. A comparative electrochemical investigation into the redox properties of cobalt complexes with the following series of modified porphyrins: *meso*-tetraphenylporphyrin (2HTPP), *meso*- tetra(sodium 4-sulfophenyl)porphyrin ($2H(Na_4TPPS)$) and octaethylporphyrin (2HOEP). Results will provide insight into the ease by which porphyrins may be involved in electron transfer reactions with axial dithizonato ligands.

It should be noted that the final aim of this overall research program in this laboratory is to inductively engineer or synthesise molecular data storing devices that operate by colour switching. The study presented in this dissertation will cover only the first part of the overall research program, due to the sheer volume of the entire project.

# 2. Literature Survey

## 2.1. Dithizone – The Ligand

### 2.1.1. Synthesis and Structure

Dithizone was first synthesised in 1878 by Emil Fischer during an investigation into a series of compounds resulting from the reactions of phenylhydrazine with carbon disulfide.[12] This remained the method of preparation until 1943.

An extensive study was undertaken by Billman and Cleland to develop an improved method.[13] Their method, a modification of the procedure followed by Fischer, involved three steps. Step 1 is the preparation of the phenylhydrazine salt of β-phenyldithiocarbazic acid (**1**), in 97% yield.

$$2PhNHNH_2 + CS_2 \rightarrow PhNHNH\text{-}C(S)\text{-}SH^{-}NH_2NHPh$$
**1**

The second step involves driving off hydrogen sulfide from the phenylhydrazine salt. No solvent is used, while the temperature has to be kept between 96 and 98°C to give up to 75% yield of diphenylthiocarbazide (**2**).

$$PhNHNH\text{-}C(S)\text{-}SH^{-}NH_2NHPh \rightarrow (PhNHNH)_2CS + H_2S$$
**2**

In the third step the carbazide is oxidised by boiling it in a methanolic solution containing potassium hydroxide for 5 minutes, yielding in excess of 75% dithizone (**3**). An over-all yield of *ca* 60% was obtained.

$$(PhNHNH)_2CS \rightarrow (PhN\overline{N}H)_2CS$$
**3**

Pelkis, Dubenko and Pupko[14] slightly modified synthetic procedures by Bamberger[15] and Tarbell.[16] In their method any of a series of ring-substituted anilines is dissolved in concentrated hydrochloric acid, and diazotised with sodium nitrite.

$$PhNH_2 + HCl + NaNO_2 \rightarrow PhN_2^{+}Cl^{-}$$
**4**

The formazyl (**5**) is prepared by coupling nitromethane and benzenediazonium chloride (**4**).

$$PhN_2^{+}Cl^{-} + CH_3NO_2 \rightarrow PhN{=}N\text{-}C(NO_2){=}N\text{-}NHPh$$
**5**

Reduction with ammonium hydrosulfide gives dihydroformazylmercaptan (**6**).

$$PhN{=}N\text{-}C(NO_2){=}N\text{-}NHPh \xrightarrow{NH_3,\ H_2S} PhNH\text{-}NH\text{-}C(SH){=}N\text{-}NHPh$$
**6**

Instead of $NH_3$ (g) and $H_2S$ (g), ammonium sulfide (20%) in ethanol can also be used.[17] Finally, the black dithizone (**7**) product is obtained by deprotonation with 2% alcoholic alkali and precipitation with 1% hydrochloric acid.

$$\text{PhNH-NH-C(SH)=N-NHPh} \xrightarrow{[O]} \underset{\mathbf{7}}{(\text{PhNHN})_2\text{CS}}$$

Dithizone itself is a violet-black solid with a metallic reflex. It is insoluble in water and sparingly soluble in most organic solvents, giving strongly coloured solutions characterised by intense absorption bands in the visible spectrum.

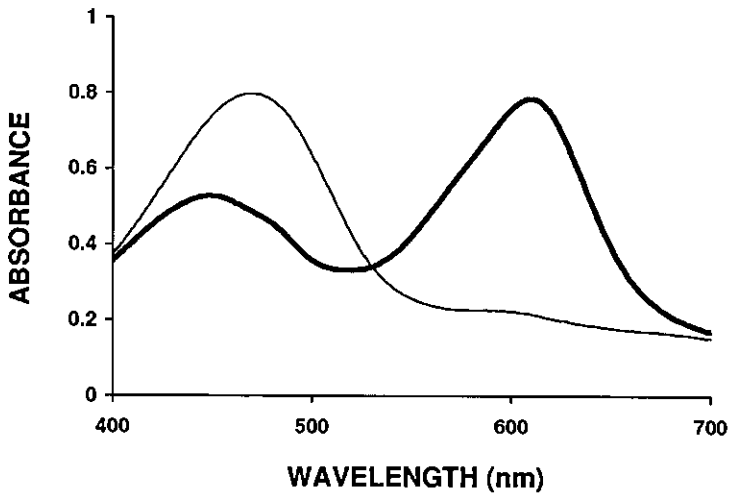


**Figure 2.1** Absorption spectra of dithizone in dichloromethane (—) and methanol (–).

Apart from metal dithizonato complexes being photochromic, the free ligand also exhibits a degree of solvatochromism. Dilute solutions in methanol are orange, with $\lambda_{max}$ = 472 nm, while dichloromethane solutions are green, with $\lambda_{max}$ = 450 and 608 nm. The presence of the two widely separated peaks gave rise to the unlikely hypothesis that in organic solvents dithizone exists as a tautomeric equilibrium between the thione and thiol forms, one of which would give rise to the peak at 450 nm, the other to the peak at 608 nm.[18] Hutton and Irving, however, conclusively argued in favour of the existence of only the symmetrical thione structure in solution.[3]


**Figure 2.2** Dithizone, $H_2Dz$, has a highly conjugated symmetrical thione structure. No experimental evidence supports the existence of the thiol form.

The above symmetrical structure also represents the X-ray crystallography established solid state structure of dithizone.[19,20] The molecule is nearly planar, with phenyl rings only slightly twisted out of the plane. It is evident from the measured bond lengths that π-electrons in the N-N-C-N-N backbone are delocalised throughout and that there are no localised single or double bonds. The N-C-N bonds are 1.34 and 1.35 Å, while the two N-N bonds are 1.29 and 1.30 Å respectively. The two imino hydrogen atoms are located as shown, both weakly hydrogen-bonded to the sulfur atom.

## 2.1.2. Derivatives

Although dithizone is practically insoluble in water, concentrated mineral acids dissolve dithizone to give red-violet solutions ($\lambda_{max}$ = 520 nm in 60% sulfuric acid), which could be used to strip the reagent from its solutions in organic solvents. On the other hand, it is readily deprotonated in the presence of a base, rendering the yellow water soluble anion, $HDz^-$. In 10 M potassium hydroxide a further colour change to red-violet occurs, which is attributed to the formation of the $Dz^{2-}$ species.

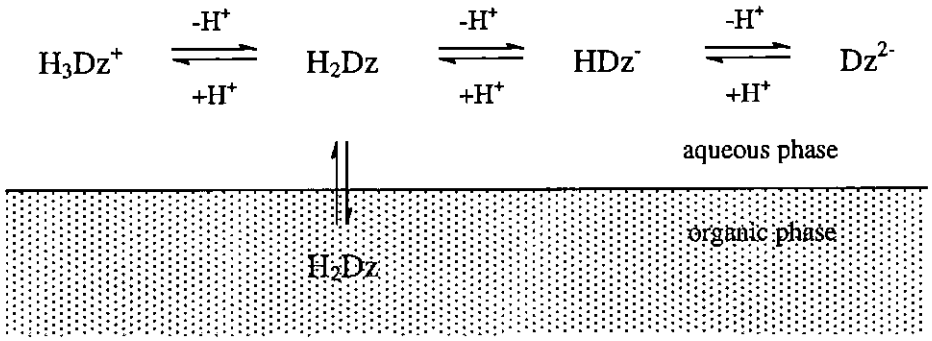


**Figure 2.3** The partition of dithizone between two miscible phases, e.g. water and organic solvent.

The second proton from dithizone is significantly labilised when the first is replaced by a metal. This is shown most convincingly by the behaviour of the yellow primary dithizonatophenylmercury(II), which gives rise to a magenta anion.

$$\text{(yellow) PhHgHDz} \rightleftharpoons \text{(magenta) PhHgDz}^- + \text{H}^+$$

A pK value of 11.46 for the above reaction could be determined by spectrophotometry in 52.8% (v/v) ethanol-water mixtures.[21,22]

The only crystal data that is available for a dithizone compound that is essentially ionic, is that of the potassium salt of dithizone,[23] prepared by addition of dithizone to *ca* 5% excess of KOH dissolved in either water or methanol.

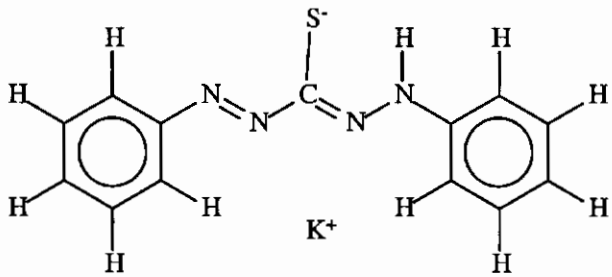


**Figure 2.4** The structure of the ionic compound, $K^+HDz^-$.

As opposed to the delocalised π-electrons in the free ligand (Figure 2.2), where no localised single or double bonds are observed, the anion clearly exhibits a high degree of localization. In the N-N-C-N-N backbone the two N-N bonds are 1.276 and 1.346 Å, while the N-C-N bonds are 1.410 and 1.320 Å respectively. The carbon-sulfur distance of 1.719 Å, however, is comparable with the 1.71 Å in the free ligand, which is indicative of some delocalization.

Aqueous alkali dithizone solutions are unstable, with the rate of decomposition increasing with pH and temperature. Decomposition is further accelerated by aeration and the presence of catalytic amounts of various metals. Addition of reducing agents such as hydroxylamine and sequestering agents such as EDTA slows the change down, but does not inhibit it.[24,25] Solutions in carbon tetrachloride are said to be stable indefinitely if the liquid is overlaid with dilute sulfurous acid, and stored in a cool dark place. The action of phosgene on dithizone in halogenated solvents led to the isolation of the yellow-brown product, 5-phenylazo-3-phenyl-1,3,4,-thiadiazole-2-one.[26]

$$CHCl_3 \xrightarrow[h\nu]{[O]} COCl_2 + HCl$$

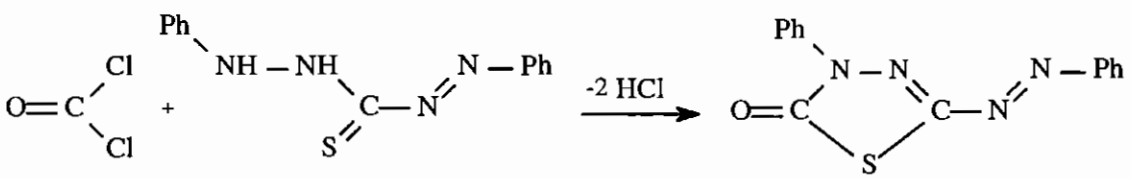


Yellow solutions of deteriorated dithizone can sometimes be reconverted into green dithizone almost quantitatively by treatment with sulfurous acid.[27] Two oxidation products, due to

deterioration of stock solutions, had been identified.[28,29] An investigation was done on the interaction of dithizone with elemental iodine, which is often used to oxidise thiols to disulfides. In dilute chloroform solutions, in the presence of water, dithizone immediately changed to a red ($\lambda_{max}$ = 420 nm) oxidised product and hydriodic acid appeared in the aqueous phase in stoichiometric amounts. The formation of the disulfide, $(HDz)_2$, is followed by a thermal fission reaction, yielding equal amounts of dithizone and a yellow compound (DDz) containing two fewer hydrogen atoms.

$$2\,H_2Dz + I_2 \rightarrow 2\,HI + (HDz)_2 \rightarrow H_2Dz + DDz$$

The fission reaction is markedly dependent on solvent polarity. At 25°C, $t_{½}$ for the disulfide increases from 10.5 minutes in acetone to 77 days in *n*-hexane. The final yellow oxidation product, DDz, was found to be identical with the tetrazolium salt, "dehydrodithizone", obtained by oxidizing dithizone with potassium hexacyanoferrate(III), or any of a variety of other oxidizing agents. In view of its polar character it has widely varied electronic spectra for different solvents, e.g. orange in acetone ($\lambda_{max}$ = 460 nm) and almost colourless in water ($\lambda_{max}$ = 380 nm).[29] Ogilvie and Corwin[30] were the first to suggest the meso-ionic structure (Figure 2.5) for orange crystalline dehydrodithizone, DDz, which was some time later confirmed by X-ray crystallography.[31]

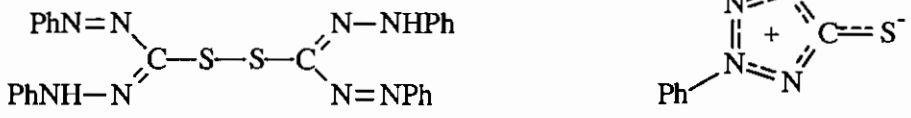


**Figure 2.5** Bis-1,5-diphenylformazan-3-yl disulfide (left), and the *meso*-ionic tetrazolium compound, dehydrodithizone, DDz (right)

Because dehydrodithizone has not extensively been studied as ligand, and its coordination characteristics are poorly defined, Walsh and coworkers[32] performed a single crystal X-ray analysis of a polypyridylruthenium(II) dehydrodithizone complex. The ligand was mono-coordinated through the sulfur atom, with no significant differences from those in the free ligand. The N-N bond lengths are 1.31 Å, compared to 1.30 Å in free dithizone, while the N-C-N bonds are 1.36 Å compared to 1.35 Å in dithizone. The C-S bond length of 1.69 Å is only slightly shorter.

Dehydrodithizone has been used as intermediate for the anchoring of dithizone on cross-linked poly(vinyl pyridine), which was eventually to be used for the preconcentration of nanogram levels of mercury.[33] Because of the enhanced nucleophilic properties of the meso-ionic

compound, displacement reactions on the chloromethylated group of the reactive polymer proceeded successfully. Opening of the heterocycle was achieved by treating the orange resin with a neutralised solution of ascorbic acid, resulting in a support carrying S-bonded dithizone. Reduction of dehydrodithizone can also be done, amongst others, with an alkaline solution of dextrose.[30]

Another well-studied S-bonded dithizone derivative is S-methyldithizone, which was originally prepared by Irving and Bell.[34] This was done by methylating dithizone in alkaline solution with $Me_2SO_4$, by the action of MeI on Ag(HDz), and by the action of NaSMe upon 1,5-diphenyl-3-chloroformazan. Freshly prepared solutions has two bands, at 270 and 550 nm ($\varepsilon_{550}$ = 1225 $dm^3.mol^{-1}.cm^{-1}$) in chloroform, which isomerises to a form with three bands, at 280, 420 ($\varepsilon_{420}$ = 1775 $dm^3.mol^{-1}.cm^{-1}$) and 540 nm. The band originally at 550 nm becomes less intense as the new band appears at 420 nm, while the colour changes from permanganate pink to yellow. Isomerisation is reversed on illumination. S-methyldithizone crystallises as a dark red solid by the concentration of solutions of either the pink or yellow forms,[35] while the *o*-tolyl homologue crystallises as yellow plates.[36]

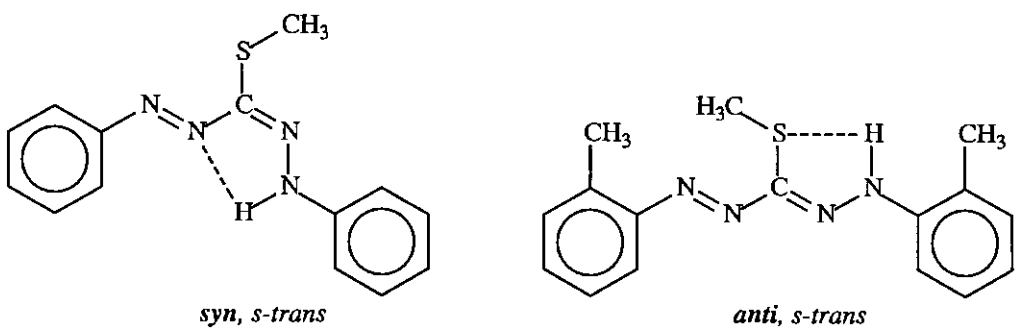


*syn, s-trans* *anti, s-trans*

**Figure 2.6** Configurational representations based on X-ray data of pink S-methyldithizone (left), and its yellow *o*-tolyl homologue (right).

One more crystal structure in this series, is that of the S-bonded carboxymethyl derivative (R-S-$CH_2COOH$),[37] which is equivalent to that of S-methyldithizone, both structurally and colourwise. Evidence from these three structures settles the origin of the different coloured species conclusively, namely that isomerisation around the -C=N- double bond yields the yellow and pink isomers.

## 2.1.3. Redox Properties

The redox properties of dithizone are governed by its thiol group and formazan structure, hence it can be both reduced and oxidised electrochemically. The fact that dithizone is a weak reducing agent is well known. Electrochemical investigations on dithizone was for the first time done by Tomcsanyi in 1975.[38] The redox behaviour of dithizone and its oxidation products were examined, and the mechanisms of the electrochemical and aerial oxidation of dithizone were considered. Both oxidation products, the disulfide and tetrazolium compounds, were followed by voltammetric methods.

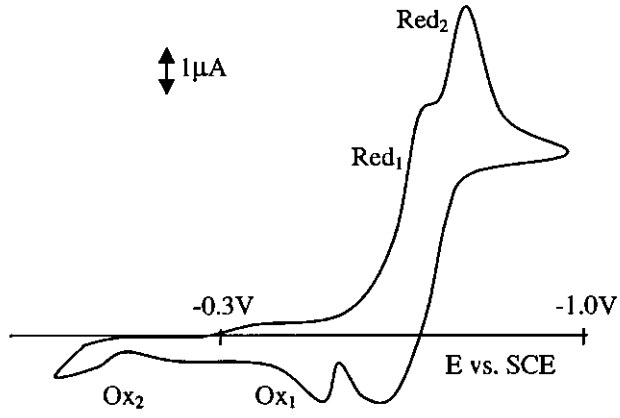


**Figure 2.7** Cyclic voltammogram of oxidised dithizone (DDz) solution at a hanging mercury drop electrode (HMDE). $Red_1$: DDz → $HDz^-$. $Red_2$: $HDz^-$ → $H_3Dz^-$. See Figure 2.4 for $HDz^-$ and Figure 2.5 for DDz structures.

The following scheme was proposed for the reduction of the autoxidised product:

$$DDz + 2e^- + H^+ \rightarrow HDz^-$$

$$HDz^- + 2e^- + 2H^+ \rightarrow H_3Dz^-$$

The oxidised product, DDz, is easily reduced to the dithizonato anion, $HDz^-$, which can then be further reduced at the N=N bond to form the corresponding colourless hydrazo compound, diphenylcarbazide, $H_3Dz^-$. In a separate experiment the $HDz^-$ → $H_3Dz^-$ reduction reaction was found to be completely reversible. Attempts to oxidise dithizone electrochemically to the tetrazolium compound, DDz, at the hanging mercury drop electrode failed. In the course of autoxidation of alkaline dithizone solutions, a new reduction polarographic wave was observed, which disappears completely in oxidised solutions. The wave corresponds to the reduction of a disulfide intermediate in the autoxidation process.

$$(HDz)_2 \rightarrow 2\,HDz^-$$

Mirkhalaf and coworkers[17] successfully attached dithizone to gold and indium tin oxide (ITO) electrodes. This was done by synthesizing a dicarboxylic acid derivative of dithizone. In this method a primary amine containing a terminal self-assembled active group (e.g. triethoxy silane for ITO and thiol for gold), without the use of coupling agents, rapidly reacted with the carboxylic acid of the synthesised compound. From the pH dependence of the cyclic voltammetric results the formation of a disulfide as the surface redox processes of the attached ligand was concluded.

A study done at the University of Baghdad[39] illustrates means by which dithizone can be stabilised against oxidation. In order to determine the acid dissociation constants and metal chelate formation equilibria of a series of dithizones, seven phenyl ring-substituted derivatives were synthesised (See Table 1). A 50% v/v aqueous dioxan solution was the medium for all absorbance measurements made in the determination of equilibrium constants. The stabilities of dioxan and chloroform solutions of the halogen substituted dithizones toward oxidation were found to decrease in the order, F > Cl > Br > I. This trend is expected when compared to the corresponding values for the acid dissociation constants, which decrease with increasing electron withdrawing ability of the substituent. A roughly linear correlation was found between the $pK_a$ values of the ligands and the value of the Hammet $\sigma$ constants of the substituents.

Metal equilibrium formation constants also follow the same trend. Variation of chelate stability with ligand basicity is in complete accord with the conventional $pK_a - \log K_f$ relationships.

**Table 2.1** Acid dissociation constants of dithizones and formation constants of their 1:1 Co(II) chelates in 50% v/v aqueous dioxan solutions of 0.10 M ionic strength at 25°C.

| **Dithizone** | **$pK_a(\lambda^*)$** | **$\log K_{f1}(\lambda^*)$** |
|---|---|---|
| Di-*p*-$CH_3$-phenyl | 6.40 | |
| Di-*o*-$CH_3$-phenyl | 6.23 | |
| Diphenyl | 5.77 | 6.43(520) |
| Di-*p*-F-phenyl | 4.99 | 5.94(440) |
| Di-*p*-Cl-phenyl | 4.63 | 5.63(440) |
| Di-*p*-Br-phenyl | 4.40 | 5.39(520) |
| Di-*p*-I-phenyl | 4.03 | 4.84(440) |
| Di-*m*-$CF_3$-phenyl | 2.57 | 3.48(580) |

* Absorbance measurements at wavelength maximum of metal complex

# 2.2. Dithizone – Metal Complexes

## 2.2.1. Analytical Applications

In 1925 Helmuth Fischer[40] showed the great potential of dithizone for the detection and determination of heavy metal ions. Through the years it has become more or less indispensable in trace metal analysis. The output of published work in this field reached a peak of about 100 publications per annum in the sixties. Since then, the role of dithizone as most sensitive reagent for the direct determination of traces of metals, by liquid-liquid extraction followed by spectrophotometry, gradually became less important. In 1977 Harry Irving did a thorough review of the whole subject.[2,41]

| | | | | | | | | | | | | | | | | | |
|---|---|---|---|---|---|---|---|---|---|---|---|---|---|---|---|---|---|
| H | | | | | | | | | | | | | | | | | He |
| Li | Be | | | | | | | | | | | B | C | N | O | F | Ne |
| Na | Mg | | | | | | | | | | | Al | Si | P | S | Cl | Ar |
| K | Ca | Sc | Ti | Y | Cr | Mn | Fe | Co | Ni | Cu | Zn | Ga | Ge | As | Se | Br | Kr |
| Rb | Sr | Y | Zr | Nb | Mo | Tc | Ru | Rh | Pd | Ag | Cd | In | Sn | Sb | Te | I | Xe |
| Cs | Ba | La | Hf | Ta | W | Re | Os | Ir | Pt | Au | Hg | Tl | Pb | Bi | Po | At | Rn |
| Fr | Ra | Ac | Th | Pa | U | | | | | | | | | | | | |

**Figure 2.8** Indicated metals can be extracted as dithizonato complexes from aqueous solution into organic solvents and precipitated as sulfides.[3]

By making use of dithizone in ethanol as extractant, Van Staden and Taljaard[42] very recently (2004) developed systems for the simultaneous sequential injection analysis of South African soil and water samples containing many different metal ions. Results comparable to that obtained by means of atomic absorption spectrometry (AAS) were obtained with this inexpensive and low maintenance technique. At the same time Comitre and Reis,[43] also utilizing dithizone as complexing agent, achieved spectrophotometric detection limits of 12 parts per billion for the analyses of lead in plant materials. Results, once again, compare well with those obtained employing inductively coupled plasma optical emission spectroscopy (ICP OES).

## 2.2.2. Structures

The structures of metal dithizonato complexes are well established with a total of eighteen X-ray data collections that have been reported up to date. Published structures include the following: $Hg(HDz)_2$,[44] $Cu(HDz)_2$,[45] $Ni(HDz)_2$,[46] PhHgHDz & MeHgHDz,[36] $Bi(HDz)_3$,[47] $Zn(HDz)_2$,[48] $In(HDz)_3$,[49] $Tl(EtOH)(Ph)_2(HDz)$,[50] $[MoO_2(Dz)(HDz)](n\text{-}Bu_4N)$,[51] [Au(Hdamp-$C^1$)(HDz)Cl]Cl

& [Au(Hdamp-$C^1$)(HDz)(Smetetraz)],[52] [{$Os_5C(CO)_{14}(\mu-\eta^2$-HDz$)_2\}_2(\mu_4$-Hg)] (**8**), [$Ru_2(CO)_4$Ph-{$\mu-\eta^2$-C(O)Ph}($\mu_2$-S)($\mu-\eta^2$-HDz')] (**9**), [$Ru_2(CO)_4${C(O)Ph}($\mu-\eta^2$-C(O)Ph}($\mu^2$-S)($\mu-\eta^2$-HDz')] (**10**) & [{$Ru_2(CO)_2$Ph}$_2(\mu-\eta^2$-HDz')$_2$] (**11**),[53] Pt{8-ethoxytricyclo(5.2.1.$0^{2,6}$)dec-3-en-9-yl} (HDz),[54] and Ru(2,2`-bipyridyl-N,N`)$(HDz)_2$.[55]

Except for slight twists of the dithizonato phenyl rings in some cases, the ligand is essentially planar in all the aforementioned structures. Ligands are bidentately coordinated to the respective metals, via S and N. An exception is found in $In(HDz)_3$, where one of its three HDz ligands is monodentately coordinated through sulfur. The same was observed for the above ruthenium complex. Ligands are in the *anti, s-trans* configuration (see Figure 2.6, p.9). The only exception is found in the osmium cluster compound **8**, where both ligands are, due to steric reasons, in the *syn, s-trans* configuration. An interesting observation made for the first time, is that the dithizonato sulfur in the four cluster compounds **8 - 11** is coordinated to two adjacent metal centers, serving as a bridge between the metals. The $M_a$-S-$M_b$ bond angles are close to 90°, depending on the cluster, with the one metal ($M_b$) lying almost perpendicular to the ligand plane. The $M_a$-S bonds are on average 0.05 to 0.09 Å shorter than the S-$M_b$ bond lengths.

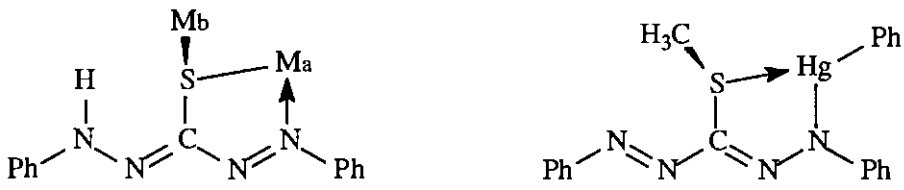


**Figure 2.9** M-S-M configuration in cluster compounds **8 - 11** (left). S-methyldithizonatophenylmercury(II) (right).

As opposed to the cluster compounds, the Hg-S-$CH_3$ bond angle in S-methyldithizonatophenylmercury(II) is expected to be closer to 109.5° (out of the plane), due to the almost tetrahedral electron orbital configuration on the sulfur atom. The bond angle is also not restricted by bonding to adjacent atoms as is the case in the clusters.

S-methyldithizonatophenylmercury(II) was for the first time synthesised by Irving and coworkers.[56] The reagent acts as a monobasic acid, as opposed to the dibasic acid, dithizone. In the complexation reaction the imino hydrogen is replaced by the cation in the presence of sodium carbonate. The bidentate ligand is expected to be coordinated through nitrogen and the methylated sulfur. Unfortunately no X-ray data collection from a compound of this type has yet been performed.

Having lost its imino proton, the deep yellow-green compound, S-methyldithizonatophenylmercury(II) does not exhibit photochromic behaviour, as does the parent compound, dithizonatophenylmercury(II).

Although the complexes under discussion lend itself ideally towards quantum computational investigation with regard to structural and electronic properties, no such work had been published as yet. Other photochromic compounds like dinuclear molybdenum complexes,[57,58] 2-(2',4'-dinitrobenzyl)pyridine,[59] and indolylfulgide[60] had been investigated by means of *ab initio* Gaussian, density functional theory (DFT) and PM3 techniques.

Geometry optimizations reproduced experimental geometries satisfactorily, thereby proving this technique to be a suitable tool for the investigation of possible photoisomers associated with photochromism. In addition, density functional theory is known as a useful tool for the theoretical study of transition metal complexes because of the feature of including electron correlation.[61-63]

In order to elucidate the mechanism of photochromism observed for $[Mo_2(\mu\text{-}S_2)(\mu\text{-}S_2C_2Ph_2)_2(S_2C_2Ph_2)_2]$, **12**,

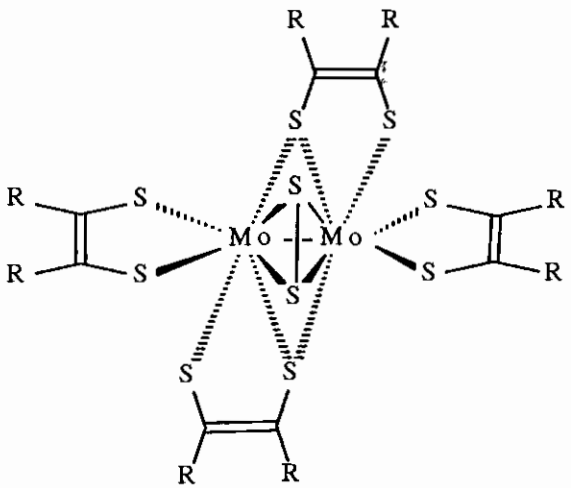


**12** (R = Ph, H or *n*-Bu)

all phenyl groups were replaced by hydrogens, and optimization done by using *ab initio* and hybrid DFT (B3LYP) programs. The authors found that B3LYP/3-21G afforded the best results. Time dependant density functional theory (TDDFT) was applied to the calculation of the electronic spectrum of the dinuclear molybdenum complex, phenyls included. This approach proved to be useful and in reasonable agreement with experimental data.

The photochromic property of $[Mo_2(\mu\text{-}S_2)(\mu\text{-}S_2C_2Ph_2)_2(S_2C_2Ph_2)_2]$ originates from the isomerisation at the lowest excited state, and the analysis of its electronic properties suggests that the charge transfer transition from the $\pi$-orbitals of the bridged ethylene-1,2-dithiolate ligand to Mo d-orbitals of **12** would trigger the isomerisation. It is well-known that the photochromism of spiropyrane (See Fig. 2.11) is also due to the photoisomerisation at the lowest excited state.[64,65]

## 2.2.3. Photochromism

Photochromism refers to a reversible phototransformation of a chemical species between two forms having different absorbance spectra. Photochromic compounds reversibly change not only the absorbance spectra under certain conditions, but also their geometrical and electronic structures. The molecular structure changes induce physical property changes of the molecules, such as fluorescence, refractive index, polarizability, electrical conductivity, and magnetism. Photoswitching of these physical properties can be accomplished by appropriate design of the molecules. By feeding back the evaluation of these physical properties to the molecular design, more sophisticated photoresponsive molecular systems can be constructed.

Metal dithizonates form an interesting class of photochromic compounds. In spite of the fact that several dyes as diarylethenes,[66] spiropyrans[67] and fulgides[68] have dominated in the world of photochromism, the interest in metal dithizonates still exists.

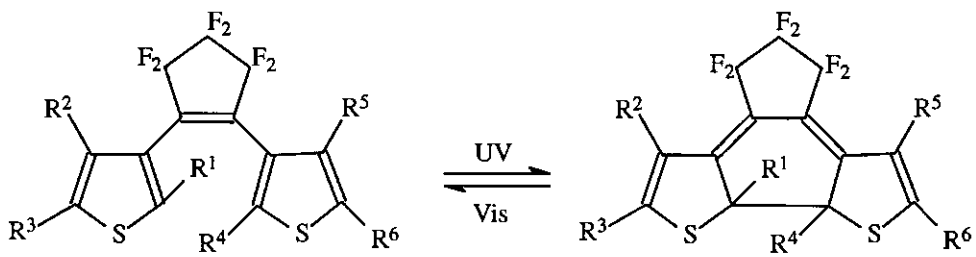


**Figure 2.10** Photochromism of diarylethene

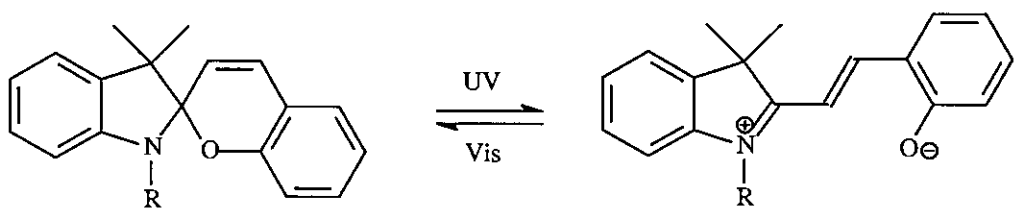


**Figure 2.11** Photochromism of spiropyrans

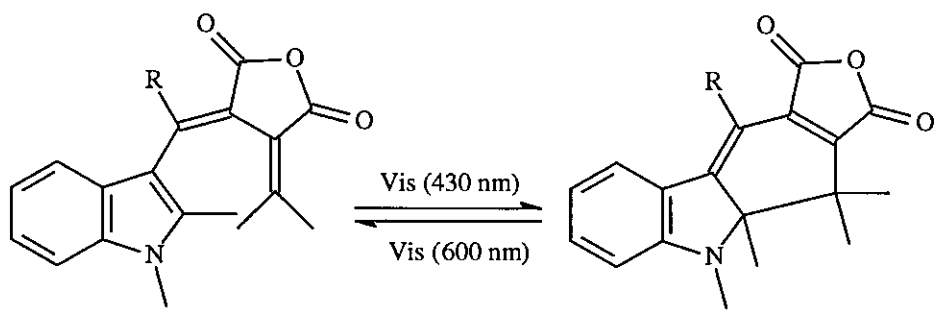


**Figure 2.12** Photochromism of indolfulgides

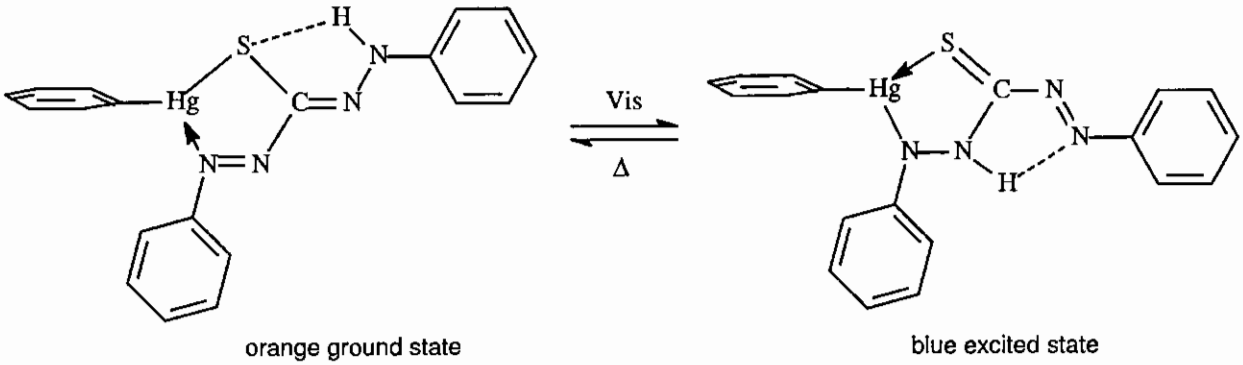


**Figure 2.13** Photochromism of dithizonatophenylmercury(II)

The reasons for the continued interest in metal dithizonates are because:

**a)** dithizone forms strongly coloured complexes with many different metals,

**b)** the synthesis of the complexes is a simple chemical process,

**c)** the photochromic cycle can be repeated many times,

**d)** the complexes are compatible with different mediums as solvents, polymers and host-guest systems, and

**e)** the complexes can be attached to polymer chains, glass surfaces, textile and paper.[69]

Around 1950 Irving and coworkers,[70] and Webb and coworkers,[71] reported independently that the dithizonatomercury(II) complex is photochromic. For 15 years these unusual findings were never followed up, until Meriwether, Breitner and Sloan did a thorough investigation which led to the discovery of a large number of photochromic metal dithizonates (Table 2.2).[7]

Metal dithizonates have very limited solubilities in the usual organic solvents. The highest solubility is usually found in chloroform, although carbon tetrachloride, dichloromethane, toluene, tetrahydrofuran, acetone and ethyl acetate are also satisfactory solvents for spectrophotometric studies. Most dithizonates are either insoluble or very slightly soluble in ethanol and methanol. They are insoluble in water. Dimethylformamide, pyridine and acetonitrile solutions also tend to have unusual colours, indicative of strong interaction with the solvent. The complexes often cannot be recovered unchanged from these polar solvents.

The photochromic property, as measured by the return rate in solution, is very sensitive to the polarity of the solvent and the presence of acids and bases. The strongest photochromic effects are observed in dry, non-polar solvents, such as the halogenated solvents, carbon disulfide and toluene. Hydroxylic solvents and organic acids and bases are generally the poorest media for observing photochromism. This results from their accelerating effect on the rate of return of the activated form to the normal form. Addition of a few drops of ethanol, acetic acid or triethylamine reduces the return reaction half-life profoundly.

**Table 2.2** Photochromic reactions of metal dithizonates.[7] The activated form results from irradiation with light .

| Complex | Solvent | Colour and absorbance maxima (nm) | | Temp. (°C) | Approx. return time (s) |
|---|---|---|---|---|---|
| | | Normal form | Activated form | | |
| $Pd(HDz)_2$ | Chloroform | Green (450, 640) | Blue (450, 520, 570, 630) | 25 | 5-10 |
| | Benzene | Green | Orange | 25 | 5-10 |
| | Dichloromethane | Green | Orange | -10 | 1-2 |
| $Pt(HDz)_2$ | Benzene & carbon tet. | Yellow (490, 708) | Red | 25 | 1-2 |
| $AgHDz{\cdot}H_2O$ | Tetrahydrofuran | Yellow (470) | Violet | 25 | 2-5 |
| | | | | 10 | 40-60 |
| $Zn(HDz)_2$ | Dichloromethane | Red (530) | Violet-blue | 25 | 1-2 |
| | Tetrahydrofuran & ethylacetate | Red | Violet-blue | -40 | < 1 |
| $Cd(HDz)_2$ | Tetrahydrofuran & acetone | Orange (500) | Violet | -80 | <1 |
| $Hg(HDz)_2$ | Benzene & chloroform | Orange (490) | Blue (605) | 25 | 30-90 |
| $Pb(HDz)_2$ | Tetrahydrofuran | Red (520) | Blue | -80 | < 1 |
| $Bi(HDz)_3$ | Dichloromethane, xylene, ethyl acetate & methanol | Orange (498) | Violet | -30 | < 1 |
| | Pyridine | Orange | Violet | -30 | 10 |
| $BiCl(HDz)_2$ | Tetrahydrofuran & dichloromethane | Orange (490) | Blue (605) | -40 | 2-5 |

Although the metal has very little effect on the colour of the activated form, it has a marked influence on the rate of return to the normal form. These return reaction rates range from a half-life of about 30 seconds for mercury compounds at 25°C, to less than 1 second for cadmium and lead compounds at -80°C. At high levels of illumination it is possible to achieve a steady-state system at 25°C in benzene containing 80-90% of the total mercury complex in the activated form. No particular significance can be drawn from the order of metals in increasing the apparent return rate: Hg < Pd < Ag < Pt ~ Zn < Bi < Cd < Pb. Failure to observe spectral changes in the remaining metal dithizonates may simply be the result of very high return reaction rates. Preliminary results of flash photolysis studies support the assumption that all metal dithizonates are photochromic. In benzene solution at 25°C $Ni(HDz)_2$ has a half-life for the return reaction of less than 50 μs, and the half-life of TlHDz is about 30 ms. Spectral changes similar to those observed in the other photochromic complexes were found.

Spectral studies of the metal dithizonates in solution over the temperature range -80 to +80°C failed to produce evidence of thermochromism. The rate of colour change from the normal to the activated form under conditions (very low temperature) where the return reaction is repressed, is a function of the intensity of activating light only. The activation reaction thus appears to be a strictly photochemical process. On the other hand, the return reaction rate displays the usual temperature dependence and is the same in the light as in the dark, indicating the absence of a photochemical return reaction. Analysis of the time-dependant spectral changes in the return of the mercury and silver complexes has revealed a single isosbestic point between the normal and the active forms, showing the absence of reaction intermediates. Therefore, the over-all photochromic reaction of metal dithizonates in solution may be described by the simple expression

$$\text{normal form} \underset{\Delta \text{ (pathway II)}}{\overset{h\nu \text{ (pathway I)}}{\rightleftharpoons}} \text{activated form}$$

in which the steady-state concentration of the normal and activated forms is a function of both temperature and activating light intensity.

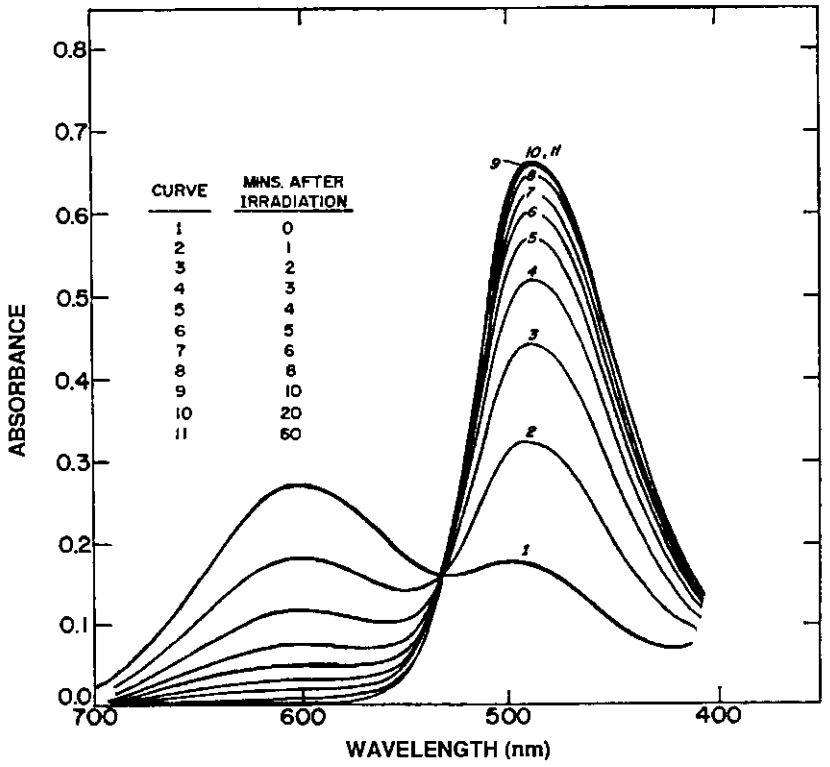


**Figure 2.14** Visible spectrum of return reaction of $Hg(HDz)_2$ ($9.4 \times 10^{-6}$ M) after irradiation in benzene at 25°C. ($\varepsilon$ = 70 000 at 490 nm for the yellow-orange isomer, and $\varepsilon$ = 39 000 at 605 nm for the blue isomer).[72]

In order to test whether free-radical species were produced in the photochromic reaction, a dilute solution of $Hg(HDz)_2$ in benzene was irradiated with visible and near-ultraviolet light at 25°C in the resonant cavity of an electron spin resonance spectrometer. No e.s.r. signals were detected. This system was also insensitive to the presence of free-radical initiators. These results coupled with the strong effect of acids and bases on the systems would suggest that we are dealing with essentially ionic processes and that any excited state species formed in the photochemical reaction must be of extremely short lifetime. More detailed studies of the return reaction of $Hg(HDz)_2$ have confirmed the ionic character of the process.[8]

All the complexes investigated by Meriwether and coworkers were stable to visible light of wavelength longer than 400 nm. Therefore, a low pressure Hg arc source was used during the experiments. With the exception of dithizone and AgHDz they were unaffected by light of $\lambda >$ 360 nm. Rapid decomposition took place when the solutions were exposed to wavelengths down to 320 and 300 nm. Since all of the complexes possess a weak absorption band at 320 nm, photochemical instability must reside in this band. As compared to the stability of the free ligand, formation of the metal complex has a strong stabilizing effect on the light tolerance of the ligand. This might perhaps be attributed to the harmless dissipation of excitation energy in the photochromic process, as observed in various ultraviolet absorbers.[73]

Together with all the above-mentioned "primary" dithizonates (MHDz), some non-photochromic "secondary" dithizonates of Pd(II), Cu(II) and Ag(I) were also synthesised by Meriwether and coworkers. The secondary complexes are formally derived from the dianion, $(PhNN)_2CS^{2-}$.

$$M^{n+} + (n/2)H_2Dz \rightarrow M(Dz)_{n/2} + nH^+$$

These complexes differ from the previously mentioned osmium and ruthenium cluster compounds wherein two metals share one primary dithizonate ligand, but are equivalent to the S-methyldithizonato metal complexes in that both protons are displaced. Elemental analyses of the secondary compounds clearly support the compositions, $Ag_2Dz$ and $PdDz{\cdot}2H_2O$. A secondary mixed-metal complex, $Hg(AgDz)_2$, was also prepared by Irving and Jankowska.[74] When a solution of primary mercury(II) dithizonato, $Hg(HDz)_2$, in chloroform is shaken with aqueous silver nitrate in excess, the typical orange colour changes to magenta ($\lambda = 512$ nm). The thus formed $Hg(AgDz)_2$ is readily reverted by 0.1 M sulfuric acid. Absorbances of chloroform solutions of primary mercury and primary silver dithizonates are additive, showing the absence of any molecular interaction.

X-ray structural determinations of these compounds are much needed.

# 2.3. Photochromic Polymers

Solid photochromic polymeric materials may be obtained by either anchoring the photochromic compound via a suitable functional group onto the polymer to give a polymer photochromophore blend, or co-dissolving the compound with a polymer, and evaporating the solvent. Pure solid dithizonatophenylmercury(II) is not photochromic at all, arguably due to space restriction in solids which prohibits the photochromic isomerisation reaction from taking place.

## 2.3.1. Functionalization of Dithizonatophenylmercury(II)

To be part of a polymeric structure, dithizonatophenylmercury(II) has to be anchored via a functional group on the mercury-bonded phenyl group. There are two reasons why the dithizone phenyl rings should not be considered for functionalization. Firstly, the synthesis of unsymmetrical dithizone ligands, i.e. with only one phenyl ring carrying a substituent, promises to be largely problematic in view of the presently known synthetic procedures. If it could be done, however, the question remains; which of the two phenyls will carry the substituent – the one closest, or furthest from the metal? (See Figure 2.13, p.16) The second reason is that due to added rigidity to the dithizonato structure, anchoring via the photochromic ligand itself might inhibit or even completely prevent the photochromic isomerisation reaction from taking place.

A large variety of organomercury(II) dithizonato complexes have already been synthesised, amongst others, the following series: $XArHg^+$, where Ar = phenyl, and X = *p*-F, *p*-Cl, *p*-Br, *p*-I, *p*-Me, *o*-MeO, *o*- and *p*-OH, *o*- and *p*-COOH, *p*-$NH_2$, *p*-$NHCOCH_3$, *p*-$NMe_2$, and also Ar = $C_6F_5$ and 2-hydroxy-3-nitrophenyl.[22, 80-81] This series demonstrates the versatility of mercury to be complexed with a diverse range of phenyl ring substituted ligands.

The following reaction scheme illustrates a convenient synthesis of an amine functionalised phenylmercury(II) acetate complex, as well as a follow-up reaction of the amino group, without destroying the mercury coordination sphere.[77,78]

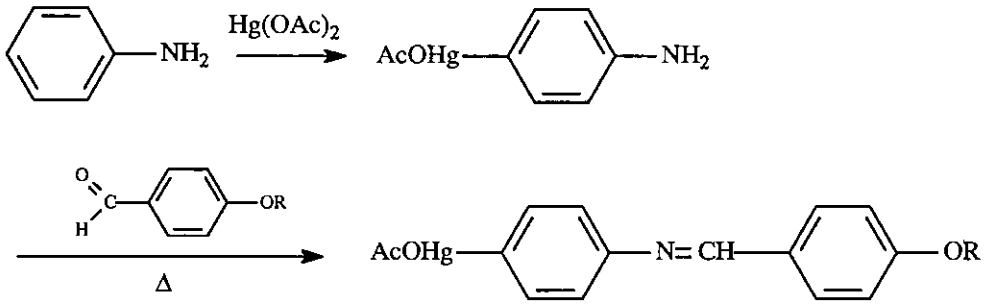


**Scheme 2.1** The synthesis of *p*-aminophenylmercury(II) acetate, a useful intermediate for anchoring mercury complexes onto organic structures. Heating the powdered amine/aldehyde mixture produces an enamine or azomethine product.

Pure *p*-aminophenylmercury(II) acetate is simply prepared by addition of two moles of freshly distilled aniline to 1 mole of mercury(II) acetate in water. The white precipitate that forms within a few minutes of stirring, is the desired product. An azomethine linkage can then be established by doing a condensation of an aldehyde with the primary amine.[77] Because *p*-aminophenylmercury(II) acetate is extremely insoluble, this reaction was done in the solid state. 4-Methoxybenzaldehyde was intimately mixed with a finely powdered sample of the mercury salt, and heated for 2 minutes at 150°C. A yield of more than 75% of the desired product was obtained.

Generally, in reactions with mercury(II), phenols and primary or secondary aromatic amines can have initial reactions occurring at the -OH or $-NH_2$ groups to give oxygen-mercury and nitrogen-mercury species. Subsequent rearrangement leads to ring substitution, particularly at low pH.

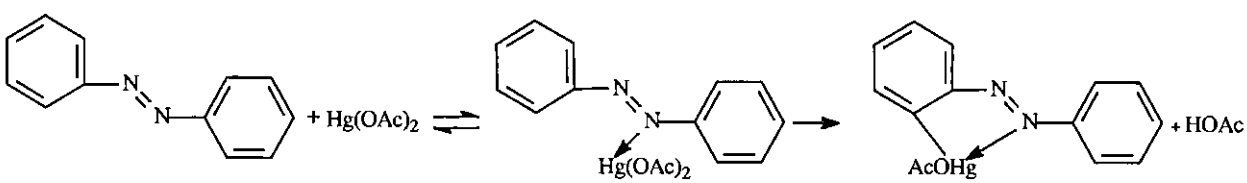


**Scheme 2.2** Complexation of azobenzene with $Hg(OAc)_2$, and the consequent rearrangement that typically takes place.

Mercuration of substituted aromatics suffers from lack of selectivity, with all possible ring substitution products frequently occurring. The usual directing effects of the substituents are operable, but the selectivity is poor. The reaction of $Hg(OAc)_2$ with refluxing toluene for example, gives 41% *ortho*-, 21% *meta*- and 37% of the *para* isomers. Additionally, reactions are often reversible and isomerisation of the initial products may result.[79]

Apart from organomercury(II) compounds forming 1:1 complexes with the monoamines,[80]

$$H_3CHg^+ + R_3N \rightarrow [H_3CHgNR_3]^+$$

organomercury(II) bases, in particular the hydroxides (e.g. PhHgOH), react with a variety of nitrogen acids, including amines, carboxamides, imines, imides, etc.[79] The ease of reaction depends on the acidity of the nitrogen acid. For reactions with less acidic compounds, such as aniline, water must be removed as an azeotrope with benzene to drive the reaction over to the product side.

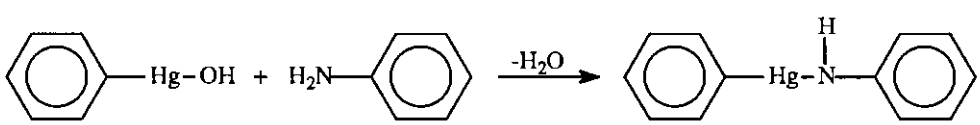

It is therefore evident that reactions of mercury(II) salts with substituted phenyls in general yield a variety of products or product mixtures, depending on reaction conditions, the phenyl substituents and the salt anion. This is quite contrary to the one pure high yield product, aminophenylmercury(II) acetate, obtained from the reaction between mercury(II) acetate and aniline, leaving it as reagent of choice with regard to polymer anchoring procedures.

Not only can the aniline functional group directly be utilised in anchoring reactions, but it may also be converted into a carboxylic acid. This may conveniently be done via its reaction with succinic anhydride.[81]

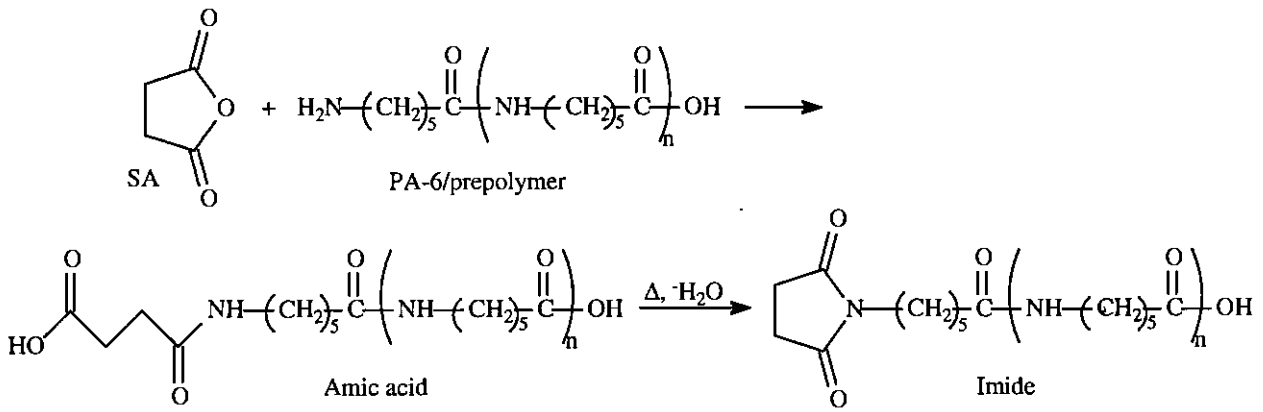


**Scheme 2.3** Amine end group modification of Nylon 6 polymer or prepolymer with succinic anhydride ( SA ).

## 2.3.2. Synthesis of functionalised polymers

Any of a wide range of polymers might have been selected for purposes of this research project. As a starting point, derivatives of polysuccinimide (PSI) as hydrophilic-, and polyepichlorohydrin (PECH) as lypophilic polymer were selected as polymeric supports for the dithizone-based photochromic moiety.

**a) Poly-DL-succinimide and derivatives**

Poly-DL-succinimide is prepared by mixing DL-aspartic acid and 85% orthophosphoric acid.[82] The reaction mixture is heated for 2½ hours while kept under reduced pressure. After dissolving the cooled reaction mixture in dimethylformamide, the solution is poured into water, and the precipitated polymer filtered, washed and dried. The solid is ground under liquid nitrogen and dried under reduced pressure over $P_2O_5$ in an Abderhalden drying tube to prevent hydrolytic ring opening reactions.

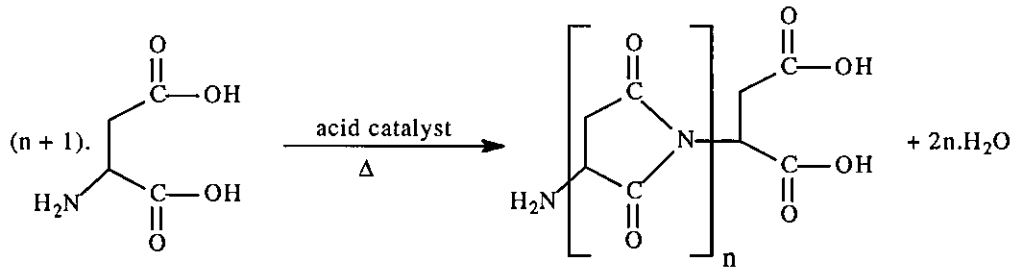


**Scheme 2.4** Synthesis of polysuccinimide from DL-aspartic acid at high temperature, using $H_3PO_4$ as acid catalyst.

The advantage of the above reaction procedure is that no solvent is additionally required and that orthophosphoric acid allows for reaction temperatures of up to 200°C. Sulfuric acid might also be used instead. An alternative method[83] of polysuccinimide synthesis allows for smaller amounts of orthophosphoric acid, though with the use of solvents like mesitylene, sulfolane, diethylbenzene or a combination of these. The water that forms during the 4½ hour polycondensation reaction is removed by means of a Dean-Stark trap, and after removal of the solvent the residue is washed with water and methanol. Reaction temperatures in excess of 160°C give yields of up to 96%.

The succinimide rings in the backbone of polysuccinimide can be easily opened by nucleophilic attack.[84] Under carefully controlled reaction conditions, these ring opening reactions could lead to polymers with functionalised side chains including amines (Scheme 2.5). The side chains themselves can be chosen from a large pool of compounds, including saccharides, nucleotides, esters, urethanes, thio-ethers and disulfides.[85] By carefully selecting the side chains that are to be introduced into polysuccinimide, the properties of the resulting polymer can be tailored to meet the requirements of a specific application. The reaction of polysuccinimide with N-(3-aminopropyl)morpholine converts the parent lypophilic polysuccinimide into a polymer that is highly water-soluble. Polysuccinimide, otherwise, is almost only soluble in dimethylformamide and dimethylsulfoxide.

Swarts and coworkers synthesised a water-soluble polymeric drug carrier system (Scheme 2.5, Compound **13**) to which the ferrocene-containing antineoplastic agent was covalently bound.[86,87] The improved water solubility of the polymeric ferrocene-containing anticancer drug led to an increase in cytotoxicity for the ferrocenyl group of almost one order of magnitude. The above ferrocene-containing molecule serves as a model for the anchoring of a suitably functionalised dithizonatophenylmercury(II) complex on a water-soluble polymeric substrate. A key feature of this reaction sequence is the coupling of a carboxylic acid-functionalised ferrocene derivative with the amine containing side chains of the polymer.

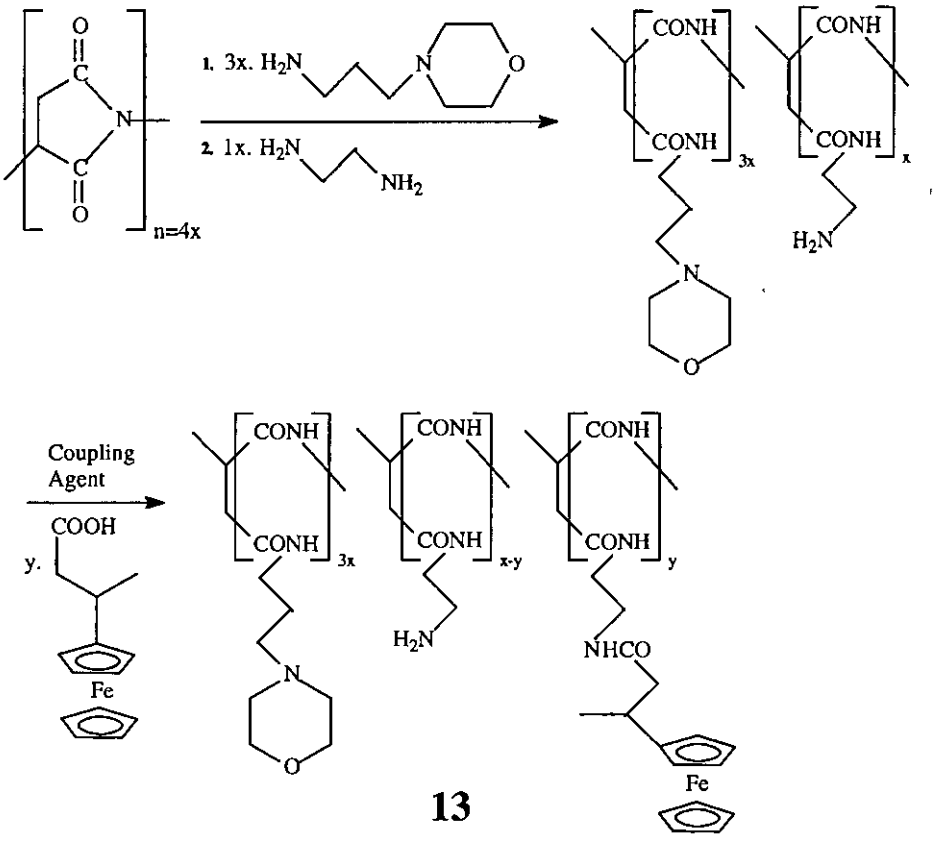


**Scheme 2.5** A water-soluble polymeric drug carrier prepared from the consecutive reactions of N-(3-aminopropyl)-morpholine, ethylenediamine and ferrocenylacetic acid with polysuccinimide. Ferrocenylbutanoic acid was coupled to the unreacted amine on the ethylenediamine side-group.

Coupling reactions between carboxylic acids and amines usually occur under forcing (high temperature) conditions or require the use of specialised coupling reagents like O-benzotriazolyl-N,N,N',N'-tetramethyluronium hexafluorophosphate. This coupling agent may be prepared in yields of up to 86%, as described by Dourtoglou.[88]

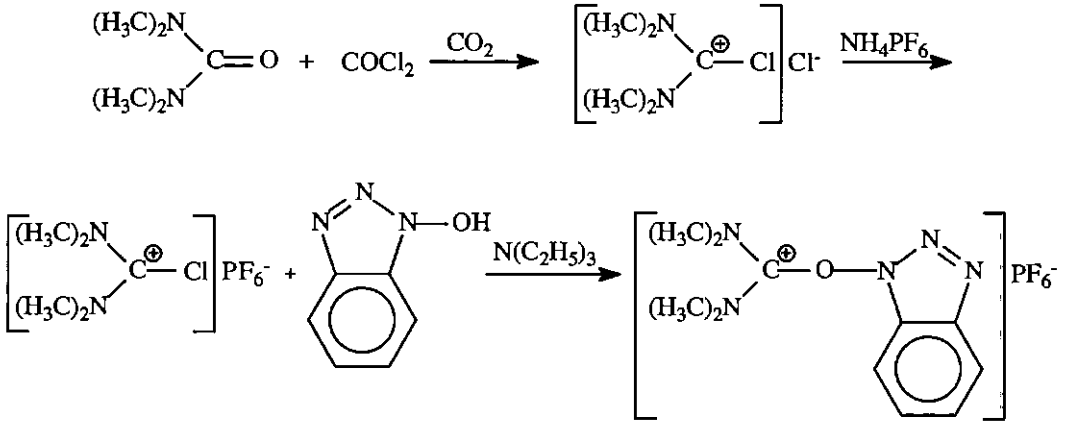


**Scheme 2.6** Synthesis of O-benzotriazolyl-N,N,N',N'-tetramethyluronium hexafluorophosphate, an ideal reagent for coupling organic acids and amines.

Reaction conditions are very simple; the coupling is achieved by mixing a solution of the acid and the amine with the coupling reagent in stoichiometric amounts in the presence of a tertiary base such as triethylamine. Reaction times are short (~15 minutes), with high yields.

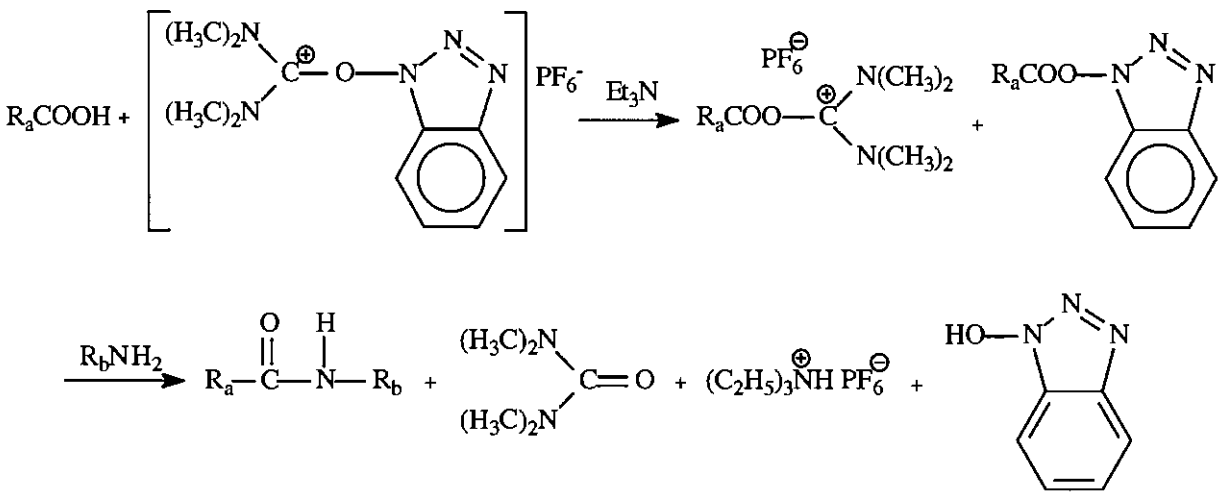

**Scheme 2.7** The coupling of carboxylic acid, $R_aCOOH$, with amine, $R_bNH_2$, by making use of the coupling reagent, O-benzotriazolyl-N,N,N',N'-tetramethyluronium hexafluorophosphate. The method involves *in situ* conversion of the acid to an activated ester, followed by coupling reactions with the primary amino group.

**b) Polyepichlorohydrin and derivatives**

Polyepichlorohydrin, on the other hand, is a lypophilic polymer, that may be substituted at the –Cl position. Polyepichlorohydrin is prepared by ring opening polymerization of the substituted oxirane monomer, namely epichlorohydrin, using different types of initiators.[89] Though three-membered epoxy ring compounds are known to undergo polymerization both by anionic and cationic mechanisms, polymerization of epichlorohydrin is usually brought about by the cationic mechanism, using Lewis acids such as $BF_3$ etherate, $SnCl_4$, $SbCl_5$ or $FeCl_3$. A protic compound such as water, alcohol or a diol is often required as co-initiator, interacting with Lewis acids like $BF_3$ etherate as shown in Scheme 2.8. In the first step, protonation of the monomer produces a secondary oxonium ion (activated monomer).

The product obtained during polymerization of epichlorohydrin depends on the type of initiator and the mechanism of propagation. There are two types of mechanistic pathways for the cationic ring opening polymerisation reaction of epichlorohydrin. In the active chain end mechanism there is always an excess of epichlorohydrin present and the growing point of the polymer is not destroyed before all the starter monomer is consumed. The reaction is hydroxyl terminated by the addition of a dialcohol.

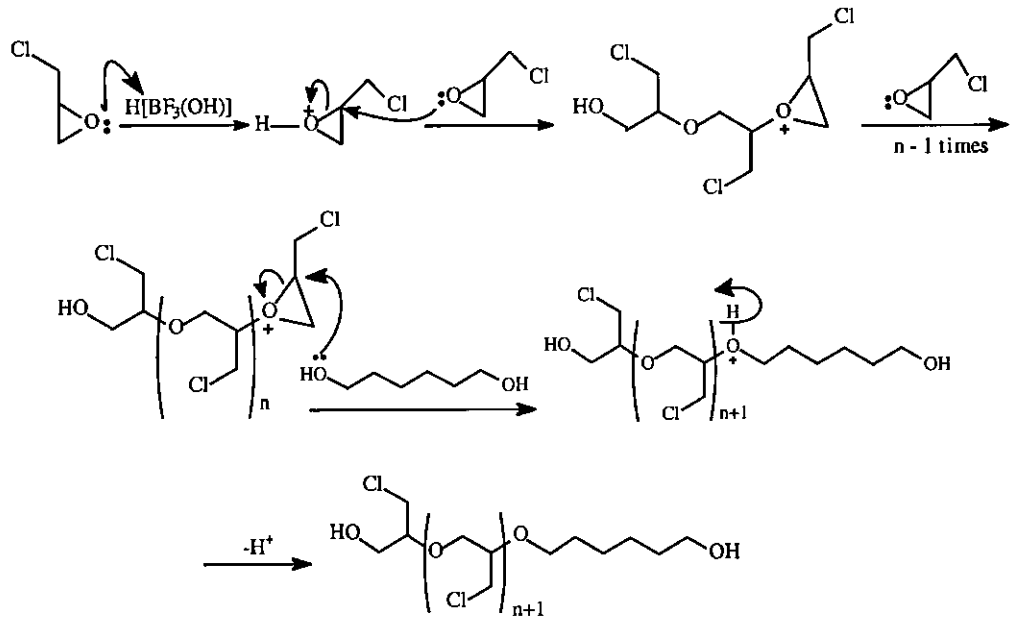


**Scheme 2.8** Epichlorohydrin polymerization. The active chain end mechanism.

A disadvantage associated with the activate chain end mechanism is that the polymer chain possesses highly reactive end groups which do not only react with the monomer but also with hetero-atoms of the polymer chains, leading to the formation of cyclic oligomers (dioxanes) and a polymer with reduced molar mass. To reduce the risk of cyclic oligomers from forming, the presence of a protic compound such as water, alcohol or diol is required as co-initiator or chain transfer agent at the outset. Protic compounds interact with Lewis acids like $BF_3$, and the protonation of the monomer produces a secondary oxonium ion (activated monomer).

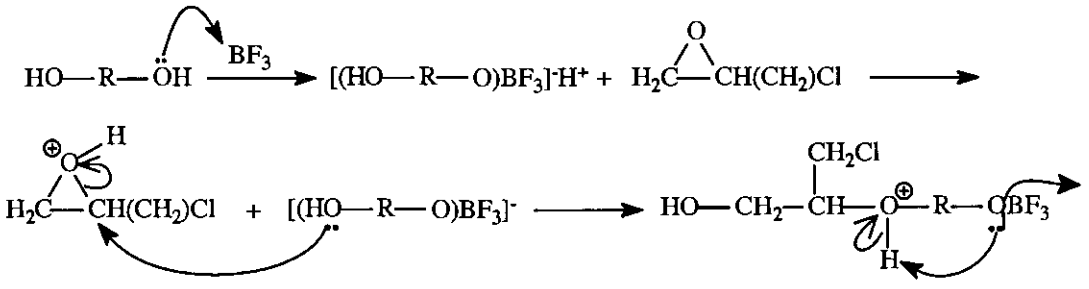


**Scheme 2.9** The interaction of a diol with borontrifluoride in the polymerisation reaction of epichlorohydrin.

The activated monomer reacts with the diol molecule to give hydroxy terminated macro-monomers. The monomers further react with the activated monomer, resulting in high molar mass polyepichlorohydrin with hydroxy end groups. This mechanism is known as the so-called active monomer mechanism (Scheme 2.10). Hereby the growing point of the polymer is terminated after each separate epichlorohydrin attack on the dialcohol.

The two mechanisms can coexist. The proportion of their contribution to chain growth depends on the oxirane monomer structure and polymerisation conditions. When the amount of epichlorohydrin is always less than the amount of dialcohol, conditions favour chain growth

according to the active monomer mechanism. The average molar mass of the formed product is governed by the final epichlorohydrin to diol reaction ratio.

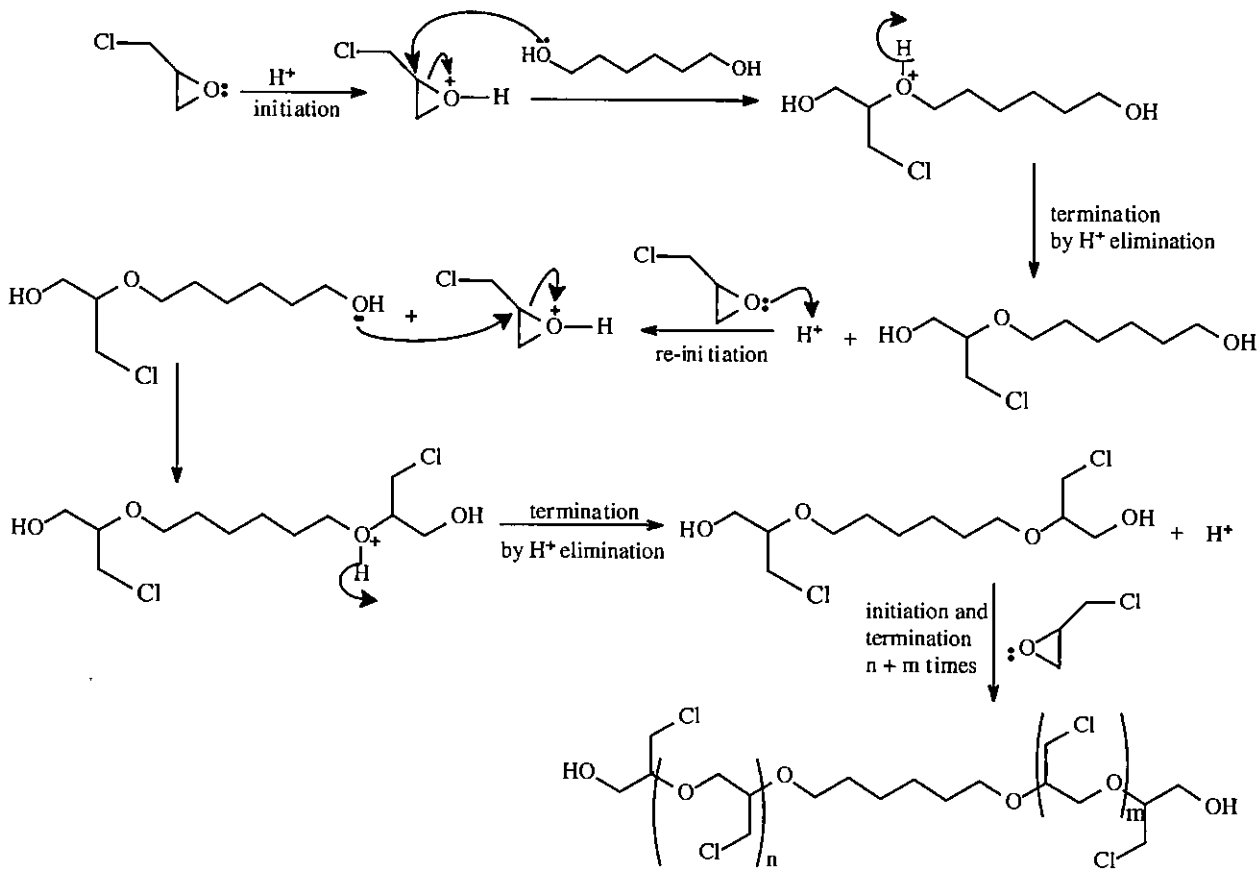


**Scheme 2.10** Epichlorohydrin polymerization. The active monomer mechanism.

The -Cl group in the side chain of polyepichlorohydrin, dissolved in chloroform or dimethylsulfoxide, reacts via nucleophilic substitution wherein –Cl is substituted by R-$NH^-$ or R-$O^-$ groups, amongst others. These reactions are temperature driven and has to be done in the presence of a base salt, like sodium bicarbonate, to remove the liberated HCl.[90,91] For the purpose of this study, the reaction between polyepichlorohydrin and an amine is appropriate.

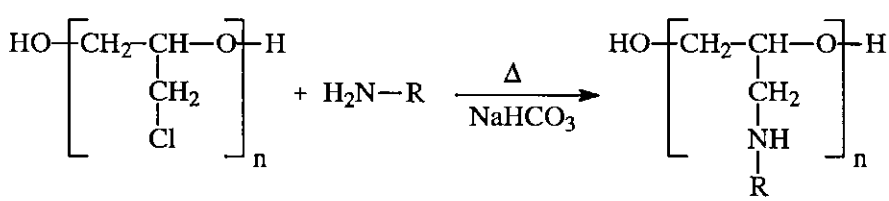


**Scheme 2.11** Anchoring reaction of an amine on polyepichlorohydrin. Sodium bicarbonate removes the liberated HCl.

## 2.3.3. Polymer anchoring reactions involving photochromic dyes

Several patents have been registered for photochromic dyes in fabrics which change colour (reversibly) in sunlight from yellow to blue,[4, 91-92] and for incorporation into resins and plastics to form photochromic films, glasses, or lenses.[93-95] Preparational procedures of these dyes are related to the above-mentioned scheme for attaching amines to polyepichlorohydrin.

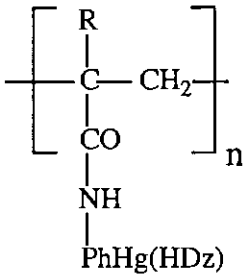


**14**

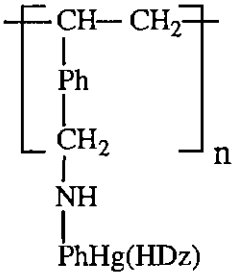


**15**

**Figure 2.15** Photochromic Polymers

The acrylamide unit containing polymer **14** is prepared in a multi-step reaction by first polymerizing acryloyl chloride.[96] Freshly distilled acryloyl chloride is mixed in a polymer tube with 3 ml pure dioxane and 50 mg α,α'-azodiisobutyronitrile. The tube is sealed under nitrogen and the mixture is warmed at 50°C for 48 hours. Evaporation of the solvent gives 84% yield of poly(acryloyl chloride) with a molar mass of about 36 000 g/mol. In a follow-up reaction, the -COCl side chains are treated with *p*-aminophenylmercury(II) acetate and dithizone, yielding the photochromic polymer **14**.[97] In agreement with the photochromic reaction of dithizonatophenylmercury(II), typical absorbance maxima shifts from 500 to 600 nm were recorded on irradiation of the polymer with light. The recovery time was fast.

Polymer **15** was synthesised by first polymerizing 1 gram mixture of *m*- and *p*-(chloromethyl) styrene in the absence of oxygen with 0.005 g azobisisobutyronitrile as initiator in 2 ml DMF at 80°C for 72 hours. A highly viscous solution was obtained from which poly(chloromethyl)-styrene was precipitated by addition of excess methanol, yielding 0.95 g polymer.[91] This polymer (0.5 g) was dissolved in 20 ml methyl ethyl ketone, stirred for 1 hour at 60°C with 0.2 g *p*-aminodithizonatophenylmercury(II) and 0.2 g sodium bicarbonate, to give 0.7 g of a red powdery product, after workup. A maximum absorbance at 490 nm in benzene was observed for this material. The absorbance maximum of the polymer film shifted to 610 nm when exposed to sunlight or fluorescent lighting. The colour of the film changed from reddish brown to dark blue via brown.

The authors reporting this reaction did not describe the workup to separate unreacted *p*-aminodithizonatophenylmercury(II) from the polymeric material. Experience obtained by the

author of the present dissertation during the course of his study showed this to be a daunting task. It is expected that the above described procedure resulted in material containing limited amounts of the photochromic reagent actually covalently bound to the polymeric carrier. It is very likely that the obtained product had a significant portion of *p*-aminodithizonatophenylmercury(II) simply embedded within the polymeric matrix of the carrier.

The blue-grey colour of the above-mentioned photochromic polymers is often found to persist for relative long times after exposure to light. In order to accelerate the reversion time several compounds were tested as so-called reversion accelerators.[108] Compounds containing poly(methyl methacrylate) and either 2-naphthoic acid, *m*-chlorobenzoic acid, phenol, stearic acid, or oxalic acid as reversion accelerators were prepared and compression molded into sunglass lenses. A mixture containing 1 mg *p*-aminodithizonatophenylmercury(II), 50 mg phenol and 1 ml of the polymer had a reversion time of 3 seconds compared to 15 minutes for a similar compound free of phenol accelerator.

In another experiment 10 g poly(methyl methacrylate) film containing 0.01 g *bis*-dithizonatomercury(II) and azobenzene were exposed to sunlight for 5 minutes to show shades of bluish violet, green, greenish brown, and dark green, for azobenzene contents 0, 0.01, 0.03-0.05, and 0.1 g respectively.[93] Similar results were observed with polyethylene and cellulose acetate as binders, and other amines and azo compounds, e.g. aniline, naphthylamine and hydrazobenzene.

A novel sample preparation technique has been developed to preserve solid *bis*-dithizonatomercury(II) in a matrix of polyvinyl chloride (PVC) for analysis by photochromism-induced photoacoustic spectrometry.[99] This technique, which begins with extraction of mercury(II) from water with dithizone, allows for the determination of mercury(II) in environmental samples. Inclusion of *bis*-dithizonatomercury(II) within the polymer matrix enhances the photochromism-induced photoacoustic spectrometry signal amplitude over that from the bare *bis*-dithizonatomercury(II) film almost sixfold.
What is equally important here is that a study conducted to monitor the change in photochromism-induced photoacoustic spectrometry signal amplitude obtained for the same sample over an extended storage period of 19 days, demonstrates that polyvinylchloride protects the integrity of the solid $Hg(HDz)_2$ sample.

As opposed to the previous anchoring reactions, the latter example has *bis*-dithizonatomercury(II) simply embedded (dissolved) in the polyvinylchloride matrix, with the photochromic reaction once again uninhibited by the surrounding polymeric carrier.

# 2.4. Porphyrins

## 2.4.1. Synthesis and Substitution Patterns

Porphyrins is a class of compounds of which the remarkably diverse bio-chemical and photo-electro properties have continued to attract the attention of researchers for well over a hundred years. Since Hans Fischer's pioneering synthesis of hemin in the 1920s,[100] applications for porphyrin derivatives have been found in the field of molecular electronic devices,[101] as photodynamic cancer therapy agents[102] and in materials chemistry,[103] to mention but a few.

Porphyrin synthetic methodology advanced significantly over the past 80 years. Most porphyrin syntheses proceed by tetramerization of monopyrrole. *Meso*-Tetraphenylporphyrin (2HTPP) was first synthesised by Rothemund,[104] which was followed by a simplified synthesis by Adler and Longo.[105-107] In the Adler method, a solution of benzaldehyde and pyrrole in a high boiling acid solvent such as propanoic acid, is heated at reflux in air so that condensation and oxidation occur simultaneously. Yields are typically 20%. The crude product contains about 3% tetraphenylchlorin. Chromatographic purification through a column of silica conveniently rids smaller amounts of product from tetraphenylchlorin. Rousseau and Dolphin found that addition of the mild oxidant, 2,3-dichloro-5,6-dicyanobenzoquinone to the reaction mixture assists the oxidation process markedly, and rids the crude product of most, if not all, tetraphenylchlorin.[108] This method saves both time and costs, especially when working with larger quantities of material.

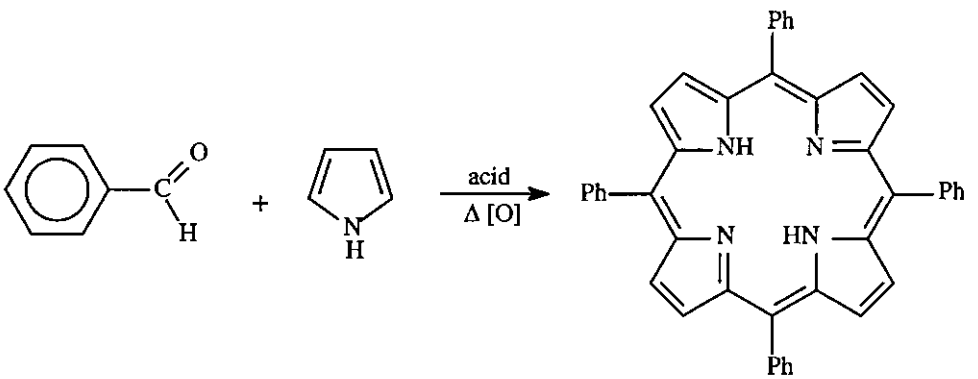


**Scheme 2.12** Adler synthesis of *meso*-tetraphenylporphyrin from benzaldehyde and pyrrole.

Nonetheless, the Adler-Longo methodology is beset with certain vexing problems. Firstly, the harsh reaction conditions result in complete failure with benzaldehydes bearing sensitive functional groups like the hydroxyethoxy-, methoxycarbonyl-, dithiacyclopentyl-, etc. groups. Secondly, the high level of tar produced presents purification problems in many instances, especially with those porphyrins that do not crystallise or precipitate at the end of the reaction. Thirdly, the batch-to-batch reproducibility of the reaction is often rather poor.

Lindsey and coworkers published results on studies of an improved method for the synthesis of some *meso*-tetraarylporphyrins and discussed a mechanistic interpretation of the reaction.[119,120] He performed reactions between aldehydes and pyrrole under nitrogen in the presence of trace amounts of acid catalysts, e.g. $BF_3$ or trifluoroacetic acid. After equilibrium is reached (1 hour), the porphyrinogen intermediate product is irreversibly oxidised to porphyrin by addition of a stoichiometric amount of *p*-chloranil. This method more than doubles the yield for *meso*-tetraphenylporphyrin compared to the Adler method, yielding up to 40%, as compared to the original 20%.

Sharghi and Hassani very recently (2004) developed yet another method for the synthesis of *meso*-tetraarylporphyrins from pyrrole and aryl aldehydes, cleanly and efficiently, in a one-pot reaction at room temperature, using an equimolar amount of trifluoromethanesulfonyl chloride ($CF_3SO_2Cl$) catalyst in the presence of air as oxidant.[111] By this method, in the absence of 2,3-dichloro-5,6-dicyanobenzoquinone, 5,10,15,20-tetraarylporphyrins can be prepared in yields of up to 67%. The first part of the reaction is performed under nitrogen, yielding the maximum amount of porphyrinogen after one hour. Thereafter the solution is oxidised for 4 hours, using filtered house air. During this time the solution turns dark purple as the porphyrinogen is converted to porphyrin.

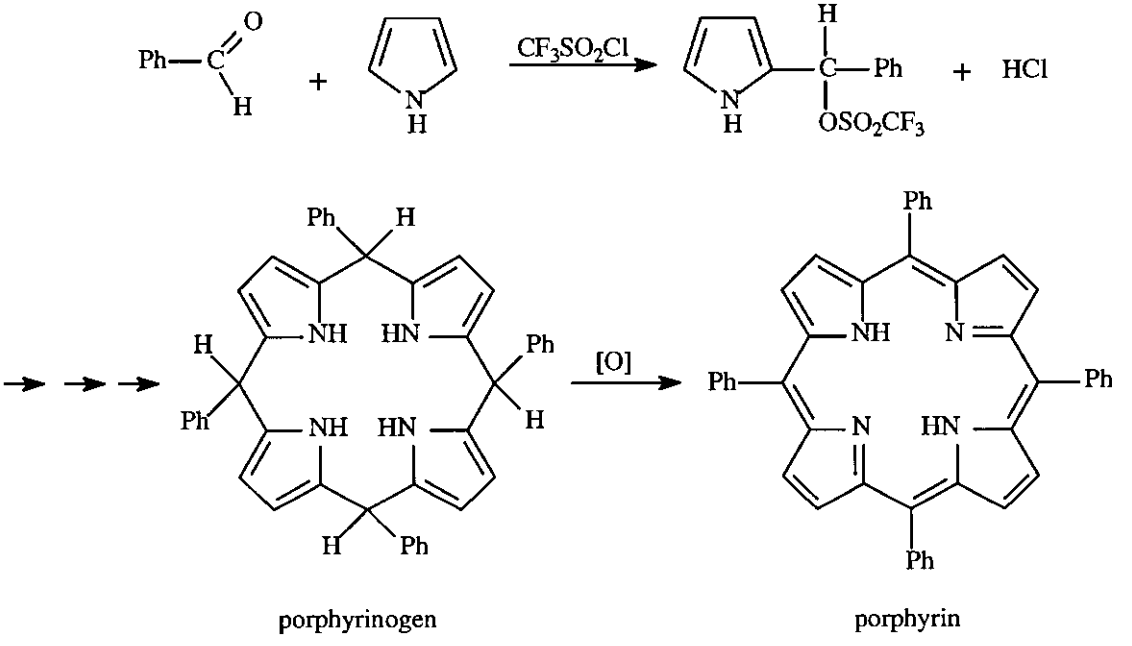


**Scheme 2.13** Sharghi synthesis of *meso*-tetraphenylporphyrin, using catalytic amounts of trifluoromethanesulfonyl chloride

To functionalise tetraphenylporphyrin at the phenyl ring, one can either use a substituted phenylaldehyde, or one can first synthesise tetraphenylporphyrin and then derivitise it. An example of such a synthetic approach is the synthesis of the water-soluble tetra(sodium 4-sulfo-

phenyl)porphyrin derivative.[112] By treating tetraphenylporphyrin with warm concentrated sulfuric acid, the sulfonic acid is formed. The tetraammonium salt is then precipitated by dissolving the acid in methanolic ammonia after which acetone is added. Further purification of the tetraammonium salt is carried out by six successive reprecipitations from a methanolic solution with acetone. Conversion to the tetrasodium salt is accomplished with the use of sodium methoxide.

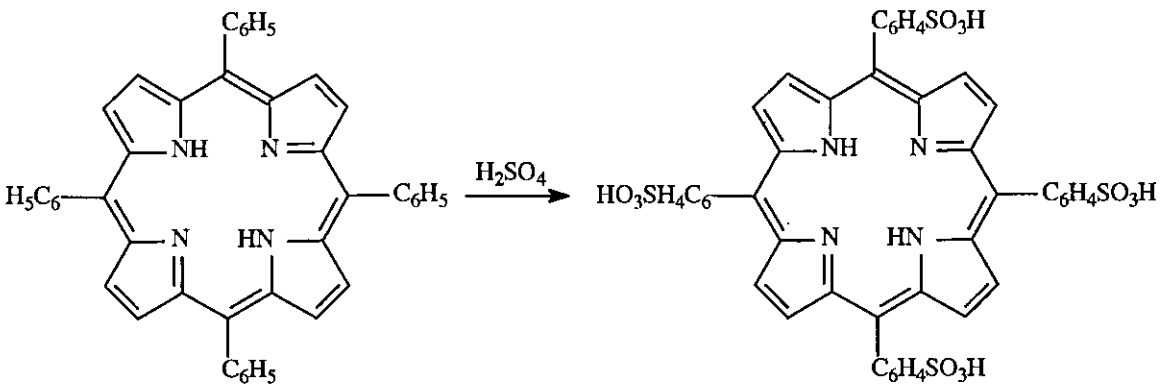


**Scheme 2.14** Functionalizing *meso*-tetraphenylporphyrin by *para* substitution of the heterocycle phenyl rings with sulfonic acid groups.

*Meso*-tetra(4-phenylcarboxylic acid)porphyrin, on the other hand, is prepared by starting off with *p*-carboxybenzaldehyde, following the procedure as for the parent compound, *meso*-tetraphenylporphyrin. Purification is done by recrystallization from methanol/chloroform.[107]

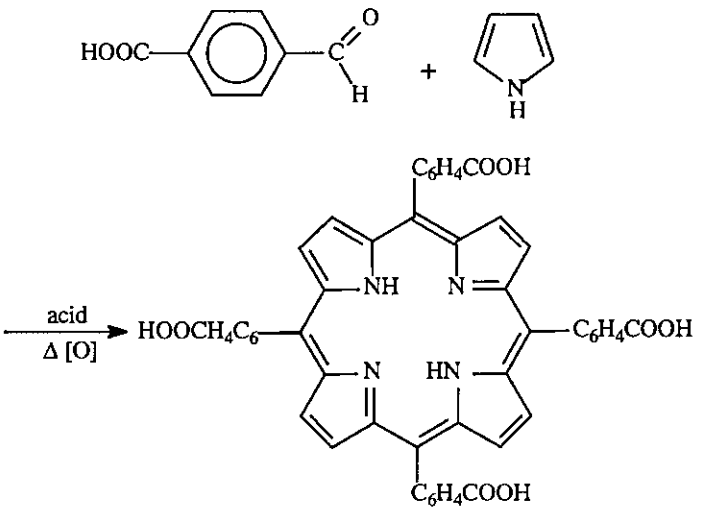


**Scheme 2.15** Functionalizing *meso*-tetraphenylporphyrin by employing a substituted reagent, *p*-carboxybenzaldehyde.

Apart from altering substituents on the phenyl rings, entirely different aldehydes may be used. Wollmann and Hendrickson synthesised *meso*-tetraferrocenylporphyrin by refluxing

formylferrocene and pyrrole in propanoic acid, yielding 40% product.[113] Characterization was done by means of elementary analysis and NMR spectroscopy.

Furthermore, substitution at the β-pyrrole positions is another possibility to obtain novel porphyrin derivatives. Octaethylporphyrin, as an example of this group, is probably the most widely used and best known compound in this series. Here 3,4-diethylpyrrole is reacted with formaldehyde. As substituted pyrroles are seldom commercially available, it has to be synthesised first. Traditionally, octaethylporphyrin has been prepared by the self-condensation of 2-N,N'-diethylaminomethyl-3,4-diethylpyrrole,[114,115] ethyl 5-N,N'-diethylaminomethyl-3,4-diethylpyrrole-2-carboxylate[116,117] or 3,4-diethyl-5-hydroxymethyl-pyrrole-2-carboxylic acid under oxidative conditions.[118] Neither of these labour intensive procedures, however, conveniently overcomes the problem associated with preparing 3,4-diethylpyrrole.

The following scheme represents a greatly improved and well tested method published by Sessler and coworkers, for the synthesis of 3,4-diethylpyrrole (Scheme 2.16).[119]

In the first step (labeled A in Scheme 2.16) 1-nitropropane is added dropwise to a solution of propionaldehyde in isopropyl alcohol containing potassium fluoride as catalyst. 4-Nitro-3-hexanol is obtained from distillation of the resulting liquid. A catalytic quantity of sulfuric acid is then added to 4-nitro-3-hexanol, followed by the slow addition of acetic anhydride. Vacuum distillation at 100°C removes the lower boiling components, after which the fraction boiling at 105-107°C/10 mm is collected, affording 3-acetoxy-2-nitrohexane in 90% yield.

In the next step (labeled B in Scheme 2.16) a flask containing anhydrous tetrahydrofuran is charged with 3-acetoxy-2-nitrohexane, ethylisocyanoacetate and isopropylalcohol. (The foul-smelling and expensive ethylisocyanoacetate may be prepared by a method described by Hartman and Weinstock, using glycine ethyl ester hydrochloride and methyl formate as starting reagents.[120]) 1,8-Diazobicyclo[5.4.0]undec-7-ene is then added to eliminate the acetate from one of the reactants, to form 3-nitro-3-hexene *in situ*, which goes on to form 3,4-diethylpyrrole-2-carboxylate. This material is not isolated, but directly decarboxylated by making use of sodium hydroxide in ethylene glycol. After extraction with hexane and concentration under reduced pressure, 3,4-diethylpyrrole is distilled off at 100°C/25 mm, yielding about 40% of the pyrrole.

In the last step (labeled C in Scheme 2.16) 3,4-diethylpyrrole, aqueous formaldehyde and *p*-toluenesulfonic acid under nitrogen are refluxed together in benzene, while water is removed by means of a Dean-Stark trap. After 8 hours oxygen is bubbled through the cooled solution for an additional 24 hours. The product is worked up and recrystallised twice from chloroform-hexane to afford 66% analytically pure 2,3,7,8,12,13,17,18-octaethylporphyrin.

A.

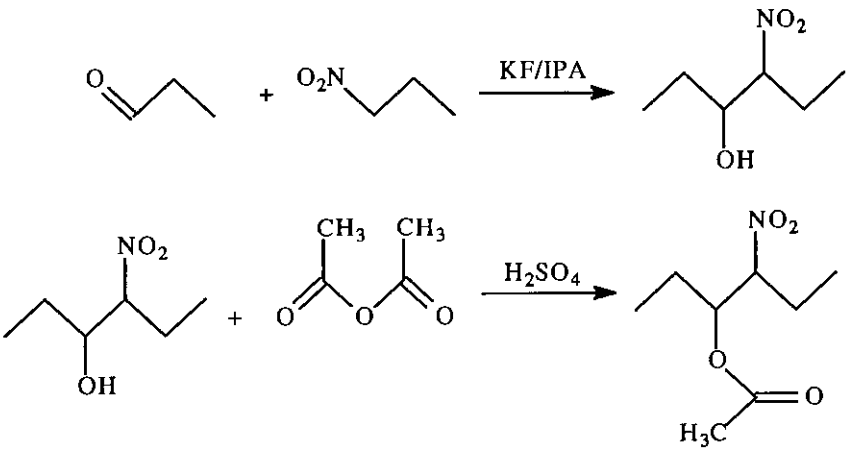


B.

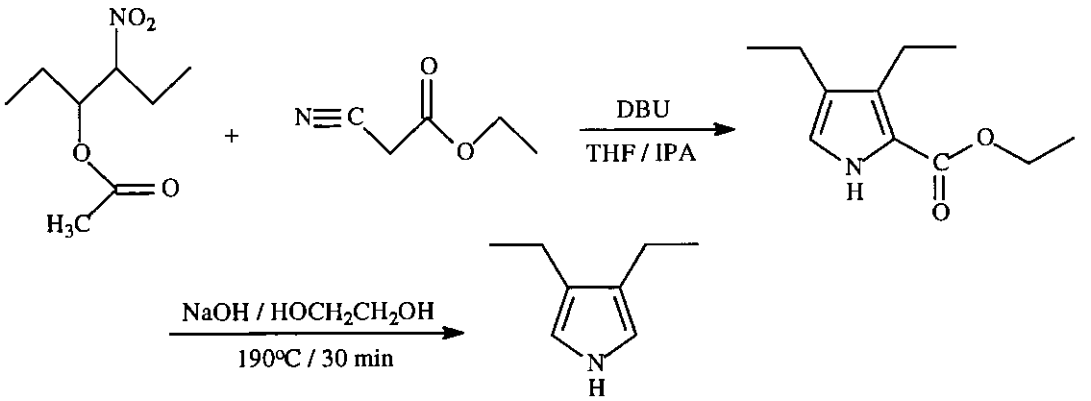


C.

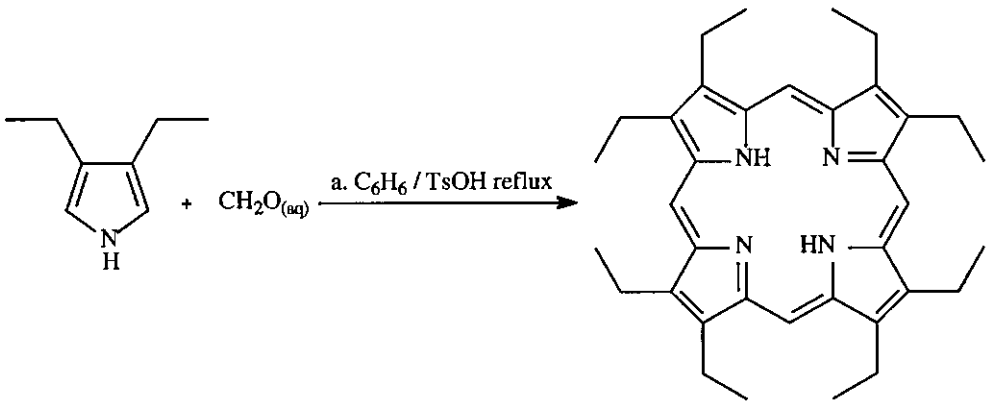


**Scheme 2.16** Sessler synthesis of octaethylporphyrin.

(IPA = isopropyl alcohol, DBU = 1,8-diazobicyclo[5.4.0]undec-7-ene, TsOH = *p*-toluenesulfonic acid)

Once again, instead of adding substituents to the pyrrole at the outset, substitution at the β-pyrrole positions may alternatively be done afterwards. Such an example is octabromoporphyrin. The method involves direct bromination of zinc(II) *meso*-tetraphenylporphyrin using liquid bromine in carbon tetrachloride, followed by demetallation of the resulting zinc(II) octabromo(*meso*-tetraphenylporphyrin) in perchloric acid to yield octabromo(*meso*-tetraphenylporphyrin), 2HTPPBr$_8$.[121]

## 2.4.2. Metal Insertion Techniques

An extensive variety of metal insertion synthetic methods to yield metal-containing porphyrins are known.[107] Amongst these are reactions of porphyrins with metallic salts, done in acidic (e.g. an acetate in acetic acid), basic (e.g. a chloride in pyridine) or in neutral media (with a specific organometallic compound, e.g. Grignard or carbonyl). While all these reactions are successful and useful, they all suffer from certain deficiencies as general or convenient methods of synthesis. Most of these problems center around the major difficulty of getting both the free base porphyrin and the metallic reagent simultaneously into the same solution under reactive conditions. This is due to the fact that good solvents for porphyrins in their unionised forms are generally poor solvents for simple metallic ions and vice versa.

An investigation in the seventies into a number of solvents lifted N,N'-dimethylformamide out as solvent of choice. The synthetic procedure consists simply of allowing the porphyrin and a divalent metal salt to react in refluxing dimethylformamide. While solubility is low at room temperature, at the reflux temperature a large variety of porphyrinic materials are soluble in excess of 1g/100ml. Most divalent metal acetates, halides, hydroxides and carbonates are also soluble. Almost all metal insertion reactions done with a stoichiometric amounts of metal salts, as tested by Adler and coworkers,[107] have shown 100% conversion to the metal product within 5 minutes. The high reflux temperature (153°C) not only facilitates rapid reaction, but readily displaces the formed product acids, thereby driving the reaction to stoichiometric completion. An equal volume of water added to the completed reaction will frequently quantitatively precipitate the product for ready filtration or enable ready extraction into a low boiling organic solvent for crystallization.

Using this method the following materials have been prepared: Zn, Cu, Ni and Fe porphyrin; Zn, Cu, Ni, Co, Fe, Cr, Mn, VO, Hg, Cd, Pb, Sn, Mg, Ba, Ca, Pd and Ag *meso*-tetraphenylporphyrin; proto, hemato, deutero, meso, phyllo, rhodo, pyrro, and hemato dimethyl ester hemins, as well as a wide variety of *para*-substituted *meso*-tetraphenylporphyrins. Even metal insertion reactions with *meso*-tetraphenylchlorins, tetraazaporphin and phthalocyanine were successful under these conditions.

A few years later (1975) Fuhrhop and Smith suggested a mixed solvent system instead.[122] There method entails the addition of a saturated solution of metal acetate in methanol to a boiling chloroform solution of the porphyrin. After a few minutes refluxing and checking by spectrophotometry, the mixture is concentrated, diluted with a little methanol, and the resulting precipitate is filtered off in virtually quantitative yield.

In yet another development, Hermann and coworkers pointed out that insolubility of metal salts should not necessarily be an obstacle.[123] Metal complexes of water-soluble and other porphyrins were prepared by a heterogeneous reaction, i.e. the porphyrin in solution reacting with the insoluble metal reactant. The heterogeneous metal insertion reaction can be carried out using metal oxides, free metals, metal sulfides, and other insoluble metal salts (e.g. $Cu_2Cl_2$) in water or in non-aqueous solvents. The method has been used successfully to prepare metal complexes of tetra(sodium 4-sulfophenyl)porphyrin, hematoporphyrin, protoporphyrin IX dimethyl ester, octaethylporphyrin and *meso*-tetraphenylporphyrin. This type of metalloporphyrin formation reaction has the obvious advantage over more conventional methods that the reactant can be removed from the product by simple filtration of the solid phase, rather than by tedious methods, often in combination with extraction, precipitation, dialysis and chromatography.

## 2.4.3. UV/visible Spectroscopy

A very convenient property of porphyrins and its corresponding metal complexes is that reactions may easily be followed spectrophotometrically.

The porphyrin macrocycle is highly conjugated and a number of resonance forms can be written.[124] There are nominally 22 π-electrons, but only 18 of these are included in any one delocalization pathway, which conforms with Hückel's 4n + 2 rule for aromaticity. Porphyrins are highly coloured and their main absorbance bands have very high extinction coefficients.

In 1883 Soret discovered an intense absorption band in hemoglobin, lying at about 400 nm. It was later observed in other porphyrins by Gamgee and others.[124] The "Soret" band is the most intense light absorption band in porphyrins and their derivatives, with molar extinction coefficients around 400 000 often being recorded. The intensity is weaker in chlorins and metallochlorins and, as might be expected, totally absent in porphyrinogens (Scheme 2.13, p.31), because the conjugation pattern is interrupted or broken. The Soret band is the UV/visible band of choice for spectrophotometric determinations. It can be measured easily in cells of 10 mm path length at concentrations around $10^{-6}$ mol.dm$^{-3}$. In typical porphyrin UV/visible spectra there are also one or more longer wavelength satellite bands, the so-called Q-bands (Figure 2.16, insert), and a band which lies in the ultraviolet ( ~ 280 nm) region.

As can be seen from these spectra, the Soret band moves from $\lambda_{max}$ = 418 to 410 nm during cobalt insertion. A further shift to 408 nm occurs with oxidation of Co(II) → Co(III). Finally,

addition of pyridine to ClCo(III)TPP, which coordinates axially to the central metal atom, brings about a red shift to about 435 nm of the Soret band in dichloromethane.

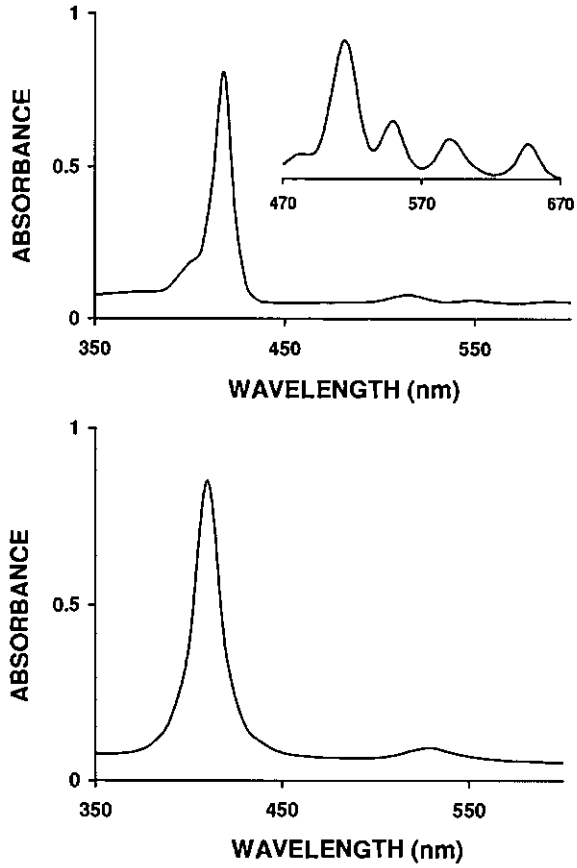


**Figure 2.16** UV/visible spectra of *meso*-tetraphenylporphyrin (top) and *meso*-tetraphenylporphyrinatocobalt(II) (bottom) in dichloromethane show the intense Soret band, observed at 418 nm and 410 nm respectively. Several bands of lower intensity appear at the right of the Soret band (insert).

In general, the simple square-planar porphyrins, i.e. divalent metal porphyrins with no axial ligands, have a Soret and at least two visible bands, called the $Q_0$ and $Q_1$ bands. Further coordination with axial ligands often generates octahedral complexes and induces a general shift of absorbance bands to longer wavelengths.

## 2.4.4. Axial Bond Formation

Five-, and to a lesser extent, six-coordinate Co(II)TPP complexes may form with a vast range of possible axial ligands. Of these, the amines are probably the most extensively studied. Walker spectrophotometrically measured the equilibrium constants and free energies of formation of a series of 1:1 complexes between amines and tetra(*p*-methoxyphenyl)porphyrinatocobalt(II) in toluene.[125] Equilibrium constants were also measured as a function of temperature. The results show axial cobalt-nitrogen bond strengths in the range 8-10 kcal/mol. A plot of log K vs. the $pK_a$ of the conjugate acid of the amine shows a linear relationship within each type of amine

(pyridines, imidazoles and aliphatic amines). Complexes with imidazoles were found to be most stable, suggesting that imidazoles are better $\pi$ acceptors from the cobalt $d_\pi$ orbitals.

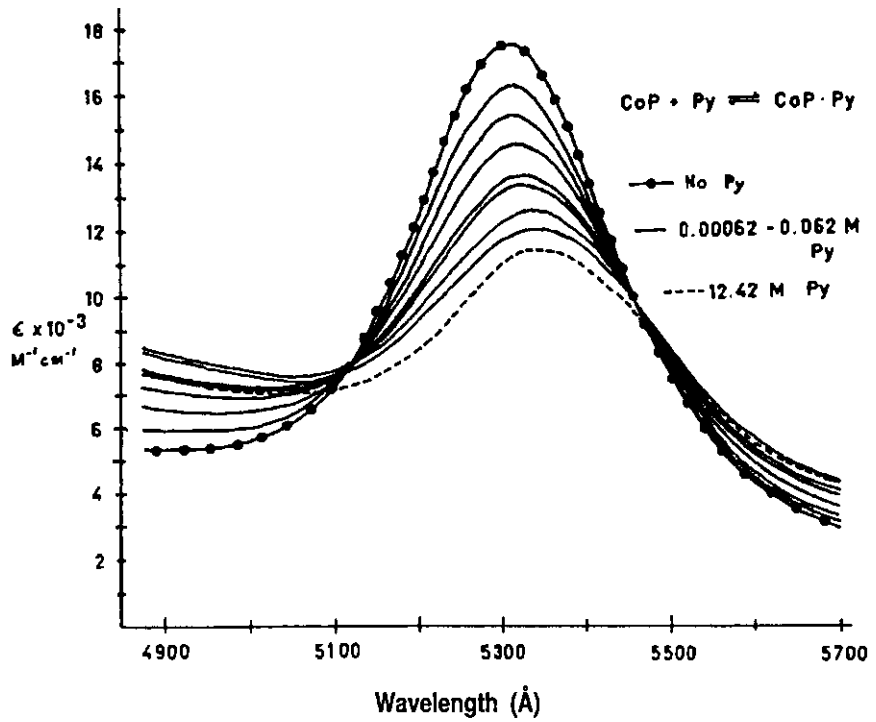


**Figure 2.17** Visible spectral changes upon addition of pyridine to Co(*p*-$OCH_3$)TPP. The top line is for Co(*p*-$OCH_3$)TPP in the absence of pyridine, with toluene as solvent. Nonisosbestic behaviour of the 12.42 M pyridine trace probably indicates spectral changes due to solvation of the five-coordinate pyridinate complex by excess pyridine, since $K_2$ is much less than 1.[126] In addition, at 12.42 M pyridine, the character of the solution might be so much different (non-ideal) compared to low concentrations, that the Beer-Lambert law may not be obeyed.

Steric factors must also be taken into account when considering bond strengths between the axial ligands and cobalt porphyrin. As can be seen from the equilibrium constants, the sterically hindered bases like quinoline, acridine and 2,4,6-trimethylpyridine (Figure 2.18) are weakly bonded as compared to imidazole and piperidine. Equilibrium constants further give some feeling for the distance cobalt will lie out of the plane of the porphyrin ring.

Bases with a wide variety of electronic and steric differences are seen to coordinate to cobalt(II) porphyrin, with bond strengths markedly dependant on these differences. Based on the above evidence, the question posed is: will dithizone / dithizonato, which harbours no less than four sterically hindered tertiary amines in its backbone, as well as the more protruded thio sulfur atom, behave as an axial ligand to cobalt in cobalt porphyrin? If not, what can be done to alter the electronic properties of either dithizone or cobalt porphyrin, or both, in order to accomplish this goal?

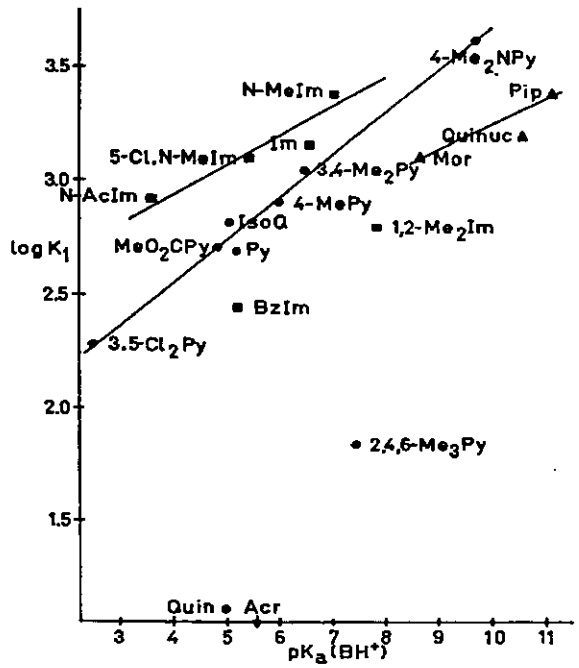


**Figure 2.18** Relationship between amine basicity (σ-donor strength) and $\log K_1$. Abbreviations are as follow: Py = pyridine, 4-MePy = 4-picoline, 3,4-$Me_2$Py = 3,4-lutidine, 4-$Me_2$NPy = 4-dimethylaminopyridine, 3,5-$Cl_2$Py = 3,5-dichloropyridine, 4-$MeO_2$CPy = 1-methylisonicotinate, 2,4,6-$Me_3$Py = γ-collidine, IsoQ = isoquinoline, Quin = quinoline, Acr = acridine, Im = imidazole, N-MeIm = 1-methylimidazole, 5-Cl-N-MeIm = 5-chloro-1-methylimidazole, N-AcIm = N-acetylimidazole, 1,2-$Me_2$Im = 1,2-dimethylimidazole, BzIm = benzimidazole, N-$SiMe_3$Im = 1-trimethylsilylimidazole, Pip = piperidine, Mor = morpholine, Quinuc = quinuclidine (1,4-ethylenepiperidine).

One means of promoting axial coordination is to enhance the electrophilic character of the central cobalt atom. That may be done by oxidizing cobalt(II) to cobalt(III). In doing so, *meso*-tetraphenylporphyrinatocobalt(II) is suspended in methanol containing a small amount of concentrated hydrochloric or perchloric acid.[127,128] The open solution is stirred over night, or else, for a much shorter period of time while bubbling oxygen through. During oxidation the suspension dissolves and turns to deep red, from which the cobalt(III) porphyrin is isolated. Axial coordination of neutral ligands to the higher oxidation state cobalt(III) metal center, or substitution of $Cl^-$ or $ClO_4^-$ with another anionic species, occurs readily and reactions are fast as compared to cobalt(II).

In line with the reactions mentioned above, and bearing the goal (Chapter 1) of this study in mind, four possible methods, A-D, compatible with the anticipated dithizone – cobalt porphyrin interaction, were identified in the literature:

**A.** Axial Coordination: Dehydrodithizone (see Figure 2.5, p.8) has not been studied extensively as ligand. For this reason Walsh and coworkers set out to synthesise polypyridyl ruthenium complexes containing a dehydrodithizone ligand.[129] An X-ray data collection was done on a crystal of the ruthenium(II) compound. The bent geometry at the sulfur atom Ru-S-C equals 115.1°, and the Ru-S bond length of 2.393 Å compares well with other complexes which also contain Ru-S bonds.[130]

As mentioned earlier (p.8), dithizone is both easily oxidised and reduced to the *meso*-ionic compound (i.e. dehydrodithizone, DDz ) and back again. It leaves the possibility that, after coordination of the *meso*-ionic ligand, it may be reduced to the original dithizone again, yet still intact as far as its bond to the metal is concerned. When considering nucleophilic attacks on sterically crowded metal centers, dehydrodithizone is of course sterically much less hindered as compared to the parent compound.

**B.** Anionic Substitution: Chen and Hung prepared an iron porphyrin compound that reacted with the sodium salt of 4-methylbenzenethiolate.[131] The thiolate anion coordinated through sulfur at the metal center, as seen from the single crystal X-ray data collection that was done. As part of a study on cytochrome P-450 monooxygenase, a natural product compound with an iron-thiolate bond, Sakurai and coworkers reacted ClFe(III)TPP with thioglycolic acid ethyl ester to form the pentacoordinate $RS^-$—FeTPP complex.[132] X-ray data collection confirmed the structure.

Schrauzer and Windgassen reported the preparation and properties of several mercaptocobaloximes, i.e. bis(dimethylglyoximato)cobalt complexes with Co-S bonds.[133] The affinity of the cobalt atom to sulfur appears to be independent of the special structure of the corrin ligand, which follows from their study of the reactions of cobaloximes with thiols, dialkyl disulfides, and sulfonium compounds. In the absence of added base, chloro- or cyanocobaloximes slowly react with mercaptans, if at all. Addition of a stoichiometric amount of base converts the chlorocobaloxime into the hydroxyl derivative, which in turn combines with the mercaptan to produce mercaptocobaloxime.

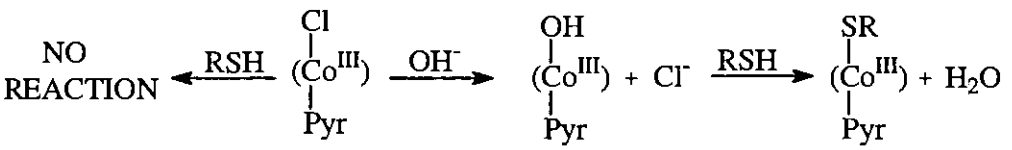


**Scheme 2.17** Axial substitution reaction of mercaptan (RSH) with cobalt(III) oxime in the presence of base.

The Co-S bond is easily cleaved by a variety of reducing agents, e.g. molecular hydrogen in mildly acidic, alkaline, or neutral solution. Thiophenols are more reactive and combine with cobaloxime to produce Co-S thiophenolatocobaloximes with simultaneous evolution of an equivalent amount of hydrogen. With molecular hydrogen, dialkyl disulfides in alkaline or neutral solution are reduced to thiols in the presence of catalytic amounts of cobaloximes(II), while in the presence of molecular oxygen, thiols are catalytically oxidised to disulfides. In general, cobaloximes(II) catalyze the oxidation of thiols and reduction of disulfides.

Other reactions comparable to the above are found amongst those done by Sugimoto and coworkers:[128]

$$[Co^{III}(TPP)(H_2O)_2]ClO_4 + Na^+X^- \rightarrow [Co^{III}(TPP)(H_2O)X],\ X = SCN^-, N_3^-, Br^- \& I^-$$

As already illustrated earlier, the anionic derivative of dithizone, $HDz^-$, lends itself ideally to coordination. It may readily be prepared by reaction with a strong base, like potassium hydroxide, to yield $K^+HDz^-$.

**C.** Transfer Intermediate: Fukuzumi and Kitano explained how alkylcobalt(III) porphyrins can be prepared by reductive alkylation of $CoTPP^+$ with mild alkylating reagents such as the tetraalkyltin compounds, in acetonitrile and / or chloroform at 298K.[134] The formation of RCoTPP is identified by the characteristic $^1H$ NMR signals in the high-field regions, due to the alkyl group bound to cobalt.

$$R_4Sn + Co(TPP)Cl \rightarrow RCoTPP + R_3SnCl$$

George and Lappert have shown that organotin-nitrogen compounds, such as dimethylaminotrimethylstannane, are compounds of exceptional reactivity (comparable to Grignard reagents), as exemplified by their reactions with protic species and unsaturated substrates,[135,136]

$$Me_3Sn\text{-}NMe_2 + H\text{-}X \rightarrow Me_3Sn\text{-}X + HNMe_2$$

$$Me_3Sn\text{-}NMe_2 + X\text{-}A \rightarrow Me_3Sn\text{-}X + ANMe_2$$

These reactions proceed in nearly quantitative yield and require mild conditions. Almost the only suitable solvents for reactions of this kind are benzene and ether. Exclusion of atmospheric moisture is necessary to avoid decomposition.

The amination reactions owe their faculty to the high donor strength of dimethylaminotrimethyltin(IV), $Me_3Sn\text{-}NMe_2$, to the weak and polar Sn-N bond, and to the large values for the heats of formation of organotin products such as $Me_3SnCl$. It is probable, therefore, that organotin compounds of general formula, $R_3SnY$, may frequently serve as intermediates for transfer of a moiety Y via Sn to another electrophilic site.

Applying this method for the reaction between dithizone, $H_2Dz$, and dimethylaminotrimethyltin(IV) may have the advantages that no base is required and that it may serve as a dithizone transfer reaction with cobalt(III) porphyrin. By not requiring a base, possible competing reactions, as far as axial substitution is concerned, are eliminated.

The tin complex further has the quality of neatly removing the substituted chloride, while simultaneously delivering the dithizonato anion to the porphyrin metal centre.

**D.** Tailed Metal Insertion: In this method the axial ligand-to-be is first bound to the metal. The metal is then inserted into the heterocyclic ligand, with the ligand "tailing behind". The following discussion illustrates this approach.

The most widely used synthetic route to organocobalt complexes is reductive alkylation, in which Co(II) or Co(III) complexes are reduced to Co(I) complexes and then treated with electrophilic alkylating agents.[137] This route has also been successful in the preparation of uncharged $CH_3Co(Por)$ compounds where the porphyrin is electron-rich and soluble in organic solvents, e.g. methylCo(III) *meso*-tetraphenylporphyrin[138] and methylCo(III) octaethyl-porphyrin.[139]

Organocobalt(III) derivatives of cationic water-soluble porphyrins such as *meso*-tetrakis(*N,N,N*-trimethylaniliniumyl)porphyrin, $[TMAP]^{4+}$, and *meso*-tetrakis(*N*-methyl-4-pyridiniumyl)-porphyrin, $[TMpyP]^{4+}$, were unknown until Trommel and Marzilli were successful in preparing the corresponding salts via a new approach never used before.[10] They started off by making use of the pentaaminemethylcobalt(III) cation. The $[Co(III)(NH_3)_5CH_3]^{2+}$ cation is the simplest organocobalt(III) compound with one organometallic bond and five coordinated nitrogen atoms. The *trans*-labilizing methyl group promotes facile amine ligand exchange. Substitution with simple ligands such as $H_2O$, $NO_2^-$, $CN^-$, and 1,2-ethylenediamine of the amine ligands in $[Co(III)(NH_3)_5CH_3]^{2+}$ has been reported.[140,141]

It was found that this substitution procedure can be extended to the tetracationic porphyrin ligands. Insertion of the Co-$CH_3$ moiety into the porphyrin requires no heat and also avoids the need for reducing conditions and the exclusion of ambient oxygen from the reaction. The study has generated good evidence that five-coordinate $[CH_3Co(III)(Por)]^{4+}$ may exist in water.

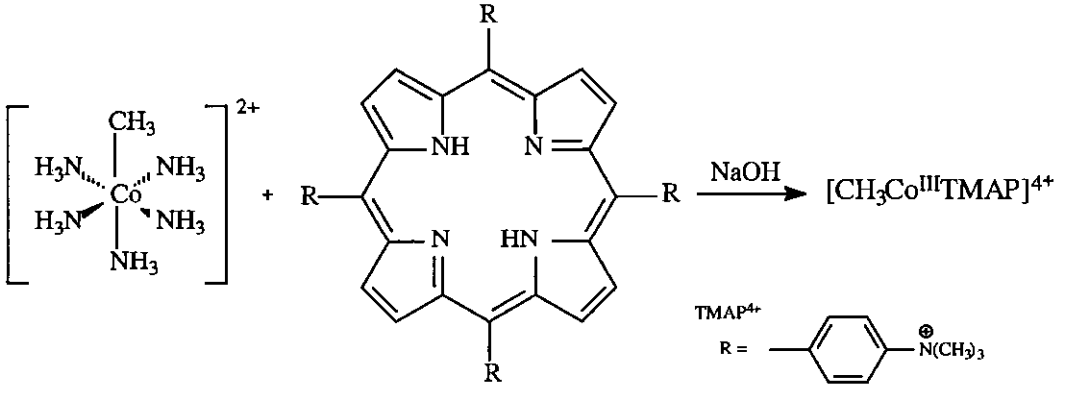


**Scheme 2.18** Pentaaminemethylcobalt(III) cation used as starting material for metal insertion into a water-soluble porphyrin, $[TMAP]^{4+}$, without loss of the methyl group.

Pentaaminemethylcobalt(III) nitrate is prepared by dissolving cobalt(II) nitrate in a little water and adding 25% ammonia, followed by methylhydrazine.[142] Exposure to atmospheric oxygen while stirring at room temperature for 4 hours is sufficient for complete cobalt(II) oxidation.

Thus, by first attaching the axial-ligand-to-be onto cobalt, and then inserting cobalt into the heterocyclic porphyrin ring - without loss of the attached moiety, an alternative method is developed for the direct transfer of a ligand.

This approach is expected to circumvent the possible problem of steric obstruction that may occur during axial coordination of dithizone to cobalt porphyrin, both being sterically hindered, to a greater or lesser degree. Regardless which procedure is followed, the isomeric form (compare the structures of the methylated derivative in Figure 2.6, p.9) which dithizone assumes during axial coordination will play an important role. The ***syn***, *s-trans* isomer leaves the possible coordination sites on dithizone much more exposed as compared to the ***anti***, *s-trans* form.

## 2.4.5. Photolytic Axial Bond Cleavage

A key feature of a molecular data storage device based on polymer-bound dithizonatophenylmercury(II) cobalt porphyrin complexes, is the capability of this complex to reversibly cleave and bind the axial dithizonatophenylmercury(II) ligand. Although this goal lies beyond the scope of the present dissertation, a brief discussion based on available research results is nevertheless included to further motivate research into opto-molecular switches of this kind.

Chlorotetraphenylporphyrinatocobalt(III) in aerated dichloromethane solution was found to undergo photooxidation to produce the porphyrin π-cation radical, $Co^{III}(TPP)^{+\cdot}Cl_2$.[143] Studies on the formation mechanism of $Co^{III}(TPP)^{+\cdot}Cl_2$ from $Co^{III}(TPP)Cl$ in aerated dichloromethane solution in a light room have revealed that:

(1) $Co^{III}(TPP)Cl$ undergoes homolytic cleavage of the Co-Cl bond in $Co^{III}(TPP)Cl$ upon Soret-band excitation to yield $Co^{II}(TPP)$ and chlorine atoms;
(2) the hydrogen abstraction of the chlorine atoms from dichloromethane molecules produces solvent radicals, which then react with oxygen molecules to form oxidant radicals;
(3) oxidant radicals are also formed by photolysis of aerated dichloromethane, and
(4) these oxidant radicals oxidise $Co^{III}(TPP)Cl$ to produce $Co^{III}(TPP)^{+\cdot}Cl_2$.

Photolytic cleavage of the cobalt(III)-axial ligand bond, as in (1) above, is well-known for the cobalt porphyrins and oximes.

The model compounds of coenzyme $B_{12}$, like 5'-deoxyadenosylcobaloxime, undergoes $Co^{III}$-C bond cleavage on light irradiation just like the $B_{12}$ coenzyme itself.[144] Complexation of adenosylcobalamin by apoenzyme results in a dramatic acceleration of the homolysis of the $Co^{III}$-C bond by $\geq 10^{10}$ relative to the uncomplexed adenosylcobalamin.[155] The "base-on" effect, which results from coordination of an axial ligand, accelerates homolysis of the $Co^{III}$-C bond by a factor of $10^2$ - $10^3$. Homolytic cleavage of the photosensitive cobalt(III)-methyl bond to produce cobalt(II) and a methyl radical in non-water-soluble $CH_3Co^{III}$(Por) complexes and a variety of other methyl-cobalt(III) complexes has been studied extensively.[10,11]

In short, a validated basis exists for both bond formation and bond breakage, as well as the desired light responses of the two moieties which should constitute the envisaged molecular switch.

## 2.5. Electrochemical Behaviour of Cobalt Porphyrins

Generally, metal free and metal porphyrin complexes of electrochemical silent metals can electrochemically undergo two ring-centered reversible or quasi-reversible oxidations, and four ring-centered reversible (quasi-reversible) reductions. This can give rise to the following general electrochemical scheme.

$$2HPor^{4-} \underset{red4}{\overset{-e^-}{\rightleftharpoons}} 2HPor^{3-} \underset{red3}{\overset{-e^-}{\rightleftharpoons}} 2HPor^{2-} \underset{red2}{\overset{-e^-}{\rightleftharpoons}} 2HPor^{-} \underset{red1}{\overset{-e^-}{\rightleftharpoons}} \underset{\text{(normal resting state)}}{2HPor} \underset{ox1}{\overset{-e^-}{\rightleftharpoons}} 2HPor^{+} \underset{ox2}{\overset{-e^-}{\rightleftharpoons}} 2HPor^{2+}$$

The 3rd and 4th reduction steps normally occur at potentials so negative that they cannot be seen in common organic solvents such as dichloromethane. Here solvents are electrochemically destroyed before the 3rd and 4th porphyrin reduction sets in. If a redox active metal, such as cobalt, is coordinated in the porphyrin macrocycle, additional oxidation and reduction waves may be observed.

## 2.5.1. Cyclic Voltammetry

A cyclic voltammogram of $ClCo^{III}TPP$ in dichloromethane containing 0.1 M TBAP is shown in Figure 2.19.[146] The reversible oxidations at E½ = 0.90 and 1.15 V are labelled as processes 2' and 3' and correspond to the two ring oxidations of the Co(III) complex. The first reduction of $ClCo^{III}TPP$ has non-coupled cathodic and anodic peaks, which are labelled as peak 1a (reduction) and peak 1b (oxidation). These peaks were spectroelectrochemically characterised as representing the Co(III)/(II) transition.

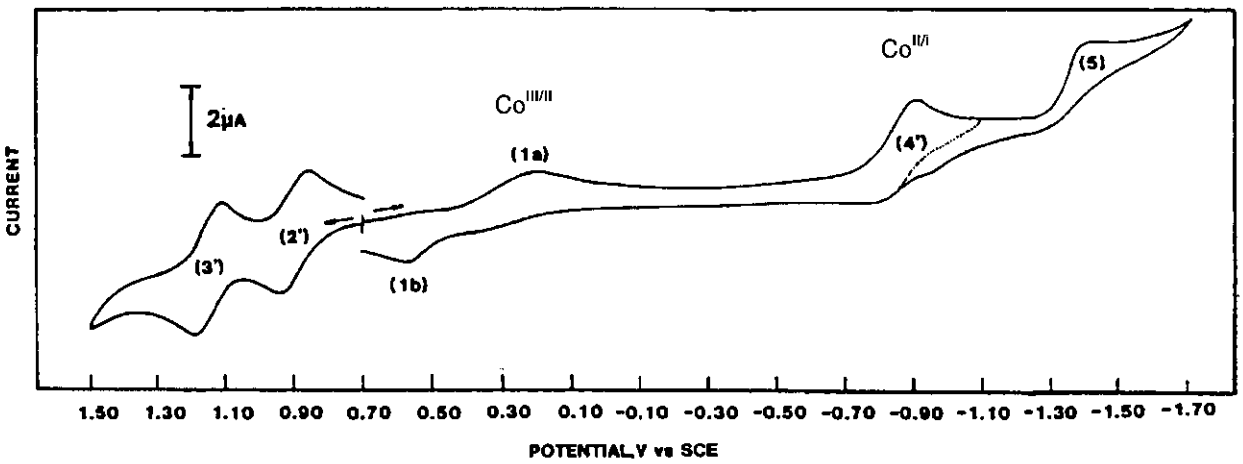


**Figure 2.19** Cyclic voltammogram of $ClCo^{III}TPP$ at a Pt electrode in $CH_2Cl_2$, 0.1 M TBAP. Scan rate = 0.10 V/s.

The non-coupled Co(III)/(II) reactions of $ClCo^{III}TPP$ can be explained by the "box mechanism" shown in Scheme 2.19.

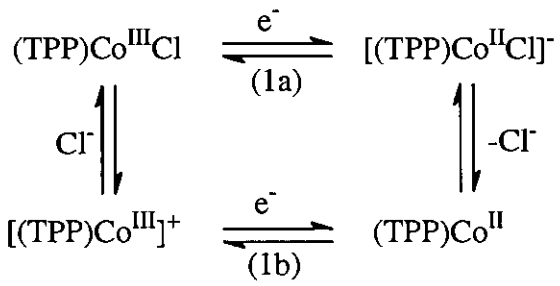


**Scheme 2.19** The redox reactions of chlorotetraphenylporphyrinatocobalt(III)

In this scheme, the $Co^{III}$ reduction and $Co^{II}$ re-oxidation of $ClCo^{III}TPP$ occur via two separate reversible electron-transfer steps, each of which is coupled to a following chemical reaction. The one-electron reduction of $ClCo^{III}TPP$ generates a transient $[ClCo^{II}TPP]^-$ species before loss of $Cl^-$ occurs (overall process 1a). The generated $Co^{II}TPP$ can then be re-oxidised to $Co^{III}TPP^+$, but this oxidation is followed by a rapid binding of $Cl^-$ to generate $ClCo^{III}TPP$ (process 1b).

The labelled processes 4' and 5 represent the 1st and 2nd reduction processes from $ClCo^{II}TPP$, where the reduction process, 4', involves the $Co^{II}/Co^{I}$ transition.

When doing voltammetric investigations of cobalt porphyrins in dichloromethane, it must be kept in mind that the solvent becomes involved in a reaction with the analyte.[146]

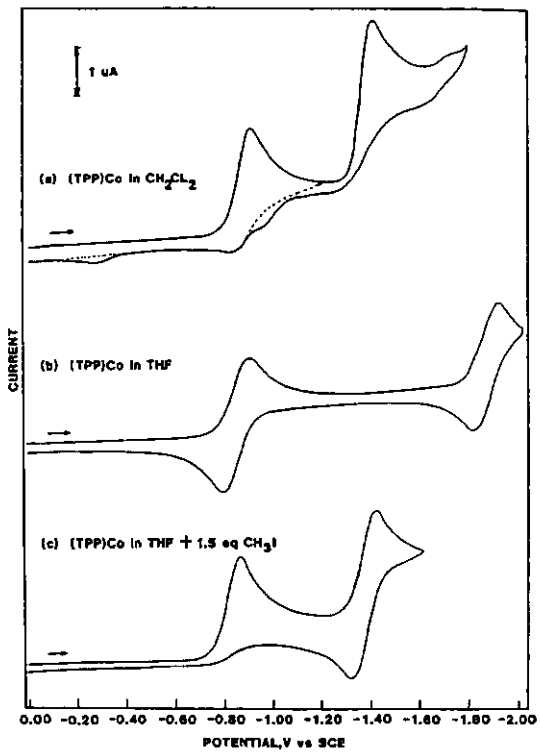


**Figure 2.20** Cyclic voltammograms of (a) CoTPP in $CH_2Cl_2$, 0.1 M TBAP; (b) CoTPP in THF, 0.1 M TBAP; and (c) CoTPP in THF, 0.1 M TBAP, plus 1.5 equivalent of $CH_3I$. Scan rate = 0.10 V/s

The first reduction of $Co^{II}TPP$ is reversible in $CH_2Cl_2$ at scan rates larger than 1.0 V/s, and corresponds to the reaction

$$Co^{II}TPP + e^- \rightleftharpoons [Co^{I}TPP]^-$$

However, the electrogenerated $[Co^{I}TPP]^-$ is not stable and rapidly reacts with $CH_2Cl_2$ to form $(CH_2Cl)CoTPP$. This is evident at slower potential scan rates and leads to a voltammogram such as that shown in Figure 2.20a. These irreversible processes are not observed in other nonaqueous solvents, which have voltammograms similar to the one for THF (Figure 2.20b).

Metalloporphyrins are subject to oxidation at both the metal and the porphyrin ligand to form metal- and porphyrin-centered oxidation products, respectively.[147] It is well documented that $Co^{II}OEP$ may be oxidised electrochemically[148] or chemically[149,150] in two successive one electron steps, first to $Co^{III}OEP{\cdot}X^-$ and then to $Co^{III}OEP^+{\cdot}2X^-$. An alternative one-electron oxidation product, the ring-centered oxidised species, $Co^{II}OEP^+{\cdot}ClO_4^-$, was for the first time observed by

Salehi and coworkers.[147] $Co^{II}OEP^{+}\cdot ClO_4^{-}$ is prepared by stirring a dry dichloromethane solution of $Co^{II}OEP$ with an excess of solid anhydrous $AgClO_4$, with a consequent Soret band shift from 391 to 376 nm. The product is only stable in anhydrous non-coordinating solvents. Addition of water or methanol to a dry dichloromethane solution of $Co^{II}OEP^{+}\cdot ClO_4^{-}$ results in a species with absorbance maxima at 409 ($\varepsilon = 1.80 \times 10^5$ $M^{-1}$ $cm^{-1}$), 522, and 558 nm. The effect of the "wet" solvent is reversible: if the solvent of the 409 nm species is evaporated to dryness and the residue is redissolved in dry dichloromethane, the 376 nm species reappears.

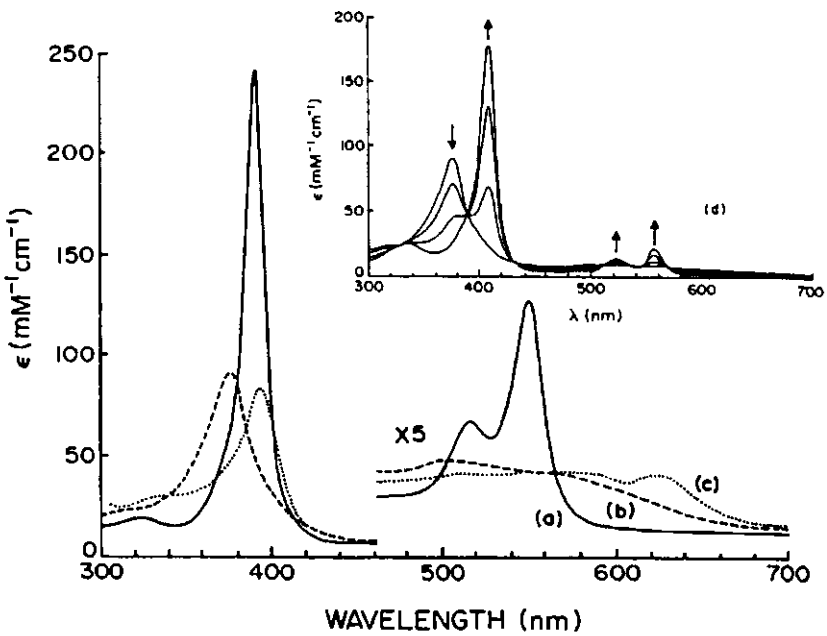


**Figure 2.21** Electronic absorbance spectra of $Co^{II}OEP$ derivatives: (a) $Co^{II}OEP$ (—); (b) $Co^{II}OEP^{+}\cdot ClO_4^{-}$ (---); (c) $Co^{III}OEP^{+}\cdot 2ClO_4^{-}$ (···), in $CH_2Cl_2$; (d) spectral changes on addition of methanol to a solution of (b) producing $Co^{III}(CH_3OH)_2OEP\cdot ClO_4^{-}$, total methanol content < 0.01%.

Electrochemical oxidation,[151] by cyclic voltammetry, of a series of $Co^{II}(p\text{-X})TPP$ complexes (where X = $OCH_3$, $CH_3$, H, F, Cl, CN and $NO_2$) yields first $[Co^{III}(p\text{-X})TPP]^{+}$, followed by the $\pi$ cation radical $[Co^{III}(p\text{-X})TPP]^{2+}$, and then the cation $[Co^{III}(p\text{-X})TPP]^{3+}$, in discrete reversible one-electron transfer steps. Reduction of the same series of compounds yields first $[Co^{I}(p\text{-X})TPP]^{-}$, followed by the $\pi$ anion radical $[Co^{I}(p\text{-X})TPP]^{2-}$, again in discrete one-electron steps.

A typical cyclic voltammogram of $Co^{II}(p\text{-X})TPP$ is shown in Figure 2.22, in which the electrochemical processes are identified by equation number (as per reference 169).

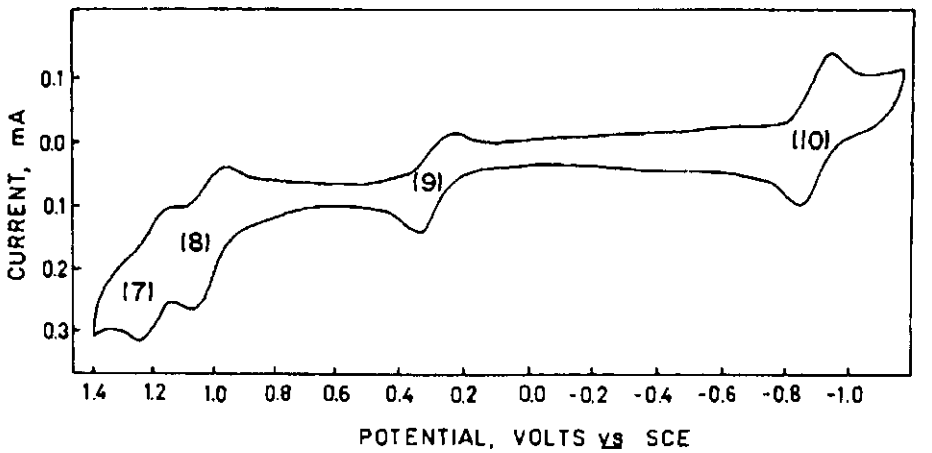


$$[Co^{III}(p\text{-}X)TPP]^{3+} + e^- \rightleftharpoons [Co^{III}(p\text{-}X)TPP]^{2+} \quad (7)$$

$$[Co^{III}(p\text{-}X)TPP]^{2+} + e^- \rightleftharpoons [Co^{III}(p\text{-}X)TPP]^{+} \quad (8)$$

$$[Co^{III}(p\text{-}X)TPP]^{+} + e^- \rightleftharpoons [Co^{II}(p\text{-}X)TPP]^{0} \quad (9)$$

$$[Co^{II}(p\text{-}X)TPP]^{0} + e^- \rightleftharpoons [Co^{I}(p\text{-}X)TPP]^{-} \quad (10)$$

**Figure 2.22** Typical cyclic voltammogram of 2.78 mM Co(*p*-$OCH_3$)TPP in butyronitrile, 0.1 M TBAP. Scan rate = 0.100 V/s. Numbers in parentheses refer to the redox process involved, and correspond to Eq. 7 to 10.

## 2.5.2. Solvent Effects

Metal oxidation or reduction is considerably more sensitive to substituents than ring oxidation or reduction. On the contrary, ring redox potentials are only slightly dependent on solvent conditions, and axial ligands. In contrast again, oxidation of cobalt(II) to cobalt(III) is markedly dependent on the coordinating ability of the solvent. This is convincingly shown in Table 2.3 where the half-wave potentials of reactions 7 to 11 (as in Figure 2.22) are listed for several solvents.

**Table 2.3** Reversible half-wave potentials for Co(*p*-X)TPP in various solvents. Waves 7-10 are as per Fig. 2.22. Wave 11 corresponds to the reaction $[Co^{I}(p\text{-}X)TPP]^- + e^- \rightarrow [Co^{I}(p\text{-}X)TPP]^{2-}$.

| | E½ (V vs. SCE)[a] Reaction | | | | |
|---|---|---|---|---|---|
| **Solvent** | **7** | **8** | **9 ($Co^{III/II}$)** | **10 ($Co^{II/I}$)** | **11** |
| Pyridine[b] | - | - | -0.214 | -1.030 | - |
| $Me_2SO$[b] | - | - | 0.130 | -0.814 | -1.870 |
| DMF[c] | - | - | 0.300 | -0.770 | -1.880 |
| Butyronitrile[b] | 1.35 | 1.16 | 0.395 | -0.812 | - |
| Benzonitrile[c] | 1.31 | 1.10 | 0.486 | -0.858 | - |
| DCM[b] | 1.20 | 1.00 | - | -0.855 | - |

[a] Not corrected for liquid junction potentials. [b] 0.1 M TBAP. [c] 0.1 M TEAP.

The coordinating ability of aprotic solvents for cations decreases from top to bottom in the above table. In the strongly coordinating solvents such as pyridine and dimethylsulfoxide a facile oxidation of cobalt(II) is observed while in solvents such as benzonitrile the oxidation is shifted anodically by 344-700 mV and become somewhat irreversible, as determined by the separation of the anodic and cathodic peak potentials. In the nonbonding solvent, dichloromethane, oxidation of Co(II) was irreversible. Basolo and coworkers have reported that the ease of oxidation of cobalt(II) complexes is directly proportional to the base strength of the bound axial ligand.[152,153] These results are in accord with Corwin and coworkers who reported that the oxidation of Co(II) is solvent dependent.[154,155]

## 2.5.3. The Effects of Axial Ligands

Costa and co-workers have found that Co(II)/(I) redox potentials are considerably more sensitive to the equatorial porphyrin ring substituents than are Co(III)/(II) redox potentials.[156,157] In contrast, the latter redox potentials are much more sensitive to axial ligand properties than the former. Addition of a variety of anions and amines to $[Co^{III}TPP]ClO_4$ by Sugimoto and coworkers brought about shifts of the redox potential for Co(III)/Co(II) to more negative values.[128] The redox couple Co(II)/Co(I), on the other hand, was almost insensitive.

**Table 2.4** Half-wave potentials for bi- and tervalent cobalt porphyrins.

| | | V *vs.* SCE | |
|---|---|---|---|
| **Compound** | **Solvent** | **Co(III)/(II)** | **Co(II)/(I)** |
| $Co^{II}TPP$ | DCM | + 0.71 | - 0.93 |
| $[Co^{III}TPP(H_2O)_2]ClO_4$ | | + 0.72 | - 1.05 |
| $[Co^{III}TPP(H_2O)Br]$ | | + 0.35 | - 1.03 |
| $[Co^{III}TPP(H_2O)Cl]$ | | + 0.27 | - 1.12 |
| $[Co^{III}TPP(H_2O)SCN]$ | | + 0.26 | - 0.94 |
| $[Co^{III}TPP(H_2O)I]$ | | + 0.23 | - 0.91 |
| $[Co^{III}TPP(H_2O)N_3]$ | | + 0.18 | - 0.89 |
| $[Co^{III}TPP(pyr)_2]ClO_4$ | | - 0.05 | - 1.14 |
| $[Co^{III}TPP(imd)_2]ClO_4$ | | - 0.31 | - 1.02 |
| $[Co^{III}TPP(H_2O)_2]ClO_4$ | DCM / EtOH | + 0.32 | - 0.95 |
| $[Co^{III}TPP(H_2O)Br]$ | | + 0.27 | - 0.96 |
| $[Co^{III}TPP(H_2O)Cl]$ | | + 0.28 | - 0.99 |
| $[Co^{III}TPP(H_2O)N_3]$ | | + 0.29 | - 0.99 |

Tetrabutylammonium perchlorate was used as supporting electrolyte. A three-electrode system was used which consisted of platimum working and counter electrodes and a commercial saturated calomel electrode. Molecular weight measurements did indicate that only $[Co^{III}TPP(H_2O)_2]ClO_4$ aggregate at higher concentrations in chloroform. In polar solvents such as methanol, all are monomeric.

The effect of strongly coordinating axial ligands on the Co(III)/(II) redox potential is clearly illustrated by the above table. Having the weakly coordinated water molecules replaced by imidazole brought about a large cathodic shift of more than 1 V in dichloromethane. Imidazole, being a much stronger base than pyridine, produces a redox potential 260 mV lower than that of pyridine.

## 2.5.4. The Effects of Peripheral Substituents

An extensive study was done by a large group of American researchers on a range of 40 free base, magnesium and zinc porphyrins in order to provide a foundation for tuning the electronic properties of monomeric porphyrins as building blocks for multichromophoric assemblies in optoelectronics and other applications.[158] According to them, the rational design of molecular photonic devices relies on the ability to select components with predictable electronic structure, excited state lifetimes and redox chemistry. This investigation included a variety of *meso*-phenyl substituted porphyrins involving halogens and methyl groups.

As far as tuning of electronic properties is concerned, Giraudeau and coworkers noted that observed shifts of reduction potential (facilitating easier reduction) is at least five times larger when pyrroles instead of only phenyls (as above) are substituted in *meso*-tetraphenylporphyrins.[159]

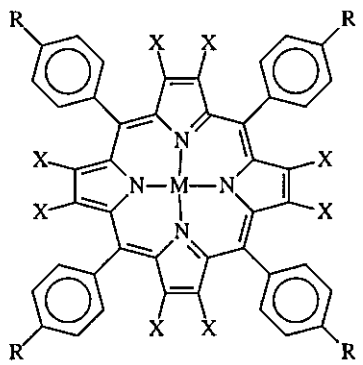


**Figure 2.23** Substituted *meso*-tetraphenylporphyrin. R = *para* positions of the four *meso*-phenyls. X = β-pyrrole positions in direct conjugation with the macrocylic π ring system.

For instance, in the first reduction step, four cyano groups induce the shift, $\Delta E_{1/2}$ = +0.96 V (referred to the half-wave potential of 2HTPP), when the pyrroles are mono-substituted, and only $\Delta E_{1/2}$ = +0.17 V when the phenyls are substituted in the *para*-position. Both types of porphyrins have been used as catalysts.[160] Cobalt porphyrin complexes, with halogen substituents on the β-pyrrole positions that are in direct conjugation with the macrocylic π ring system, show

exceptional oxidative catalytic ability towards organic substrates. But cobalt *meso*-tetraphenylporphyrins with halogen substituents on the pyrrole positions as well as the phenyl rings show even greater catalytic ability, although the relationship is not linear, due to deterring steric effects.

Typically, electron-releasing substituents induce cathodic shifts of reduction potentials whereas electron-withdrawing substituents exert the opposite effect. Positive centers on the porphyrin periphery, as is the case with the electron withdrawing halogen and pseudohalide cyano substituents, cause the delocalised $\pi$ electron cloud to be more diffused over the surface of the molecule. On the other hand, negative or electron donating groups, lead to a partial localization of electron density near the center.[161] Higher oxidation states of the central metal is thereby stabilised, as opposed to the former more electron poor centers.

Comparison of the relative Co(III)/(II) redox potentials of the following more general case further illustrates the aforementioned stabilization effect:[162]

$$[Co(H_2O)_6]^{3+} + e^- \rightarrow [Co(H_2O)_6]^{2+} \qquad E^o = +1.84\ V \text{ vs. S.H.E}$$

$$[Co(NH_3)_6]^{3+} + e^- \rightarrow [Co(NH_3)_6]^{2+} \qquad E^o = +0.108\ V$$

$$[Co(CN)_6]^{3-} + e^- \rightarrow [Co(CN)_5]^{3-} + CN^- \qquad E^o = -0.8\ V$$

From the above, in the presence of coordinating ligands other than water, Co(III) is stabilised relative to Co(II), i.e. the higher valent species are no longer strong oxidizing agents. Hexaaqua complexes exist naturally in the Co(II) oxidation state, while the more basic hexaammine and negative cyano ligands stabilise the higher valent Co(III) oxidation state, with consequent stronger metal-ligand bonds.

Van Eldik and coworkers illustrated how even metal porphyrin complexes with higher electron density around the metal center, like iron(III) tetra(sodium 4-sulfophenyl)porphyrin with its negatively charged peripheral $—SO_3^-$ groups, nevertheless still maintain oxidative catalytic ability.[163,164] Its ability, however, is substantially weaker, with the consequence that only traditionally strong reducing agents such as ascorbate and thiourea dioxide may be catalytically oxidised. Like ascorbic acid, dithizone is also a diprotic species with relative reducing strength of each species in the order: $H_2Dz < HDz < Dz$.

In basic medium ascorbate is able to reduce Fe(III)TPPS, and a redox cycle can be performed by addition of oxygen, with immediate reoxidation of Fe(II)$Na_4$TPPS to Fe(III)$Na_4$TPPS. In a weakly acidic medium, on the other hand, oxidation of the Fe(III)$Na_4$TPPS monomer to the Fe(III)$Na_4$TPPS$^{\cdot+}$ radical cation, and partial formation of Fe(II)$Na_4$TPPS was observed, but there

was no indication of a redox cycle. (As mentioned earlier, acids are usually used to oxidise cobalt(II) porphyrins to cobalt(III).)

Kinetic investigations have shown that an axial ligand like the thiocyanate ion adds about 500 times faster to diaquatetra(sodium 4-carboxyphenyl)porphyrinatocobalt(III), $[Co(TCP)(H_2O)_2]^{3-}$, than to $[CoTMpyP(H_2O)_2]^{5+}$, with TMpyP = α,β,γ,δ-tetra(4-N-methylpyridyl)porphyrin. For $[Co(TPPS)(H_2O)_2]^{3-}$, the rate of thiocyanate coordination is about 100 times faster compared to $[CoTMpyP(H_2O)_2]^{5+}$. There is more available electron density that could interact with cobalt(III) in $[Co(TCP)(H_2O)_2]^{3-}$ and $[Co(TPPS)(H_2O)_2]^{3-}$ than in $[CoTMpyP(H_2O)_2]^{5+}$, and this increased electron density increases the lability of cobalt(III). It is clear that porphyrins induce a *cis*-labilizing effect with regard to axial substitution on cobalt(III).[165] As a matter of fact, anation reactions with cobalt(III) porphyrins are about $10^9$ times faster than with the corresponding cobalt(III) pentaamine complexes, e.g. with pyridine, $NCS^-$ or $I^-$.[161] The increased amount of electron density placed upon cobalt(III) by the porphyrin makes cobalt(III) less positive, more like cobalt(II), and stabilises five-coordinate reactive intermediates during substitution reactions.

Boucher and Garber did an informative study on the effect of seven different porphyrins on the redox potential of the Mn(III)/Mn(II) transition.[166] They noted that varying the substituents on the porphyrin ring changes the redox potential by as much as 0.22 V (Figure 2.24 and Table 2.5). Etioporphyrin, with the largest number of electron donating methyl and ethyl groups, stabilises Mn(III) most, as opposed to the weakest donor, tetraphenylporphyrin. The observed order corresponds closely to the $pK_a$ order of porphyrins.[167] The higher the basicity towards the proton, the higher the $pK_a$ (for the dissociation of the protonated form of the porphyrin) and the more negative the half-wave potential, i.e. the stronger the porphyrin-manganese interaction.

Inamo and coworkers gave the estimated absolute $pK_a$ values for the conjugate acids of the following neutral bases in acetonitrile as: pyridine (12.33) > 2HOEP (12.17) > 2HTPP (10.23) > 2H(*p*-Cl)TPP (9.76).[168] The electronic properties of etioporphyrin is expected to be largely similar to that of octaethylporphyrin (OEP), as the latter has ethyl groups instead of the methyl groups of the former. In this regard it should be noted that the electronic inductive properties of alkyl substituents are all approximately the same;

$\sigma_m = -0.7$ for methyl, ethyl, and isopropyl groups, and –0.10 for *tert*-butyl.[169]

It should, however, be kept in mind that varying the peripheral alkyl substituents might alter steric crowding, resulting in nonplanar distortions of metalloporphyrins. It has been shown that such distortions can significantly alter chemical and photophysical properties of metalloporphyrins.[170] Of particular importance for an electron-transport protein like cytochrome

c is the modification of the oxidation-reduction properties of the heme by nonplanar distortion. Specifically, protein-controlled ruffling of the heme provides a mechanism by which the structure of the surrounding protein can regulate heme reduction potentials.

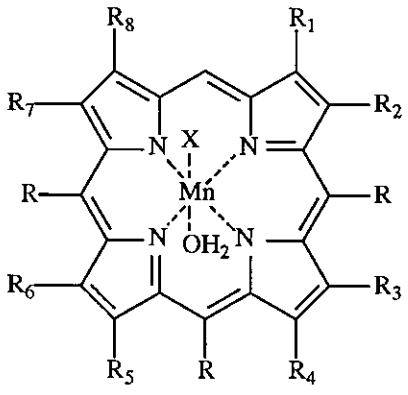


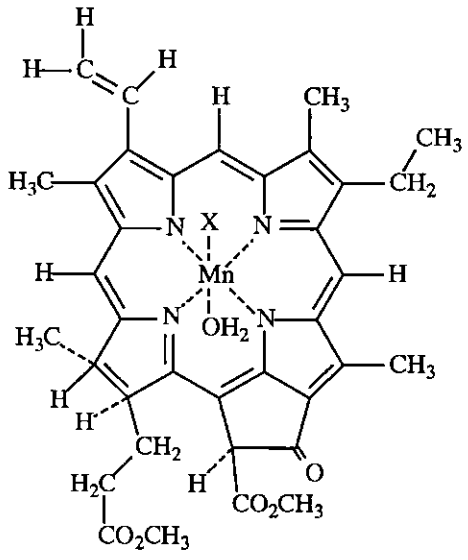


| Compound[a] | | Substituents[b] | | | | | | | | |
|---|---|---|---|---|---|---|---|---|---|---|
| | | R | $R_1$ | $R_2$ | $R_3$ | $R_4$ | $R_5$ | $R_6$ | $R_7$ | $R_8$ |
| DeuteroporphyrinIXdimethylester | DMDepor | H | M | H | M | H | M | PrM | PrM | M |
| MesoporphyrinIXdimethylester | DMMesopor | H | M | E | M | E | M | PrM | PrM | M |
| HematoporphyrinIXdimethylester | DMHPor | H | M | ME | M | ME | M | PrM | PrM | M |
| ProtoporphyrinIXdimethylester | DMPrpor | H | M | V | M | V | M | PrM | PrM | M |
| Etioporphyrin | Etio | H | M | E | M | E | M | E | M | E |
| Tetraphenylporphyrin | TPP | Ph | H | H | H | H | H | H | H | H |
| Pheophorbide a monomethylester | MePheo | Figure on right | | | | | | | | |

[a] x = anion

[b] M = $CH_3$; E = $CH_2CH_3$; V = $CH{=}CH_2$; ME = $CHOHCH_3$; PrM = $CH_2CH_2CO_2CH_3$; Ph = $C_6H_5$

**Figure 2.24** Structural representation of manganese porphyrin complexes with variation of peripheral groups.

**Table 2.5** Mn(III) → Mn(II) half-wave potentials (vs. SCE) of ClMnIII(Por)H2O

| Porphyrin | E½, (V) in acetonitrile | E½, (V) in dimethylformamide |
|---|---|---|
| Etio | -0.45 | -0.40 |
| DM Mesopor | -0.43 | -0.40 |
| DM Depor | -0.38 | -0.33 |
| DM Hpor | -0.37 | -0.32 |
| DM Prpor | -0.35 | -0.31 |
| TPP | -0.23 | -0.22 |
| Mepheo | -0.23 | -0.21 |

As seen above, octaethylporphyrin is the most suitable of general synthetic porphyrins for stabilization of the higher oxidation states of cobalt. Beyond the cobalt +III oxidation state corroles have to be employed to stabilise the metal. Octaethylcorrole (2HOEC) for example, is structurally similar to octaethylporphyrin except for the omission of one *meso*-carbon; i.e. two adjacent pyrroles being directly linked. The contracted heterocyclic ring stabilises cobalt oxidation states of up to +V. Will and coworkers reported the synthesis, electrochemistry, spectroscopy and X-ray structural characterization of some high-valent phenyl σ-bonded iron and cobalt corroles. The central cobalt ions are in the +IV and +V oxidation states.[171] Very little work has otherwise been done on these and related compounds.

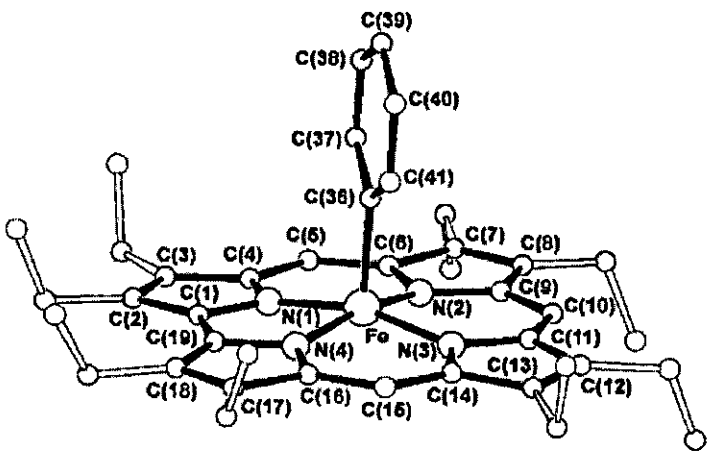


**Figure 2.25** ORTEP diagram of the cation of the octaethylcorrole, $[(OEC)Fe(C_6H_5)]ClO_4 \cdot 0.5C_2H_4Cl_2$ (perspective view, hydrogen atoms omitted for clarity). Notice the "omitted" carbon between C(1) and C(19).

# 3. Results and Discussion

## 3.1. Introduction

In order to realise the relevance of the approaches and results presented in this chapter, it is important to first picture the anticipated final aim or molecular assembly of this research project, regardless the fact that it was, due to the sheer volume of the work, only partially achieved. The operational principle of the anticipated light-switching device is demonstrated in Figure 3.1.

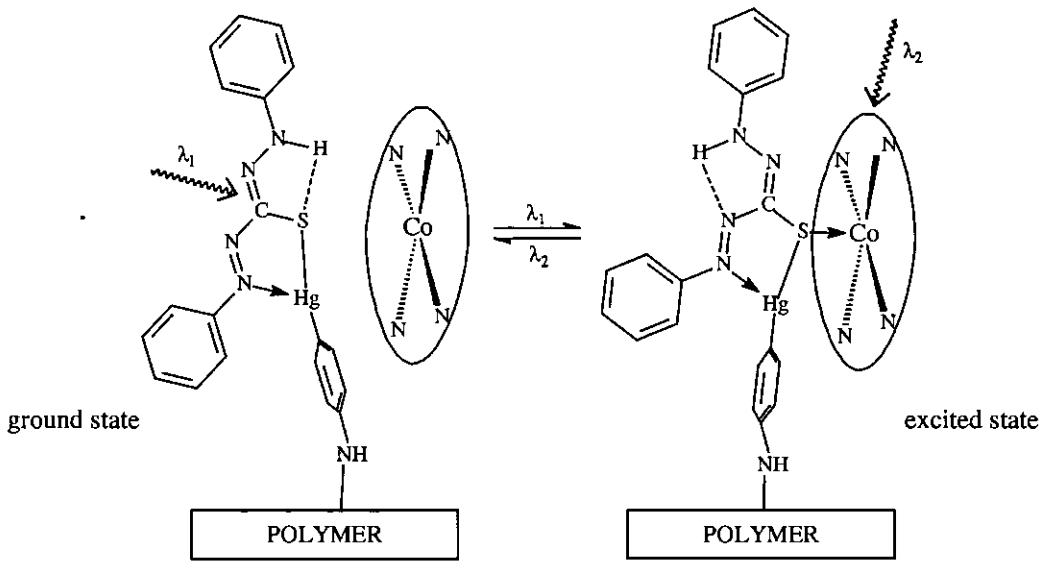


**Figure 3.1** Anticipated interaction between dithizonatophenylmercury(II) and a cobalt porphyrin. Irradiation with light ($\lambda_1$), causing the ornage→blue photochromic reaction to occur, results in larger exposure of the non-bonding electron pairs on sulfur. The sulfur therefore becomes more readily available for coordination to a suitable cobalt-containing porphyrin (right). Absorbance by the porphyrin of light of a different frequency ($\lambda_2$) causes bond homolysis in the axial position, allowing the trapped excited state photochromic moiety to relax to its original ground state (left). Dithizonatophenylmercury(II) is anchored onto a polymer via the amine moiety. The polymer support, which can be either hydrophilic or lypophilic, may or may not be bound to cobalt porphyrin.

This chapter is organised firstly to discuss the synthetic approaches that were pursued, namely (1) the synthesis of relevant dithizone derivatives, (2) reactions involved in anchoring the mercury dithizonate complex onto different polymers, (3) synthesis of a variety of cobalt porphyrins, and (4) an initial investigation into the interactions between dithizone and the various cobalt porphyrins. (Goals 1 & 2, Chapter 1.) As the final envisaged molecular assembly is relying on effective light induced conformational changes, UV/visible spectroscopy was extensively used as qualitative tool throughout.

Single crystal X-ray data from dithizonate complexes of tin and cobalt determined in this study are compared to other related structures, while its relevance to the present study is highlighted. (Goal 3, Chapter 1.)

Thirdly, results from quantum chemical computations on the methylated and unmethylated dithizonatophenylmercury(II) complexes are presented, evaluated, and related to earlier work in this chapter. (Goal 4, Chapter 1.)

Lastly, results from electrochemical studies of the redox potentials of a series of halogenated dithizones, as well as the different cobalt porphyrins are given and discussed. (Goals 5 & 6, Chapter 1.) This study was done to determine what parameters control the redox stability of these two redox active species.

# 3.2. Synthesis

## 3.2.1. Dithizone Derivatives

### 3.2.1.1. S-methyldithizonatophenylmercury(II) as model compound

Before attempting axial coordination of the mercury dithizonate complex to cobalt porphyrin, as illustrated in Figure 3.1, it was considered important to first explore how substituted dithizone derivatives interact with mercury. Selected for this purpose was the derivative of dithizone where-in sulfur was methylated. Eventually, in the final anticipated molecular assembly, the methyl group will be replaced by a cobalt porphyrin in bonding to the dithizone sulfur.

For the purpose of methylation, an excess of methyl iodide was added to the potassium salt of dithizone, **19**. After removal of the solvent (acetone) and any excess methyl iodide under reduced pressure, the product, **17**, was dissolved in the non-polar solvent, dichloromethane, to separate it from any unreacted potassium dithizonate and the formed sodium iodide. Recrystallization from ethanol yielded well-formed black needle crystals with a bronze reflex. This procedure was followed due to availability of ample amounts of potassium dithizonate.

For comparison purposes the methylation reaction was repeated according to a published method.[172] In this method, dimethylsulfate served as source of methyl groups. Addition of a small amount of sodium hydroxide singly deprotonated the dibasic acid, $H_2Dz$, **16**. The mixture had to be heated to destroy any excess of dimethylsulfate, and a chloroform extract was washed several times with dilute aqueous ammonia to remove the unmethylated dithizone. Removal of the solvent left impure S-methylated dithizone, which had to be purified by chromatography on 100 g of silica, and recrystallised from ethanol.

The visible and NMR spectra, as well as the melting points of the products obtained from both the methyl iodide and the dimethylsulfate methods are mutually consistent, indicating pure products. Clearly, with its tedious purification steps, the dimethylsulfate method is more cumbersome than the new methyl iodide path.

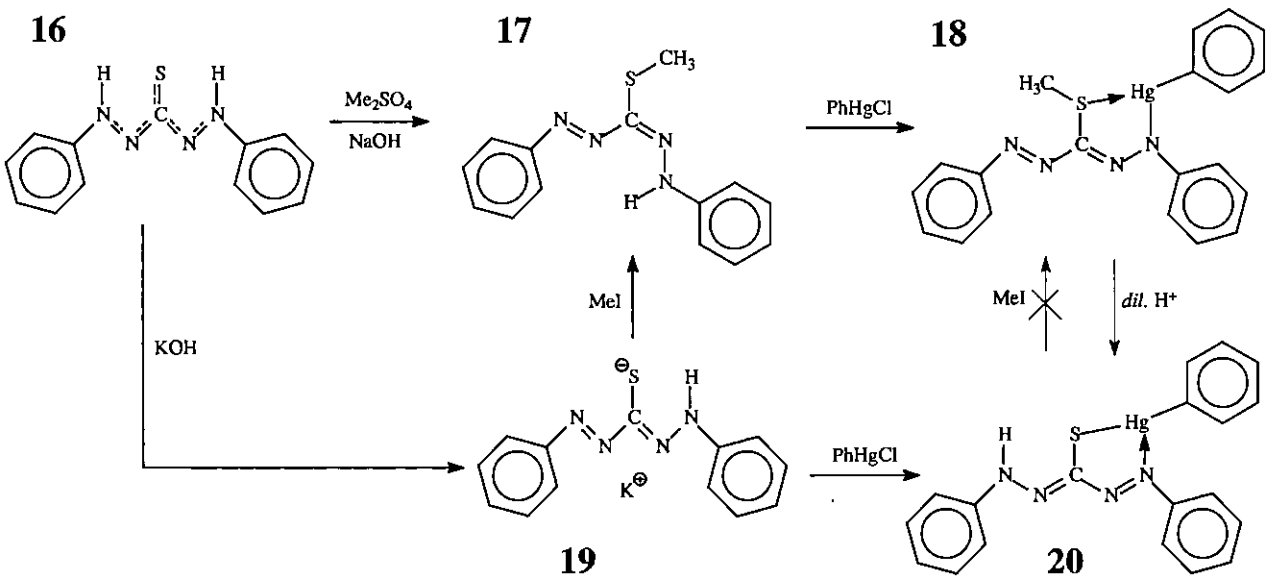


**Scheme 3.1** Synthesis of S-methyldithizonatophenylmercury(II), **18**.

Evidence for two structural isomers of **17** were found in deuterated chloroform. The following $H^1$ NMR spectrum shows two methyl peaks. The sum of the integrals (at 2.41 and 2.55 ppm) of these two peaks gives the required value of three, for the three methyl protons. The same can be seen for the amine proton (at 9.53 and 10.27 ppm).

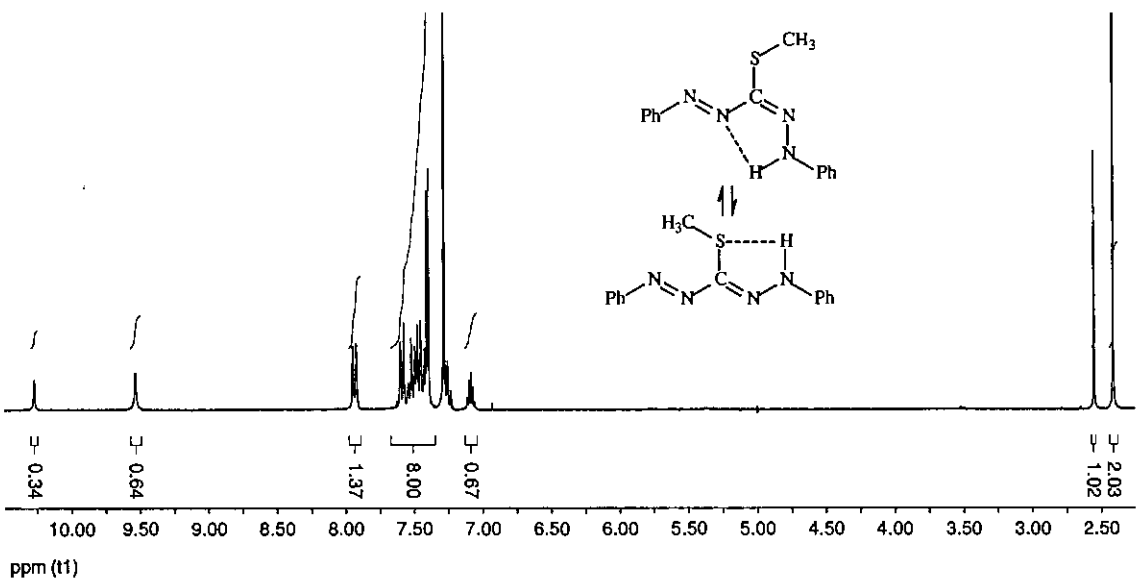


**Figure 3.2** $H^1$ NMR of S-methyldthizone in $CDCl_3$. The peaks at 2.41 & 2.55 are indicative of two structural isomers of **17**.

Before complexation of S-methyldithizone with phenylmercury chloride is discussed, it must be stated at this point that NMR spectroscopy is not always very conclusive in characterizing dithizone derivatives, as molecular changes due to chemical reactions usually only involve the dithizone backbone with its amine protons that are hardly detectable. On the contrary, the electronic spectra (UV/visible) are highly sensitive to any chemical changes, and very typical of

each derivative. To demonstrate, an acetone solution of the starting material has a typical almost blue-green colour (**16**, $\lambda_{max}$ = 444 & 612 nm), which changes to orange-red when stripped of one proton (**19**, $\lambda_{max}$ = 502 nm). Methylation changes the colour to purple (**17**, $\lambda_{max}$ = 541 nm), while consequent complexation with phenylmercury(II) results in a deep green colour (**18**, $\lambda_{max}$ = 442 & 600 nm). Solutions for spectrophotometric investigations of most compounds under investigation in this research project had to be highly diluted due to its intense colour and very high molar absorption coefficients.

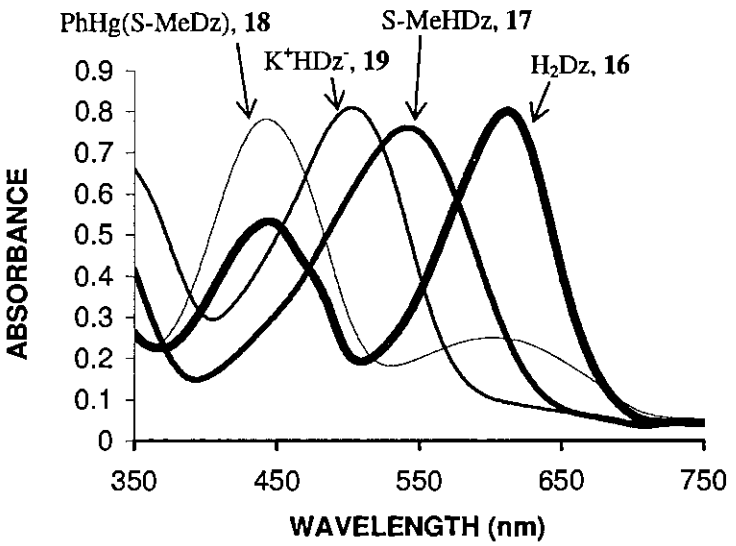


**Figure 3.3** Visible spectra ($\lambda_{max}$, from right to left) of Dithizone, $H_2Dz$; S-Methyldithizone, S-MeHDz; Potassium Dithizonate, $K^+HDz^-$, and S-Methyldithizonatophenylmercury(II), PhHg(S-MeDz), in acetone. (Concentrations were not similar.)

Complexation of S-methyldithizone with phenylmercury(II) chloride dissolved in dichloromethane was accomplished in the presence of an aqueous layer of sodium hydroxide (0.2 M), yielding a dark green product, **18**. The "second" dithizone proton (S-MeDz-**H**) is much stronger bound to the ligand than the "first" proton (**H**Dz-H), and therefore required the stronger base, sodium hydroxide, to remove it. In the complexation reaction of the unmethylated dithizone, much weaker bases like triethylamine or ammonia proved to be sufficient to singly deprotonate dithizone to accomplish mercury coordination. All attempts to methylate the mercury dithizonate complex directly, failed.

Crystallization attempts of **18** in dichloromethane layered over with ethanol, yielded crystals that were too small for an X-ray data collection. Other solvent systems in the hands of the author failed to provide crystals. Synthesizing the analogous chloro(S-methyldithizonato)-mercury compound for the purpose of growing sufficiently large crystals also only yielded at most very tiny radial crystal blooms. It was therefore decided to embark the computational chemistry route in order to get an indication of the most likely structure of **18** (Paragraph 3.4). The reason why it

was considered important to establish the structure of the mercury-containing derivative of dithizone, **18**, was to know in advance the molecular geometry of the photochromic moiety when connected to cobalt porphyrin. This would allow the author to predict whether the ligand will still be bidentately coordinated to mercury through nitrogen and sulfur, or perhaps through two nitrogens.

The synthetic procedure yielded pure product in high yield (94 %), therefore paving the way for a similar approach in construction of the molecular switch, i.e. first coordinating dithizone via sulfur to the metal porphyrin, followed by complexation with phenylmercury to form the bimetallic complex. The published structure of the uncomplexed S-methyldithizone[35] proved that it is indeed sulfur that is methylated, and not any of the four nitrogens. Sulfur is therefore also the anticipated point of attachment with cobalt porphyrin.

In conclusion it must be mentioned that the methyl-sulfur bond is not very strong. This was derived from the observed colour change from green (colour of **18**) to orange (colour of dithizonatophenylmercury(II) ) in deuterated chloroform. Chloroform often typically contains minute amounts of acid due to photochemical decomposition. Ligand protonation therefore readily results in the loss of the relatively labile methyl group.

### 3.2.1.2. Oxidation products of dithizone

Irving[28] reported eight different methods to oxidise dithizone to the fully deprotonated compound, dehydrodithizone, **21**. Only the two methods that were reported to give the highest yields were studied here, namely oxidation of dithizone with potassium hexacyanoferrate(III), and iodine (Scheme 3.2).

The reason for the synthesis of the oxidation product of dithizone was to convert it into a ligand that would be sterically less crowded, thereby enhancing the possibility of axial ligation with cobalt porphyrins, as compared to dithizone (**16**), or the dithizonate anion (**19**). After coordination to cobalt porphyrin dehydrodithizone may be reduced again, with an alkaline solution of dextrose, amongst others.[173]

The iodine-base oxidation method proved to be inconvenient since it was found to give a mixture of products. Iodine oxidation generates disulfides [28] which, in the case of the dithizone dimer, $(HDz)_2$, **22**, lead to spontaneous fission into equimolar amounts of dehydrodithizone and dithizone. In contrast, use of the iron(III) salt, $K_3[Fe(CN)_6]$, yielded pure dehydrodithizone, **21**. Oxidation was achieved by stirring a chloroform solution of dithizone together with an aqueous solution of potassium hexacyanoferrate(III) and potassium carbonate. In essence, cyclisation of

dithizone to dehydrodithizone firstly involves generation of **19** by removal of one proton, before the second proton is removed during oxidation to generate **21**.

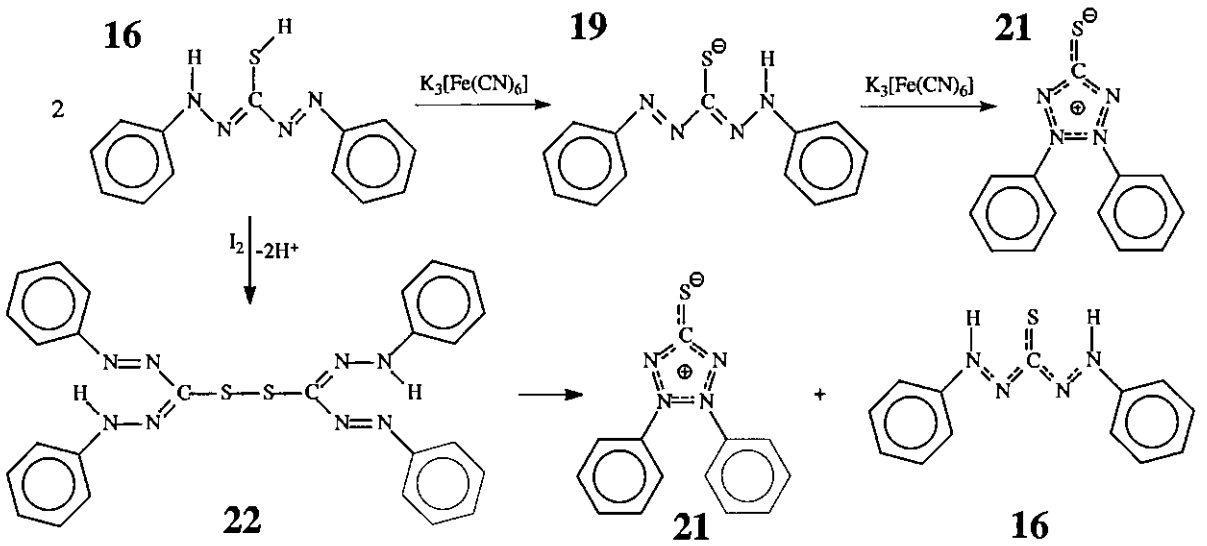


**Scheme 3.2** Complete oxidation of dithizone, **16**, to dehydrodithizone, **21**, is achieved with $K_3[Fe(CN)_6]$. Iodine only partially oxidises **16**.

Recrystallization of the product from hot acetone and water yielded large orange crystals. Care must be taken in exposure of this tetrazolium salt, **21**, to high heat, as it exploded violently at 173°C while melting point determination was under way. Both solubility and visible spectra serve as a good indication of whether dithizone is only partially deprotonated to **19**, or fully oxidised and deprotonated to **21**. An acetone solution of the latter is lighter yellow in colour ($\lambda_{max}$ = 456 nm) than the singly deprotonated compound ($\lambda_{max}$ = 501 nm). Furthermore, dehydrodithizone is insoluble in water, as opposed to the dithizonate auion.

When considering substitution reactions involving the displacement of axial ligands on cobalt(III) porphyrin complexes with dithizonates, e.g. substituting chlorine on a cobalt(III) porphyrin, it has to be kept in mind that the original dithizone has to be converted into its anionic form, **19**, which obviously requires a base. The problem with bases, especially the amines, is their strong coordination tendency to cobalt(III) porphyrins. Apart from generating the anionic form of dithizone, **19**, the base molecules or ions will also form axial bonds with cobalt in cobalt porphyrin macrocycles, which will prevent dithizone from coordinating axially instead. For this reason it was decided to synthesise the dithizonate anion beforehand, and more, to attempt the deprotonation of the dithizonatophenylmercury(II) complex, PhHgHDz, itself, generating the $PhHgDz^-$ anion, which might be used directly in axial substitution reactions involving cobalt porphyrins.

Two approaches for deprotonation (without oxidation) were tested. Oxidation results in product **21**.

The first method used strong bases like sodium or potassium hydroxide. The second method utilised sodium metal in direct contact with dithizone in tetrahydrofurane (Scheme 3.3). In the case of the former, the amount of base required was determined titrimetrically with dithizone acting as self-indicator. The endpoint of the titration, however, was not clearly identifiable. The colour of an acetone solution of dithizone (0.0152 mol.dm$^{-3}$) changed from green through grey to orange-red with addition of a methanolic solution of potassium hydroxide (0.38 mol.dm$^{-3}$). The first appearance of a translucent solution with an orange-red colour was taken to be indicative of the complete conversion of $H_2Dz$ to $K^+HDz^-$, **19**. A 37 % excess of potassium hydroxide was required for this purpose. For the actual synthesis of **19** a 40% excess was used. The dried product was twice redissolved in acetone, and filtered, to get rid of the excess potassium hydroxide, which is insoluble in acetone.

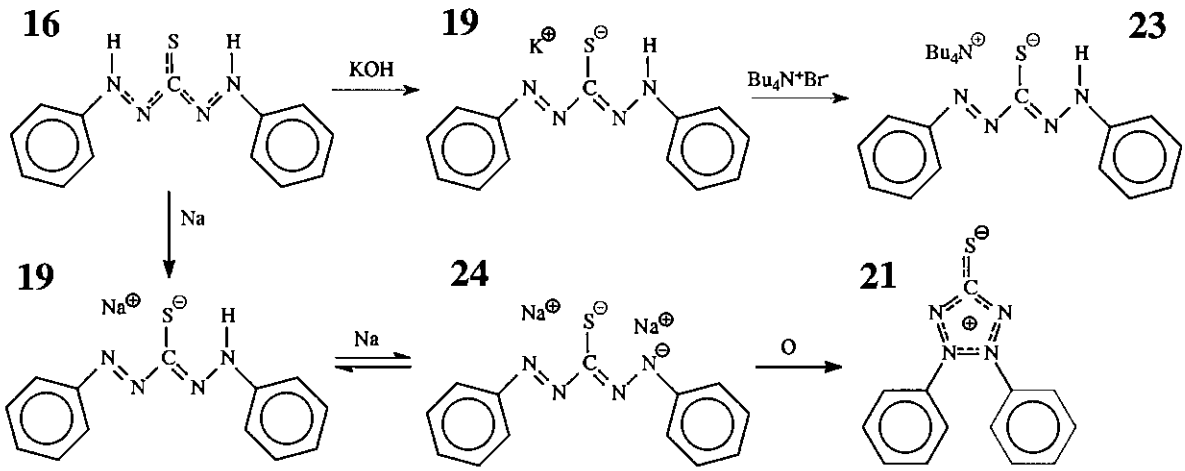


**Scheme 3.3** Peparation of dithizonate salts that are soluble in water (**19**), and soluble in non-polar solvents (**23**). Sodium wire easily deprotonates $H_2Dz$ completely (**24**).

As opposed to dithizone, potassium dithizonate is only soluble in polar solvents, including water. $K^+HDz^-$ does not melt, only blackening of the material above 200°C was observed. Initial tests to determine whether only one or both protons were replaced by potassium were done with the aid of a flame photometer for determination of the potassium content of **19**, using standard solutions of potassium chloride. The results clearly showed that only one proton has been replaced, i.e. compound **19** was pure.

Under this approach a biphasic method was also followed, in that an acetone solution of dithizone was refluxed in the presence of potassium hydroxide pellets. The desired colour change did occur, but the product was oily. However, extensive workup to clean an impure product resulted in the reverse reaction, namely reprotonation of the dithizonate to dithizone itself.

In the last approach dithizone was added to dried tetrahydrofurane containing sodium wire. After refluxing the solution for 10 – 15 minutes, the green colour was changed into orange,

indicative of single deprotonation (forming NaHDz, **19**, $\lambda_{max}$ = 501 nm in acetone). Refluxing the solution for a longer period of time gradually resulted in a solution that was magenta coloured – indicative of double deprotonation (forming $Na_2Dz$, **24**, $\lambda_{max}$ = 530 nm in acetone). The exact point where the dithizonate solution had to be removed from sodium wire was difficult to determine. However, since the di-sodium salt is hard to preserve, it readily reverted back to the mono-sodium salt. $Na_2Dz$, **24**, required the absolute exclusion of any protic solvents. This left acetone as almost the only inert solvent in which **24** was soluble and stable for at least 12 hours. The same was found for the deprotonated form, **25**, of dithizonatophenylmercury(II), **20**. The sodium salt of **20** was also found to be magenta coloured ($\lambda_{max}$ = 532 nm in acetone), which clearly distinguished it from the orange parent compound, **20** ($\lambda_{max}$ = 469 nm in acetone).

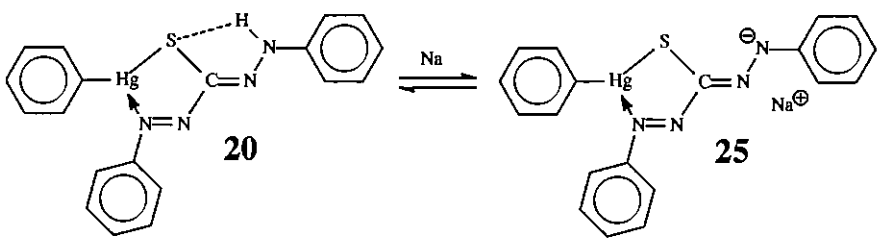


$Na^+PhHgDz^-$ was equally hard to preserve, as it also involves removal of the "second" dithizone proton. The instability of **24** and **25** led us not to pursue these compounds any further as possible precursors to porphyrin coordination.

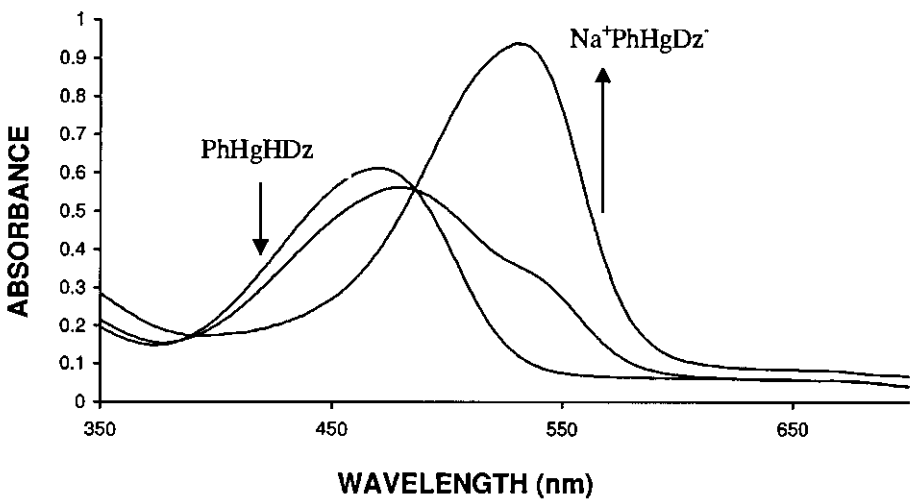


**Figure 3.4** Deprotonation of dithizonatophenylmercury(II) with Na metal, KOH or NaOH in acetone results in the gradual disappearance of the peak at $\lambda_{max}$ = 469 nm, while a new peak appears at 532 nm.

Crystallography quality NaHDz crystals were grown from an acetone / carbon disulfide solvent mixture, overlayed with hexane. No data collection was attempted, however, since the structure of KHDz was already published.[174] Leaving the magenta $Na_2Dz$ acetone solution to crystallise, yielded pure dehydrodithizone, **21**, crystals. Although not pursued per se, yet another method for the complete oxidation of dithizone was thereby discovered. An attempt to grow crystals of

$Na^+PhHgDz^-$, **25**, from acetone only resulted in the salt reverting back to the original complex, dithizonatophenylmercury(II), PhHgHDz, **20**. The latter complex proved to be photochromic, which allowed its positive identification. Synthesis of $K^+PhHgDz^-$ on addition of a threefold excess of potassium hydroxide was also successful, but was eventually also abandoned due to the difficulty of preservation of $K^+PhHgDz^-$.

From the above work only the mono-sodium and potassium salts of dithizone were considered to be stable enough for useful synthetic application. Availability of these salts not only eliminates the use of bases in follow-up reactions, but also makes dithizone water-soluble.

The poor solubility of potassium dithizonate in non-polar solvents implies it can not conveniently be used for reactions in these solvents. To overcome this problem, tetrabutylammonium dithizonate, $Bu_4N^+HDz^-$, **23**, ($\lambda_{max}$ = 501 nm in acetone) was synthesised (Scheme 3.3). Addition of tetrabutylammonium bromide to $K^+HDz^-$, **19**, dissolved in acetone, gave **23** in good yield (77%). This salt is also soluble in non-polar solvents such as dichloromethane.

### 3.2.1.3. Dithizonato metal complexes

**MERCURY:** The reported procedure for synthesis of mercury complexes of dithizone utilised an aqueous ammonia layer in the presence of a mercury salt dissolved together with dithizone in benzene.[175] Instead of using this tedious separating funnel procedure it was decided to simplify the synthesis by rather employing triethylamine as base to deprotonate dithizone in the presence of a small excess of phenylmercury chloride dissolved in dichloromethane.

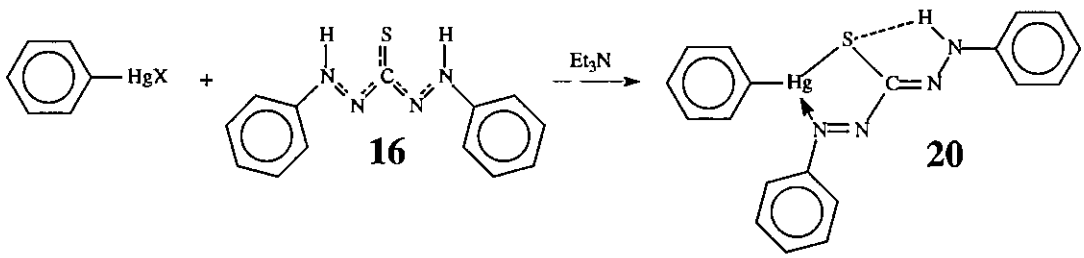


**Scheme 3.4** Synthesis of dithizonatophenylmercury(II) (**20**). (X = $Cl^-$ or $CH_3COO^-$)

Recrystallization was done from dichloromethane and ethanol, resulting in large orange crystals of dithizonatophenylmercury(II), **20**, in very high yield (93 %). Typically, a relatively long half-life ( > 1 minute ) of the blue photo-excited state, **26**, in dichloromethane is a good indication of both compound and solvent purity. This was indeed found to be the case (Figure 3.3), over and above the fact that the NMR spectrum and melting point were in agreement with the published data.

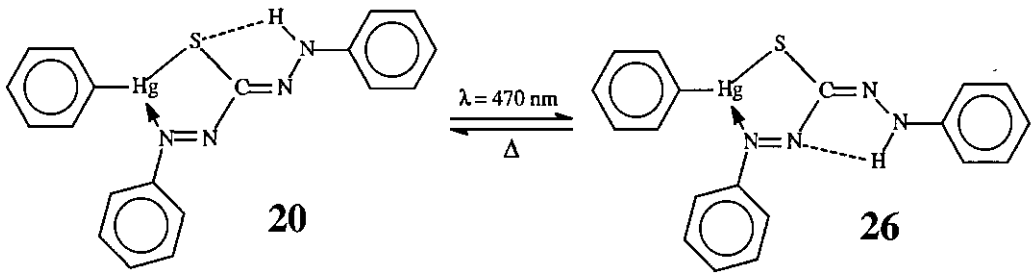


**20** **26**

The blue photo-excited state, **26**, was generated by irradiation of the dilute orange dichloromethane solution ($1.56 \times 10^{-5}$ mol.dm$^{-3}$) of the photochromic compound, **20**, with a 400 W mercury-halide lamp, which radiates mainly in the visible region of the electromagnetic spectrum. Photo-conversion from orange to blue is however more efficient when the mercury dithizonate is exposed to direct sunlight. (Radiation from the sun peaks in the blue-green region of the spectrum, which coincides with the absorbance peak of orange mercury dithizonates.)

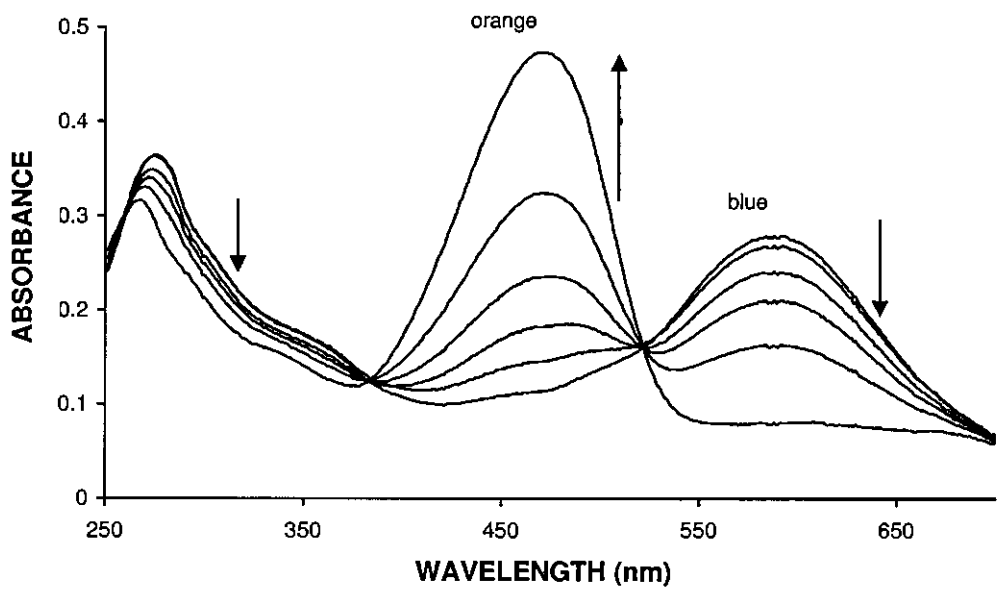


**Figure 3.5** The photochromic back-reaction of excited (blue form, **26**) dithizonatophenylmercury(II) in dichloromethane. The blue photo-excited state ($\lambda_{max}$ = 583 nm, $\varepsilon$ = 18 000 dm$^3$.mol$^{-1}$.cm$^{-1}$) reverts back to the orange ground state ($\lambda_{max}$ = 470 nm, $\varepsilon$ = 30 000 dm$^3$.mol$^{-1}$.cm$^{-1}$), with characteristic isosbestic points at 381 nm & 521 nm. Spectra were recorded at 5 sec., 2 min., 6 min., 12 min., 24 min. & 120 min. after exposure to light.

**TIN:** Dithizonatotrimethyltin(IV), **28**, was synthesised for the purpose of serving as possible transfer intermediate in the axial ligation reaction of dithizonate with cobalt(III) porphyrin. To our knowledge, this led to the first ever synthesis and structure determination of the tin dithizonate complex. Dimethylaminotrimethyltin(IV), **27**, was used as reagent together with dithizone to synthesise dithizonatotrimethyltin(IV), **28**. Due to the high reactivity of the organo-tin liquid, reaction media are limited to non-protic, non-coordinating, non-halogen containing solvents like diethylether or hydrocarbons.

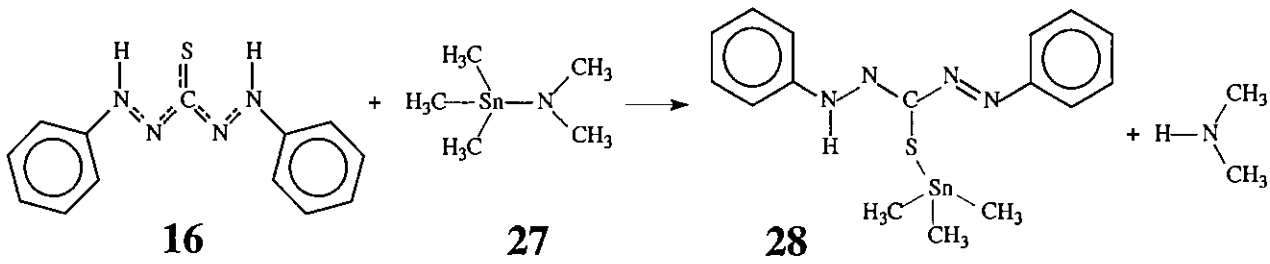


**Scheme 3.5** Synthesis of dithizonatotrimethyltin(IV) (**28**)

On coordination of dithizone to tin in diethylether, the weak and polar Sn-N bond in $(CH_3)_3$-Sn-$N(CH_3)_2$ broke, with the liberation of dimethylamine, which quickly evaporated, leaving a product that did not require further purification. Neat orange crystals, suitable for X-ray crystallography, were grown from a diethylether solution covered with parafilm. The structural elucidation is discussed in Paragraph 3.3.2. $\lambda_{max}$ = 438 nm in diethylether. (See Figure 3.6, p.66)

**COBALT:** The last metal dithizonate investigated in this research project, was the cobalt dithizonate complex. The initial aim of attempting mono-coordination of dithizone to cobalt was to do a so-called tailed metal insertion reaction as presented in the following scheme, based on work done by Ogoshi and Trommel.[176]

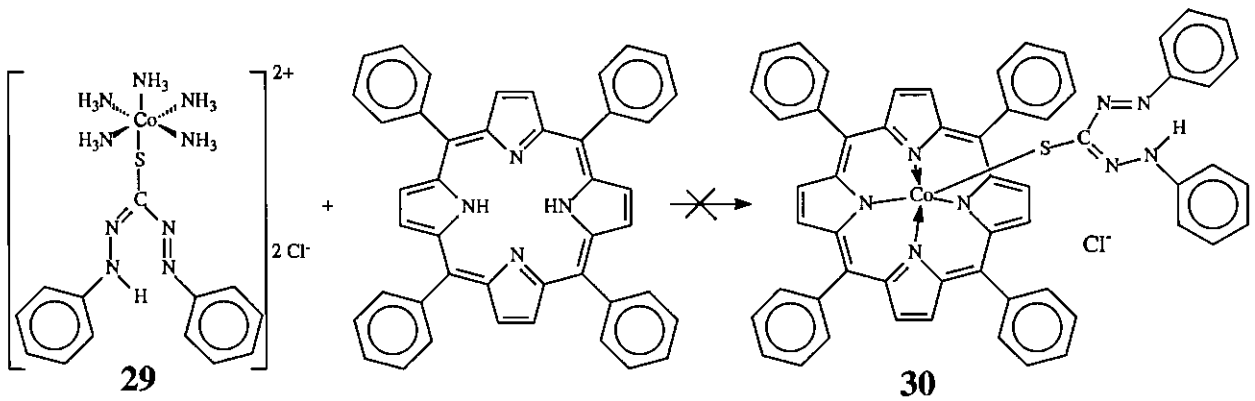


**Scheme 3.6** Proposed tailed metal insertion reaction whereby cobalt may be inserted into the porphyrin heterocycle, without the loss of the dithizonate ligand (**30**). This reaction might only be feasible with dithizone being mono-coordinated to cobalt (**29**).

This approach, however, was quickly eliminated as method for porphyrin cobalt axial coordination of the bulky dithizonate ligand, because the required reagent, **29**, could not be synthesised. Regardless whether stoichiometric excesses of the pentaamine-, hexaamine- or hexaaqua cobalt complexes were used as starting reagent, reaction with potassium dithizonate always resulted in the *tris*-coordinated dithizonatocobalt(III) product, **33**. The structure of $Co(HDz)_3$, **33**, was solved by an X-ray data collection (see Paragraph 3.3.3.) that was done on a crystal grown from the hexaaqua reaction.

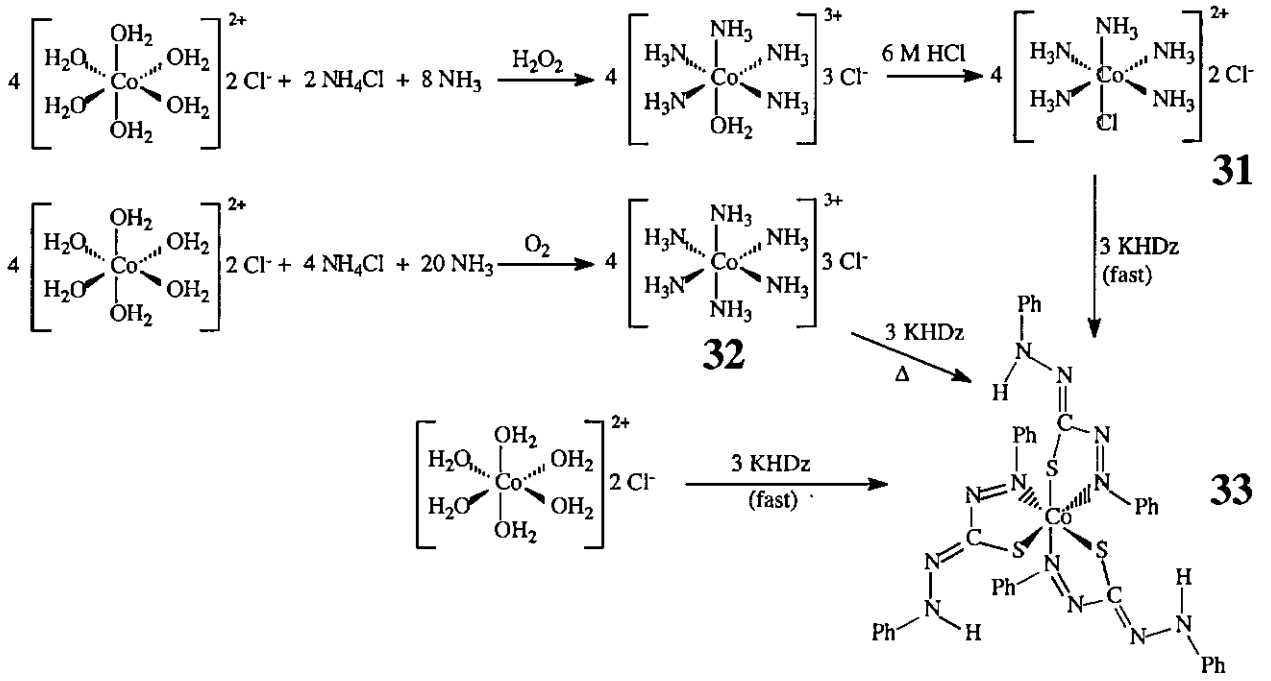


**Scheme 3.7** Three approaches leading to one product, $Co(HDz)_3$ (**33**), regardless the use of equimolar amounts of the cobalt salt and potassium dithizonate, in acetone.

Visible spectra ($\lambda_{max}$ = 549 nm in diethyl ether), melting points (175°C) and elemental analysis of the final products (**33**) from all three the above reactions were similar and consistent with *tris*-coordination.

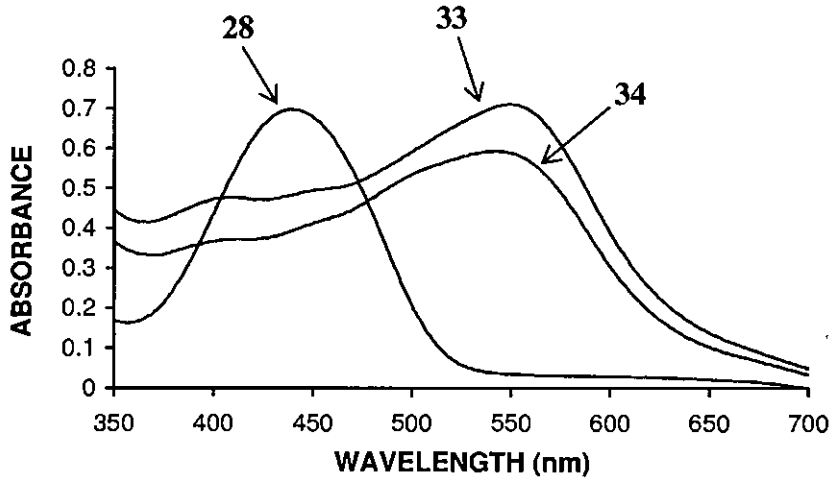


**Figure 3.6** Visible spectra of dithizonatotrimethyltin(IV) (**28**); *tris*(dithizonato)cobalt(III), $Co(HDz)_3$ (**33**), and the dithizonatophenylmercury(II) cobalt complex (**34**) in diethylether. (Concentrations were not similar.)

The reaction of potassium dithizonate with the pentaamine cobalt salt,[177] **31**, was almost instantaneous at room temperature, where as the reaction with the hexaamine salt,[178] **32**, hardly proceeded without heating and stirring the mixture over 30 minutes. Such behaviour must be explained in terms of the one chloride in the pentaamine salt, **31**, that is directly coordinated to cobalt. The chloride is a better leaving group, compared to the $NH_3$ group. Relatively strong Co-$NH_3$ bonds, in the case of the hexaamine salt, occupy the entire inner coordination sphere around cobalt, and therefore impede the room temperature reaction with dithizone.

In view of the fast coordination of dithizone that also occurred when using the hexaaqua cobalt salt, it was decided to briefly extend the investigation to dithizonatophenylmercury(II), **20**, as ligand, as well. Some interesting and promising observations were then made. When the hydrated cobalt salt, $[Co(H_2O)_6]Cl_2$, was dissolved in acetone, giving a bright blue solution, there was an immediate reaction on addition of dithizonatophenylmercury(II). The solution colour changed to deep purple-red, with a UV/visible spectrum that compares closely to that of **33** ($\lambda_{max}$ = 543 nm in diethyl ether). In contrast, when the cobalt salt was dissolved in methanol, giving a light pink solution, no reaction seemed to take place on addition of the mercury complex. This was also in contrast to both dithizone and potassium dithizonate, that *did* react with cobalt in methanol.

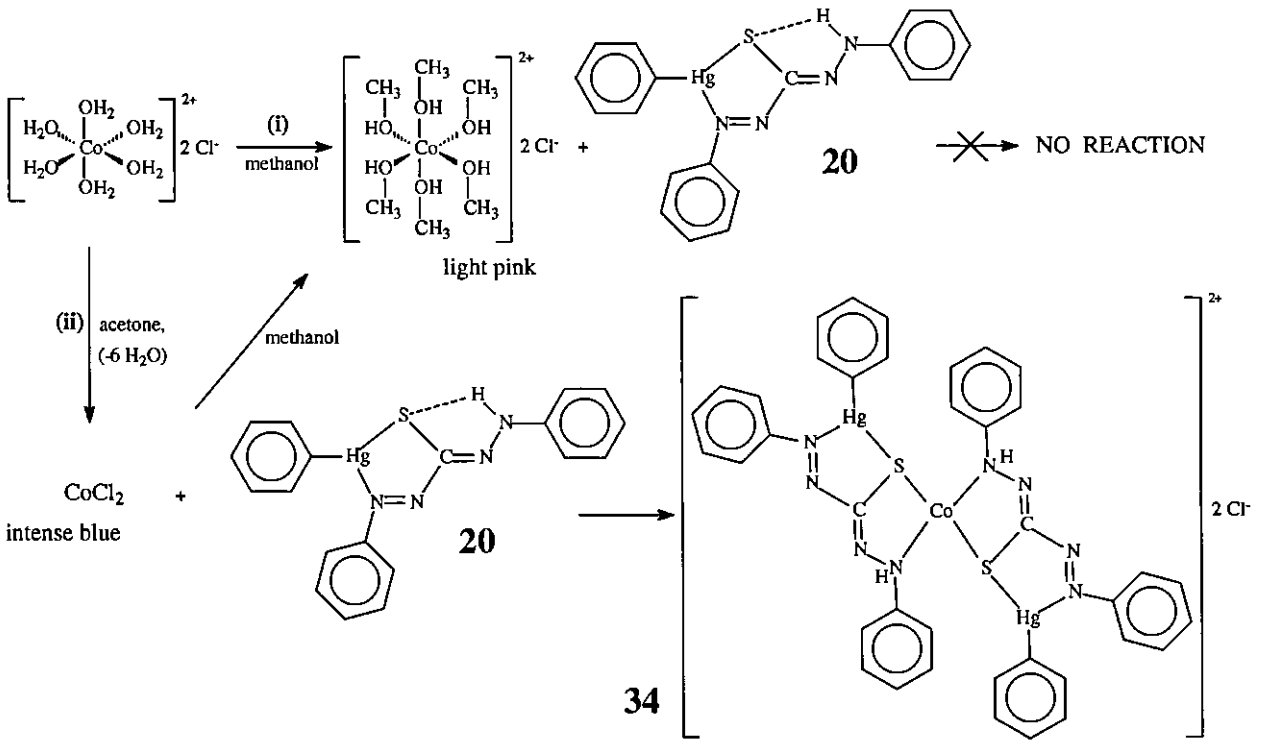


**Scheme 3.8** Two approaches, using different solvents, to complex dithizonatophenylmercury(II) with cobalt. Only in acetone a reaction was observed, yielding a product considered to be $[Co(PhHgHDz)_2]Cl_2$ (**34**).

Two aspects are of key importance in explaining these observations. Firstly, cobalt(II) cations are known to form light pink $[Co(H_2O)_6]^{2+}$ solvated octahedral complexes in water. Dissolution in acetone removes the crystal water, allowing chloride to enter the inner coordination sphere, forming intense blue $CoCl_2$. Based on the observation that methanolic solutions of cobalt chloride are also light pink, it is concluded that the crystal water is displaced by methanol to form a similar complex, $[Co(CH_3OH)_6]^{2+}$, which, as in the case of the aqua complex, allows for strong hydrogen bonding between H and O of adjacent solvated methanol molecules.

It must further be noted that addition of the solid hydrated salt to methanol was observed to initially have a bright blue colour surrounding the salt crystals in the solvent. The colour

changed to pink when the salt dissolved. The explanation is that initial liberation of coordinated water around cobalt, with the consequent entry of $Cl^-$ into the cobalt coordination sphere, causes the blue colour. Thereafter the cation became methanol solvated, changing to pink again. This behaviour is demonstrated in Scheme 3.8.

All the above observations are in line with the fact that both the coordinating ability and polarity, and the solvents' abilities to form interlocking hydrogen bonds around the central metal, lie in the order: acetone < methanol < water.

Secondly, in explaining the different behaviour in methanol and acetone, it must be kept in mind that the phenylmercury dithizonate complex is a much weaker and sterically more obstructed ligand as compared to dithizone. Although the reaction with dithizone did occur in methanol, the methanol solvation around cobalt is sufficient to prevent the mercury complex to coordinate, as opposed to unsolvated $CoCl_2$ in acetone. Hydrogen bonds between solvent molecules and the dithizonate nitrogens are further expected to inhibit coordination by the mercury complex.

These observations are most significant, since it proved that the mercury dithizonate complex as a whole may serve as a ligand in reactions with cobalt. In addition, coordination is extremely labile, as illustrated by the competing reaction with methanol. A relatively weak Co-S bond would certainly be an important requirement in any molecular switch assembly. As opposed to the above Co-S,N ligation (**34**), Co-N,N ligation was not considered to take place, since it would require photo-induced rotation around the C=N double bond, which clearly was not a requirement for the observed reaction. Further evidence in support of this notion is to be found in the mode of coordination observed in the X-ray crystal structure of $Co(HDz)_3$, **33**, where coordination is only Co-S,N (see paragraph 3.3.3).

By now the question must be posed; was mercury not perhaps displaced by cobalt in the acetone solution, thereby rendering the photochromic dithizonate complex useless for reversible switching? (Photochromism has not been observed in the cobalt dithizonate complex, **34**.)

Two further observations answered this question conclusively.
Firstly, while passing a dichloromethane solution of **34** through a silica column, the colour gradually changed from purple to orange. The orange eluent was typically photochromic, changing from orange to blue and back after irradiation with visible light. This proved that mercury was not displaced, but that the complex was simply locked in a different colour state by the cobalt cation. By passing the non-polar solvent solution through silica, the purple product was stripped of the ionic cobalt chloride.

Secondly, dimethylsulfoxide was observed to permit similar behaviour to that of acetone, namely a blue DMSO cobalt solution that allowed reaction of cobalt with the mercury complex. Interestingly, addition of water to the purple product solution (**34**) changed it to orange, the

standard colour of the photochromic moiety. Boiling the water away again, reverted the solution back to purple. This could be repeated many times, indicating complete reversibility. Competing solvation reactions therefore proved to be sufficient to dislocate dithizonatophenyl-mercury(II) from being locked by cobalt in the purple form.

The above question is therefore conclusively answered: Hg-Co interchange did not take place, but a new purple-red Co-PhHgHDz adduct formed. The observations that were made gave a clear indication that the overall direction of this research is well-founded and in the right direction. Further research is required to establish the exact nature and structure of the new $[Co(HDz)_2]Cl_2$ complex. This would include isolation and crystal structure determination.

One aspect, namely the ligand-to-metal ratio was nevertheless unambiguously solved in this study. The so-called mole-ratio method [179] was used to establish the metal-to-ligand ratio in the above reaction. A series of solutions were prepared in which the analytical concentration of the cation, $Co^{2+}$, was held constant while that of the ligand, PhHg(HDz), was varied. A plot of absorbance versus mole ratio of the reactants was then made (Fig.3.7). The two straight lines of the different slopes intersect at a mole ratio corresponding to the combining ratio in the complex.

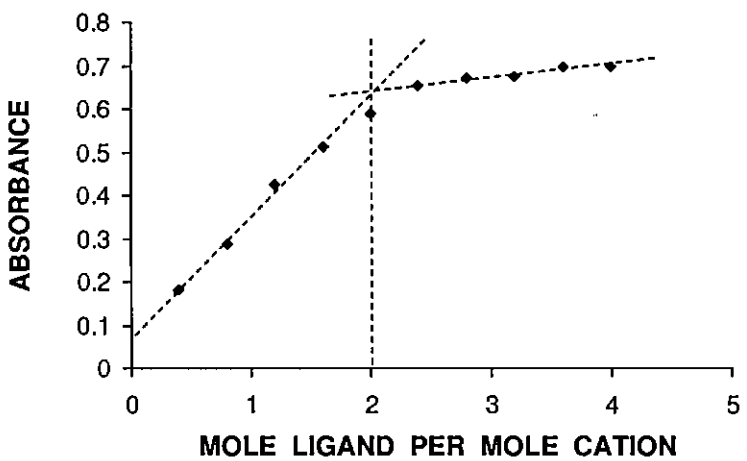


**Figure 3.7** Plot of absorbance versus mole ligand per mole cation (at 547 nm). $[Co^{2+}] = 1.89 \times 10^{-5}$ mol.dm$^{-3}$.

From the intersect, the mole ligand to mole cation ratio was unmistakably derived to be 2 : 1, which suggested structure **34,** as in Scheme 3.8, namely $[Co(PhHgHDz)_2]Cl_2$. Formation constants can be evaluated from the data in the curved portion of the mole-ratio plot where the reaction is least complete. This, however, is left for later investigations.

### 3.2.1.4. Halogenated dithizones

As seen from paragraph 3.2.1.2, it is clear that the dithizonate ligand may very easily be oxidised by a variety of mildly oxidizing agents. It was therefore decided to investigate ways to stabilise the ligand without loosing its photochromic property, and to quantify the measures that were

taken with regard to relative stabilization strengths. This investigation is further validated by the fact that any molecular switch assembly will be highly dependent on subtle differences in electronic effects.

To address the question of oxidation ease, a series of phenylhalogenated dithizones were synthesised and electrochemically investigated (Paragraph 3.5). The series included the *para*-chloro-, *para*-fluoro-, *meta*-fluoro-, *ortho*-fluoro-, 3,4-difluoro- and 3,5-difluoro-dithizones. Halogenation was symmetrical, i.e. on both phenyl rings. The synthetic method followed for dithizone that was according to Pelkis, Dubenko and Pupko.[14]

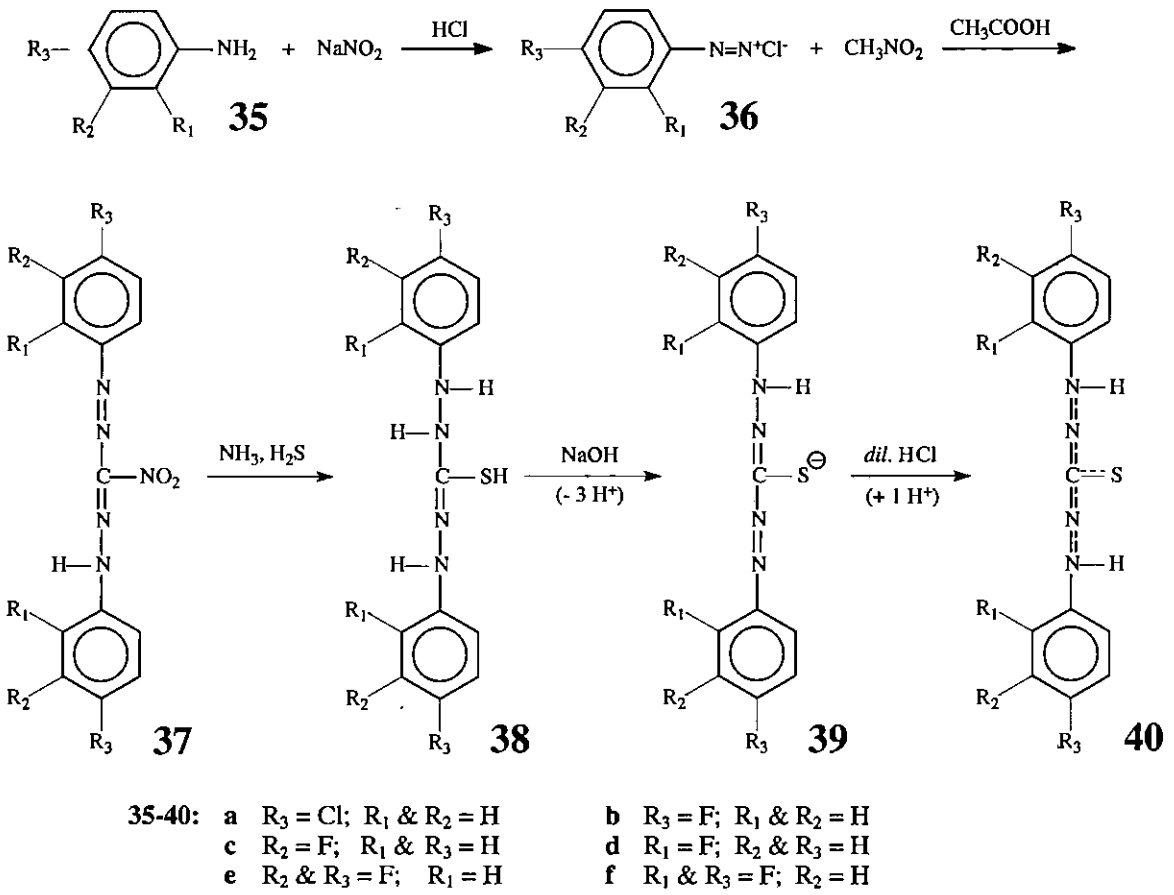


**35-40:** **a** $R_3 = Cl$; $R_1$ & $R_2 = H$ **b** $R_3 = F$; $R_1$ & $R_2 = H$
**c** $R_2 = F$; $R_1$ & $R_3 = H$ **d** $R_1 = F$; $R_2$ & $R_3 = H$
**e** $R_2$ & $R_3 = F$; $R_1 = H$ **f** $R_1$ & $R_3 = F$; $R_2 = H$

**Scheme 3.9** The synthesis of halogenated dithizones from the corresponding halogenated anilines.

En route to halogenated dithizones, the first reaction was the diazotization of the halogenated anilines by the addition of sodium nitrite in the presence of hydrochloric acid. The nitroformazans, **37**, were made by reacting the diazo compound, **36**, with nitromethane in the presence of acetic acid. The red formazyl products, **37**, thus precipitated, were filtered off and washed with copious amounts of water. NMR spectra of the uncrystallised and recrystallised products agreed exactly, thus making further purification of products in which no impurities were observed, pointless.

In the next step the thiocarbazones, **38**, were made. This was accomplished by consecutively bubbling ammonia and hydrogen sulfide gas through an ethanolic solution of the nitroformazan.

After mercaptan introduction was complete, as indicated by a change of colour from red to orange-yellow, the solution was added to water to precipitate a dirty-white thiocarbazide, **38**. The unstable thiocarbazide was immediately oxidised to the orange-red thiocarbazone, **39**, by the addition of cold 2 % methanolic sodium hydroxide solution. The thiocarbazone was purified by precipitation from a methanolic sodium hydroxide solution, with the addition of dilute hydrochloric acid. Repeating the latter procedure about five times yielded sufficiently pure, dark green dithizone derivatives, **40**, not requiring the use of column chromatography for further purification. The di-fluorinated dithizones gave orange solutions in dichloromethane, with broad UV/visible peak maxima at *ca* 400 nm. The mono-fluorinated dithizones, on the contrary, are all dark green in solution, with two peak maxima, *ca* 447 nm and 620 nm, in dichloromethane.

The corresponding potassium dithizonate and dithizonatophenylmercury(II) compounds were then synthesised, the former for use in reactions with cobalt porphyrins, and the latter, to test for photochromicity (also a measure of purity). It was found that all the mono-halogenated (i.e. one halogen per phenyl) mercury dithizonate complexes were still photochromic. After exposure to light, the existence times of the blue excited states in dichloromethane were visibly inspected, and found to be in the order;

PhHgHDz > PhHg(*p*-F)HDz = PhHg(*p*-Cl)HDz >> PhHg(*m*-F)HDz = PhHg(*o*-F)HDz

In toluene, diethylether and tetrahydrofurane the order was found to be:

PhHgHDz > PhHg(*p*-F)HDz > PhHg(*p*-Cl)HDz > PhHg(*m*-F)HDz > PhHg(*o*-F)HDz

The above observed order is mostly (apart from *p*-F and *p*-Cl, that are reversed) in line with the expected capacity of the halogenated phenyls to withdraw electron density from the semi-conjugated dithizonate backbone. These observations are in good agreement with work done by Al-Salihy & Freiser[180], where the $pK_a$ values, i.e. their propensity to resist oxidation, were determined (see also Table 2.1.):

$H_2Dz$ (5.77) > (*p*-F)$H_2Dz$ (4.99) > (*p*-Cl)$H_2Dz$ (4.63) > (*m*-$CF_3$)$H_2Dz$ (2.57)

These observations will later further be compared to electrochemical data (Paragraph 3.5).

The author had not been able to successfully prepare any of the di-fluorinated dithizone mercury complexes, with the consequence that no di-fluorinated photochromic compound could be isolated. By going from the green mono- to the orange di-fluorinated dithizones the barrier had therefore been crossed within which photochromism was still observed. Single crystal X-ray crystallography is envisaged for the purpose of solving the structure of the di-halogenated compounds, but lies outside the scope of the present investigation.

## 3.2.2. Polymer Syntheses and Anchoring Reactions

For the purpose of this dissertation it was decided to start the investigation into a suitable receptacle for the molecular switch by anchoring the photochromic moiety via the phenyl amine onto examples of both hydrophilic- and lypophilic polymers. Poly-DL-succinimide was selected as a polymer that may readily be converted into a water-soluble polymer. Side-chains of polysuccinimide may conveniently be functionalised for anchoring purposes. Polyepichlorohydrin, on the other hand, is a lypophilic polymer which may be used directly in anchoring reactions. Derivatives of both the above polymers required either amine or carboxylic acid functional groups on the mercury phenyl in the subsequent coupling reactions.

### 3.2.2.1. Functionalization of phenylmercury(II) complexes

*Para*-aminophenylmercury(II) acetate, $H_2NPhHg(OAc)$, known for more than a 100 years,[77, 181] is conveniently synthesised and yields a pure product in high yield. The phenyl amine group offers a convenient handle for anchoring mercury complexes onto polymeric substrates via the amide bond. In this reaction two moles of aniline were added to one mol of mercury acetate in water, with the formation of a white precipitate, *p*-aminophenylmercury(II) acetate, **41**. The additional equivalent of aniline serves as base to capture the liberated acid.

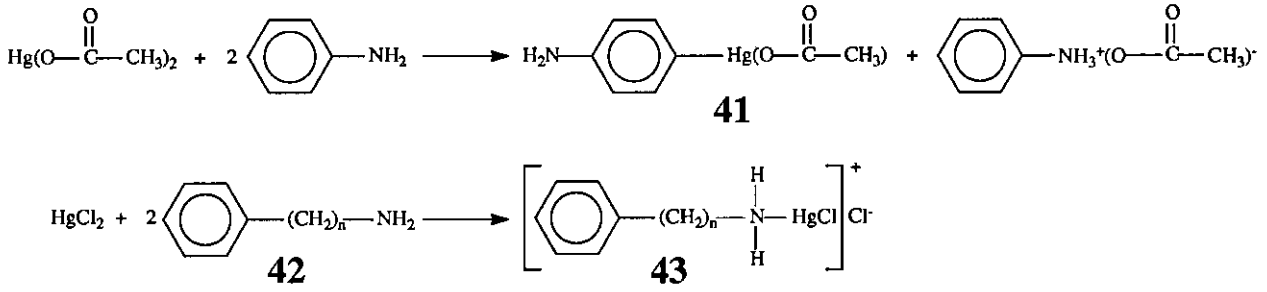


**Scheme 3.10** Aromatic amines, coordinating in different ways to mercury(II) salts.

Contrary to the successful synthesis of **41**, but in agreement with literature, none of the $H_2N(CH_2)_nPhHgCl$ complexes (n = 1, 2, 3 & 4) could be isolated using the respective amines and mercury chloride (or -acetate) as reagents. The NMR spectrum of $H_2N(CH_2)PhHgCl$ (see Spectrum A14, Appendix 1) indicates five protons on the phenyl, quite contrary to the two neatly split phenyl doublets (Spectrum A13) of **41**, representing four protons. The compounds of **43** therefore coordinated with mercury via the amine, behaviour which was also tested and observed for aliphatic amines, like dimethylamine, triethylamine, etc. This observation is consistent with work done by Alderighi *et al*,[182] wherein ethylenediamine coordinated to a mercury salt via the amine, as illustrated in the following reaction.

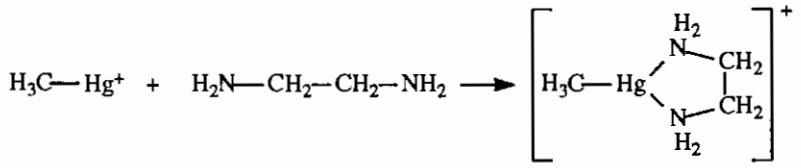

In aniline it is the strongly activating influence of the $-NH_2$ group (*ortho*- and *para*-directing) that contributes towards *para* Hg coordination of the phenyl, as opposed to the $-(CH_2)_n-$ groups on the phenyls of **42** that are merely weakly activating. The NMR spectrum of **41** further clearly indicates formation of only the *para*-aminophenylmercury compound. This is contrary to reported cases where other substituents are used on the phenyl ring, which almost always result in a mixture of products, i.e. mercury coordinates at different phenyl ring positions.[82] For the purpose of functionalizing mercury complexes, aniline therefore still proved to be one of the most suitable and convenient reagents.

In subsequent reactions the amine was used for preparation of compounds with a carboxylic acid functional group. For this purpose succinic anhydride was employed as reagent. A test was first done by reacting uncomplexed phenylethylamine with succinic anhydride in acetone. A white precipitate immediately formed, and washing of the filtered product with cold acetone yielded the desired pure 4-oxo-4-[(2-phenylethyl)amino]butanoic acid, **42**, as confirmed by NMR (Spectrum A15).

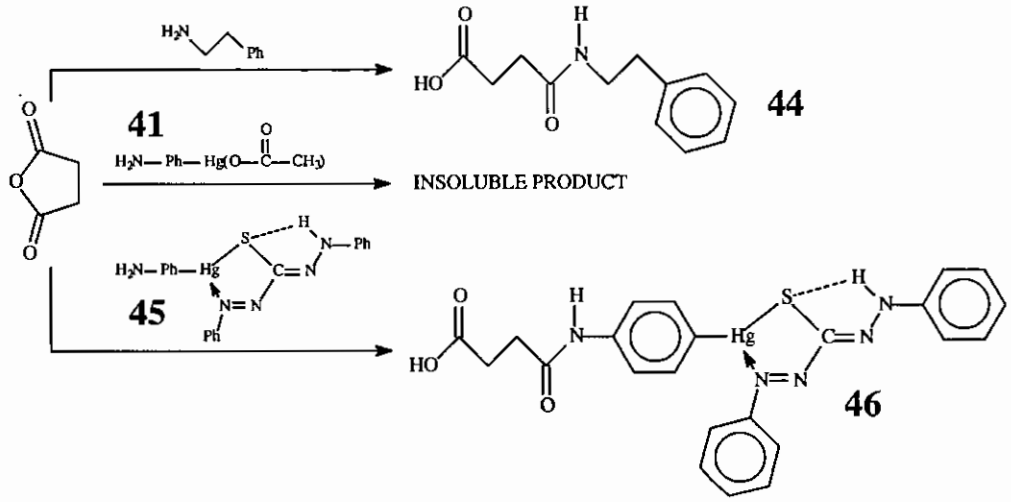


**Scheme 3.11** Preparation of a carboxylic acid functional group by using succinic anhydride. Synthesis of *p*-aminophenyldithizonatomercury(II), **45**, was done similarly to that of dithizonatophenylmercury(II), **20** (Scheme 3.4).

The next reaction with succinic anhydride was attempted with *p*-aminophenylmercury(II) acetate, **41**, but the product that formed was completely insoluble, and most probably a polymer of some kind. Repeating the same reaction with the corresponding dithizonate complex, **45**, gave the required product, *p*-anilino-4-oxobutanoic acid(dithizonato)mercury(II), **46**, in high yield (80 %). A dramatic increase in melting point of the product over the reagent was observed.

The reagent complex, **45**, melted at 130°C, while product **46** melted at 228°C. Both compounds are photochromic in dichloromethane. $\lambda_{max}$ for the orange isomer of **45** is 475.5 nm, and for the blue isomer 588 nm, while $\lambda_{max}$ for the orange isomer of **46** is 489 nm, and for the blue isomer 601 nm.

### 3.2.2.2. Poly-DL-succinimide, and the anchoring of *p*-anilino-4-oxo-butanoic acid(dithizonato)mercury(II)

In the high yield synthesis (Scheme 3.12) of poly-DL-succinimide, **48**, DL-aspartic acid, **47**, was heated to 190°C in the presence of concentrated *ortho*-phosphoric acid.[183] The reaction mixture was kept under vacuum for the purpose of removing water molecules that were liberated during polymerization. Precipitation of polysuccinimide was accomplished by very slowly pouring a dimethylformamide solution of the reaction mixture into rapidly stirring water. Polysuccinimide prepared in this way is reported to have a molar mass of 57 000 g/mol.[184, 185]

Polysuccinimide in itself is not water-soluble, but was converted into a hydrophilic polymer by anchoring 4-(3-aminopropyl)morpholine onto 75 % of the polymeric repeating units. An excess of ethylenediamine was then reacted for the purpose of functionalizing the 25 % remaining repeating units to give the amino-containing polymer **49**. The crude reaction mixture was dialyzed (12 000 molar mass cut-off membrane tubing) for two days, and freeze-dried to yield the light-yellow water-soluble polymer, **49**. NMR signals (see Paragraph 4.4.2.7, p.160) were in good agreement with structure **49**, as presented in the following scheme. Polymer **49** has the potential to bind the carboxylic acid mercury complex, **46**.

Finally, reaction of the polymer amine with the mercury dithizonate carboxylic acid required a coupling reagent, O-benzotriazolyl-N,N,N',N'-tetramethyluronium hexafluorophosphate. The dark brick-red polymer, **50**, was very soluble in water, giving an orange-red solution. Dithizonatophenylmercury(II) was therefore successfully coupled to the hydrophilic polymer, polysuccinimide.

Based on the $^1$H NMR integral values from the phenyl rings of the mercury complex, *ca* 70 % of available amines on polymer **49** reacted with compound **46** as the dithizone derivative. An integral value of only 9.93 (out of a potential of 14) for the 14 dithizone phenyl protons was observed (see Spectrum A19). An elemental analysis performed on polymer **50** showed a 13.3% mercury content. The calculated requirements for 70 % mercury dithizone content on polymer **50** shows the mercury content should be 10.56 %. A 100 % successful anchoring reaction of **46** onto **49** would in theory give **50** with a 13.3 % mercury content.

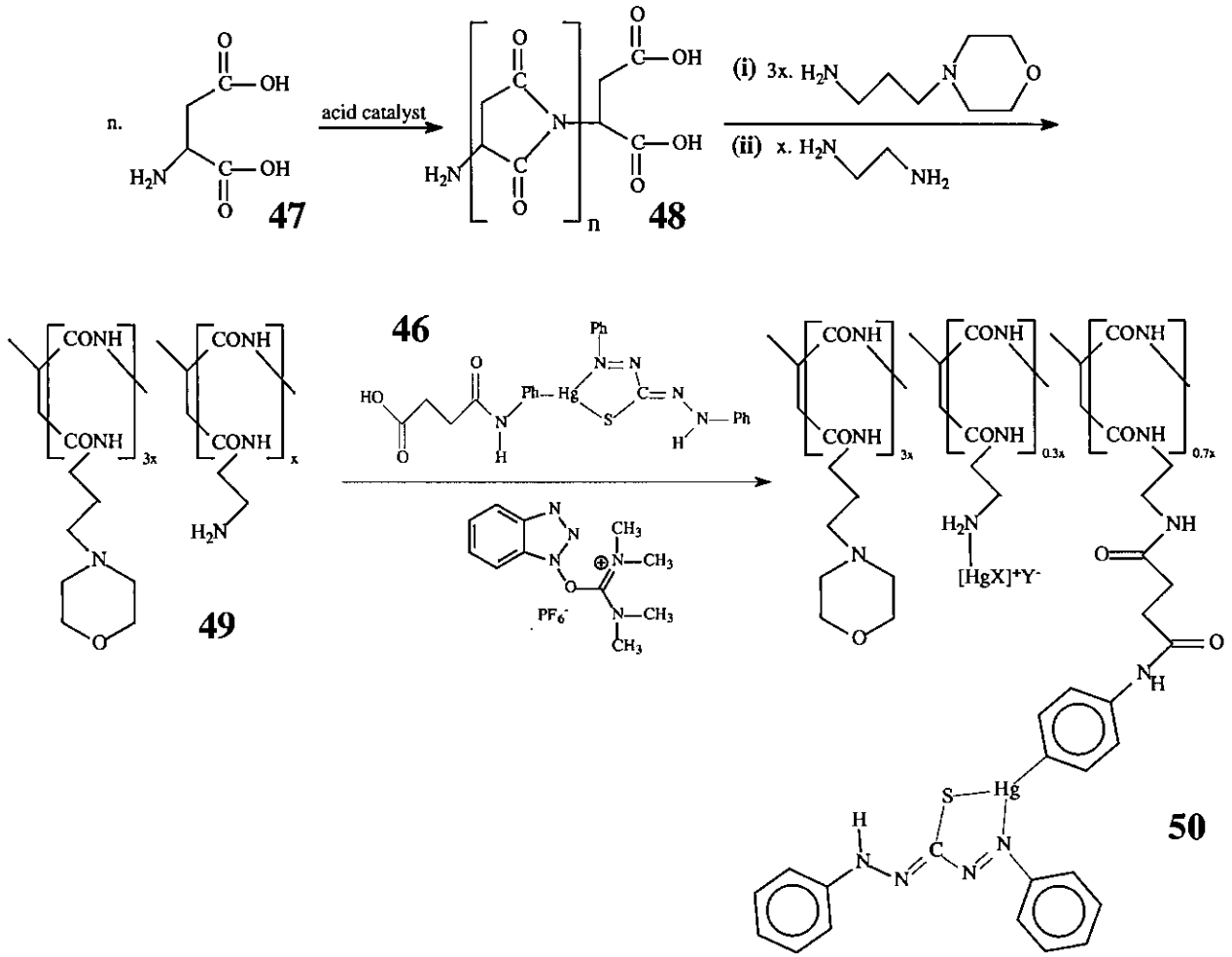


**Scheme 3.12** Polymerization of aspartic acid, **47**, to form polysuccinimide, **48**, is followed by the addition of 4-(3-aminopropyl)morpholine, which enhances water solubility, while the ethylenediamine reactant provides a side-chain functional group on polymer **49**. Anchoring of the photochromic moiety, **46**, on **49**, takes place with the aid of a coupling reagent, to form polymer, **50**. X and Y are unknown $Hg^{2+}$ ligands that are bound to Hg following partial decomposition of the Hg dithizonato fragment of polymer **50**.

From the values for the elemental analysis it can be seen that the mercury content in the polymer is a few percentage points higher than what would be expected from $^1$H NMR data. Simultaneously, the values for the remaining elements, C, N & H, are lower than the calculated requirement. This discrepancy may be explained in terms of the relative instability of the mercury dithizonate complex in polar solvents, keeping in mind that the coupling reaction had been done in DMF, and water dialysis lasted for a full day. Partial decomposition could therefore be expected, although the typical orange colour of the photochromic moiety nevertheless still indicated a large degree of stability while being coupled onto the polymer. Any mercury that might have liberated from decomposition of the dithizonatomercury(II) fragment of **50** might readily have coordinated with the remaining unreacted amine sites, as shown in Scheme 3.10, thereby explaining the higher mercury content in the polymer. At the same time would decomposition have led to the shedding of the organic parts of the mercury complex, with the consequent decrease in percentage of elements C, N & H. The limited understanding of what

exactly did happen during the partial decomposition process is yet to be investigated, but lies outside the scope of the present research project. No photochromism was observed for this product, neither in the solid state, nor in solution.

### 3.2.2.3. Polyepichlorohydrin, and the anchoring of *p*-aminophenyl-dithizonatomercury(II)

Polyepichlorohydrin, **52**, with target $M_r$ = 20 000 g/mol, was prepared by the polymerization of epichlorohydrin, **51**, via a cationic ring-opening mechanism in the presence of trifluoroboron etherate as initiator, and phenol as co-initiator.[89] Slow addition of epichlorohydrin to the reaction mixture was done over a period of 24 hours while tightly controlling the temperature to between 24 and 27°C. The product was obtained as a colourless and highly viscous liquid that is soluble in dichloromethane.

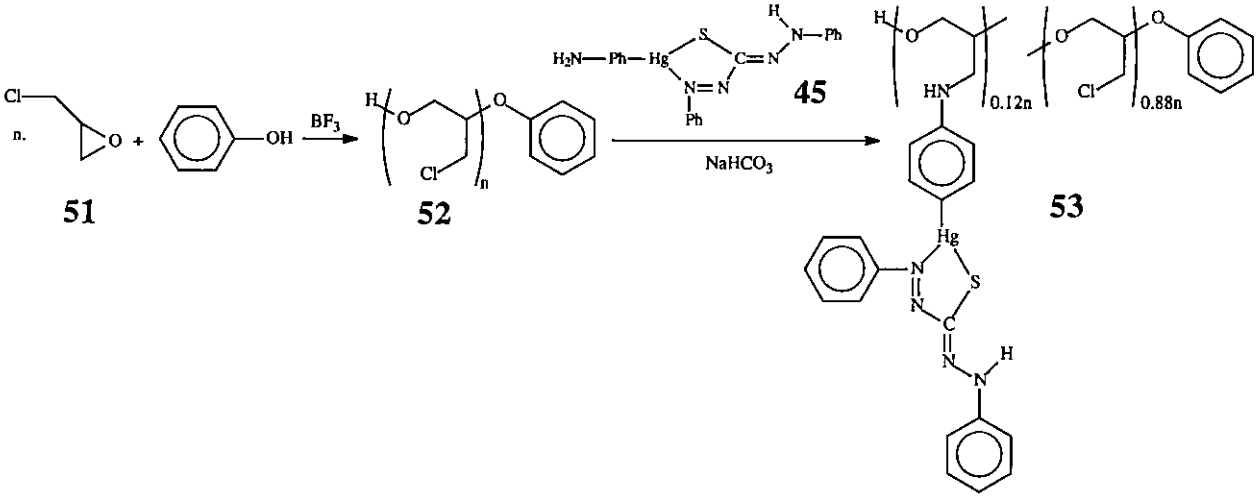


**Scheme 3.13** Polymerization of epichlorohydrin, **51**, to form polyepichlorohydrin, **52**, was followed by the anchoring of the photochromic moiety, **45**, in the presence of sodium bicarbonate, to yield the photochromic lypophilic polymer, **53**.

In the $^1$H NMR spectrum (Spectrum A20) the five protons of the epichlorohydrin repeating unit (see **52**) are represented by two signals lying very close together, in the region 3.5 – 4.05 ppm. Comparing integral values of the terminal phenyl ring to that of the former five protons, provide a means to calculate the molar mass of **52**. Setting the integral value of the phenyl protons to 5, to correspond to the 5 phenyl protons, resulted in the polymer repeating unit proton integral value changing to 1251. There is only one terminal phenyl on every polymeric unit, with the consequence that the number of repeating units in the polymer may be calculated, i.e. 1251 / 5 = 250 repeating units. The molar mass of the polymer is thus: (250 × 92.52 g/mol) + 94.11 g/mol = 23 224 g/mol. This value is slightly higher than the target molar mass of 20 000 g/mol, but sufficiently close for purposes of this research.

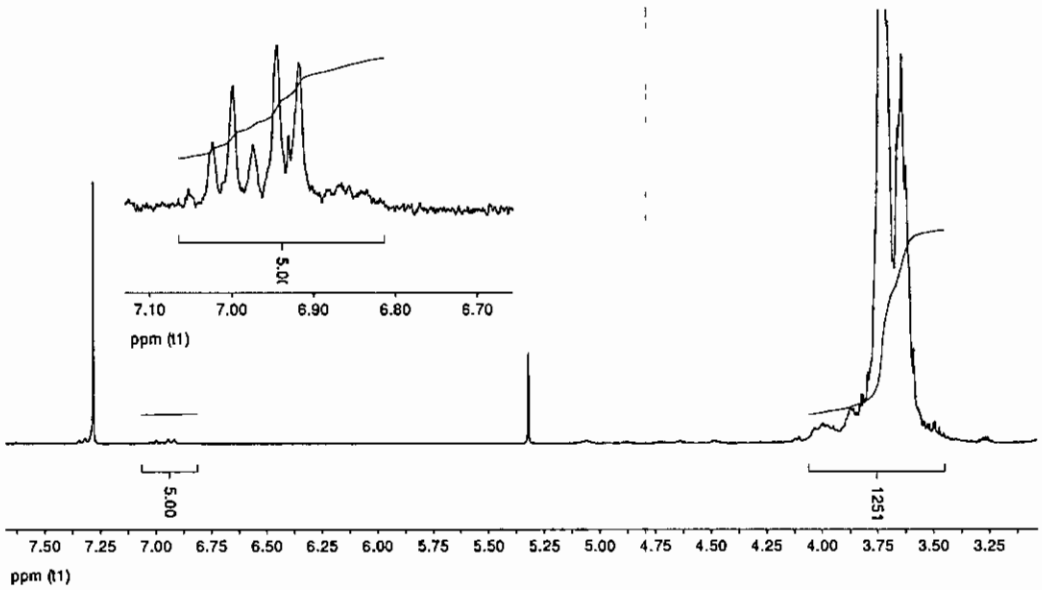


**Figure 3.8** NMR spectrum of polyepichlorohydrin, **52**, in $CDCl_3$. The insert is an expansion of the region where the phenyl group resonates.

In the final step, polyepichlorohydrin and the mercury dithizonate amine, **45**, was reacted in dimethylsulfoxide. Sodium bicarbonate was used to neutralise the HCl liberated as a consequence of the displacement of the polymer-Cl by the amine of the photochromic moiety. Precipitation of the final product was accomplished by pouring the solution into vigorously stirring lukewarm water, and the crude product was filtered off. Unreacted dithizonatophenyl-mercury(II) was extracted from the solid polymer by briefly boiling the suspended polymer in vigorously stirring hexane, and decanting the orange hexane solution containing the dithizonate. The extraction procedure was repeated three times, the third solution remaining clear.

The dichloromethane solution of the polymeric product, **53**, that remained after the hexane extraction, proved to be completely photochromic on exposure to sunlight. As opposed to the previous hydrophilic polymer, **50**, the lypophilic polymer, **53**, is also photochromic in the solid state, changing to grey-blue on exposure to direct sunlight. The back-reaction, i.e. back-isomerisation from blue to orange, was much slower in the solid polymer, as the colour returned to the original orange only over a period of about 24 hours.

Based on the $^1H$ NMR integral values from the phenyl rings of the mercury complex, *ca* 12 % of the polymeric repeating units effectively anchored compound **43**. An integral value of 1.7 (out of a potential of 14) for the 14 phenyl protons was observed (see Spectrum A21). Elemental analysis performed on a product sample gave: C, 40.34; H, 3.81; N, 7.95 & Hg, 15.8 %. The calculated requirements based on 12 % anchoring are: C, 41.1; H, 4.5; N, 5.5 & Hg, 15.6 % for $(C_{22}H_{21}N_5OSHg)_{0.12}(C_3H_5OCl)_{0.88}$. Apart from N, these sets of values are in good agreement. The nitrogen content was found to be much higher than the calculated value. In view of the fact that all the other elements are in good agreement with the expected percentages of analysis, and

that a solution of product **51** is completely photochromic, it may be concluded that the nitrogen analysis was wrong. The presence of possible sources of nitrogen, e.g. DMF or amines, would have prevented the photochromic reaction from taking place.

## 3.2.3. Porphyrin Derivatives and their Cobalt Complexes

### 3.2.3.1. Tetraphenylporphyrin and some anionic derivatives

Tetraphenylporphyrin (and its complexes) is probably the most well researched derivative in the porphyrinic group of compounds. For this reason, as well as for its relative ease of synthesis, tetraphenylporphyrin was selected as starting material in researching the interaction of dithizone and its derivatives with cobalt porphyrin complexes.

The synthetic procedure followed for tetraphenylporphyrin was in accordance with the method described by Adler *et al.*[105] Benzaldehyde and pyrrole in refluxing propionic acid reacted to form 5,10,15,20-tetraphenylporphyrin, together with a small amount of chlorin. The chlorin was removed on a silica column. Material from the main band was recrystallised from dichloromethane and ethanol, yielding the glistening purple crystalline product, **54**, having $\lambda_{max}$ (Soret band) at 417 nm in dichloromethane.

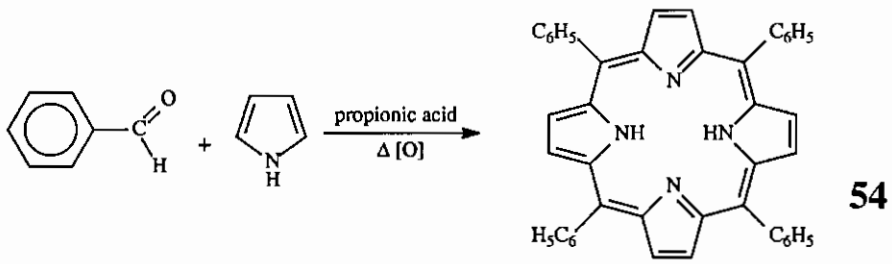


**54**

**Scheme 3.14** Synthesis of tetraphenylporphyrin, **54**.

The relative ease with which dithizone and its derivatives are oxidised, had to be inhibited, since oxidation will irreversibly destroy the photochromic moiety. Knowing that $Co^{III}$ porphyrins often act as oxidation catalysts,[161,163,186] ways had to be found by which its oxidation capability could be decreased. That may be done by placing more electron density on the metal centre, i.e. by substituting the heterocyclic ring with electron donating groups. Towards this goal the sodium salt of tetra(4-sulfophenyl)porphyrin, **57**, was synthesised. Here, four negative ions were placed at the *para* positions on the phenyl rings. These anionic groups were expected to change the electron density on the central cobalt(III) metal,[187] and thereby its oxidation strength.

Preparation of the anionic compound, **57**, was started by the direct sulfonation of tetraphenylporphyrin with concentrated sulfuric acid (Scheme 3.15).[112] The fine suspension that formed on addition to water could only be separated by means of centrifugion. Repeated addition to water and centrifugion rid the bright green compound (**55**) of remaining sulfuric acid.

After drying, the tetra-sulfonic acid, **55**, was neutralised by dissolution in methanolic ammonia, yielding the ammonium salt, **56**. Precipitation of the brown ammonium salt was achieved by addition of acetone. For the purpose of purification, six repeated precipitations from hot methanol were done.

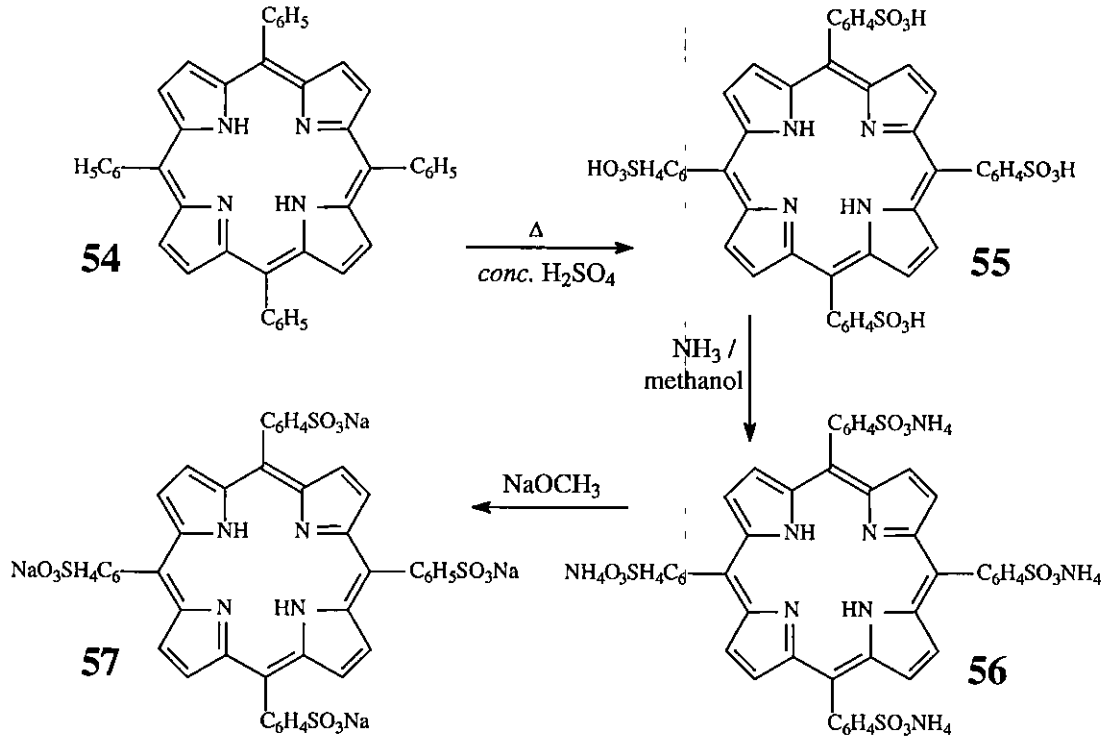


**Scheme 3.15** Synthesis of tetra(sodium 4-sulfophenyl)porphyrin, 2H($Na_4$TPPS) (**57**).

Eventually, the dried ammonium salt was added to a sodium methoxide solution, yielding an olive green precipitate of the tetra-sodium salt, **57**, which was filtered off and washed with ethanol. 2H($Na_4$TPPS).16$H_2O$ is very soluble in water. The Soret band was found to be at 414 nm in water.

Starting off with the synthetic procedure for **54**, tetra(sodium 4-carboxyphenyl)porphyrin was also prepared in good yield (Scheme 3.16). Contrary to the previous porphyrin, **57**, where substitution of the phenyls were done after having prepared tetraphenylporphyrin, a substituted benzaldehyde reagent was used here, namely *para*-carboxybenzaldehyde.

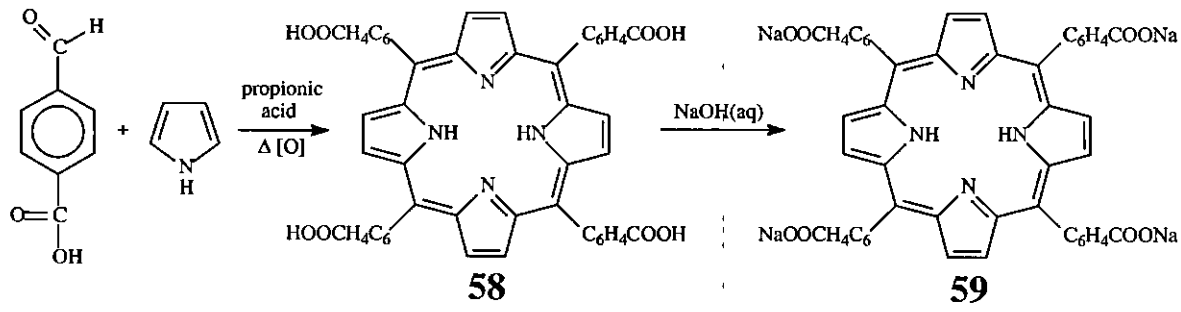


**Scheme 3.16** Synthesis of tetra(sodium 4-carboxyphenyl)porphyrin, 2H($Na_4$TCP) (**59**).

The tetra-carboxylic acid, **58**, was soluble in methanol, but completely insoluble in both water and chloroform. Treatment of the acid with a slight excess of sodium hydroxide resulted in the sodium salt, **59**, which is highly soluble in water, with $\lambda_{max}$ being at 415 nm. It would be interesting to note that while this salt is soluble in methanol, it is completely insoluble in even hot ethanol.

### 3.2.3.2. Porphyrins containing electron donating substituents

Ferrocene, containing Fe(II), is one of the most powerful electron donating moieties that may be attached to the heterocycle. The resulting product, tetraferrocenylporphyrin, **60,** is therefore expected to be more basic than any other synthetic porphyrin. For the synthesis, ferrocene aldehyde first had to be prepared. This was done by the reaction of N-methylformanilide and phoshorous oxychloride with ferrocene.[188] The crude product was purified by passing through a silica column, yielding formylferrocene in good yield (69 %). Condensation of the ferrocene aldehyde with pyrrole was done as with tetraphenylporphyrin, **54**.[189] Purification was performed by passing a chloroform solution of the crude product through a silica column. The third band (black) contained tetraferrocenylporphyrin, **60**. The porphyrin adsorbed strongly onto the silica, and had to be removed by elution with dimethylsulfoxide.

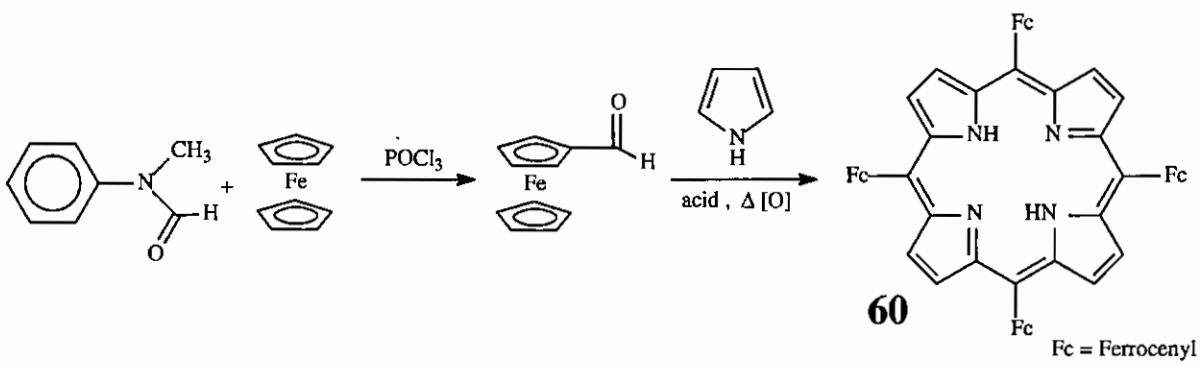


**Scheme 3.17** Synthesis of tetraferrocenylporphyrin (**60**).

Elemental analysis bears evidence of a product containing one molecule of dimethylsulfoxide. The Soret band of **60** underwent a significant blue-shift to 328 nm, compared to the 417 nm found for tetraphenylporphyrin. The Soret band peak of **60** is, however, much wider than what is normally found for porphyrins (Figure 3.9). Unfortunately the product was rather insoluble and dissolution appeared to promote aggregation, a problem typically encountered with many porphyrins. The result was that recovery from solution yielded a solid mass that was insoluble in all the standard laboratory solvents, which also rendered it useless as far as the consequent metal insertion reaction was concerned.

The last porphyrin to be synthesised for purposes of this dissertation was octaethylporphryin, **66**. The octaethyl free-base porphyrin, 2HOEP ($pK_a$ = 12.17), is almost a 100 times more basic than the tetraphenyl free-base porphyrin, 2HTPP ($pK_a$ = 10.23).[190] Due to its consequent stronger ligand-to-metal electron donating ability, octaethylporphyrin was selected as the next porphyrin in the present series of study.

The approach followed here was according to the tested method by Sessler *et al*,[191] which mainly deals with an efficient way to synthesise the substituted pyrrole, **66** (Scheme 3.20). To synthesise 3,4-diethylpyrrole, 3-nitro-4-hexanol, **61**, was firstly prepared from propionaldehyde and 1-nitropropane in the presence of potassium fluoride as catalyst. The recovered oily product was distilled at 88 - 90°C (2 mm), yielding **61**, which was used directly in the next step. Sulfuric acid and acetic anhydride was added to **61**. After the reaction was complete, the lower boiling point components were driven off on a rotary evaporator. Reasonably pure 3-acetoxy-4-nitrohexane, **59**, was obtained from the fraction boiling at 98 – 100°C (1 mm), in almost quantitative yield. Attempts to purify it further by column chromatography and redistillation failed.

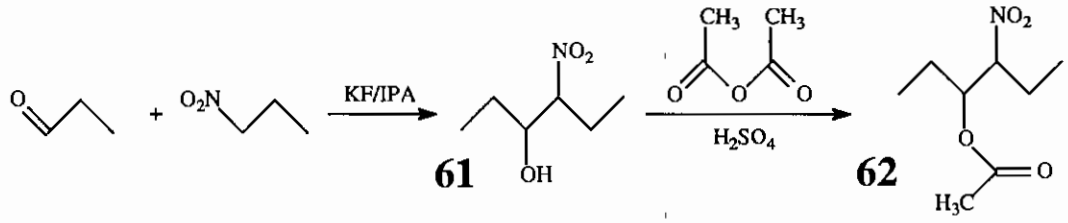


**Scheme 3.18** Synthesis of 3-nitro-4-hexanol (**61**) and 3-acetoxy-4-nitrohexane (**62**).

In the subsequent step, ethyl isocyanoacetate was required as reagent. For the preparation of ethyl isocyanoacetate, **64**, glycine ethyl ester hydrochloride was reacted with methyl formate in the presence of triethylamine. To the distillation product, N-formylglycine ethyl ester, **63**, was once more added triethylamine, followed by phosporous oxychloride and anhydrous sodium carbonate. The organic layer was washed with water and a sodium chloride solution, after which the remaining brown oil was distilled, yielding pure ethyl isocyanoacetate in good yield (69 %).

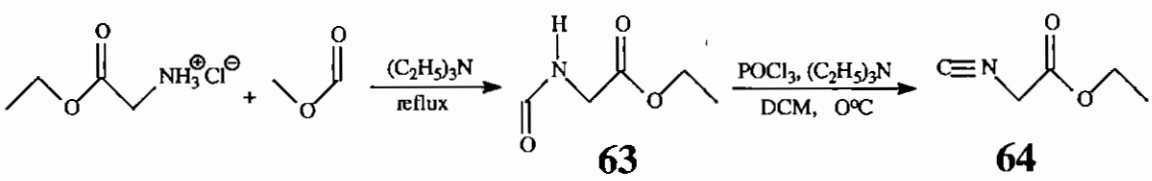


**Scheme 3.19** Synthesis of ethyl isocyanoacetate (**64**).

While ensuring dry reaction conditions, ethyl isocyanoacetate, 3-acetoxy-4-nitrohexane, isopropyl alcohol and the base, 1,8-diazabicyclo[5.4.0] undec-7-ene (DBU) were added together

in tetrahydrofuran. The resulting crude product, ethyl 3,4-diethylpyrrole-2-carboxylate, **65**, was used directly in the next step. Refluxing a mixture of **65** and sodium hydroxide in ethylene glycol at 190°C yielded the reagent needed for the synthesis of octaethylporphyrin, namely 3,4-diethylpyrrole, **65**. The pure product was obtained by distillation (71°C, 2 mm), and purity was confirmed by $H^1$ NMR. The pyrrole, **66**, was stored in a deep-freeze, but turned brown after a few weeks. It therefore had to be distilled afresh before further use.

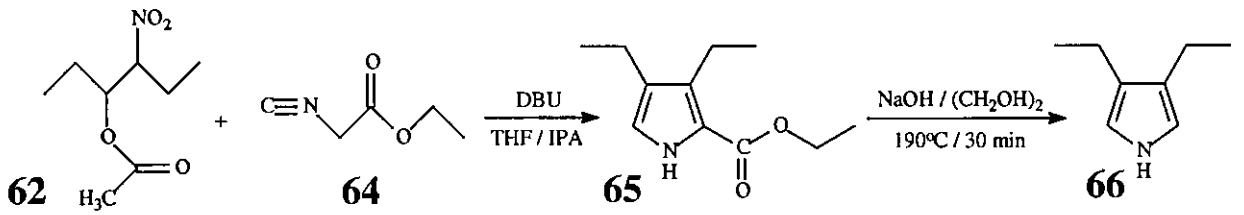


**Scheme 3.20** Synthesis of 3,4-diethylpyrrole (**66**).

In the last step of this reaction sequence, namely the condensation of 3,4-diethylpyrrole and formaldehyde in the presence of *p*-toluenesulfonic acid, water had to be removed constantly by means of a Dean-Stark trap while refluxing in benzene. Optimum product yield required low reagent concentrations (*ca* 0.025 mol.dm$^{-3}$). After having bubbled oxygen through the solution for a period of 24 hours, and work-up of the product, analytically pure 2,3,7,8,12,13,17,18-octaethylporphyrin, **67**, was obtained by recrystallization from chloroform-hexanes (66 %).

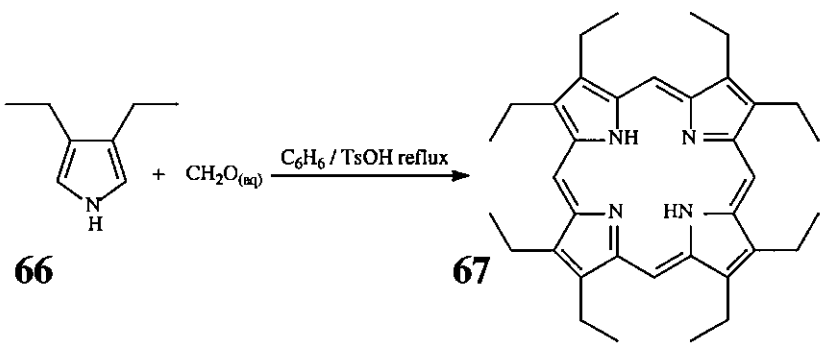


**Scheme 3.21** Synthesis of octaethylporphyrin (**67**).

In agreement with all the porphyrins synthesised in this investigation, no melting was observed below the melting point apparatus temperature maximum of 230°C. The NMR signal of the ethyl protons (-C<u>H</u>$_2$CH$_3$) bordering the heterocyclic ring underwent a large shift from 2.47 ppm for the pyrrole reagent to 4.14 ppm for the porphyrin product in deuterated chloroform. The $CH_3$ signal displayed only a small shift to 1.95 ppm compared to the pyrrole value of 1.24 ppm. The former large shift towards higher frequency is the result of deshielding by the electron-delocalised heterocyclic ring.

As for the UV/visible spectrum, the Soret band was found to be at 397 nm in dichloromethane, which is 17 nm lower than that of tetraphenylporphyrin. The observed blue-shift occurs due to

increased charge donation from the eight ethyl groups to the heterocycle. Red-shifts, on the other hand, occur when porphyrins are substituted with electron-withdrawing groups like halogens or cyano groups. Figure 3.9 illustrates the shifts in the Soret band maxima of the porphyrins synthesised in this investigation.

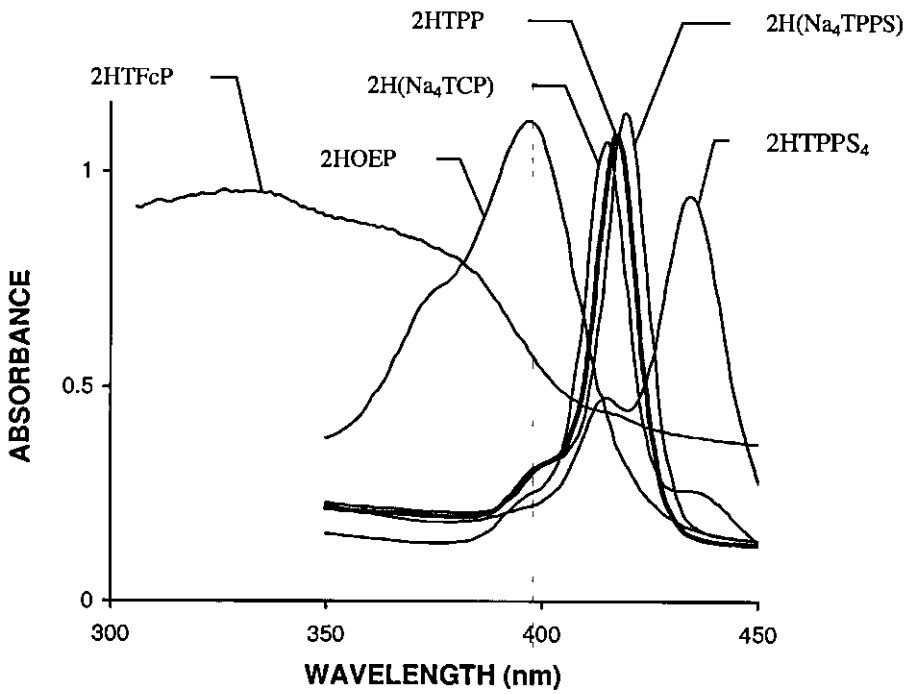


**Figure 3.9.** UV/visible Soret band spectra in dimethylformamide (except otherwise specified), of 2HTFcP (**60**) in dichloromethane, 2HOEP (**67**), 2H($Na_4$TCP) (**59**) in water, 2HTPP (**54**), 2H($Na_4$TPPS) (**57**) & 2HTPPS (**55**). (Concentrations are not the same.)

Soret band peak positions are in the order: (shortest wavelength) 2HTFcP (328 nm) < 2HOEP (397 nm) < 2H($Na_4$TCP) (415 nm) < 2HTTP (417 nm) < 2H($Na_4$TPPS) (419 nm) < 2HTPPS (448 nm) (longest wavelength). The anionic substituents, $-SO_3^-$ and $-COO^-$, on the porphyrin phenyls are seen to have only a very minor influence on the electron density of the heterocylic ring. Although much stronger an electron donor than the free sulfonic acid derivative, 2HTPPS, the corresponding sodium salt, 2H($Na_4$TPPS), is still less basic than 2HTPP. At first glance the sodium salt of the carboxyphenylporphyrin seems to be more basic than 2HTPP, but that may not be said conclusively, since the 2H($Na_4$TCP) spectrum was drawn from an aqueous solution. 2H($Na_4$TCP) is not soluble in dimethylformamide, in which 2HTPP was dissolved.

The conclusion, namely to correlate $\lambda_{max}$ with how electron rich the heterocyclic ring (origin of Soret band electronic spectrum) is, was investigated by means of cyclic voltammetry in this study (see Paragraph 3.5). An increase in electron density on the ring is expected to have Soret band blue-shifts to go hand in hand with a less positive redox potential, i.e. an increase in the ease of oxidation. In contrast to 2H($Na_4$TPPS), the significant red-shift of the tetra-sulfonic acid, 2HTPPS, was in agreement with expectation. The sulfonic acid group, $-SO_3H$, exerts a strong

electron withdrawing effect on the heterocyclic ring electron density, even via the phenyl ring to which it is attached. This species, however, was a reaction intermediate (see Scheme 3.15), and was merely included here for comparison purposes.

Comparisons between these relative commonly used porphyrins are not to be found in the literature, most probably due to incompatible solubilities. In this investigation dimethylformamide was found to be the only solvent in which most of the above free-base porphyrins were soluble to at least a certain extent.

### 3.2.3.3. Cobalt Porphyrin Complexes

Three different approaches were followed for metal insertion into the above metal free porphyrins.

Tetraphenylporphyrin in methanol was refluxed together with an equimolar amount of the metal acetate for 30 minutes.[192] After dilution with methanol, the product was filtered off in quantitative yield.

$$2HTPP + M(OAc)_2 \xrightarrow[\Delta]{MeOH} M^{II}TPP, \qquad M = Co\ (\mathbf{68}),\ Cu\ (\mathbf{69})$$

The heterogeneous reaction method was followed for cobalt insertion into the anionic porphyrins.[193] The porphyrin was refluxed for 2 hours in water containing the insoluble cobalt(II) carbonate salt. After filtering off the excess cobalt salt, the cobalt porphyrin complex was obtained in quantitative yield on removal of the solvent.

$$2H(Por) + Co(CO_3)_2 \xrightarrow[\Delta]{H_2O} Co^{II}(Por), \qquad Por = Na_4TPPS\ (\mathbf{70}),\ Na_4TCP\ (\mathbf{71})$$

Lastly, metal insertion into octaethylporhyrin was accomplished by actively refluxing a dimethylformamide solution of the porphyrin together with the metal chloride for 30 minutes.[107] Addition of water resulted in the product precipitating out. Good yields of more than 90 % were obtained.

$$2HOEP + MCl_2 \xrightarrow[\Delta]{DMF} M^{II}OEP, \qquad M = Co\ (\mathbf{72}),\ Cu\ (\mathbf{73})$$

The cobalt complexes described here were targeted due to the axial binding capabilities of the Co(II) and Co(III) complexes. From a scientific point of view it was also considered relevant to compare the electrochemical behaviour of the present series of porphyrins when a redox silent, non-axial binding metal is inserted in the porphyrin cavity. For this purpose, the Cu complexes, CuTPP, **69**, and CuOEP, **73**, were synthesised. The synthetic routes for the Cu complexes did not require any different techniques from the Co complexes, but they were easier to purify.

Obtaining $H^1$ NMR spectra of compounds **68**, **69**, **72** and **73** (Spectra A30 – 32) were subject to the paramagnetic influences of Co(II) and Cu(II). The presence of paramagnetic metals in metallo-organic compounds may cause proton chemical shifts of more than 200 ppm.[194] Such chemical shifts may be positive or negative, depending on the electron distribution. The following table illustrates the extent to which an unpaired electron on the respective metal centers caused aromatic and aliphatic protons to resonate at energies significantly different to what is typical for each type.

In both the octaethyl- and tetraphenylporphyrin complexes the individual chemical shifts of the free-base porphyrins correspond closely to related values of their Co(III) complexes. Co(III) is diamagnetic, with electron configuration, $[Ar]3d^6$. Although diamagnetic metals do influence its organic surroundings, the influence is very small. Significant shifts, however, were observed in cases where the divalent, paramagnetic metals, Cu(II) ( $[Ar]3d^9$ ) and Co(II) ( $[Ar]3d^7$ ) occupied the porphyrin cavities. (Paramagnetic metals are known for causing large $H^1$ NMR shifts of even up to 150 ppm.) The most pronounced chemical shift recorded in the above table is for the aliphatic protons of $Co^{II}OEP$, $-C\underline{H}_2CH_3$, with an up-field shift of 4.66 ppm as compared to its corresponding free-base, 2HOEP. It is lastly noteworthy to point out that the aromatic phenyls in tetraphenylporphyrin seems to be lessoning the paramagnetic effect, which, in the case of the aliphatic protons in octaethylporphyrin, is rather large.

**Table 3.1** A comparison of the $H^1$ NMR chemical shifts (ppm) observed for selected free-base porphyrins and their corresponding copper and cobalt complexes.

| | *o*-$C_6H_5$ | *m,p*-$C_6H_5$ | | -$C\underline{H}_2CH_3$ | $CH_2C\underline{H}_3$ |
|---|---|---|---|---|---|
| **2HTPP** | 8.24 | 7.79 | **2HOEP** | 4.14 | 1.95 |
| **$Cu^{II}$TPP** | 7.66 | 7.51 | ***$Cu^{II}$OEP** | - | - |
| **$Co^{II}$TPP** | 9.78 | 9.97 | ***$Co^{II}$OEP** | 8.80 | 6.14 |
| **$Co^{III}$TPP** | 8.22 | 7.88 | **$Co^{III}$OEP** | 4.27 | 1.90 |

* Apart from solvent peaks, no recognizable resonances were observed for $Cu^{II}OEP$. Peak positions are unusual because $Cu^{II}$ and $Co^{II}$ are paramagnetic.

β-pyrrole resonant frequencies were omitted since these values often lie outside the 0 – 10 ppm range that was investigated.

Oxidation of $Co^{II}$ to $Co^{III}$ was done in the same way for all the cobalt porphyrins. To every 100 mg of cobalt(II) porphyrin 100 ml of methanol containing 1 ml concentrated perchloric acid was added.[127,128] Exposed to atmospheric oxygen, the solutions were stirred for 3 hours at room temperature.

$$Co^{II}Por \xrightarrow[O_2]{HClO_4} [Co^{III}Por(MeOH)_2]ClO_4\ ,\quad Por = TPP(\mathbf{74}),\ Na_4TPPS(\mathbf{75}),\ Na_4TCP(\mathbf{76}),\ OEP(\mathbf{77})$$

Addition of water resulted in the precipitation of the $Co^{III}$ complex. Acetone, instead of water, was used in the case of the water-soluble porphyrins, $[Co^{III}(Na_4TPPS)(MeOH)_2]ClO_4$ and $[Co^{III}(Na_4TCP)(MeOH)_2]ClO_4$. Yields were in excess of 80 %. The large degree of sensitivity of the typical sharp Soret band peak to minute electronic alterations in the molecule makes it possible for reaction progress to be followed conveniently by means of UV/visible spectroscopy.

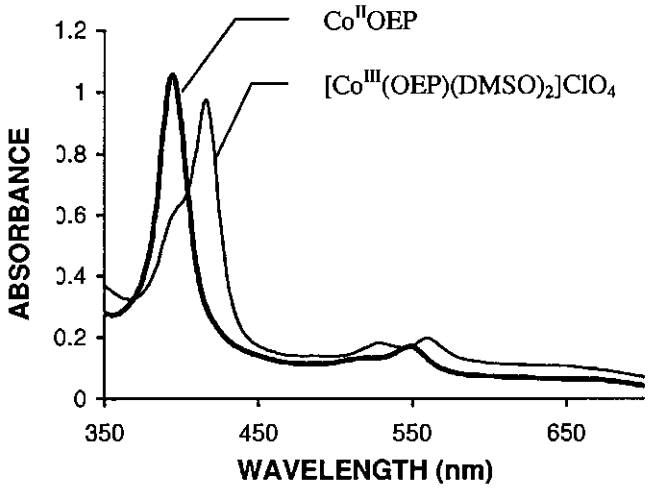


**Figure 3.10** UV/ visible spectra of $Co^{II}OEP$ and $[Co^{III}(OEP)(DMSO)_2]ClO_4$ in dimethylsulfoxide. (Concentrations were not the same.)

The Soret band red-shift observed during oxidation of the metal centre is in line with red-shifts that occur on substitution of the macrocycle with halogens. In both cases electron density is withdrawn from the electron delocalised ring structure. The following table gives corresponding Soret band peak maxima of the above porphyrins and their metal complexes.

**Table 3.2** Wavelengths (nm) at the absorbance maxima of the free-base porphyrins and their corresponding metal complexes. Solvents are given in parentheses.

| | **M-OEP** | **M- $Na_4TCP$** | **M-TPP** | **M- $Na_4TPPS$** |
|---|---|---|---|---|
| **M = $2H^+$** | 397 *(dmf)* | 415 *(aq)* | 417 *(dmf)* | 419 *(dmf)* |
| **M = $Co^{II}$** | 394 *(dmso)* | 415 *(aq)* | 415 *(dmso)* | 421 *(dmso)* |
| **M = $Co^{III}$** | 416 *(dmso)* | 426 *(aq)* | 434 *(dmso)* | 435 *(dmso)* |
| **M = $Cu^{II}$** | 398 *(dcm)* | | 415 *(dcm)* | |

The above data illustrates that $\lambda_{(M\text{-}OEP)} < \lambda_{(M\text{-}Na_4TCP)} \leq \lambda_{(M\text{-}TPP)} < \lambda_{(M\text{-}Na_4TPPS)}$ for all four cases, i.e. M = $2H^+$, $Co^{II}$, $Co^{III}$ and $Cu^{II}$. It must therefore be concluded that the decrease in electron density on the different porphyrin ligands also lie in the same order, i.e. tetra(sodium 4-sulfophenyl)porphyrin actually being the least electron rich of the four complexes. If the differences in $\lambda_{max}$ values are indeed an indication of the relative electron densities of the ligands, i.e. their ease to undergo oxidation, then tetra(sodium 4-sulfophenyl)porphyrin is only

slightly less electron rich than tetraphenylporphyrin, which in turn is much more electron poor than octaethylporphyrin. Similarly, the octaethylporphyrin system is much more electron rich than the $Na_4TPPS$ series of compounds. It follows that cobalt(III) would be much more resistant to spontaneous reduction in OEP complexes than in $Na_4TPPS$, TPP and $Na_4TCP$ complexes. This striking result is further elucidated in the electrochemical study reported in Paragraph 3.5.

## 3.2.4. Axial Coordination Reactions

Reactions of metal porphyrins with dithizone and its derivatives are for the first time reported in this study.

Based on the known reversible reactions of cobalt(II) porphyrins with oxygen,[195] as well as the relative ease with which many amines coordinate axially to cobalt(II) tetraphenylporphyrins,[125] tetraphenylporphyrinatocobalt(II), **68**, was selected as starting reagent in this investigation. Interactions of **68** with dithizone, the dithizonate anion, dehydrodithizone and dithizonatophenylmercury(II) were investigated. Before doing so, known reactions were first tested in order to establish the effect of axial coordination on the porphyrin complex Soret band. Shifts in the position of the Soret band, as mentioned earlier, often conveniently serve as sufficient measure for the progress of a reaction.

Axial ligation of $Co^{II}TPP$ with the amine, pyridine, was the first reaction that was tested. A 100-fold excess of pyridine was added to a dichloromethane solution of **68** at room temperature. A red-shift was observed during which the Soret band moved from 410 nm to 434 nm (Figure 3.11a). As in the case of the pyridine nitrogen, the nitrogens in the dithizone ligand are, apart from sulfur, also potential coordination sites, but are sterically considerably more obstructed with regard to coordination to large planar complexes like metal porphyrins.

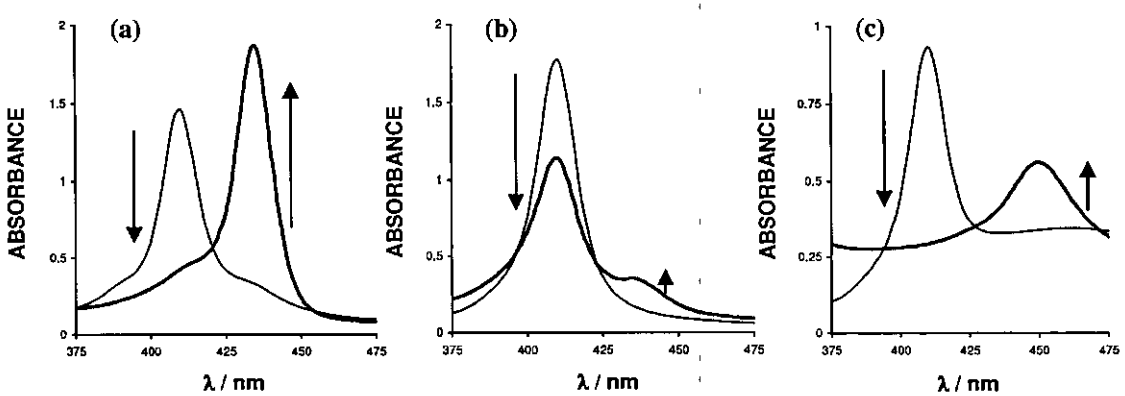


**Figure 3.11** UV / visible spectra of $Co^{II}TPP$ + R at t = 0 s, and t = 100 hrs., where (a) R = pyridine, (b) R = thiophene (reaction incomplete), and (c) R = dehydrodithizone, in dichloromethane.

For the reason of investigating the effect of a ligand that might also coordinate through sulfur, thiophene was secondly employed. Although thiophene was used in 100-fold excess, and the

reaction mixture left for 100 hours, only a small percentage axial coordination took place, as may be seen from the partial decrease of the 410 nm peak in Figure 3.11b. The coordination product peak started forming at *ca* 435 nm. As for dithizone, **16**, the dithizonate anion, **19**, or dithizonatophenylmercury(II), **20**, not even a slight reaction was observed with tetraphenylporphyrinatocobalt(II). The only exception here was the sterically favourable dehydrodithizone, **21**. Using similar reaction conditions as before, the reaction was complete within 75 hours (Figure 3.11c). Instead of the original narrow peak at 410 nm, a new broad peak appeared at 450 nm. As compared to dithizone, dehydrodithizone did therefore indeed react better with regard to coordination, as was espected.

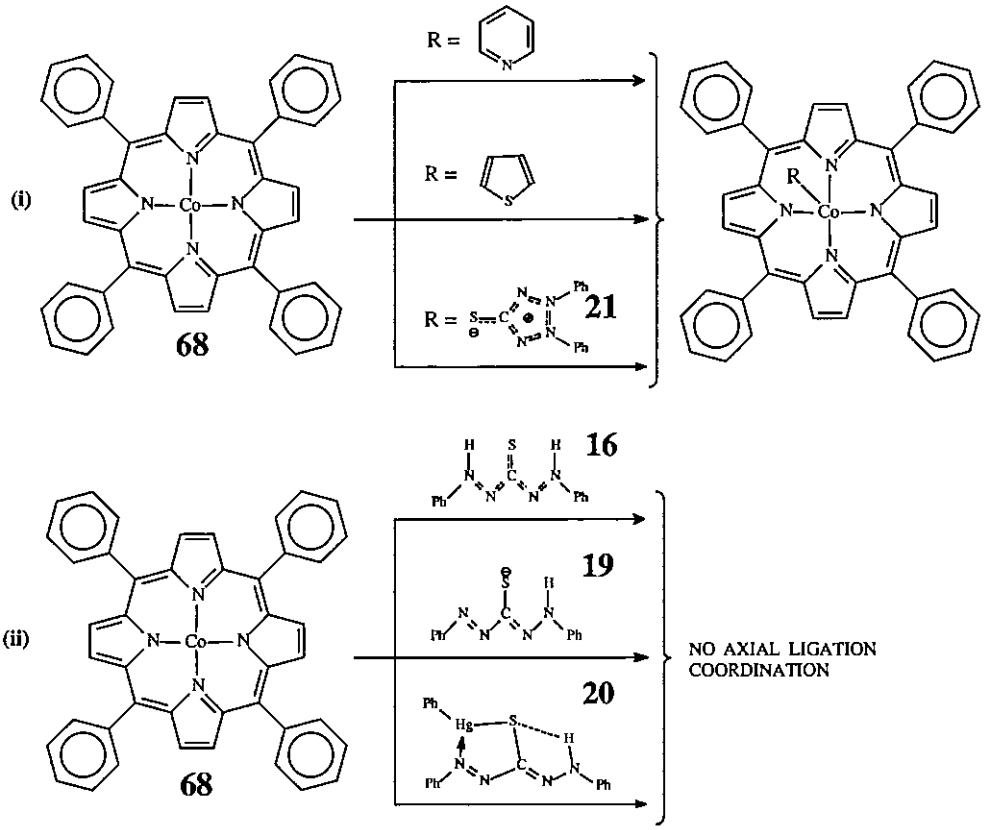


**Scheme 3.22** Tetraphenylporphyrinatocobalt(II) (**68**) dissolved in dichloromethane, axially coordinate (i) pyridine, thiophene (weakly) and dehydrodithizone, but not, (ii) the sterically hindered compounds, $H_2Dz$ (**16**), $HDz^-$ (**19**) and PhHgHDz (**20**).

Based on the above observations it was concluded that the electrophilic character of the Co(II) oxidation state was not sufficient for axial coordination of dithizone and its derivatives to readily take place. Although dehydrodithizone did indeed coordinate to the metal centre, the reaction required a large excess of ligand and a very long reaction time. A 10-fold ligand excess was found to be too little for the reaction to proceed meaningfully at all.

It was therefore decided to increase the electrophilicity of the metal centre by oxidizing Co(II) to Co(III). Oxidation of cobalt porphyrins may be done by a number of inorganic acids in the presence of atmospheric oxygen. For purposes of this study perchloric acid was chosen, thereby

largely excluding interference from a reactive anion. The perchlorate anion, $ClO_4^-$, has the advantage of being very poorly coordinative, and would therefore also not block the axial positions on the cobalt porphyrin complex, $[Co^{III}TPP(MeOH)_2]ClO_4$, **74**, via a coordinate bond. The axial ligands are usually weakly coordinating solvent molecules originating from the solvent from which the complex was recovered after oxidation or recrystallization, here methanol.

Coordination of dehydrodithizone to the Co(III) complex, **74**, was as expected, much faster as compared to coordination with the Co(II) complex.

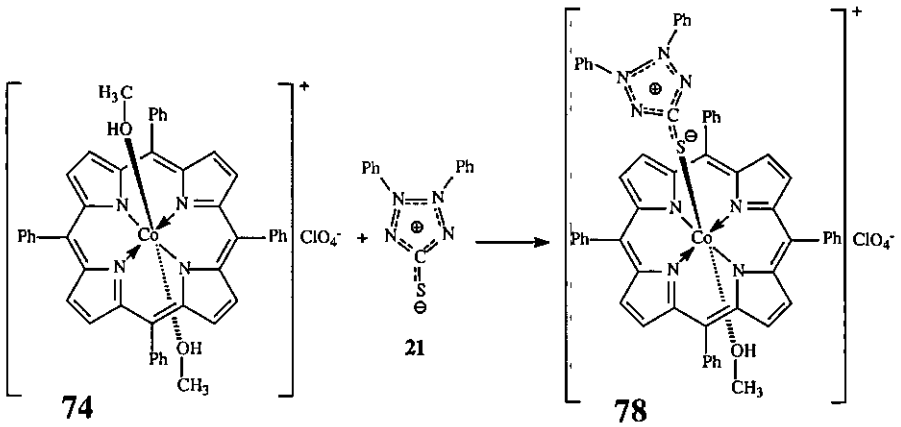


**Scheme 3.23** Tetraphenylporphyrinatocobalt(III) perchlorate (**74**) axially coordinates dehydrodithizone to form product **78**.

As opposed to the Co(II) complex, where a large excess and a long reaction time was required, addition of an *equimolar* amount of the ligand to **74** ($\lambda_{max}$ = 428 nm, in acetone) resulted in an immediate spectral change as depicted in Figure 3.12 (**78**: $\lambda_{max}$ = 437 nm). Adding the ligand in 10-fold excess had only an insignificant influence on the spectrum of the product, $[Co^{III}TPP(DDz)(MeOH)]ClO_4$, **78**. It is therefore concluded that the product curve, as seen in Figure 3.12, is indeed representative of the final complex, **78**, and that the reaction was probably complete.

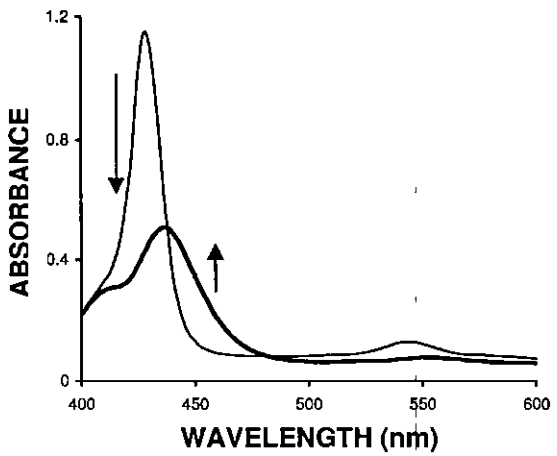


**Figure 3.12** Axial ligation of dehydrodithizone (**21**) with $[Co^{III}TPP(MeOH)_2]ClO_4$ (**74**) in acetone results in a shift of the Soret band from 428 nm to 437 nm. Absorbance contribution of the equimolar amount of **21** ($\lambda_{max}$= 456 nm) to the product peak is negligible.

The decrease in peak maximum (smaller molar absorption coefficient) due to coordination via the sulfur of the dithizone derivative, is noted to be a further characteristic of the new complex. The same was observed for the related Co(II) complex (Figure 3.11c). The opposite is true for coordination through an amine nitrogen (Figure 3.11a), i.e. the peak maximum increased. This observation may therefore serve as a possible crude diagnostic test to distinguish between sulfur and nitrogen coordination, which indeed is relevant in the case of dithizone with its dual coordination sites. To confirm that this diagnostic test is valid, it should be noted that the author observed similar trends for the N-coordinating ligands, piperidine and *n*-butylamine (increase in molar absorption coefficient), and the S-coordinating ligands, sodium diethyl dithiocarbamate and thiourea (decrease in molar absorption coefficient). Scheme 3.24 and Figure 3.13 illustrate behaviour of the S-bonding of ligands to cobalt(III) porphyrin complexes.

A $H^1$ NMR spectrum of crystals grown from compound **78** confirmed its composition (Spectrum A35), but also revealed that coordination was only *ca* 75 % successful, information which could not be deduced from the UV / visible spectrum alone (Figure 3.12). The unsubstituted porphyrinic reagent, **74**, has β-pyrrole protons resonating at 9.18 ppm (Spectrum A33). The substituted product, **78**, with expected increase in shielding of the β-pyrrole protons, has the new resonant frequency at 8.94 ppm. This peak integrated for only 75 %, while the peak remaining at 9.18 ppm integrates for 25 % of the β-pyrrole protons.

Contrary to dehydrodithizone, dithizone itself reduced Co(III) to Co(II) in tetraphenylporphyrin. The same was true for the derivatives; S-methyldithizone, the dithizonate anion, dithizonatophenylmercury(II) and dithizonatotrimethyltin(IV).

$$\underset{\mathbf{74}}{[Co^{III}TPP(MeOH)_2]ClO_4} + R \longrightarrow \underset{\mathbf{68}}{Co^{II}TPP}, \quad R = H_2Dz, \text{ S-MeHDz}, HDz^-, \text{ PhHgHDz}, Me_3SnHDz$$

On addition of these compounds to **74** in dichloromethane, the characteristic Soret band peak at 427 nm, related to Co(III), disappeared immediately while the Co(II) peak at 412 nm appeared. Whereas the electron affinity of the cobalt(II) metal centre was too weak for "pulling in" the dithizone ligand, the electron affinity of the cobalt(III) metal centre proved to be much too strong, as a matter of fact, so strong that it rid dithizone of some of its electrons. The consequence was that the designated photochromic moiety was rendered useless through oxidation, while the metal centre lost its ability with regard to dithizonate coordination. It is therefore also evident why pursuing the dehydrodithizone route, with compound **78** as intermediate towards axially bonding dithizone onto the porphyrin metal center, was henceforth also eliminated as a workable option towards a photochromic switch. Although it is possible to reduce dehydrodithizone back to its parent compound, **16**, the reduction process would be

indiscriminate, with the consequence that Co(III) will be reduced as well. Additionally, the reduced dithizone product itself is also to emerge as reductant.

The tetraphenylporphyrin complex of cobalt served as a springboard in this investigation, having given valuable information with regard to the direction further molecular engineering was to take. From the previous paragraph it can be seen that the desired electron affinity of cobalt, i.e. its ability to bind dithizone without oxidizing it, is to lie somewhere between that of Co(II) and Co(III) when inserted in tetraphenylporphyrin. Fortunately porphyrins are highly versatile with regard to peripheral substitution, thereby being readily tunable with respect to charge donation towards its inserted metals. Substitution of electron donating groups on the heterocyclic ring will have the effect of more electron density being donated to the metal centre. In the case of cobalt(III) the electrophilic character of the metal will therefore decrease towards that of cobalt(II), and thereby also decrease its potential for redox reactions to take place, i.e. dithizone being oxidised and Co(III) being reduced.

As a consequence the sodium salt of tetra(4-sulfophenyl)porphyrin seemed to be the next practical choice, since it could readily be synthesised from available stock of tetraphenylporphyrin. Furthermore, the anionic $-SO_3^-$ groups which are *para*-substituted on the four phenyl rings were expected to alter the inductive effect of the porphyrin on cobalt(III). Experimentation, however, revealed no significant change over that of the parent compound, tetraphenylporphyrinatocobalt(III). In the reaction of potassium dithizonate with $Co^{III}(Na_4TPPS)$, **75**, reduction of Co(III) was again observed. The Soret peak shifted from 426 nm to 414 nm (Fig.3.13a), the latter being characteristic of the Co(II) compound in water. This result proves quite conclusively that the electron density on a porphyrin can be judged from the position of its Soret band as shown in Table 3.2. From Table 3.2. it can therefore be predicted that $Co^{III}(Na_4TCP)$, $Co^{III}TPP$ and $Co^{III}(Na_4TPPS)$ would all undergo reduction upon dithizone addition because the free base Soret band maxima are all clustered close together (415 – 419 nm).

To confirm this prediction $Co^{III}(Na_4TCP)$, **76**, was also studied. Based on the observations by Pasternack and Ashley,[196,197] that thiocyanate adds about 400 times faster to **76** than to **75**, it was decided to investigate the interaction between **76** and dithizone. The faster binding of thiocyanate was attributed to more available porphyrin electron density. More electron density on the central cobalt would also mean a lesser tendency to be reduced by dithizone. Nevertheless, the change in converting from sulfonate to carboxylate proved to be insignificant with regard to the oxidation of dithizonate. Addition of an excess of potassium dithizonate to **76** once again resulted in the immediate reduction of Co(III), as signified by the Soret band blue-shift from 427 nm to 415 nm (Fig.3.13b).

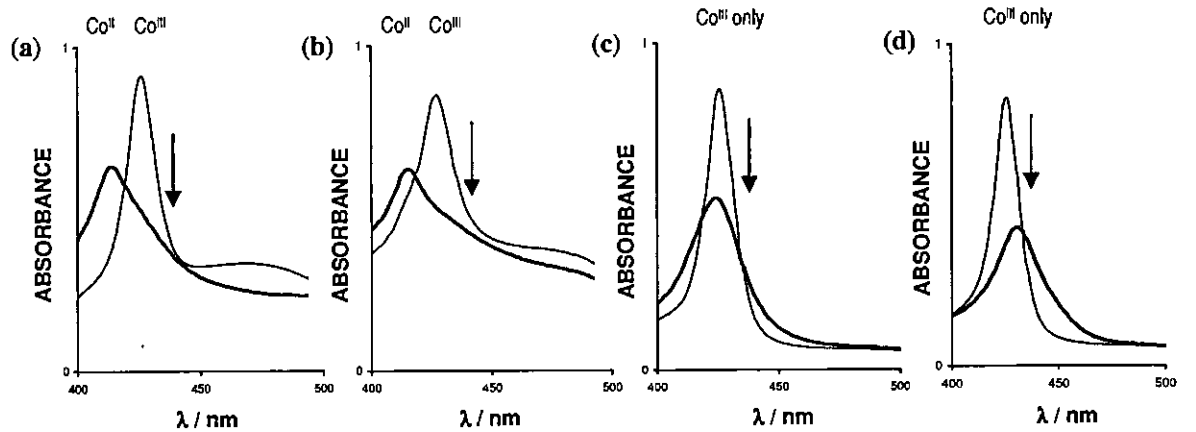


**Figure 3.13** UV / visible spectra of $Co^{III}P$ + R at t = 0 s, and t = 30 min. (all reactions complete), where (a) P = $Na_4TPPS$ & R = KHDz, (b) P = $Na_4TCP$ & R = KHDz, (c) P = $Na_4TPPS$ & R = $NaSC(S)N(C_2H_5)_2$, and (d) P = $Na_4TPPS$ & R = $SC(NH_2)_2$, in water. R was used in 10-fold excess over the cobalt(III) porphyrin. Spectra (a) and (b) show $Co^{II}$ formation as seen from the $\lambda_{max}$ blue-shift. Spectra (c) and (d ) show S-ligation to $Co^{III}$ without reduction, as seen from the smaller ε-values and absence of the typical $Co^{III} \rightarrow Co^{II}$ $\lambda_{max}$ blue-shift.

As a further means of verification of the above results it was decided to employ two non-reducing S-coordinating ligands. Sodium diethyl dithiocarbamate was an available anionic analogous to potassium dithizonate, while thiourea was the neutral compound that was tested in its reaction with **75** (Scheme 3.24). During both these reactions no indication of $Co^{III} \longrightarrow Co^{II}$ reduction was observed. Addition of the sodium salt to **75** resulted in a gradual peak shift towards 424 nm (as seen in Fig.3.13c), the reaction being largely complete at *ca* 20 minutes. The reaction with thiourea was instantaneous, with a product peak at 431 nm (Fig.3.13d).

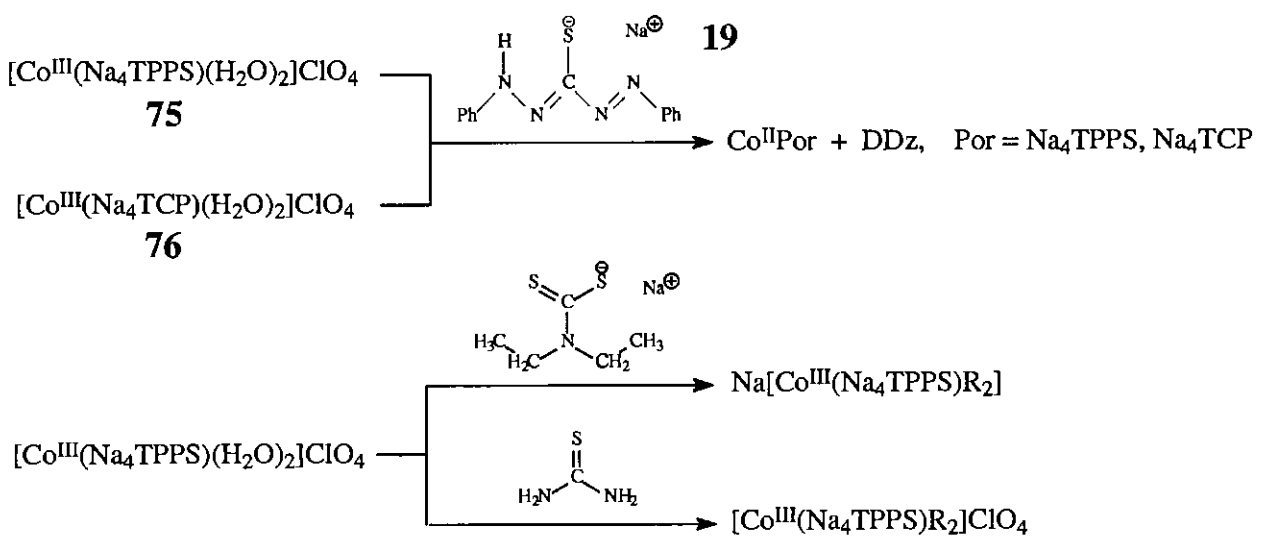


**Scheme 3.24** The cobalt(III) porphyrins, **75** & **76**, dissolved in water, are reduced to their cobalt(II) analogues by potassium dithizonate (**19**). The S-coordinating compounds, R = sodium diethyl dithiocarbamate and thiourea, coordinate axially without reduction of cobalt(III).

It can therefore convincingly be argued that the dithizonate anion did indeed reduce Co(III) and that the product peak was not a coincident equivalent to the Co(II) peak, since;

1) non-reducing axial ligation would have resulted in peak shifts comparable to the above two test compounds, and
2) the product peaks resulting from reactions with the anionic cobalt porphyrins, **75** & **76**, are both exact matches of the corresponding Co(II) peaks. Co(II) also has, as with the above axially ligated compounds, a molar absorption coefficient lower than that of Co(III) porphyrins.

As a further method to prevent the problem of Co(III) reduction in porphyrins with dithizone derivatives, the dithizone phenyls were substituted with halogens in a series of ways. If dithizone could be altered to "hold more tight" to its electrons, i.e. making dithizone electron poor, Co(III) reduction in $Co^{III}$TPP and analogous compounds might be prevented. For this reason the series of halogenated dithizones described at the end of Paragraph 3.2.1 were used. The halogens Cl and especially F exert a strong electronic pull on the dithizone phenyls, and therefore also on the dithizone backbone. In this way dithizone might be prevented from reducing cobalt(III) in the axial ligation reaction.

Unfortunately none of these measures proved to be sufficient in preventing the redox process from taking place. Interactions of all the mono-halogenated dithizones and dithizonates with the aforementioned cobalt(III) porphyrins involved the flow of electrons from dithizone to the Co(III) porphyrin derivatives. This was once again confirmed by blue-shifts typical of the $Co^{III} \rightarrow Co^{II}$ conversion, as seen in Figures 3.13 a & b. The effect of the different halogens substituted on various phenyl positions on the reduction potential of dithizone was quantified by means of the technique of cyclic voltammetry, as discussed in Paragraph 3.5.

The last compound that was considered for purposes of this dissertation, was octaethylporphyrinatocobalt(III), **77**. From Table 3.2, in noting the short Soret band wavelength of OEP complexes, and from the results just described, it was now considered that $Co^{III}$OEP would have the best chance of coordinating dithizone without involving Co(III) reduction. The hypothecy that was hoped to be confirmed was that electron-donating β-pyrrole substituents would be more effective in making the Co(III) porphyrin system electron rich than do phenyl derivatives substituted at the *meso* positions. Compound **77** was the target compound to be investigated.

The result was striking. For the first time now an axial ligation reaction was observed wherein dithizonate substituted axial solvent ligands, without alteration of the Co(III) oxidation state in the porphyrin heterocycle.

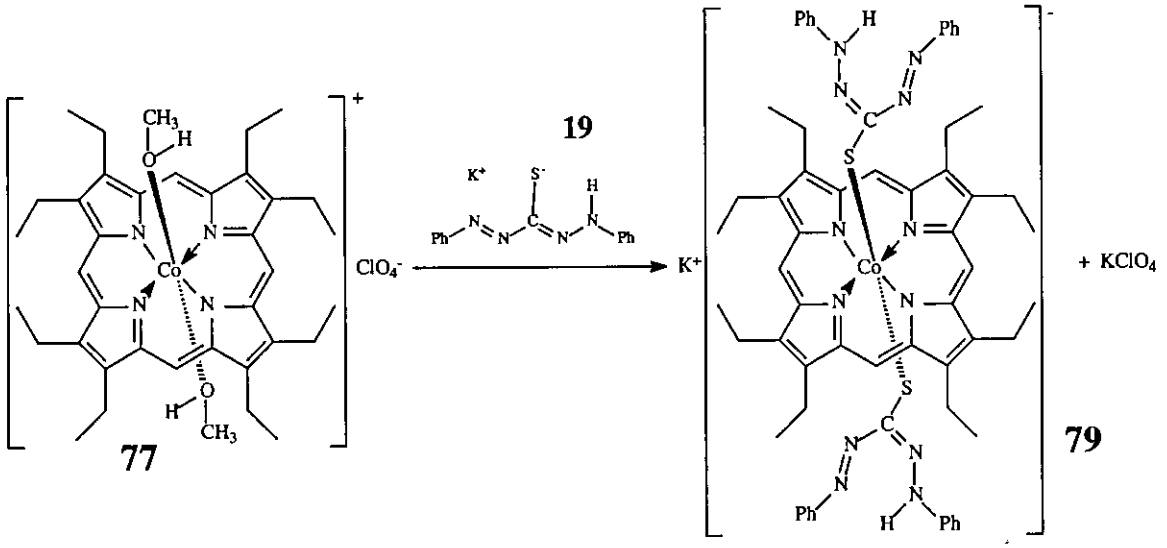


**Scheme 3.25** Octaethylporphyrinatocobalt(III) perchlorate, **77**, reacts with potassium dithizonate to form the Co(III) *bis*-dithizonato porphyrin complex, **79**. An excess of **19** was used to prevent the formation of a mixture of reaction products.

The $H^1$ NMR spectrum (Spectrum A36) of compound **79** integrated for four phenyls, i.e. two dithizonate ligands being attached to the central cobalt. Compared to the reagent, **77**, both the signals for the $-C\underline{H}_2CH_3$ (1.90 → 1.80 ppm) and the $-CH_2C\underline{H}_3$ (4.27 → 4.02 & 3.84 ppm) protons experienced a shift towards lower field, the result of being more shielded. The *meso*-protons followed the same tendency by shifting from an unknown value higher than 10.5 ppm, to 10.13 ppm. These results are consistent with electron density being donated to the cobalt porphyrin, and thus, dithizonate being axially bonded to cobalt.

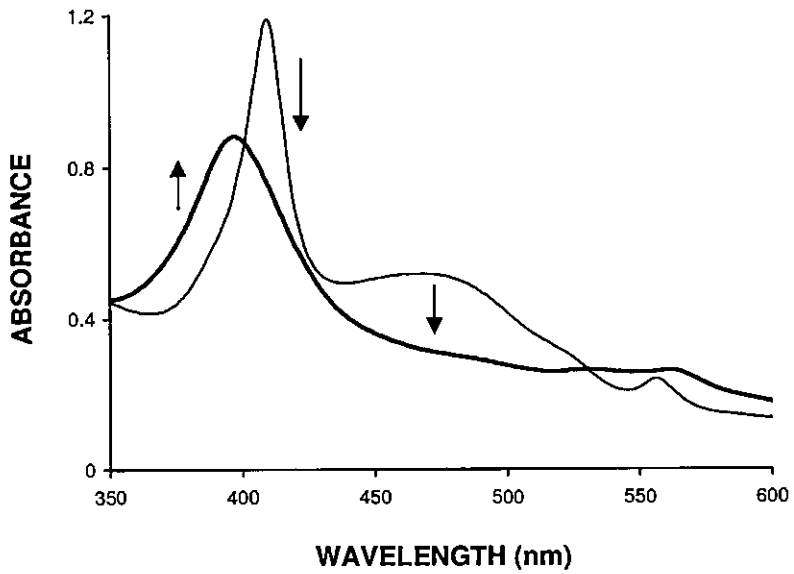


**Figure 3.14** UV/visible spectra of methanol solutions of $[Co^{III}OEP(CH_3OH)_2]ClO_4$ (–) and $K[Co^{III}OEP(HDz)_2]$, (—), at 25°C. The product peak settled at 398 nm within 10 minutes after addition of 3 equivalents of KHDz, and was monitored over a period of two hours for stability. The $Co^{III}$–complex concentration was $5 \times 10^{-6}$ mol.dm$^{-3}$. A double-walled quartz cuvette was used.

UV/visible spectroscopy confirmed this result, namely that dithizonate axially coordinated to the cobalt complex, without reducing it. The reagent, **77**, has a Soret band peak maximum at 409 nm in methanol, while that of the $K[Co^{III}OEP(HDz)_2]$ product, **79**, peaks at 398 nm. No indication of the typical 392 nm Co(II)OEP peak was observed. By undergoing a small blue-shift of 9 nm the spectrum of product **79** bears evidence of added electron density. This may be expected in view of the ease with which the electron rich dithizonate ligand reduced other Co(III) porphyrins.

The above observation was repeated for all the mono-halogenated dithizonates, with the only difference being the rate of coordination. The *meta-* and *ortho-* fluorinated dithizonates visibly coordinated slower than the *para*-halogenated derivatives.

With regard to dithizonatotrimethyltin(IV), as a final remark it must be mentioned that this compound did not prove to be a suitable transfer intermediate, due to the tendency of Sn(IV) to react with most solvents, e.g. chloroform, methanol, acetone and dimethylsulfoxide. Dissolution in these solvents, amongst others, resulted in partial or complete liberation of the ligand, as seen from the protonation reaction wherein the orange dithizonate turned into green dithizone. A less expensive and more versatile alternative is the tetrabutylammonium salt of dithizone, compound **23**. The latter compound, however, underwent blackening in air over time and appeared to be more hygroscopic than the corresponding potassium salt.

# 3.3. X-Ray Crystallography

## 3.3.1. Introduction

As a follow-up, to learn more of the structural properties of dithizone complexes of this study, the structures **28**, dithizonatotrimelthyltin(IV), and **33**, *tris*-dithizonatocobalt(III) was solved by means of single crystal X-ray diffractometry.

Hutton studied the existence of a tautomeric equilibrium for dithizone in solution that includes the thione, thiol and mesomeric forms.[198]

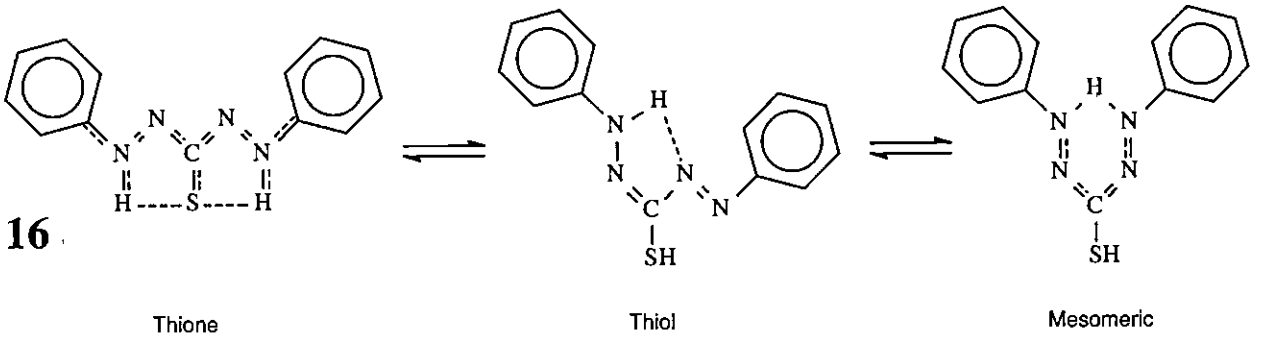


**Figure 3.15** Possible tautomeric forms of dithizone (**16**)

While the thione is the validated structure representation of dithizone,[199] it also corresponds to the basic geometry of reported metal-dithizonates. The only present exception is in the osmium cluster compound synthesised by Kong & Wong.[200] Due to steric effects in the cluster, dithizonate is held in the thiol form, which coincidentally also corresponds to the blue isomeric form of photochromic dithizonatophenylmercury(II) (see Figure 2.13, p.16). Metal dithizonate structures similar to the mesomeric form has to date never been reported. Due to lack of structural evidence it was speculated in 1961 (Irving *et al*) that $R_3Sn(HDz)$ could be of the mesomeric form.[201] The presently reported structure, $Me_3SnHDz$, now conclusively proves a ligand geometry similar to the thione form. Irving rightfully argued that the ligand should be monodentate, coordinated through sulfur only. The reason given was that tin has a maximum coordination number of four. However, it soon became known afterwards that Sn(IV) can even be 8-coordinated.[202]

## 3.3.2. Dithizonatotrimethyltin(IV)

Crystal and structure refinement detail for dithizonatotrimethyltin(IV), **28**, are summarised in Table 3.3, while selected bond and torsion angles and bond lengths can be found in Tables 3.4 - 3.6. Figure 3.16 shows the structure and atom labelling for **28**.

**Table 3.3** Crystal data and structure refinement

| | |
|---|---|
| Empirical formula | $C_{16}H_{20}N_4SSn$ |
| Formula weight | 419.11 |
| Temperature | 183(2)K |
| Wavelength | 0.7107Å |
| Crystal system | Monoclinic |
| Space group | $P2_1/n$ |
| Unit cell dimensions | a = 11.1(1)Å α = 90° |
| | b = 7.2(1)Å β = 101.0(7)° |
| | c = 22.4(1)Å γ = 90° |
| Volume | 1765(29)Å$^3$ |
| Z | 4 |
| Density (calculated) | 1.577 Mg/m$^3$ |
| Absorption coefficient | 1.567 mm$^{-1}$ |
| F(000) | 840 |
| Crystal size | 0.45 x 0.22 x 0.18 mm |
| Theta range for data collection | 2.78° to 30.09° |
| Index ranges | 0<=h<=15, 0<=k<=10, -31<=l<=31 |
| Reflections collected | 5831 |
| Independent reflections | 5185 [R(int)=0.1178(0.0476,1σ data)] |
| Absorption correction | Psi-scan |
| Max. and min. transmission | 0.999 and 0.938 |
| Refinement method | Full-matrix least-squares on $F^2$ |
| Data / restraints / parameters | 5185 / 0 / 202 |
| Goodness-of-fit on $F^2$ | 1.152 |
| Final R indices [I>2σ(I)] | R1 = 0.0329, wR2 = 0.1046 |
| R indices (all data) | R1 = 0.0551, wR2 = 0.1181 |
| Extinction coefficient | 0.0004(2) |
| Largest diff. peak and hole | 1.221 and -1.957 e.Å$^{-3}$ |

The structure revealed distorted tetrahedral coordination geometry around tin. Tetrahedral coordination would naturally have been expected, but when considering the varied bond angles sulfur makes with the three methyl carbons through the metal, i.e. 110.5(4)°, 105.0(4)° and 98.0(9)°, it is clear that coordination is at most pseudo-tetrahedral.

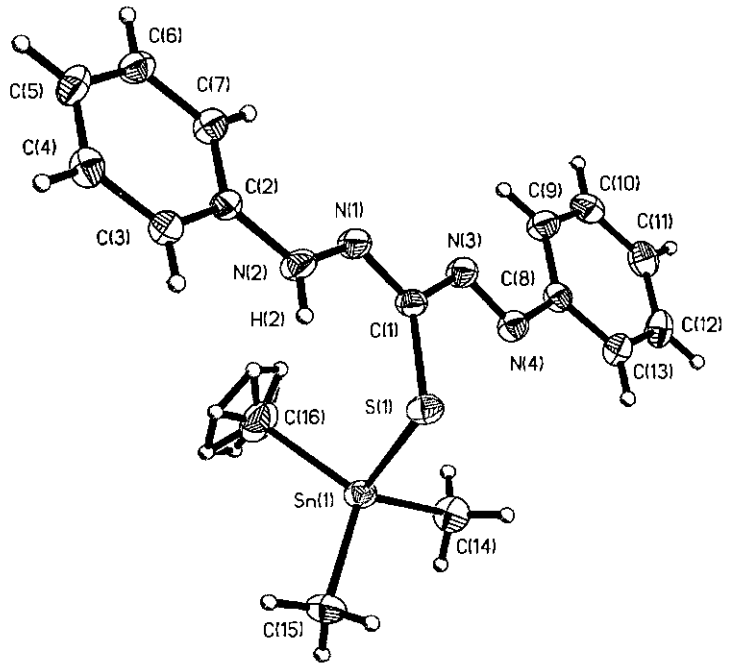


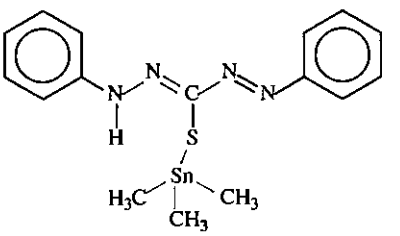

**28**

**Figure 3.16** Left: Molecular structure of dithizonatotrimethyltin(IV), showing 50% probability displacement ellipsoids. The metal lies out of the plane of the ligand. Right: The structure of **28**, indicating double bonds.

Contrary to most bidentate metal-dithizonate complexes, but with the exception of one ligand in $In(HDz)_3$ [203] and in an osmium carbonyl cluster compound,[200] coordination of dithizone to trimethyltin(IV) was found to be monodentate, through a sulfur atom alone (Figure 3.16). Torsion angles along the dithizonate ligand, summarised in Table 3.4, clearly illustrate the high degree of planarity, as opposed to the cobalt dithizonate complex (Par.3.3.3). The 120° bond angles around nitrogen atom, N2, deviates from the 109.5° angle expected for $sp^3$ hybridization, but agree exactly with the trigonal planar geometry of $sp^2$ hybrid orbitals. These bond angles typify a high degree of conjugation along the ligand backbone, and explain the planarity observed. The ligand backbone is linear, comparable to that of uncoordinated dithizone (Fig.2.2, p.5).

**Table 3.4** Selected torsion angles [°]

| | | | |
|---|---|---|---|
| C14 - Sn1 - S1 - C1 | 84.78 ( 0.65) | N4 - N3 - C1 - S1 | 4.49 ( 0.52) |
| C16 - Sn1 - S1 - C1 | -36.41 ( 0.44) | N1 - N2 - C2 - C7 | 4.45 ( 0.62) |
| C15 - Sn1 - S1 - C1 | -156.82 ( 0.32) | N3 - N4 - C8 - C9 | -7.85 ( 0.59) |
| N2 - N1 - C1 - S1 | -1.99 ( 0.57) | | |

The Sn-S bond length of 2.47(3) Å agrees well with the value of 2.433(2) Å in a related compound, 4,6-dimethylpyrimidine-2-thione triphenyltin(IV), $Ph_3Sn(Me_2Pymt)$, reported by Fernandes *et al.*[204] The less bulky pyrimidine-thione ligand, however, is bidentately coordinated to Sn through both sulfur and nitrogen, forming a four-membered ring as opposed to the usual

5-membered metal-dithizonate rings, as for PhHgHDz. In the case of $Me_3Sn(HDz)$, the metal lies completely outside the ligand plane, whereas in most other metal-dithizonates the carbon-sulfur-metal angle is in the direction of the nitrogen (N4) that does not carry the imine proton (H2). The three methyl carbons, being at bond distances of 2.13(2) Å, holds the metal in the sterically more favourable out-of-plane position.

**Table 3.5** Selected bond angles [°]

| | | | |
|---|---|---|---|
| C(14)-Sn(1)-C(16) | 112.2(7) | N(1)-N(2)-C(2) | 120.0(7) |
| C(14)-Sn(1)-C(15) | 113.1(6) | N(1)-N(2)-H(2) | 120.0 |
| C(16)-Sn(1)-C(15) | 116.6(6) | C(2)-N(2)-H(2) | 120.0 |
| C(14)-Sn(1)-S(1) | 110.5(4) | N(4)-N(3)-C(1) | 113.8(7) |
| C(16)-Sn(1)-S(1) | 105.0(4) | N(3)-N(4)-C(8) | 113.9(7) |
| C(15)-Sn(1)-S(1) | 98.0(9) | N(1)-C(1)-N(3) | 112.1(7) |
| C(1)-S(1)-Sn(1) | 100.8(8) | N(1)-C(1)-S(1) | 124.2(6) |
| C(1)-N(1)-N(2) | 117.4(7) | N(3)-C(1)-S(1) | 123.7(6) |

**Table 3.6** Selected bond lengths [Å]

| | | | |
|---|---|---|---|
| Sn(1)-C(14) | 2.13(2) | N(1)-N(2) | 1.327(14) |
| Sn(1)-C(16) | 2.13(2) | N(2)-C(2) | 1.398(10) |
| Sn(1)-C(15) | 2.13(2) | N(2)-H(2) | 0.8600 |
| Sn(1)-S(1) | 2.47(3) | N(3)-N(4) | 1.267(9) |
| S(1)-C(1) | 1.774(14) | N(3)-C(1) | 1.40(2) |
| N(1)-C(1) | 1.308(9) | N(4)-C(8) | 1.42(2) |

The bond lengths along the ligand backbone are neither typically single nor double bond in character. However, the N3-N4 bond length of 1.267(9) Å and the N1-C1 bond length of 1.308(9) Å are close to typical double bond lengths of 1.25 Å and 1.29 Å respectively. Even the N1-N2 bond (1.327(14) Å), which is expected to be a single bond, has more double bond character than single. N-N single bonds are typically 1.45 Å in length. The N3-C1 bond length of 1.40(2) Å is shorter than a typical N-C single bond length of 1.47 Å. The observed deviations from typical single and double bond distances is further evidence of the high degree of electron delocalization along the dithizonate backbone.

The fact that dithizone is only mono-coordinated to tin results in a relatively labilised ligand as compared to bidentately ligated complexes. Additionally, the Sn-S bond length is also *ca* 0.1 Å longer than the corresponding Hg-S bond (see Table 3.13) regardless the significantly smaller ionic radius of tin(IV) (ionic radius of $Sn^{IV}$ = 0.71 Å; ionic radius of $Hg^{II}$ = 1.10 Å).[205] As this longer bond distance is indicative of a weaker bond interaction, it is concluded that the overall Sn – dithizonate bond interaction is weak and that the ligand may easily be displaced by other

incoming species, like $Cl^-$, which tin has a natural affinity for. This evidence points therefore favourably towards the purpose for preparing dithizonatotrimethyltin(IV), namely for use in anionic substitution reactions in non-coordinating and non-halogen containing solvents.

The N2-H2...S1 hydrogen-bond interaction was again observed, with a distance of 2.49 Å, which is only slightly longer than estimated by Hutton *et al* [36] for the corresponding H...S hydrogen bond in PhHg(HDz) (2.4 Å) and Niven *et al*[206] for $Bi(HDz)_3$ (2.4 Å). Ligand bond distances and bond angles otherwise compare well with those in both the aforementioned complexes, regardless the fact that both are bidentately coordinated, as opposed to monodentate in the present tin complex.

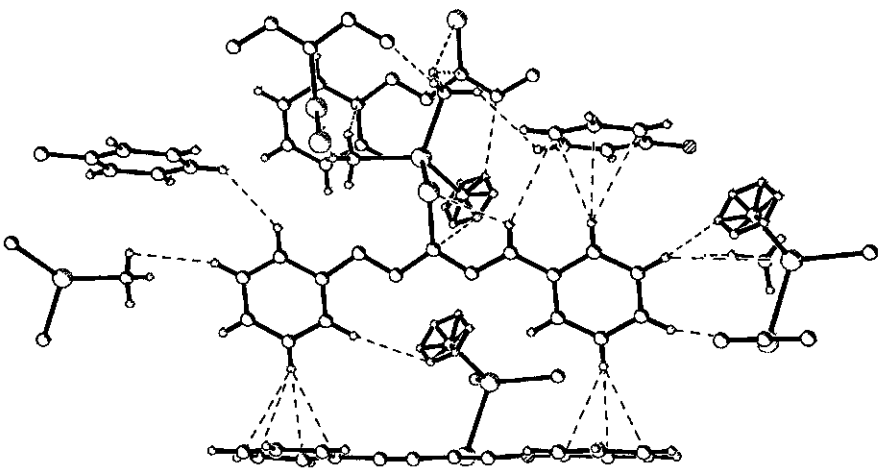

**Figure 3.17** Partial packing diagram, showing some intermolecular and intramolecular S-H, C-H and H-H atomic interactions (dashed lines).

**Table 3.7** Selected contact distances [Å] and bond angles [°]. Specified hydrogen bonds and other intermolecular contacts (with esds, except fixed and riding H).

| | D-H | H...A | D...A | <(DHA) |
|---|---|---|---|---|
| N2-H2...S1 | 0.86 | 2.49 | 2.931(17) | 112.3 |
| C3-H3...C6_$1 | 0.93 | 2.82 | 3.72(3) | 162.9 |
| C4-H4...H16A_$2 | 0.93 | 2.42 | 3.27(4) | 153.0 |
| C12-H12...H14C_$4 | 0.93 | 2.64 | 3.51(3) | 156.4 |
| C13-H13...H5_$5 | 0.93 | 2.53 | 3.34(2) | 145.9 |
| C15-H15A...H4_$1 | 0.96 | 2.50 | 3.25(2) | 134.5 |
| C15-H15B...N4_$7 | 0.96 | 2.91 | 3.86(3) | 169.2 |

Only a few of many more inter and intramolecular interactions are shown above. From this multitude of relatively short interactions very closely packed molecules in crystalline form are observed.

## 3.3.3. *Tris*-dithizonatocobalt(III)

Crystal and structure refinement detail for *tris*-dithizonatocobalt(III), **33**, is summarised in Table 3.8, while selected bond and torsion angles and bond lengths can be found in Tables 3.9 -3.12. Figure 3.18 shows the structure and atom labelling for **33**.

**Table 3.8** Crystal data and structure refinement

| | | |
|---|---|---|
| Empirical formula | $C_{39}H_{33}CoN_{12}S_3$ | |
| Formula weight | 824.88 g/mol | |
| Temperature | 213 K | |
| Wavelength | 0.7107 Å | |
| Crystal system | Triclinic | |
| Space group | P -1 | |
| Unit cell dimensions | a = 13.559(3) Å | α = 109.61(1)° |
| | b = 15.068(2) Å | β = 106.91(2)° |
| | c = 10.901(2) Å | γ = 71.84(1)° |
| Volume | 1949.7(7) $Å^3$ | |
| Z | 2 | |
| Density (calculated) | 1.405 $Mg/m^3$ | |
| Absorption coefficient | 0.647 $mm^{-1}$ | |
| F(000) | 852.00 | |
| Crystal size | 0.22 x 0.16 x 0.14 $mm^3$ | |
| Theta range for data collection | 2.81 to 30.10° | |
| Index ranges | 0<=h<=16, -20<=k<=20, -15<=l<=14 | |
| Reflections collected | 11106 | |
| Independent reflections | 10662 [R(int) = 0.06580] | |
| Completeness to theta = 30.10° | 92.8 % | |
| Absorption correction | Psi-scan | |
| Max. and min. transmission | 1.000 and 0.946 | |
| Refinement method | Full-matrix least-squares on $F^2$ | |
| Data / restraints / parameters | 10662 / 231 / 499 | |
| Goodness-of-fit on $F^2$ | 0.952 | |
| Final R indices [I>2sigma(I)] | R1 = 0.0474, wR2 = 0.1324 | |
| R indices (all data) | R1 = 0.1935, wR2 = 0.2002 | |
| Largest diff. peak and hole | 0.847 and -0.944 $e.Å^{-3}$ | |

*Tris*-dithizonatocobalt(III), Co{PhNHNC(S)NNPh}$_3$, has an octahedral coordination geometry. To our knowledge only two other *tris*-dithizonate complexes were reported, namely Bi(HDz)$_3$ [206] and In(HDz)$_3$.[203] The cobalt complex is rather similar to the bismuth complex, with all three dithizonate ligands acting as bidentate ligands, coordinating through the N and S atoms. The indium complex, on the other hand, has only two bidentate ligated dithizonates and one that is

monodentately coordinated. As in the case with bismuth, the three dithizonate ligands in $Co(HDz)_3$ are all *cis*-coordinated, i.e. the sulfur atoms are coordinated on one side of the metal and the nitrogens on the other side.

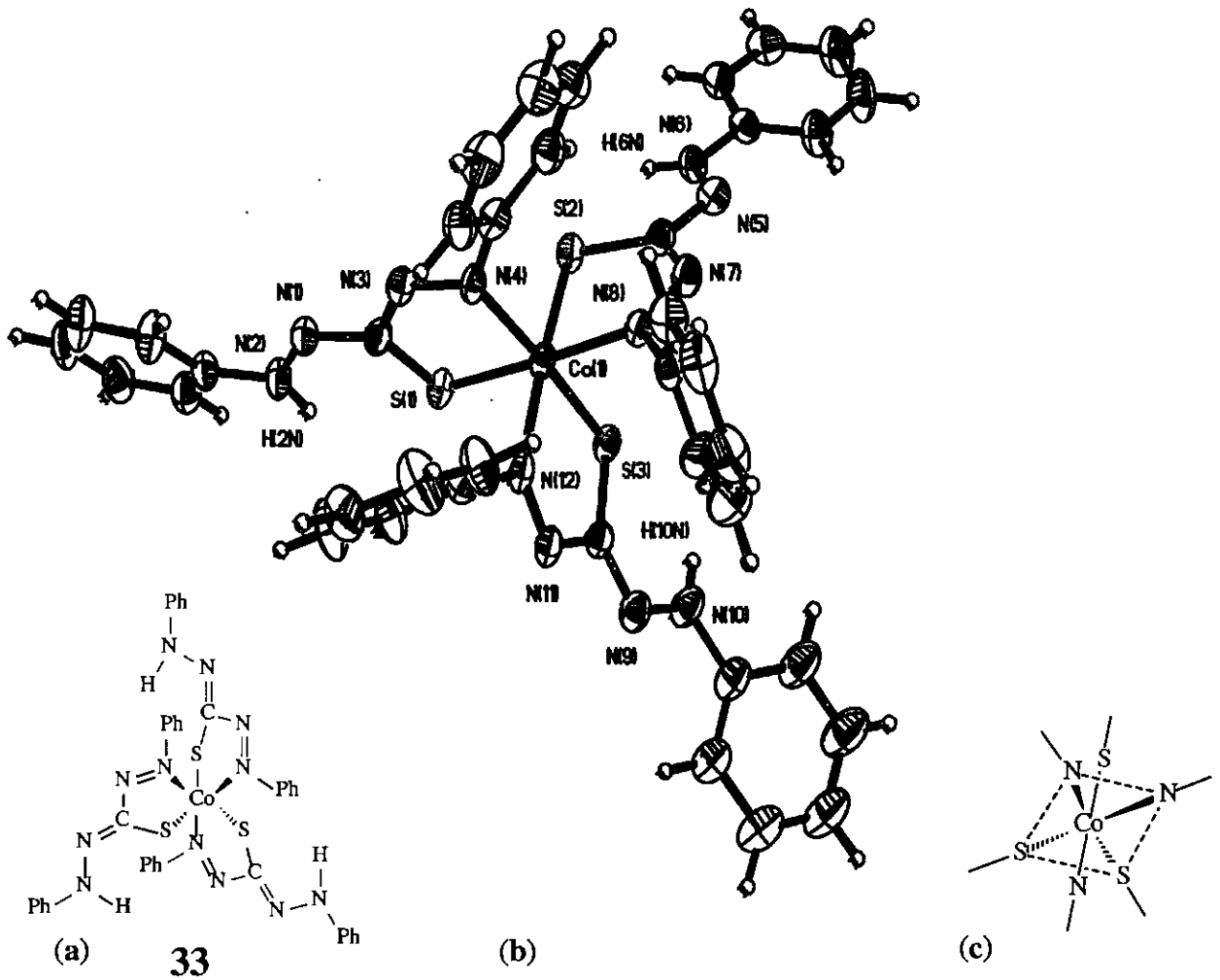


**Figure 3.18** (a) The structure of *tris*-dithizonatocobalt(III), **33**, indicating double bonds. (b) Molecular structure of **33**, showing 50% probability displacement ellipsoids. The three Co-N phenyls lie above the plane defined by atoms S1-N4-N8-S3, while the peripheral phenyls (above perspective) lie below the plane, clearly illustrating *cis*-coordination (c).

In the small deviations from 180° and 90° of the *trans*- and *cis*- L-Co-L bond angles, it can be seen that the octahedral coordination is slightly distorted, but in a lesser degree as compared to bismuth. The axial S(2)-Co(1)-N(12) bond angle of 170.52(11)° is the furthest from 180°, while the S-Co-S angles are amongst the closest to 90°, namely 89.71(5)°, 89.66(5)° and 86.30(5)°.

**Table 3.9** Metal-centered bond angles [°]

| | | | | | |
|---|---|---|---|---|---|
| *S(1)-Co(1)-S(2) | 89.71(5) | S(1)-Co(1)-N(8) | 174.76(10) | N(4)-Co(1)-N(8) | 96.86(15) |
| S(1)-Co(1)-S(3) | 89.66(5) | S(2)-Co(1)-N(12) | 170.52(11) | N(4)-Co(1)-N(12) | 95.44(14) |
| S(2)-Co(1)-S(3) | 86.30(5) | S(3)-Co(1)-N(4) | 174.45(11) | N(8)-Co(1)-N(12) | 97.52(14) |

**Table 3.10** Selected torsion angles [°]

| Ligand 1 | | Ligand 2 | | Ligand 3 | |
|---|---|---|---|---|---|
| Co1-N4-C8-C9 | -124.08 ( 0.39) | Co1-N8-C21-C22 | -105.22 ( 0.44) | Co1-N12-C34-C39 | -85.59 ( 0.50) |
| N1-N2-C2-C3 | 161.34 ( 0.43) | N5-N6-C15-C16 | 14.53 ( 0.66) | N9-N10-C28-C29 | -156.74 ( 0.49) |
| N4-N3-C1-N1 | -179.77 ( 0.36) | N8-N7-C14-N5 | -172.63 ( 0.38) | N12-N11-C27-N9 | 166.55 ( 0.38) |
| N4-N3-C1-S1 | -2.61 ( 0.53) | N8-N7-C14-S2 | 5.80 ( 0.55) | N12-N11-C27-S3 | -13.40 ( 0.53) |

**Table 3.11** Selected bond angles [°]

| Ligand 1 | | Ligand 2 | | Ligand 3 | |
|---|---|---|---|---|---|
| N(4)-Co(1)-S(1) | 84.81(11) | N(8)-Co(1)-S(2) | 85.24(10) | N(12)-Co(1)-S(3) | 84.71(11) |
| C(1)-S(1)-Co(1) | 94.81(16) | C(14)-S(2)-Co(1) | 94.52(14) | C(27)-S(3)-Co(1) | 95.52(15) |
| N(3)-N(4)-Co(1) | 121.9(3) | N(7)-N(8)-Co(1) | 122.2(3) | N(11)-N(12)-Co(1) | 123.1(3) |
| C(1)-N(1)-N(2) | 117.0(4) | C(14)-N(5)-N(6) | 115.6(4) | C(27)-N(9)-N(10) | 116.0(4) |
| N(1)-C(1)-N(3) | 112.4(4) | N(5)-C(14)-N(7) | 111.8(4) | N(9)-C(27)-N(11) | 112.7(4) |
| N(1)-C(1)-S(1) | 125.8(4) | N(5)-C(14)-S(2) | 127.1(3) | N(9)-C(27)-S(3) | 127.2(3) |
| N(3)-C(1)-S(1) | 121.8(3) | N(7)-C(14)-S(2) | 121.1(3) | N(11)-C(27)-S(3) | 120.1(3) |
| N(4)-N(3)-C(1) | 115.5(4) | N(8)-N(7)-C(14) | 115.0(4) | N(12)-N(11)-C(27) | 115.3(4) |

**Table 3.12** Selected bond distances [Å]

| Ligand 1 | | Ligand 2 | | Ligand 3 | |
|---|---|---|---|---|---|
| Co(1)-S(1) | 2.2386(13) | Co(1)-S(2) | 2.2332(13) | Co(1)-S(3) | 2.2379(13) |
| Co(1)-N(4) | 1.979(4) | Co(1)-N(8) | 1.964(3) | Co(1)-N(12) | 1.974(4) |
| S(1)-C(1) | 1.741(4) | S(2)-C(14) | 1.742(4) | S(3)-C(27) | 1.746(4) |
| N(1)-C(1) | 1.322(5) | N(5)-C(14) | 1.314(5) | N(9)-C(27) | 1.295(6) |
| N(1)-N(2) | 1.323(5) | N(5)-N(6) | 1.320(5) | N(9)-N(10) | 1.336(5) |
| N(2)-C(2) | 1.402(6) | N(6)-C(15) | 1.401(5) | N(10)-C(28) | 1.407(6) |
| N(2)-H(2N) | 0.8666 | N(6)-H(6N) | 0.8663 | N(10)-H(10N) | 0.8748 |
| N(3)-N(4) | 1.276(5) | N(7)-N(8) | 1.273(5) | N(11)-N(12) | 1.266(5) |
| N(3)-C(1) | 1.364(6) | N(7)-C(14) | 1.389(5) | N(11)-C(27) | 1.389(5) |
| N(4)-C(8) | 1.449(6) | N(8)-C(21) | 1.451(5) | N(12)-C(34) | 1.454(5) |

Concerning the dithizonate ligand, a large degree of planarity is the norm in most structural reports, except in the case of the gold complex, [Au($PhCH_2NHCH_2CH_3$)(HDz)Cl], where the Au-N phenyl ring is twisted against the coordination plane by 75.1(2)°.[207] $Co(HDz)_3$ now is also observed to have a large degree of phenyl rotation, with Co-N-C-C torsion angles of -124.08(0.39)°, -105.22(0.44)° and -85.59(0.50)°. This might be explained in terms of the relatively short metal-ligand bond distances observed for cobalt as compared to bismuth (see Table 3.13), where the corresponding phenyl rings lie co-planar with the ligand. The consequence is that an increased amount of steric crowding exists between the ligands in

$Co(HDz)_3$. Having observed the twisted phenyl rings, the adjoining -N-Ph bond distances were naturally expected to be longer, as conjugation between this phenyl ring and the ligand backbone can no longer take place. That is indeed seen to be the case, with N(4)-C(8) bond distances of *ca* 1.45 Å, as opposed to the phenyl ring at the opposite end of the ligand that lies co-planar with the backbone, having a bond length of *ca* 1.40 Å.

In this regard it must further be noted that the purple colour of $Co(HDz)_3$ is altogether different to the orange colour of KHDz (**19**), $Me_3SnHDz$ (**28**) and PhHgHDz (**20**) (with planar HDz ligands), and that this significant colour change may be attributed to the degree of conjugation along the dithizonate backbone in each complex. The conjugation, in turn, will be affected by the degree of rotation that exists for the peripheral phenyl rings. Further confirmation for this hypothesis is yet to be obtained by critical evaluation of UV/visible spectra of all available metal dithizonate complexes and the degree of rotation found for the phenyl rings of each. The metal naturally will also have an influence on the colour of its dithizonate complex, but the exact extent is yet to be researched.

Table 3.13 is compiled from published crystallographic data, placing the coordination bond lengths in the cobalt complex in relation to other metal dithizonates. Co-S bond lengths vary from 2.233(1) to 2.239(1) Å and Co-N bond lengths from 1.964(3) to 1.979(4) Å, which are amongst the shortest as compared to the other listed metals. In going from Hg to Co, there is only a slight length decrease of *ca* 0.14 Å in the metal-S bond, which is quite contrary to the marked increase in bond strength as far as the metal-N bond is concerned; a decrease of *ca* 0.66 Å was observed. Bi-S- and Bi-N- bond lengths are the longest reported values; *ca* 2.61 Å and 2.7 Å respectively. On the other hand, $Cu(HDz)_2$ has coordination bond lengths that are by far the shortest, with Cu-S being 2.00 Å and Cu-N 1.85 Å.[208]

**Table 3.13** Comparison between bond distances of different metal dithizone complexes. [Å]

| Period* | Atom | M-S | M-N |
|---|---|---|---|
| 4 | $Co^{III}$ | 2.24 | 1.97 |
| | $Ni^{II}$ [209] | 2.19 | 1.87 |
| | $Cu^{II}$ [208] | 2.00 | 1.85 |
| | $Zn^{II}$ [210] | 2.27 | 2.07 |
| 5 | $Mo^{VI}$ [211] | 2.5 | 2.1-2.4 |
| | $In^{III}$ [210] | 2.47 | 2.35 |
| | $Sn^{IV}$ | 2.47 | |
| 6 | $Os^{III}$ [200] | 2.5 | |
| | $Au^{III}$ [207] | 2.25 | 2.13 |
| | $Hg^{II}$ [212] | 2.38 | 2.63 |
| | $Bi^{III}$ [206] | 2.61 | 2.7 |

* Period on the Periodic Table

The -N-N- and -C-N- single bonds are normally *ca* 1.47 Å long, while -N=N- and -C=N- double bonds are *ca* 1.25 Å and *ca* 1.27 Å respectively.[213] Hence N(3)-N(4) (1.266 – 1.276 Å) corresponds strongly to a localised double bond (Table 3.12), while N(1)-N(2) (1.323 – 1.336 Å) and N(1)-C(1) (1.295 – 1.322 Å) are largely double bond in character, typically of what is expected for a conjugated system. The phenyl-N bond lengths are, although shorter than typical single bonds, nevertheless also single bond in character. As compared to the mercury complex, the cobalt complex shows a slightly larger degree of electron delocalization around the C=N conjugated double bond – the axis around which photochromic isomerisation is known to take place.

| | | C(2) ··· N(2) ··· N(1) ═ C(1) ··· N(3) = N(4) ··· C(8) | | | | | |
|---|---|---|---|---|---|---|---|
| **Co:** | (purple complex) | 1.40 | **1.32** | **1.32** | **1.36** | 1.28 | 1.45 Å |
| **Hg:** | (yellow complex) | 1.38 | **1.34** | **1.29** | **1.41** | 1.28 | 1.43 Å |

As opposed to mercury and other dithizonate complexes (see Table 2.2, p.17), no photochromism is observed in the cobalt complex. Sterical hindrance can evidently not be attributed as reason for this phenomenon (see peripheral phenyls in Figures 3.18 & 3.19). It will therefore have to be explained in terms of electronic effects – an aspect which calls for further investigation.

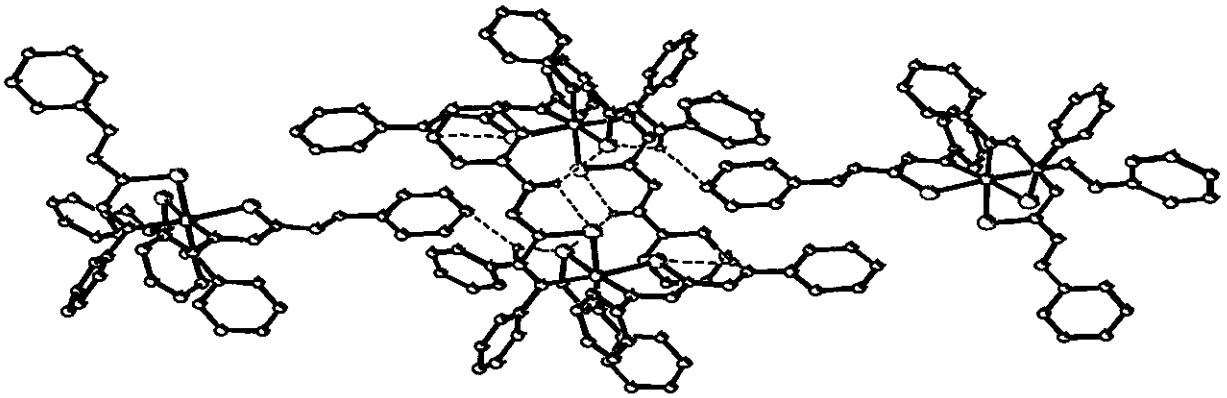

**Figure 3.19** Partial packing diagram, showing the hydrogen bonds (dashed lines). Inter- and intramolecular S-H and C-H bonds are shown.

The characteristic dithizone N2-H2...S1 hydrogen-bonds were observed, with distances of 2.50 - 2.53 Å, which agrees with the only other experimentally observed value of 2.49 Å, in the $Me_3Sn(HDz)$ complex (see Paragraph 3.3.2). Other dithizonate bond distances and -angles are typical and agree well with those of reported structures.

# 3.4. Quantum Computational Chemistry

## 3.4.1. Introduction

The main purpose of this study was to construct a dithizonatophenylmercury – cobalt porphyrin conjugate capable of trapping the photochromic system in the blue excited state. However, since the structure of the blue form is not even known yet, PhHg(S-Me)Dz, **18**, was prepared to obtain a crude model of such a system with the porphyrin group replaced by a methyl group. The synthesis of **18** was successful but all attempts to obtain crystals suitable for X-ray single crystal structure determination failed. It was therefore decided to follow the quantum computational approach to address as much of the structurally based unanswered questions as possible.

To make the quantum chemical study as meaningful as possible within the borders of this Ph.D. research program, some goals were set.

1. The quantum chemical approach had to be validated as accurate. This was addressed by theoretically solving the structures of the orange forms of MeHgHDz and PhHgHDz, **20**, and then comparing the calculated data with the structural data of MeHgHDz and PhHgHDz, which were experimentally determined by means of single crystal X-ray diffraction methods. Whether artificially generated atomic coordinates, or coordinates obtained from X-ray data collections were used in the input files, the relevant calculated molecular energies always converged to the same values.
2. Having then proved that the quantum chemical approach gives structures for the orange form of MeHgHDz and PhHgHDz that almost exactly correspond to the experimentally determined structures, the structure of the blue isomer of PhHgHDz was solved by theoretical means.
3. The structure of the model compound PhHg(S-Me)Dz, **18**, was then solved. Two preferential isomers of **18** were considered; the one corresponds to the orange form of PhHgHDz, **20**, the other corresponds to the blue form. Key differences between **18** and **20** could be related to the absence of a hydrogen-bonding H-atom (which was replaced with a $CH_3$ group) in the S-methyldithizonato backbone of **18**.
4. The quantum chemically optimised structures of PhHg(S-Me)Dz, **18**, PhHgHDz, **20** and $H_2Dz$, **16**, were then utilised to predict the electronic (UV/visible) spectra by utilizing the time-dependent Amsterdam Density Function (ADF) computational package. Fair to good results were obtained, which may serve as a useful starting point for future refinements and/or improvements as our understanding of these systems increases.
5. By following the quantum computational approach the energy required for the orange to blue isomerisation of **20** to take place were calculated, as well as the shapes of corresponding

HOMO and LUMO orbitals . The results led to a better understanding of photochromism as observed in dithizonato complexes of mercury.

6. Finally, calculations were done of a hypothetical PhHgHDz - porphyrin complex to determine if the blue form of such an adduct had indeed a realistic chance of being trapped after isomerisation from the corresponding orange form took place. This was done by comparing overall molecular energies.

The Amsterdam Density Functional (ADF) program package version 2004.01 with the PW91 functional and the triple ζ plus polarization basis set, ZORA/TZP, which includes relativistic effects, was used. Density functional theory (DFT) is known as a useful tool for theoretical studies of transition metal complexes because electron correlation is taken into account.[214-216] Usage of the quadruple ζ ZORA/QZ4P basis set afforded no improvement in result accuracy but lengthened CPU runtimes by *ca* 10 times. It was thus decided not to use the ZORA/QZ4P basis set, which employs 16 times more functions than ZORA/TZP.

The Gaussian program package version 0.3 (G03) with the B3LYP functional and the CEP-31G basis set was also employed. CPU run times, using this program, proved to be 10 – 25 times shorter when compared to similar calculations done using the ADF program.

No symmetry limitations were imposed, i.e. all calculations were done in the C1 (NO-SYM) mode.

## 3.4.2. Dithizonatophenylmercury(II) – the orange isomer, and Dithizonatomethylmercury(II)

Figures 3.20 and 3.21 give graphical illustrations, comparing ADF and G03 quantum computational bond lengths and bond angles to experimental X-ray crystal data of PhHgHDz and MeHgHDz.[36] R values are given as a measure of the average accuracy of all the (*gas-phase*) computed bond lengths and angles under consideration, with the numerical value of one being representative of results that agree exactly with experimental (*solid state*) crystal data.

The following expression was used to calculate R values,

$$n^{-1} \times \sum[(x_{ei} - |x_{ci} - x_{ei}|)/x_{ei}], \quad i = 1 \rightarrow n$$

where n = number of data points, $x_{ei}$ = experimental data point *i*, and $x_{ci}$ = calculated data point *i*.

Table 3.14 lists the X-ray structural data and calculated parameters obtained from ADF and G03 geometry optimizations of the methylmercury- and phenylmercury dithizonate complexes.

By the following illustrations (Figures 3.20 and 3.21) an indication of the general degree of accuracy of computational results is given.

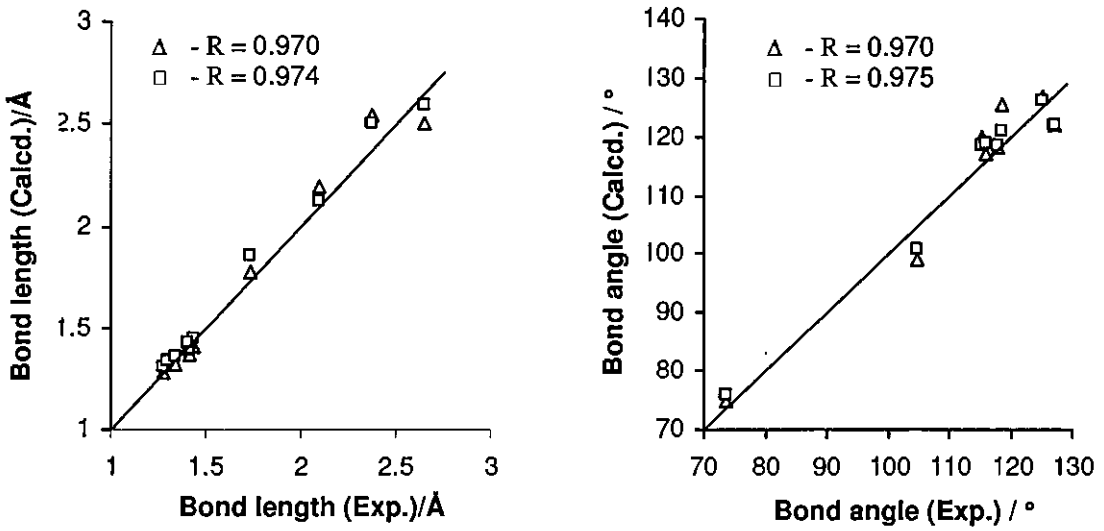


**Figure 3.20** Plots of experimental versus calculated bond lengths and bond angles of dithizonatophenylmercury(II), **PhHgHDz**, using the ADF(PW91)/ZORA/TZP (Δ) and G03(B3LYP)/CEP-31G (□) systems. Data points correspond to values in Table 3.14.

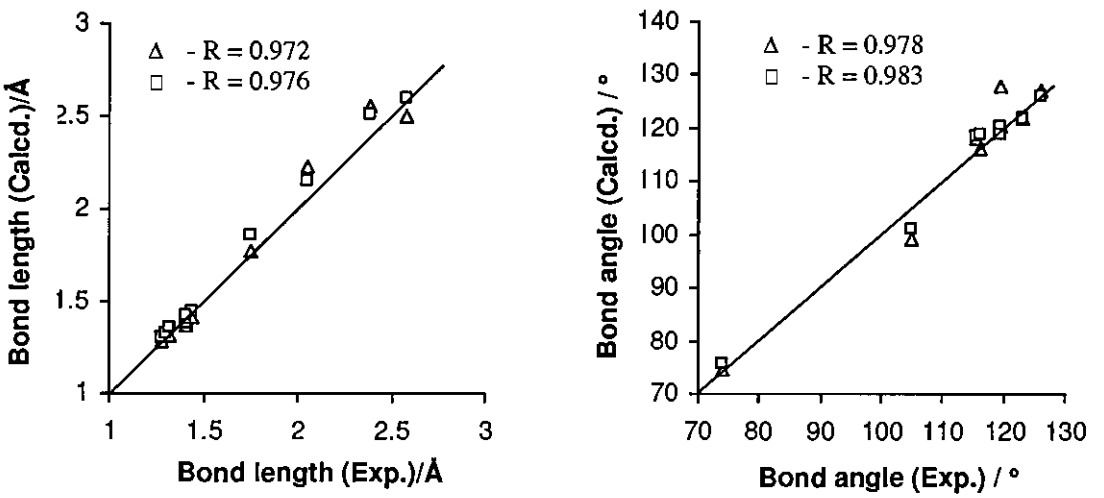


**Figure 3.21** Plots of experimental versus calculated bond lengths and bond angles of dithizonatomethylmercury(II), **MeHgHDz**, using the ADF(PW91)/ZORA/TZP (Δ) and G03(B3LYP)/CEP-31G (□) systems. Data points correspond to values in Table 3.14. Note: Dithizonatomethylmercury(II), MeHgHDz, is not to be confused with S-methyldithizonatophenylmercury(II), PhHg(S-Me)Dz.

All the above R values correspond to average accuracies ≥ 97 %. Gaussian optimizations consistently gave bond length and bond angles that agree slightly better with experimental data than optimizations with ADF. This, however, is not true for torsion angles, as will be seen later. It must be pointed out that all the above R values will improve significantly if bond lengths and angles of the phenyl groups are included, since phenyl parameters are generally calculated accurately, as was also the case here. These results were not included, since they do not involve aspects directly under consideration in this section.

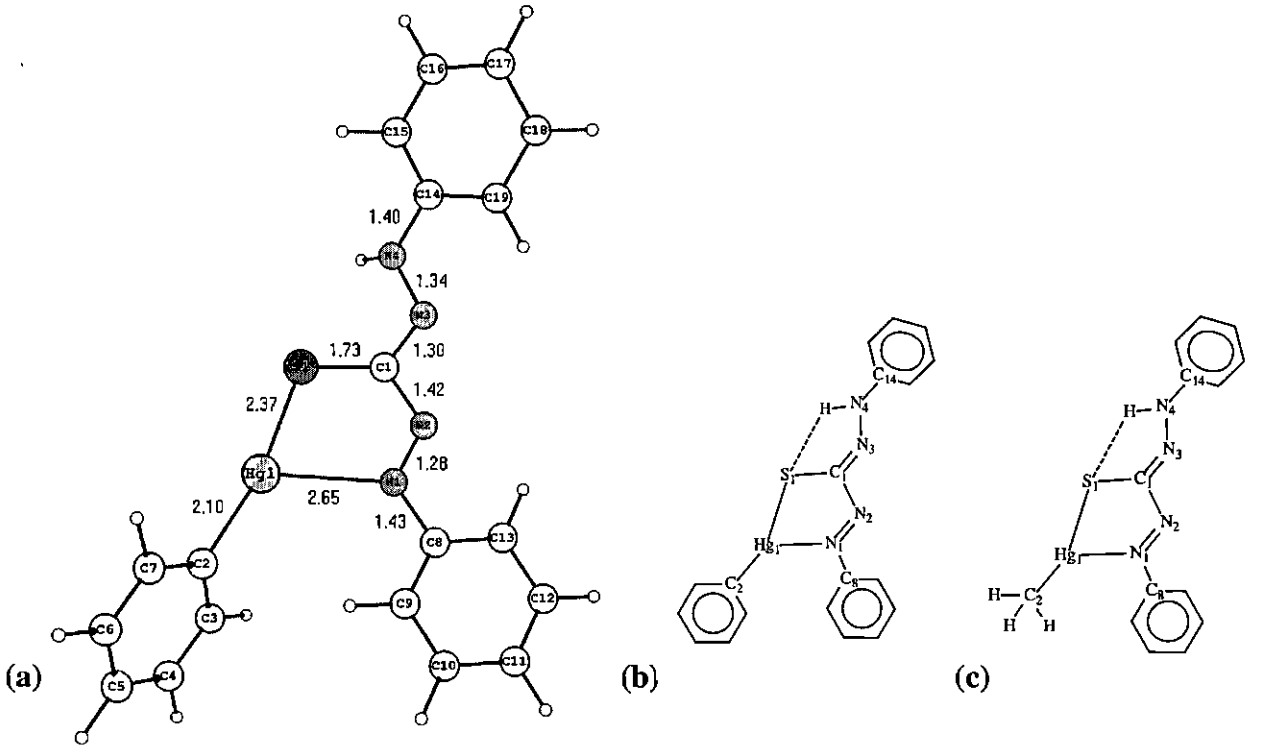


**Figure 3.22** (a) X-ray crystal structure of dithizonatophenylmercury(II), PhHgHDz (orange), **20**, indicating atom labels and bond lengths (Å), (b) PhHgHDz double bonds and hydrogen bond. (c) MeHgHDz double bonds and hydrogen bond.

**Table 3.14** X-ray crystal data and calculated bond lengths and bond angles of dithizonatophenylmercury(II) and dithizonatomethylmercury(II).

| | PhHgHDz | | | MeHgHDz | | |
|---|---|---|---|---|---|---|
| | **Crystal** | **ADF*** | **G03#** | **Crystal** | **ADF** | **G03** |
| **Bond lengths (Å)** | | | | | | |
| **Hg1-S1** | 2.37 | 2.54 | 2.50 | 2.39 | 2.56 | 2.51 |
| **Hg1-C2** | 2.10 | 2.19 | 2.13 | 2.06 | 2.23 | 2.15 |
| **Hg1-N1** | 2.65 | 2.50 | 2.59 | 2.58 | 2.50 | 2.60 |
| **N1-N2** | 1.28 | 1.28 | 1.31 | 1.28 | 1.28 | 1.31 |
| **N1-C8** | 1.43 | 1.41 | 1.44 | 1.44 | 1.41 | 1.44 |
| **N2-C1** | 1.42 | 1.37 | 1.40 | 1.41 | 1.37 | 1.40 |
| **C1-S1** | 1.73 | 1.77 | 1.86 | 1.75 | 1.77 | 1.85 |
| **C1-N3** | 1.30 | 1.33 | 1.34 | 1.30 | 1.34 | 1.33 |
| **N3-N4** | 1.34 | 1.31 | 1.35 | 1.33 | 1.31 | 1.35 |
| **N4-C14** | 1.40 | 1.40 | 1.42 | 1.41 | 1.39 | 1.42 |
| **Bond Angles (°)** | | | | | | |
| **Hg1-S1-C1** | 105 | 99 | 101 | 105 | 99 | 101 |
| **S1-Hg1-N1** | 74 | 75 | 76 | 74 | 75 | 76 |
| **N1-Hg1-C2** | 118 | 125 | 121 | 119 | 128 | 121 |
| **Hg1-N1-N2** | 115 | 120 | 119 | 120 | 121 | 119 |
| **N1-N2-C1** | 118 | 118 | 119 | 116 | 118 | 119 |
| **N2-C1-S1** | 125 | 127 | 126 | 126 | 127 | 126 |
| **S1-C1-N3** | 127 | 122 | 122 | 123 | 122 | 122 |
| **C1-N3-N4** | 116 | 117 | 119 | 116 | 116 | 119 |

Geometry optimization times: * - *ca* 80 hrs, # - *ca* 5 hrs

From the above table it can be seen that bond lengths around mercury were not very accurately calculated. The Hg-S and Hg-C bonds were consistently calculated too long, while the Hg-N bonds are too short. The only exception is the longer Hg-N1 bond (2.60 Å) in the G03 calculation for MeHgHDz. The deviations in bond lengths must therefore be attributed to the underlying theory in both the ADF and G03 programs. It must also be pointed out that all computations done in this study simulated gas-phase conditions, with the consequent exclusion of intermolecular interactions and forces. The result is that bond lengths in general tend to be longer in the *gas-phase* computational optimizations than in the corresponding *solid state* crystal structures. The G03 program nevertheless calculated the bond lengths around the metal more accurately.

The opposite is true for the remaining bonds in the dithizonate ligand. Here, ADF optimised bond lengths were without exception all shorter than the corresponding G03 lengths. Only in the case of the C1-S1 bond it can be said that ADF (1.77 Å) gave a significant improvement over G03 (1.86 Å) in accuracy. The experimental C1-S1 length is 1.73 Å. The C-N and N-N bond lengths, in close agreement with structural data, all reveal a high degree of conjugation along the dithizonate backbone.

No specific tendency in bond angle size, or accuracy of the one program over the other with regard to bond angles, was observed. The biggest deviation is seen for the N1-Hg1-C2 bond angle. ADF calculated this angle to be 125°, while G03 gave a value of 121°, which is closer to the correct value of 118°. This bond involves the Hg-phenyl, which has less movement restrictions than the bidentate dithizonate ligand. In general, bond angles in both cases agreed closely to experimental values.

The slightly bent conformation of PhHgHDz (see Figure 3.23**a**), as compared to the planar MeHgHDz (**d**) may initially be explained both in terms of sterical constraints in the crystal structure, and possibly the small differences in group electronegativity between the phenyl ring ($\chi_{Ph}$ = 2.21) and the methyl group ($\chi_{Me}$ = 2.34). ADF optimised PhHgHDz to a similar bent molecular shape (**b**), but not for the methylmercury analogous (**e**), which might point towards an explanation in terms of electronic effects. ADF, an electron density approach, does take electronic effects better into account than the *ab initio* G03 approach. In both cases (**b** & **e**) ADF obviously gave a more accurate representation of the overall correct molecular shape than G03. Even the slightly twisted ligand phenyl ring in the case of the methylmercury compound (compare **e** to **d**) was more accurately optimised by ADF.

Otherwise, ligand phenyl rings are all co-planar with the ligand, which are indicative, together with relevant bond lengths, of a high degree of conjugation between the phenyls and the dithizonate Ph-N-N-C-N-N-Ph backbone. Hereby the phenyl $\pi$-orbitals may overlap with

adjacent unhybridised nitrogen p-orbitals directed vertically to the ligand plane. This phenomenon may further be seen in the shortened Ph-N bond lengths (N4-C14) of *ca* 1.40 Å. In general, C-N single bonds are typically 1.47 Å, while double bonds are 1.29 Å.

The following figure gives an illustration of the degree of planarity observed and calculated for both compounds under discussion.

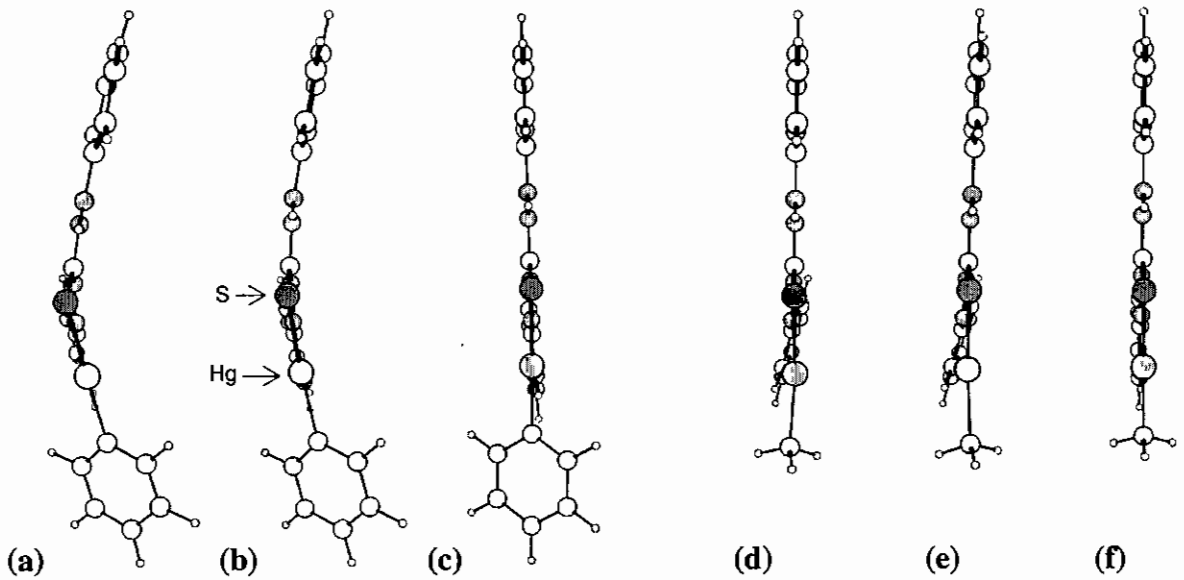


**Figure 3.23** Sideviews of the orange isomer of PhHgHDz (**a-c**) and MeHgHDz (**d-f**), based on X-ray crystal data (**a, d**) and geometry optimizations using the ADF(PW91)ZORA/TZP (**b, e**), and G03(B3LYP)CEP-31G (**c, f**) programs. In this regard, the better structural optimization obtained by ADF over G03 when compared to the crystal structure, is evident.

Evidence presented in this section illustrated the relatively high degree of accuracy attained by the use of quantum computational programs like ADF and G03 in geometry optimizations of mercury dithizonate complexes. Whether artificially generated atomic coordinates, or coordinates obtained from X-ray crystal data were used in the input files, optimization energies ended up being the same in both cases. Further structural data computed for related compounds may therefore now with confidence be presented at an extrapolative equally high degree of accuracy.

## 3.4.3. Dithizonatophenylmercury(II) – the blue isomer

No conclusive evidence has as yet been presented in the literature as far as the structure of the photo-excited blue metal dithizonate isomer is concerned. The intuitively predicted structure favoured by most, is the one presented in Paragraph 2.2.3 (p. 16). Figure 3.24**b** also shows the same structure (henceforth referred to as structure N(2)H), together with two other alternatives (**a** & **c**) also investigated by means of computational chemistry. In the first structure (**a**) the proton

is bonded to N4 ( Structure N(4)H ). This structure is in essence equivalent to the orange isomer, apart from 180° rotation around the C1–N3 bond. The third possibility (**c**) is related to Isomer **2** of the S-methylated mercury dithizonate complex, with the proton in the position where the methyl group is attached ( Structure S(1)H ). (See also Figure 3.28a)

Geometry optimizations using both the ADF and G03 programs were performed on all three possibilities and the energy of each optimised structure was calculated. A decision first had to be made with regard to the most viable (blue) structure, before anything could be said about the mechanism, orbitals involved in the photo-isomerisation reaction, and oscilator strengths (UV/visible spectra) of compound **20**.

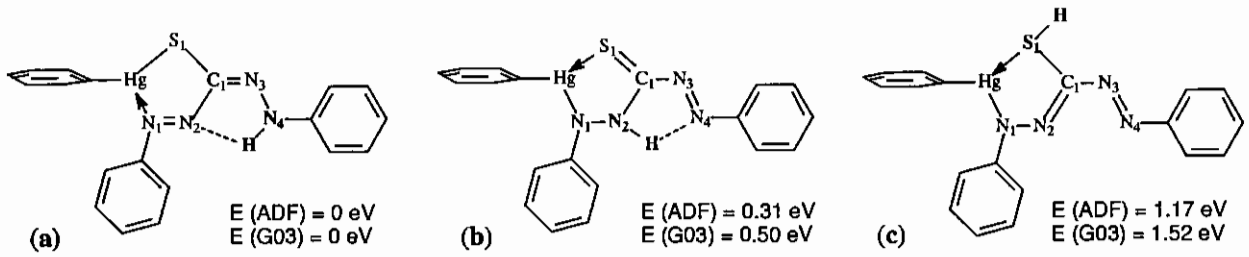


**Figure 3.24** Possible photo-excited structural isomers of PhHgHDz (blue), **20**. Structure **a** is labeled N(4)H in the text, structure **b** is N(2)H, and structure **c**, S(1)H. Optimization energy differences are indicated. The ADF computed energy for structure N(4)H (**a**) was -264.34 eV, while G03 optimised to -8711.55 eV.

Clearly, structure S(1)H has the highest energy, and is therefore immediately excluded as a possibility for the blue isomer of **20**. Structure N(2)H, the structure most widely supported by previous researchers, has the second highest energy. The ADF calculated relative energy is 0.31 eV (ADF), while G03 gave 0.50 eV, both significantly higher than the energy of structure N(4)H. In general, an energy difference larger than 0.3 eV is regarded as significant (personal communication, Prof. A. Ghosh, Quantum Chemistry, University of Tromso, Norway). Based on the above shown relative energies, the N(4)H structure of the blue isomer of **20** is therefore considered to be the most stable one.

Figure 3.25 gives the full numbering system of the ADF optimised blue isomer, structure N(4)H, and the corresponding orange isomer of compound **20**. Table 3.15 compares bond distances and angles of the ADF and G03 geometry optimised blue isomer with corresponding data of the orange isomer. Apart from two small differences, both the ADF and G03 bond angles and bond lengths of the blue isomer are in very close agreement with corresponding values in the orange isomer of **20**. The angle around the -C1–N3- axis of rotation, namely the N2-C1-N3 bond angle, increased by 6° on going from orange to the blue form. Furthermore, the Hg1-N1 bond length increased by about 0.05 Å.

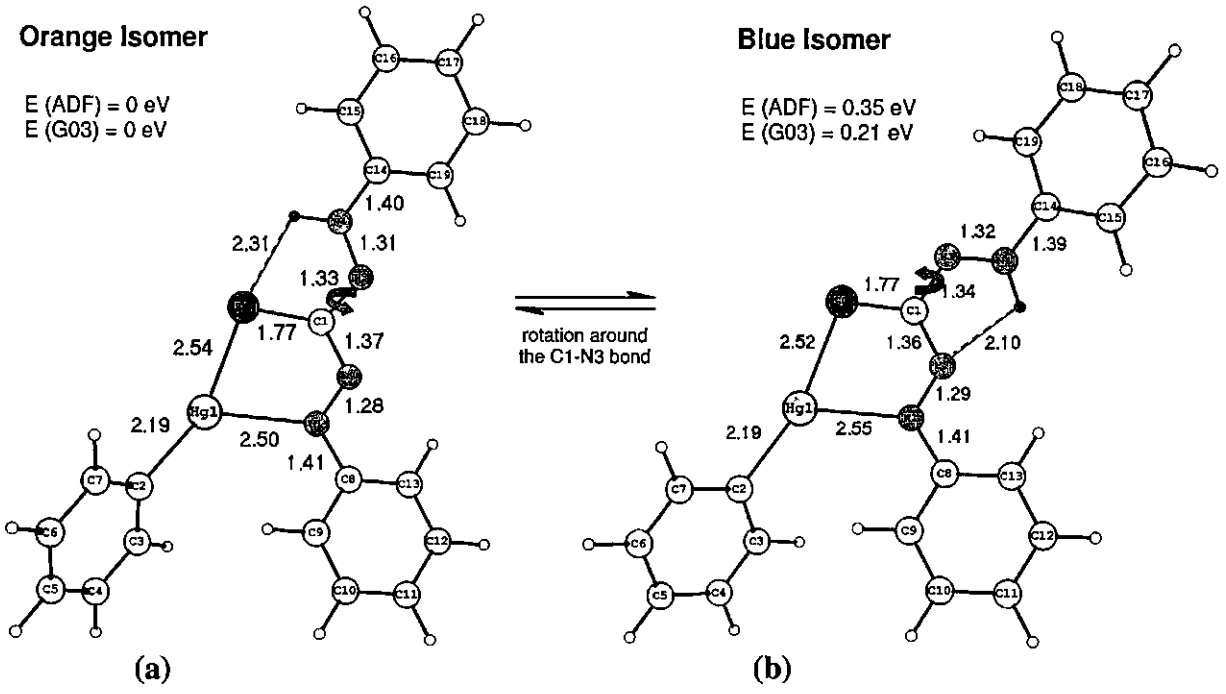


**Figure 3.25** ADF optimised geometries of (**a**) the orange isomer of dithizonatophenylmercury(II), PhHgHDz, and (**b**) the corresponding blue N(4)H isomer of **20**. Atom labelling, selected bond and hydrogen bond lengths, as well as optimization energy differences are indicated. The ADF computed energy for the orange isomer (**a**) was -264.69 eV while G03 optimised to -8711.76 eV. The structural difference between the blue and orange isomers involve rotation about the C1-N3 axis. This results in hydrogen bonding between N4–H---S1 in the orange form, and between N4–H---N2 in the blue form.

**Table 3.15** Calculated bond lengths and bond angles of the blue isomer, structure N(4)H, compared to corresponding data from the orange isomer of dithizonatophenylmercury(II), **20**.

| | Orange Isomer | | Blue Isomer (N(4)H) | |
|---|---|---|---|---|
| | **ADF** | **G03** | **ADF*** | **G03#** |
| **Bond lengths (Å)** | | | | |
| **Hg1-S1** | 2.54 | 2.50 | 2.52 | 2.47 |
| **Hg1-C2** | 2.19 | 2.13 | 2.19 | 2.13 |
| **Hg1-N1** | 2.50 | 2.59 | 2.55 | 2.67 |
| **N1-N2** | 1.28 | 1.31 | 1.29 | 1.31 |
| **N1-C8** | 1.41 | 1.44 | 1.41 | 1.44 |
| **N2-C1** | 1.37 | 1.40 | 1.36 | 1.40 |
| **C1-S1** | 1.77 | 1.86 | 1.77 | 1.85 |
| **C1-N3** | 1.33 | 1.34 | 1.34 | 1.34 |
| **N3-N4** | 1.31 | 1.35 | 1.32 | 1.36 |
| **N4-C14** | 1.40 | 1.42 | 1.39 | 1.42 |
| **Bond Angles (°)** | | | | |
| **Hg1-S1-C1** | 99 | 101 | 99 | 102 |
| **S1-Hg1-N1** | 75 | 76 | 75 | 76 |
| **N1-Hg1-C2** | 125 | 121 | 120 | 116 |
| **Hg1-N1-N2** | 120 | 119 | 117 | 116 |
| **N1-N2-C1** | 118 | 119 | 119 | 119 |
| **N2-C1-N3** | 111 | 112 | 117 | 118 |
| **C1-N3-N4** | 117 | 119 | 117 | 120 |

Geometry optimization times: * - *ca* 70 hrs, # - *ca* 7 hrs

The intramolecular distance between atoms N2 and N4 of 2.55 Å in the ADF computed blue isomer is 0.32 Å shorter than the distance of 2.87 Å between N4 and S1 in the orange isomer. The direct consequence is that, apart from the fact that N—H---N hydrogen bonds are much stronger than N—H---S hydrogen bonds, the hydrogen bonding distance in the blue form is shorter and therefore also for this reason much stronger. The ADF calculated hydrogen bond distance in the blue isomer is 2.10 Å. In the orange isomer the distance is 2.31 Å.

The degree of planarity to which the ADF and G03 programs optimised the N(4)H isomer of compound **20** followed the same trends observed during geometry optimizations of the orange isomer (see Figures 3.23 and 3.26). For reasons already mentioned the ADF geometry is considered to be the more realistic of the two in this regard.

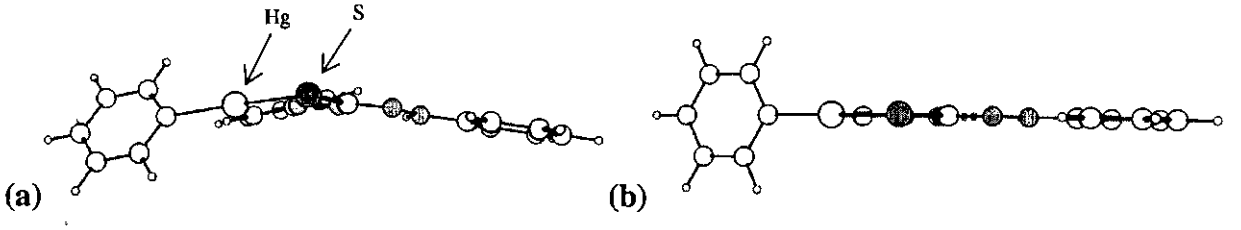


**Figure 3.26** Side views of (**a**) ADF and (**b**) G03 optimised structures of the N(4)H blue isomer of compound **20**.

## 3.4.4. Dithizonatophenylmercury(II) – the S-methyl derivative

The structures of both possible isomers of the solvatochromic compound, S-methyldithizonato-phenylmercury(II), **18**, were optimised utilizing the same computational methods that were used for the unmethylated parent compound, PhHgHDz, **20**. Table 3.16 gives the ADF and G03 optimised bond angles and bond lengths of both isomers.

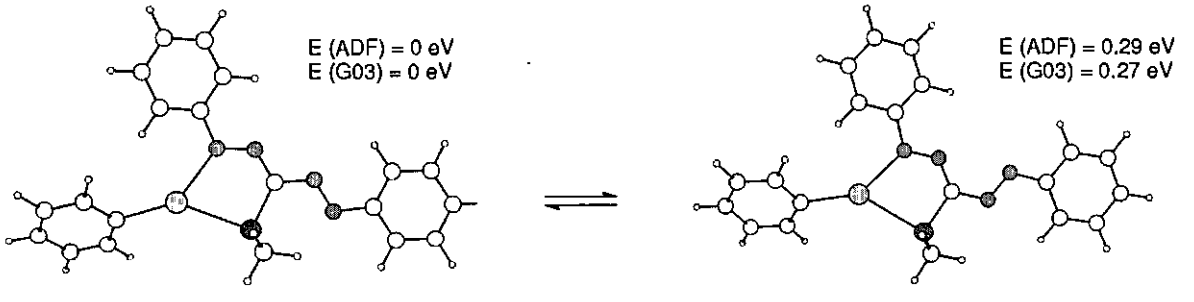


**Isomer 1** of compound **18**
(structurally equivalent to orange isomer of **20**.
See Figure 3.25)

**Isomer 2** of compound **18**
(structurally equivalent to blue isomer of **20**.
See Figure 3.25)

**Figure 3.27** (**a**) Possible isomers of S-methyldithizonatophenylmercury(II), PhHg(S-Me)Dz, **18**. Optimization energy differences are indicated. The ADF computed energy for Isomer **1** was -280.05 eV while G03 optimised to -8896.70 eV.

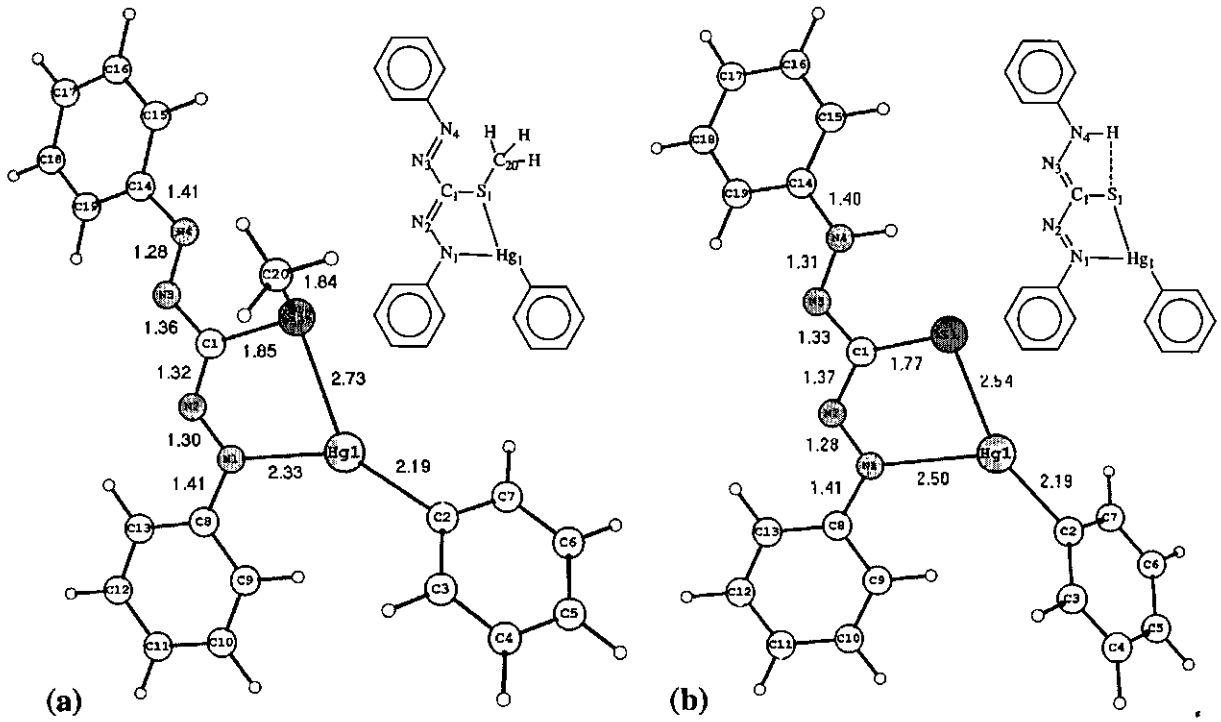


**Figure 3.28** ADF optimised structural geometries of (a) PhHg(S-Me)Dz, **18**, and (b) PhHgHDz, **20** (orange). Atom labelling, bond distances and bond orders are indicated.

**Table 3.16** Calculated bond lengths and bond angles of the two isomers of S-methyldithizonatophenylmercury(II), **18**, compared to the orange isomer of dithizonatophenylmercury(II), **20**.

| | Orange Isomer of compound 20 | | | Isomer 1 of compound 18 | | Isomer 2 of compound18 | |
|---|---|---|---|---|---|---|---|
| | Crystal | ADF* | G03# | ADF* | G03# | ADF | G03 |
| **Bond lengths (Å)** | | | | | | | |
| **Hg1-S1** | 2.37 | 2.54 | 2.50 | 2.74 | 2.95 | 2.78 | 2.99 |
| **Hg1-C2** | 2.10 | 2.19 | 2.13 | 2.19 | 2.11 | 2.19 | 2.11 |
| **Hg1-N1** | 2.65 | 2.50 | 2.59 | 2.33 | 2.17 | 2.31 | 2.16 |
| **N1-N2** | 1.28 | 1.28 | 1.31 | 1.30 | 1.35 | 1.30 | 1.36 |
| **N1-C8** | 1.43 | 1.41 | 1.44 | 1.41 | 1.45 | 1.41 | 1.45 |
| **N2-C1** | 1.42 | 1.37 | 1.40 | 1.32 | 1.32 | 1.31 | 1.31 |
| **C1-S1** | 1.73 | 1.77 | 1.86 | 1.85 | 1.90 | 1.82 | 1.89 |
| **C1-N3** | 1.30 | 1.33 | 1.34 | 1.36 | 1.40 | 1.38 | 1.42 |
| **N3-N4** | 1.34 | 1.31 | 1.35 | 1.28 | 1.31 | 1.28 | 1.31 |
| **N4-C14** | 1.40 | 1.40 | 1.42 | 1.41 | 1.44 | 1.41 | 1.44 |
| **S1-C20** | | | | 1.84 | 1.92 | 1.84 | 1.91 |
| **Bond Angles (°)** | | | | | | | |
| **Hg1-S1-C1** | 105 | 99 | 101 | 95 | 88 | 94 | 88 |
| **S1-Hg1-N1** | 74 | 75 | 76 | 74 | 76 | 74 | 75 |
| **N1-Hg1-C2** | 118 | 125 | 121 | 143 | 172 | 145 | 173 |
| **Hg1-N1-N2** | 115 | 120 | 119 | 124 | 126 | 124 | 126 |
| **N1-N2-C1** | 118 | 118 | 119 | 123 | 126 | 124 | 126 |
| **N2-C1-N3** | 125 | 111 | 112 | 124 | 115 | 125 | 124 |
| **C1-N3-N4** | 116 | 117 | 119 | 117 | 117 | 116 | 117 |
| **Hg1-S1-C20** | | | | 108 | 111 | 107 | 118 |

Geometry optimization times: * *ca* 180 hrs, # *ca* 7 hrs

Geometry optimization of **18** (Isomer **1**) was initiated from the X-ray atomic coordinates of compound **20**, with the addition of methyl to sulfur, while the imine dithizonate proton was omitted. The geometry of Isomer **2** was computed by starting from the optimised structure of Isomer **1**, but having the C1-N3 bond rotated by 180°. The fact that both programs optimised isomer **1** to a lower energy is an indication that isomer **1** represents the favoured configuration. The difference between the energies of the two isomers for the ADF calculations is 0.29 eV, while the difference for G03 is 0.27 eV. The energy differences are large enough to favour isomer **1** significantly, but not so large that the existence of isomer **2** can categorically be excluded under all circumstances. For the latter to be true one would expect $\Delta E$ values > 0.3 eV. It might therefore reasonably be concluded that under the right conditions both isomers might exist in solution. This will be further discussed in Paragraph 3.4.5.2.

The first aspect seen from the bond lengths of **18** in the above table is the dramatic increase in Hg1-S1 bond lengths as compared to compound **20**. ADF gave an increase of 0.18 Å, while G03 gave 0.45 Å. Hg1-N1 bond lengths, on the other hand, decreased in distance. With the methyl group bonded to sulfur a consequent weakening in the Hg1-S1 bond is expected, which is compensated for by a stronger Hg1-N1 bond. With the replacement of the imine or sulfur proton with a methyl group, a larger degree of double bond character in PhHg(S-Me)Dz moved from N1-N2 to N2-C1, as well as from C1-N3 to N3-N4. Single bond distances are nevertheless shorter than the typical C-N (1.47 Å) and N-N (1.45 Å) bond lengths, while double bonds are longer than the typical C=N (1.29 Å) and N=N (1.25 Å) bond distances. This indicates that also the methylated derivative is subject to a degree of electron delocalization along the ligand backbone.

In molecule **18**, PhHg(S-Me)Dz, there is a striking similarity between ligand bond lengths of the two isomers, **1** and **2** (See Table 3.16). Due to the fact that the C1-N3 bond (ADF: 1.36 Å, G03: 1.40 Å) of the solvatochromic compound, **18**, has greater single bond character than in the photochromic compound **20**, PhHgHDz, free rotation around this bond may more readily take place when **18** is dissolved than in the case of the corresponding double bond (1.30 Å) of the photochromic parent compound, **20**. This, in part, explains why **18** is solvatochromic (colour dependent on medium), and why it does not require photochemical excitation, as with **20**, for a colour change (isomerisation) to occur. The latter is to be discussed extensively in Paragraph 3.4.5.

Bond angles of ADF and G03 are in close agreement, as far as the S-methyldithizonate ligand is concerned. The same is true for a comparison between the two isomers. The one profound discrepancy observed in all computations involves the Hg-phenyl, where the N1-Hg1-C2 G03-calculated bond angle was almost 30° larger than the corresponding ADF angle. Both programs

nevertheless are consistent with regard to bending of the *trans* Hg-phenyl group towards the sulfur atom.

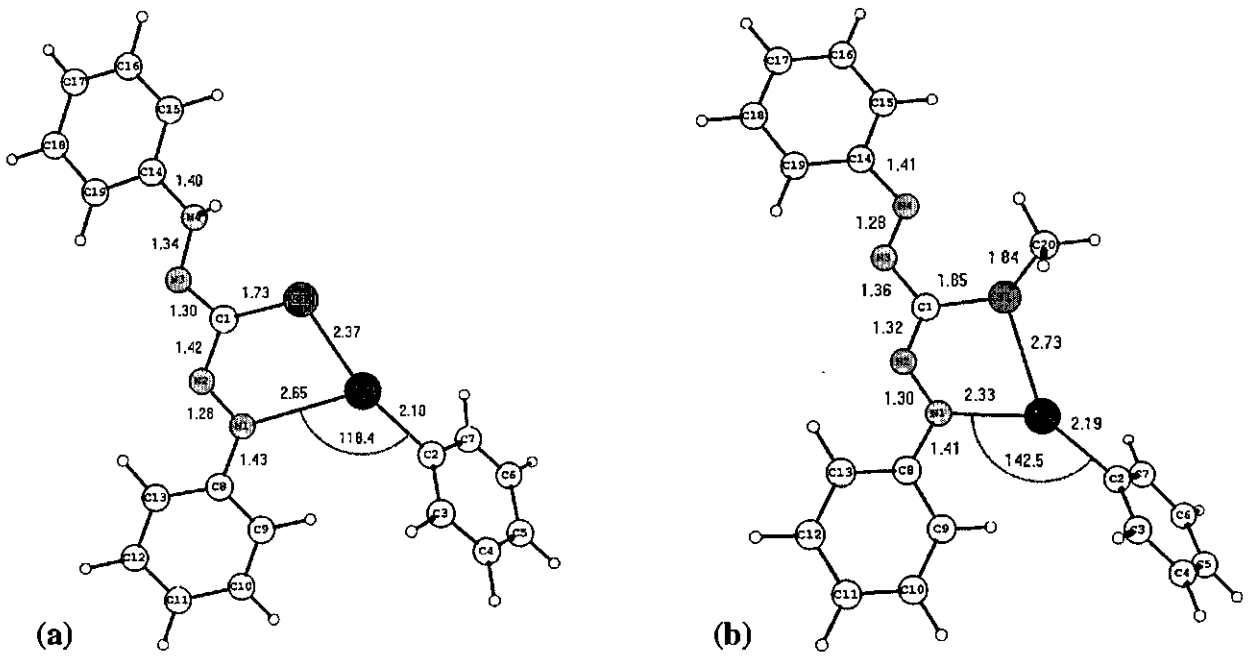


**Figure 3.29** (**a**) X-ray crystal structure of the orange isomer of PhHgHDz, **20**, and (**b**) the ADF optimised structure of PhHg(S-Me)Dz, **18** (Isomer **1**). Bond lengths and the change in N1-Hg1-C2 bond angle are illustrated. Figure 3.28 compares the *calculated* structure of orange **20** with the *calculated* structure of **18**.

The weakening of the Hg1-S1 bond, as compared to **20**, and the strengthening of the Hg1-N1 bond went hand in hand with a change of a largely trigonal planar configuration around mercury towards a linear configuration for **18**. The G03 N1-Hg1-C2 bond angle (172°) shows almost complete linearity, as opposed to the ADF bond angle of 143°. In compound **20** this corresponding G03 bond angle is 121°.

Apart from having shed light on some structural aspects, to an extrapolated average accuracy of *ca* 97 %, geometry optimizations of compound **18** and its isomers now also serve to reasonably predict the geometry of the envisaged, but yet, hypothetical mercury dithizonate – cobalt porphyrin complex, as depicted in the Introduction of Chapter 3. This extrapolation is made by assuming the cobalt porphyrin, when it binds to S1, will be approximately situated in 3-dimensional space where the methyl group of PhHg(S-Me)Dz is. The first feature that stands out is the fact that the methyl group (which is bonded in the position where cobalt porphyrin is also to be bonded) lies almost perpendicular to the largely flat plane of the mercury complex (See Figure 3.28a). The Hg1-S1-C20 bond angle optimised to 108°, which was expected due to the tetrahedral $3s^2 3p^4$ valence orbital arrangement around the sulfur atom. This "sideways" staggered bonding pattern is therefore also expected for the coordination of PhHgHDz via sulfur to a cobalt porphyrin complex.

The premise of this entire investigation, of which this dissertation forms only the onset, is that the blue isomer of compound **20** would be sterically more favourable than the orange isomer with regard to coordination to a large planar complex like a metal porphyrin. Figure 3.30 (bottom), by means of the model compound, **18**, illustrates how that is indeed the case. In Figure 3.30 the methyl carbon (C20) has been replaced with a hypothetical cobalt porphyrin ligand lying perpendicular to the plane of the paper, as represented by plane **a**. Isomer **1**, which is sterically equivalent to the orange form of **20**, has its H(C16) proton almost touching plane **a**, i.e. the hypothetical axially coordinated porphyrin ligand. Isomer **2**, which is sterically equivalent to the blue form of PhHgHDz, **20**, has the closest atom, H(C18), due to isomerisation around the C1-N3 bond , removed from plane **a** by a distance of *ca* 0.88 Å, i.e. the distance between planes **a** and **b**.

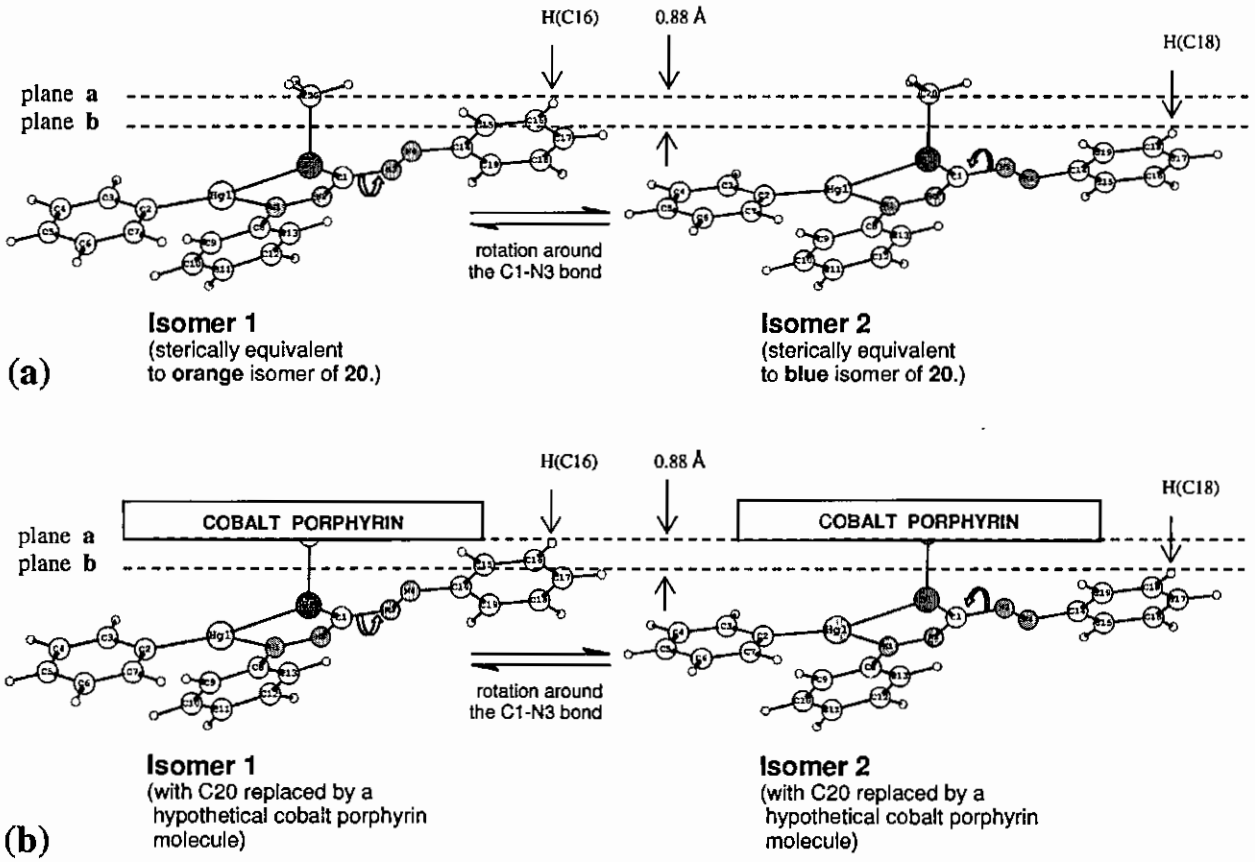


**Figure 3.30** (a) ADF optimised structural isomers of PhHg(S-Me)Dz. Plane **a** represents the plane which bisects the C20 atom of the $CH_3$ group that is bound to S1. In Isomer **1**, plane **a** also lies adjacent to the closest atom of the dithizonate backbone of the structural equivalent of **18** to the *orange* form of **20**, namely the H-atom on C16. In Isomer **2**, plane **b** lies adjacent to the closest atom of the structural equivalent of **18** to the *blue* form of **20**, namely the H-atom on C18. Illustration (**b**) corresponds to (**a**), but with the $CH_3$ group on S1 replaced by a hypothetical cobalt porphyrin running through plane **a**. The porphyrin is not drawn according to scale, but the cobalt center is assumed to ligate axially to S1 in much the same way as C20 is bonded to S1. For this illustration the Co-S1 bond distance was assumed to be the same as the calculated C20-S1 bond distance (1.84 Å), although porphyrin Co-S bond distances has been shown to be 2.35 Å.[217]

From the above illustration it can therefore clearly be seen that the blue isomer of **20**, as represented by Isomer **2** of compound **18**, may well be the sterically favoured isomer for coordination to cobalt porphyrins. This observation is based solely on ADF optimised structural parameters of **18**, not taking into account that the phenyl ring (of which H(C18) forms part of) might rotate slightly, or that the C20-S1-C1 bond angle might be distorted, which both may increase the measured distance of 0.88 Å even further.

## 3.4.5. A Possible Mechanism for Photo-Induced Isomerisation

### 3.4.5.1. Introduction

At the basis of photochromic reactions lies the absorption of light photons of specific energies by the highest occupied molecular orbitals in a molecule. The absorbed quanta supply the energy required to overcome the energy barrier which lies between the initial ground state (global molecular energy minimum) and a new state of slightly higher energy (local minimum). Experimental UV/visible spectra supply the researcher with an indication of the energies required for such photo-transformations to take place. Calculations of the discrete energies underlying the experimental UV/visible spectra of the different possible isomers of compound **20** are reported in this section. From the optimised parameter sets of the ground and excited states, the molecular orbitals of each isomer could be constructed, which aided in finding the reason why rotation is possible in the photo-excited state of the dithizonate complex, as opposed to its ground state.

Time Dependent Density Functional Theory (TDDFT), as implemented in the ADF version 2004.01, was used to calculate excitation energies. To validate the accuracy of the TDDFT(PW91)/TZP method, simpler, but related known compounds were investigated with regard to their calculated and experimentally observed UV/visible spectra. Therefore, before considering dithizonatophenylmercury(II), **20**, itself, computed electronic transitions of solvatochromic (colour determined by type of solvent) uncomplexed dithizone, **16**, as well as S-methyldithizonatophenylmercury(II), **18**, were compared to the experimental spectra of these compounds. Dithizone was selected because, like PhHgHDz, **20**, it also has the potential to isomerise, while its protons are involved in hydrogen bonding between nitrogen and sulfur atoms. Compound **18**, on the other hand, may isomerise, but without any protons and the consequent possibility of intramolecular proton transfer along the ligand backbone.

### 3.4.5.2. TDDFT calculations of Dithizone and S-methyldithizonatophenyl-mercury(II)

Figures 3.31 **a-d** give both the calculated and super-imposed experimentally obtained UV/visible spectra of the four isomers of free dithizone that had been considered. Dilute methanol solutions of dithizone are orange, absorbing at 466 nm, while dichloromethane solutions are blue-green, with absorbance peaks at 441 and 608 nm. Hutton argued that there is no reason for a single species in solution not to give two strong absorption bands.[198] Although being in support of one structural form in solution (**a**), as is the case for the solid, he nevertheless expressed the need for properly explaining the marked solvatochromism of dithizone. The computational results of this study clearly revealed the existence of different tautomers (two or more structural isomers that exist in equilibrium and are readily converted from one isomeric form to another) in solution. Not only is there good agreement between calculated and observed peak energies (wavelengths) of dithizone solutions, but oscillator strengths also corresponded remarkably.

Before attempting to be more specific, it should be emphasised that computations simulate the gas phase. Absorbance maxima in dithizone are highly medium dependent. One may therefore safely argue that the relative energies (E) of the gas-phase optimizations and the corresponding spectra, as indicated in Figure 3.31, for each proposed dithizone structure, are not in an absolute sense indicative of the favoured isomeric form of dithizone in solution, but that it may nevertheless strongly approximate it.

Since the calculated and experimentally determined electronic spectra in methanol for the dithizone structures shown in Figure 3.31 **a**, **b** and **c** all agree well, one may consider these structures as possible tautomers of dithizone in methanol solutions. However, based on the fact that the energy of **a** (-195.79 eV) is the lowest of the four structures, while **b** (0.34 eV higher than **a**) and **c** (0.63 eV higher than **a**) are both significantly higher energy structures, **a** must be regarded as the *dominant* isomer in methanol solution. The strongest oscillator peak, lying at 451 nm, is in close agreement with the experimental peak maximum of 466 nm. The strongest calculated peak of **b** lies at 473 nm, which is also close to 466 nm. The two other strong peaks, at 381 and 398 nm, that coincide with the experimentally determined absorbance minimum at 380 nm implies **b** makes a contribution to the spectrum. If it did not, the experimental minimum at 380 nm would have zero absorbance rather than a finite value. That isomer **c** must also make a small contribution to the spectrum of dithizone is evident by the strong oscillator peak at 355 nm which corresponds to the experimentally determined low wavelength shoulder below 350 nm.

A striking agreement of the calculated spectra of dithizone with the experimentally determined spectrum in dichloromethane as solvent, is shown in Figure. 3.31**d**.

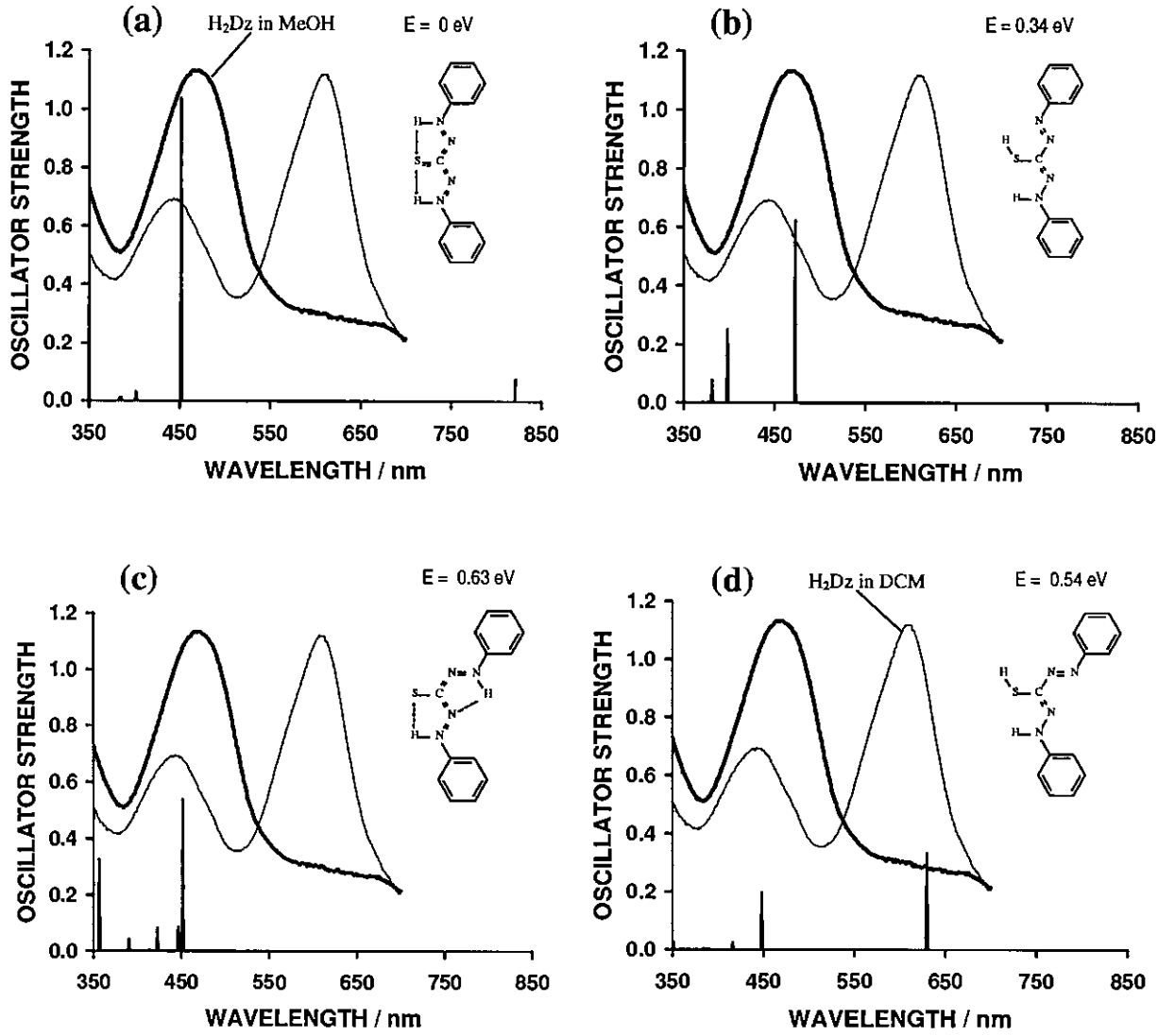


**Figure 3.31** ADF calculated electronic spectra (bars) and experimentally determined spectra (continuous wave lines) [$\lambda_{max}$(MeOH) = 466 nm (–), $\lambda_{max}$(DCM) = 441 & 608 nm (–)] of different possible isomers of dithizone, $H_2Dz$. Hydrogen bonding patterns and optimization energy differences are indicated. The relative molecular energy of the isomer shown in **a** is -195.79 eV. Experimental spectra showed no peaks between 700 & 850 nm.

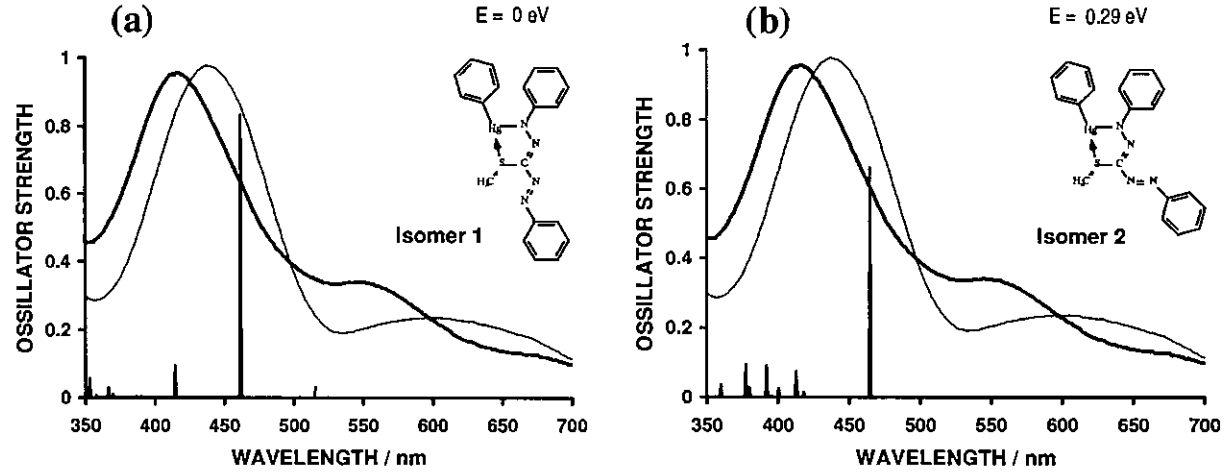


**Figure 3.32** ADF calculated electronic spectra (bars) and experimental spectra (lines) [$\lambda_{max}$(MeOH) = 415 nm (–), $\lambda_{max}$(DCM) = 441 & 620 nm (–)] of two possible isomers of S-methyldithizonatophenylmercury(II), PhHg(S-Me)Dz. Hydrogen bonding patterns and optimization energy differences are indicated. The relative energy of isomer **1** was calculated to be -280.05 eV.

Oscillator peak positions were calculated to be at 448 nm (exp.: 441nm) and 630 nm (exp.: 608 nm). If the 630 nm oscillator and 608 nm experimental peaks are scaled to a value of 1, then the value for the 448 nm oscillator peak is 0.59 and the 441 nm experimental peak is 0.61. This is in extraordinary good agreement with each other. Computed evidence therefore indicates structure **d** as by far the dominant species in dichloromethane solution.

Figure 3.32 above gives both the calculated and superimposed experimental electronic spectra of the two possible isomers of the second solvatochromic compound, PhHg(S-Me)Dz, **18**. The calculated absorbance spectra for both isomers of **18** show only one strong oscillator peak that red-shifts by 3 nm in going from isomer **1** to isomer **2** (462 to 465 nm). The experimental absorbance maximum of **18** red-shifts by 26 nm from 415 nm in methanol to 441 nm in dichloromethane. The same trend was observed for dithizone. In dithizone (Figure 3.31**d**) both the calculated peaks were found at longer wavelengths (7 and 22 nm) than the observed experimental peaks in dichloromethane. The same was also found for compound **18**, with the calculated peak being 21 nm higher than the experimentally observed peak in dichloromethane. TDDFT calculated electronic spectra of the proposed $H_2Dz$ and PhHg(S-Me)Dz isomers presented above are in strong agreement with the solvatochromic properties of these compounds.

Based on results from the above two test compounds it may therefore safely be concluded that TDDFT computations of electronic spectra are to a large degree accurate for the class of compounds here investigated, and that additional structural information can readily be extracted from data thus acquired.

### 3.4.5.3. TDDFT calculations of Dithizonatophenylmercury(II)

Figure 3.33 gives the calculated and super-imposed experimental electronic spectra of the orange and blue isomers of the photochromic compound, PhHgHDz, **20**. Fair agreement between the calculated and experimental spectra is observed at especially the lower wavelengths, i.e. below the isosbestic point of 381 nm. At these wavelengths there is an increase in both oscillator strength and absorbance in going from the orange to the blue form. Also at the higher wavelength region, the two oscillator peaks appearing at 470 and 500 nm agree closely with the two small shoulders (*ca* 450 and 495 nm) observed in the experimental spectrum of the blue isomer (Figure 3.33**b**).

The peak appearing at 777 nm is at much lower energy than the observed maximum at 587 nm. This phenomenon may be explained on basis of the fact that the calculated spectrum is that of the ground state of the blue isomer, where-as the blue form probably is an excited state species. All attempts to calculate the electronic spectrum of the excited state blue isomer of PhHgHDz failed. If the blue form is indeed an excited state species, the 777 nm peak is expected to fall away,

since the HOMO orbital will in fact be empty, while the LUMO orbital will be occupied (orbitals to be discussed in more detail in paragraph 3.4.5.4.). The HOMO-1 orbital is then becoming the next possible origin for the electronic transition responsible for the experimental absorbance peak maximum observed at 587 nm. The small calculated HOMO-1 peak lies at 582 nm (Figure 3.33**b**), and is indeed agreeing remarkably well with the observed experimental maximum of 587 nm. The HOMO-2 peak is also lying very close to the HOMO-1 peak, namely at 564 nm. Not only may these two close lying electronic transitions be responsible for the broadened blue isomer absorbance peak, as compared to the orange, but these orbitals are also rather similar in geometry and with regard to the atoms they involve (see Figure 3.35 or the extended graphical depictions of orbitals in Appendix 3, Table A3-19, p.XXXV).

With no absorbance peak indeed appearing in the experimentally observed spectrum around or close to 777 nm, the above observations may therefore be presented as the first trace of evidence in favour of the blue form of PhHgHDz existing in the excited state.

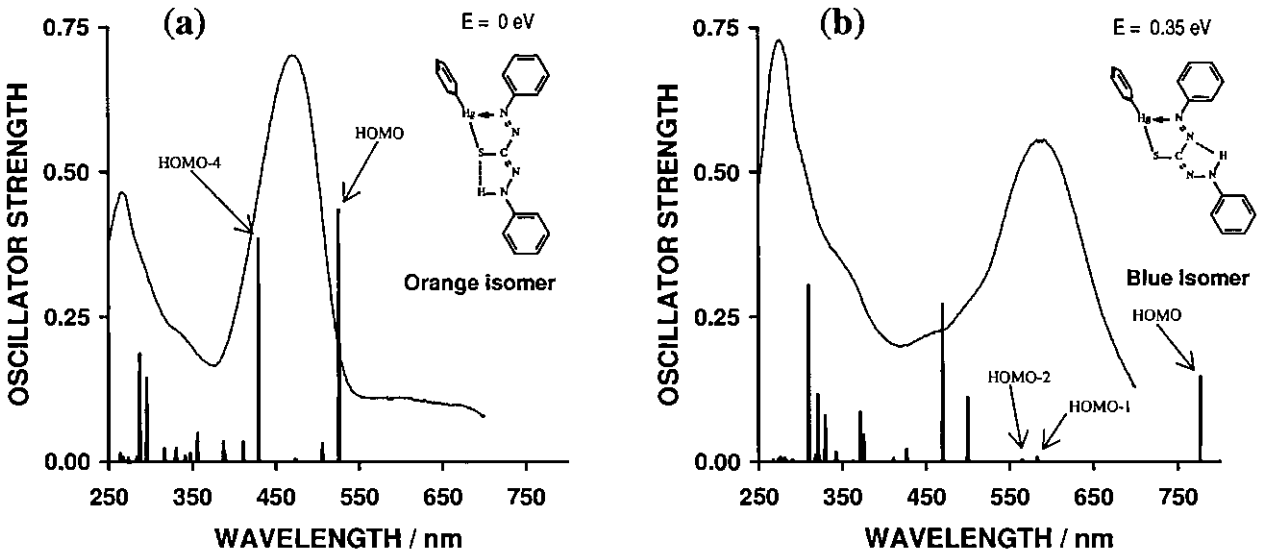


**Figure 3.33** ADF calculated electronic spectra (bars) and experimental spectra (lines) of the isomers of dithizonato-phenylmercury(II), PhHgHDz. (**a**) Orange isomer [$\lambda_{max}$(DCM) = 264 & 467 nm]. (**b**) Blue isomer - Structure N(4)H [$\lambda_{max}$(DCM) = 272 & 583 nm]. Hydrogen bonding patterns and optimization energy differences are indicated. The relative molecular energy of the orange isomer is -264.69 eV. Oscillator peaks related to selected orbitals are indicated. If the blue isomer is to exist in the excited state, the HOMO oscillator peak will fall away since it will then be empty, while the LUMO orbital will be filled. Experimental spectra showed no peaks between 700 & 850 nm.

The strong oscillator peak calculated for the orange isomer, appearing at 430 nm, is related to the HOMO-4 orbital, while the peak at 526 nm relates to the HOMO orbital. The experimentally observed peak at 467 nm may be the resultant of these two oscillator peaks. The peak appearing at 526 nm lies 59 nm higher than the experimental peak maximum of 467 nm. It alone may also be the sole source of the experimental peak at 467 nm. Although the deviation is the highest

here, the red-shift is consistent with the general trend observed in this study for calculated peaks to lie at lower energies (longer λ) than what is experimentally observed. Not only were these red-shifts seen for $H_2Dz$ and PhHg(S-Me)Dz, but also for all the oscillator peaks of both the orange and blue isomers of PhHgHDz.

### 3.4.5.4. Electronic structure of Dithizonatophenylmercury(II)

Figure 3.34 graphically illustrates the shapes of the highest occupied (HOMO) and lowest unoccupied (LUMO) molecular orbitals associated with the orange and blue ground and excited state isomers of compound **20**, PhHgHDz. The suggested photo-induced isomerisation path and the electronic occupancies of the accompanying states resulting from this study are indicated.

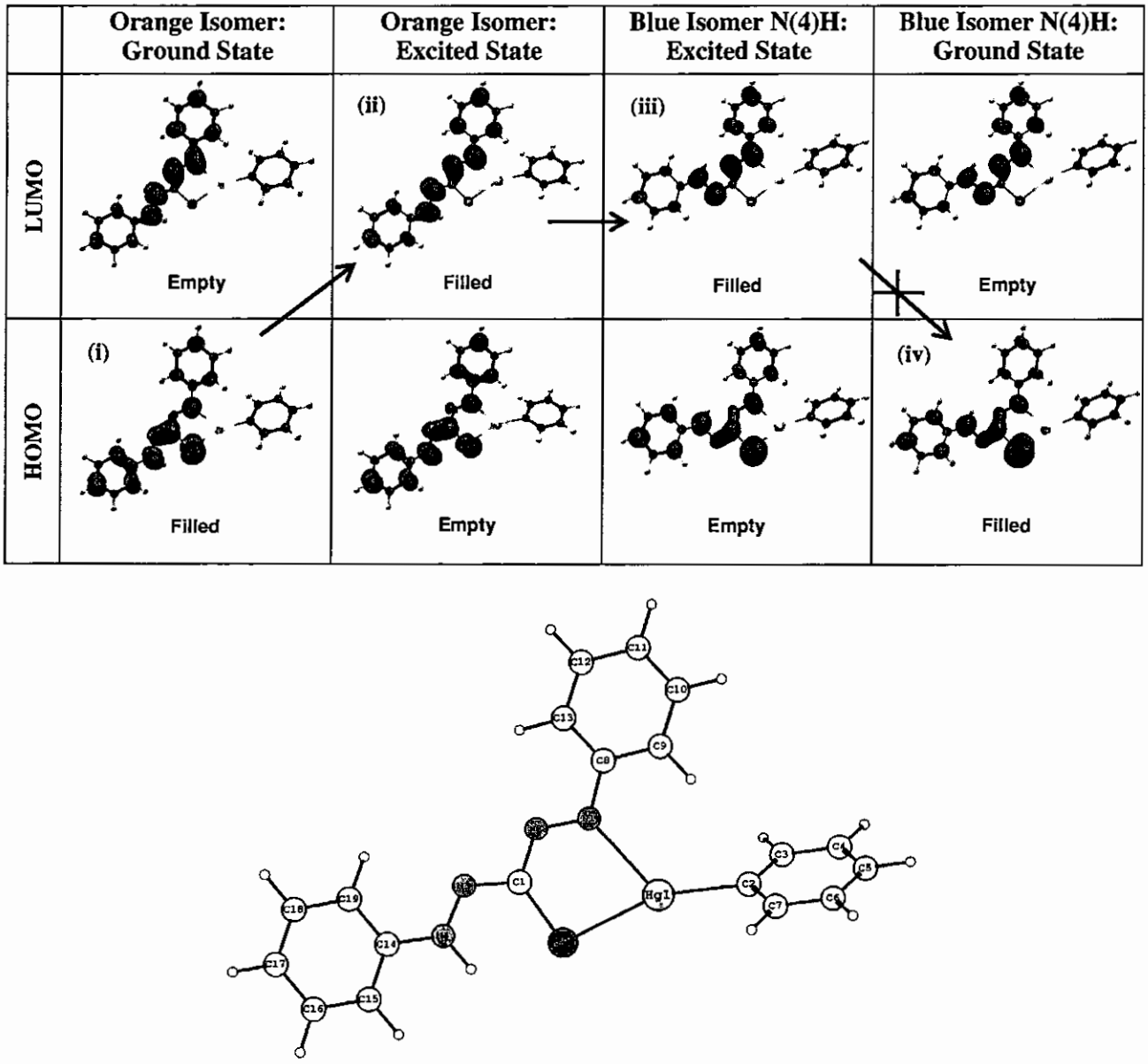


**Figure 3.34** Above: Selected molecular orbitals associated with dithizonatophenylmercury(II), **20**. Bonding and anti-bonding orbitals are differentiated by colour. Below: Atom labeling of PhHgHDz.

On inspection of all the HOMO to HOMO-7 orange ground state orbitals (see Appendix 3 for an expanded list, Table A3-19) the outstanding feature is that only the HOMO and LUMO orbitals involve the –C1=N3– bond around which rotation is to take place during photo-isomerisation. Both orbitals stretch along the entire length of the ligand, i.e. including the ligand backbone as well as both phenyl rings. This dispersion of the HOMO orbital is indicative of the fact that the phenyls sustain a molecular orbital of the right energy to allow photochromism to take place. The result is consistent with experimental observations that substitution of one or both phenyls by methyl or other groups prevents photochromism from taking place.

The second important feature to be noted is the appearance of double and single bonds. The orange ground state (Figure 3.34**i**) clearly shows the strong interaction (double bond caused by overlapping of π-orbitals) between C1 and N3. The excited state (LUMO, **ii** ), on the other hand, has anti-bonding orbitals neighbouring the bonding orbitals between C1 and N3, i.e. being out of phase. Photochemical excitation transformed the –C1=N3– double bond into a single bond, allowing free rotation to take place. The blue ground state (HOMO, **iv** ), as opposed to the blue excited state (LUMO, **iii** ) has the –C1=N3– double bond forming again. Such a structure would not be consistent with the ease with which the thermal radiationless back reaction takes place. The implication would be that the double bond has to gain energy from somewhere after light irradiation is stopped, in order for the –C1=N3– double bond of the ground state blue form to degenerate into a single bond before free rotation back to the orange isomer around this bond can again take place. Based on the fact that the blue PhHgHDz isomer oscillator peak at 777 nm could not be experimentally detected, it was suggested in paragraph 3.4.5.3 that the blue isomer exists in the excited state and does not relax to its corresponding ground state. The result described above, namely that the blue form probably exists in the excited state based on orbital investigations is therefore mutually consistent with the conclusion drawn based on evidence from the calculated electronic spectra.

Further evidence in favour of the blue excited state, based on the requirement of a –C1–N3– single bond, as is the case in the LUMO structure (**iii**) of the blue isomer, can be found upon quantifying the energy requirements for the possible transitions. Figure 3.35 gives a summary of the relative energies (eV) of the top five occupied (HOMO) and the lowest unoccupied (LUMO) molecular orbitals of both isomers. As seen from the diagram, the energy required to raise the orange ground state isomer (HOMO) to its excited state (LUMO), is about 1.63 eV. From this point rotation may take place, with a drop in energy of about 0.17 eV in going from the orange to the blue LUMO orbital. If the system is to relax further it would mean an additional drop of 1.11 eV to the blue ground state. This would give a new ground state that is 0.35 eV higher in energy than the original orange form.

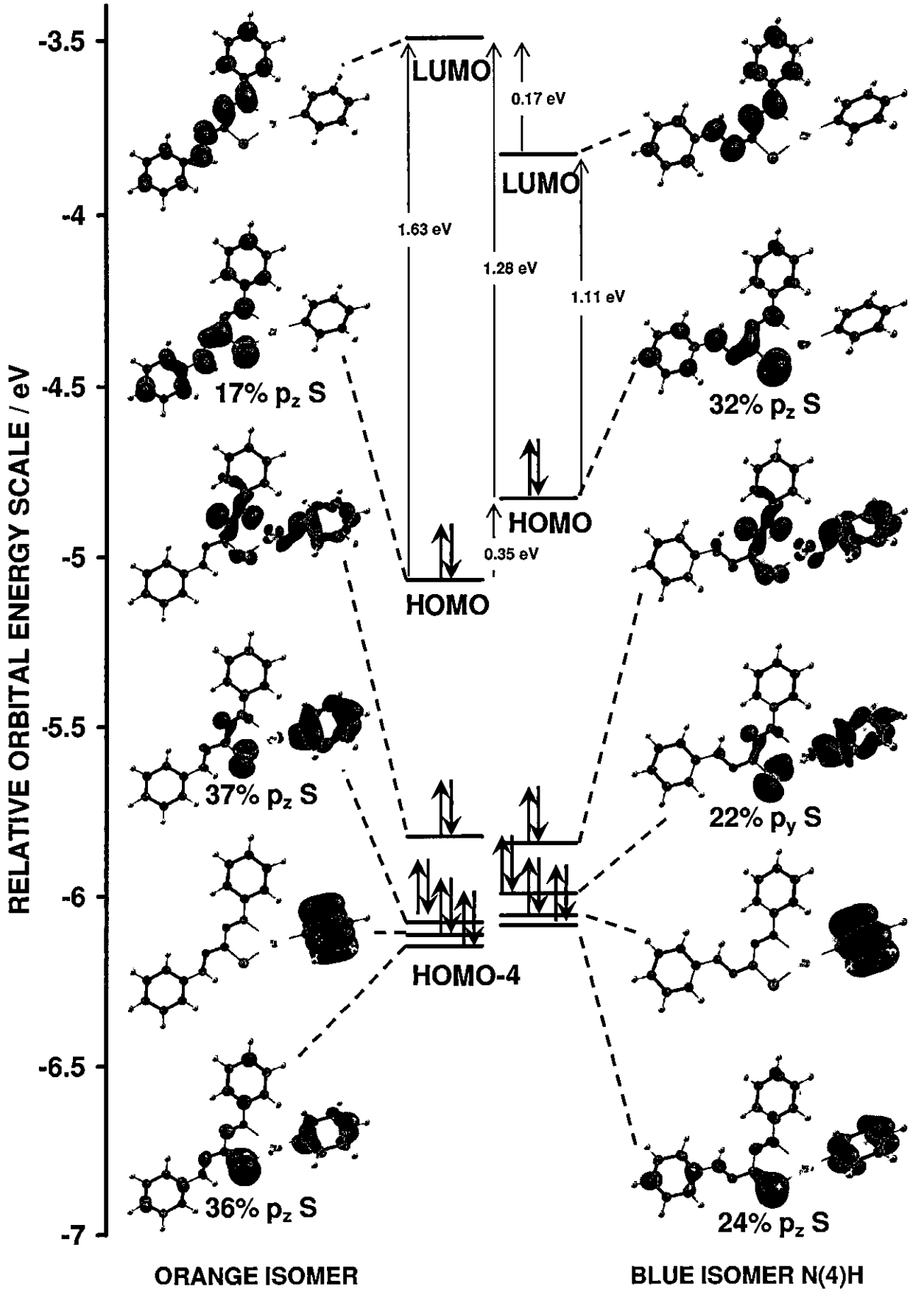


**Figure 3.35** Correlation diagram for the top five occupied (HOMO) and the lowest unoccupied (LUMO) molecular orbitals (MO's) of dithizonatophenylmercury(II), **20**, with the orbital energy scale in electronvolt (eV).

In further support of the suggestion that the blue form exists in the excited state, it is now further argued that the energy required (1.28 eV) for the reverse reaction to take place, i.e. to overcome the energy barrier, is too high to occur without external excitation. (The back reaction is experimentally observed to take place at low temperatures and in complete exclusion of light.) If instead the blue isomer is to exist in its excited state, the energy that has to be acquired is only the difference between the blue and orange LUMO orbitals, namely 0.17 eV. This calculated energy difference is insignificant as compared to the blue HOMO to orange LUMO transition requiring 1.28 eV, and is it therefore once again plausible to suggest that the ground state blue form may be excluded as the correct state. The LUMO blue state fulfills energy requirements of experimentally observed colour changes much better.

### 3.4.5.5. Rotation of Dithizonatophenylmercury(II) from the Orange to the Blue Isomeric Forms

Figure 3.36(**a**) relates both the ground and excited state energies with the dihedral angle, i.e. the angle through which rotation takes place around the –C1–N3– bond during the photo-induced isomerisation of PhHgHDz, **20** from the orange to the blue form. Figure 3.36(**b**) relates the dihedral angle to the length of the –C1–N3– bond. ADF geometry optimizations of both the ground and excited states of compound **20** were done at rotational angle increments of approximately 0°, 45°, 90°, 135° and 180°.

**Table 3.17** Calculated ground and excited state energies, as well as C1-N3 bond lengths for selected angles of rotation during photochromic isomerisation of compound **20**.

| Ground State | | | Vertical Excitation | Excited State Geometry Relaxed | |
|---|---|---|---|---|---|
| **Dihedral angle (S1 C1 N3 N4)/ °** | **Energy / eV** | ***d* (C1, N3) / Å** | **Energy / eV** | **Dihedral angle (S1 C1 N3 N4)/ °** | ***d* (C1, N3) / Å** |
| 1.4 | -264.69 | 1.3313 | -263.06 | -2.3 | 1.3702 |
| 44.7 | -264.18 | 1.3433 | -262.93 | 44.9 | 1.3859 |
| 89.7 | -262.93 | 1.4053 | -262.82 | *- | - |
| 135.2 | -264.00 | 1.3522 | -262.97 | 135.1 | 1.3924 |
| 178.3 | -264.34 | 1.3395 | -263.23 | 179.1 | 1.3655 |

* ADF optimization of the geometry relaxed excited state failed at the 90° dihedral angle.

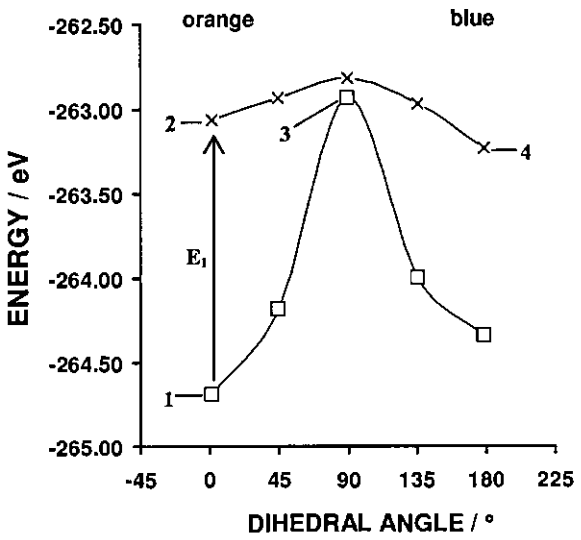


**Figure 3.36** (a) Correlation of the isomerisation dihedral angle of PhHgHDz with the corresponding ground state (□) and excited state (×) energies.

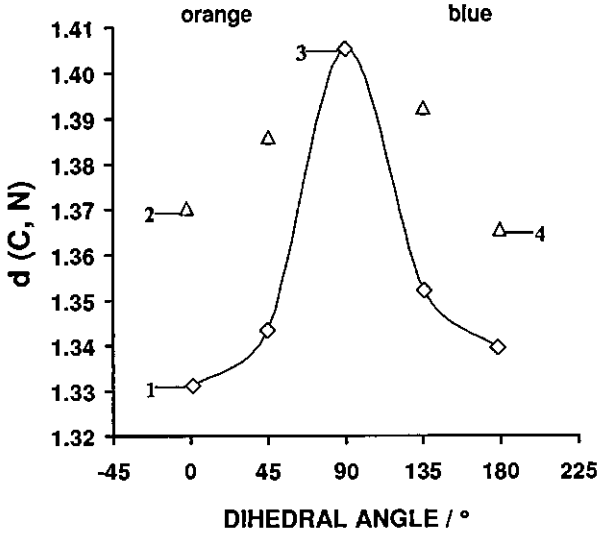


**Figure 3.36** (b) Correlation of the isomerisation dihedral angle of PhHgHDz with both the ground state (◊) and the excited state (Δ) C1–N3 bond lengths (Å).

In order for photochromism (photo-induced isomerisation) to take place at all, the energy of excitation ($E_I$, **1**→**2**, Fig.3.36a) should at least be equal to, or more than the ground state rotational peak (**3**) energy of the molecule. The calculated data above is in very good agreement with this requirement, allowing for computational error. The ground state energy of compound **20** peaks at a rotational angle of 90° (**3**), with an energy of -262.93 eV, while the energy of the vertically excited state molecule (**2**) is -263.06 eV. The difference of 0.13 eV is not meaningful. (A minimum of 0.3 eV energy difference is regarded as meaningful.) For all practical purposes $E_I$ (vertical excitation of the orange isomer ground state / HOMO, to its excited state / LUMO) may thus be considered as indicative of the barrier peak energy.

In view of the above and preceding arguments the following path is now proposed for the reversible photochromic reaction of PhHgHDz. (Compare Figure 3.34, page 124.)

Forwards reaction: (**1**, 0°, orange ) → (**2**, 0° ) → (**3**, 90° ) → (**4**, 180°, blue ), and

back reaction: (**4**, 180°, blue ) → (**3**, 90° ) → (**1**, 0°, orange )

In Figure 3.36(b) a striking agreement is seen between the length of the -C1–N3- bond and the energy curve in Figure 3.36(a). Photo-induced excitation results in the degeneration of the π -C1=N3- double bond, with immediate elongation from 1.33 to 1.37 Å. This is only about a 50 % increase in bond length of what is required at 90°, where the -C1–N3- bond reaches a length of more than 1.40 Å. Single electron excitation, however, provides sufficient energy to overcome the rotational energy barrier, as seen in Figure 3.36(a).

## 3.4.6. Co(III) Porphyrin – PhHgHDz adducts

As a provisional final test for the viability of using compound **20** together with cobalt(III) porphyrin as a molecular switch, two last geometry optimizations have been done. The purpose was to, (i) explore the possible existence of a yet unknown Co(III) porphyrin - PhHgHDz adduct, and (ii) to see if the energy of the blue isomer axially ligated to Co(III) porphyrin will indeed be lower or at least in the same order than that of the orange isomer. This was expected, based on steric considerations alone, as was seen from the crude model compound, PhHg(S-Me)Dz, in Figure 3.30. In order to try and save on computational time a porphyrin without any peripheral substituents was used. The geometry optimizations nevertheless took almost 2000 hours each. Figure 3.37 represents the two optimised geometries, including their corresponding energies.

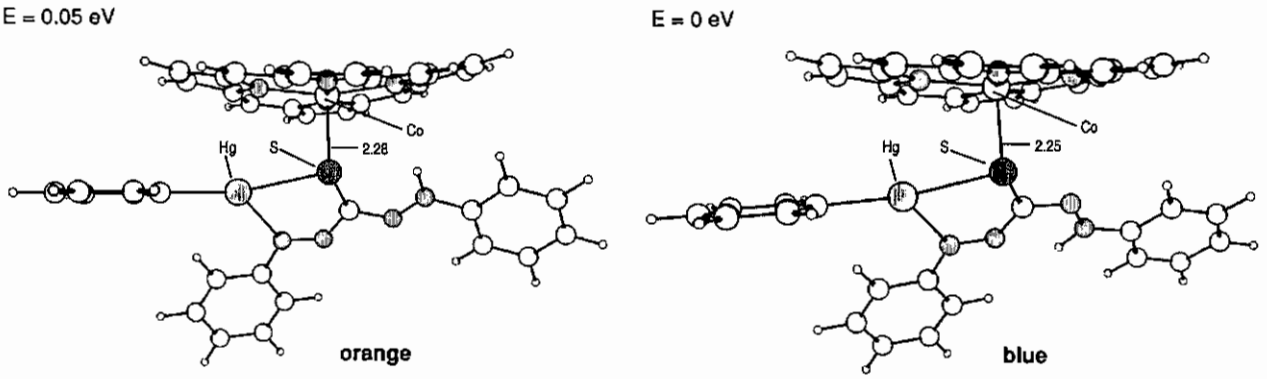


**Figure 3.37** ADF geometry optimised structures of the orange and blue isomers of dithizonatophenylmercury(II), **20**, hypothetically axially coordinated to cobalt(III) porphyrin.

The ADF optimised energy preference of the blue isomer was only 0.05 eV. In the absence of a porphyrin ligand the orange isomer is favoured by 0.35 eV. Using the optimised PW91 electron densities for the blue and orange states performed above, non-iterative post-SCF energies of the different spin states with a wide variety of functionals, including BLYP,[218,219] RPBE,[220] revPBE,[221] OLYP,[222,219] mPBE,[223] OPBE,[224-226] B3LYP(VWN5),[227-229] and O3LYP(VWN5)[230] were also determined. All functionals indicate the blue state is of comparable stability to the orange form, if not slightly favoured. Newer pure functionals such as OLYP and OPBE appeared to reproduce the PW91 energy preference as shown in Table 3.18. The analysis of new pure functionals, including OLYP and OPBE, suggests a more pronounced bias in favour of the blue geometry than the older PW91 and B3LYP functionals, and largely reproduce the energetics obtained with the hybrid density functional B3LYP. These encouraging results suggest that the blue geometry of cobalt porphyrin – PhHgHDz adducts may indeed be slightly more stable than the orange geometry.

**Table 3.18** Total Bonding Energy (E, eV) from PW91/ADF calculations (which was used for the geometry optimization) and post-SCF energies of different functionals such as B3LYP, O3LYP, etc. of PHgHDz-Co(III)Por.

| Energy Functional | ΔE* (eV) |
|---|---|
| **PW91** | 0.04 |
| **BLYP** | 0.08 |
| **RPBE** | 0.08 |
| **revPBE** | 0.07 |
| **OLYP** | 0.13 |
| **mPBE** | 0.04 |
| **OPBE** | 0.11 |
| **B3LYP(VWN5)** | 0.11 |
| **O3LYP(VWN5)** | 0.14 |

* Energy of orange isomer - Co(III)Por adduct relative to the blue isomer adduct.

For the blue form to be significantly more stable than the orange porphyrin-PhHgHDz conjugate, the blue form needs to be at least 0.3 eV lower in energy. This, however, is not necessarily a requirement for the proposed optical molecular switch, since an energy difference that is too large might prevent the subtle switching mechanism from taking place reversibly from the blue form to the orange form and back again.

# 3.5. Electrochemistry

## 3.5.1. Introduction

From the discussions in Paragraph 3.2 (Synthesis) it is evident that both reagents, i.e. dithizone and its derivatives, and the cobalt(III) porphyrin complexes, are readily involved in electron transfer (redox) reactions. During interactions between these two groups of compounds, the axial ligand, dithizone, usually oxidises while the latter, the cobalt(III) porphyrin moiety, is reduced. For reasons already discussed, different measures were undertook to prevent this flow of electrons from taking place. As for the axial ligand, halogenated dithizone derivatives were synthesised to try and increase its resistance against oxidation, while the porphyrinic macrocycle, on the other hand, were substituted with electron donating groups in an attempt to stabilise the higher trivalent oxidation state of cobalt against reduction.

This electrochemical study was performed to quantify the measures taken by determining reduction potentials, and to establish some of the fundamental electrochemical properties of these systems. Cyclic voltammetry was employed as technique to measure the relative changes that had been brought about with regard to redox potentials of the chemically altered species. Oster Young square wave voltammetry (SW) and linear sweep voltammetry (LSV) supplemented cyclic voltammetry, although no new insight was obtained from these two techniques. Dichloromethane was mostly used as solvent, but where comparisons had to be drawn between lypophilic and hydrophilic porphyrins, dimethylsulfoxide was used as solvent. In order to determine whether the extremely non-coordinating electrolyte, $[NBu_4][B(C_6F_5)_4]$, would enhance peak resolution as compared to the more commonly used $[NBu_4][PF_6]$ electrolyte, selected compounds were measured in each, and the results compared. All potentials were measured against an in-house constructed Ag/AgCl reference electrode, while potentials were reported versus $Fc/Fc^+$ as internal standard, as recommended by IUPAC.[231]

## 3.5.2. Dithizone and its derivatives

The electrochemical behaviour of dithizone, **16**, its halogenated derivatives, **40a-d**, dithizonatophenylmercury(II), **20**, and *tris*-dithizonatocobalt(III), **33**, is for the first time extensively reported here.

Before the redox waves in the respective voltammograms were assigned, investigations were done with regard to the most suitable solvent and electrolyte for purposes of this study. Figure 3.38 gives a comparison between cyclic voltammograms drawn for dithizone in dimethylsulfoxide and dichloromethane, with $[NBu_4][PF_6]$ as electrolyte. Anodic and cathodic peak potentials for voltammograms obtained at a scan rate of 200 mV/s are listed in Table 3.19

(at end of Paragraph 3.5.2). Figure 3.39 gives the voltammograms of dithizone in dichloromethane, but with $[NBu_4][B(C_6F_5)_4]$ as electrolyte. Peak potentials are listed in Table 3.20.

The effect of the coordinating polar solvent, dimethylsulfoxide (DMSO), can be seen to have a drastic lowering in the anodic peak potentials ($\mathbf{E_{I\ \&\ 2}}$) of dithizone to 152 mV versus $Fc/Fc^+$, as compared to the value of 705 mV in dichloromethane (DCM). Apart from this peak, almost all the other redox waves are less well defined. The reduction waves, $\mathbf{E_{III}}$ and $\mathbf{E_{IV}}$, on the contrary, may be seen to have moved to only slightly higher values (-1058 & -1284 mV) in DMSO as compared to dichloromethane (-1083 & -1341 mV). The effect of DMSO is therefore to narrow down the range over which the oxidation and reduction waves span, in this case, by about 610 mV ($\Delta E$ between $\mathbf{E_I}$ and $\mathbf{E_{IV}}$). Regardless the *ca* 550 mV lowering in the value of $\mathbf{E_I}$, the second anodic peak still does not fall completely within the electrochemically inactive/usable range for DMSO (*ca* -2900 to 700 mV versus $Fc/Fc^+$). For this reason and because peaks are poorly defined, as well as the fact that DMSO is a strongly coordinating solvent, especially towards oxidised electron poor species (it may therefore interact with the different oxidised species under investigation), it was decided to continue the electrochemical studies by rather using DCM as solvent. Since DCM is not redox active within the range of about -2300 to 1500 mV, it allows for investigations of oxidation processes at higher potentials. DCM is also a non-coordinating solvent, with the consequence that little or no interaction is expected between the solvent and the species under investigation. Figure 3.38(b) shows in general both better peak resolution and scanning width as compared to the DMSO runs in Figure 3.38(a).

Even in DCM as solvent peak resolution still was not good when compared to the result obtained when changing the electrolyte from $[NBu_4][PF_6]$ to $[NBu_4][B(C_6F_5)_4]$ (See Figure 3.39). The latter electrolyte has the advantage of a much larger $[B(C_6F_5)_4]^-$ anion, which inevitably has the anionic negative charge distributed over a much larger volume than in $[PF_6]^-$. Using the $[NBu_4][B(C_6F_5)_4]$ electrolyte did not only allow for much improved peak resolution, but also for the appearance of the otherwise completely absent cathodic peaks, $\mathbf{E_I}$ and $\mathbf{E_{IIa,b}}$, without which accurate description of the redox cycle would have been impossible.

Assignment of the different redox waves, with the simultaneous description of the chemical changes involved, nevertheless proved to be still difficult without also viewing the cyclic voltammograms of $Co(HDz)_3$, **33**, and PhHgHDz, **20**, (Figure 3.40) in conjunction with that of $H_2Dz$, **16**. This is so because the cyclic voltammogram of **33**, $Co(HDz)_3$, showed additional re-oxidation waves at the peak labelled, **2a-c**, that was not seen in the cyclic voltammograms of dithizone or PhHgHDz. In addition, the cyclic voltammogram of **33**, $Co(HDz)_3$, shows the characteristic splitting of single peaks into three distinct features, **a**, **b** and **c**, for the oxidation waves **1**, **2** and **3**, as well as for the reduction waves **I** and **II**. The sub-waves **a**, **b** and **c** in **33** is a result of **33** having three dithizonato ligands coordinated to it.

**Figure 3.38**

Cyclic voltammograms of 0.001 mol.dm$^{-3}$ $H_2Dz$, **16**, recorded at scan rates of 100, 200, 300, 400 & 500 mV/s, using 0.1 mol.dm$^{-3}$ **[$NBu_4$][$PF_6$]** as supporting electrolyte, and a glassy carbon working electrode at 20°C, in

(**a**) $(CH_3)_2SO$, and

(**b**) $CH_2Cl_2$.

Assigned oxidation and reduction peaks correspond to Schemes 3.26 - 28.

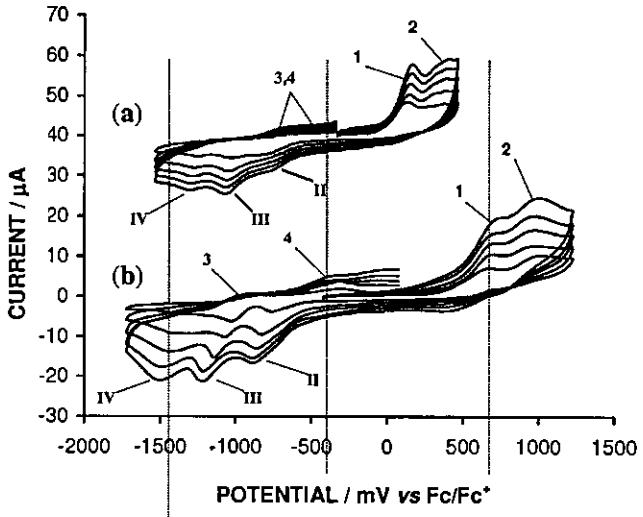


**Figure 3.39**

(**a**) Cyclic voltammograms of 0.001 mol.dm$^{-3}$ $H_2Dz$ showing the *ferrocene* wave as internal standard. The scan rate was 100 mV/s.

(**b**) Cyclic voltammograms of 0.001 mol.dm$^{-3}$ $H_2Dz$, **16**, recorded at scan rates of 100, 200, 300, 400 & 500 mV/s, using 0.1 mol.dm$^{-3}$ **[$NBu_4$][$B(C_6F_5)_4$]** as supporting electrolyte, and a glassy carbon working electrode at 20°C, in $CH_2Cl_2$.

Assigned oxidation and reduction peaks correspond to Schemes 3.26 - 28

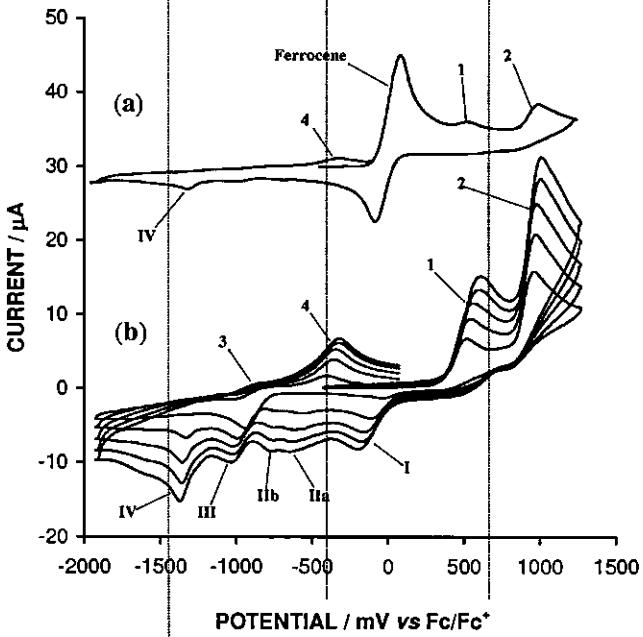


**Figure 3.40**

Cyclic voltammograms of 0.001 mol.dm$^{-3}$

(**a**) $Co(HDz)_3$, **33**, and

(**b**) PhHgHDz, **20**,

recorded at a scan rate of 500 mV/s, using 0.1 mol.dm$^{-3}$ [$NBu_4$][$B(C_6F_5)_4$] as supporting electrolyte, and a glassy carbon working electrode at 20°C, in $CH_2Cl_2$.

Assigned oxidation and reduction peaks for (**a**) correspond to Scheme 3.29, and (**b**) Scheme 3.30. Vertical dotted lines coincide with peaks $E_{III}$, $E_3$ and $E_1$ of PhHgHDz (**b**).

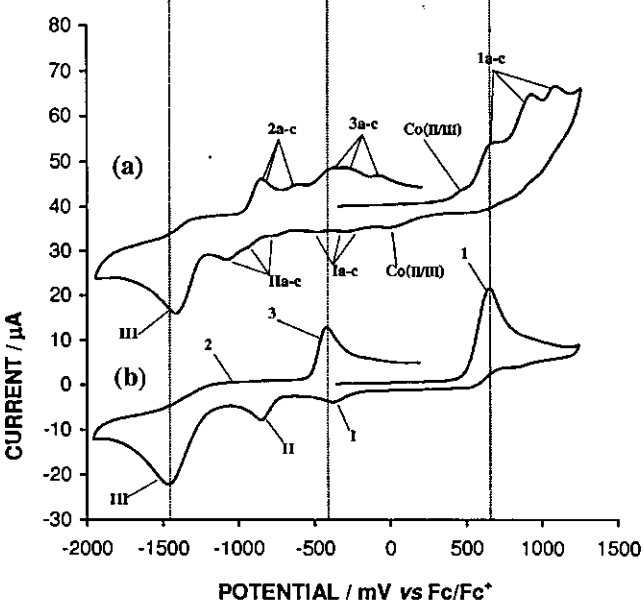

The splitting of a single peak into multiple peaks, here labelled **a**, **b** and **c**, when intermediate mixed valent species are formed, is a subject that was well studied and documented, amongst others, by our own group,[232] by Geiger and by Taube.[233-236] PhHgHDz, **20**, has only one dithizonato ligand and hence, like dithizone, **16**, itself, does not show this peak splitting. The assigned oxidation and reduction waves correspond to Schemes 3.26 - 3.30.

The large degree of similarity between the voltammograms here under consideration (Figure 3.39(b), Figure 3.40(a) and 3.40(b)) is noticeable. One important difference, however, is dithizone having *two* distinct oxidation peaks ($\mathbf{E}_{1\ \&\ 2}$) and *four* reduction processes ($\mathbf{E}_{I\text{-}IV}$), as opposed to *one* oxidation ($\mathbf{E}_1$) and *three* reduction processes for the mercury and cobalt complexes. This is explained in terms of the fact that the free dithizone ligand has got two acidic protons that may be removed during the oxidation sequence. In the metal complexes the dithizonate anion holds only one proton.

With all the above evidence at hand the following schemes for the complete redox cycles of $H_2Dz$, PhHgHDz and $Co(HDz)_3$ may now be suggested.

In the first step of the oxidation of dithizone ($\mathbf{E}_1$, 624 mV), two $H_2Dz$ molecules each loose both one electron and one proton to form the disulfide, $(HDz)_2$, **22**. During the second step ($\mathbf{E}_2$, 1026 mV) every monomer once again looses both an electron and a proton, with consequent ring-closure to form the completely oxidised dithizone species, a tetrazolium salt, dehydrodithizone (DDz), the monomers of which correspond to **21**. The disulfide, **22**, is known to cleave disproportionately to give DDz, **21**, and $H_2Dz$, **16**. It is expected that **21-21** will behave likewise, but these disproportionation reactions were not researched. The two dithizone waves are much more pronounced than any of the remaining waves, which may in itself be indicative of the fact that each of these processes involves the transfer of two electrons.

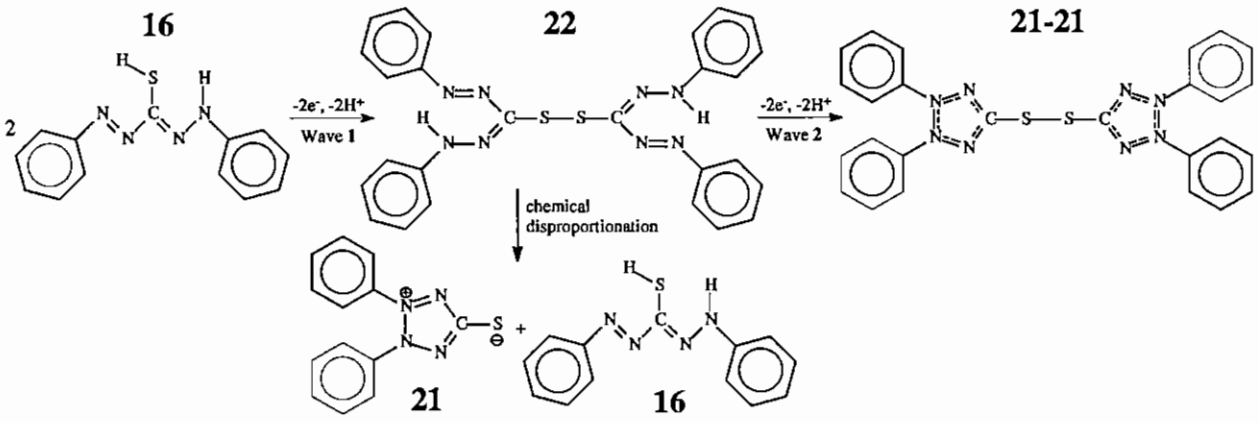


**Scheme 3.26** The proposed complete oxidation of dithizone, **16**, to the tetrazolium dimer, *di*-dehydrodithizone, (monomer = **21**) is a two-step process, via the disulfide, **22**: $2H_2Dz \rightarrow (HDz)_2 \rightarrow (DDz)_2$. The disulfide, **22**, is known to chemically disproportionate into **21** and **16**. For clarity only one isomer of **16** and one canonical form of **21** is shown. Wavenumbers correspond to wavenumbers in the CV's shown in Figures 3.38, 3.39 & 3.42.

In the subsequent reduction sequence the above order is reversed (Scheme 3.27). At the first reduction wave ($E_I$, -210 mV) the tetrazolium rings are expected to open on addition of electrons. Dehydrodithizone is a stable compound, which explains why the potential difference between $E_2$ and $E_I$ is large, namely 1236 mV. Addition of the first proton is expected to be fast, forming the HDz-DDz$^-$ species, **22a**, while the second proton will add more slowly to give $(HDz)_2$, **22**. These latter two newly formed species are suggested to be the origin of reduction waves $E_{IIa}$ & $E_{IIb}$. On further reduction of species **22a** and **22** the neutral compound, $(HDz)_2$, **22**, will add electrons more readily ($E_{IIa}$, -662 mV) than **22a**, HDz-DDz$^-$ ($E_{IIb}$, -778 mV). Peaks **IIa** and **IIb** lying so close to each other is also consistent with the interpretation that **22a** converts slowly to **22**. Alternatively **22a** may be in equilibrium with **22**, but we do not favour this explanation as we cannot see that the equilibrium between —NH— and [—N$^-$— + H$^+$] will lie significantly to the amide side.

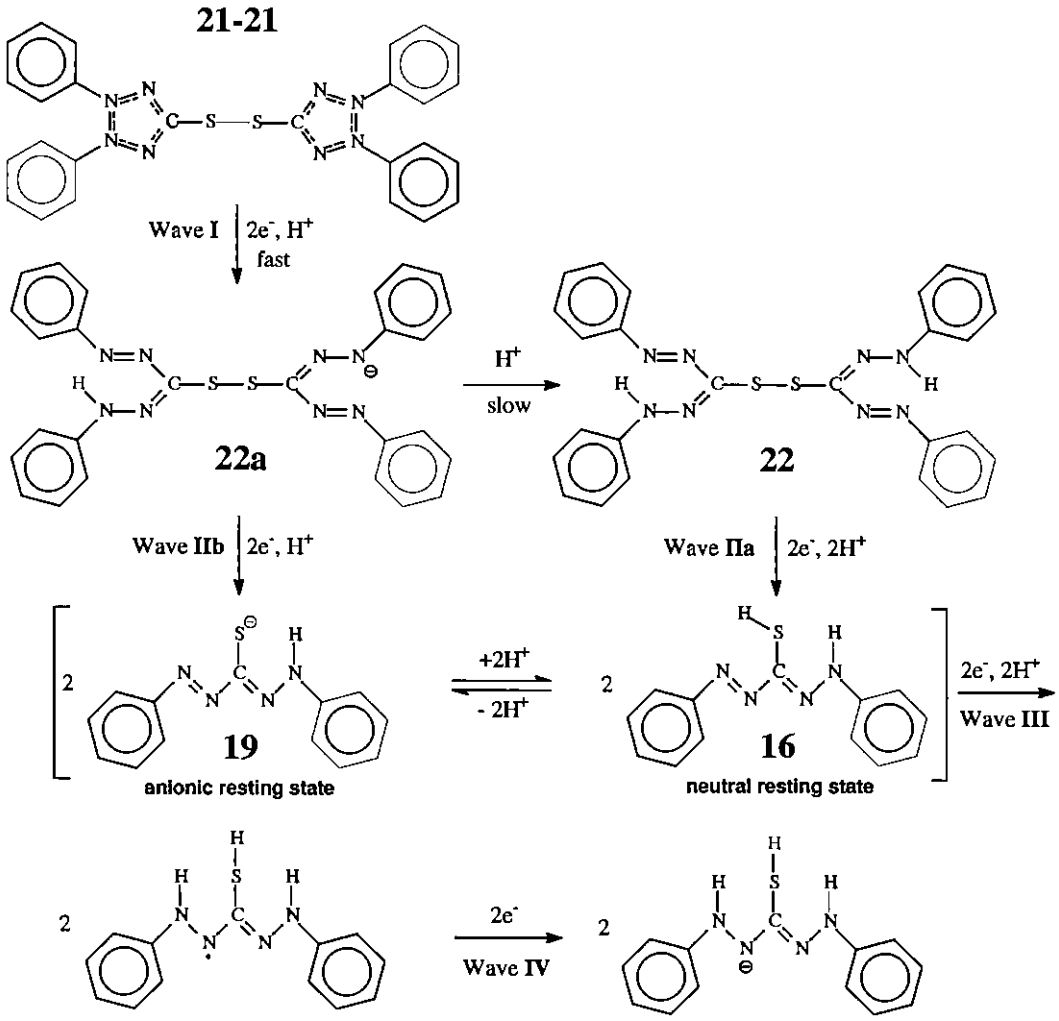


**Scheme 3.27** The complete reduction of *di*-dehydrodithizone is essentially a four-step process: $(DDz)_2 \rightarrow 2(HDz)_2 \rightarrow 2H_2Dz \rightarrow 2H_3Dz \rightarrow 2H_3Dz^-$. Acid-base equilibria are anticipated between the protonated and deprotonated species resulting from reduction steps **III** and **IV**, but are not shown. For the sake of clarity single canonical forms of most intermediates are shown. Wavenumbers correspond to wavenumbers in the CV's shown in Figures 3.38, 3.39 & 3.42.

On the CV timescale, when the potential associated with reduction waves **IIa** and **IIb** is reached, it is expected that **22a** has not yet fully converted to **22** because of the low supply of protons. The disulfide S-S bond breaks at these potentials (waves **IIa** and **IIb**) to form the dithizonate anion, $HDz^-$, **19**, and the neutral parent compound, $H_2Dz$, **16**. The intermediate species, **19**, then also chemically reacts with protons to form **16** in an equilibrium process. The source of $H^+$ is either the liberated $H^+$ resulting from the oxidation process as shown in Scheme 3.26, or it comes from $H_2Dz$ in the bulk solution ($pK_a = 5.77$ [40]).

In the next step ($E_{III}$, -1048 mV) the tri-protonated species, $H_3Dz$, may form upon one electron reduction. $H_3Dz$, again is expected to exist in equilibrium, with the anion, $H_2Dz^-$. Addition of strong acids to $H_2Dz$ turns the blue-green colour of dithizone to magenta, the colour of tri-protonated $H_3Dz$. In the last step the $H_3Dz^-$ anion forms ($E_{IV}$, -1382 mV). This is in agreement with suggestions made by Tomcsanyi in 1977 (see page 10).[39]

Scheme 3.28 represents the last part of the dithizone cyclic voltammogram, namely the two-step re-oxidation of $H_3Dz^-$ to $H_2Dz$. Loss of the $H_3Dz^-$ electron is estimated to take place at about -850 mV. No clear peak **3** is observed here, and this estimation is only made, as argued earlier, on basis of analogous peaks appearing at a similar position on the $Co(HDz)_3$ cyclic voltammogram. The final oxidation step ($E_4$) has a well defined oxidation wave at -304 mV, the product being the parent compound, $H_2Dz$.

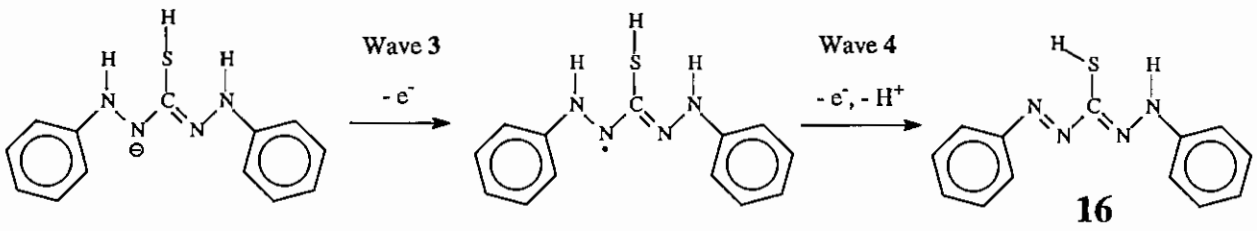


**Scheme 3.28** Re-oxidation of the reduced species, $H_3Dz^-$, to dithizone, $H_2Dz$, **16**, is a two-step process, with the loss of two electrons and a proton: $H_3Dz^- \rightarrow H_3Dz \rightarrow H_2Dz$. Wavenumbers correspond to wavenumbers in the CV's shown in Figures 3.38, 3.39 & 3.42.

All the above redox processes are electrochemically irreversible because $\Delta E$ values are larger than 59 mV.

The electrochemistry of dithizonatophenylmercury(II), **20** (see Figure 3.40b and Tables 3.21 & 3.22), may be explained along the same lines as above. It is important to recognise that PhHgHDz does not have a free mercaptan group that can dimerise to the disulfide bridge as is the case with free dithizone. Upon complexation with mercury, the free mercaptan became a stable "metal thioether", Hg-S-C, which effectively prevent disulfide formation. In addition, as

mentioned earlier, PhHgHDz has only one proton to lose ($E_1$, 669 mV) in order to form the tetrazolium adduct, as depicted in the following scheme. It must be noted that the metal has a significant labilizing effect on the remaining dithizonate proton, as observed from $pK_a$ experiments done by Irving *et al* (see page 6).[22,23]. This peak ($E_1$) lies 357 mV lower than the corresponding peak ($E_2$) on the dithizone voltammogram.

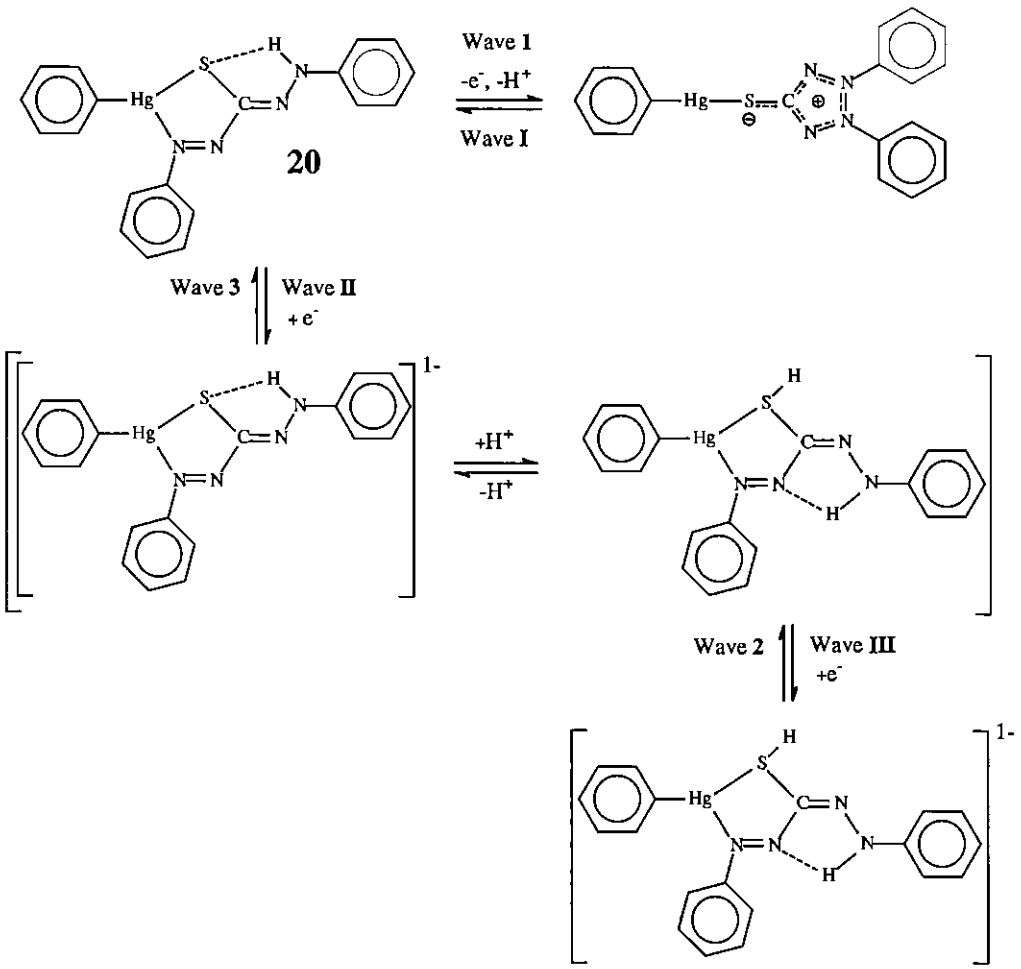


**Scheme 3.29** Dithizonatophenylmercury(II), **20**, is oxidised in one step to the tetrazolium adduct: **20**, PhHgHDz → PhHgDz. Reduction of PhHgDz is essentially a three-step process: PhHgDz → PhHgHDz → $PhHgH_2Dz$ → $PhHgH_2Dz^{\cdot}$. Wavenumbers correspond to wavenumbers in the CV shown in Figure 3.40(b).

Reduction, associated with ring-opening ($E_I$) takes place at -391 mV, which is 181 mV lower than for the free ligand, once again indicative of a compound much more electron rich than free dithizone. The next two reduction waves ($E_{II\ \&\ III}$) lie at -865 and -1479 mV respectively. the re-oxidation wave, $E_2$, is estimated to lie at *ca* -900 mV, while $E_3$ lies at -405 mV. With all the PhHgHDz peaks consistently lying at lower potentials than what is observed for dithizone, all of them may rightfully be attributed to the undissociated mercury dithizonate complex. Dissociation of dithizonate only takes place on protonation of complex **20** in acidic media.

The electrochemistry scheme of *tris*-dithizonatocobalt(III), **33**, is, apart from two distinct differences, to a large degree similar to that of PhHgHDz (see Scheme 3.30, Figure 3.40a and Tables 3.21 & 3.22). As with PhHgHDz, $Co(HDz)_3$ does not have a free mercaptan group that can be oxidised to form disulfide bridges. It also has only one proton per dithizonato ligand that can be removed upon oxidation to form tetrazolium rings. The one difference, as mentioned earlier, is the three ligands that successively undergo oxidation (or reduction) to three tetrazolium rings. The second difference is the $Co^{II} \rightarrow Co^{III}$ transition that is observed at about 490 mV. This value is in close agreement with the $Co^{II} \rightarrow Co^{III}$ anodic peak potential value of 420 mV reported later in this dissertation (Table 3.24) for tetraphenylporphyrinatocobalt(II). The $Co^{II/III}$ peak appears as a very small shoulder on the $Co(HDz)_3$ cyclic voltammogram (Figure 3.40a). The weak intensity (small current) of the shoulder is expected in view of the fact that $Co^{III}$ is octahedrally coordinated by sterically large dithizonate ligands, which to a large degree isolates the metal from the electrode upon oxidation or reduction. The result is a less prominent oxidation wave. In line with what is observed for the octahedrally coordinated $CoTPP.Pyr_2$ complex (see Figure 3.47), no $Co^{III} \rightarrow Co^{II}$ reduction peak could unambiguously be identified. However, our results are consistent with the $Co^{II/III}$ peak (-10 mV) being the reduction of $Co^{III}$. The potentials at which the redox waves, $\mathbf{E_1}$, $\mathbf{E_{III}}$ and $\mathbf{E_3}$ are observed, are in almost exact agreement with corresponding values for PhHgHDz. The complete electrochemical profile of $Co(HDz)_3$ is shown in Scheme 3.30.

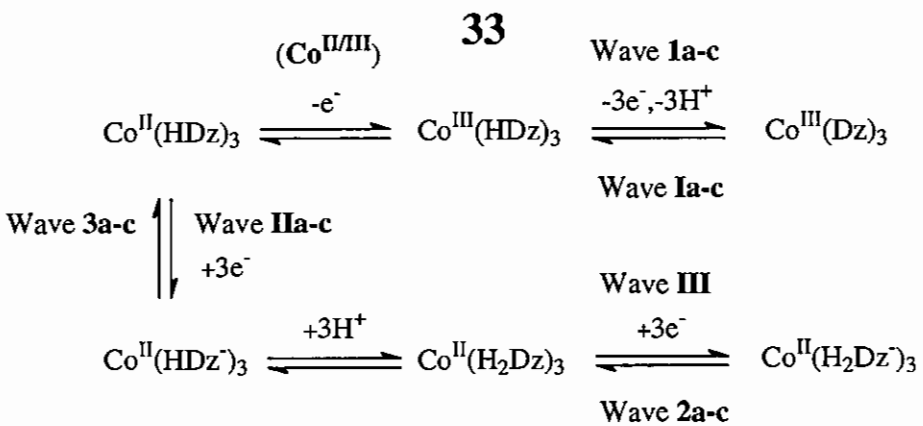


**Scheme 3.30** Starting the cyclic voltammogram for *tris*-dithizonatocobalt(III), **33**, at 0 V, results in $Co^{III}(HDz)_3$ being reduced to $Co^{II}(HDz)_3$ in an electrolysis process, after which it is re-oxidised to $Co^{III}$, followed by the oxidation of the dithizonate ligands to the tetrazolium species. Apart from the three dithizonato ligands, each oxidising or reducing in three successive steps (**a-c**), and the $Co^{II} \leftrightarrow Co^{III}$ transition taking place, the redox cycle for **33** agrees with that of **20**. Wavenumbers correspond to wavenumbers in the CV shown in Figure 3.40(a).

Having elucidated the electrochemical behaviour of dithizone and two of its metal complexes, PhHgHDz and $Co(HDz)_3$, the results of the main aim for investigating dithizone electrochemically is now reported, namely the relative ease with which different halogenated dithizones may be oxidised.

Figure 3.41 compares the cyclic voltammograms of $H_2Dz$, **16**, (*p*-Cl)$H_2Dz$, **40a**, (*p*-F)$H_2Dz$, **40b**, (*o*-F)$H_2Dz$, **40c** & (*m*-F)$H_2Dz$, **40d**. Anodic and cathodic peak potentials are reported in Table 3.20.

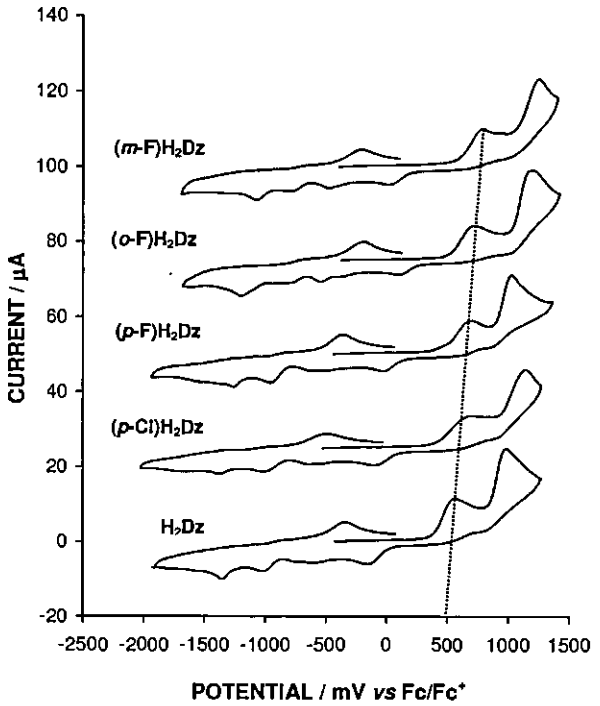


**Figure 3.41**

Cyclic voltammograms recorded at scan rates of 300 mV/s, using 0.1 mol.dm$^{-3}$ $[NBu_4][B(C_6F_5)_4]$ as supporting electrolyte, and a glassy carbon working electrode at 20°C, in $CH_2Cl_2$, of 0.001 mol.dm$^{-3}$ of $H_2Dz$, **16**, (*p*-Cl)$H_2Dz$, **40a**, (*p*-F)$H_2Dz$, **40b**, (*o*-F)$H_2Dz$, **40d** & (*m*-F)$H_2Dz$, **40c**.

All cyclic voltammograms were referenced against ferrocene as internal standard. The dotted line indicates the increase in potential of the first oxidation peak of the series of dithizones.

The increase in the first oxidation potential ($E_1$) of the above series of dithizones lie in the order (potential values in brackets are given in millivolt, for a scan rate of 300 mV/s):

$H_2Dz$ (576) < (*p*-Cl)$H_2Dz$ (716) < (*p*-F)$H_2Dz$ (717) < (*o*-F)$H_2Dz$ (741) < (*m*-F)$H_2Dz$ (805)

This order is in general agreement with the $pK_a$ values determined by Al-Salihy and Freiser (see Table 2.1, p.11). In both the electrochemical and $pK_a$ studies the *meta*-substituted derivatives have the best stability against oxidation. Both the *para*-substituted derivatives (*p*-Cl and *p*-F) are comparatively similar in their abilities to stabilise the ligand, with the *ortho*-F derivative being only slightly better. Halogens are known to be deactivating towards the *ortho*- and *para*-directions. This might be the reason why the potentials ($E_1$) of the *ortho*- and *para* derivatives lie in close proximity to each other.

The *meta*-fluoro dithizone, being the best stabilised against mercaptan oxidation, has an anodic peak potential of 805 mV. This is 229 mV higher than the corresponding $H_2Dz$ value of 576 mV. Although the difference is significant, it nevertheless proved to be insufficient to prevent these dithizone derivatives from being oxidised by $Co^{III}TPP$, $Co^{III}TCP$ and $Co^{III}TPPS$.

**Table 3.19** Cyclic voltammetry data obtained from voltammograms (*vs* $Fc/Fc^+$) of dithizone, **16**, in dimethylsulfoxide and dichloromethane, with 0.1 mol.dm$^{-3}$ $[NBu_4][PF_6]$ as electrolyte and a glassy carbon working electrode, at a scan rate of 200 mV/s, at 20°C. Anodic peak potentials ($E_{I-4}$) and cathodic peak potentials ($E_{I-IV}$) are given.

| | $E_I$ | $E_2$ | $E_I$ | $E_{IIa}$ | $E_{IIb}$ | $E_{III}$ | $E_{IV}$ | $E_3$* | $E_4$ |
|---|---|---|---|---|---|---|---|---|---|
| **$(CH_3)_2SO$:** | 152 | - | - | - | - | -1058 | -1284 | - | - |
| **$CH_2Cl_2$:** | 705 | 991 | - | - | -841 | -1083 | -1341 | -850 | -303 |

* Estimated value
- Redox process expected, but not observed.

**Table 3.20** Cyclic voltammetry data obtained from voltammograms (*vs* $Fc/Fc^+$) of dithizone, **16**, and the four halogenated derivatives, **40a-d**, in $CH_2Cl_2$/0.1 mol dm$^{-3}$ $[NBu_4][B(C_6F_5)_4]$ with a glassy carbon working electrode at 20°C. Scan rates ($v$), anodic peak potentials ($E_{I-4}$), and cathodic peak potentials ($E_{I-IV}$) are given.

| | $v$/mV.s$^{-1}$ | $E_I$ | $E_2$ | $E_I$ | $E_{IIa}$ | $E_{IIb}$ | $E_{III}$ | $E_{IV}$ | $E_3$* | $E_4$ |
|---|---|---|---|---|---|---|---|---|---|---|
| | **100** | 536 | 978 | -70 | - | - | -966 | - | -850 | -382 |
| | **200** | 558 | 990 | -130 | -572 | - | -996 | -1342 | -850 | -344 |
| **$H_2Dz$:** | **300** | 576 | 998 | -168 | -620 | - | -1024 | -1360 | -850 | -326 |
| | **400** | 604 | 1016 | -190 | -644 | -766 | -1036 | -1372 | -850 | -310 |
| | **500** | 624 | 1026 | -210 | -662 | -778 | -1048 | -1382 | -850 | -304 |
| | **100** | 698 | 1110 | -106 | - | - | -1012 | - | -900 | -550 |
| | **200** | 708 | 1134 | -112 | -644 | -526 | -1018 | -1378 | -900 | -506 |
| **(*p*-Cl)$H_2Dz$:** | **300** | 716 | 1158 | -118 | -650 | -530 | -1030 | -1388 | -900 | -476 |
| | **400** | 718 | 1170 | -120 | -660 | -552 | -1042 | -1396 | -900 | -466 |
| | **500** | 724 | 1184 | -122 | -666 | -564 | -1050 | -1406 | -900 | -460 |
| | **100** | 717 | 1023 | - | - | - | -927 | - | -800 | -383 |
| | **200** | 719 | 1035 | -27 | -495 | -617 | -947 | -1243 | -800 | -363 |
| **(*p*-F)$H_2Dz$:** | **300** | 717 | 1041 | -39 | -523 | -637 | -967 | -1273 | -800 | -345 |
| | **400** | 717 | 1051 | -59 | -563 | -653 | -991 | -1301 | -800 | -333 |
| | **500** | 717 | 1065 | -75 | -575 | -663 | -999 | -1319 | -800 | -325 |
| | **100** | 749 | 1217 | 67 | - | - | -765 | - | -690 | -241 |
| | **200** | 787 | 1247 | 35 | -390* | -473 | -779 | -1065 | -690 | -209 |
| **(*m*-F)$H_2Dz$:** | **300** | 805 | 1267 | 3 | -390* | -485 | -799 | -1077 | -690 | -193 |
| | **400** | 817 | 1285 | -15 | -390* | -497 | -811 | -1093 | -690 | -183 |
| | **500** | 829 | 1297 | -29 | -390* | -501 | -821 | -1101 | -690 | -173 |
| | **100** | 739 | 1173 | - | - | - | -765 | - | -660 | -199 |
| | **200** | 741 | 1191 | 127 | - | -531 | -779 | -1177 | -660 | -187 |
| **(*o*-F)$H_2Dz$:** | **300** | 741 | 1205 | 91 | -391 | -559 | -809 | -1209 | -660 | -179 |
| | **400** | 745 | 1211 | 61 | -421 | -577 | -819 | -1231 | -660 | -177 |
| | **500** | 749 | 1217 | 33 | -441 | -597 | -823 | -1255 | -660 | -175 |

* Estimated values
- Redox process expected, but not observed.

**Table 3.21** Cyclic voltammetry data obtained from voltammograms (*vs* $Fc/Fc^+$) of dithizonatophenylmercury(II), **20**, and *tris*-dithizonatocobalt(III), **33**, in $CH_2Cl_2$/0.1 mol.dm$^{-3}$ $[NBu_4][B(C_6F_5)_4]$ with a glassy carbon working electrode at 20°C. Scan rates ($v$) and **anodic** peak potentials ($E_{I-4}$) are given.

| | $v$/mV.s$^{-1}$ | $Co^{II/III}$ | $E_{1a}$ | $E_{1b}$ | $E_{1c}$ | $E_{3a,b}$ | $E_{3c}$ | $E_{4a}$ | $E_{4b}$ | $E_{4c}$ |
|---|---|---|---|---|---|---|---|---|---|---|
| | **100** | | 710 | | | -900* | | - | | |
| | **200** | | 708 | | | -900* | | -349 | | |
| **PhHgHDz:** | **300** | | 703 | | | -900* | | -371 | | |
| | **400** | | 685 | | | -900* | | -387 | | |
| | **500** | | 669 | | | -900* | | -405 | | |
| | **100** | 490* | 690* | 950 | 1102 | - | - | - | - | - |
| | **200** | 490* | 690* | 948 | 1102 | -826 | - | -374 | -276 | - |
| **$Co(HDz)_3$:** | **300** | 490* | 690* | 948 | 1102 | -830 | - | -364 | -274 | -70 |
| | **400** | 490* | 690* | 948 | 1102 | -834 | -586 | - | - | -66 |
| | **500** | 490* | 690* | 948 | 1102 | -836 | -588 | - | - | -64 |

* Estimated values
\- Redox process expected, but not observed.

**Table 3.22** Cyclic voltammetry data obtained from voltammograms (*vs* $Fc/Fc^+$) of dithizonatophenylmercury(II), **20**, and *tris*-dithizonatocobalt(III), **33**, in $CH_2Cl_2$/0.1 mol dm$^{-3}$ $[NBu_4][B(C_6F_5)_4]$ with a glassy carbon working electrode at 20°C. Scan rates ($v$) and **cathodic** peak potentials ($E_{I-III}$) are given.

| | $v$/mV s$^{-1}$ | $Co^{II/III}$ | $E_{Ia}$ | $E_{Ib}$ | $E_{Ic}$ | $E_{IIa}$ | $E_{IIb}$ | $E_{IIc}$ | $E_{III}$ |
|---|---|---|---|---|---|---|---|---|---|
| | **100** | | - | | | - | | | -1429 |
| | **200** | | -215 | | | -749 | | | -1435 |
| **PhHgHDz:** | **300** | | -295 | | | -781 | | | -1443 |
| | **400** | | -339 | | | -815 | | | -1451 |
| | **500** | | -391 | | | -865 | | | -1479 |
| | **100** | - | - | - | - | - | -912 | - | -1428 |
| | **200** | -10 | - | -236 | -472 | -758 | -928 | -1074 | -1430 |
| **$Co(HDz)_3$:** | **300** | -30 | - | -288 | -492 | -778 | -934 | -1088 | -1432 |
| | **400** | -50 | - | -318 | -506 | -790 | -940 | -1102 | -1440 |
| | **500** | -70 | 250* | -338 | -516 | -800 | -948 | -1112 | -1450 |

* Estimated value
\- Redox process expected, but not observed.

In conclusion to this paragraph it is to be mentioned that Oster-Young square wave (**SW**) and linear sweep voltammograms (**LSV**) were obtained for all the compounds electrochemically investigated in this study. Figure 3.42 compares the **CV**, **SW**'s and **LSV**'s of dithizone. Normally **SW** scans may assist in finding peaks that do not clearly appear in the **CV**, while **LSV**'s may serve as an indication of the amount of electrons being transferred at a given potential. By inspecting the following comparison it is clear that no additional information, over and above that which may be obtained from the **CV**, can be extracted from the **SW** and **LSV**'s.

**Figure 3.42**

Cyclic voltammogram (**CV**, 300 mV/s scan rate), Oster-Young square wave (**SW**, 100Hz) and linear sweep voltammograms (**LSV**, 2 mV/s) of 0.001 mol.dm$^{-3}$ $H_2Dz$, **16**, using 0.1 mol.dm$^{-3}$ $[NBu_4][B(C_6F_5)_4]$ as supporting electrolyte, and a glassy carbon working electrode, at 20°C, in $CH_2Cl_2$ (R: scan from low to high potential, L: scan from high to low potential).

Assigned oxidation and reduction peaks correspond to Schemes 3.26 - 28.

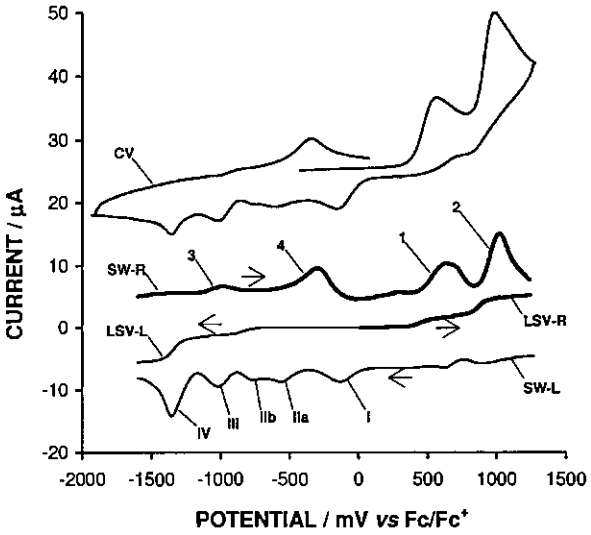


## 3.5.3. Cobalt Porphyrin

As opposed to dithizone, its derivatives and its complexes, the electrochemistry of cobalt porphyrins is well-known. Comparing even well investigated compounds nevertheless remains a problem, since a variety of conditions, e.g. temperatures, electrode systems, electrolytes, solvents, scan rates, etc., which all have an effect on individual redox waves, makes comparisons very unsatisfactory. In order, therefore, to comparatively quantify electrochemical data from a group or groups of compounds it is a prerequisite to make use of a preselected set of conditions that remain unchanged right through the duration of the experiment(s). For this reason cyclic voltammograms of the following well-known cobalt porphyrins had to be obtained anew. The comparisons and conclusions drawn here could not be found in published literature.

As was the case for dithizone, brief investigations were done with regard to suitable electrolytes and solvents for purposes of this study. Figures 3.43/4 and 3.45 give comparisons between cyclic voltammograms drawn for several cobalt porphyrins in dichloromethane (Figures 3.43 & 3.44) and dimethylsulfoxide (Figure 3.45), with both $[NBu_4][B(C_6F_5)_4]$ (Figure 3.43) and $[NBu_4][PF_6]$ (Figures 3.44 & 3.45) as supporting electrolytes. Corresponding anodic ($E_{pa}$) and cathodic ($E_{pc}$) peak potentials, formal reduction potentials ($E^{0'}$, where $E^{0'} = (E_{pa} + E_{pc})/2$), anodic peak currents ($i_{pa}$) and anodic/cathodic peak current relationships ($i_{pa}/i_{pc}$) are listed in Tables 3.23 - 3.26 (at end of Paragraph 3.5.3).

Although $[NBu_4][B(C_6F_5)_4]$ gave cyclic voltammograms with slightly improved peak resolution (Figure 3.43) over that obtained in the presence of $[NBu_4][PF_6]$ (Figure 3.44), redox waves, in the case of the former, are observed to drift towards lower potentials at higher scan rates. For this reason, and due to the high cost of $[NBu_4][B(C_6F_5)_4]$, it was decided to continue the cobalt

porphyrin study using $[NBu_4][PF_6]$ as electrolyte. One set of data based on the use of $[NBu_4][B(C_6F_5)_4]$ as supporting electrolyte (Table 3.23) is enough for overall comparison purposes. The formal reduction potential, $\mathbf{E^{0'}}$, of the first oxidation peak appears here at a slightly higher value of 430 mV, as compared to the value of 360 mV when $[NBu_4][PF_6]$ was used as electrolyte. As for the rest of oxidation and reduction potentials, $[NBu_4][B(C_6F_5)_4]$ has a spreading effect on these values; consecutive waves being further removed from each other. In the presence of $[NBu_4][PF_6]$ the difference between $\mathbf{E_1^{0'}}$, and $\mathbf{E_2^{0'}}$ is 236 mV, while in the presence of $[NBu_4][B(C_6F_5)_4]$ the difference is 405 mV. This effect may contribute towards outermost potentials not being able to be observed properly, as seen for $\mathbf{E_V}$ in Figure 3.43(b). Ion paring with $PF_6^-$, but not with $[B(C_6F_5)_4]^-$, may in part be causing the observed effect.

Before commenting further on the characteristics of individual cyclic voltammograms, an explanation is first given of Scheme 3.31, a general overall oxidation/reduction scheme for cobalt porphyrins (See also Paragraph 2.5.1).[163, 169] As will be proven later, the first electronic change that occurs during oxidation of $Co^{II}$TPP or $Co^{II}$OEP, is the loss of an electron by $Co^{II}$, getting oxidised to $Co^{III}$ ($\mathbf{E_1^{0'}}$). Subsequent loss of electrons occurs at the porphyrin ring ($\mathbf{E_2^{0'}}$ and $\mathbf{E_3^{0'}}$). On reduction the above process reverses, followed by metal-centered redox reactions occurring in successive steps, i.e. $Co^{III} \rightarrow Co^{II} \rightarrow Co^{I}$ ($\mathbf{E_{III}^{0'}}$ & $\mathbf{E_{IV}^{0'}}$). In the last reduction step (Wave **V**) the ring is reduced. Re-oxidation (Waves **4** and **5**) first involves the loss of the electron taken up by the ring in the previous step, followed by the oxidation of the metal center; $Co^{I} \rightarrow Co^{II}$.

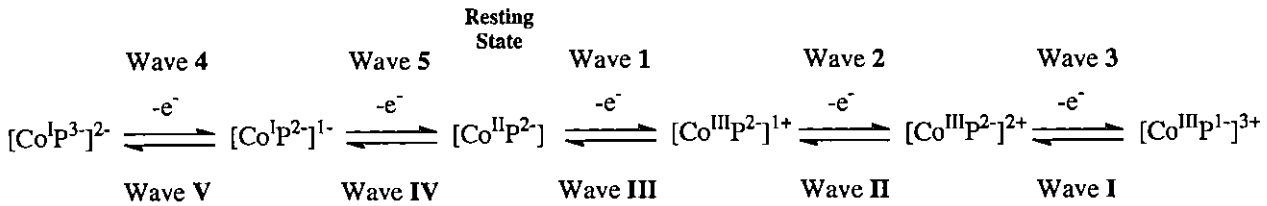


**Scheme 3.31** All the cobalt porphyrins (**68, 72, 74, 75 77**) electrochemically investigated in this study underwent the same redox cycle, as presented in the above scheme. P = TPP, TPPS & OEP. Wavenumbers correspond to wavenumbers in CV's shown in Figures 3.43 - 48.

In this study all redox active couples involving reduction waves $\mathbf{E_{I\text{-}IV}}$ behaved quasi-reversible (90 mV < $\Delta\mathbf{E_{peak}}$ < 150 mV) at scan rates of 100 - 300 mV/s, for tetraphenylporphyrinato-cobalt(II), **68**, and octaethylporphyrinatocobalt(II), **72**. The $\mathbf{E_V}$ couples were electrochemically irreversible, i.e. > 150 mV. Furthermore, since $i_{pc}/i_{ac} \approx 1$ for all processes here involving cobalt porphyrins, these reactions are all chemically reversible.

**Figure 3.43**

(a) All cyclic voltammograms were referenced against ferrocene as internal standard. This CV was recorded at a scan rate of 500 mV/s, and shows the redox wave associated with ferrocene as internal standard.

(b) Cyclic voltammograms of 0.001 mol.dm$^{-3}$ CoTPP, **68**, recorded at scan rates of 100, 200, 300, 400 & 500 mV/s, using 0.1 mol.dm$^{-3}$ **[NBu$_4$][B(C$_6$F$_5$)$_4$]** as supporting electrolyte, and a glassy carbon working electrode at 20°C, in $CH_2Cl_2$.

Assigned oxidation and reduction peaks correspond to Scheme 3.31, and are similar for all voltammograms involving porphyrins.

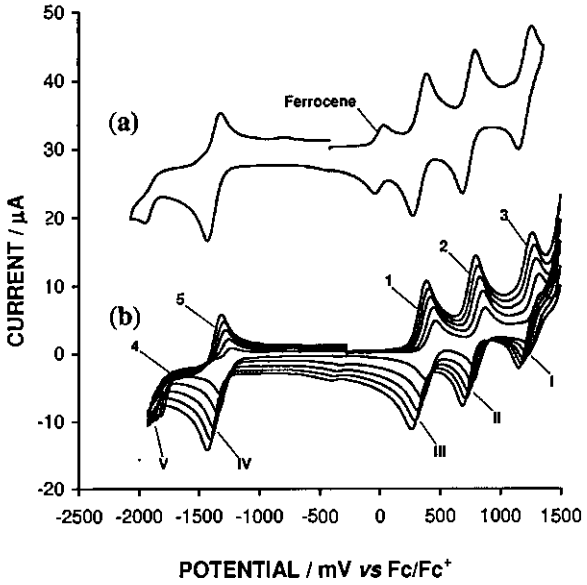


**Figure 3.44**

(a) All cyclic voltammograms were referenced against ferrocene as internal standard. This CV was recorded at a scan rate of 100 mV/s, and shows the redox wave associated with ferrocene as internal standard.

Cyclic voltammograms recorded at scan rates of 100, 200, 300, 400 & 500 mV/s, using 0.1 mol.dm$^{-3}$ **[NBu$_4$][PF$_6$]** as supporting electrolyte, and a glassy carbon working electrode at 20°C, in $CH_2Cl_2$, of 0.001 mol.dm$^{-3}$ (b) CoTPP, **68** and (c) CoOEP, **72**,.

Assigned oxidation and reduction peaks correspond to Scheme 3.31. Dotted lines indicate the Co(II/III) oxidation potential increase in going from CoOEP to CoTPP.

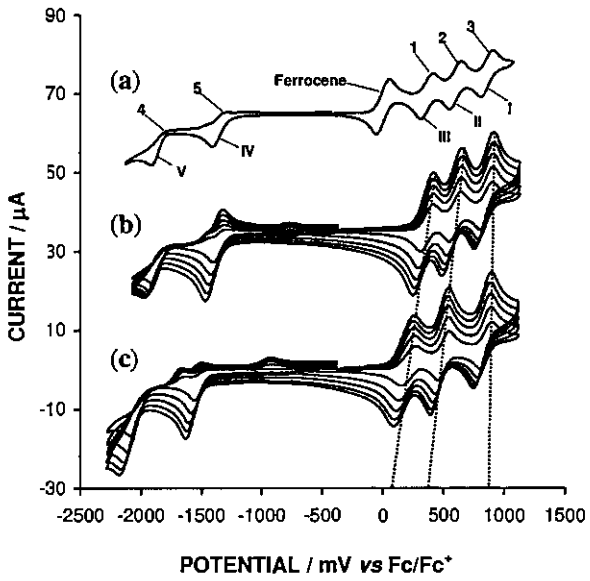


**Figure 3.45**

Cyclic voltammograms recorded in **DMSO**, at a scan rate of 200 mV/s, using 0.1 mol.dm$^{-3}$ [NBu$_4$][PF$_6$] as supporting electrolyte, and a glassy carbon working electrode at 20°C, of 0.001 mol.dm$^{-3}$

(a) [Co$^{III}$(TPPS)(DMSO)$_2$]ClO$_4$, **75**,

(b) [Co$^{III}$(TPP)(DMSO)$_2$]ClO$_4$, **74**, and

(c) [Co$^{III}$(OEP)(DMSO)$_2$]ClO$_4$, **77**.

The dotted line indicates the small Co(II/III) oxidation potential increase in going from CoOEP to CoTPP to CoTPPS.

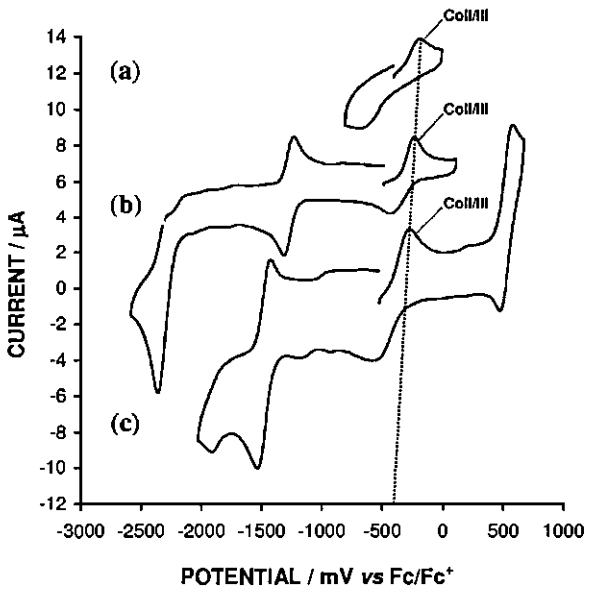

The observation for electrochemical quasi-irreversibility in the cobalt porphyrins is contrary to what was seen for dithizone and its derivatives, where all redox couples are electrochemically irreversible. Whereas the $Co^{II/III}$ redox couples in cobalt(II) porphyrins were still quasi-reversible in character, the opposite is true for axially ligated cobalt(III) porphyrins. (See Figure 3.45 and Table 3.26 for DMSO as axial ligand, and Figures 3.47 & 3.48 and Table 3.27 for pyridine as axial ligand.)

In an attempt to unambiguously assign the $Co^{II/III}$ redox wave, two approaches were followed. The first approach was to replace cobalt with copper, which is redox inactive within the potential range under investigation. Thereby the cobalt(II/III) redox wave would be eliminated, and if the porphyrin ligand were to behave electrochemically relatively unaffected by the replacement, the $Co^{II/III}$ peak may, by this indirect means of elimination, be identified. As seen in Figure 3.46 this proved not to be a workable option since replacing cobalt by copper also significantly affected the potentials of remaining ring centered redox waves, with the consequence that the original $Co^{II/III}$ couple could still not be assigned unequivocally.

The second approach was to incrementally add 0.25, 0.5, 1.0 and 2.0 equivalents of pyridine to solutions of both CoTPP and CoOEP (Figures 3.47 & 3.48 and Table 3.27), obtaining cyclic voltammograms after each such addition. Addition of l0 equivalents of pyridine effected no further observable change to the cyclic voltammogram. In general, Co(II) tetraphenylporphyrins form 1:1 complexes with amines at amine excesses of less than a 1000 times.[125, 237] Addition of electron donating bases like the amines, is known to significantly stabilise the higher $Co^{III}$ oxidation state. The consequence is that the relevant $Co^{II/III}$ redox couple would:

1) move to lower potentials,
2) become less pronounced because of the now inner-sphere reaction being shielded from its surroundings and the contact electrode, and
3) its reversible or quasi-reversible character should become electrochemically irreversible.

The relevant voltammograms showed indeed such behaviour, namely agreement with all three the above points. The stepwise addition of pyridine resulted in the gradual disappearance of the redox wave assigned, $\mathbf{E_1}$ (422 mV, bottom **CV**), while a new weaker peak appeared simultaneously at -52 mV (top **CV**), giving a total shift of 474 mV to lower potentials. The corresponding shift for CoOEP agrees closely, with a value of 432 mV. At the same time the cathodic peak potentials for the $Co^{II/III}$ couple moved down by 1130 mV and 1236 mV respectively, to peak **III**. The two additional ring-centered oxidation peaks ($\mathbf{E_2}$ & $\mathbf{E_3}$) moved to higher values by more than 100 mV in each case. The $\mathbf{E_{IV}}$ and $\mathbf{E_V}$ redox couples were relatively unaffected.

Considering the above evidence, therefore, the $Co^{II/III}$ redox couple is unambiguously assigned to the first oxidation/reduction wave, $\mathbf{E_1}$.

**Figure 3.46**

Cyclic voltammograms of 0.001 mol.dm$^{-3}$ CoOEP (**72**), CuOEP (**73**), CoTPP (**68**) and CuTPP (**69**), recorded at a scan rate of 100 mV/s, using 0.1 mol.dm$^{-3}$ [$NBu_4$][$PF_6$] as supporting electrolyte, and a glassy carbon working electrode at 20°C, in $CH_2Cl_2$.

Corresponding porphyrin ring oxidation waves are indicated by dotted lines.

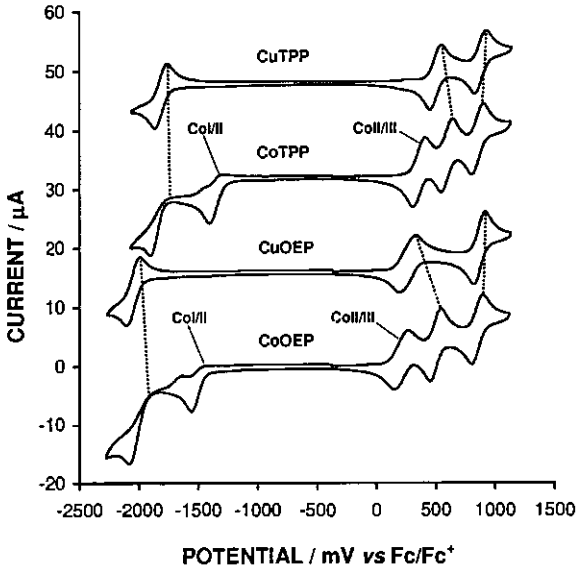


**Figure 3.47**

Cyclic voltammograms of 0.001 mol.dm$^{-3}$ **CoTPP, 68,** recorded at scan rates of 100 mV/s, using 0.1 mol.dm$^{-3}$ [$NBu_4$][$PF_6$] as supporting electrolyte, and a glassy carbon working electrode at 20°C, in $CH_2Cl_2$. Voltammograms (from bottom to top) represent the addition of 0, 0.20, 0.5, 1.0 and 2.0 equivalents of pyridine. The insert at peak **III** (top) shows $Co^{III}$ reduction of the pyridine adduct with $i_p$ magnified 5 times.

Assigned oxidation and reduction peaks correspond to Scheme 3.31.

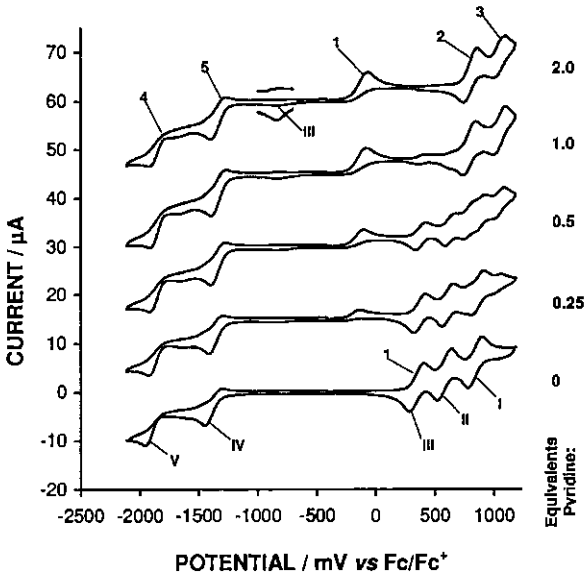


**Figure 3.48**

Cyclic voltammograms of 0.001 mol.dm$^{-3}$ **CoOEP, 72,** recorded at scan rates of 100 mV/s, using 0.1 mol.dm$^{-3}$ [$NBu_4$][$PF_6$] as supporting electrolyte, and a glassy carbon working electrode at 20°C, in $CH_2Cl_2$. Voltammograms (from bottom to top) represent the addition of 0, 0.20, 0.5, 1.0 and 2.0 equivalents of pyridine. The insert at peak **III** (top) shows $Co^{III}$ reduction of the pyridine adduct with $i_p$ magnified 5 times.

Assigned oxidation and reduction peaks correspond to Scheme 3.31.

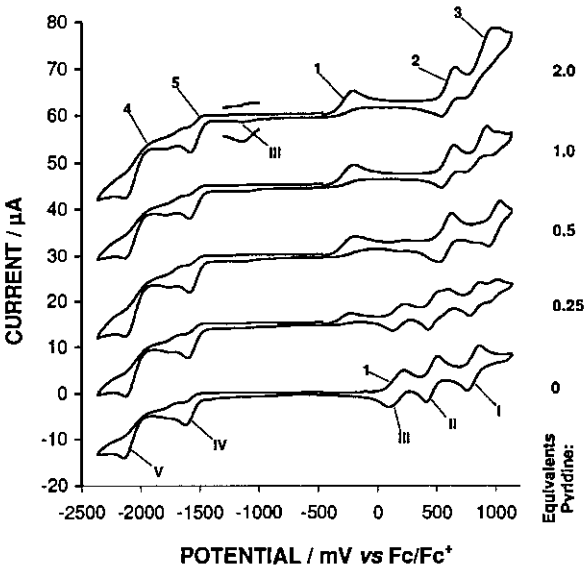

Having now also elucidated the electrochemical behaviour of cobalt porphyrins, the results of the main aim for investigating different cobalt porphyrins electrochemically is now reported, namely the relative resistance the different cobalt(III) porphyrins exert against becoming reduced, while simultaneously oxidizing the incoming dithizonate ligand.

As for replacing tetraphenylporphyrin with octaethylporphyrin, a significant drop of 157 mV (from 360 to 203 mV) was observed for the $Co^{II/III}$ formal reduction potential, using dichloromethane as solvent. The only way to quantitatively compare the $Co^{II/III}$ reduction potentials of the CoTPP, **68**, and CoOEP, **72**, lypophilic cobalt porphyrins to the water soluble tetra-sulfonated compound, **75**, was to dissolve their corresponding cobalt(III) complexes in dimethylsulfoxide. The cobalt(II) analogues of these compounds are not all soluble in DMSO, as was the case for $Co^{II}$TCP and $Co^{III}$TCP, **76**. The tetra-carboxyphenylporphyrin complex, **76**, is only soluble in water and could therefore not be evaluated. Nevertheless, only a small increase in the $E_1$ anodic peak potentials was observed, namely (in mV):

$$Co^{III}OEP\ (-261) < Co^{III}TPP\ (-223) < Co^{III}TPPS\ (-179)$$

The observed order is in agreement with earlier observations where the Soret bands of the respective complexes were found to lie in the same order (see Paragraph 3.2.3.2, page 83).

**Table 3.23** Cyclic voltammetry data obtained from voltammograms (*vs* $Fc/Fc^+$) of CoTPP, **68**, in $CH_2Cl_2$/ 0.1 mol.dm$^{-3}$ **[NBu$_4$][B(C$_6$F$_5$)$_4$]** with a glassy carbon working electrode at 20°C. Scan rates, $E_{pa}$ (anodic peak potentials), $\Delta E_p$ (difference between the anodic and cathodic peak potentials), $E^{0'}$ (formal reduction potentials, $E^{0'} = (E_{pa} + E_{pc})/2$), $i_{pa}$ (anodic peak currents) and $i_{pa}/i_{pc}$ (anodic/cathodic peak current relationship) are shown. Redox wave numbers correspond to numbers in Figure 3.43.

| Redox wave | $v$ / mV s$^{-1}$ | $E_{pa}$ / mV | $E_{pc}$ / mV | $\Delta E_p$ / mV | $E^{0'}$ / mV[a] | $i_{pa}$ / µA | $i_{pc}$ / µA | $i_{pc}/i_{pa}$ |
|---|---|---|---|---|---|---|---|---|
| **1** | **100** | 479 | 381 | 98 | 430 | 6.0 | 5.5 | 0.92 |
| **2** | **100** | 887 | 783 | 104 | 835 | 4.4 | 4.3 | 0.98 |
| **3** | **100** | 1327 | 1239 | 88 | 1283 | 3.8 | 3.6 | 0.95 |
| **IV** | **100** | -1327 | -1215 | 112 | -1271 | 5.2 | 1.9 | 0.37 |
| **V** | **100** | -1839 | -1675 | 164 | -1757 | 5.5 | 1.1 | 0.20 |

**Table 3.24** Cyclic voltammetry data obtained from voltammograms (*vs* $Fc/Fc^+$) of **CoTPP, 68**, in $CH_2Cl_2$/ 0.1 mol.dm$^{-3}$ **[NBu$_4$][PF$_6$]** with a glassy carbon working electrode at 20°C. Scan rates, $E_{pa}$ (anodic peak potentials), $\Delta E_p$ (difference between the anodic and cathodic peak potentials), $E^{0'}$ (formal reduction potentials, $E^{0'} = (E_{pa} + E_{pc})/2$), $i_{pa}$ (anodic peak currents) and $i_{pa}/i_{pc}$ (anodic/cathodic peak current relationship) are shown. Redox wave numbers correspond to numbers in Figure 3.44.

| Redox wave | $v$ / mV s$^{-1}$ | $E_{pa}$ / mV | $E_{pc}$ / mV | $\Delta E_p$ / mV | $E^{0'}$ / mV[a] | $i_{pa}$ / µA | $i_{pc}$ / µA | $i_{pc}/i_{pa}$ |
|---|---|---|---|---|---|---|---|---|
| | **100** | 420 | 299 | 121 | 360 | 8.1 | 7.1 | 0.88 |
| | **200** | 420 | 285 | 135 | 353 | 8.8 | 8.1 | 0.92 |
| **1** | **300** | 420 | 271 | 149 | 346 | 10.6 | 9.9 | 0.93 |
| | **400** | 420 | 257 | 163 | 339 | 12.1 | 11.3 | 0.93 |
| | **500** | 420 | 245 | 175 | 333 | 13.6 | 12.3 | 0.90 |
| | **100** | 653 | 539 | 114 | 596 | 5.3 | 4.9 | 0.92 |
| | **200** | 653 | 523 | 130 | 588 | 8.5 | 7.4 | 0.87 |
| **2** | **300** | 655 | 507 | 148 | 581 | 10.6 | 9.2 | 0.87 |
| | **400** | 656 | 497 | 159 | 577 | 12.7 | 9.9 | 0.78 |
| | **500** | 656 | 485 | 171 | 571 | 14.4 | 10.9 | 0.76 |
| | **100** | 913 | 797 | 116 | 855 | 5.3 | 4.5 | 0.85 |
| | **200** | 913 | 783 | 130 | 848 | 8.8 | 6.2 | 0.70 |
| **3** | **300** | 915 | 769 | 146 | 842 | 11.6 | 6.3 | 0.54 |
| | **400** | 917 | 759 | 158 | 838 | 14.8 | 7.5 | 0.51 |
| | **500** | 917 | 751 | 166 | 834 | 16.2 | 7.7 | 0.48 |
| | **100** | -1403 | -1305 | 98 | -1354 | 6.2 | 2.5 | 0.40 |
| | **200** | -1431 | -1307 | 124 | -1369 | 8.9 | 3.6 | 0.40 |
| **IV** | **300** | -1451 | -1310 | 141 | -1381 | 10.6 | 4.5 | 0.42 |
| | **400** | -1465 | -1315 | 150 | -1390 | 12.2 | 5.7 | 0.47 |
| | **500** | -1477 | -1317 | 160 | -1397 | 13.5 | 6.8 | 0.50 |
| | **100** | -1917 | -1759 | 158 | -1838 | 9.1 | 1.3 | 0.14 |
| | **200** | -1939 | -1765 | 174 | -1852 | 9.7 | 1.9 | 0.20 |
| **V** | **300** | -1959 | -1773 | 186 | -1866 | 9.5 | 2.1 | 0.22 |
| | **400** | -1973 | -1781 | 192 | -1877 | 9.3 | 2.3 | 0.25 |
| | **500** | -1987 | -1797 | 190 | -1892 | 8.6 | 2.5 | 0.29 |

**Table 3.25** Cyclic voltammetry data obtained from voltammograms (*vs* $Fc/Fc^+$) of **CoOEP, 72**, in $CH_2Cl_2$/ 0.1 $mol.dm^{-3}$ $[NBu_4][PF_6]$ with a glassy carbon working electrode at 20°C. Scan rates, $E_{pa}$ (anodic peak potentials), $\Delta E_p$ (difference between the anodic and cathodic peak potentials), $E^{0'}$ (formal reduction potentials, $E^{0'} = (E_{pa} + E_{pc})/2$), $i_{pa}$ (anodic peak currents) and $i_{pa}/i_{pc}$ (anodic/cathodic peak current relationship) are shown. Redox wave numbers correspond to numbers in Figure 3.44.

| Redox wave | $v$ / $mV\,s^{-1}$ | $E_{pa}$ / mV | $E_{pc}$ / mV | $\Delta E_p$ / mV | $E^{0'}$ / mV[a] | $i_{pa}$ / µA | $i_{pc}$ / µA | $i_{pc}/i_{pa}$ |
|---|---|---|---|---|---|---|---|---|
| | **100** | 267 | 139 | 128 | 203 | 5.9 | 5.7 | 0.97 |
| | **200** | 267 | 127 | 140 | 197 | 8.2 | 8.0 | 0.98 |
| **1** | **300** | 265 | 107 | 158 | 186 | 9.9 | 9.6 | 0.97 |
| | **400** | 265 | 93 | 172 | 179 | 10.7 | 10.5 | 0.98 |
| | **500** | 267 | 85 | 182 | 176 | 12.1 | 11.8 | 0.98 |
| | **100** | 547 | 449 | 98 | 498 | 5.9 | 5.4 | 0.92 |
| | **200** | 547 | 427 | 120 | 487 | 9.0 | 7.9 | 0.88 |
| **2** | **300** | 547 | 407 | 140 | 477 | 11.5 | 9.3 | 0.81 |
| | **400** | 547 | 395 | 152 | 471 | 13.5 | 10.4 | 0.77 |
| | **500** | 547 | 387 | 160 | 467 | 15.5 | 11.3 | 0.73 |
| | **100** | 901 | 801 | 100 | 851 | 5.4 | 4.5 | 0.83 |
| | **200** | 899 | 775 | 124 | 837 | 8.7 | 6.8 | 0.78 |
| **3** | **300** | 899 | 761 | 138 | 830 | 11.8 | 8.7 | 0.74 |
| | **400** | 899 | 747 | 152 | 823 | 14.4 | 10.1 | 0.70 |
| | **500** | 901 | 743 | 158 | 822 | 16.3 | 11.3 | 0.69 |
| | **100** | -1561 | -1439 | 122 | -1500 | 6.1 | 2.6 | 0.43 |
| | **200** | -1583 | -1461 | 122 | -1522 | 8.8 | 3.8 | 0.43 |
| **IV** | **300** | -1607 | -1471 | 136 | -1539 | 10.6 | 4.9 | 0.46 |
| | **400** | -1621 | -1483 | 138 | -1552 | 12.1 | 5.9 | 0.49 |
| | **500** | -1629 | -1491 | 138 | -1560 | 13.5 | 7.0 | 0.52 |
| | **100** | -2091 | -1905 | 186 | -1998 | 12.0 | 3.9 | 0.33 |
| | **200** | -2119 | -1910 | 209 | -2015 | 15.3 | 5.0 | 0.33 |
| **V** | **300** | -2147 | -1914 | 233 | -2031 | 16.2 | 5.4 | 0.33 |
| | **400** | -2167 | -1916 | 251 | -2042 | 18.4 | 6.1 | 0.33 |
| | **500** | -2181 | -1919 | 262 | -2050 | 19.1 | 6.8 | 0.36 |

**Table 3.26** Cyclic voltammetry data obtained from voltammograms (*vs* $Fc/Fc^+$) of $[Co(OEP)(DMSO)_2]ClO_4$, **77**, $[Co(TPP)(DMSO)_2]ClO_4$, **74**, and $[Co(TPPS)(DMSO)_2]ClO_4$, **75**, in **DMSO**/0.1 $mol.dm^{-3}$ $[NBu_4][PF_6]$ with a glassy carbon working electrode at a scan rate of 200 mV/s, at 20°C. The $Co^{II/III}$ $E_{pa}$ (anodic peak potential), $E_{pc}$ (cathodic peak potential) and $\Delta E_p$ (difference between the anodic and cathodic peak potentials) values are shown, corresponding to Figure 3.45.

| | $E_{pa}$ / mV | $E_{pc}$ / mV | $\Delta E_p$ / mV |
|---|---|---|---|
| **$[Co(OEP)(DMSO)_2]ClO_4$** | -261 | -594 | 333 |
| **$[Co(TPP)(DMSO)_2]ClO_4$** | -223 | -442 | 219 |
| **$[Co(TPPS)(DMSO)_2]ClO_4$** | -179 | -689 | 510 |

**Table 3.27** Cyclic voltammetry data obtained from voltammograms (*vs* $Fc/Fc^+$) of [CoTPP, **68**]* and [CoTPP + 2 equivalents **pyridine**]#, and of [CoOEP, **72**]* and [CoOEP + 2 equivalents **pyridine**]# in $CH_2Cl_2$/0.1 mol.dm$^{-3}$ $[NBu_4][PF_6]$ with a glassy carbon working electrode, at a scan rate of 100 mV/s, at 20°C. $E_{pa}$ (anodic peak potentials), $\Delta E_p$ (difference between the anodic and cathodic peak potentials), $E^{0'}$ (formal reduction potentials, $E^{0'} = (E_{pa} + E_{pc})/2$), $i_{pa}$ (anodic peak currents) and $i_{pa}/i_{pc}$ (anodic/cathodic peak current relationship) are shown. CoTPP oxidation wave numbers correspond to numbers in Figure 3.45. CoOEP reduction wave numbers correspond to numbers in Figure 3.47. Data is tabled for 0 and 2 equivalents of pyridine added.

| | Redox wave | Eq. Pyr. | $E_{pa}$ / mV | $E_{pc}$ / mV | $\Delta E_p$ / mV | $E^{0'}$ / mV[a] | $i_{pa}$ / µA | $i_{pc}$ / µA | $i_{pc}/i_{pa}$ |
|---|---|---|---|---|---|---|---|---|---|
| | 1 | 0* | 422 | 274 | 148 | 348 | 5.1 | 4.7 | 0.92 |
| | | 2# | -52 | -856 | 804 | -454 | 4.7 | 0.5 | 0.11 |
| | 2 | 0 | 652 | 508 | 144 | 580 | 5.8 | 5.3 | 0.91 |
| | | 2 | 872 | 728 | 144 | 800 | 6.5 | 4.9 | 0.75 |
| CoTPP | 3 | 0 | 914 | 766 | 148 | 840 | 5.9 | 5.1 | 0.86 |
| | | 2 | 1112 | 982 | 130 | 1047 | 6.2 | 2.8 | 0.45 |
| | IV | 0 | -1458 | -1288 | 170 | -1373 | 5.7 | 2.8 | 0.49 |
| | | 2 | -1414 | -1258 | 156 | -1336 | 6.9 | 3.6 | 0.52 |
| | V | 0 | -1968 | -1750 | 218 | -1859 | 5.9 | 1.4 | 0.24 |
| | | 2 | -1936 | -1740 | 196 | -1838 | 5.2 | 2.1 | 0.40 |
| | 1 | 0* | 242 | 84 | 158 | 163 | 4.2 | 3.7 | 0.88 |
| | | 2# | -190 | -1152 | 962 | -671 | 3.9 | 0.5 | 0.13 |
| | 2 | 0 | 528 | 378 | 150 | 453 | 4.2 | 4.0 | 0.95 |
| | | 2 | 634 | 492 | 142 | 563 | 6.2 | 4.2 | 0.68 |
| CoOEP | 3 | 0 | 838 | 736 | 102 | 787 | 4.2 | 3.7 | 0.88 |
| | | 2 | 954 | 706 | 248 | 830 | 8.8 | 3.6 | 0.41 |
| | IV | 0 | -1636 | -1502 | -134 | -1569 | 5.0 | 1.8 | 0.36 |
| | | 2 | -1596 | -1458 | -138 | -1527 | 6.0 | 2.4 | 0.40 |
| | V | 0 | -2148 | -1952 | -196 | -2050 | 8.3 | 2.6 | 0.31 |
| | | 2 | -2154 | -1960 | -194 | -2057 | 9.1 | 3.1 | 0.34 |

**Table 3.28** Cyclic voltammetry data obtained from voltammograms (*vs* $Fc/Fc^+$) of **CuTPP**, **68**, and **CuOEP**, **72**, in $CH_2Cl_2$/0.1 mol.dm$^{-3}$ $[NBu_4][PF_6]$ with a glassy carbon working electrode at a scan rate of 100 mV/s, at 20°C. $E_{pa}$ (anodic peak potentials), $\Delta E_p$ (difference between the anodic and cathodic peak potentials), $E^{0'}$ (formal reduction potentials, $E^{0'} = (E_{pa} + E_{pc})/2$), $i_{pa}$ (anodic peak currents) and $i_{pa}/i_{pc}$ (anodic/cathodic peak current relationship) are shown. Reduction wave numbers correspond to numbers in Figure 3.48.

| | Redox wave | $E_{pa}$ / mV | $E_{pc}$ / mV | $\Delta E_p$ / mV | $E^{0'}$ / mV[a] | $i_{pa}$ / µA | $i_{pc}$ / µA | $i_{pc}/i_{pa}$ |
|---|---|---|---|---|---|---|---|---|
| | 1 | 565 | 442 | 123 | 504 | 5.3 | 5.1 | 0.96 |
| CuTPP | 2 | 945 | 840 | 105 | 893 | 5.3 | 4.3 | 0.81 |
| | IV | -1874 | -1746 | 128 | -1810 | 5.1 | 4.6 | 0.90 |
| | 1 | 349 | 185 | 164 | 267 | 5.2 | 4.6 | 0.88 |
| CuOEP | 2 | 931 | 829 | 102 | 880 | 6.1 | 5.5 | 0.90 |
| | IV | -2113 | -1977 | 136 | -2045 | 7.0 | 4.6 | 0.66 |

# 4. Experimental

## 4.1. Introduction

Experimental procedures, reaction conditions and techniques used during the course of this investigation are reported in this chapter.

## 4.2. Materials

Solid reagents were purchased from Sigma-Aldrich, and used without further purification. Liquid reagents and solvents were distilled prior to use. Doubly distilled water was used. Melting points (uncorrected) of products were determined on a Reichert Thermopan microscope with a Koffler hot-stage. The upper temperature limit of this instrument is 230°C. Elemental analyses of selected products were performed by the Canadian Microanalytical Service.

## 4.3. Spectrometry

Nuclear magnetic resonance proton spectra were recorded on a 300 MHz Bruker Avance DPX 300 NMR spectrometer, at 298 K. Chemical shifts are reported relative to $SiMe_4$ (0 ppm). Spectral processing was done by means of the MestReC v.4.5.9.1 NMR software for Windows. Ultraviolet and visible spectra were recorded on a Varian Cary 50 Probe UV/visible spectrophotometer. Spectra were drawn from dilute solutions in double-walled quartz cuvettes. Mixing reagent solutions contained in the separate cuvette compartments ensured unaltered reagent absorption coefficients. All relevant compounds obey Beer's law at the experimental concentrations utilised. Spectral processing was done with Microsoft Excel.

## 4.4. Synthesis

### 4.4.1. Dithizone Derivatives

#### 4.4.1.1. S-methyldithizone, S-MeHDz [17] (Scheme 3.1, p.57)

**Methyliodide Method**: Methyliodide (0.05 g, 0.34 mmol) was added to potassium dithizonate (0.05 g, 0.17 mmol) dissolved in acetone (40 ml). While stirring the solution at room temperature for 1 hour, the orange colour changed to deep purple. The reaction mixture was filtered and the solvent removed under reduced pressure. The residue was dissolved in benzene (100 ml), leaving potassium iodide and any unreacted potassium dithizonate behind. After a second filtration the solvent was removed under reduced pressure, and recrystallization done from ethanol (100 ml). The black S-methylated dithizone crystals were washed with 1 M

aqueous ammonia (to remove unmethylated dithizone), followed by water, and a small amount of ice cold ethanol to give 0.0269 g (58 %) pure **17**.

M.p. 118-120°C, $\lambda_{max}$/nm (dichloromethane) 542, $\delta_H$ (300 MHz, $CDCl_3$, Spectrum A1)/ppm: 2.41 & 2.55 (3 H, 2 × s, C<u>H</u>$_3$ ), 7.05 – 7.97 (10 H, 3 × m, C$_6$<u>H</u>$_5$), 9.53 & 10.27 (1 H, 2 × s, N<u>H</u>).

**Dimethylsulfate Method** (Irving *et al* [238]): A solution of dithizone (5.0 g, 19.5 mmol) in aqueous sodium hydroxide (0.5 M, 100 ml) was shaken well with dimethylsulfate (1.9 ml, 2.6 g, 20.6 mmol) (caution, carcinogenic) in a glass stoppered flask. The initial orange colour of the solution rapidly disappeared and a black solid separated almost immediately. A further portion of the NaOH solution (15 ml, 2 M) was added, and the mixture was heated gently on a water bath for 30 minutes to destroy any excess of dimethylsulfate. On cooling, the mixture was extracted with chloroform and the organic extract was washed several times with dilute aqueous ammonia (to remove unmethylated dithizone) and with water, and finally the organic extract was dried ($Na_2SO_4$). Removal of the solvent left impure S-methylated dithizone, which was purified by chromatography on 100 g silica, using chloroform as eluent. The dark brown product band, running ahead, was followed by narrower light brown, light green, and pink bands. Recrystallization from warm ethanol (700 ml) gave 3.48 g black S-methylated dithizone needles with a bronze reflex (66 %). Characterization data agrees with the former methyl iodide method.

### 4.4.1.2. S-Methyldithizonatophenylmercury(II), PhHg(S-Me)HDz [18] (Scheme 3.1, p.57)

Phenylmercury(II) chloride (0.58 g, 1.85 mmol) and S-methyldithizone (0.5 g, 1.85 mmol) was dissolved in dichloromethane (100 ml) in a separating funnel. An aqueous solution of sodium hydroxide (0.2 M, 100 ml) was added, and the funnel shaken well. The organic layer was washed several times with distilled water and dried by filtration through sodium sulfate. The solvent was removed under reduced pressure and recrystallization done from dichloromethane and ethanol, yielding 0.95 g (94 %) of **18**.

M.p. 143 °C, $\lambda_{max}$/nm (dichloromethane) 441, $\delta_H$ (300 MHz, $CDCl_3$, Spectrum A2)/ppm: 2.53 (3 H, s, C<u>H</u>$_3$), 7.02 – 7.98 ( 15 H, m, 3 × C$_6$<u>H</u>$_5$ )

### 4.4.1.3. Dehydrodithizone, DDz [21] [28] (Scheme 3.2, p.60)

A solution of dithizone (1 g, 3.9 mmol) in dichloromethane (300 ml) was stirred (2 hours) with a solution of potassium hexacyanoiron(III) (3.2 g) and potassium carbonate (3 g) in water (100 ml). The organic layer was removed and the solvent evaporated under reduced pressure. The product residue, on recrystallization from a minimum hot acetone and 30 % water, gave 0.52 g orange-red crystals of **21** (52 %).

M.p. 173°C (explode), $\lambda_{max}$/nm (acetone) 456, $\delta_H$ (300 MHz, $(CD_3)_2SO$, Spectrum A3)/ppm: 7.52 – 7.67 (6 H, m, *m,p*-$C_6\underline{H}_5$), 7.72 (4 H, 2 × d, *o*-$C_6H_5$)

### 4.4.1.4. Potassium dithizonate, $K^+HDz^-$ [19] (Scheme 3.3, p.61)

Potassiumhydroxide (0.4 g, 7 mmol) dissolved in hot methanol (100 ml) was added dropwise to dithizone (1.0 g, 3.9 mmol) dissolved in dichloromethane (300 ml) while stirring. The solution changed from dark green to deep orange-red. The solvents were removed under reduced pressure, followed by extractions of the product residue, first with acetone (80 ml), and then with methanol (40 ml). After every extraction the solution was gravity-filtered through filter paper and the solvent evaporated under reduced pressure. The orange potassium salt of dithizone was ground fine and dried over night at 100°C to ultimately give 1.12 g (41 %) yield of **19**.

Testing for potassium, using a flame photometer, indicated a 1 : 1 ratio for $K^+$ : $HDz^-$.

M.p. 200°C (decomposed), $\lambda_{max}$/nm (methanol) 471, (acetone) 501, $\delta_H$ (300 MHz, $(CD_3)_2SO$, Spectrum A4)/ppm: 6.70 – 7.75 (10 H, m, $C_6\underline{H}_5$)

### 4.4.1.5. Tetrabutylammonium dithizonate, $Bu_4N^+HDz^-$ [23] (Scheme 3.3, p.61)

Tetrabutylammonium bromide (0.05 g, 0.155 mmol) and potassium dithizonate (0.046 g, 0.155 mmol) was dissolved in acetone (50 ml) and stirred for 1 hour. The solvent was removed under reduced pressure, after which the product was again dissolved in acetone. The insoluble white potassium bromide salt was filtered off and the solvent removed under reduced pressure. This procedure was repeated twice. The resulting orange tetrabutylammonium dithizonate product was dried overnight at 50°C to give 0.06 g (77 %) pure compound.

M.p. 71 °C, $\lambda_{max}$/nm (acetone) 501, $\delta_H$ (300 MHz, $CDCl_3$, Spectrum A5)/ppm: 0.92 – 1.02 (12 H, t, $CH_2CH_2CH_2C\underline{H}_3$), 1.33 – 1.47 (8 H, m, $CH_2CH_2C\underline{H}_2CH_3$), 1.51 – 1.65 (8 H, m, $CH_2C\underline{H}_2CH_2CH_3$), 3.15 – 3.35 (8 H, t, $C\underline{H}_2CH_2CH_2CH_3$), 7.10 – 8.05 (10 H, m, $C_6\underline{H}_5$),

### 4.4.1.6. Dithizonatophenylmercury(II), PhHgHDz [20] (Scheme 3.4, p.63)

Triethylamine (0.51 g, 5 mmol) was added to a solution of dithizone (1.025 g, 4 mmol) and phenylmercury(II) chloride (1.315 g, 4.2 mmol) in dichloromethane (300 ml). After stirring for 15 minutes the solvent was removed under reduced pressure. Recrystallization of dithizonatophenylmercury(II) was done from dichloromethane and ethanol, to liberate 1.98 g (93 %) of pure **20**.

M.p. 166 °C, $\lambda_{max}$/nm (dichloromethane) 470, $\delta_H$ (300 MHz, $CDCl_3$, Spectrum A6)/ppm: 7.60 – 8.00 (15 H, 3 × m, $C_6\underline{H}_5$). Passing $CDCl_3$ through basic alumina to remove trace amounts of acid that are often present in chloroform, resulted in additional impurities being observed around 1 ppm. Acids protonate the ligand with consequent decomposition of the complex.

### 4.4.1.7. Dithizonatotrimethyltin(IV), $Me_3SnHDz$ [28] (Scheme 3.5, p.65)

Dithizone (0.1 g, 0.39 mmol) was dissolved in dry benzene (100 ml) and dimethylamino-trimethyltin (0.082 g, 0.394 mmol) was added under nitrogen. The solvent was removed under reduced pressure, yielding 0.157 g (97 %) dithizonatotrimethyltin(IV), after recrystallization from ether.

M.p. 134°C, $\lambda_{max}$/nm (ether) 442, $\delta_H$ (300 MHz, $C_6D_6$, Spectrum A7)/ppm: 0.47 (6 H, s, 2 × $C\underline{H}_3$), 0.54 (3 H, s, $C\underline{H}_3$), 6.85 – 8.09 (10 H, 3 × m, $C_6\underline{H}_5$), Crystallographic data (Par.3.3.2)

### 4.4.1.8. Chloropentaamminecobalt(III) chloride, $[Co(NH_3)_5Cl]Cl_2$ [31] [177] (Scheme 3.7, p.66)

Ammoniumchloride (5 g, 93.5 mmol) was dissolved in concentrated aqueous ammonia (30 ml, *ca* 0.44 mol) in a 250 ml flask. The solution was stirred while finely powdered cobalt(II) chloride hexahydrate (10 g, 42 mmol) was added in small portions, each portion being dissolved before the next was added. To this slurry, 30 % hydrogen peroxide (8 ml, 49 mmol) was slowly added with a pasture pipette while stirring the solution, resulting in a vigorous exothermic reaction with effervescence. When the effervescence had virtually ceased, a deep red solution of the aquopentaamine salt has formed. To this, concentrated hydrochloric acid (30 ml, 12 M) was added slowly. The mixture was heated for 15 minutes on a steam bath, cooled to room temperature, and filtered by suction. The precipitated product was washed with several portions of ice cold water totalling 50 ml, followed by an equal volume of cold hydrochloric acid (6 M). After an alcohol wash and an acetone wash, the product was heated at 100 to 110°C for 2 hours to facilitate drying. In this manner 9.6 g ( 91 %) of pure **31** was isolated.

M.p. > 230 °C, $\lambda_{max}$/nm (water) 363, 531.

### 4.4.1.9. Hexaamminecobalt(III) chloride, $[Co(NH_3)_6]Cl_3$ [32] [178] (Scheme 3.7, p.66)

Cobalt(II) chloride hexahydrate (12 g, 83 mmol) and ammonium chloride (8 g, 150 mmol) were added to water (10 ml). The mixture was shaken until most of the salts were dissolved. Then activated decolourising charcoal (0.2 g) and concentrated ammonia (25 ml) were added. Air was vigorously bubbled through the mixture until the red solution turned yellow-brown (after about 4 hours). The crystals and carbon were filtered on a Büchner funnel and then added to a solution

of concentrated hydrochloric acid in water (1 ml HCl in 75 ml $H_2O$). The mixture was heated on a hot plate to effect complete solution, and was filtered hot. The hexaamminecobalt(III) chloride was precipitated by addition of concentrated hydrochloric acid (20 ml) and slowly cooling to 0°C. The orange-yellow precipitate was filtered, washed with 60 % ethanol, and then with 95 % ethanol, and dried at 90°C to give 10.9 g (81 %) of pure **32**.

M.p. > 230 °C, $\lambda_{max}$/nm (water) 334, 486.

### 4.4.1.10. *Tris*-dithizonatocobalt(III), $Co(HDz)_3$ [33] (Scheme 3.7, p.66)

**Hexaaqua Method**: Cobalt(II) chloride hexahydrate (0.0810 g, 0.34 mmol) and potassium dithizonate (0.3 g, 1 mmol) was dissolved in acetone (100 ml) and stirred for 15 minutes. A dark purple solution immediately formed. The solution was filtered and the solvent removed under reduced pressure. The cobalt dithizonate complex was twice more dissolved in dichloromethane, filtered, and the solvent removed under reduced pressure. Using dichloromethane as eluent, the product was passed through a column containing silica. The main purple band was collected and the product recrystallised from ether to give 0.262 g (90 %) of pure **33**.

M.p. 175 °C, (Found: C, 55.88; H, 4.04; N, 19.08. $(C_{13}H_{11}N_4S)_3Co$ requires C, 54.66; H, 3.88; N, 19.61 %); $\lambda_{max}$/nm (dichloromethane) 545, $\delta_H$ (300 MHz, $CDCl_3$, Spectrum A8)/ppm: 6.40 – 7.45 (30 H, 3 × m, $C_6\underline{H}_5$), 9.49 (1 H, s, N$\underline{H}$). Crystallographic data is presented in Par.3.3.3.

**Pentaamine Method**: Chloropentaamminecobalt(III) chloride (0.17g, 0.68 mmol) and potassium dithizonate (0.2 g, 0.68 mmol) was dissolved in water (100 ml) and stirred for 15 minutes. The insoluble black product was filtered off, thoroughly washed with water, and dried at 50°C to give 0.15 g (100 %) of pure **33**, with characterization as in the above hexaaqua method.

**Hexaamine Method**: Except for the use of hexaamminecobalt(III) chloride as reagent, the synthetic procedure was as above. The reaction mixture, however, had to be heated slightly (60°C), and a longer period of stirring was required (1 hour) before 0.14 g (99 %) of product **33** was isolated. 0.2 g KHDz reagent was used. Characterization was as in the hexaaqua method.

### 4.4.1.11. *Para*-chlorophenyldithizone, $(p\text{-ClPhNHN})_2CS$ [40a] [14] (Scheme 3.9, p.70)

**Nitroformazan [37a]**: In a 100 ml beaker, *para*-chloroaniline (5 g, 39 mmol) was added to a mixture of concentrated hydrochloric acid (20 ml) and water (35 ml) at 0°C. Diazotization was done by the slow addition of sodium nitrite (3.5 g, 50 mmol), stirring, until (*ca* 1 hour) all the aniline was dissolved. In a 500 ml beaker, the diazo solution was added, with stirring, to a cold mixture of sodium acetate (80 g, *ca* 1 mol), glacial acetic acid (45 ml, 0.75 mol) and water (25 ml). Nitromethane (6.8 g, 111 mmol) was added after 10 minutes. After stirring for 2 hours

at room temperature the volume was increased with water to 400 ml. After stirring for another 1 hour the red formazyl derivative was filtered in a large Büchner funnel, washed with copious amounts of water and then with a small amount of ethanol and ether. Drying of the nitroformazan product was done in a vacuum oven at 70°C (5.54 g, 41 %).

**Thiocarbazone [38a]**: Nitroformazan (1.2 g) was suspended in absolute ethanol (150 ml) in a 200 ml Erlenmeyer flask. The mixture was saturated (20 minutes) with ammonia gas. Then, for a period of 3 hours, hydrogen sulfide gas, with the use of a Gibbs apparatus, was passed through the solution, resulting in the formation of thiocarbazide. After reduction was complete as indicated by a change of colour from red to orange-yellow, while manually stirring, the solution was slowly added to a water/ice (500 ml) mixture. The dirty-white carbazide was filtered off by suction on a Büchner funnel, and washed with water. The unstable thiocarbazide compound was oxidised to red thiocarbazone by adding cold 2 % methanolic potassium hydroxide solution (50 ml). Stirring was continued until complete dissolution.

***Para*-chlorophenyldithizone [40a]**: Dark green dithizone was precipitated by addition of the thiocarbazone to dilute hydrochloric acid (1 %, 100 ml). The product was filtered and again precipitated from an alcoholic alkali solution to which diluted hydrochloric acid was added. The product was washed with water, followed by a little ethanol and ether.

A crude product sample was dissolved in chloroform and passed through a short silica column using toluene as eluent. A yellow impurity ran ahead of the green product band, while some impurities stayed behind at the origin. Alternatively, instead of running a column, repeating the aforementioned precipitation procedure five times, yielded pure 0.51 g (44 %) *para*-chlorophenyldithizone, as monitored by the use of TLC plates and NMR spectroscopy.

M.p. 175 °C, $\lambda_{max}$/nm (dichloromethane) 447, 625, $\delta_H$ (300 MHz, $CDCl_3$, Spectrum A10)/ppm: 7.50 (4 H, d, $J_{a'b'}$ = 8 Hz, *o*-$C_6\underline{H}_4Cl$), 7.68 (4 H, d, $J_{b'a'}$ = 8 Hz, *m*-$C_6\underline{H}_4Cl$)

### 4.4.1.12. *Para*-fluorophenyldithizone, (*p*-FPhNHN)$_2$CS [40b] (Scheme 3.9, p.70)

Synthetic procedure as for *para*-chlorophenyldithizone (4.4.1.11).

(a) Nitroformazan product yield, 3.98 g (25 %)

(b) Dithizone product yield, 0.3 g (26 %) 1.2 g nitroformazan reagent was used.

M.p. 174 °C, $\lambda_{max}$/nm (dichloromethane) 444, 609, $\delta_H$ (300 MHz, $CDCl_3$, Spectrum A10)/ppm: 7.24 (4 H, m, *o*-$C_6\underline{H}_4F$), 7.73 (4 H, m, *m*-$C_6\underline{H}_4F$)

### 4.4.1.13. *Meta*-fluorophenyldithizone, (*m*-FPhNHN)$_2$CS [40c]

Synthetic procedure as for *para*-chlorophenyldithizone (4.4.1.11).

(a) Nitroformazan product yield, 2.38 g (17 %)

(b) Dithizone product yield, 0.58 g (51 %) 1.2 g nitroformazan reagent was used.

M.p. 112 °C, $\lambda_{max}$/nm (dichloromethane) 447, 615, $\delta_H$ (300 MHz, $CDCl_3$, Spectrum A11)/ppm: 7.03 – 7.16 & 7.35 – 7.63 (8 H, 2 × m, $C_6\underline{H}_4F$)

### 4.4.1.14. *Ortho*-fluorophenyldithizone, (*o*-FPhNHN)$_2$CS [40d]

Synthetic procedure as for *para*-chlorophenyldithizone (4.4.1.11).

(a) Nitroformazan product yield, 1.03 g (7.4 %)

(b) Dithizone product yield, 0.22 g (26 %) 0.9 g nitroformazan reagent was used.

M.p. 114 °C, $\lambda_{max}$/nm (dichloromethane) 450, 621, $\delta_H$ (300 MHz, $CDCl_3$, Spectrum A12)/ppm: 7.41 – 7.29 & 8.02 – 8.10 (8 H, 2 × m, $C_6\underline{H}_4F$)

### 4.4.1.15. 3,4-difluorophenyldithizone, (3,4-F$_2$PhNHN)$_2$CS [40e]

Synthetic procedure as for *para*-chlorophenyldithizone (4.4.1.11).

(a) Nitroformazan product yield, 1.1 g (17 %)

(b) Product yield, 0.2 g (18 %) 1.1 g nitroformazan reagent was used.

M.p. 83 °C, $\lambda_{max}$/nm (dichloromethane) 404, $\delta_H$ (300 MHz, $CDCl_3$)/ppm: 7.50 (3 H, m, $C_6\underline{H}_3F_2$)

### 4.4.1.16. 3,5-difluorophenyldithizone, (3,5-F$_2$PhNHN)$_2$CS [40f]

Synthetic procedure as for *para*-chlorophenyldithizone (4.4.1.11).

(a) Nitroformazan product yield, 1.36 g (21 %)

(b) Product yield, 0.5 g (41 %) 1.2 g nitroformazan reagent was used.

M.p. 138 °C, $\lambda_{max}$/nm (dichloromethane) 401, $\delta_H$ (300 MHz, $CDCl_3$)/ppm: 7.00 (3 H, m, $C_6\underline{H}_3F_2$)

### 4.4.1.17. (*p*-Cl)dithizonatophenylmercury(II), PhHg(*p*-Cl)HDz (Scheme 3.4, p.63)

Synthetic procedure as for dithizonatophenylmercury(II) (4.4.1.6).

Product yield, 0.15 g (81 %). 0.1 g *p*-chlorophenyldithizone reagent was used.

M.p. 188 °C, $\lambda_{max}$/nm (dichloromethane) 482, $\delta_H$ ($CDCl_3$)/ppm: 7.33 -7.91 (13 H, m, 2 × $C_6\underline{H}_4Cl$ & 1 × $C_6\underline{H}_5$ )

### 4.4.1.18. (*p*-F)dithizonatophenylmercury(II), PhHg(*p*-F)HDz

Synthetic procedure as for dithizonatophenylmercury(II) (4.4.1.6).

Product yield, 0.16 g (82 %). 0.1 g *p*-fluorophenyldithizone reagent was used.

M.p. 208 °C, $\lambda_{max}$/nm (dichloromethane) 471, $\delta_H$ (300 MHz, $CDCl_3$)/ppm: 7.06 – 7.99 (13 H, m, 2 × $C_6\underline{H}_4F$ & 1 × $C_6\underline{H}_5$ )

### 4.4.1.19. (*m*-F)dithizonatophenylmercury(II), PhHg(*m*-F)HDz

Synthetic procedure as for dithizonatophenylmercury(II) (4.4.1.6).

Product yield, 0.11 g (56 %). 0.1 g *m*-fluorophenyldithizone reagent was used.

M.p. 143 °C, $\lambda_{max}$ (dichloromethane) 472 nm, $\delta_H$ (300 MHz, $CDCl_3$)/ppm: 6.75 – 7.79 (13 H, m, $2 \times C_6\underline{H}_4F$ & $1 \times C_6\underline{H}_5$)

### 4.4.1.20. (*o*-F)dithizonatophenylmercury(II), PhHg(*o*-F)HDz

Synthetic procedure as for dithizonatophenylmercury(II) (4.4.1.6).

Product yield, 0.15 g (77 %). 0.1 g *o*-fluorophenyldithizone reagent was used.

M.p. 163 °C, $\lambda_{max}$/nm (dichloromethane) 471, $\delta_H$ (300 MHz, $CDCl_3$)/ppm: 6.99 – 7.88 (13 H, m, $2 \times C_6\underline{H}_4F$ & $1 \times C_6\underline{H}_5$)

### 4.4.1.21. 3,4-difluorophenyldithizonatophenylmercury(II), PhHg(3,4-$F_2$)HDz

Attempted synthetic procedure as for dithizonatophenylmercury(II) (4.4.1.6).

Product yield, 0.06 g (31 %). 0.1 g 3,4-difluorophenyldithizone reagent was used.

Product not photochromic. No further characterization done.

### 4.4.1.22. 3,5-difluorophenyldithizonatophenylmercury(II), PhHg(3,5-$F_2$)HDz

Attempted synthetic procedure as for dithizonatophenylmercury(II) (4.4.1.6).

Product yield, 0.04 g (20 %). 0.1 g 3,5-difluorophenyldithizone reagent was used.

Product not photochromic. No further characterization done.

## 4.4.2. Polymer Synthesis and Anchoring Reactions

### 4.4.2.1. *para*-Aminophenylmercury(II) acetate, $H_2$NPhHg(OAc) [41] [77,78] (Scheme 3.10, p.72)

Freshly distilled aniline (5.84 g, 62.7 mmol) was added to a solution of mercury(II) acetate (10.0g, 31.4 mmol) in water (50 ml) and stirred at room temperature for 3 hours, during which time a white precipitate formed. The white precipitate that formed was filtered off, washed with water, and dried overnight to give 4-aminophenylmercury(II) acetate (7.35 g, 67 %).

M.p. 162 °C, $\delta_H$ (300 MHz, $(CD_3)_2SO$, Spectrum A13)/ppm: 1.91 (3 H, s, $C\underline{H}_3$ ), 5.00 (2 H, s, $N\underline{H}_2$ ), 6.53 (2 H, d, $J_{a'b'}$ = 8 Hz, *o*-$C_6\underline{H}_4$), 6.99 (2 H, d, $J_{b'a'}$ = 8 Hz, *m*-$C_6\underline{H}_4$)

### 4.4.2.2. Benzylaminomercury(II) chloride, $PhCH_2NH_2HgCl$ [43] (Scheme 3.10, p.72)

To mercury(II) acetate (2 g, 6.28 mmol) dissolved in water (20 ml), benzylamine (1.350 g, 12.6 mmol) was added and stirred for 3 hours, while a light yellow-white precipitate formed. The product was filtered off, washed with a small amount of water (product soluble), and dried overnight at 50°C (1.45 g, 64 %).

M.p. 136 °C, (Found: C, 22.11; H, 2.32; N, 3.66. $C_6H_5CH_2NH_2HgCl{\cdot}HCl$ requires C, 22.20; H, 2.40; N, 3.70 %); $\delta_H$ (300 MHz, $(CD_3)_2SO$, Spectrum A14)/ppm: 3.91 (2 H, s, $C\underline{H}_2$ ), 7.29 – 7.42 (5 H, m, $C_6\underline{H}_5$)

The complete series, $[H_2N(CH_2)_nPhHgCl]Cl$, where n = 1, 2, 3 & 4, was synthesised according to the above method. Due to insolubility of products, NMR spectra could not be recorded for the $H_2N(CH_2)_nPhHgCl$ complexes with n = 2, 3 & 4.

### 4.4.2.3. *p*-Aminophenyldithizonatomercury(II), $H_2NPhHgHDz$ [45] (Scheme 3.4, p.63)

The synthetic procedure was as for dithizonatophenylmercury(II) (4.4.1.6).

Product yield, 1.95 g (91 %). 1.025 g dithizone reagent was used.

M.p. 130 °C, $\lambda_{max}$/nm (dichloromethane) 475.5, $\delta_H$ (300 MHz, $CDCl_3$)/ppm: 6.70 – 8.05 (14 H, m, $2 \times C_6\underline{H}_5$ & $1 \times C_6\underline{H}_4NH_2$ )

### 4.4.2.4. 4-oxo-4-[(2-phenylethyl)amino]butanoic acid [44] (Scheme 3.11, p.73)

Succinic anhydride (0.810 g, 8.25 mmol) was dissolved in acetone (50 ml). 2-Phenylethylamine (1g, 8.25 mmol) was added, and the reaction mixture stirred for 30 minutes. The solution immediately turned milky. The precipitate was filtered off and washed with cold acetone until the light yellow colour disappeared, giving 0.4 g pure **44**.

M.p. 104 °C, $\delta_H$ (300 MHz, ($D_2O$, Spectrum A15)/ppm: 2.37 (4 H, s, $OCC\underline{H}_2C\underline{H}_2CO$), 2.85 (2H, t, $PhCH_2C\underline{H}_2NH$), 3.13 (2 H, t, $PhC\underline{H}_2CH_2NH$), 7.15 – 7.29 (5 H, m, $C_6\underline{H}_5$)

### 4.4.2.5. *p*-Anilino-4-oxobutanoic acid(dithizonato)mercury(II) $HOOCCH_2CH_2CONHPhHg(HDz)$ [46] (Scheme 3.11, p.73)

*Para*-aminophenyl(dithizonato)mercury(II) (0.5 g, 0.91 mmol) was dissolved in acetone (200 ml), and succinic anhydride (0.27 g, 2.7 mmol) added. The solution was stirred for 30 minutes at 50°C. Water (100 ml) was added and the acetone removed under reduced pressure.

A small amount of floating impurities were decanted and the product filtered off, washed with ample amounts of water, and dried. Recrystallization was done from a minimum of acetone and ethanol, to give 0.47 g (80 %) of pure **46**.

M.p. 228 °C, $\lambda_{max}$/nm (dichloromethane) 489, $\delta_H$ (300 MHz, $(CD_3)_2CO$, Spectrum A16)/ppm: 2.70 (4 H, s, $OCC\underline{H}_2C\underline{H}_2CO$), 7.03 – 8.02 (14 H, m, $2 \times C_6\underline{H}_5$ & $C_6\underline{H}_4$), 9.23 (1 H, s, $PhN\underline{H}N$), 9.91 (1H, s, $PhN\underline{H}CO$)

### 4.4.2.6. Poly-DL-succinimide [48] [82] (Scheme 3.12, p.75)

Finely powdered DL-aspartic acid (10.00 g, 75.14 mmol) and 85% *ortho*-phosphoric acid (10.00 g, 102 mmol) were thoroughly mixed in a 250 ml round bottom flask. The flask (connected to a rotary evaporator fitted with a vacuum pump) was carefully submerged, at atmospheric pressure, into an oil bath preheated to 200°C, with slow rotation. After 5 minutes of rotation, the oil bath temperature was lowered slightly and maintained at 170-190°C for 2½ hours, while the pressure was reduced to below 5 torr. After the flask was cooled down to room temperature, dimethylformamide (60 ml) was poured onto the reaction mixture. The flask was slowly rotated on the rotary evaporator overnight, to afford a homogeneous light gold solution. The solution was very slowly poured, with vigorous stirring, into a beaker containing water (1000 ml, 35°C). The resulting polymer suspension was filtered through a large Büchner funnel, thoroughly washed with water (5 × 250 ml), and dried overnight in a vacuum oven at 50°C.

The solid was ground under liquid nitrogen and then further dried (30 hours) at 56°C under reduced pressure over phosphor pentoxide in an Abderhalden (incl. vacuum pump & $N_2$ trap) drying tube, using boiling acetone as a heat source, to give 6.25 g (86 %) white poly-DL-succinimide, having an average molar mass of 57 000 $g.mol^{-1}$.

$\delta_H$ (300 MHz, $(CD_3)_2SO$, Spectrum A17)/ppm: 5.27 (1 H, s, $C\underline{H}$), 3.17 (2 H, s, $C\underline{H}_2$), 2.70 (2 H, s, $C\underline{H}_2$)

### 4.4.2.7. 4 : 3 : 1 Polysuccinimide : 4-(3-aminopropyl)morpholine : ethylenediamine adduct [49] [84] (Scheme 3.12, p.75)

To a solution of polysuccinimide (1.164 g, 12 mmol) in anhydrous dimethylsulfoxide (15 ml, 5°C), 4-(3-aminopropyl)morpholine (1.298 g, 9 mmol) was added over a period of 10 minutes. The reaction mixture was stirred at room temperature for 20 hours, cooled down, and ethylenediamine (0.24 g, 4 mmol, 25 % excess) added. After 8 hours of stirring, a dialyses tube was charged with the mixture to which 50 ml of water was added, and dialysed over 48 hours.

After freeze-drying, 0.8 g (30 %) of the white water-soluble amine-functionalised polymer was obtained.

$\delta_H$ (300 MHz, $D_2O$, Spectrum A18)/ppm: 1.59 (6 H, s, β-C<u>H</u>$_2$), 2.29 (6 H, s, δ-C<u>H</u>$_2$), 2.42 (12 H, s, γ-C<u>H</u>$_2$), 2.66 (8 H, s, 4 asp-C<u>H</u>$_2$), 3.08 (6H, s, α-C<u>H</u>$_2$), 3.62 (12 H, s, ε-C<u>H</u>$_2$), 4.28 - 4.62 (4 H, s, asp-C<u>H</u>), 2.96 (2 H, s, α'-$CH_2$), 3.35 (2 H, s, β'-$CH_2$); $M_r > 12\,000$ g.mol$^{-1}$.

### 4.4.2.8. Polymer 49 adduct bearing *p*-anilino-4-oxobutanoic acid (dithizonato)mercury(II) [50] (Scheme 3.12, p.75)

To a solution of polymer **49** (0.2 g, 0.23 mmol) (Par. 4.4.2.7. product) in water (1 ml), in this order, was added triethylamine (0.03 g, 0.3 mmol), *p*-anilino-4-oxobutanoic acid(dithizonato) mercury(II) (0.147 g, 0.23 mmol) in dimethylformamide (5 ml), and the coupling reagent, O-benzotriazolyl-N,N,N',N'-tetramethyluronium hexafluorophosphate (0.1 g, 0.26 mmol). The reaction mixture was stirred for 3 hours at room temperature, dialysed for 22 hours (12000 molar mass cut-off membrane tubing), and freeze-dried, to give 0.3 g (85 %) of **50**.

Found: C, 43.18; H, 5.24; N, 13.74; Hg, <u>13.3</u> %. If only 70% anchoring of **50** occurred, as NMR suggests, then $(C_{11}H_{19}N_3O_3)_3(C_6H_{11}N_3O_2)_{0.3}(C_{29}H_{30}N_8O_4SHg)_{0.7}$ requires C, 50.55; H, 6.16; N, 16.32; Hg, 10.56 %). If 100 % anchoring occurred, then $(C_{11}H_{19}N_3O_3)_3$ $(C_{29}H_{30}N_8O_4SHg)_1$ requires C, 49.28; H, 5.80; N, 15.76; Hg, <u>13.3</u> %

$\lambda_{max}$/nm (water) 484, $\delta_H$ (300 MHz, $D_2O$, Spectrum A19)/ppm: 1.57 (6 H, s, β-C<u>H</u>$_2$), 1.98 – 3.82 (52 H, m, remaining aliphatic <u>H</u>), 4.27 – 4.60 (4 H, asp-C<u>H</u>), 6.24 – 8.04 (14 H, m, 2 × C$_6$<u>H</u>$_5$ & 1 × C$_6$<u>H</u>$_4$) (70 % of the polymeric amine sites bonded to the photochromic moiety).

$M_r > 12000$ g.mol$^{-1}$. From the elemental analyses and NMR data it is concluded that 30 % mercury dithizonate decomposition occurred, and that this Hg bonded to free –$NH_2$ chains in an as yet undetermined manner.

### 4.4.2.9. Polyepichlorohydrin [52] [89] (Scheme 3.13, p.76)

Phenol (0.0941 g, 1 mmol) was added to a mixture of pentane (10 ml) and hexane (10 ml) in a 500 ml three-necked round-bottom flask, equipped with an overhead stirrer. A solution of epichlorohydrin (18.84 g, 204 mmol) in hexane (40 ml) was prepared and 0.5 ml of this solution was added to the flask, using a dropping funnel. After the internal temperature of the reaction mixture was set to 25°C, freshly distilled trifluoroboron etherate (0.08 ml) was added to the stirring solution. The remaining epichlorohydrin solution in a dropping funnel was then added over a period of 24 hours, while maintaining the temperature between 24 and 27°C. Subsequent to addition, the reaction mixture was stirred for a further 30 minutes. The hexane phase was decanted and water (100 ml) was added. After stirring for 30 minutes, the water was decanted

and the precipitate was dissolved in dichloromethane (100 ml). Following thorough washing of the dichloromethane phase with water (6 × 100 ml), the organic phase was dried over magnesium sulfate and removal of the solvent under reduced pressure gave 11 g of polyepichlorohydrin, as a colourless highly viscous liquid.

$\delta_H$ (300 MHz, $CDCl_3$, Spectrum A20)/ppm: 3.58 – 3.68 (2 H, m, $C\underline{H_2}Cl$), 3.68 – 4.01 (3 H, m, $C\underline{H}C\underline{H_2}O$); $M_r$ = 23 224 g/mol.

### 4.4.2.10. *p*-Aminophenyldithizonatomercury(II) polyepichlorohydrin [53] (Scheme 3.13, p.75)

Polyepichlorohydrin (0.1 g, 1.08 mmol) was dissolved in dimethylsulfoxide (2 ml), and sodium bicarbonate (0.12 g, 1.4 mmol) added. *p*-Aminophenyldithizonatomercury(II) (0.197 g, 0.36 mmol) was then added, and the reaction mixture stirred for 3 hours at 80°C. The product solution was poured into vigorously stirring lukewarm water (100 ml), and the precipitated polymer filtered off (0.16 g). Remaining unreacted dithizonate complex was thrice extracted from the crude product, using hot hexane, leaving the photochromic polymer behind (0.038 g).

Found: C, 40.34; H, 3.81; N, 7.95; Hg, 15.8 %. $(C_{22}H_{21}N_5OSHg)_{0.33}(C_3H_5OCl)_{0.67}$ requires C, 42.60; H, 10.36; N, 8.84; Hg, 25.33 %. As per NMR, $(C_{22}H_{21}N_5OSHg)_{0.123}(C_3H_5OCl)_{0.877}$ requires C, 41.24; H, 7.02; N, 5.54; Hg, 15.8 %.

$\lambda_{max}$/nm (dichloromethane) 472.5, $\delta_H$ (300 MHz, $CDCl_3$, Spectrum A21)/ppm: 3.60 – 3.68 (2 H, m, $C\underline{H_2}Cl$), 3.68 – 3.99 (3 H, m, $C\underline{H}C\underline{H_2}O$), 6.70 – 8.11 (14 H, m, 2 × $C_6\underline{H_5}$ & 1 × $C_6\underline{H_4}$) (12.3 % of the –Cl groups on the polymer reacted with the photochromic moiety. This represents 36.9 % of the available mercury complex.

## 4.4.3. Porphyrin Derivatives and their Cobalt Complexes

### 4.4.3.1. *meso*-Tetraphenylporphyrin, 2HTPP [54] [105] (Scheme 3.14, p.78)

Benzaldehyde (9.5 g, 90 mmol) and pyrrole (6 g, 90 mmol) were added to refluxing propionic acid (250 ml). The mixture was refluxed for 30 minutes and left overnight at room temperature for the crystalline product to settle. Purple crystals were filtered off and washed with water and methanol (2.86 g, 21 %). The product was rid of impurities and the small percentage chlorin present, by passing through a column of silica, using chloroform as eluent, collecting the first band (purple). Recrystallization was done from dichloromethane / ethanol, yielding 2.63 g (92 %) lustrous purple crystals.

M.p. > 230 °C, $\lambda_{max}$/nm (dichloromethane) 417, $\delta_H$ (300 MHz, $CDCl_3$, Spectrum A22)/ppm: 7.73 – 7.84 (12 H, m, 4 × *m,p*-$C_6\underline{H_5}$ ), 8.21 – 8.27 (8 H, m, 4 × *o*-$C_6\underline{H_5}$ ), 8.87 (8 H, s, β-pyrrole)

### 4.4.3.5. Tetra(sodium 4-sulfophenyl)porphyrin, 2H($Na_4$TPPS) [57] [112] (Scheme 3.15, p.79)

Tetraphenylporphyrin (2.0 g, 3.2 mmol) and concentrated sulfuric acid (20 ml) were ground into a homogeneous paste with a mortar and pestle. The slurry was transferred into a 250 ml beaker and 50 ml of concentrated sulfuric acid was added. The mixture was kept at 100°C for 4 hours and then allowed to stand at room temperature for 48 hours. While slowly stirring, the filtrate was cautiously added to two volumes of water. The bright green suspension was centrifuged (10000 rpm, 20 minutes, 10°C), the liquid decanted, and the precipitate a few times gently washed with distilled water. Separation in water (250 ml) by means of centrifugion was done three more times, ridding the product from any remaining sulfuric acid. The porphyrin sulfonic acid was then dried overnight at 100°C.

Methanolic ammonia (250 ml) was added to the flask, stirring for one hour to dissolve the porphyrin sulfonic acid. Precipitation of the neutralised porphyrin sulfonic acid as the brown ammonium salt was accomplished by the addition of 3 volumes of acetone. The porphyrin ammonium salt was then filtered off, and purified by six successive precipitations, i.e. by dissolving the product in warm methanol (150 ml), followed by the addition of acetone (500 ml). The product was dried at 80°C for 3 hours, yielding 1.65 g (51 %) of the brown ammonium salt. The dry ammonium salt was added to a sodium methoxide solution (250 ml), and stirred for 2 hours. (The sodium methoxide solution was obtained by reaction of *ca* 1 g of sodium wire with 250 ml dry methanol.) The ensuing olive green precipitate was filtered off and thoroughly washed with ethanol, to give 1.68 g (100 %) *meso*-tetra(sodium 4-sulfophenyl)porphyrin.
M.p. > 230 °C, $\lambda_{max}$/nm (water) 414, $\delta_H$ (300 MHz, $D_2O$, Spectrum A23)/ppm: 7.16 & 8.71 (8 H, 2 × s, β-pyrrole), 7.59 (8 H, d, $J_{a'b'}$ = 8 Hz, 4 × *m*-$C_6\underline{H}_4$), 8.09 (8 H, d, $J_{b'a'}$ = 8 Hz, 4 × *o*-$C_6\underline{H}_4$)

### 4.4.3.2 Tetra(sodium 4-carboxyphenyl)porphyrin, 2H($Na_4$TCP) [59] [239] (Scheme 3.16, p.79)

*Para*-carboxybenzaldehyd (8 g, 53 mmol) and pyrrole (3.575 g, 53 mmol) were added to refluxing propionic acid (100 ml). The mixture was refluxed for 2 hours. Purple micro-crystals precipitated on cooling. The crystals were filtered off, washed with acetone, and dried, to give 4.8 g (46 %) of tetra(4-phenylcarboxylic acid)porphyrin.

The porphyrin carboxylic acid (2.0 g, 2.52 mmol) was neutralised by the addition of 10 % excess of aqueous sodium hydroxide (0.44 g, 11 mmol) solution (100 ml). The reaction mixture was stirred for 30 minutes and the solvent removed under reduced pressure. The crude product was twice refluxed in ethanol to remove (dissolve) the excess sodium hydroxide. (2H($Na_4$TCP) is

not soluble in ethanol.) After extraction of the alkali, the product was filtered off and dried, to give pure **59** in quantitative yield.

M.p. > 230 °C, $\lambda_{max}$/nm (water) 415, $\delta_H$ (300 MHz, $D_2O$, Spectrum A24)/ppm: 6.55 & 8.77 (8 H, 2 × s, β-pyrrole), 7.48 (8 H, m, 4 × *m*-$C_6\underline{H}_4$ ), 8.21 – 8.27 (8 H, m, 4 × *o*-$C_6\underline{H}_4$ )

### 4.4.3.3. *meso*-Tetraferrocenylporphyrin, 2HTFcP [60] (Scheme 3.17, p.80)

**Formylferrocene**:[188] A solution of N-methylformanilide (2.16 g, 160 mmol) and phoshorous oxychloride (15.3 g, 100 mmol) was stirred vigorously in a 500 ml two-necked flask, while finely ground ferrocene (11.16 g, 60 mmol) was added in small portions over a period of 30 minutes. The purple viscous mixture was stirred for 1 hour at room temperature and then for 3 hours under nitrogen atmosphere at 65 – 70°C. Hereafter the reaction mixture was cooled to 0°C before a solution of sodium acetate (50 g, 609.5 mmol in 400 ml water) was added. Stirring continued overnight before the mixture was extracted with diethyl ether (3 × 300 ml). The ether extracts were combined and washed with equal volumes of 1 mol.dm$^{-3}$ HCl (114 ml/liter), water, saturated sodium bicarbonate solution and finally with water (all saturated with sodium chloride). The ether phase was dried by passing it through a little magnesium sulfate, and in a fume hood evaporated to a volume of about 100 ml. The product was purified at low ambient temperature by passing two successive 50 ml portions through a silica (300 ml) column with ether : hexane (1:2) as eluent. The light orange band running ahead is unreacted ferrocene, followed by the red-brown product band. Evaporation of the solvent yielded 8.90 g (69 %) reddish-brown crystals of formylferrocene.

M.p. 111 °C. $\delta_H$(300 MHz, $CDCl_3$)/ppm: 9.95(1H, s, $C_{10}H_9C\underline{H}O$), 4.80 (2H, s, CH), 4.62 (2H, s, CH), 4.30 (5H, s, $C_5H_5$).

***meso*-Tetraferrocenylporphyrin**:[240] Formylferrocene (1 g, 4.6 mmol) was dissolved in refluxing propanoic acid (5 ml). With stirring, pyrrole (0.312 g, 4.6 mmol) was added dropwise. The solution was vigorously stirred for 30 minutes, rapidly cooled, and filtered (1.22 g). The resulting black glass was thoroughly washed with methanol until the washings were colourless. After drying, the black solid was dissolved in minimum chloroform (50 ml) and chromatographed on a silica column. Elution with chloroform resulted in the separation of three bands. The 1$^{st}$ band was yellow-greenish-black, the 2$^{nd}$ was reddish black, and the 3$^{rd}$ was black. The 1$^{st}$ two bands were rapidly removed from the column with chloroform. The 3$^{rd}$ band, which was adsorbed strongly, was removed from the column by elution with dimethylsulfoxide. The resulting solution was four times washed with water. The organic layer was then evaporated, washed with methanol, and dried to give 0.27 g (21 %) of pure *meso*-tetraferrocenylporphyrin.

M.p. > 230 °C, (Found: C, 66.05; H, 4.43; N, 4.84; . $(C_{60}H_{46}N_4Fe_4)(C_2H_6SO)$ requires C, 66.21; H, 4.67; N, 4.98 %); $\lambda_{max}$/nm (dichloromethane) 328. Due to insolubility of the aged product NMR characterization could not be done.

### 4.4.3.4. Octaethylporphyrin, 2HOEP [67] [191] (Schemes 3.18-21, p.81)

**3-Nitro-4-hexanol [61]**: To a 1 liter 2-necked round-bottom flask equipped with a mechanical stirrer, thermometer, dropping funnel, and drying tube were added distilled propionaldehyde (87 g, 1.5 mol) and isopropyl alcohol (225 ml). The solution was stirred while finely ground potassium fluoride (12.5 g, 0.075 mol) was added to the flask. 1-Nitropropane (133.65 g, 1.5 mol) was then added dropwise with stirring, while keeping the temperature below 40°C. Stirring was continued for 20 hours. The catalyst was then removed by filtration and the filtrate concentrated under reduced pressure. The residue was poured into water (250 ml) and the oil extracted with ether (3 × 150 ml). The ethereal layer was dried over anhydrous sodium sulfate and the solvent removed under reduced pressure. The remaining liquid was distilled under reduced pressure and the fraction boiling at 88-90°C (2 mm) was collected in a pre-weighed round bottom flask (500 ml), yielding 100 g (45 %) 3-nitro-4-hexanol, **61**. (The flask containing the product was used directly in the next step.

**3-Acetoxy-4-nitrohexane [62]**: To the above flask, containing 3-nitro-4-hexanol (100 g, 0.679 mol), concentrated sulfuric acid (0.3 ml) was added. To the contents of the flask acetic anhydride (72.73 g, 0.712 mol) was added in portions while stirring, keeping the temperature of the reactants below 60°C. Stirring was continued for another hour. The lower boiling components were removed on a rotary evaporator (20 mm) by gradually heating the flask to 96°C. Hereafter the system was cooled, attached to a vacuum pump, and carefully heated. The fraction boiling at 98 – 100°C (1 mm) was collected, affording 120 g (98 %) impure 3-acetoxy-4-nitrohexane, **62**. Attempts to further purify this compound lead to decomposition.

$\delta_H$ (300 MHz, $CDCl_3$, Spectrum A25)/ppm: 0.99 (6 H, m, $C\underline{H}_3$), 1.62 (2 H, m, $CH_3COCHC\underline{H}_2CH_3$), 1.80 ($O_2NCHC\underline{H}_2CH_3$), 2.06 (3 H, m, $CH_3CO_2$), 4.56 (1 H, m, $CH_3CO_2C\underline{H}$), 5.12 & 5.27 (1H, 2 × m, $C\underline{H}NO_2$)

**N-formylglycine ethyl ester[63]**:[241] A 1 liter 2-necked round-bottom flask fitted with a mechanical stirrer, a pressure equalizing dropping funnel, and a reflux condenser bearing a calcium chloride drying tube was charged with glycine ethyl ester hydrochloride (69.5 g, 0.495 mol) and methyl formate (250 ml). The suspension was stirred and heated at reflux while triethylamine (55.0 g, 0.544 mol) was added. The resulting mixture was heated under reflux for 20 hours, cooled to room temperature, and filtered through a Büchner funnel, removing triethylamine hydrochloride. The filtrate was concentrated on a rotary evaporator and left to stand for a few hours. The crystals that formed were filtered off, and the remaining clear oil was

distilled under reduced pressure (2 mm, 138°C) yielding 41.5 g (63 %) pure N-formylglycine ethyl ester, **63**.

B.p. 138°C (2 mm), $\delta_H$ (300 MHz, $CDCl_3$, Spectrum A26)/ppm: 1.29 (3 H, t, $CH_2C\underline{H}_3$), 4.08 (2 H, d, $NHC\underline{H}_2$), 4.23 (2 H, q, $C\underline{H}_2CH_3$), 6.44 (1 H, s, N<u>H</u>), 8.26 (1 H, s, C<u>H</u>O)

**Ethyl isocyanoacetate [64]:** A 1 liter 2-necked round-bottom flask equipped with a thermometer, a mechanical stirrer, and a pressure-equalizing dropping funnel bearing a nitrogen inlet was charged with N-formylglycine ethyl ester (41.0 g, 0.31 mol), triethylamine (78.24 g, 0.772 mol), and dichloromethane (300 ml), and the apparatus was flushed with nitrogen. The resulting solution was stirred and cooled to below 0°C in an ice-salt bath, and newly opened phosporous oxychloride (47.89 g, 0.312 mol) was added dropwise over 30 minutes while the temperature was kept at 0°C. The mixture turned orange while it was stirred and kept cool (0°C) for an additional 2 hours. Stirring was continued as a solution of anhydrous sodium carbonate (62.6 g) in water (250 ml) was added dropwise at a rate such that the temperature of the mixture was maintained at 25-30°C. Foaming and temperature increase occurred after a while. The 2-phased mixture was stirred for another 30 minutes, after which water was added until the volume of the aqueous layer was brought to 600 ml. The aqueous layer was separated and extracted with two 150 ml portions of dichloromethane. The dichloromethane solutions were combined, washed with saturated sodium chloride solution, and dried over anhydrous potassium carbonate. Evaporation of the solvent under reduced pressure, and distillation of the remaining brown oil afforded 24.1 g (69 %) pure ethyl isocyanoacetate, **64**.

B.p. 73°C (2 mm), $\delta_H$ (300 MHz, $CDCl_3$, Spectrum A27)/ppm: 1.43 (3 H, t, $CH_2C\underline{H}_3$), 4.25 (2 H, s, $NCC\underline{H}_2$), 4.31 (2 H, q, $C\underline{H}_2CH_3$)

**Ethyl 3,4-diethylpyrrole-2-carboxylate [65]**: A 1 liter, 2-necked, round-bottom flask was equipped with a magnetic stirrer bar, dropping funnel, thermometer, and drying tube, and charged with 3-acetoxy-4-nitrohexane (90.89 g, 0.48 mol), ethyl isocyanoacetate (44.74 g, 0.40 mol), anhydrous tetrahydrofuran (280 ml), and anhydrous isopropyl alcohol (115 ml). 1,8-Diazabicyclo[5.4.0] undec-7-ene, DBU, (135 g, 0.88 mol) was then added, keeping the temperature between 20°C and 30°C with the aid of an ice bath. When addition of DBU was complete, the orange solution was stirred for 4 hours at room temperature. The solvent was removed under reduced pressure and the residue poured into a 1 liter beaker and diluted with warm water (300 ml). To this biphasic mixture was added diethyl ether (300 ml). The contents of the beaker was poured into a separatory funnel. The aqueous layer was drawn off and extracted with an additional two portions of ether (300 ml). The ether layers were combined and washed with aqueous 10 % hydrochloric acid (2 × 300 ml) and dried over magnesium sulfate. The ether was removed under reduced pressure in a pre-weighed 1 liter round-bottomed flask,

leaving approximately 88 g of crude ethyl 3,4-diethylpyrrole-2-carboxylate, **65**, which was used directly in the next step.

**3,4-Diethylpyrrole [66]**: To the previous crude product, **65,** (88 g) was added sodium hydroxide (28 g, 0.7 mol) and ethylene glycol (300 ml). The contents was held at reflux (190°C) under nitrogen for 1 hour, cooled, transferred to a 2 liter separatory funnel, and diluted with water (500 ml) and hexane (600 ml). The layers were separated, and the aqueous layer further extracted with hexane (3 × 300 ml). The hexane layers were combined, dried over magnesium sulfate, and concentrated under reduced pressure. The residue was distilled under reduced pressure, and the fraction boiling at 71°C (2 mm) was collected, yielding 22 g (42 %) 3,4-diethylpyrrole, **66**. This compound has to be stored cold, in the dark, to slow down photochemical decomposition.

$\delta_H$ (300 MHz, $CDCl_3$, Spectrum A28)/ppm: 1.24 (6 H, t, $CH_2C\underline{H}_3$), 2.47 (4 H, q, $C\underline{H}_2CH_3$), 6.57 (2 H, d, pyrrole C<u>H</u>), 7.85 (1 H, s, pyrrole N<u>H</u>).

**2,3,7,8,12,13,17,18-Octaethylporphyrin [67]**: A 1 liter round-bottomed flask was wrapped with aluminium foil and equipped with a reflux condenser with a Dean-Stark trap, mechanical stirrer, and nitrogen inlet. The flask was charged with 3,4-diethylpyrrole (2 g, 16.2 mmol), benzene (600 ml), a 37 % solution of aqueous formaldehyde (1.46 ml, 17.8 mmol), and *p*-toluenesulfonic acid (0.06 g, 3.4 mmol). The mixture was stirred and heated at reflux under nitrogen using an oil bath, and the water was removed by means of a Dean-Stark trap. After 8 hours the solution was cooled, and the Dean-Stark trap and condenser were replaced with a fritted glass aerator/bubbler. Oxygen was bubbled through the brown mixture while stirring for *ca* 24 hours. Benzene was removed under reduced pressure, and the residue dissolved in chloroform (40 ml). The solution was washed with 1 M sodium hydroxide and water. The chloroform solution was concentrated to 10 ml in a 100 ml round-bottom flask, carefully layered over with methanol (100 ml), and allowed to stand for 48 hours. The resulting solid was collected by filtration, and dried overnight at 40°C.

The crude material was twice recrystallised from chloroform-hexanes (effected by dissolving in chloroform (20 ml), layering over with hexanes (140 ml), and allowing to stand overnight). The final precipitate was collected by filtration, and dried, yielding 1.44 g (66.4 %) analytically pure 2,3,7,8,12,13,17,18-octaethylporphyrin, **67**, as a purple amorphous powder.

M.p. > 230 °C, $\lambda_{max}$/nm (dichloromethane) 397, $\delta_H$ (300 MHz, $CDCl_3$, Spectrum A29)/ppm: 1.95 (24 H, t, 4 × $CH_2C\underline{H}_3$), 4.14 (16 H, q, $C\underline{H}_2CH_3$), 1.95 (4 H, s, *meso*-H)

### 4.4.3.5. Tetraphenylporphyrinatocobalt(II), $Co^{II}TPP$ [68] [107] (p.84)

To tetraphenylporphyrin (0.5 g, 0.81 mmol) in boiling chloroform (100 ml) was added a saturated solution (20 ml) of cobalt(II) acetate (0.203 g, 0.81 mmol) in methanol.

After 30 minutes of refluxing, the mixture was concentrated, diluted with a little methanol, and after cooling, 0.54 g tetraphenylporphyrinatocobalt(II) was filtered off in virtually quantitative yield (100 %).

M.p. > 230 °C, $\lambda_{max}$/nm (dichloromethane) 410, $\delta_H$ (300 MHz, $CDCl_3$, Spectrum A30)/ppm: 9.76 (8 H, broad s, 4 × *o*-$C_6\underline{H}_5$ ), 9.97 (12 H, broad s, *m,p*-$C_6\underline{H}_5$).

### 4.4.3.6. Tetraphenylporphyrinatocopper(II), $Cu^{II}$TPP [69] (p.84)

The synthetic procedure was as for tetraphenylporphyrinatocobalt(II) (Paragraph 4.4.3.5).

Product yield, 0.108 g (98 %). 0.100 g 2HTPP reagent was used.

M.p. > 230 °C, $\lambda_{max}$/nm (dichloromethane) 415, $\delta_H$ (300 MHz, $CDCl_3$, Spectrum A31)/ppm: 7.51 (12 H, broad s, 4 × *m,p*-$C_6\underline{H}_5$ ), 7.66 (8 H, broad s, *o*-$C_6\underline{H}_5$).

### 4.4.3.7. Octaethylporphyrinatocobalt(II), $Co^{II}$OEP [72] [107] (p.84)

In a 500 ml 2-necked flask, cobalt chloride (0.6 g, 2.52 mmol) and octaethylporphyrin (0.6 g, 1.12 mmol) were dissolved in dimethylformamide (300 ml). The solution was brought to the boil and actively refluxed for 30 minutes under nitrogen while stirring. The solution was cooled down and an equal volume of water added. The cobalt porphyrin complex was filtered off, washed with ample amounts of water, and dried overnight at 40°C, to give 0.61 g (92 %) of pure **72**.

M.p. > 230 °C, $\lambda_{max}$/nm (dichloromethane or methanol) 392, $\delta_H$ (300 MHz, $CDCl_3$, Spectrum A32) 6.14 ( 24 H, broad s, $CH_2C\underline{H}_3$ ), 8.80 ( 16 H, broad s, $C\underline{H}_2CH_3$ ). Unusual shifts of the aliphatic peaks are attributed to the paramagnetic effect of Co(II).

### 4.4.3.8. Octaethylporphyrinatocopper(II), $Cu^{II}$OEP [73] (p.84)

The synthetic procedure was as for octaethylporphyrinatocobalt(II) (Paragraph 4.4.3.7).

Product yield, 0.103 g (92 %). 0.100 g 2HOEP was used.

M.p. > 230 °C, $\lambda_{max}$/nm (dichloromethane) 398. No NMR spectrum of Cu(II)OEP could be obtained due to the paramagnetic effect of Cu(II).

### 4.4.3.9. Tetraphenylporphyrinatocobalt(III) perchlorate, $[Co^{III}(TPP)(H_2O)_2]ClO_4$ [74] [127,128] (p.85)

Tetraphenylporphyrinatocobalt(II) (0.3 g, 0.45 mmol) was suspended in methanol (300 ml) containing concentrated perchloric acid (70 %, 3 ml). The solution was stirred in an open beaker for 3 hours. After 30 minutes the suspension has dissolved and the solution turned deep red. The solution was concentrated to *ca* 25 ml under reduced pressure, water (50 ml) added, and the

precipitate filtered off and washed with water and a 1:1 water : methanol mixture. Recrystallization from minimum dichloromethane and methanol yielded 0.32 g (92 %) lustrous purple crystals.

M.p. > 230 °C, $\lambda_{max}$/nm (dichloromethane) 427, $\delta_H$ (300 MHz, $(CD_3)_2SO_3$, Spectrum A33)/ppm: 7.84 – 7.92 (12 H, m, 4 × *m,p*-$C_6\underline{H}_5$ ), 8.18 – 8.26 (8 H, m, 4 × *o*-$C_6\underline{H}_5$ ), 9.18 (8 H, s, β-pyrrole)

### 4.4.3.10. Tetra(sodium 4-sulfophenyl)porphyrinatocobalt(III) perchlorate, $[Co^{III}(Na_4TPPS)(H_2O)_2]ClO_4.16H_2O$ [75] [128] (p.85)

Tetra(sodium 4-sulfophenyl)porphyrin (0.05 g, 0.049 mmol) was added to refluxing, doubly distilled water (100 ml) containing cobalt carbonate (0.5 g, insoluble) in a 250 ml 2-necked flask, and refluxed for 2 hours. The excess insoluble cobalt salt was filtered off and the solvent removed under reduced pressure (0.067 g, 100 %)

The cobalt (0.3 g, 0.22 mmol) porphyrin complex was suspended in methanol (300 ml) containing concentrated perchloric acid (70 %, 3 ml). The solution was stirred in an open beaker for 3 hours. The solution was concentrated to *ca* 25 ml under reduced pressure, acetone (50 ml) added, and the precipitate filtered off and washed with acetone, to give 0.32 g (96 %) of compound **75**.

M.p. > 230 °C, $\lambda_{max}$/nm (water) 425, $\delta_H$ (300 MHz, $D_2O$)/ppm: 8.13 (8 H, d, $J_{a'b'}$ = 8 Hz, 4 × *o*-$C_6\underline{H}_5$), 8.32 (8 H, d, $J_{b'a'}$ = 8 Hz, 4 × *m*-$C_6\underline{H}_5$), 9.26 (8 H, s, β-pyrrole)

### 4.4.3.11. Tetra(sodium 4-carboxyphenyl)porphyrinatocobalt(III) perchlorate, $[Co^{III}(Na_4TCP)(H_2O)_2]ClO_4$ [76] [128] (p.85)

The synthetic procedure was as for tetra(sodium 4-sulfophenyl)porphyrinatocobalt(III) perchlorate (4.4.3.10.), to give 0.21 g (94 %) of pure **76**. 0.172 g 2H($Na_4$TCP) reagent was used.

M.p. > 230 °C, $\lambda_{max}$/nm (water) 426, $\delta_H$ (300 MHz, $D_2O$)/ppm: 8.13 (8 H, d, $J_{a'b'}$ = 8 Hz, 4 × *o*-$C_6\underline{H}_5$), 8.32 (8 H, d, $J_{b'a'}$ = 8 Hz, 4 × *m*-$C_6\underline{H}_5$), 9.26 (8 H, s, β-pyrrole)

### 4.4.3.12. Octaethylporphyrinatocobalt(III) perchlorate $[Co^{III}(OEP)(H_2O)_2]ClO_4$ [77] [193] (p.85)

70% perchloric acid (1.0 ml) was added to methanol (100 ml), followed by octaethyl-porphyrinatocobalt(II) (0.1 g, 0.19 mmol). The open mixture was vigorously stirred overnight. Water (10 ml) was added and the volume reduced to 15 ml, with the cobalt(III) complex crystallizing out. The purple crystals were filtered off and thoroughly washed with water, to give 0.11 g (80 %) of pure **77**.

M.p. > 230 °C, $\lambda_{max}$/nm (dichloromethane) 377, (methanol) 409, $\delta_H$ (300 MHz, $(CD_3)_2SO$, Spectrum A34) 1.90 (24 H, t, $CH_2C\underline{H}_3$), 4.27 (16 H, q, $C\underline{H}_2CH_3$)

### 4.4.3.13. Dehydrodithizone(tetraphenylporphyrinato)cobalt(III) perchlorate, $[Co^{III}(TPP)(DDz)(MeOH)]ClO_4$ [78] (Scheme 3.23, p.89)

Dehydrodithizone, DDz (0.0316 g, 14 mmol) and tetraphenylporphyrinatocobalt(III) perchlorate (0.1 g, 13 mmol) was dissolved in methanol (60 ml). Purple-black crystals grew from this solution, after having been left in a closed desiccator, including an open beaker containing water. The product yield of 0.102 g (78 %) contained *ca* 75 % of **78** and *ca* 25 % of **77**.

M.p. > 230 °C, $\lambda_{max}$/nm (dimethylsulfoxide) 438, $\delta_H$ (300 MHz, $(CD_3)_2SO_3$, Spectrum A35)/ppm: 6.98 – 8.24 (30 H, m, 6 × $C_6\underline{H}_5$ ), 8.94 (75 % of 8 H, s, β-pyrrole), 9.18 (25 % of 8 H, s, β-pyrrole) - 25 % unsubstituted.

### 4.4.3.14. *Bis*-dithizonato(octaethylporphyrin)cobalt(III) $[Co^{III}(OEP)(HDz)_2]$ [79] (Scheme 3,25, p.94)

Octaethylporphyrinatocobalt(III) perchlorate (0.050 g, 0.07 mmol) was dissolved in methanol (50 ml), and potassium dithizonate (0.0597 g, 0.2 mmol) added. The solution was stirred for 15 minutes at room temperature, water (100 ml) was added, and the methanol allowed to evaporate in a fumehood. The product was filtered off and washed with water and water / methanol to remove unreacted potassium dithizonate and formed potassium perchlorate. Drying of the product was done at 40°C overnight, to yield 0.058 g (93 %) of pure **79**.

M.p. > 230 °C, $\lambda_{max}$/nm (methanol) 398, $\delta_H$ (300 MHz, $(CD_3)_2SO$, Spectrum A36) 1.80 (24 H, t, $CH_2C\underline{H}_3$), 3.84 & 4.02 (16 H, 2 × q, $C\underline{H}_2CH_3$), 7.49 – 7.75 (10 H, m, $C_6\underline{H}_5$), 10.13 (4 H, s, *meso*-H)

### 4.4.3.15 $Co^{III}$ / $Co^{II}$ porphyrin reduction / recovery

Cobalt(III) tetraphenyl- and octaethylporphyrins were dissolved in tetrahydrofurane (150 ml) containing sodium wire. The mixture was refluxed for 30 minutes under nitrogen. Cobalt(II) porphyrin was precipitated by decanting the solution into lukewarm water (200 ml) while stirring. The precipitate was filtered off and washed with ample amounts of water. Hundred percent recovery of the cobalt(II) porphyrin complexes was achieved by using this method.

# 4.5. X-Ray Diffractometry

## 4.5.1. Dithizonatotrimethyltin(IV)

**Data Collection**

An orange needle crystal of $C_{16}H_{20}N_4SSn$ having approximate dimensions of 0.18 × 0.22 × 0.45 mm was mounted on a glass fiber. All measurements were made on a Rigaku AFC5R diffractometer with graphite monochromated Mo-Kα radiation and a rotating anode generator.

Cell constants and an orientation matrix for data collection, obtained from a least-squares refinement using the setting angles of 25 carefully centered reflections in the range $38.83 < 2\theta < 40.75°$ corresponded to a primitive monoclinic cell with dimensions:

a = 11.1(1) Å
b = 7.2(1) Å $\quad \beta = 101.0(7)°$
c = 22.4(1) Å
V = 1765(29) Å$^3$

For Z = 4 and F.W. = 419.11, the calculated density is 1.58 g/cm$^3$. The systematic absences of:

h0l: h+l ± 2n
0k0: k ± 2n

uniquely determine the space group to be:

$P2_1/n$ (#14)

The data were collected at a temperature of -90 ± 1°C using the ω-2θ scan technique to a maximum 2θ value of 60.2°. Omega scans of several intense reflections, made prior to data collection, had an average width at half-height of 0.21° with a take-off angle of 6.0°. Scans of (1.68 + 0.35 tan θ)° were made at a speed of 16.0°/min (in ω). The weak reflections ($I < 15.0\sigma(I)$) were rescanned (maximum of 6 scans) and the counts were accumulated to ensure good counting statistics. Stationary background counts were recorded on each side of the reflection. The ratio of peak counting time to background counting time was 2:1. The diameter of the incident beam collimator was 1.0 mm, the crystal to detector distance was 285 mm, and the detector aperture was 9.0 x 6.0 mm (horizontal x vertical).

**Data Reduction**

Of the 5831 reflections collected, 5573 were unique ($R_{int}$ = 0.118). The intensities of three representative reflections were measured after every 150 reflections. No decay correction was applied.

The linear absorption coefficient, μ, for Mo-Kα radiation is 15.7 $cm^{-1}$. An empirical absorption correction based on azimuthal scans of several reflections was applied which resulted in transmission factors ranging from 0.94 to 1.00. The data were corrected for Lorentz and polarization effects. A correction for secondary extinction was applied (coefficient = 1.15772e-007).

**Structure Solution and Refinement**

The structure was solved by direct methods and expanded using Fourier techniques. The non-hydrogen atoms were refined anisotropically. Hydrogen atoms were included but not refined. They were placed in geometrically calculated positions and allowed to ride on the heavy atom to which they were bonded with Uiso equal to 1.2Ueq of the heavy atom (1.5Ueq for methyl hydrogens).

## 4.5.2. *Tris*-dithizonatocobalt(III)

**Data Collection**

A dark brown block crystal of $C_{39}H_{33}N_{12}S_3Co_1$ having approximate dimensions of 0.14 × 0.16 × 0.22 mm was mounted on a glass fiber. All measurements were made on a Rigaku AFC5R diffractometer with graphite monochromated Mo-Kα radiation and a rotating anode generator.

Cell constants and an orientation matrix for data collection, obtained from a least-squares refinement using the setting angles of 23 carefully centered reflections in the range $9.92 < 2\theta < 39.80°$ corresponded to a primitive triclinic cell with dimensions:

| | |
|---|---|
| a = 13.559(3) Å | α = 109.61(1)° |
| b = 15.068(2) Å | β = 106.91(2)° |
| c = 10.901(2) Å | γ = 71.84(1)° |
| V = 1949.7(7) $Å^3$ | |

For Z = 2 and F.W. = 824.88, the calculated density is 1.40 $g/cm^3$. Based on a statistical analysis of intensity distribution, and the successful solution and refinement of the structure, the space group was determined to be:

P-1 (#2)

The data were collected at a temperature of -60 ± 0.25°C using the ω-2θ scan technique to a maximum 2θ value of 60.1°. Omega scans of several intense reflections, made prior to data collection, had an average width at half-height of 0.21° with a take-off angle of 6.0°. Scans of

(0.79 + 0.35 tan θ)° were made at a speed of 16.0°/min (in ω). The weak reflections (I < 15.0σ(I)) were rescanned (maximum of 6 scans) and the counts were accumulated to ensure good counting statistics. Stationary background counts were recorded on each side of the reflection. The ratio of peak counting time to background counting time was 2:1. The diameter of the incident beam collimator was 1.0 mm, the crystal to detector distance was 285 mm, and the detector aperture was 9.0 x 6.0 mm (horizontal x vertical).

**Data Reduction**

Of the 11106 reflections collected, 10662 were unique ($R_{int}$ = 0.066). The intensities of three representative reflections were measured after every 150 reflections. No decay correction was applied. The linear absorption coefficient, μ, for Mo-Kα radiation is 6.5 $cm^{-1}$. An empirical absorption correction based on azimuthal scans of several reflections was applied, which resulted in transmission factors ranging from 0.95 to 1.00. The data were corrected for Lorentz and polarization effects.

**Structure Solution and Refinement**

The structure was solved by direct methods and expanded using Fourier techniques. The non-hydrogen atoms were refined anisotropically. Hydrogen atoms were included but not refined. The H(C) atoms were placed in geometrically calculated positions and allowed to ride on the heavy atom to which each was bonded with Uiso equal to 1.2Ueq of the heavy atom. The positions for the H(N) atoms were located in the final difference Fourier map. These were also placed using a riding model but the H-N distance was allowed to refine after restraining it to a value of 0.87(0.015)Å. The phenyl C-C bond lengths were restrained to a distance of 1.38(0.015)Å. A rigid bond restraint was placed over the entire molecule. In addition, one phenyl ring, C(28)-C(33), was restrained to have similar Uij components for all atoms. A total of 231 restraints were applied to the refinement.

## 4.6. Computational Chemistry

All ADF (Amsterdam Density Functional) calculations were carried out using DFT (Density Functional Theory) with the PW91 (Perdew-Wang, 1991) exchange and correlation functional. Relativistic effects have been taken into account. ZORA (Zero Order Regular Approximation) / TZP (Tripple ζ polarised) basis set including scalar relativistic effects, a fine mesh for numerical integration, a spin-unrestricted formalism and full geometry optimization with tight convergence criteria as implemented in the ADF program system version 2004.01, was used. TDDFT (Time-Dependent Density Functional Theory) PW91/ZORA/TZP implemented in the ADF version 2004.01 was used for calculation of excitation energies. Gaussian full geometry optimization was done with tight convergence criteria as implemented in the Gaussian program package, version 03, using the B3LYP (B3 Becke 3-parameter exchange and Lee-Yang-Parr correlation) functional, for both exchange and correlation and the CEP-31G (Stevens/Barch/Krauss effective core potential triple-split) basis set.

## 4.7. Electrochemistry

Electrochemical measurements were done on a BAS100B Electrochemical Analyzer linked to a personal computer. Measurements were done at 293 K, under Argon. Sigma-Aldrich A.C.S. spectrophotometric grade solvents (dichloromethane and dimethylsulfoxide) and $TBAPF_6$ (tetra-*n*-butylammonium hexafluorophosphate) electrolyte, purchased from Fluka, were used. The tetra-*n*-butylammonium tetrakispentafluoroboron electrolyte was synthesised locally, and twice recrystallised before use. (The author acknowledges Dr E. Erasmus for samples of this electrolyte.) Supporting electrolyte concentrations were hundred times (0.1 M) the concentration of the analytes (0.001 M) investigated.

Three-electrode cells were employed. A platinum auxiliary electrode, a glassy carbon (surface area, 3.14 $mm^2$) working electrode and a silver wire (coated with silver chloride) reference electrode were used. The reference electrode was prepared as follows: Two silver wires were connected to the positive and negative poles of a DC power source and submersed into a dilute HCl (0.1 M) solution. A 700 mA current was passed through the solution with evolution of $H_2$ gas at the cathode. After the anode has acquired a uniform dark colour (deposition of AgCl), the wire was removed and washed with water, methanol and acetone – now being ready for use. After obtaining cyclic voltammograms of a series of compounds, the AgCl was removed from the reference electrode by washing with concentrated ammonia, and following the same preparation method as described above for the next set of cyclic voltammograms. Data processing was done with Microsoft Excel.

# 5. Summary and Future Perspective

In the initial research towards constructing an optical molecular switch, a significant amount of basic research had to be done on aspects of the photochromic compound, dithizonatophenylmercury(II), PhHgHDz, as well as cobalt porphyrin, which was identified as a possible "trap" for locking PhHgHDz in its photo-excited state.

Several methods were considered to axially ligate dithizone, which is sterically hindered with regard to coordination to the large planar cobalt porphyrins. The fully oxidised product of dithizone was first of all prepared. As a sterically favourable ligand, coordination with tetraphenylporphyrinatocobalt(II) & (III) was observed, albeit slow in the case of $Co^{II}$, but fast in the case of $Co^{III}$. Secondly, the anionic dithizonate species, $K^+HDz^-$ and $Bu_4N^+HDz^-$, to be used in axial substitution reactions with $Co^{III}$ porphyrins in *polar* media, were synthesised. Thirdly the very weakly coordinated dithizonate tin complex, $Me_3Sn^{IV}HDz$, was synthesised as an alternative to the above, to be used in axial substitution reactions in *non-polar* media.

The last approach was to attempt so-called tailed metal insertion, i.e. by first preparing a mono-coordinated dithizonate cobalt(III) pentaamine complex, and then inserting the metal into a porphyrin cavity. This was to be done with retention of the dithizonate, but with loss of the amines. The method was shown to be unworkable by the growth and X-ray structure determination of a crystal, which proved to be the stable *tris*-coordinated $Co(HDz)_3$ compound. Simultaneously the ligation capabilities of PhHgHDz itself to cobalt(II) chloride was researched. Orange PhHgHDz was observed to coordinate reversibly with $Co^{II}$ to form a complex of similar colour to the purple $Co(HDz)_3$ compound.

The single crystal X-ray structure of $Me_3Sn^{IV}HDz$ was also solved. The structure revealed the dithizonate ligand to be uniquely monodentate coordinated. The low stability of this complex in most solvents, however, made this compound less suitable for use in follow-up coordination reactions with cobalt porphyrins.

Initial experiments showed that dithizone, its anion, and its mercury complex do not axially bind with tetraphenylporphyrinatocobalt(II). The $Co^{III}$ analogues proved to have such a strong electron affinity that it oxidised the dithizone species in solution, while $Co^{III}$ itself became reduced to $Co^{II}$. For this reason the resistance of $Co^{III}$ in the porphyrin ligand against reduction was enhanced by substituting the porphyrin ring with electron donating groups. This resulted in an increased amount of electron density on the central $Co^{III}$ atom. Synthesis of the water-soluble tetra(sodium-sulfophenyl) and tetra(sodium-carboxyphenyl) porphyrin derivatives was found not to improve the resistance of $Co^{III}$ against reduction by dithizone, i.e. the peripheral anionic $-SO_3^-$ and $-COO^-$ groups did not add a greater amount of electron density onto the central metal.

A powerful electron donating group, ferrocene, was then *meso*-substituted on the porphyrin heterocycle, but the product, tetraferrocenylporphyrin, aggregated to such a high degree that it was rendered useless with regard to follow-up reactions. The last porphyrin synthesised was the β-substituted octaethylporphyrin. Its $Co^{III}$ complex was not reduced in the presence of dithizone, with the consequence that the first cobalt porphyrin - dithizone adduct, $K[Co^{III}(OEP)(HDz)_2]$, could be identified.

Other attempts to stabilise dithizone against oxidation by $Co^{III}$ porphyrins, included the synthesis of *para*-chloro-, *para*-fluoro-, *meta*-fluoro-, *ortho*-fluoro-, 3,4-difluoro- and 3,5-difluorophenyl dithizones. No significant observable change with regard to the resistance of these species against $Co^{III}$ oxidation was observed. As for the di-fluoro dithizones, their mercury complexes proved to be no longer photochromic, as opposed to all the mono-fluoro mercury dithizonates.

In order to quantify overall electronic changes brought about by the above chemical alterations, extensive electrochemical investigations were done on all the relevant species. For the first time an overall description was given with regard to all the oxidised and reduced species of dithizone, PhHgHDz and $Co(HDz)_3$ within the potential range, -2000 to 1500 mV, using dichloromethane as solvent and the non-coordinating supporting electrolyte, $[NBu_4][B(C_6F_5)_4]$. The first reduction potential with regard to the oxidation of the halogenated dithizones were compared. The most significant change was seen in (*meta*-fluoro)dithizone, with its reduction potential 229 mV higher than that of dithizone itself. Use of the above supporting electrolyte, as opposed to $[NBu_4][PF_6]$, proved to significantly improve peak resolution, without which a comprehensive description of the redox process associated with the cyclic voltammogram would not have been possible.

As for the porphyrins, the resistance against $Co^{III}$ reduction was significant enough when moving from cobalt tetraphenyl- to cobalt octaethylporphyrin to prevent $Co^{III}$ reduction by dithizone. In dichloromethane the decrease in reduction potential associated with $Co^{II/III}$ oxidation was 157 mV, and in dimethylsulfoxide, the anodic peak potential decrease was 38 mV on going from tetraphenyl- to octaethylporphyrin. Stepwise fractional addition of pyridine assisted in clearly identifying the $Co^{II/III}$ oxidation wave, which could otherwise also have been done by the much more tedious bulk electrolysis spectro-electrochemical technique.

In view of the eventual requirement of having the desired molecular switch embedded into a suitable polymer, functionalization of PhHgHDz was initiated through the Hg-phenyl molecular fragment. Functionalization was achieved by complexing aniline at the *para* position to mercury acetate. All attempts to lengthen the phenyl - amine chain by complexing mercury with amines that has methylene groups in between the phenyl and the amine, were unsuccessful. The aniline $-NH_2$, however, could be converted into a longer chain carboxylic acid functionalised derivative

by reaction with succinic anhydride. This reaction was unsuccessful with the aniline mercury salt, but it was successful with the corresponding dithizonate complex, $H_2NPhHgHDz$.

Both hydrophilic and lypophilic polymers were synthesised for the purpose of embedding the photochromic species into a polymer. For the former, polysuccinimide was prepared and made water-soluble by partial ring opening with 4-(3-aminopropyl)morpholine. An anchoring site for dithizonato derivatives on this polymer was put in place by further reaction of the polymer with ethylenediamine. The carboxylic acid mercury dithizonate complex was coupled to the amine-functionalised hydrophilic polymer at an estimated 70 % success rate. The resulting mercury dithizonato functionalised polymer, although dark red-orange in colour, was not photochromic in both the solid state and in solution.

The lypophilic polymer, polyepichlorohydrin, was then reacted with $H_2NPhHgHDz$ to obtain a lypophhilic polymer being 16 % functionalised with the mercury dithizonato derivative. In solution the polymer showed an orange-blue photochromic colour change on irradiation with light. The colour of the solid state orange polymer changed to blue-grey under direct light.

The S-methylated derivative of dithizone and its phenylmercury complex was prepared as crude model for the envisaged PhHgHDz - cobalt porphyrin adduct. Because all efforts to grow crystals and solve the structure of the PhHg(S-Me)Dz complex failed, it was decided to follow the quantum computational route, simultaneously solving related outstanding issues with regard to the PhHgHDz photochromic reaction as well.

The methyl group in PhHg(S-Me)Dz was seen to be bound sideways, almost perpendicular to the plane of the molecule, which then is also the way in which PhHgHDz is expected to coordinate axially to cobalt porphyrin. The isomer of PhHg(S-Me)Dz corresponding to the photo-excited blue isomer of PhHgHDz was calculated to be structurally more favorable towards axial ligation with cobalt porphyrin than is the case with the isomer corresponding to the orange form.

In general, agreement between the ADF and Gaussian computational program results and experimentally obtained data, both as far as structural data, and the electronic spectra of these species are concerned, was good. Together with optimised molecular energies, comparisons between calculated and experimental spectra of different tautomers or isomers proved to be a valuable tool towards finding the particular structure responsible for a specific spectrum.

Molecular orbital calculations of the orange and blue isomer ground and excited states, as well as energy comparisons of the 45° incremental rotamers lying in between the orange and blue forms, gave improved understanding of the photochromic reaction mechanism. The HOMO to LUMO excitation proved to be responsible for the photo-induced isomerisation reaction, with the C=N

double bond around which rotation is to take place, degenerating into a single bond on excitation, thereby allowing rotation to take place.

As a provisional final test to establish whether in the PhHgHDz - cobalt porphyrin assembly the blue isomer adduct is more stable when compared to the orange adduct, complete ADF geometry optimizations were done on both the orange and blue structures. Results showed a significant increase in stability of the blue isomer assembly, but energy differences between the orange and blue isomer porphyrin adduct were not sufficient to predict which isomer dominates. In contrast, in the absence of adduct formation with cobalt porphyrin, the orange form is clearly the dominant isomer.

Having completed the research herein reported, a multitude of avenues have opened up, not just as far as the specific application here envisaged is concerned, but also with regard to basic academic research in all the fields described, namely synthesis, X-ray crystallography, electrochemistry and quantum computational chemistry.

As for a potential molecular switch, the next step already in progress is the further complexation of the above mentioned $K[Co^{III}(OEP)(HDz)_2]$ complex with phenylmercury(II) to try and obtain the complete photochromic moiety - cobalt porphyrin assembly. If further redox problems persists (transfer of electrons are not desired at this point, because the photochromic moiety gets altered irreversibly), a number of alternative research avenues exist. One option would be to, instead of the former tetraferrocenylporphyrin, synthesise the di- or tri-ferrocenyl octaethyl pophyrins, which should significantly add towards the stabilization of the higher $Co^{III}$ state. Having the ferrocenes bound to the porphyrin ring has the added benefit of intramolecular redox reactions that may be beneficial, and therefore needs to be investigated.

Using entirely new ligands like the corroles, may prove to be even more beneficial. The corroles have a profound ability to stabilise even the rare, higher $Co^{IV}$ and $Co^{V}$ oxidation states. It may well be that corroles may therefore prevent dithizone-induced $Co^{III}$ reduction in these macrocycles.

The cobalt metal, however, may also be replaced by another suitable metal, i.e. one that possesses a high enough electron affinity to coordinate dithizone, but simultaneously low enough not to be oxidised in the process. Here lies much potential for further electrochemical investigations, i.e. comparing a range of metals with regard to their own reduction potentials, as well as their influence on the porphyrin ring reduction potentials.

It is also known that axial ligands to a large degree stabilise the higher oxidation states, as was inferred form the addition of pyridine to cobalt porphyrins during the course of this study.

Varying both σ- and π-donating and accepting abilities by changing the axial ligands has a profound influence on the electrochemical behaviour of metal porphyrins.

As for the phenylmercury dithizonato complexes, the di-fluoro derivatives were no longer photochromic in nature. This implies a boundary had been reached in stabilizing the dithizonato ligand against oxidation. By changing mercury to other metals also leaves much scope for interesting research. Such metal changes may invoke different colour changes, as well as different photo-excited state half-lives. These metal alterations may also bring about new possibilities for quantum computational research, as would further substitution on the phenyl rings, on the S-position, and even replacing the phenyl rings by entirely new groups. The physical length of the HOMO orbital in the ligand may hereby be altered, and thereby also the subtle energy changes involved in allowing the photochromic reaction to take place. Twisting one or both dithizonate phenyl rings, e.g. in the $Co(HDz)_3$ complex, is a related phenomenon that is already under further quantum chemical investigation.

The last potential future field of investigation to be mentioned here, concerns the vast field of polymers. Further research is underway to couple the entire PhHgHDz - cobalt porphyrin assembly onto a suitable lypophilic polymer. Investigations may also be done into the possibility of coupling both the photochromic and porphyrin moieties onto a polymer. The influence of different polymers on PhHgHDz, whether the latter is only dissolved or actually coupled to the polymeric chain, is a further outstanding matter to be researched.

Once success in reversibly coordinating a photochromic metal dithizonate to a metal porphyrin, -corrole or phthalocyanine has been attained, much research still lies ahead in determining the correct energies required for the so-called "read", "write" and "erase" mechanisms en route to this product becoming commercially viable as an information storage device.

The potential data storage capacity based on molecular switches of this kind, is about 3 terabytes.cm$^{-2}$, or 280 terabytes on the surface of a 120 mm DVD disc. At present DVD's store at most 17 gigabytes (double sided/dual layer) of data, which is about 17 000 times less than the former.

# ABSTRACT

A series of dithizones were synthesised, including its oxidation products, and the S-methylated and phenyl halogenated derivatives. Phenylmercury(II) complexes have been prepared from all these dithizonate ligands, while cobalt(III) and tin(IV) complexes were prepared from dithizone alone. X-ray crystal structure determinations were performed on the latter two complexes, revealing valuable information with regard to coordination number, $\pi$-conjugation patterns along the dithizonate backbone, and coordination bond strengths. A bi-metallic cobalt-mercury-dithizonate complex was for the first time identified, illustrating reversible coupling between the mercury dithizonate complex and cobalt.

The lypophilic polymer, polyepichlorohydrin, and a hydrophilic polymer, a morpholine derivative of polysuccinimide, were synthesised. Both polymers, as well as dithizonatophenylmercury(II), PhHgHDz, were suitably functionalised to allow successful coupling of the photochromic compound, PhHgHDz, on both polymers. PhHgHDz remained photochromic in the lypophilic polymer, but not in the hydrophilic polymer.

A series of porphyrins were synthesised, including tetraphenyl-, tetra(sodium 4-sulfophenyl)-, tetra(sodium 4-carboxyphenyl)-, tetraferrocenyl- and octaethylporphyrin. Apart from the ferrocenyl derivative, cobalt(II) and cobalt(III) complexes were prepared from all these porphyrins, while copper(II) complexes were prepared from tetraphenyl- and octaethylporphyrin. Interactions between the cobalt porphyrins and the above-mentioned dithizone derivatives were extensively studied by means of UV/visible spectroscopy. This revealed the redox nature often encountered in these complexes.

Extensive ADF and Gaussian quantum chemical computations were done on dithizone, dithizonatophenylmercury(II) and its S-methylated derivative. Results highlighted the most probable structures of these compounds. The photochromic mechanism of PhHgHDz and its orbitals and transition energies involved, were also clarified. Computations on the adduct of the orange and blue isomers of PhHgHDz with cobalt porphyrin revealed results that were consistent with the expectation that the blue form might be at least as stable (or more stable) than the orange form.

Electrochemical elucidation of the redox behaviour of dithizone, its derivatives, and mercury(II) and cobalt(III) complexes were researched for the first time. The relative resistance of the halogenated dithizones against oxidation was compared. Cobalt complexes of octaethyl-, tetraphenyl- and its sulfophenyl porphyrin derivatives were also electrochemically investigated, and there resistance against reduction compared. A comparative solvent study on the electrochemical behaviour of the substrate was performed, utilizing dimethylsulfoxide, dichloromethane and pyridine. The effect of supporting electrolyte on the electrochemical behaviour of dithizone and porphyrin derivatives was investigated, utilizing $[NBu_4][PF_6]$ and $[NBu_4][B(C_6F_5)_4]$.

# SAMEVATTING

'n Reeks ditisone is gesintetiseer, insluitend ditisoon se oksidasieprodukte, en die S-gemetileerde en feniel gehalogeneerde derivate. Fenielkwik(II)komplekse van al hierdie ditisoonligande is berei, terwyl kobalt(III)- en tin(IV)komplekse van ditisoon alleen berei is. X-straalkristalstruktuurbepalings wat op laasgenoemde twee komplekse gedoen is, het waardevolle inligting rakende koördinasiegetal, π-konjugasie-patrone langs die ditisoonruggraat, en koördinasiebindingssterktes gegee. 'n Bi-metalliese kobalt-kwik-ditisoon kompleks is vir die eerste keer geïdentifiseer, wat omkeerbare koppeling tussen die kwik-ditisoon-kompleks en kobalt geopenbaar het.

Die lipofiliese polimeer, poliepichlorohidrien, en 'n hidrofiliese polimeer, 'n morfolienderivaat van polisuksinimied, is gesintetiseer. Beide polimere, sowel as ditisonatofenielkwik(II), PhHgHDz, is sodaning gefunksionaliseer dat suksesvolle koppeling tussen die fotochromiese verbinding, PhHgHDz, en beide polimere bewerkstellig is. PhHgHDz was steeds fotochromies in die lipofiliese polimeer, maar nie in die hidrofiliese polimeer nie.

'n Reeks porfiriene is ook gesintetiseer, insluitend die tetrafeniel-, tetra(natrium 4-sulfofeniel)-, tetra(natrium 4-karboksiefeniel)-, tetraferroseniel- en oktaetielporfiriene. Behalwe vir die ferrosenielderivaat is kobalt(II)- en kobalt(III)komplekse van al hierdie porfiriene berei, terwyl koper(II)komplekse berei is met tetrafeniel- en oktaetielporfirien. Interaksies tussen kobaltporfiriene en bogenoemde ditisoonderivate is deeglik ondersoek met behulp van UV/sigbare spektroskopie. Hierdeur is die redokskarakter wat dikwels in hierdie komplekse voorkom, geopenbaar.

Uitgebreide ADF en Gaussiese kwantumchemiese berekenings is uitgevoer op ditisoon, ditisonatofenielkwik(II) en die S-gemetileerde derivaat. Resultate het die mees waarskynlike strukture van hierdie verbindings uitgewys. Die fotochromiese reaksiemeganisme van PhHgHDz, die orbitale en oorgangsenergieë betrokke was is ook opgeklaar. Rekenaarberekenings op die addukte van die oranje en blou isomere van PhHgHDz met kobaltporfirien was in ooreenstemming met die verwagting dat die blou vorm minstens net so stabiel, (of stabieler) as die oranje vorm sal wees.

Elektrochemiese toeligting met betrekking tot die redoksgedrag van ditisoon, sy derivate, en kwik(II)- en kobalt(III)komplekse is vir die eerste keer nagevors. Die relatiewe weerstand van die gehalogeneerde ditisone teen oksidasie is vergelyk. Kobaltkomplekse van oktaetiel-, tetrafeniel- en die sulfofenielporfirien derivate is elektrochemies ondersoek, en hulle weerstand teen reduksie onderling vergelyk. 'n Vergelykende oplosmiddelstudie op die elektrochemiese gedrag van die substraat is met behulp van dimetielsulfoksied, dichlorometaan en piridien uitgevoer. Die effek van die hulpelektroliet op die elektrochemiese gedrag van ditisoon en porfirienderivate is met behulp van $[NBu_4][PF_6]$ en $[NBu_4][B(C_6F_5)_4]$ nagevors.

# Bibliography


1. H. M. N. H. Irving in *Dithizone*, Analytical Sciences Monographs No.**5**, The Chemical Society, London, 1977
2. H. M. N. H. Irving, *CRC Crit. Rev. Anal. Chem.*, 321, **8** (1980)
3. A. T. Hutton, *Polyhedron*, 13, **6** (1987)
4. Y. Shimano and P. Yap, 70 50 355, *Chem. Abs.*, 97 349h, **80** (1974)
5. J. A. Davis and M. Thomas (San Diego State University) in *Photochromic Materials Study*, Rome Air Development Centre, Final Technical Report No. RADC-TR-85-177, Sept. 1985
6. K. Ichimura in *Photochromic Materials and Photoresists in Photochromism: Molecules and Systems*, H. Durr and H. Bouas-Laurent, Studies in Organic Chemistry 40, Elsevier, Amsterdam, 1990, p 903
7. L. S. Meriwether, E. C. Breitner and C. L. Sloan, *J. Am. Chem. Soc.*, 4441, **87** (1965)
8. L. S. Meriwether, E. C. Breitner and N. B. Colthup, *J. Am. Chem. Soc.*, 4448, **87** (1965)
9. K. F. Purcell and J. C. Kotz in *Inorganic Chemistry*, Holt-Saunders Int. Ed., 1985, p 1050
10. J. S. Trommel and L. G. Marzilli, *Inorg. Chem.*, 4374, **40** (2001)
11. P.J. Toscana and L.G. Marzilli, *Prog. Inorg. Chem.*, 105, **31** (1984)
12. E. Fischer, *Annalen*, 67, **190** (1878); 316, **212** (1882)
13. J. H. Billman and E. S. Cleland, *J. Am. Chem. Soc.*, 1300, **65** (1943)
14. P. S. Pelkis, R. G. Dubenko and L. S. Pupko, *J. Org. Chem. USSR*, 2190, **27** (1957)
15. E. Bamberger, F. Padova and E. Ormerod, *Lieb. Ann.*, 307, **260** (1926)
16. D. Tarbell, C. W. Todd, M. C. Paulson, E. G. Lindstrom and W. P. Wystrach, *J. Am. Chem. Soc.*, 1381, **70** (1948)
17. F. Mirkhalaf, D. Whittaker and D. J. Schiffrin, *J. Electroanal. Chem.*, 203, **452** (1998)
18. H. M. N. H. Irving in *Dithizone*, Analytical Sciences Monographs, The Chemical Society, London, 1977, pp 4 and 82, for comprehensive background and references
19. M. Laing, *J. Org. Chem., Perkin Trans. 2*, 1248, (1977)
20. F. H. Herbstein and W. Schwotzer, *J. Am. Chem. Soc.*, 2367, **106** (1984)
21. H. M. N. H. Irving in *Dithizone*, Analytical Sciences Monographs, Chem. Soc., London, 1977, pp 8-22
22. H. M. N. H. Irving and A. M. Kiwan, *Anal. Chim. Acta.*, 271, **45** (1969)
23. H. Noda, C. Pakawatchai, J. M. Patrick, A. H. White, J. M. Harrowfield and L. M. Engelhardt, *Bull. Chem. Soc. Jpn.*, 2385, **58** (1985)
24. G. Iwantscheff in *Das Dithizon und seine Anwendung in der Mikro- und Spuren-analyse*, 2nd Edition, Verlag Chemie, Weinheim, 1972
25. H. M. N. H. Irving, S. J. H. Cooke, S. C. Woodger and R. J. P. Williams, *J. Chem. Soc.*, 1847 (1949)
26. H. M. N. H. Irving and D. C. Rupainwar, *Anal. Chim. Acta*, 187, **48** (1969)
27. P. A. Clifford, *J. Assoc. Offic. Agric. Chemists*, 695, **21** (1938)
28. H. M. N. H. Irving, A. M. Kiwan, D. C. Rupainwar and S. S. Sahota, *Anal. Chim. Acta*, 205, **56** (1971)
29. A. M. Kiwan and H. M. N. H. Irving, *J. Chem. Soc.*, 898, **B** (1971)
30. J. W. Olgilvie, A. H. Corwin, *J. Am. Chem. Soc.*, 5023, **83** (1961)
31. Y. Kushi and Q. Fernando, *J. Chem. Soc.*, 1240 (1969)
32. J. L. Walsh, R. McCracken and A. T. McPhail, *Polyhedron*, 3221, **17** (1998)
33. R. Shah and S. Devi, *Reactive & Functional Polymers*, 1, **31** (1996)
34. H. M. N. H. Irving and C. F. Bell, *J. Chem. Soc.*, 4253 (1954)
35. Von J. Preuss and A. Gieren, *Acta Cryst.*, 1276, **B31** (1975)
36. A. T. Hutton, H. M. N. H. Irving and L. R. Nassimbeni, *Acta Cryst.*, 2071, **B36** (1980)

37. A. T. Hutton and H. M. N. H. Irving and L. R. Nassimbeni, *Acta Cryst.*, 1354, **B35** (1979)
38. L. Tomcsanyi, *Anal. Chim. Acta*, 411, **70** (1974); 371, **88** (1977) and 409, **89**, (1977)
39. A. R. Al-Salihy and H. Freiser, *Talanta*, 182, **17** (1970)
40. H. Fischer, *Wiss. Veröffentlich. Siemens-Werken*, 158, **4** (1925)
41. H. M. N. H. Irving in *Dithizone*, Analytical Sciences Monographs No.**5**, The Chemical Society, London, 1977
42. J. F. van Staden and R. F. Taljaard, *Talanta*, 1203, **64** (2004)
43. A. L. D. Comitre, B. F. Reis, *Talanta* at www.sciencedirect.com (2004)
44. M. M. Harding, *J. Chem. Soc.*, 4136 (1958)
45. R. F. Bryan and P. M. Knopf, *Proc. Chem. Soc.*, 203 (1961)
46. M. Laing, *J. Chem. Soc. Perkin Trans. 2*, 1247 (1977)
47. M. L. Niven, H. M. N. H. Irving and L. R. Nassimbeni, *Acta Cryst,*, 2140, **B38** (1982)
48. J. McB. Harrowfield, C. Pakawatchai and A. H. White, *Aust. J. Chem.*, 825, **36** (1983)
49. J. McB. Harrowfield, C. Pakawatchai and A. H. White, *J. Chem. Soc. Dalton Trans.*, 1109 (1983)
50. A. Irving and H. M. N. H. Irving, *J. Cryst. Spec. Res.*, 495, **16** (1986)
51. L. Shuncheng and J. Zubieta, *Polyhedron*, 677, **8** (1989)
52. K. Ortner and U. Abram, *Polyhedron*, 749, **18** (1999)
53. F. Kong and W. Wong, *J. Chem. Soc. Dalton Trans.*, 2497 (1999)
54. A. A. Pasynskii, A. V. Romanenkov, Y. V. Torubaev, P. V. Belousov and K. A. Lysenko, *Russ. J. Inorg. Chem.*, 2004, **47** (2002)
55. G. L. Seamans, J. L. Walsh, T. William, *Acta Cryst., Sect. C: Cryst. Struct. Comm.*, m268, **59** (2003)
56. H. M. N. H. Irving, A. H. Nabilsi and S. S. Sahota, *Anal. Chim. Acta*, 135, **67** (1973)
57. K. Wakamatsu, K. Nishimoto and T. Shibahara, *Inorg. Chim. Acta*, 180-188, **295** (1999)
58. K. Wakamatsu, K. Nishimoto and T. Shibahara, *Inorg. Chem. Comm.*, 677-679, **3** (2000)
59. G. N. Andreev, B. Schrader, D. A. Hristozova, V. B. Dlechev, J. S. Petrov and P. Rademacher, *J. Mol. Struct.*, 77-87, **645** (2003)
60. J. Abe, N. Nemoto, Y. Nagase and Y. Shirai, *Chem. Phys. Lett.*, 450-454, **276** (1997)
61. T. Ziegler, *Chem. Rev.*, 651, **91** (1991)
62. B. G. Johnson, P. M. W. Gill, J. A. Pople, *J. Chem. Phys.*, 5612, **93** (1996)
63. P. E. M. Siegbahn, *Adv. Chem. Phys.*, 333, **93** (1996)
64. G. H. Brown, *Photochromism*, Wiley Interscience, New York, 1971
65. H. Dürr, H. Bouas-Laurent (Eds.), *Photochromism, Molecules and Systems*, Elsevier, Amsterdam, 1990
66. K. Matsuda and M. Irie, *J. Photochem. & Photobiol. C: Photochem. Rev.*, 169, **5**, (2004)
67. G. J. Ashwell, *Nature*, 617, **347**, (1990)
68. M. A. Wolak N. B. Gillespie, C. J. Thomas, R. R. Birge and W. J. Lees, *J. Photochem. & Photobiol. A: Chem.*, 39, **147**, (2002)
69. N. Sertova, I. Petkov and J. M. Nunzi, *J. Photochem. & Photobiol. A: Chem.*, 163, **134** (2000)
70. H. Irving, G. Andrew and E. J. Risdon, *J. Chem. Soc.*, 541 (1949)
71. J. L. A. Webb, I. S. Bhatia, A. H. Corwin and A. G. Sharp, *J. Am. Chem. Soc.*, 91, **72** (1950)
72. H. M. N. H. Irving in *Dithizone*, Analytical Sciences Monographs, The Chemical Society, London, 1977, p 38
73. G. S. Hammond, N. J. Turro and P. A. Leermakers, *J. Phys. Chem.*, 1144, **66**, (1962)
74. H. M. N. H. Irving and T. Nowicka-Jankowska, *Anal. Chim. Acta*, 55, **54** (1971)
75. H. M. N. H. Irving and J. J. Cox, *J. Chem. Soc.*, 466 (1963)
76. H. M. N. H. Irving and A. M. Kiwan, *J. Chem. Soc.*, 4288 (1963)
77. N.L. Cromhout and A.T. Hutton, *Appl. Organomet. Chem.* 66, **14** (2000)

78. O. Dimroth, *Chem. Ber.*, 2032, **35** (1902)
79. J. L. Wardell, *Comp. Organomet. Chem.*, 874, **2** (1982)
80. L. Alderighi, *Inorg. Chim. Acta*, 8, **356**, (2003)
81. J. M. de Gooijer , M. Scheltus , H. W. Lösch , R. Staudt , J. Meuldijk and C. E. Koning, *J. Supercritical Fluids*, 129-152, **29** (2004)
82. P. Neri and G. Antoni, *Macromol. Synth.*, 25, **8** (1982)
83. M. Tomida, T. Nakato, S. Matsunami and T. Kakuchi, *Polymer*, 4733, **38** (1997)
84. P. Neri, *J. Med. Chem.*, 893, **16** (1973)
85. B. V. Erlanger, *Pharmacol. Rev.*, 271, **25** (1973)
86. J. C. Swarts, D. M. Swarts, D. M. Maree, E. W. Neuse, C. La Madeleine and J. E. van Lier, *Anticancer Research*, 2033, **21** (2001)
87. J. C. Swarts, E. W. Neuse and G. J. Lamprecht, *J. Inorg. & Organomet. Pol.*, 143, **4** (1994)
88. V. Dourtoglou and B. Gross, *Synthesis*, 572-573 (1984)
89. A. U. Francis, S. Venkatachalam, M. Kanakavel, P. V. Ravindran, K. N. Ninan, *Eur. Pol. J.*, 831, **39** (2003)
90. M. S. Eroglu, B. M. Baysal and O. Guven, *Polymer*, 1945, **38** (1997)
91. H. Kamogawa and Hiroyoshi, *Chem. Abs.*, 60393s, **80** (1974)
92. M. S. Eroglu, B. M. Baysal and O. Guven, *Polymer*, 1945, **38** (1997)
93. Y. Sumitomo, K. Tsuboshima and H. Hayakawa, *Chem. Abs.*, 15494g, **76** (1972)
94. P. Silver, *Chem. Abs.*, 60576d, **80** (1974)
95. Nuclear Research Associates, *Chem. Abs.*, 120017c & 120018d, **70** (1969)
96. W. R. Sorenson, T. W. Campbell, *Preparative Methods of Polymer Chemistry*, Interscience Publishers, 1961
97. H. Kamogawa and Hiromi, *Chem. Abs.*, 71563y, **80** (1974)
98. Nuclear Research Associates, *Chem. Abs.*, 120018d, **70** (1969)
99. E. P. C. Lai, B. Wong and V. A. van der Noot, *Talanta*, 1097, **40** (1993)
100. A. D. Adler in *The chemical and physical behaviour of porphyrin compounds and related structures.* Annales, New York Academy of Science, 206, 1973
101. C. M. Drain, J. M. Lehn, *J. Chem. Soc. Chem. Commun.*, 2313 (1994) & 2337 (1996)
102. J. A. Hartley, S. M. Forrow and R. L. Souhami, *Cancer Res.*, 1936, **50** (1990)
103. K. Kadish, K. Smith and R. Guilard in *The Porphyrin Handbook*, Academic: NY, 2000, Vol. 3, pp 43-131
104. P. Rothemund, *J. Am. Chem. Soc.*, 2912, **61** (1931)
105. A.D. Adler, F. R. Longo, J. D. Finarelli, J. Goldmacher, J. Assour and L. Korsakoff, *J. Org. Chem.*, 476, **32** (1967)
106. F. R. Longo, J. D. Finarelli, J. Kim, *J. Heterocycl. Chem.*, 927, **6** (1969)
107. A.D. Adler, F. R. Longo, F. Kampas and J. Kim, *J. Inorg. Nucl. Chem.*, 2443, **32** (1970)
108. K. Rousseau and D. Dolphin, *Tetrahedron*, 4251, **48** (1974)
109. J.S. Lindsey, H. C. Hsu and I. C. Schreiman, *Tetrahedron*, 4969, **27** (1986)
110. J.S. Lindsey, I. C. Schreiman, H. C. Hsu, P. C. Kearney and A. M. Margueretaz, *J. Org. Chem.*, 827, **52** (1987)
111. H. Sharghi and A. H. Nejad, *Tetrahedron*, 1863, **60** (2004)
112. E. B. Fleischer and J. M. Palmer, *J. Am. Chem. Soc.*, 3162, **93** (1971)
113. R. G. Wollmann and D. N. Hendrickson, *Inorg. Chem.*, 3079, **16** (1977)
114. U. Eiser, R. P. Linstead, E. A. Parkes and E. Stephen, *J. Chem. Soc.*, 733 (1957) and 1655 (1956)
115. H. W. Whitlock and R. Hanauer, *J. Org. Chem.*, 2169, **33** (1968)
116. J. B. Paine, W. B. Kirshner and D. W. Moskowitz, *J. Org. Chem.*, 3857, **41** (1976)
117. C. B. Wang and C. K. Chang, *Synthesis*, 548 (1979)

118. H. H. Inhoffen, *Ann Chem.*, 133, **695** (1966)
119. J. L. Sessler, A. Mozaffari and M. R. Johnson, *Org. Synth.*, 68, **70** (1992)
120. G. D. Hartman and L. M. Weinstock, *Org. Synth.*, 620, **6** (1988)
121. P. Byrappa and V. Krishnan, *Inorg. Chem.*, 239, **36** (1991)
122. K. M. Smith, J. H. Fuhrhop in *Porphyrins and Metalloporphyrins*, Elsevier Scient. Publ. Comp., 1975, p 798
123. O. Herrmann, S. H. Mehdi and A. Corsini, *Can. J. Chem.*, 1084, **56** (1978)
124. K. M. Smith and J. H. Fuhrhop in *Porphyrins and Metalloporphyrins*, Elsevier Scient. Publ. Comp., 1975, pp 10, 19-25
125. F. A. Walker, *J. Am. Chem. Soc.*, 1150, **95** (1973)
126. F. A. Walker, *J. Am. Chem. Soc.*, 1142, **95** (1973)
127. T. Sakurai, K. Yamamoto, H. Naito, N. Nakamoto, *Bull. Chem. Soc. Jpn.*, 3042, **49** (1976)
128. H. Sugimoto, N. Ueda and M. Mori, *Bull. Chem. Soc. Jpn.*, 3425, **54** (1981)
129. J. L. Walsh, R. McCracken and A. T. McPhail, *Polyhedron*, 3221, **17** (1998)
130. S. Jeannin, *Transition Met. Chem. (Weinhein Ger.)*, 192, **1** (1976)
131. W. Chen and C. Hung, *Inorg. Chem.*, 5070, **40** (2001)
132. H. Sakurai, K. Ishizu and K. Okada, *Inorg. Chim. Acta*, L9, **91** (1984)
133. G. N. Schrauzer and R. J. Windgassen, *J. Am. Chem. Soc.*, 3607, **89** (1967)
134. S. Fukuzumi and T. Kitano, *Inorg. Chem.*, 2558, **29** (1990)
135. K. Jones and M. F. Lappert, *Proc. Chem. Soc.*, 22 (1964)
136. T. A. George and M. F. Lappert, *Chem. Comm.*, 463, **14** (1966)
137. K. L. Brown and S. Peck in *Organometallic Syntheses*, Elsevier: Amsterdam, 1988, vol. 14, p 304
138. M. Perree-Fauvet, *J. Organomet. Chem.*, 439, **120** (1976)
139. H. Ogoshi, E. Watanabe, N. Koketsu and Z. Yoshida, *Bull. Chem. Soc. Japan*, 2529, **49** (1976)
140. P. Kofod, P. Harris and S. Larsen, *Inorg. Chem.*, 2258, **36** (1997)
141. M. S. A. Hamza, C. Ducker-Benfer and R. van Eldik, *Inorg. Chem.*, 3777, **39** (2000)
142. P. Kofod, *Inorg. Chem.*, 2768, **34** (1995)
143. K. Yamamoto, M. Hoshino, M. Kohno and H. Ohya-Nishiguchi, *Bull. Chem. Soc. Jpn.*, 351, **59** (1986)
144. G. N. Schrauzer and J. W. Silbert, *J. Am. Chem. Soc.*, 1022, **92** (1970)
145. J. S. Summers, J. L. Peterson and A. M. Stolzenberg, *J. Am. Chem. Soc.*, 7189, **116** (1994)
146. K. M. Kadish, X. Q. Lin and B. C. Han, *Inorg. Chem.*, 4161, **26** (1987)
147. A. Salehi, W. A. Oertling, G. T. Babcock and C. K. Chang, *J. Am. Chem. Soc.*, 5630, **108** (1986)
148. D. Dolphin, *Proc. Nat. Acad. Sci.*, USA, 614, **68** (1971)
149. A. W. Johnson and I. T. Kay, *J. Chem. Soc.*, 2979 (1960)
150. R. H. Felton, D. Dolphin, D. C. Borg and J. Fajer, *J. Am. Chem. Soc.*, 196, **91** (1969)
151. F. A. Walker, D. Beroiz and K. M. Kadish, *J. Am. Chem. Soc.*, 3484, **98** (1976)
152. F. Basolo, *J. Chem. Soc., Chem. Commun.*, 810 (1973)
153. F. Basolo, D. P Rillema and M. J. Carter, *J. Am. Chem. Soc.*, 392, **96**(1974)
154. A. H. Corwin, D. G. Whitten, E. W. Baker and G. G. Kleinspehn, *J. Am. Chem. Soc.*, 3621, **85** (1963)
155. A. H. Corwin, E. W. Baker and D. G. Whitten, *J. Org. Chem.*, 2363, **28** (1963)
156. G. Costa, *Pure Appl. Chem.*, 335, **30** (1971)
157. G. Costa, A. Ruxeddu and E. Reisenhofer, *J. Chem. Soc., Dalton Trans.*, 1519 (1972)
158. S. I. Yang, J. Seth, J. Strachan, S. Gentemann, D. Kim, D. Holten, J. S. Lindsey and D. F. Bocian, *J. Porphyrins and Phthalocyanines*, 117, **3** (1999)
159. A. Giraudeau, H. J. Callot, J. Jordan, I. Ezhar and M. Gross, *J. Am. Chem. Soc*, 3857, **101** (1979)

160. F. D'Souza, A. Villard, E. van Caemelbecke, M. franzen, T. Boschi, P. Tagliatesta and K. M. Kadish, *Inorg. Chem.*, 4042, **32** (1993)
161. J. G. Leipoldt, R. van Eldik and H. Kelm, *Inorg. Chem.*, 4146, **22** (1983)
162. K. F. Purcell and J. C. Kotz in *Inorganic Chemistry*, W. B. Saunders Company, 1985, p 744
163. R. van Eldik and V. Lepentsiotis, *J. Chem. Soc., Dalton Trans.*, 999 (1998)
164. V. Lepentsiotis, R. van Eldik, D. M. Stulov and S. V. Makarov, *J. Chem. Soc., Dalton Trans.*, 2915 (1998)
165. K. R. Ashley and S. Au-Young, *Inorg. Chem.*, 1937, **15** (1976)
166. L. J. Boucher and H. K. Garber, *Inorg. Chem.*, 2644, **9** (1970)
167. W. S. Caughey, *Biochemistry*, 3830, **5** (1966)
168. M. Inamo, T. Kohagura, *Inorg. Chim. Acta*, 90, **340** (2002)
169. C. Hansch and A. Leo in *Substituent Constants for Correlation Analysis in Chemistry and Biology*, J. Wiley Sons: New York, 1979, Chapter 6
170. W. Jentzen, *J. Am. Chem. Soc.*, 11085, **117** (1995)
171. S. Will, J. Lex, E. Vogel, V. A. Adamian, E. van Caemelbecke, K. M. Kadish, *Inorg. Chem.*, 5577, **35** (1996)
172. H. M. N. H. Irving and C. F. Bell, *J. Chem. Soc.*, 4253 (1954)
173. J. W. Olgilvie, A. H. Corwin, *J. Am. Chem. Soc.*, 5023, **83** (1961)
174. H. Noda, L. Meinhardt, J. Harrowfield, *Bull. Chem. Soc. Jpn.*, 2385, **58** (1985)
175. A. T. Hutton and H. M. N. H. Irving, *J. Chem. Soc. Dalton Trans.*, 2299 (1982)
176. H. Ogoshi, E. Watanabe, N. Koketsu and Z. Yoshida, *Bull. Chem. Soc. Japan*, 2529, **49** (1976)
177. G. G. Schlessinger, *Inorg. Synth.*, 160-161, **9** (1960)
178. J. Bjerrum and J. P. McReynolds, *Inorg. Synth.*, 217, **2** (1941)
179. D. A. Skoog, D. M. West, F. J. Holler & S. R. Crouch, *Fundamentals of Analytical Chemistry*, Thompson Brooks/Cole, 8th Ed., 2004, p.805
180. A. R. Al-Salihy and H. Freiser, *Talanta*, 182, **17** (1970)
181. O. Dimroth, *Chem. Ber.*, 2032, **35** (1902)
182. L. Alderighi, P. Gans, S. Midollini & Vacca, *Inorg. Chim. Acta*, , **356** (2003
183. J. L. Wardell, *Comp. Organomet. Chem.*, 874, **2** (1982)
184. G. Giammona, B. Carlisi, G. Cavallaro, I. Donato, F. Pinio and V. Turco Liveri, *Int. J. Pharm.*, 239, **64** (1990)
185. F. Castelli, G. Giammona, A. Raudino and G. Puglisi, *Int. J. Pharm.*, 43, **70** (1991)
186. V. Lepentsiotis, R. van Eldik, D. M. Stulov and S. V. Makarov, *J. Chem. Soc., Dalton Trans.*, 2915 (1998)
187. K. R. Ashley and S. Au-Young, *Inorg. Chem.*, 1937, **15** (1976)
188. D.E. Bublitz and K.L. Rinehart Jr., *Org. Reactions*, 76, **17**, (1969)
189. R.G. Wollman and D. Hendrickson, *Inorg. Chem.*, 3079-89, **16** (1977)
190. M. Inamo, T. Kohagura, *Inorg. Chim. Acta*, 90, **340** (2002)
191. J. L. Sessler, A. Mozaffari and M. R. Johnson, *Org. Synth.*, 68, **70** (1992)
192. K. M. Smith and J. H. Fuhrhop, *Porphyrins and Metalloporphyrins*, Elsevier Scient. Publ. Comp., 1975, p.798
193. O. Herrmann, S. H. Mehdi and A. Corsini, *Can. J. Chem.*, 1084, **56** (1978)
194. E. D. Becker, *High Resolution NMR – Theory and Chemical Applications*, Academic Press, Inc., 1969, p.80
195. D. V. Stynes, H. C. Stynes, J. A. Ibers & B. R. James, *J. Am. Chem. Soc.*, 1142, **95** (1973)
196. R. F. Pasternack, M.A. Cobb and N. Sutin, *Inorg. Chem.*, 866, **14** (1975)
197. K. R. Ashley and S. Au-Young, *Inorg. Chem.*, 1937, **15** (1976)
198. A. T. Hutton, *Polyhedron*, 13-23, **6** (1987)
199. M. Laing, *J. Chem. Soc. Perkin II*, 1248-1252, **II** (1977)
200. F. Kong and W. Wong, *J. Chem. Soc. Dalton Trans.*, 2497 (1999)

201. H. Irving and J. J. Cox, *J. Chem. Soc.*, 1470 (1961)

202. F. A. Cotton and G. Wilkinson, *Basic Inorganic Chemistry*, John Wiley & Sons, (1976) p.268

203. J. McB. Harrowfield, C. Pakawatchai and A. H. White, *J. Chem. Soc. Dalton Trans.*, 1109-1113 (1983)

204. R. M. Fernandes, E. S. Lang, E. M. V. Lopez, G. F. De Souza, *Polyhedron*, 1149-1153 , **21** (2002)

205. K. F. Purcell and J. C. Kotz, *Inorganic Chemistry*, Holt-Saunders Int. Ed., (1977) p.284

206. M. L. Niven, H. M. N. H. Irving, L. R. Nassimbeni and A. T. Hutton, *Acta Cryst.*, 2140-2145, **B38** (1982)

207. K. Ortner and U. Abram,. *Polyhedron*, 749-754, **18** (1999)

208. R. F. Bryan and P. M. Knopf, *Proc. Chem. Soc.*, 203 (1961)

209. M. Laing, *J. Chem. Soc. Perkin Trans. 2*, 1247 (1977)

210. J. McB. Harrowfield, C. Pakawatchai and A. H. White, *Aust. J. Chem.*, 825, **36** (1983)

211. L. Shuncheng and J. Zubieta, *Polyhedron*, 677, **8** (1989)

212. M. M. Harding, *J. Chem. Soc.*, 4136 (1958)

213. M. Burke-Laing and J. B. Mann, *Acta Cryst.*, 3216-3224, **B32** (1976)

214. T. Ziegler, *Chem. Rev.*, 651, **91** (1991)

215. B. G. Johnson, P. M. W. Gill and J. A. Pople, *J. Chem. Phys.*, 5612, **98** (1993)

216. P. E. M. Siegbahn, *Adv. Chem. Phys.*, 333, **93** (1996)

217. P. Doppelt, J. Fischer and R. Weiss, *J. Am. Chem. Soc.*, 5188, **106** (1984).

218. A.D. Becke, *Phys. Rev.*, 3098-3100, **A38** (1988)

219. Lee, W. Yang, R.G. Parr, *Phys. Rev.*, 785-789, **B37** (1988)

220. Hammer, L.B. Hansen, J.K. Norskov, *Phys. Rev.*, 7413-7421, **B59** (1999)

221. Y. Zhang and W. Yang,. *Rev. Lett.*, 890, **80** (1998)

222. N.C. Handy, A.J. Cohen *Mol. Phys.*, 403-412, **99** (2001)

223. C. Adamo, V. Barone, *J. Chem. Phys.*, 5933-5940, **116** (2002)

224. N.C. Handy, A.J. Cohen *Mol. Phys.*, 403-412, **99** (2001)

225. J.P. Perdew, K. Burke, M. Ernzerhof, *Phys. Rev. Lett.*, 3865-3868, **77** (1996)

226. J.P. Perdew, K. Burke, M. Ernzerhof, *Phys. Rev. Lett.*, 1396, **78** (1997)

227. P.J. Stephens, F.J. Devlin, C.F. Chabalowski, M.J. Frisch, *J. Phys. Chem.*, 11623-11627, **98** (1994)

228. M.A. Watson, N.C. Handy, A.J. Cohen, *J. Chem. Phys.*, 6475-6481, **119** (2003)

229. R.H. Hertwig, W. Koch, *Chem. Phys. Lett.*, 345-351, **268** (1997)

230. A.J. Cohen, N.C. Handy *Mol. Phys.*, 607-615, **99** (2001)

231. G. Gritzner and J. Kuta, *Pure Appl. Chem.*, 461, **56** (1984)

232. J. Conradie, T. S. Cameron, M. A. S. Aquino, G. J. Lamprecht and J. C. Swarts, *Inorg. Chim. Acta*, 2530, **358** (2005)

233. C. Creutz and H. Taube, *J. Am. Chem. Soc.*, 3988, **91** (1969)

234. W. E. Geiger, N. van Order, D. T. Pierce, T. E. Bitterwolf, A. L. Reingold and N. D. Chasteen, *Organometallics*, 2403, **10** (1991)

235. N. van Order, W. E. Geiger, T. E. Bitterwolf, A. L. Reingold, *J. Am. Chem. Soc.*, 5680, **109** (1987)

236. D. T. Pierce and W. E. Geiger, 373, **33** (1994)

237. X. Q. Lin, B. Boisselier-Cocolios and K. M. Kadish, *Inorg. Chem.*, 3242, **25** (1986)

238. A. T. Hutton and H. M. N. H. Irving, *J. Chem. Soc. Perkin Trans. II*, 1117-1121 (1982)

239. F. A. Walker, E. Hui and J. M. Walker, *J. Am. Chem. Soc.*, 2390, **97** (1975)

240. R.G. Wollman and D. Hendrickson, *Inorg. Chem.*, 3079-89, **16** (1977)

241. G. D. Hartman and L. M. Weinstock, *Org. Synth.*, 620-623, **6** (1988)

# Appendix 1: NMR Spectra

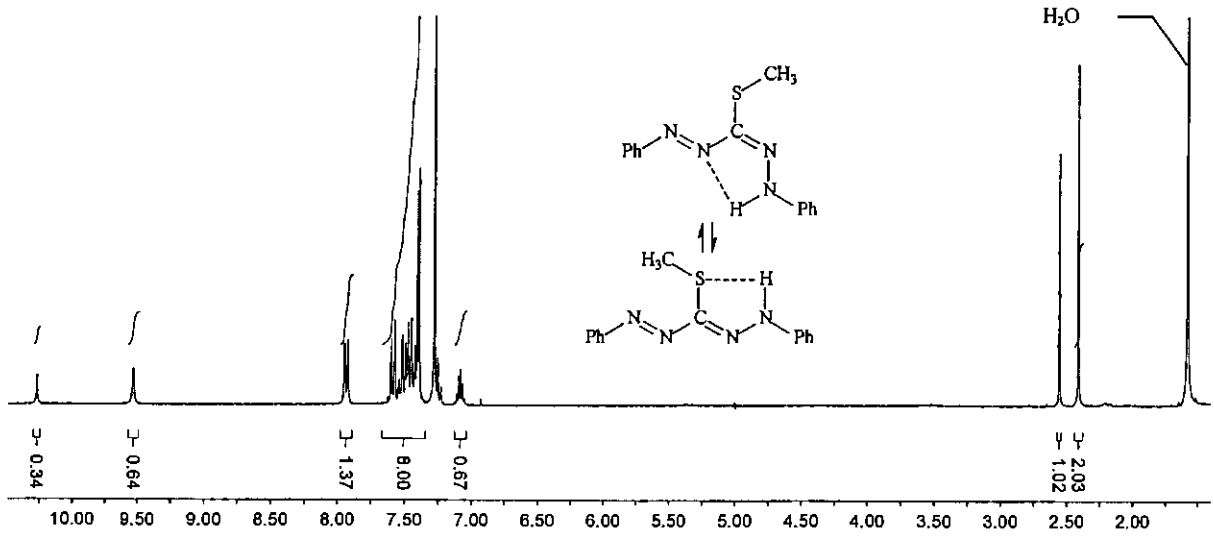


**Spectrum A1**. S-methyldithizone, **17** ($CDCl_3$)

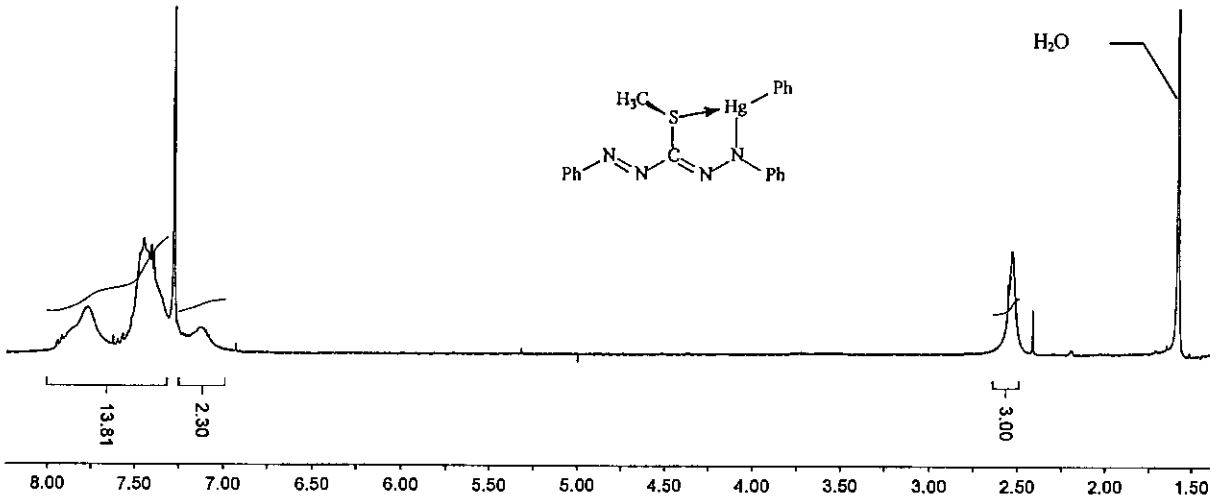


**Spectrum A2**. S-Methyldithizonatophenylmercury(II), **18** ($CDCl_3$)

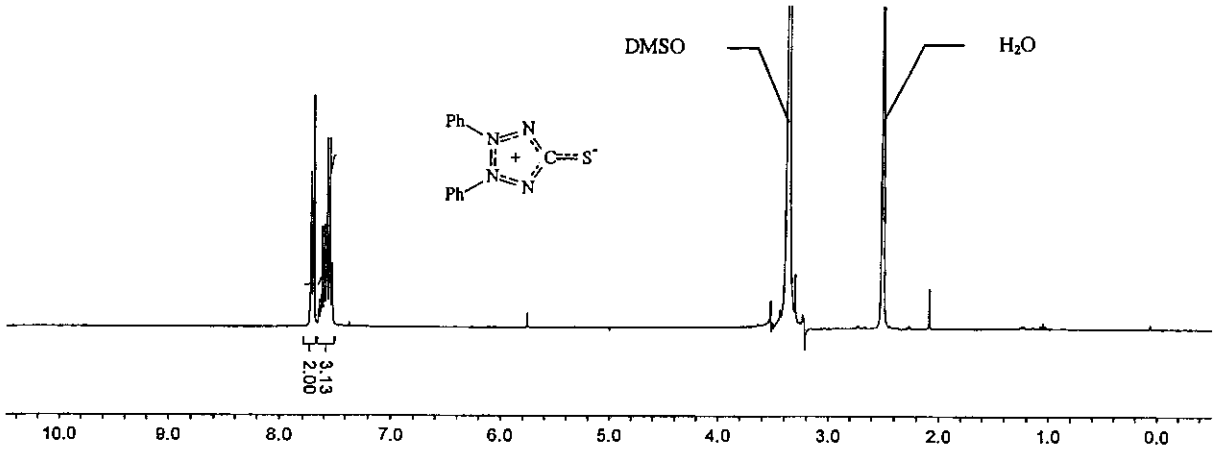


**Spectrum A3**. Dehydrodithizone, **21** ( $(CD_3)_2SO$ )

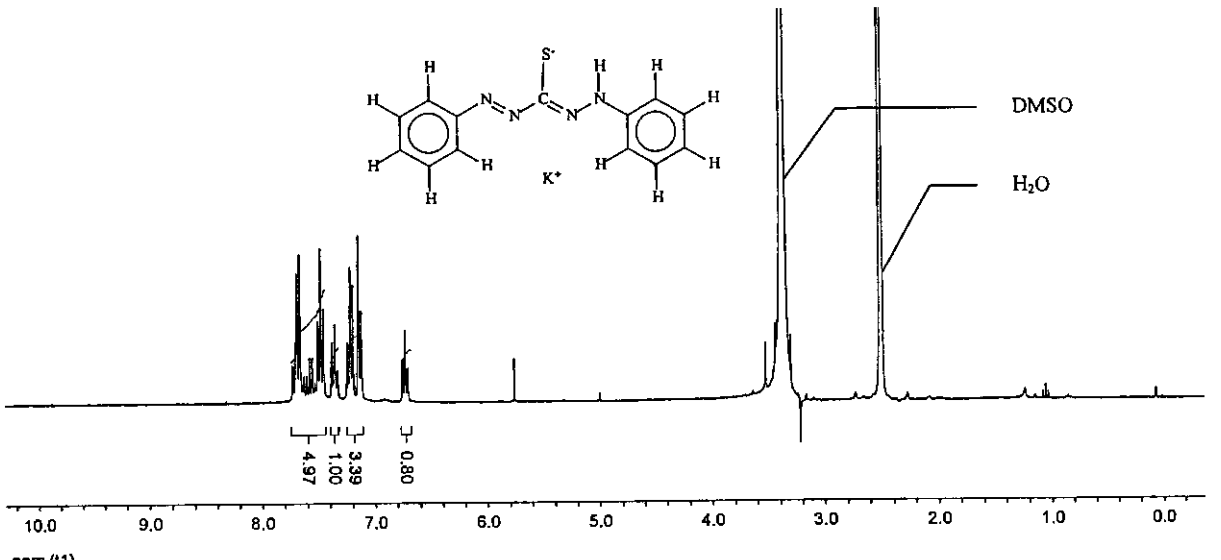


**Spectrum A4.** Potassium dithizonate, **19** ( $(CD_3)_2SO$ )

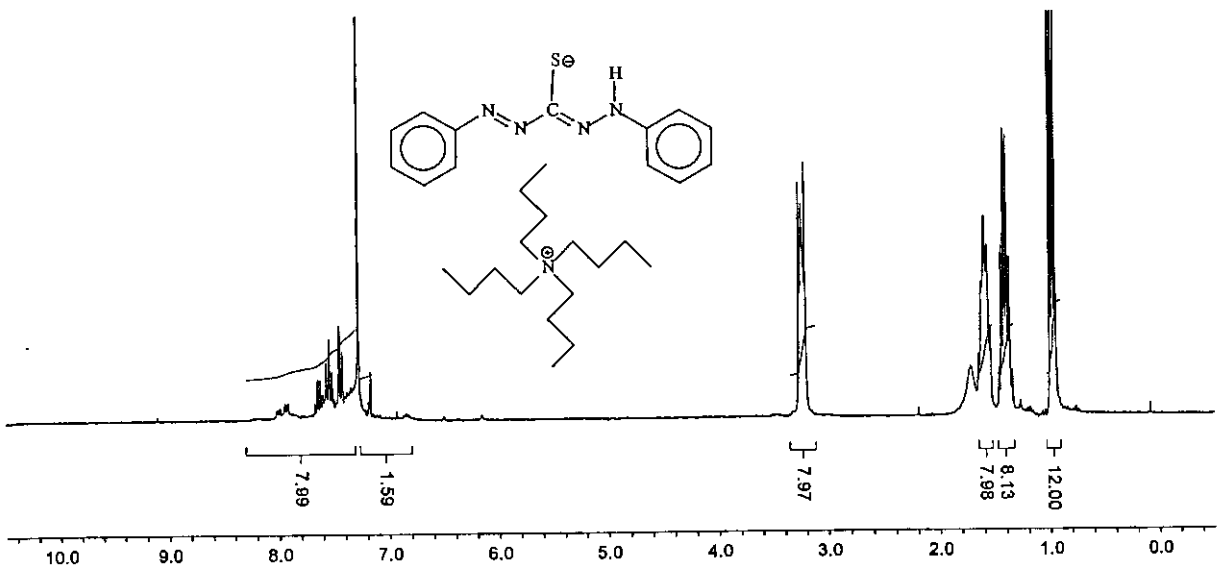


**Spectrum A5.** Tetrabutylammonium dithizonate, **23** ($CDCl_3$)

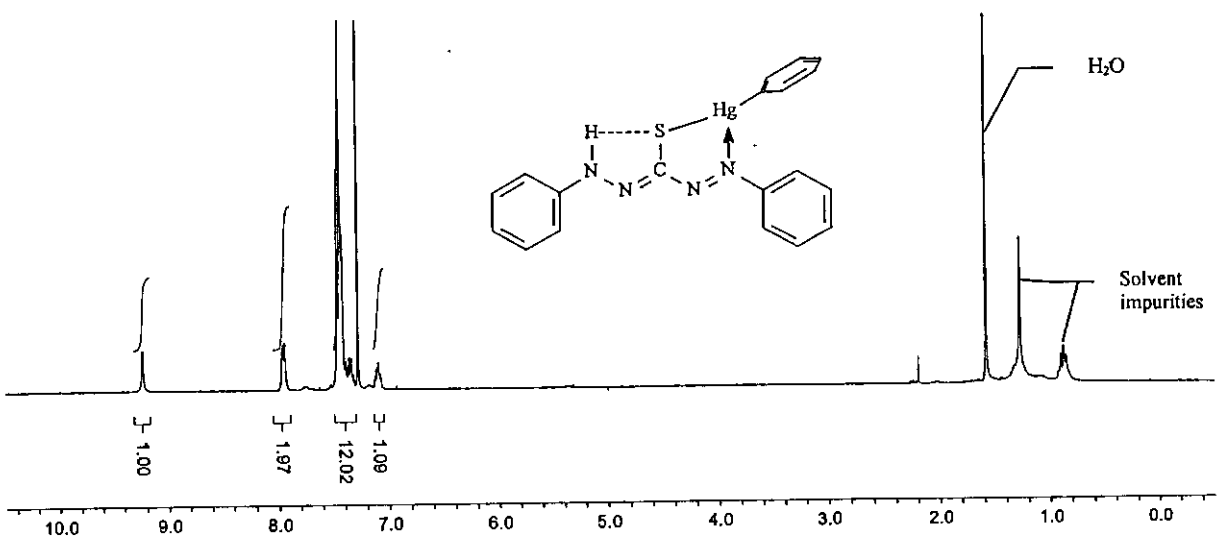


**Spectrum A6.** Dithizonatophenylmercury(II), **20** ($CDCl_3$).

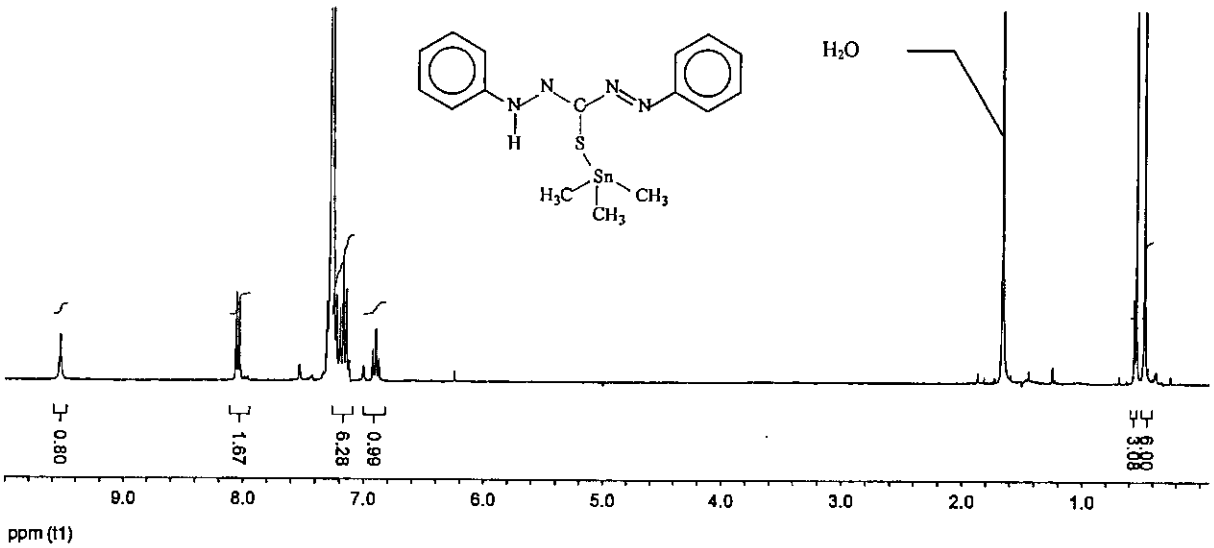


**Spectrum A7.** Dithizonatotrimethyltin(IV), **28** ($C_6D_6$)

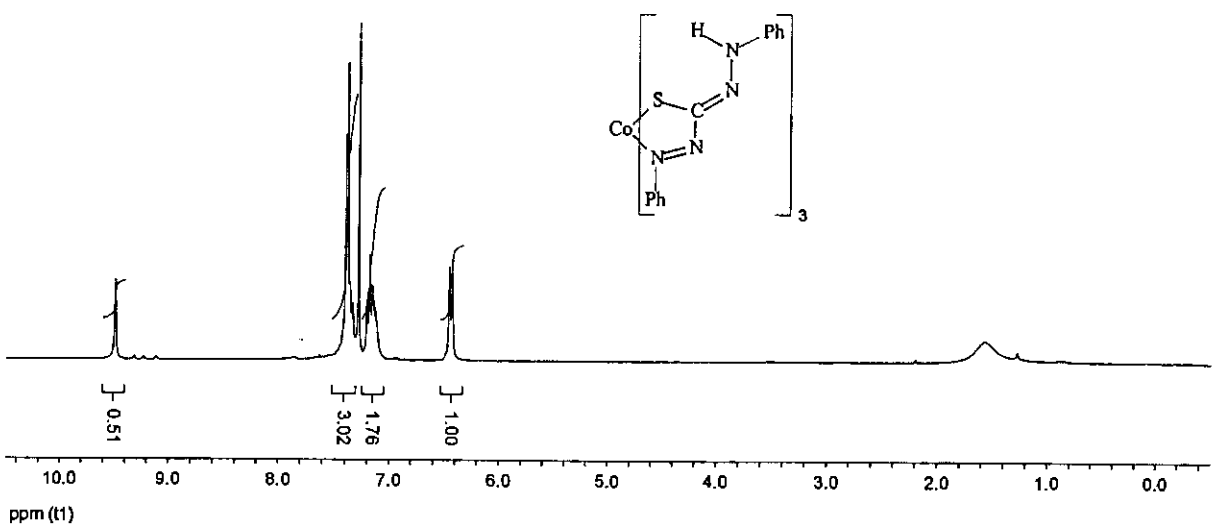


**Spectrum A8.** *Tris*-dithizonatocobalt(III), **33** ($CDCl_3$)

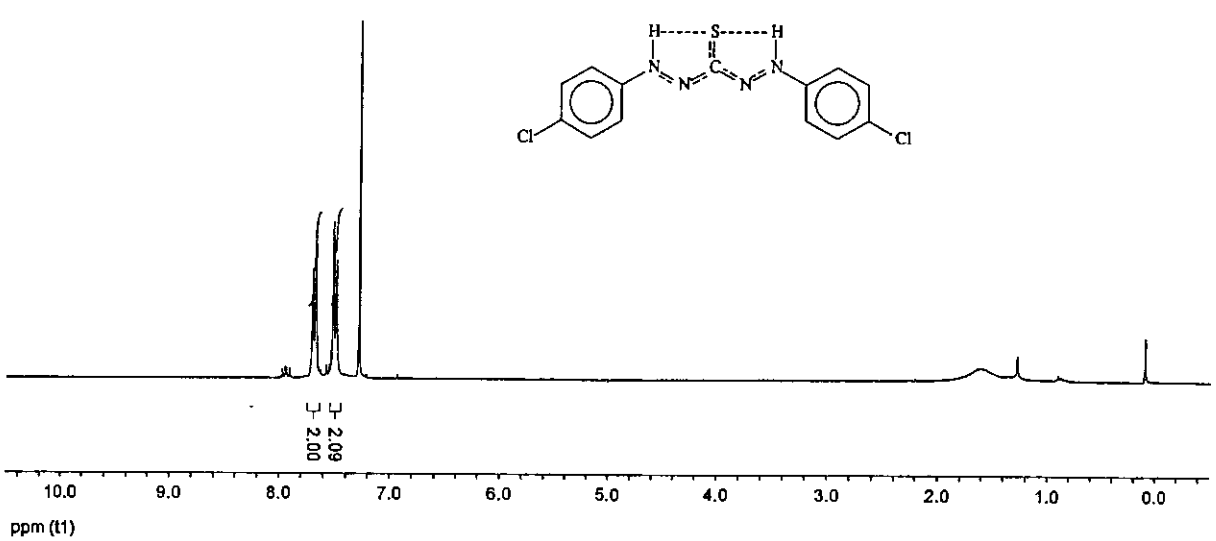


**Spectrum A9.** *p*-Chlorophenyldithizone, **40a** ($CDCl_3$)

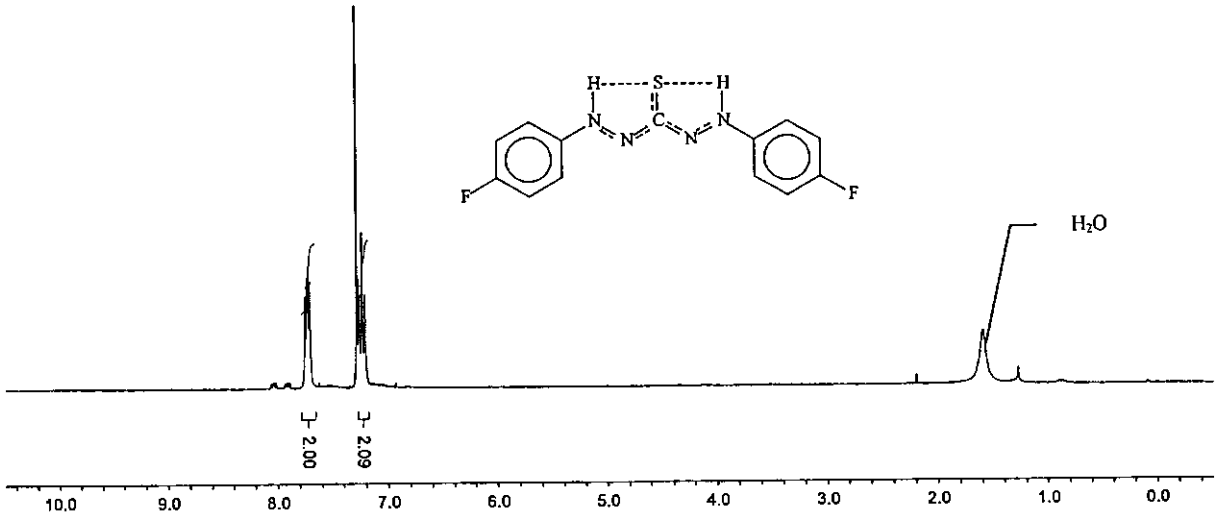


**Spectrum A10.** *p*-Fluorophenyldithizone, **40b** ($CDCl_3$)

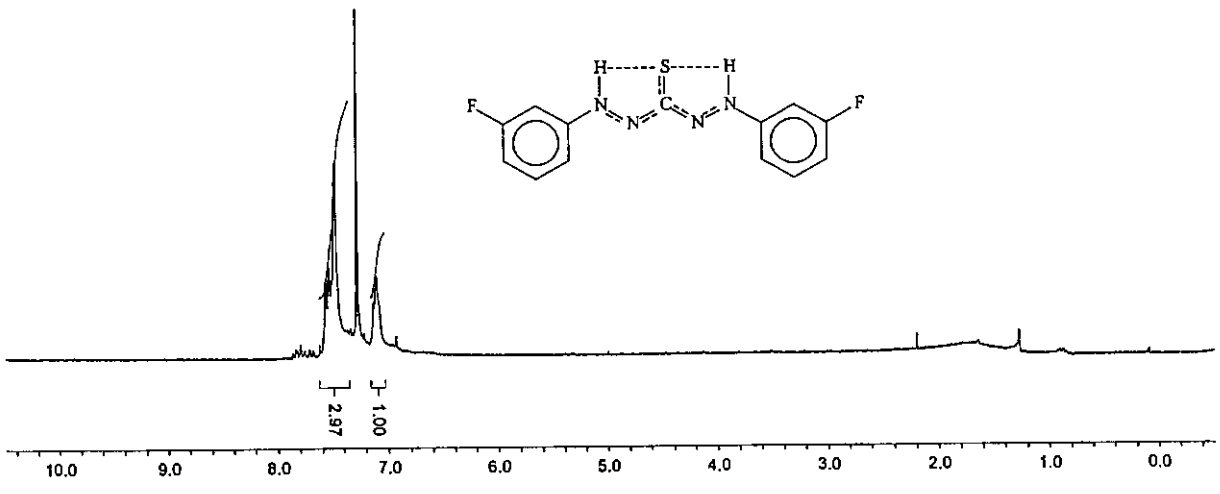


**Spectrum A11.** *m*-Fluorophenyldithizone, **40c** ($CDCl_3$)

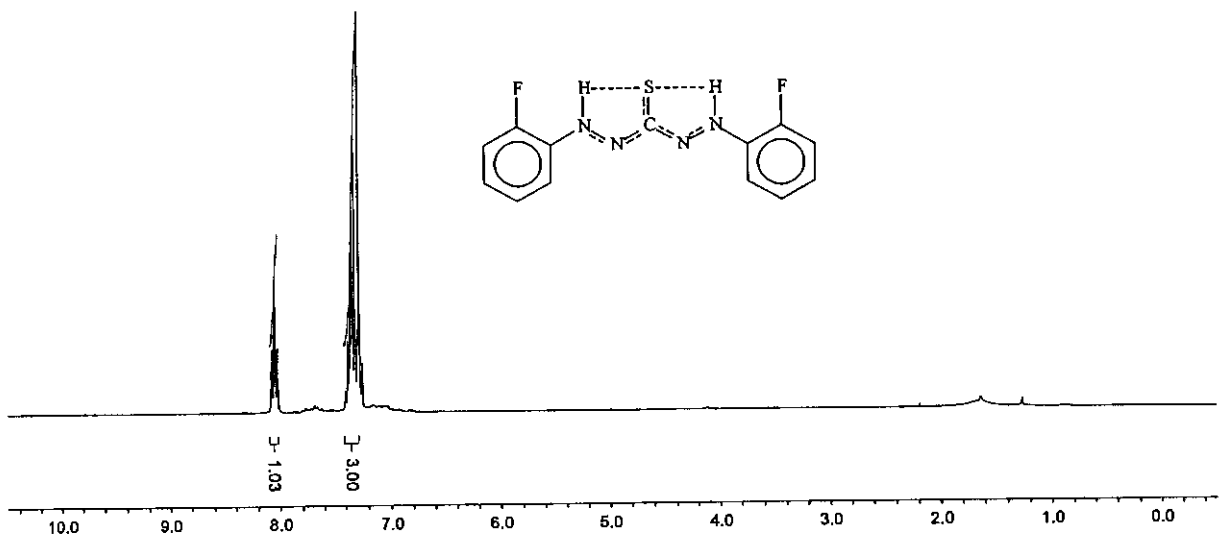


**Spectrum A12.** *o*-Fluorophenyldithizone, **40d** ($CDCl_3$)

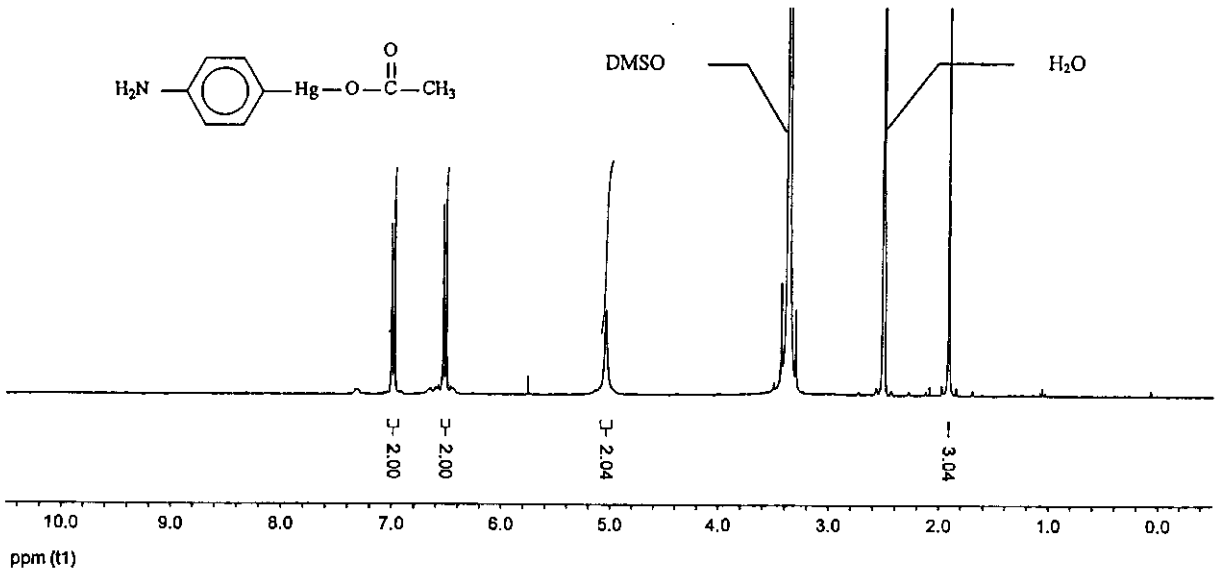


**Spectrum A13.** *p*-Aminophenylmercury(II) acetate, **41** ( $(CD_3)_2SO$ )

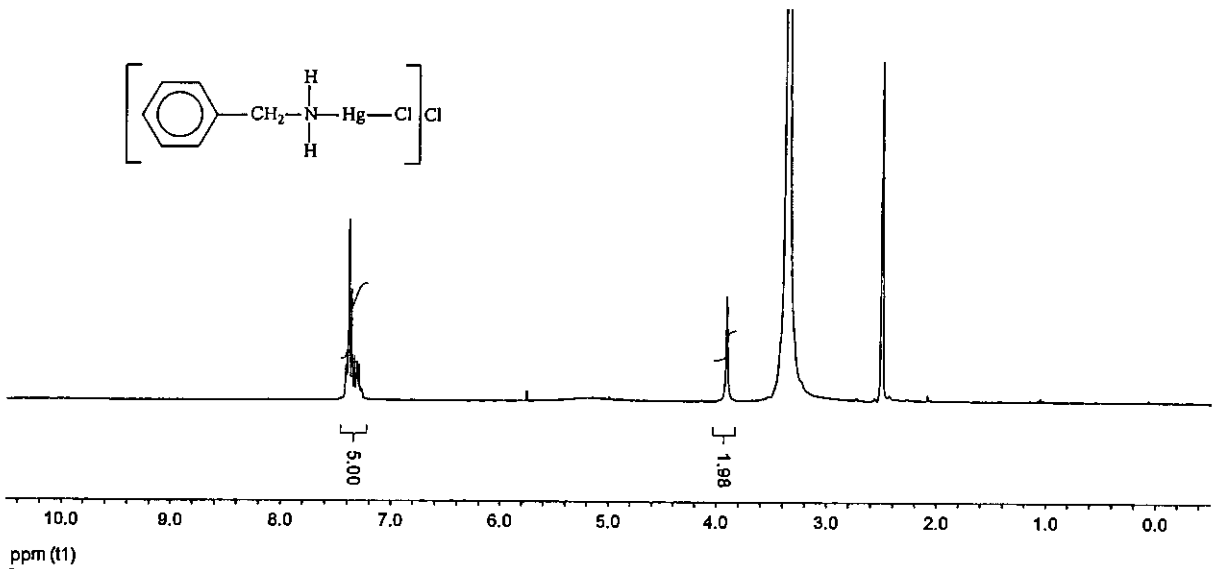


**Spectrum A14.** Benzylaminomercury(II) chloride, **43** ( $(CD_3)_2SO$ )

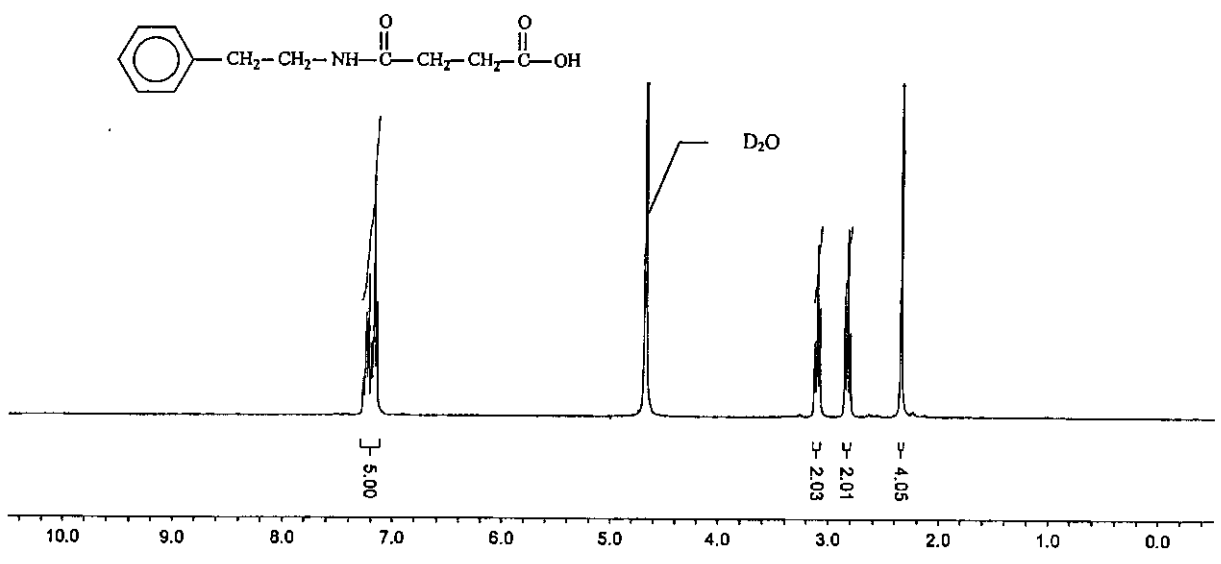


**Spectrum A15.** 4-Oxo-4-[(2-phenylethyl)amino]butanoic acid, **44** ($D_2O$)

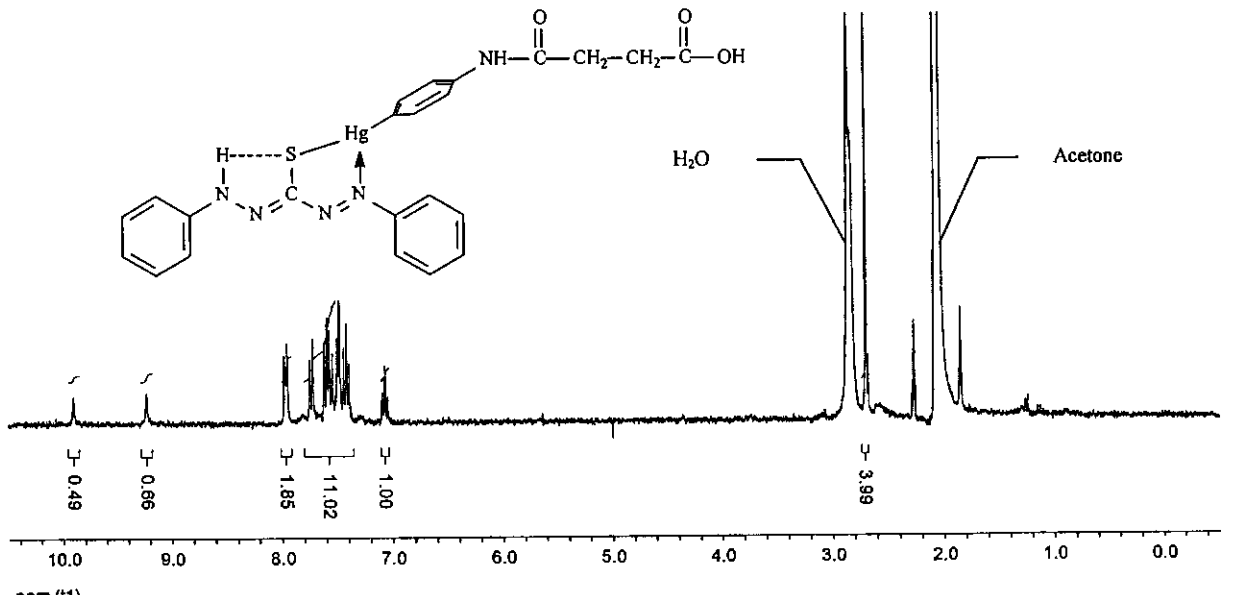


**Spectrum A16.** *p*-Anilino-4-oxobutanoic acid(dithizonato)mercury(II), **46** ( $(CD_3)_2CO$ )

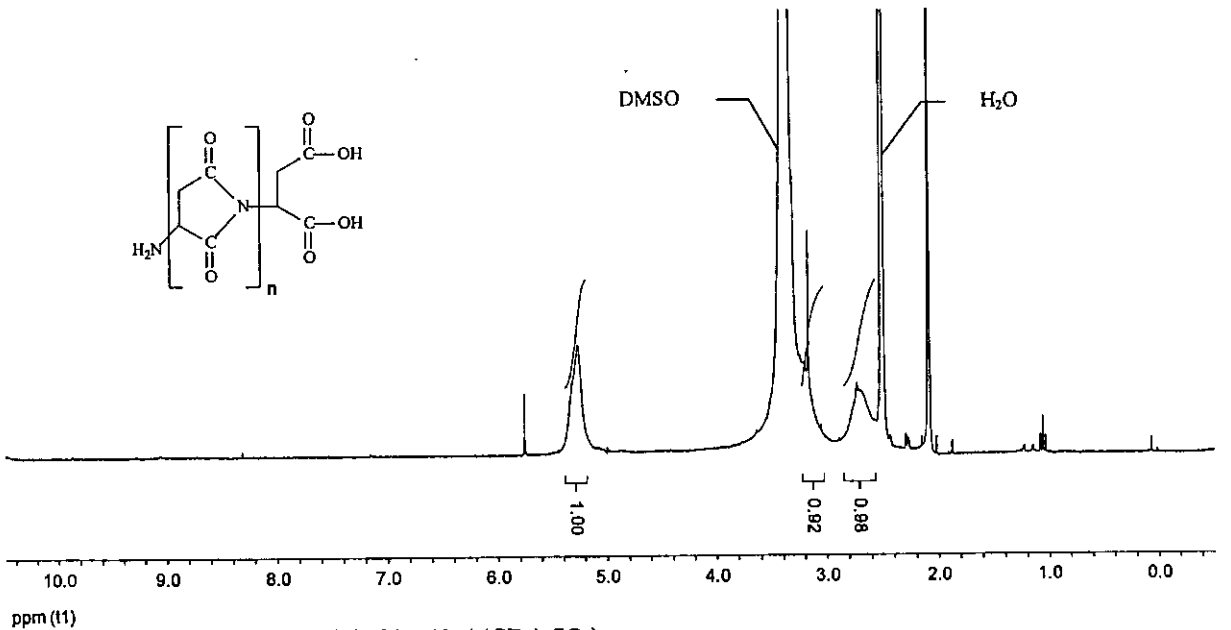


**Spectrum A17.** Poly-DL-succinimide, **48** ( $(CD_3)_2SO$ )

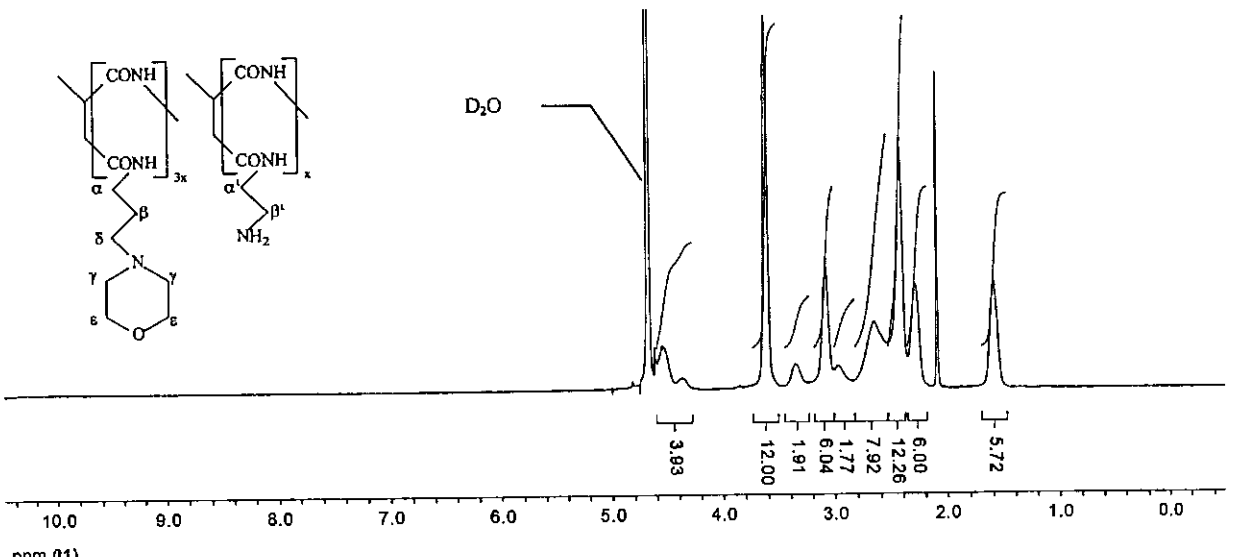


**Spectrum A18.** 4:3:1 Polysuccinimide : 4-(3-aminopropyl)morpholine : ethylenediamine, **49** ($D_2O$)

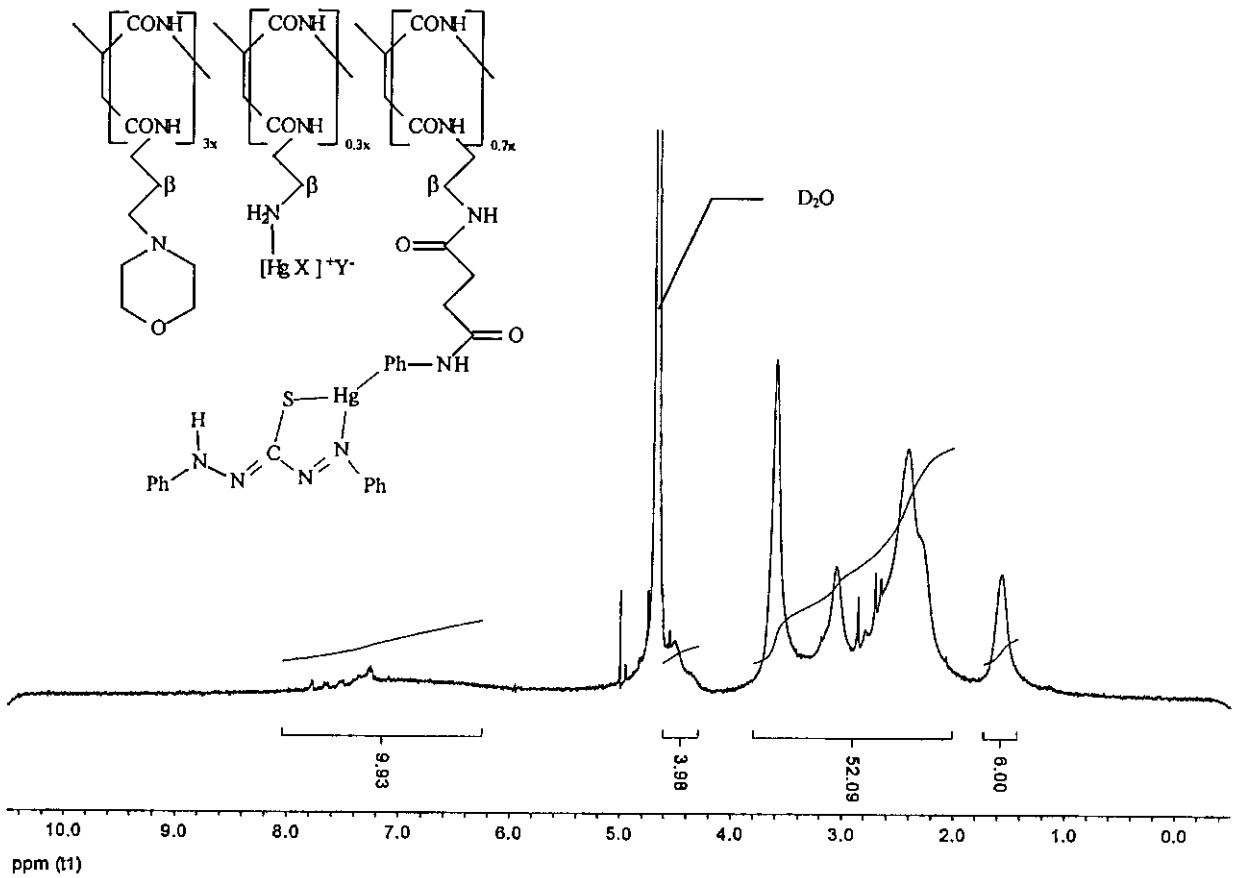


**Spectrum A19.** 1:1 Polymer 24 : *p*-Anilino-4-oxobutanoic acid(dithizonato) mercury(II), **50** ($D_2O$)

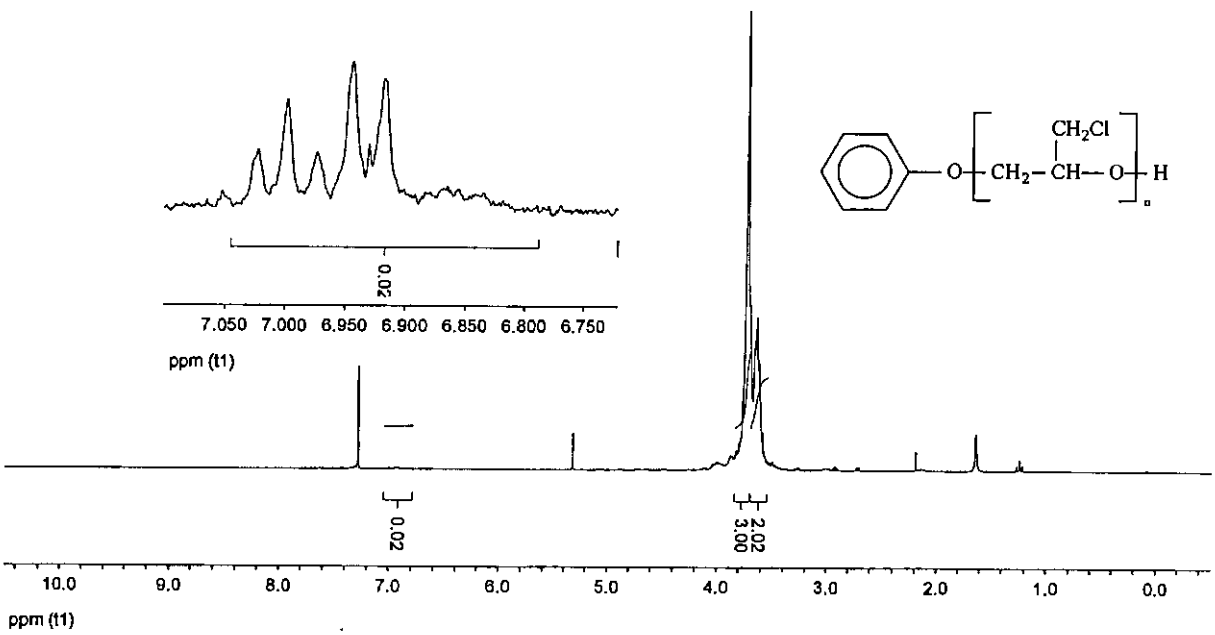


**Spectrum A20.** Polyepichlorohydrin, **52** ($CDCl_3$)

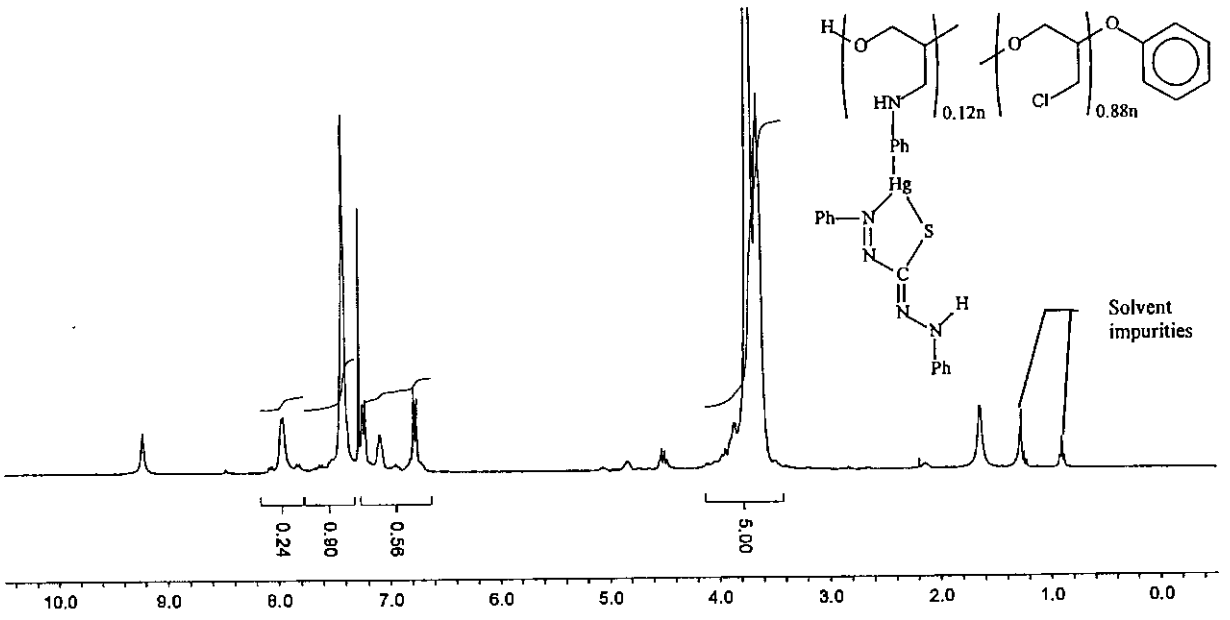


**Spectrum A21**. *p*-Aminophenyldithizonatomercury(II) polyepichlorohydrin, **53** ($CDCl_3$)

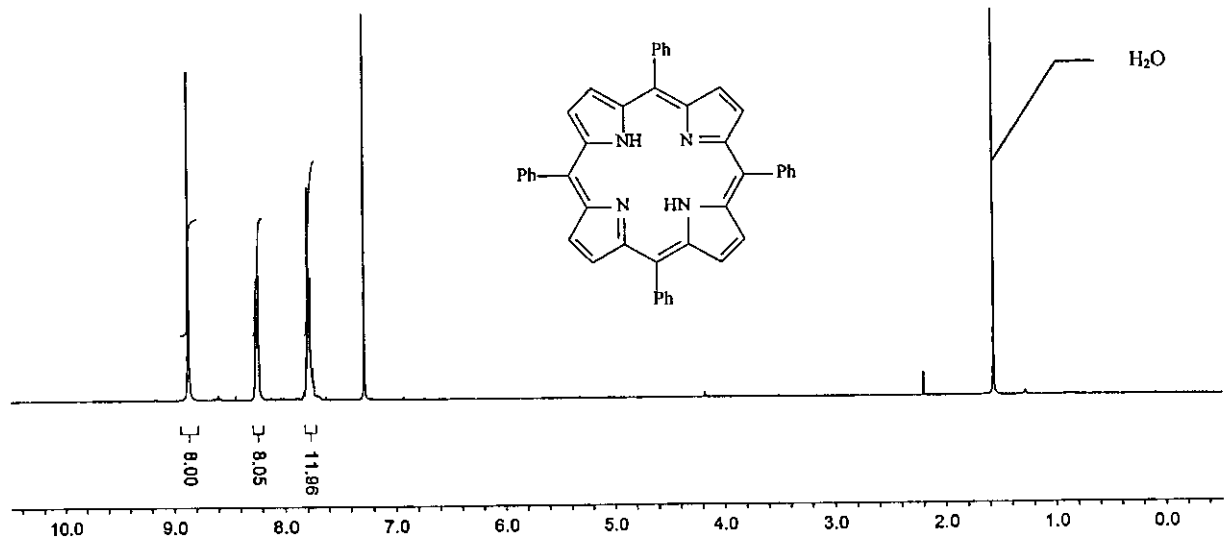


**Spectrum A22**. *meso*-Tetraphenylporphyrin, **54** ($CDCl_3$)

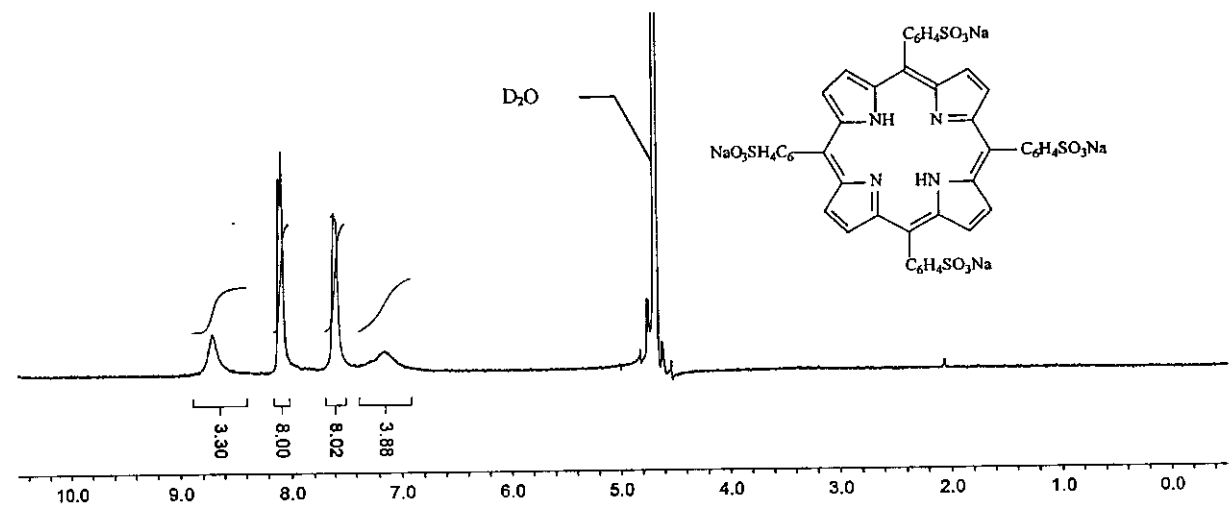


**Spectrum A23**. Tetra(sodium 4-sulfophenyl)porphyrin, **57** ($D_2O$)

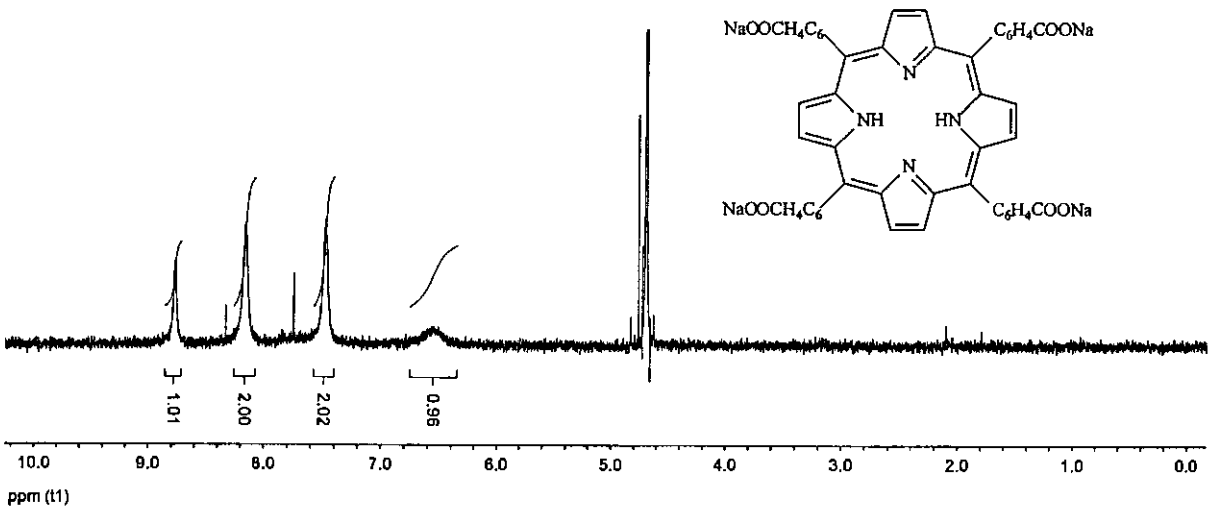


**Spectrum A24.** Tetra(sodium 4-carboxyphenyl)porphyrin, **59** ($D_2O$)

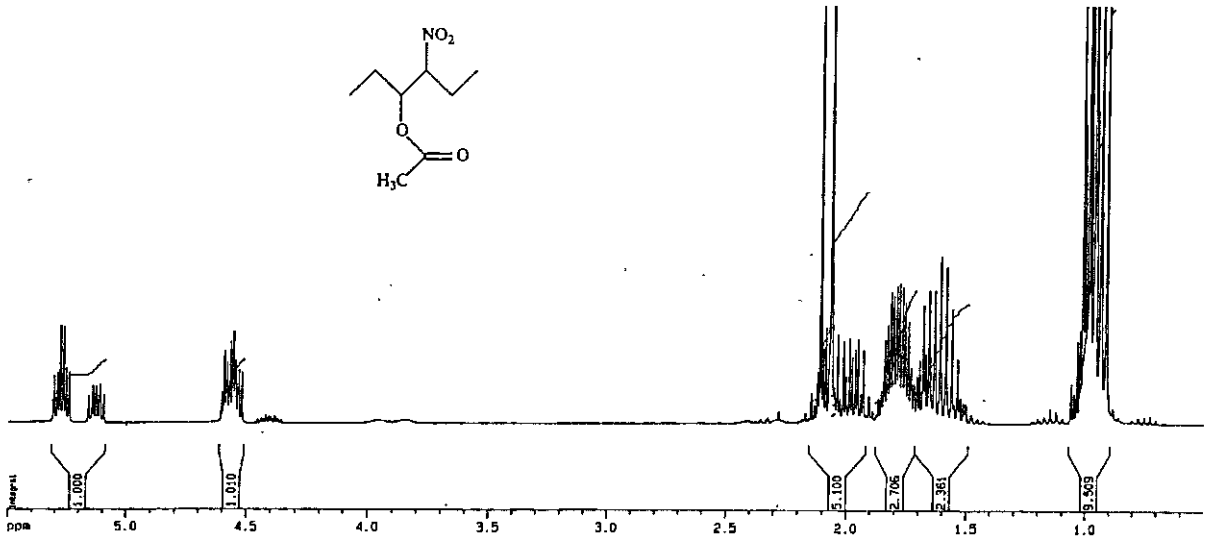


**Spectrum A25.** 3-Acetoxy-2-nitrohexane, **62** ($CDCl_3$)

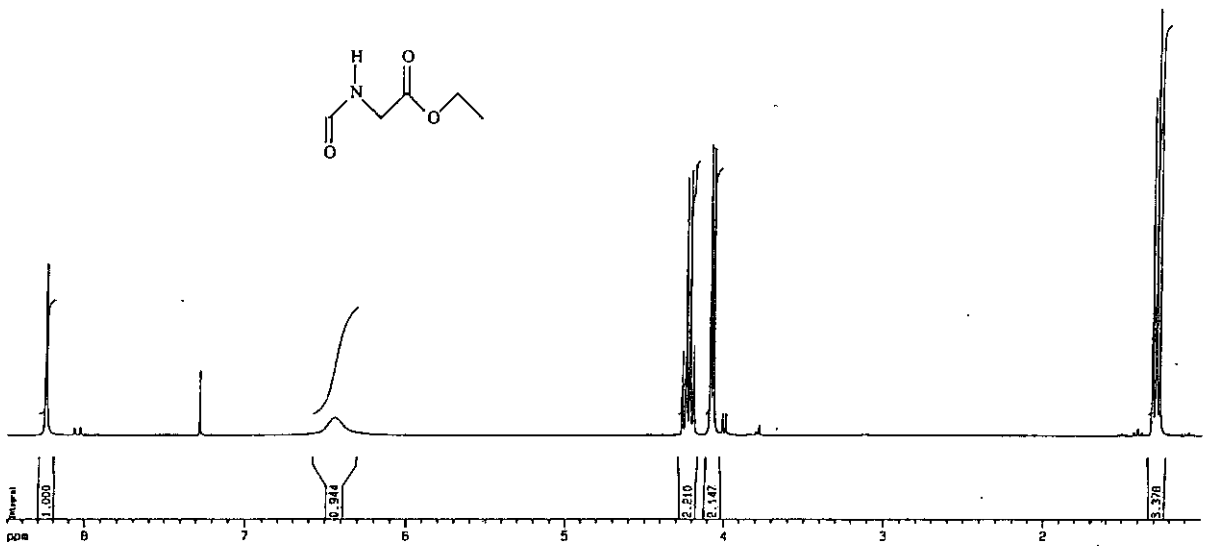


**Spectrum A26.** N-Formylglycine ethyl ester, **63** ($CDCl_3$)

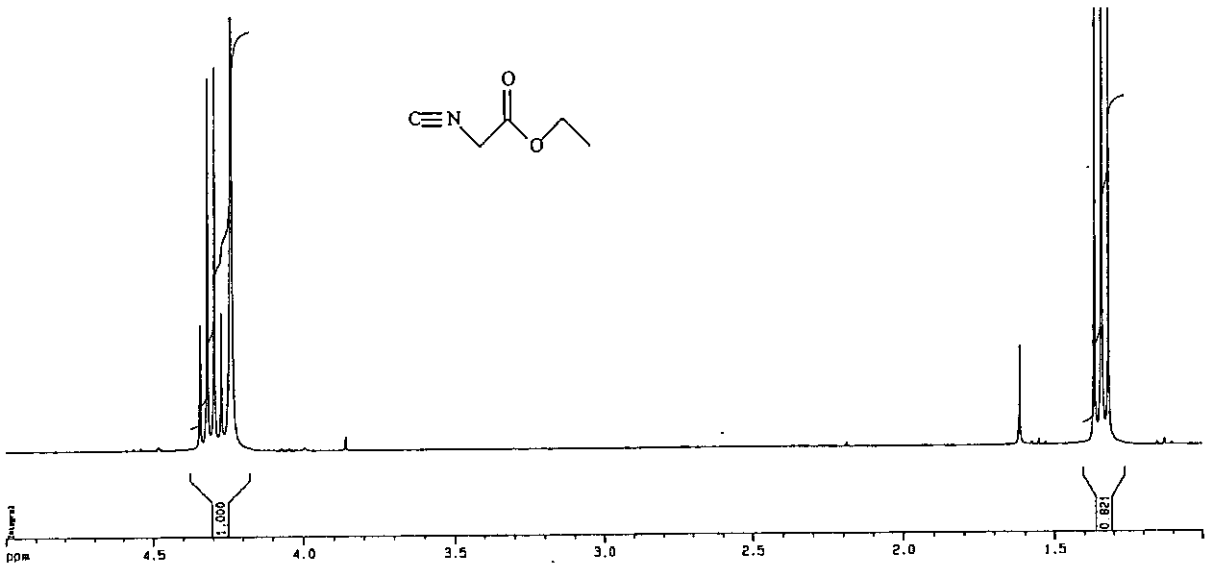


**Spectrum A27**. Ethyl isocyanoacetate, **64** ($CDCl_3$)

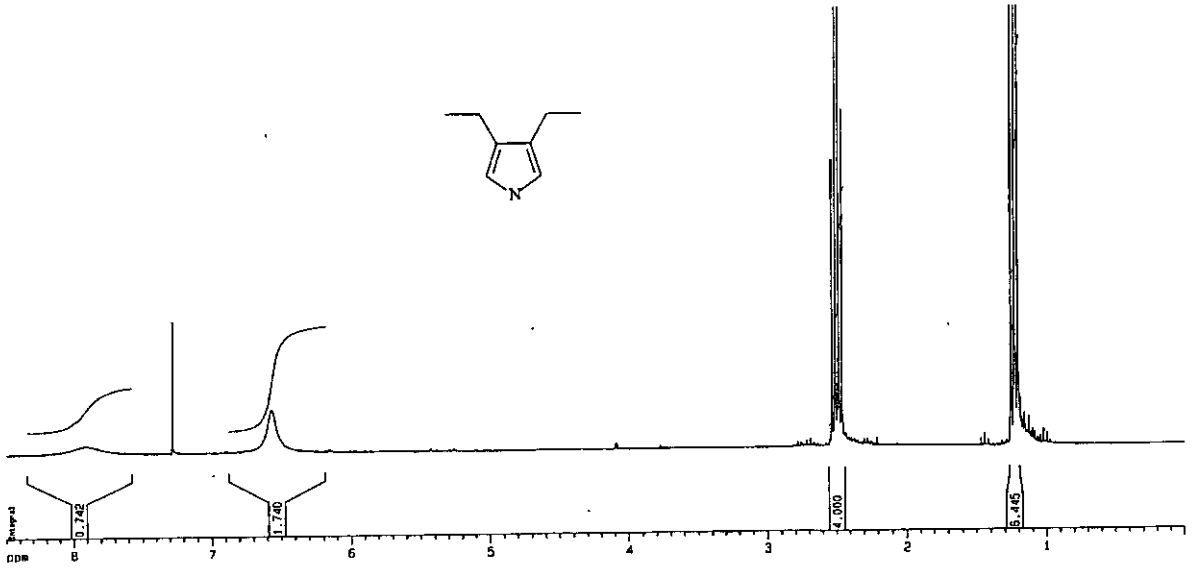


**Spectrum A28**. 3,4-Diethylpyrrole, **66** ($CDCl_3$)

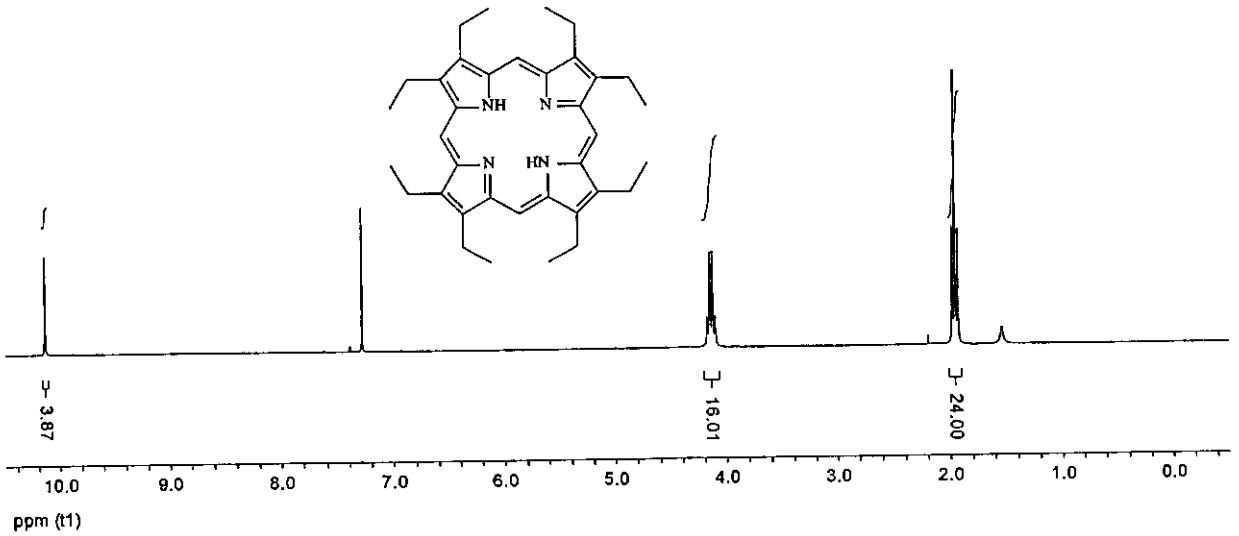


**Spectrum A29**. Octaethylporphyrin, **67** ($CDCl_3$)

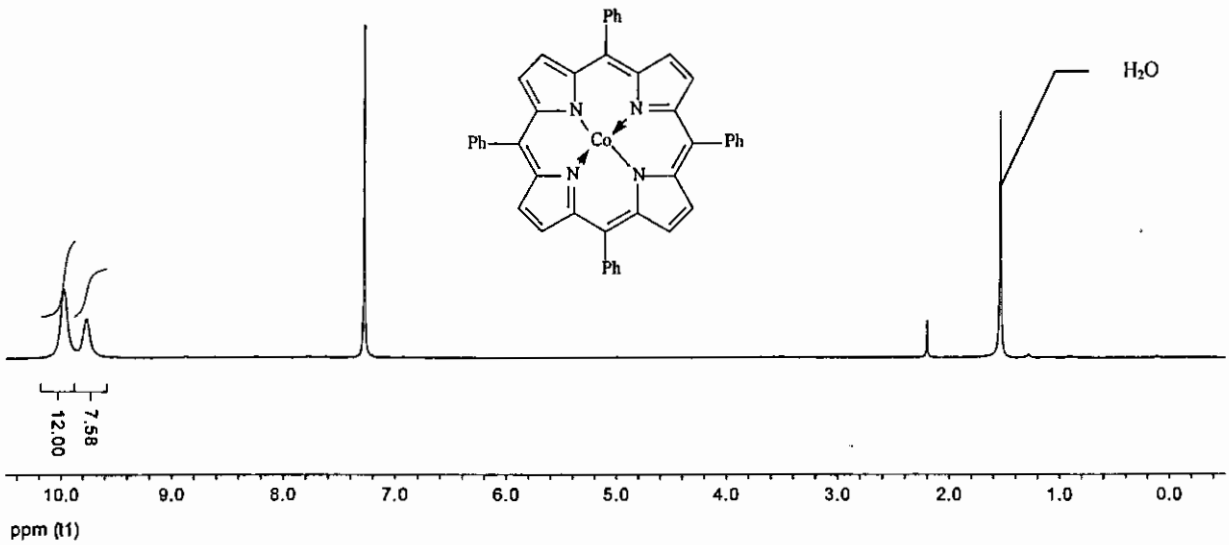


**Spectrum A30**. Tetraphenylporphyrinatocobalt(II), **68** ($CDCl_3$)

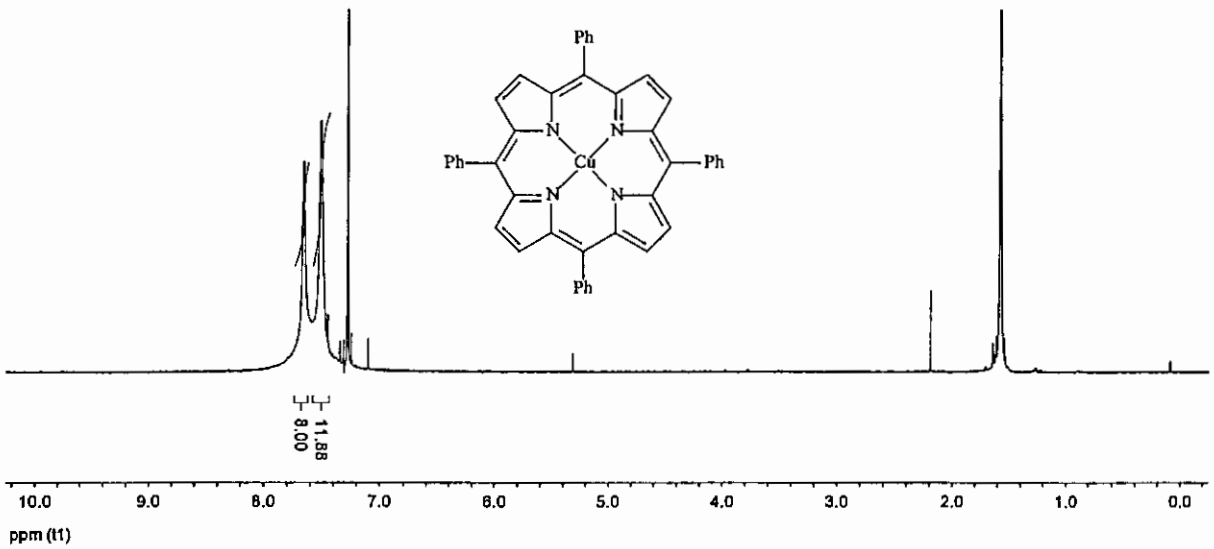


**Spectrum A31**. Tetraphenylporphyrinatocopper(II), **68** ($CDCl_3$)

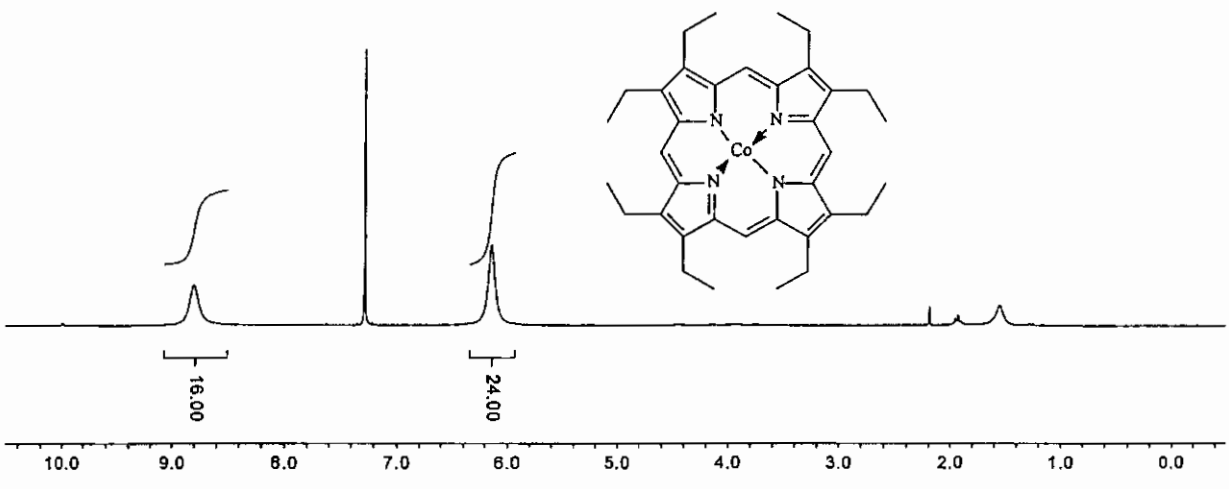


**Spectrum A32**. Octaethylporhyrinatocobalt(II), **72** ($CDCl_3$)

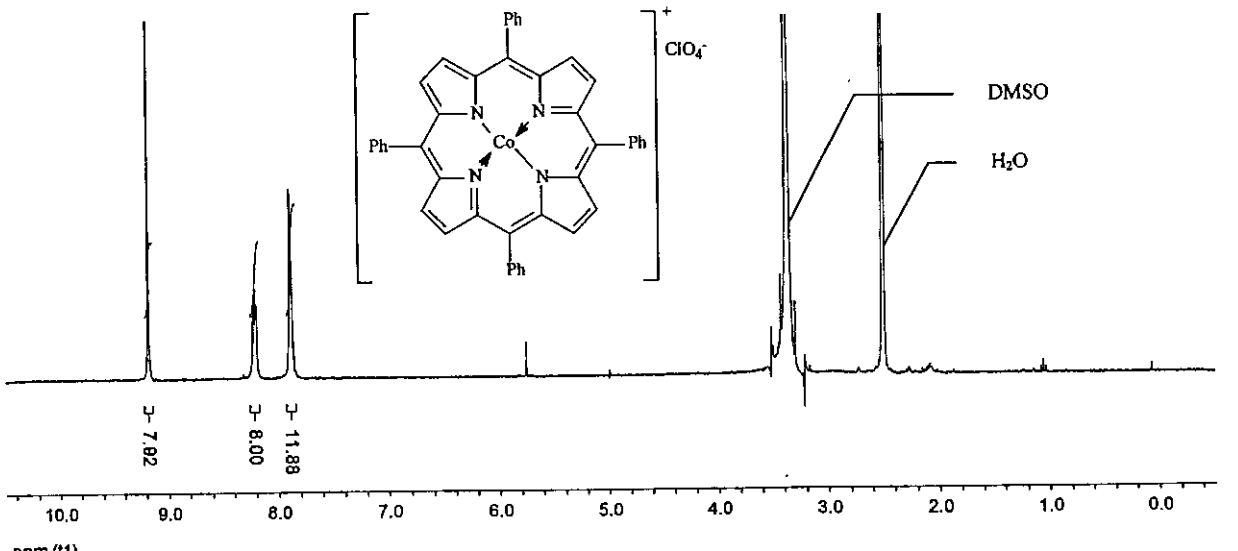


**Spectrum A33.** Tetraphenylporphyrinatocobalt(III) perchlorate, **74** ($(CD_3)_2SO$)

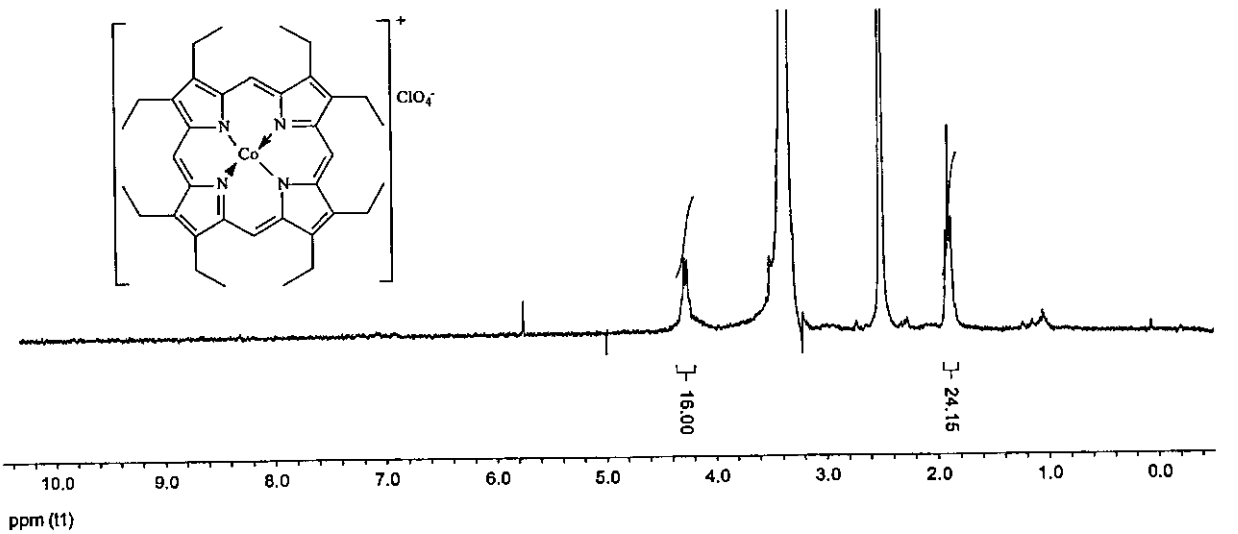


**Spectrum A34.** Octaethylporphyrinatocobalt(III) perchlorate, **77** ( $(CD_3)_2SO$)

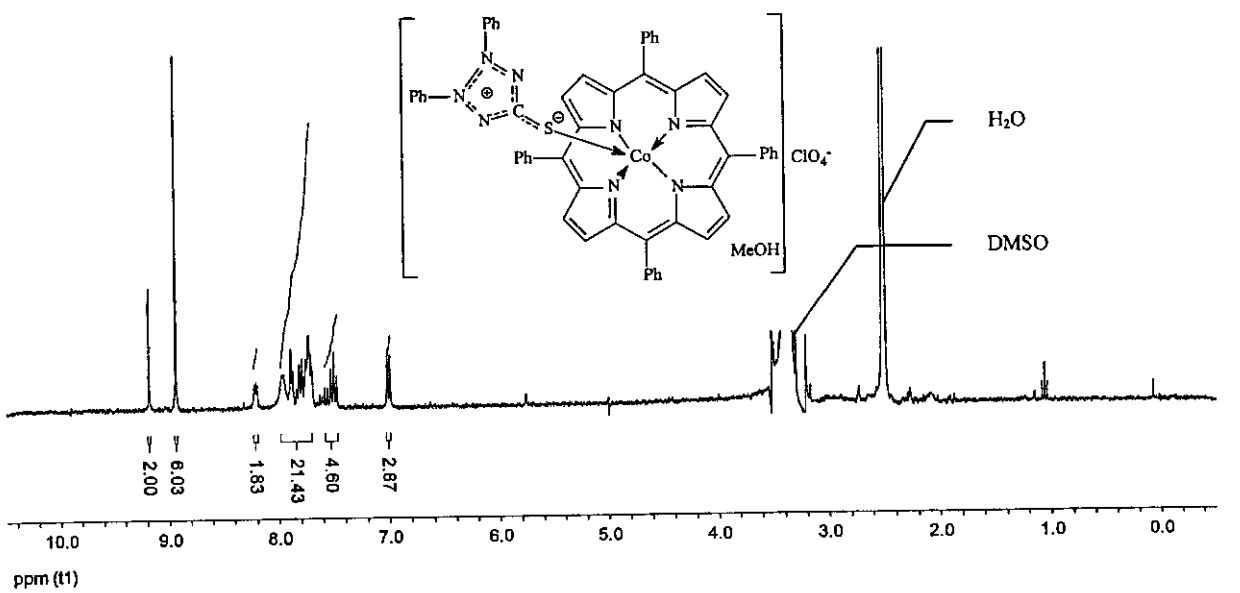


**Spectrum A35.** 75% coordinated dehydrodithizone(tetraphenylporphyrinato)cobalt(III) perchlorate, **78** ($(CD_3)_2SO$)

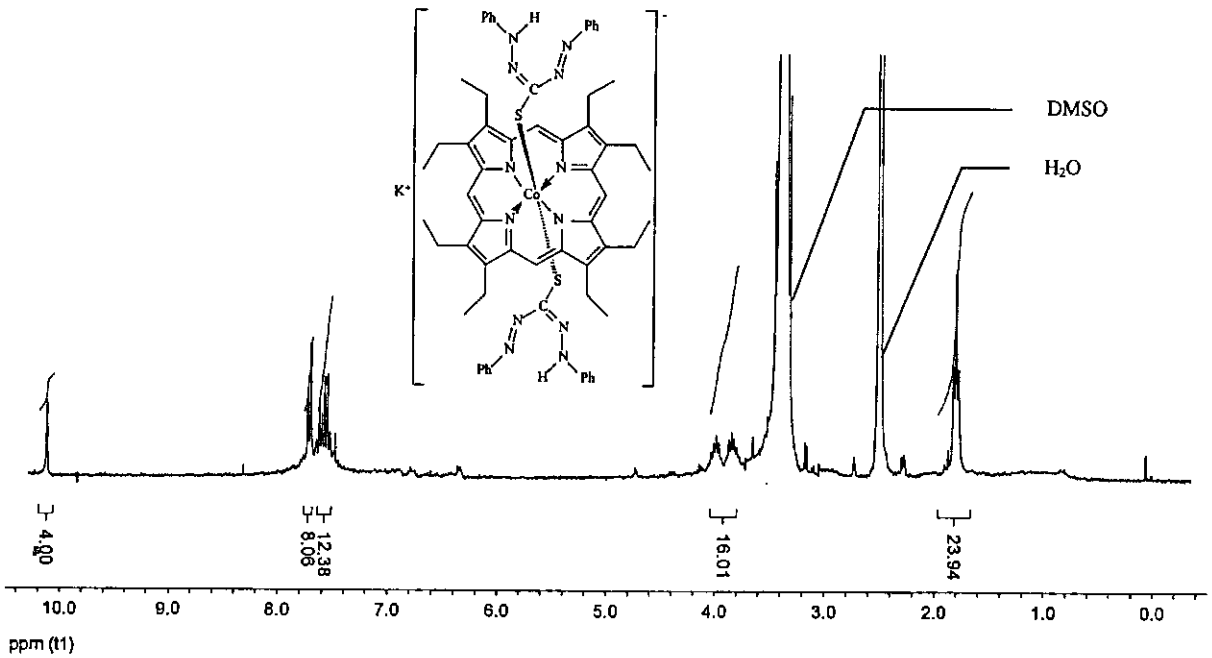


**Spectrum A36**. *Bis*-dithizonato(octaethylporphyrin)cobalt(III) $(CD_3)_2SO$ )

# Appendix 2: Crystallographic Data

## A. Dithizonatotrimethyltin(IV)

**Table A2-1** Atomic coordinates ( x $10^4$) and equivalent isotropic displacement parameters ($Å^2$ x $10^3$). U(eq) is defined as one third of the trace of the orthogonalised Uij tensor.

| Atom | x | y | z | U(eq) |
|---|---|---|---|---|
| Sn(1) | 4146(1) | 7270(1) | 3964(1) | 24(1) |
| S(1) | 5174(1) | 4230(1) | 4154(1) | 25(1) |
| N(1) | 4600(3) | 2231(5) | 3105(2) | 26(1) |
| N(2) | 5715(3) | 2700(5) | 3024(2) | 28(1) |
| N(3) | 3068(3) | 2247(5) | 3630(2) | 25(1) |
| N(4) | 2683(3) | 2864(5) | 4088(2) | 24(1) |
| C(1) | 4246(3) | 2859(5) | 3590(2) | 22(1) |
| C(2) | 6104(3) | 2204(5) | 2489(2) | 22(1) |
| C(3) | 7309(3) | 2646(6) | 2444(2) | 24(1) |
| C(4) | 7723(4) | 2213(6) | 1916(2) | 27(1) |
| C(5) | 6963(4) | 1333(6) | 1440(2) | 29(1) |
| C(6) | 5766(4) | 894(6) | 1490(2) | 27(1) |
| C(7) | 5330(4) | 1329(6) | 2009(2) | 26(1) |
| C(8) | 1467(3) | 2285(5) | 4119(2) | 23(1) |
| C(9) | 679(4) | 1331(6) | 3664(2) | 28(1) |
| C(10) | -495(4) | 886(6) | 3745(2) | 32(1) |
| C(11) | -885(4) | 1393(7) | 4274(2) | 34(1) |
| C(12) | -95(4) | 2333(7) | 4730(2) | 33(1) |
| C(13) | 1083(4) | 2781(6) | 4653(2) | 27(1) |
| C(14) | 2646(4) | 7457(7) | 4426(2) | 33(1) |
| C(15) | 5665(4) | 8974(6) | 4354(2) | 32(1) |
| C(16) | 3568(5) | 7417(9) | 3004(2) | 44(1) |

**Table A2-1** Bond lengths [Å]

| | | | |
|---|---|---|---|
| Sn(1)-C(14) | 2.13(2) | C(8)-C(9) | 1.393(12) |
| Sn(1)-C(16) | 2.13(2) | C(8)-C(13) | 1.394(10) |
| Sn(1)-C(15) | 2.13(2) | C(9)-C(10) | 1.39(2) |
| Sn(1)-S(1) | 2.47(3) | C(9)-H(9) | 0.9300 |
| S(1)-C(1) | 1.774(14) | C(10)-C(11) | 1.388(11) |
| N(1)-C(1) | 1.308(9) | C(10)-H(10) | 0.9300 |
| N(1)-N(2) | 1.327(14) | C(11)-C(12) | 1.390(13) |
| N(2)-C(2) | 1.398(10) | C(11)-H(11) | 0.9300 |
| N(2)-H(2) | 0.8600 | C(12)-C(13) | 1.39(2) |
| N(3)-N(4) | 1.267(9) | C(12)-H(12) | 0.9300 |
| N(3)-C(1) | 1.40(2) | C(13)-H(13) | 0.9300 |
| N(4)-C(8) | 1.42(2) | C(14)-H(14A) | 0.9600 |
| C(2)-C(7) | 1.393(12) | C(14)-H(14B) | 0.9600 |
| C(2)-C(3) | 1.40(2) | C(14)-H(14C) | 0.9600 |
| C(3)-C(4) | 1.386(10) | C(15)-H(15A) | 0.9600 |
| C(3)-H(3) | 0.9300 | C(15)-H(15B) | 0.9600 |
| C(4)-C(5) | 1.383(12) | C(15)-H(15C) | 0.9600 |
| C(4)-H(4) | 0.9300 | C(16)-H(16A) | 0.9600 |
| C(5)-C(6) | 1.39(2) | C(16)-H(16B) | 0.9600 |
| C(5)-H(5) | 0.9300 | C(16)-H(16C) | 0.9600 |
| C(6)-C(7) | 1.381(10) | C(16)-H(16D) | 0.9600 |
| C(6)-H(6) | 0.9300 | C(16)-H(16E) | 0.9600 |
| C(7)-H(7) | 0.9300 | C(16)-H(16F) | 0.9600 |

**Table A2-3** Bond angles [°].

| | | | |
|---|---|---|---|
| C(14)-Sn(1)-C(16) | 112.2(7) | C(10)-C(11)-C(12) | 120.2(7) |
| C(14)-Sn(1)-C(15) | 113.1(6) | C(10)-C(11)-H(11) | 119.9 |
| C(16)-Sn(1)-C(15) | 116.6(6) | C(12)-C(11)-H(11) | 119.9 |
| C(14)-Sn(1)-S(1) | 110.5(4) | C(13)-C(12)-C(11) | 119.9(7) |
| C(16)-Sn(1)-S(1) | 105.0(4) | C(13)-C(12)-H(12) | 120.1 |
| C(15)-Sn(1)-S(1) | 98.0(9) | C(11)-C(12)-H(12) | 120.1 |
| C(1)-S(1)-Sn(1) | 100.8(8) | C(12)-C(13)-C(8) | 119.7(7) |
| C(1)-N(1)-N(2) | 117.4(7) | C(12)-C(13)-H(13) | 120.1 |
| N(1)-N(2)-C(2) | 120.0(7) | C(8)-C(13)-H(13) | 120.1 |
| N(1)-N(2)-H(2) | 120.0 | Sn(1)-C(14)-H(14A) | 109.5 |
| C(2)-N(2)-H(2) | 120.0 | Sn(1)-C(14)-H(14B) | 109.5 |
| N(4)-N(3)-C(1) | 113.8(7) | H(14A)-C(14)-H(14B) | 109.5 |
| N(3)-N(4)-C(8) | 113.9(7) | Sn(1)-C(14)-H(14C) | 109.5 |
| N(1)-C(1)-N(3) | 112.1(7) | H(14A)-C(14)-H(14C) | 109.5 |
| N(1)-C(1)-S(1) | 124.2(6) | H(14B)-C(14)-H(14C) | 109.5 |
| N(3)-C(1)-S(1) | 123.7(6) | Sn(1)-C(15)-H(15A) | 109.5 |
| C(7)-C(2)-C(3) | 120.4(7) | Sn(1)-C(15)-H(15B) | 109.5 |
| C(7)-C(2)-N(2) | 122.3(7) | H(15A)-C(15)-H(15B) | 109.5 |
| C(3)-C(2)-N(2) | 117.3(7) | Sn(1)-C(15)-H(15C) | 109.5 |
| C(4)-C(3)-C(2) | 119.1(7) | H(15A)-C(15)-H(15C) | 109.5 |
| C(4)-C(3)-H(3) | 120.4 | H(15B)-C(15)-H(15C) | 109.5 |
| C(2)-C(3)-H(3) | 120.4 | Sn(1)-C(16)-H(16A) | 109.5 |
| C(5)-C(4)-C(3) | 120.8(7) | Sn(1)-C(16)-H(16B) | 109.5 |
| C(5)-C(4)-H(4) | 119.6 | H(16A)-C(16)-H(16B) | 109.5 |
| C(3)-C(4)-H(4) | 119.6 | Sn(1)-C(16)-H(16C) | 109.5 |
| C(4)-C(5)-C(6) | 119.5(7) | H(16A)-C(16)-H(16C) | 109.5 |
| C(4)-C(5)-H(5) | 120.2 | H(16B)-C(16)-H(16C) | 109.5 |
| C(6)-C(5)-H(5) | 120.2 | Sn(1)-C(16)-H(16D) | 109.5 |
| C(7)-C(6)-C(5) | 120.7(7) | H(16A)-C(16)-H(16D) | 141.1 |
| C(7)-C(6)-H(6) | 119.6 | H(16B)-C(16)-H(16D) | 56.3 |
| C(5)-C(6)-H(6) | 119.6 | H(16C)-C(16)-H(16D) | 56.3 |
| C(6)-C(7)-C(2) | 119.4(7) | Sn(1)-C(16)-H(16E) | 109.5 |
| C(6)-C(7)-H(7) | 120.3 | H(16A)-C(16)-H(16E) | 56.3 |
| C(2)-C(7)-H(7) | 120.3 | H(16B)-C(16)-H(16E) | 141.1 |
| C(9)-C(8)-C(13) | 120.4(7) | H(16C)-C(16)-H(16E) | 56.3 |
| C(9)-C(8)-N(4) | 125.2(6) | H(16D)-C(16)-H(16E) | 109.5 |
| C(13)-C(8)-N(4) | 114.4(7) | Sn(1)-C(16)-H(16F) | 109.5 |
| C(10)-C(9)-C(8) | 119.5(7) | H(16A)-C(16)-H(16F) | 56.3 |
| C(10)-C(9)-H(9) | 120.3 | H(16B)-C(16)-H(16F) | 56.3 |
| C(8)-C(9)-H(9) | 120.3 | H(16C)-C(16)-H(16F) | 141.1 |
| C(9)-C(10)-C(11) | 120.3(7) | H(16D)-C(16)-H(16F) | 109.5 |
| C(9)-C(10)-H(10) | 119.8 | H(16E)-C(16)-H(16F) | 109.5 |
| C(11)-C(10)-H(10) | 119.8 | | |

**Table A2-4** Selected torsion angles [°].

| | | | |
|---|---|---|---|
| C14 - Sn1 - S1 - C1 | 84.78 ( 0.65) | C3 - C4 - C5 - C6 | 0.65 ( 0.65) |
| C16 - Sn1 - S1 - C1 | -36.41 ( 0.44) | C4 - C5 - C6 - C7 | 0.07 ( 0.65) |
| C15 - Sn1 - S1 - C1 | -156.82 ( 0.32) | C5 - C6 - C7 - C2 | -0.53 ( 0.64) |
| C1 - N1 - N2 - C2 | -174.49 ( 0.38) | C3 - C2 - C7 - C6 | 0.27 ( 0.62) |
| C1 - N3 - N4 - C8 | 178.22 ( 0.33) | N2 - C2 - C7 - C6 | 179.28 ( 0.39) |
| N2 - N1 - C1 - N3 | -179.00 ( 0.36) | N3 - N4 - C8 - C9 | -7.85 ( 0.59) |
| N2 - N1 - C1 - S1 | -1.99 ( 0.57) | N3 - N4 - C8 - C13 | 173.22 ( 0.37) |
| N4 - N3 - C1 - N1 | -178.49 ( 0.36) | C13 - C8 - C9 - C10 | 0.41 ( 0.65) |
| N4 - N3 - C1 - S1 | 4.49 ( 0.52) | N4 - C8 - C9 - C10 | -178.46 ( 0.40) |
| Sn1 - S1 - C1 - N1 | 108.75 ( 0.56) | C8 - C9 - C10 - C11 | 0.21 ( 0.69) |
| Sn1 - S1 - C1 - N3 | -74.58 ( 0.58) | C9 - C10 - C11 - C12 | -0.71 ( 0.71) |
| N1 - N2 - C2 - C7 | 4.45 ( 0.62) | C10 - C11 - C12 - C13 | 0.57 ( 0.71) |
| N1 - N2 - C2 - C3 | -176.51 ( 0.38) | C11 - C12 - C13 - C8 | 0.05 ( 0.68) |
| C7 - C2 - C3 - C4 | 0.43 ( 0.60) | C9 - C8 - C13 - C12 | -0.54 ( 0.64) |
| N2 - C2 - C3 - C4 | -178.63 ( 0.37) | N4 - C8 - C13 - C12 | 178.45 ( 0.39) |
| C2 - C3 - C4 - C5 | -0.89 ( 0.62) | | |

**Table A2-5** Selected contact distances [Å] and angles [°] and best plane calculations.
Specified hydrogen bonds and other intermolecular contacts (with esds except fixed and riding H)

| | D-H | H...A | D...A | <(DHA) |
|---|---|---|---|---|
| N2-H2...S1 | 0.86 | 2.49 | 2.931(17) | 112.3 |
| N2-H2...C5_$1 | 0.86 | 2.97 | 3.71(3) | 145.9 |
| C3-H3...C4_$1 | 0.93 | 3.06 | 3.60(4) | 118.8 |
| C3-H3...C5_$1 | 0.93 | 2.85 | 3.64(3) | 143.3 |
| C3-H3...C6_$1 | 0.93 | 2.82 | 3.72(3) | 162.9 |
| C3-H3...C7_$1 | 0.93 | 3.01 | 3.77(3) | 139.8 |
| C4-H4...Sn1_$2 | 0.93 | 3.49 | 4.31(4) | 148.1 |
| C4-H4...H16A_$2 | 0.93 | 2.42 | 3.27(4) | 153.0 |
| C5-H5...S1_$2 | 0.93 | 3.28 | 3.97(3) | 133.0 |
| C6-H6...C8_$3 | 0.93 | 2.89 | 3.68(3) | 143.2 |
| C6-H6...C12_$3 | 0.93 | 2.93 | 3.73(3) | 144.8 |
| C6-H6...C13_$3 | 0.93 | 2.81 | 3.72(3) | 167.0 |
| C9-H9...H16E_$3 | 0.93 | 2.62 | 3.49(2) | 156.6 |
| C10-H10...C2_$3 | 0.93 | 3.02 | 3.81(3) | 142.8 |
| C10-H10...C3_$3 | 0.93 | 2.91 | 3.82(3) | 168.3 |
| C10-H10...C4_$3 | 0.93 | 2.90 | 3.73(3) | 149.8 |
| C10-H10...C5_$3 | 0.93 | 3.04 | 3.66(4) | 125.4 |
| C12-H12...H14C_$4 | 0.93 | 2.64 | 3.51(3) | 156.4 |
| C13-H13...H5_$5 | 0.93 | 2.53 | 3.34(2) | 145.9 |
| C14-H14A...C8_$6 | 0.96 | 2.93 | 3.74(4) | 143.3 |
| C14-H14B...S1_$7 | 0.96 | 3.03 | 3.81(3) | 140.3 |
| C15-H15A...H4_$1 | 0.96 | 2.50 | 3.25(2) | 134.5 |
| C15-H15B...N4_$7 | 0.96 | 2.91 | 3.86(3) | 169.2 |
| C15-H15C...S1_$6 | 0.96 | 3.03 | 3.85(5) | 144.6 |
| C15-H15C...C1_$6 | 0.96 | 2.88 | 3.50(3) | 123.5 |
| C16-H16E...Cl | 0.96 | 3.01 | 3.57(4) | 118.5 |
| C16-H16F...N1_$6 | 0.96 | 2.85 | 3.66(4) | 142.4 |

**Table A2-6** Anisotropic displacement parameters ($Å^2 \times 10^3$).
The anisotropic displacement factor exponent takes the form:
$-2\pi^2 [ h^2 a^{*2} U11 + ... + 2 h k a^* b^* U12 ]$

| | U11 | U22 | U33 | U23 | U13 | U12 |
|---|---|---|---|---|---|---|
| Sn(1) | 21(1) | 26(1) | 25(1) | -4(1) | 5(1) | -2(1) |
| S(1) | 22(1) | 27(1) | 27(1) | -6(1) | 4(1) | 1(1) |
| N(1) | 24(2) | 28(2) | 28(2) | -6(1) | 10(1) | -4(1) |
| N(2) | 24(2) | 35(2) | 26(2) | -11(1) | 10(1) | -8(1) |
| N(3) | 24(2) | 27(2) | 26(2) | -4(1) | 10(1) | -2(1) |
| N(4) | 22(2) | 28(2) | 25(2) | -1(1) | 7(1) | 0(1) |
| C(1) | 22(2) | 21(2) | 24(2) | -4(1) | 7(1) | -2(1) |
| C(2) | 24(2) | 22(2) | 23(2) | -2(1) | 8(1) | 1(1) |
| C(3) | 21(2) | 26(2) | 24(2) | -1(1) | 4(1) | -1(1) |
| C(4) | 22(2) | 27(2) | 33(2) | 3(2) | 10(2) | 4(2) |
| C(5) | 32(2) | 34(2) | 23(2) | 1(2) | 12(2) | 6(2) |
| C(6) | 31(2) | 26(2) | 22(2) | -3(2) | 2(2) | 2(2) |
| C(7) | 20(2) | 31(2) | 26(2) | -3(2) | 6(1) | -1(1) |
| C(8) | 21(2) | 22(2) | 26(2) | 1(1) | 6(1) | 0(1) |
| C(9) | 28(2) | 31(2) | 26(2) | -5(2) | 5(2) | -3(2) |
| C(10) | 30(2) | 27(2) | 37(2) | -2(2) | 3(2) | -6(2) |
| C(11) | 27(2) | 36(2) | 40(2) | 6(2) | 12(2) | -5(2) |
| C(12) | 32(2) | 41(2) | 29(2) | 7(2) | 14(2) | 0(2) |
| C(13) | 27(2) | 32(2) | 23(2) | 1(2) | 6(1) | 0(2) |
| C(14) | 25(2) | 36(2) | 39(2) | -3(2) | 12(2) | 4(2) |
| C(15) | 29(2) | 27(2) | 38(2) | -8(2) | 5(2) | -6(2) |
| C(16) | 43(3) | 64(4) | 23(2) | -1(2) | -1(2) | -8(2) |

**Table A2-7** Hydrogen coordinates ( x $10^4$) and isotropic displacement parameters ($Å^2$ x $10^3$).

| | x | y | z | U(eq) |
|---|---|---|---|---|
| H(2) | 6198 | 3309 | 3301 | 33 |
| H(3) | 7828 | 3222 | 2765 | 29 |
| H(4) | 8521 | 2519 | 1881 | 32 |
| H(5) | 7250 | 1037 | 1088 | 35 |
| H(6) | 5254 | 301 | 1171 | 32 |
| H(7) | 4526 | 1041 | 2039 | 31 |
| H(9) | 939 | 994 | 3309 | 34 |
| H(10) | -1024 | 245 | 3444 | 38 |
| H(11) | -1676 | 1103 | 4324 | 40 |
| H(12) | -356 | 2662 | 5086 | 40 |
| H(13) | 1614 | 3409 | 4957 | 33 |
| H(14A) | 2553 | 8716 | 4546 | 49 |
| H(14B) | 2800 | 6681 | 4779 | 49 |
| H(14C) | 1907 | 7060 | 4161 | 49 |
| H(15A) | 6189 | 9157 | 4065 | 47 |
| H(15B) | 6121 | 8382 | 4710 | 47 |
| H(15C) | 5368 | 10150 | 4464 | 47 |
| H(16A) | 4271 | 7326 | 2814 | 66 |
| H(16B) | 3159 | 8575 | 2897 | 66 |
| H(16C) | 3014 | 6417 | 2869 | 66 |
| H(16D) | 2692 | 7552 | 2906 | 66 |
| H(16E) | 3804 | 6304 | 2823 | 66 |
| H(16F) | 3949 | 8462 | 2851 | 66 |

Symmetry transformations used to generate equivalent atoms:
$1 -x+3/2, y+1/2, -z+1/2
$2 -x+3/2, y-1/2, -z+1/2
$3 -x+1/2, y-1/2, -z+1/2
$4 -x, -y+1, -z+1
$5 x-1/2, -y+1/2, z+1/2
$6 x, y+1, z
$7 -x+1, -y+1, -z+1

## B. *Tris*-dithizonatocobalt(III)

**Table B2-1** Atomic coordinates ( x $10^4$) and equivalent isotropic displacement parameters ($Å^2$x $10^3$). U(eq) is defined as one third of the trace of the orthogonalised $U^{ij}$ tensor.

| | x | y | z | U(eq) |
|---|---|---|---|---|
| Co(1) | 8645(1) | 2423(1) | 992(1) | 24(1) |
| S(1) | 7738(1) | 1559(1) | 1365(1) | 29(1) |
| S(2) | 8902(1) | 1287(1) | -902(1) | 30(1) |
| S(3) | 10158(1) | 1568(1) | 1973(1) | 29(1) |
| N(1) | 5576(3) | 2178(3) | 912(4) | 33(1) |
| N(2) | 5604(3) | 1493(3) | 1436(4) | 35(1) |
| N(3) | 6377(3) | 2971(3) | 249(4) | 30(1) |
| N(4) | 7237(3) | 3094(2) | 148(4) | 27(1) |
| N(5) | 10505(3) | 1301(2) | -1953(4) | 30(1) |
| N(6) | 10433(3) | 412(2) | -2667(4) | 29(1) |
| N(7) | 10014(3) | 2651(2) | -376(4) | 31(1) |
| N(8) | 9490(3) | 3072(2) | 544(3) | 25(1) |
| N(9) | 10964(3) | 2385(3) | 4578(4) | 35(1) |
| N(10) | 11882(3) | 1760(3) | 4358(4) | 40(1) |
| N(11) | 9292(3) | 3116(3) | 3825(4) | 31(1) |
| N(12) | 8585(3) | 3265(2) | 2813(4) | 28(1) |
| C(1) | 6495(3) | 2269(3) | 845(4) | 29(1) |
| C(2) | 4653(3) | 1281(3) | 1376(5) | 34(1) |
| C(3) | 4695(4) | 407(3) | 1558(5) | 40(1) |
| C(4) | 3765(4) | 148(4) | 1413(5) | 46(1) |
| C(5) | 2792(4) | 764(4) | 1092(6) | 49(1) |
| C(6) | 2757(4) | 1647(4) | 930(6) | 56(2) |
| C(7) | 3685(4) | 1912(4) | 1085(6) | 46(1) |
| C(8) | 7020(3) | 3796(3) | -594(4) | 31(1) |
| C(9) | 6364(4) | 4700(3) | -218(5) | 36(1) |
| C(10) | 6176(4) | 5366(4) | -925(6) | 47(1) |
| C(11) | 6620(4) | 5112(4) | -2019(6) | 49(1) |
| C(12) | 7261(4) | 4195(4) | -2401(5) | 43(1) |
| C(13) | 7469(4) | 3532(3) | -1690(5) | 36(1) |
| C(14) | 9852(3) | 1741(3) | -1128(4) | 28(1) |
| C(15) | 11141(3) | -149(3) | -3508(4) | 30(1) |
| C(16) | 12061(4) | 101(3) | -3412(5) | 40(1) |
| C(17) | 12732(4) | -489(4) | -4255(6) | 52(2) |
| C(18) | 12497(4) | -1320(4) | -5186(6) | 53(2) |
| C(19) | 11587(4) | -1567(3) | -5276(5) | 42(1) |
| C(20) | 10889(4) | -976(3) | -4447(4) | 34(1) |
| C(21) | 9693(3) | 4018(3) | 1295(4) | 29(1) |
| C(22) | 9163(4) | 4809(3) | 793(5) | 40(1) |
| C(23) | 9347(4) | 5712(3) | 1551(6) | 48(1) |
| C(24) | 10031(5) | 5818(4) | 2749(5) | 52(2) |
| C(25) | 10561(5) | 5024(4) | 3231(6) | 59(2) |
| C(26) | 10404(4) | 4111(4) | 2487(5) | 47(1) |
| C(27) | 10181(3) | 2378(3) | 3556(4) | 29(1) |
| C(28) | 12790(4) | 1809(4) | 5388(5) | 44(1) |
| C(29) | 13777(4) | 1437(4) | 5042(6) | 58(1) |
| C(30) | 14682(5) | 1488(5) | 6020(6) | 67(1) |
| C(31) | 14606(5) | 1913(4) | 7311(6) | 63(1) |
| C(32) | 13645(4) | 2274(4) | 7670(6) | 56(1) |
| C(33) | 12725(4) | 2212(4) | 6693(5) | 48(1) |
| C(34) | 7670(3) | 4018(3) | 3206(4) | 28(1) |
| C(35) | 6994(4) | 3807(3) | 3721(5) | 43(1) |
| C(36) | 6120(4) | 4526(4) | 4090(6) | 54(2) |
| C(37) | 5957(4) | 5436(4) | 3979(6) | 51(1) |
| C(38) | 6655(5) | 5644(4) | 3493(6) | 57(2) |
| C(39) | 7510(4) | 4931(3) | 3077(6) | 48(1) |

**Table B2-2.** Bond lengths [Å]

| | | | |
|---|---|---|---|
| Co(1)-N(8) | 1.964(3) | C(8)-C(13) | 1.381(6) |
| Co(1)-N(12) | 1.974(4) | C(9)-C(10) | 1.382(6) |
| Co(1)-N(4) | 1.979(4) | C(9)-H(9) | 0.9400 |
| Co(1)-S(2) | 2.2332(13) | C(10)-C(11) | 1.379(7) |
| Co(1)-S(3) | 2.2379(13) | C(10)-H(10) | 0.9400 |
| Co(1)-S(1) | 2.2386(13) | C(11)-C(12) | 1.383(6) |
| S(1)-C(1) | 1.741(4) | C(19)-H(19) | 0.9400 |
| S(2)-C(14) | 1.742(4) | C(20)-H(20) | 0.9400 |
| S(3)-C(27) | 1.746(4) | C(21)-C(26) | 1.368(6) |
| N(1)-C(1) | 1.322(5) | C(21)-C(22) | 1.382(6) |
| N(1)-N(2) | 1.323(5) | C(22)-C(23) | 1.391(6) |
| N(2)-C(2) | 1.402(6) | C(22)-H(22) | 0.9400 |
| N(2)-H(2N) | 0.8666 | C(23)-C(24) | 1.356(7) |
| N(3)-N(4) | 1.276(5) | C(23)-H(23) | 0.9400 |
| N(3)-C(1) | 1.364(6) | C(24)-C(25) | 1.374(7) |
| N(4)-C(8) | 1.449(6) | C(24)-H(24) | 0.9400 |
| N(5)-C(14) | 1.314(5) | C(25)-C(26) | 1.390(6) |
| N(5)-N(6) | 1.320(5) | C(25)-H(25) | 0.9400 |
| N(6)-C(15) | 1.401(5) | C(26)-H(26) | 0.9400 |
| N(6)-H(6N) | 0.8663 | C(28)-C(33) | 1.364(7) |
| N(7)-N(8) | 1.273(5) | C(28)-C(29) | 1.390(7) |
| N(7)-C(14) | 1.389(5) | C(29)-C(30) | 1.375(7) |
| N(8)-C(21) | 1.451(5) | C(29)-H(29) | 0.9400 |
| N(9)-C(27) | 1.295(6) | C(30)-C(31) | 1.356(8) |
| N(9)-N(10) | 1.336(5) | C(30)-H(30) | 0.9400 |
| N(10)-C(28) | 1.407(6) | C(31)-C(32) | 1.364(7) |
| N(10)-H(10N) | 0.8748 | C(31)-H(31) | 0.9400 |
| N(11)-N(12) | 1.266(5) | C(32)-C(33) | 1.390(7) |
| N(11)-C(27) | 1.389(5) | C(32)-H(32) | 0.9400 |
| N(12)-C(34) | 1.454(5) | C(33)-H(33) | 0.9400 |
| C(2)-C(3) | 1.378(6) | C(34)-C(35) | 1.363(6) |
| C(2)-C(7) | 1.382(6) | C(34)-C(39) | 1.373(6) |
| C(3)-C(4) | 1.383(6) | C(35)-C(36) | 1.388(6) |
| C(3)-H(3) | 0.9400 | C(35)-H(35) | 0.9400 |
| C(4)-C(5) | 1.383(7) | C(36)-C(37) | 1.360(7) |
| C(4)-H(4) | 0.9400 | C(36)-H(36) | 0.9400 |
| C(5)-C(6) | 1.383(7) | C(37)-C(38) | 1.366(7) |
| C(5)-H(5) | 0.9400 | C(37)-H(37) | 0.9400 |
| C(6)-C(7) | 1.385(6) | C(38)-C(39) | 1.381(6) |
| C(6)-H(6) | 0.9400 | C(38)-H(38) | 0.9400 |
| C(7)-H(7) | 0.9400 | C(39)-H(39) | 0.9400 |
| C(8)-C(9) | 1.377(5) | | |

**Table B2-3** Hydrogen bonds [Å and °].

| D-H...A | d(D-H) | d(H...A) | d(D...A) | <(DHA) |
|---|---|---|---|---|
| N(2)-H(2N)...S(1) | 0.87 | 2.53 | 2.950(4) | 110.6 |
| N(2)-H(2N)...C(16)#1 | 0.87 | 3.06 | 3.899(7) | 164.7 |
| N(2)-H(2N)...C(17)#1 | 0.87 | 2.99 | 3.712(8) | 142.1 |
| N(6)-H(6N)...S(2) | 0.87 | 2.50 | 2.943(4) | 112.5 |
| N(6)-H(6N)...S(3)#1 | 0.87 | 2.99 | 3.672(4) | 137.1 |
| N(10)-H(10N)...S(3) | 0.87 | 2.53 | 2.948(4) | 110.5 |
| N(10)-H(10N)...C(5)#2 | 0.87 | 3.04 | 3.777(7) | 143.5 |

**Table B2-4** Bond angles [°].

| | | | |
|---|---|---|---|
| N(8)-Co(1)-N(12) | 97.52(14) | C(2)-C(7)-H(7) | 120.2 |
| N(8)-Co(1)-N(4) | 96.86(15) | C(6)-C(7)-H(7) | 120.2 |
| N(12)-Co(1)-N(4) | 95.44(14) | C(9)-C(8)-C(13) | 121.2(4) |
| N(8)-Co(1)-S(2) | 85.24(10) | C(9)-C(8)-N(4) | 120.2(4) |
| N(12)-Co(1)-S(2) | 170.52(11) | C(13)-C(8)-N(4) | 118.6(4) |
| N(4)-Co(1)-S(2) | 93.22(11) | C(8)-C(9)-C(10) | 119.5(5) |
| N(8)-Co(1)-S(3) | 88.62(11) | C(8)-C(9)-H(9) | 120.3 |
| N(12)-Co(1)-S(3) | 84.71(11) | C(10)-C(9)-H(9) | 120.3 |
| N(4)-Co(1)-S(3) | 174.45(11) | C(11)-C(10)-C(9) | 119.9(5) |
| S(2)-Co(1)-S(3) | 86.30(5) | C(11)-C(10)-H(10) | 120.1 |
| N(8)-Co(1)-S(1) | 174.76(10) | C(9)-C(10)-H(10) | 120.1 |
| N(12)-Co(1)-S(1) | 87.24(11) | C(10)-C(11)-C(12) | 120.0(5) |
| N(4)-Co(1)-S(1) | 84.81(11) | C(10)-C(11)-H(11) | 120.0 |
| S(2)-Co(1)-S(1) | 89.71(5) | C(12)-C(11)-H(11) | 120.0 |
| S(3)-Co(1)-S(1) | 89.66(5) | C(13)-C(12)-C(11) | 120.5(5) |
| C(1)-S(1)-Co(1) | 94.81(16) | C(13)-C(12)-H(12) | 119.7 |
| C(14)-S(2)-Co(1) | 94.52(14) | C(11)-C(12)-H(12) | 119.7 |
| C(27)-S(3)-Co(1) | 95.52(15) | C(12)-C(13)-C(8) | 118.9(4) |
| C(1)-N(1)-N(2) | 117.0(4) | C(12)-C(13)-H(13) | 120.6 |
| N(1)-N(2)-C(2) | 119.3(4) | C(8)-C(13)-H(13) | 120.6 |
| N(1)-N(2)-H(2N) | 120.3 | N(5)-C(14)-N(7) | 111.8(4) |
| C(2)-N(2)-H(2N) | 120.4 | N(5)-C(14)-S(2) | 127.1(3) |
| N(4)-N(3)-C(1) | 115.5(4) | N(7)-C(14)-S(2) | 121.1(3) |
| N(3)-N(4)-C(8) | 111.0(3) | C(16)-C(15)-C(20) | 120.6(4) |
| N(3)-N(4)-Co(1) | 121.9(3) | C(16)-C(15)-N(6) | 121.7(4) |
| C(8)-N(4)-Co(1) | 127.1(3) | C(20)-C(15)-N(6) | 117.7(4) |
| C(14)-N(5)-N(6) | 115.6(4) | C(17)-C(16)-C(15) | 118.8(4) |
| N(5)-N(6)-C(15) | 120.5(4) | C(17)-C(16)-H(16) | 120.6 |
| N(5)-N(6)-H(6N) | 119.8 | C(15)-C(16)-H(16) | 120.6 |
| C(15)-N(6)-H(6N) | 119.8 | C(16)-C(17)-C(18) | 121.2(5) |
| N(8)-N(7)-C(14) | 115.0(4) | C(16)-C(17)-H(17) | 119.4 |
| N(7)-N(8)-C(21) | 112.4(3) | C(18)-C(17)-H(17) | 119.4 |
| N(7)-N(8)-Co(1) | 122.2(3) | C(19)-C(18)-C(17) | 119.8(5) |
| C(21)-N(8)-Co(1) | 125.0(3) | C(19)-C(18)-H(18) | 120.1 |
| C(27)-N(9)-N(10) | 116.0(4) | C(17)-C(18)-H(18) | 120.1 |
| N(9)-N(10)-C(28) | 118.6(4) | C(18)-C(19)-C(20) | 120.1(4) |
| N(9)-N(10)-H(10N) | 120.7 | C(18)-C(19)-H(19) | 119.9 |
| C(28)-N(10)-H(10N) | 120.6 | C(20)-C(19)-H(19) | 119.9 |
| N(12)-N(11)-C(27) | 115.3(4) | C(15)-C(20)-C(19) | 119.4(4) |
| N(11)-N(12)-C(34) | 110.8(3) | C(15)-C(20)-H(20) | 120.3 |
| N(11)-N(12)-Co(1) | 123.1(3) | C(19)-C(20)-H(20) | 120.3 |
| C(34)-N(12)-Co(1) | 125.3(3) | C(26)-C(21)-C(22) | 121.2(4) |
| N(1)-C(1)-N(3) | 112.4(4) | C(26)-C(21)-N(8) | 119.4(4) |
| N(1)-C(1)-S(1) | 125.8(4) | C(22)-C(21)-N(8) | 119.4(4) |
| N(3)-C(1)-S(1) | 121.8(3) | C(21)-C(22)-C(23) | 118.3(5) |
| C(3)-C(2)-C(7) | 120.2(4) | C(21)-C(22)-H(22) | 120.9 |
| C(3)-C(2)-N(2) | 118.7(4) | C(23)-C(22)-H(22) | 120.9 |
| C(7)-C(2)-N(2) | 121.1(4) | C(24)-C(23)-C(22) | 121.1(5) |
| C(2)-C(3)-C(4) | 120.0(5) | C(24)-C(23)-H(23) | 119.4 |
| C(2)-C(3)-H(3) | 120.0 | C(22)-C(23)-H(23) | 119.4 |
| C(4)-C(3)-H(3) | 120.0 | C(23)-C(24)-C(25) | 120.0(5) |
| C(5)-C(4)-C(3) | 120.3(5) | C(23)-C(24)-H(24) | 120.0 |
| C(5)-C(4)-H(4) | 119.8 | C(25)-C(24)-H(24) | 120.0 |
| C(3)-C(4)-H(4) | 119.8 | C(24)-C(25)-C(26) | 120.1(5) |
| C(4)-C(5)-C(6) | 119.3(5) | C(24)-C(25)-H(25) | 119.9 |
| C(4)-C(5)-H(5) | 120.3 | C(26)-C(25)-H(25) | 119.9 |
| C(6)-C(5)-H(5) | 120.3 | C(21)-C(26)-C(25) | 119.2(5) |
| C(5)-C(6)-C(7) | 120.5(5) | C(21)-C(26)-H(26) | 120.4 |
| C(5)-C(6)-H(6) | 119.7 | C(25)-C(26)-H(26) | 120.4 |
| C(7)-C(6)-H(6) | 119.7 | N(9)-C(27)-N(11) | 112.7(4) |
| C(2)-C(7)-C(6) | 119.6(5) | N(9)-C(27)-S(3) | 127.2(3) |
| N(11)-C(27)-S(3) | 120.1(3) | C(35)-C(34)-C(39) | 121.0(4) |
| C(33)-C(28)-C(29) | 119.9(5) | C(35)-C(34)-N(12) | 119.1(4) |
| C(33)-C(28)-N(10) | 122.1(5) | C(39)-C(34)-N(12) | 119.8(4) |
| C(29)-C(28)-N(10) | 118.0(5) | C(34)-C(35)-C(36) | 118.9(5) |
| C(30)-C(29)-C(28) | 119.7(6) | C(34)-C(35)-H(35) | 120.5 |
| C(30)-C(29)-H(29) | 120.2 | C(36)-C(35)-H(35) | 120.5 |
| C(28)-C(29)-H(29) | 120.2 | C(37)-C(36)-C(35) | 120.6(5) |
| C(31)-C(30)-C(29) | 119.9(6) | C(37)-C(36)-H(36) | 119.7 |
| C(31)-C(30)-H(30) | 120.1 | C(35)-C(36)-H(36) | 119.7 |
| C(29)-C(30)-H(30) | 120.1 | C(36)-C(37)-C(38) | 119.8(5) |

| | | | |
|---|---|---|---|
| C(30)-C(31)-C(32) | 121.3(5) | C(36)-C(37)-H(37) | 120.1 |
| C(30)-C(31)-H(31) | 119.4 | C(38)-C(37)-H(37) | 120.1 |
| C(32)-C(31)-H(31) | 119.4 | C(37)-C(38)-C(39) | 120.5(5) |
| C(31)-C(32)-C(33) | 119.4(6) | C(37)-C(38)-H(38) | 119.7 |
| C(31)-C(32)-H(32) | 120.3 | C(39)-C(38)-H(38) | 119.7 |
| C(33)-C(32)-H(32) | 120.3 | C(34)-C(39)-C(38) | 119.0(5) |
| C(28)-C(33)-C(32) | 119.9(5) | C(34)-C(39)-H(39) | 120.5 |
| C(28)-C(33)-H(33) | 120.1 | C(38)-C(39)-H(39) | 120.5 |
| C(32)-C(33)-H(33) | 120.1 | | |

**Table B2-5** Selected torsion angles [°].

| | | | |
|---|---|---|---|
| N8 - Co1 - S1 - C1 | -117.03 ( 1.22) | S3 - Co1 - N8 - C21 | -98.04 ( 0.32) |
| N12 – Co1 - S1 - C1 | 87.47 ( 0.18) | S1 - Co1 - N8 - C21 | -168.87 ( 1.02) |
| N4 - Co1 - S1 - C1 | -8.24 ( 0.18) | C27 - N9 - N10 - C28 | 172.88 ( 0.44) |
| S2 - Co1 - S1 - C1 | -101.51 ( 0.15) | C27 - N11 - N12 - C34 | 177.26 ( 0.35) |
| S3 - Co1 - S1 - C1 | 172.19 ( 0.15) | C27 - N11 - N12 - Co1 | 6.97 ( 0.50) |
| N8 - Co1 - S2 - C14 | 10.71 ( 0.18) | N8 - Co1 - N12 - N11 | -87.31 ( 0.34) |
| N12 - Co1 - S2 - C14 | -96.66 ( 0.66) | N4 - Co1 - N12 - N11 | 175.02 ( 0.33) |
| N4 - Co1 - S2 - C14 | 107.33 ( 0.18) | S2 - Co1 - N12 - N11 | 19.09 ( 0.90) |
| S3 - Co1 - S2 - C14 | -78.21 ( 0.15) | S3 - Co1 - N12 - N11 | 0.59 ( 0.32) |
| S1 - Co1 - S2 - C14 | -167.88 ( 0.15) | S1 - Co1 - N12 - N11 | 90.50 ( 0.32) |
| N8 - Co1 - S3 - C27 | 91.88 ( 0.18) | N8 - Co1 - N12 - C34 | 103.82 ( 0.33) |
| N12 - Co1 - S3 - C27 | -5.80 ( 0.18) | N4 - Co1 - N12 - C34 | 6.15 ( 0.34) |
| N4 - Co1 - S3 - C27 | -97.56 ( 1.10) | S2 - Co1 - N12 - C34 | -149.78 ( 0.51) |
| S2 - Co1 - S3 - C27 | 177.20 ( 0.15) | S3 - Co1 - N12 - C34 | -168.28 ( 0.32) |
| S1 - Co1 - S3 - C27 | -93.06 ( 0.15) | S1 - Co1 - N12 - C34 | -78.37 ( 0.31) |
| C1 - N1 - N2 - C2 | -171.83 ( 0.40) | N2 - N1 - C1 - N3 | 177.87 ( 0.36) |
| C1 - N3 - N4 - C8 | 175.29 ( 0.35) | N2 - N1 - C1 - S1 | 0.85 ( 0.60) |
| C1 - N3 - N4 - Co1 | -7.05 ( 0.49) | N4 - N3 - C1 - N1 | -179.77 ( 0.36) |
| N8 - Co1 - N4 - N3 | -174.72 ( 0.31) | N4 - N3 - C1 - S1 | -2.61 ( 0.53) |
| N12 - Co1 - N4 - N3 | -76.45 ( 0.32) | Co1 - S1 - C1 - N1 | -174.63 ( 0.38) |
| S2 - Co1 - N4 - N3 | 99.69 ( 0.30) | Co1 - S1 - C1 - N3 | 8.61 ( 0.36) |
| S3 - Co1 - N4 - N3 | 14.79 ( 1.31) | N1 - N2 - C2 - C3 | 161.34 ( 0.43) |
| S1 - Co1 - N4 - N3 | 10.27 ( 0.30) | N1 - N2 - C2 - C7 | -15.90 ( 0.68) |
| N8 - Co1 - N4 - C8 | 2.55 ( 0.34) | C7 - C2 - C3 - C4 | 1.75 ( 0.76) |
| N12 - Co1 - N4 - C8 | 100.82 ( 0.33) | N2 - C2 - C3 - C4 | -175.51 ( 0.43) |
| S2 - Co1 - N4 - C8 | -83.04 ( 0.32) | C2 - C3 - C4 - C5 | -0.27 ( 0.78) |
| S3 - Co1 - N4 - C8 | -167.94 ( 0.90) | C3 - C4 - C5 - C6 | -0.66 ( 0.82) |
| S1 - Co1 - N4 - C8 | -172.46 ( 0.32) | C4 - C5 - C6 - C7 | 0.11 ( 0.88) |
| C14 - N5 - N6 - C15 | -175.45 ( 0.39) | C3 - C2 - C7 - C6 | -2.29 ( 0.80) |
| C14 - N7 - N8 - C21 | 179.96 ( 0.35) | N2 - C2 - C7 - C6 | 174.91 ( 0.48) |
| C14 - N7 - N8 - Co1 | 6.65 ( 0.52) | C5 - C6 - C7 - C2 | 1.36 ( 0.89) |
| N12 - Co1 - N8 - N7 | 158.88 ( 0.33) | N3 - N4 - C8 - C9 | 53.44 ( 0.52) |
| N4 - Co1 - N8 - N7 | -104.68 ( 0.34) | Co1 - N4 - C8 - C9 | -124.08 ( 0.39) |
| S2 - Co1 - N8 - N7 | -12.00 ( 0.33) | N3 - N4 - C8 - C13 | -125.46 ( 0.42) |
| S3 - Co1 - N8 - N7 | 74.40 ( 0.33) | Co1 - N4 - C8 - C13 | 57.02 ( 0.51) |
| S1 - Co1 - N8 - N7 | 3.58 ( 1.47) | C13 - C8 - C9 - C10 | -1.94 ( 0.70) |
| N12 - Co1 - N8 - C21 | -13.56 ( 0.35) | N4 - C8 - C9 - C10 | 179.20 ( 0.42) |
| N4 - Co1 - N8 - C21 | 82.88 ( 0.34) | C8 - C9 - C10 - C11 | 1.76 ( 0.75) |
| S2 - Co1 - N8 - C21 | 175.56 ( 0.33) | C9 - C10 - C11 - C12 | -0.53 ( 0.81) |
| C10 - C11 - C12 - C13 | -0.55 ( 0.81) | N8 - C21 - C26 - C25 | -177.16 ( 0.48) |
| C11 - C12 - C13 - C8 | 0.39 ( 0.73) | C24 - C25 - C26 - C21 | -2.11 ( 0.88) |
| C9 - C8 - C13 - C12 | 0.86 ( 0.69) | N10 - N9 - C27 - N11 | -173.27 ( 0.37) |
| N4 - C8 - C13 - C12 | 179.74 ( 0.40) | N10 - N9 - C27 - S3 | 6.68 ( 0.64) |
| N6 - N5 - C14 - N7 | 177.24 ( 0.35) | N12 - N11 - C27 - N9 | 166.55 ( 0.38) |
| N6 - N5 - C14 - S2 | -1.07 ( 0.61) | N12 - N11 - C27 - S3 | -13.40 ( 0.53) |
| N8 - N7 - C14 - N5 | -172.63 ( 0.38) | Co1 - S3 - C27 - N9 | -168.07 ( 0.41) |
| N8 - N7 - C14 - S2 | 5.80 ( 0.55) | Co1 - S3 - C27 - N11 | 11.87 ( 0.37) |
| Co1 - S2 - C14 - N5 | 165.87 ( 0.40) | N9 - N10 - C28 - C33 | 22.82 ( 0.75) |
| Co1 - S2 - C14 - N7 | -12.30 ( 0.37) | N9 - N10 - C28 - C29 | -156.74 ( 0.49) |
| N5 - N6 - C15 - C16 | 14.53 ( 0.66) | C33 - C28 - C29 - C30 | -0.75 ( 0.91) |
| N5 - N6 - C15 - C20 | -165.73 ( 0.40) | N10 - C28 - C29 - C30 | 178.81 ( 0.57) |
| C20 - C15 - C16 - C17 | -0.73 ( 0.76) | C28 - C29 - C30 - C31 | -0.96 ( 1.03) |
| N6 - C15 - C16 - C17 | 179.00 ( 0.48) | C29 - C30 - C31 - C32 | 1.58 ( 1.05) |
| C15 - C16 - C17 - C18 | 0.09 ( 0.89) | C30 - C31 - C32 - C33 | -0.49 ( 0.96) |
| C16 - C17 - C18 - C19 | -0.21 ( 0.96) | C29 - C28 - C33 - C32 | 1.85 ( 0.82) |
| C17 - C18 - C19 - C20 | 0.96 ( 0.88) | N10 - C28 - C33 - C32 | -177.70 ( 0.50) |
| C16 - C15 - C20 - C19 | 1.47 ( 0.71) | C31 - C32 - C33 - C28 | -1.24 ( 0.86) |
| N6 - C15 - C20 - C19 | -178.27 ( 0.42) | N11 - N12 - C34 - C35 | -74.42 ( 0.51) |
| C18 - C19 - C20 - C15 | -1.58 ( 0.77) | Co1 - N12 - C34 - C35 | 95.61 ( 0.48) |

| | | | |
|---|---|---|---|
| N7 - N8 - C21 - C26 | -98.38 ( 0.52) | N11 - N12 - C34 - C39 | 104.38 ( 0.50) |
| Co1 - N8 - C21 - C26 | 74.71 ( 0.51) | Co1 - N12 - C34 - C39 | -85.59 ( 0.50) |
| N7 - N8 - C21 - C22 | 81.69 ( 0.50) | C39 - C34 - C35 - C36 | 1.42 ( 0.81) |
| Co1 - N8 - C21 - C22 | -105.22 ( 0.44) | N12 - C34 - C35 - C36 | -179.80 ( 0.48) |
| C26 - C21 - C22 - C23 | -1.86 ( 0.73) | C34 - C35 - C36 - C37 | -1.98 ( 0.91) |
| N8 - C21 - C22 - C23 | 178.07 ( 0.41) | C35 - C36 - C37 - C38 | 0.35 ( 0.99) |
| C21 - C22 - C23 - C24 | 0.28 ( 0.77) | C36 - C37 - C38 - C39 | 1.85 ( 1.00) |
| C22 - C23 - C24 - C25 | 0.33 ( 0.84) | C35 - C34 - C39 - C38 | 0.73 ( 0.84) |
| C23 - C24 - C25 - C26 | 0.58 ( 0.90) | N12 - C34 - C39 - C38 | -178.04 ( 0.51) |
| C22 - C21 - C26 - C25 | 2.76 ( 0.79) | C37 - C38 - C39 - C34 | -2.40 ( 0.95) |

**Table B2-6** Anisotropic displacement parameters ($Å^2 x\ 10^3$). The anisotropic displacement factor exponent takes the form: $-2\pi^2[ h^2a^{*2}U^{11} + ... + 2\ h\ k\ a^*\ b^*\ U^{12} ]$

| | $U^{11}$ | $U^{22}$ | $U^{33}$ | $U^{23}$ | $U^{13}$ | $U^{12}$ |
|---|---|---|---|---|---|---|
| Co(1) | 18(1) | 21(1) | 30(1) | 1(1) | 7(1) | -4(1) |
| S(1) | 20(1) | 27(1) | 40(1) | 9(1) | 5(1) | -6(1) |
| S(2) | 27(1) | 24(1) | 35(1) | -3(1) | 12(1) | -9(1) |
| S(3) | 20(1) | 25(1) | 35(1) | 2(1) | 6(1) | -3(1) |
| N(1) | 25(2) | 39(2) | 35(2) | 9(2) | 7(2) | -10(2) |
| N(2) | 22(2) | 42(2) | 46(2) | 15(2) | 9(2) | -9(2) |
| N(3) | 21(2) | 32(2) | 36(2) | 7(2) | 6(2) | -6(1) |
| N(4) | 21(2) | 23(2) | 33(2) | -2(1) | 10(2) | -6(1) |
| N(5) | 30(2) | 23(2) | 33(2) | 4(2) | 7(2) | -4(1) |
| N(6) | 29(2) | 25(2) | 34(2) | 2(2) | 13(2) | -6(1) |
| N(7) | 27(2) | 26(2) | 37(2) | -1(2) | 12(2) | -6(1) |
| N(8) | 23(2) | 23(2) | 28(2) | 2(1) | 7(1) | -6(1) |
| N(9) | 26(2) | 32(2) | 40(2) | 4(2) | 7(2) | -4(2) |
| N(10) | 23(2) | 39(2) | 41(2) | 0(2) | 2(2) | -1(2) |
| N(11) | 21(2) | 29(2) | 38(2) | 0(2) | 8(2) | -8(1) |
| N(12) | 16(2) | 25(2) | 39(2) | 4(2) | 7(2) | -6(1) |
| C(1) | 19(2) | 34(2) | 31(2) | 6(2) | 4(2) | -6(2) |
| C(2) | 27(2) | 42(3) | 38(3) | 9(2) | 11(2) | -11(2) |
| C(3) | 37(3) | 40(3) | 43(3) | 4(2) | 13(2) | -13(2) |
| C(4) | 47(3) | 44(3) | 53(3) | 0(2) | 19(3) | -24(2) |
| C(5) | 36(3) | 57(3) | 55(3) | -6(3) | 23(3) | -24(2) |
| C(6) | 30(3) | 58(3) | 78(4) | 13(3) | 17(3) | -7(2) |
| C(7) | 27(2) | 43(3) | 69(4) | 15(3) | 13(2) | -7(2) |
| C(8) | 25(2) | 28(2) | 37(3) | 7(2) | 3(2) | -7(2) |
| C(9) | 28(2) | 31(2) | 46(3) | 8(2) | 14(2) | 0(2) |
| C(10) | 38(3) | 36(3) | 63(4) | 18(2) | 6(2) | -2(2) |
| C(11) | 47(3) | 39(3) | 62(4) | 23(3) | 7(3) | -7(2) |
| C(12) | 36(3) | 48(3) | 45(3) | 16(2) | 7(2) | -6(2) |
| C(13) | 29(2) | 33(2) | 42(3) | 5(2) | 9(2) | -6(2) |
| C(14) | 24(2) | 26(2) | 29(2) | 2(2) | 7(2) | -7(2) |
| C(15) | 31(2) | 27(2) | 30(2) | 8(2) | 11(2) | -1(2) |
| C(16) | 36(3) | 31(2) | 51(3) | 2(2) | 20(2) | -7(2) |
| C(17) | 42(3) | 52(3) | 63(4) | -5(3) | 30(3) | -15(2) |
| C(18) | 50(3) | 46(3) | 58(4) | -4(3) | 35(3) | -4(2) |
| C(19) | 50(3) | 31(2) | 36(3) | -3(2) | 14(2) | -6(2) |
| C(20) | 35(3) | 31(2) | 33(3) | 4(2) | 10(2) | -7(2) |
| C(21) | 31(2) | 25(2) | 34(2) | -3(2) | 14(2) | -14(2) |
| C(22) | 41(3) | 28(2) | 48(3) | 1(2) | 17(2) | -8(2) |
| C(23) | 54(3) | 27(2) | 69(4) | -1(2) | 35(3) | -12(2) |
| C(24) | 71(4) | 35(3) | 57(3) | -15(2) | 34(3) | -33(3) |
| C(25) | 74(4) | 55(3) | 51(3) | -5(3) | 8(3) | -44(3) |
| C(26) | 56(3) | 40(3) | 44(3) | 3(2) | 3(2) | -27(2) |
| C(27) | 22(2) | 29(2) | 32(2) | 3(2) | 6(2) | -6(2) |
| C(28) | 32(2) | 43(2) | 49(2) | 11(2) | 0(2) | -8(2) |
| C(29) | 35(2) | 59(2) | 58(2) | 3(2) | -2(2) | -5(2) |
| C(30) | 40(2) | 67(2) | 65(2) | 4(2) | -5(2) | -4(2) |
| C(31) | 45(2) | 58(2) | 63(2) | 8(2) | -12(2) | -11(2) |
| C(32) | 50(2) | 48(2) | 55(2) | 10(2) | -7(2) | -13(2) |
| C(33) | 42(2) | 44(2) | 50(2) | 11(2) | 0(2) | -11(2) |
| C(34) | 26(2) | 24(2) | 28(2) | -1(2) | 10(2) | -3(2) |
| C(35) | 42(3) | 33(2) | 58(3) | 10(2) | 29(3) | -1(2) |
| C(36) | 46(3) | 45(3) | 78(4) | 8(3) | 42(3) | -1(2) |
| C(37) | 40(3) | 44(3) | 61(4) | 13(3) | 27(3) | 13(2) |
| C(38) | 64(4) | 32(3) | 82(4) | 19(3) | 41(3) | 9(2) |
| C(39) | 50(3) | 34(2) | 68(4) | 14(3) | 33(3) | 0(2) |

**Table B2-7** Hydrogen coordinates ( x $10^4$) and isotropic displacement parameters ($Å^2$x $10^3$).

| | x | y | z | U(eq) |
|---|---|---|---|---|
| H(2N) | 6205(11) | 1180(6) | 1813(8) | 42 |
| H(6N) | 9946(9) | 176(5) | -2615(4) | 35 |
| H(10N) | 11918(3) | 1329(8) | 3589(14) | 48 |
| H(3) | 5354 | -14 | 1780 | 48 |
| H(4) | 3796 | -450 | 1534 | 56 |
| H(5) | 2161 | 585 | 984 | 59 |
| H(6) | 2097 | 2069 | 712 | 67 |
| H(7) | 3657 | 2518 | 992 | 55 |
| H(9) | 6048 | 4863 | 514 | 43 |
| H(10) | 5745 | 5990 | -660 | 57 |
| H(11) | 6488 | 5562 | -2506 | 58 |
| H(12) | 7558 | 4023 | -3153 | 52 |
| H(13) | 7908 | 2910 | -1947 | 44 |
| H(16) | 12228 | 666 | -2782 | 48 |
| H(17) | 13361 | -324 | -4195 | 62 |
| H(18) | 12963 | -1714 | -5755 | 63 |
| H(19) | 11430 | -2137 | -5901 | 50 |
| H(20) | 10253 | -1136 | -4522 | 41 |
| H(22) | 8691 | 4738 | -39 | 48 |
| H(23) | 8991 | 6258 | 1227 | 58 |
| H(24) | 10143 | 6435 | 3250 | 63 |
| H(25) | 11030 | 5100 | 4065 | 71 |
| H(26) | 10782 | 3563 | 2800 | 56 |
| H(29) | 13825 | 1152 | 4145 | 70 |
| H(30) | 15353 | 1229 | 5794 | 81 |
| H(31) | 15228 | 1960 | 7971 | 76 |
| H(32) | 13605 | 2563 | 8570 | 67 |
| H(33) | 12059 | 2448 | 6932 | 57 |
| H(35) | 7118 | 3184 | 3824 | 51 |
| H(36) | 5636 | 4383 | 4420 | 65 |
| H(37) | 5365 | 5920 | 4236 | 61 |
| H(38) | 6553 | 6278 | 3440 | 69 |
| H(39) | 7976 | 5068 | 2711 | 58 |

Symmetry transformations used to generate equivalent atoms:
$1 -x+2, -y, -z
$2 x+1, y, z

# Appendix 3: Quantum Computational Data

**Atomic coordinates and molecular orbitals here included pertains to geometry optimised structures.**
**Atomic numbers* of corresponding elements are listed in the first column of each table, i.e. Hg(80), Co(27), S(16), N(7), C(6) & H(1).**

**Table A3-1** Dithizonatophenylmercury(II) - orange (ADF)

| *Atom nr*.* | *x* | *y* | *z* |
|---|---|---|---|
| 80 | 1.052574000 | 12.103418000 | 0.095572000 |
| 16 | 2.262220000 | 10.063281000 | 0.999683000 |
| 7 | -0.016915000 | 11.636682000 | 2.307853000 |
| 7 | 0.475875000 | 10.737652000 | 3.074948000 |
| 6 | 1.536877000 | 10.006725000 | 2.618618000 |
| 7 | 2.026176000 | 9.220856000 | 3.575413000 |
| 7 | 3.089355000 | 8.510464000 | 3.273033000 |
| 6 | 0.610423000 | 13.822028000 | -1.189297000 |
| 6 | -0.688684000 | 14.095857000 | -1.642604000 |
| 6 | -0.960856000 | 15.221257000 | -2.425983000 |
| 6 | 0.065876000 | 16.099285000 | -2.779016000 |
| 6 | 1.370941000 | 15.835940000 | -2.345895000 |
| 6 | 1.635409000 | 14.706122000 | -1.563301000 |
| 6 | -1.105270000 | 12.358517000 | 2.845228000 |
| 6 | -1.533442000 | 13.490020000 | 2.133524000 |
| 6 | -2.593057000 | 14.258046000 | 2.608597000 |
| 6 | -3.242370000 | 13.899146000 | 3.791680000 |
| 6 | -2.821819000 | 12.765854000 | 4.498659000 |
| 6 | -1.760504000 | 11.996703000 | 4.037237000 |
| 6 | 3.791870000 | 7.775596000 | 4.230828000 |
| 6 | 4.953533000 | 7.095633000 | 3.829800000 |
| 6 | 5.700737000 | 6.386008000 | 4.768897000 |
| 6 | 5.297301000 | 6.343985000 | 6.107604000 |
| 6 | 4.132395000 | 7.016893000 | 6.499384000 |
| 6 | 3.374880000 | 7.733332000 | 5.575734000 |
| 1 | 3.474874000 | 8.602675000 | 2.321467000 |
| 1 | -1.518130000 | 13.436991000 | -1.382262000 |
| 1 | -1.983150000 | 15.412683000 | -2.761565000 |
| 1 | -0.144845000 | 16.981583000 | -3.386894000 |
| 1 | 2.186234000 | 16.511515000 | -2.616578000 |
| 1 | 2.661663000 | 14.531221000 | -1.240230000 |
| 1 | -1.017694000 | 13.776442000 | 1.216131000 |
| 1 | -2.907421000 | 15.141599000 | 2.054447000 |
| 1 | -4.073232000 | 14.497768000 | 4.163426000 |
| 1 | -3.329820000 | 12.481908000 | 5.419886000 |
| 1 | -1.420481000 | 11.115510000 | 4.576300000 |
| 1 | 5.271928000 | 7.136336000 | 2.784871000 |
| 1 | 6.607424000 | 5.868774000 | 4.451620000 |
| 1 | 5.888160000 | 5.795469000 | 6.842569000 |
| 1 | 3.813867000 | 6.990540000 | 7.543243000 |
| 1 | 2.474821000 | 8.272552000 | 5.868254000 |

**Table A3-2** Dithizonatophenylmercury(II) - orange (G03)

| *Atom nr.* | *x* | *y* | *z* |
|---|---|---|---|
| 80 | -1.311571000 | -1.019865000 | 0.001979000 |
| 16 | 1.132524000 | -1.533617000 | -0.027066000 |
| 7 | -0.181577000 | 1.311752000 | -0.061608000 |
| 7 | 1.123984000 | 1.373785000 | -0.043452000 |
| 6 | 1.851530000 | 0.178052000 | -0.024784000 |
| 7 | 3.174037000 | 0.397193000 | -0.008358000 |
| 7 | 4.007857000 | -0.668668000 | 0.009520000 |
| 6 | -3.428224000 | -1.203255000 | 0.053438000 |
| 6 | -4.176479000 | -0.666447000 | 1.148908000 |
| 6 | -5.594878000 | -0.796414000 | 1.189475000 |
| 6 | -6.282683000 | -1.460596000 | 0.135434000 |
| 6 | -5.547916000 | -1.998247000 | -0.958259000 |
| 6 | -4.128970000 | -1.873696000 | -0.998508000 |
| 6 | -0.844868000 | 2.594676000 | -0.083364000 |
| 6 | -2.270104000 | 2.579104000 | -0.175561000 |
| 6 | -2.989991000 | 3.803051000 | -0.202914000 |
| 6 | -2.295052000 | 5.043270000 | -0.134982000 |
| 6 | -0.870496000 | 5.054524000 | -0.041569000 |
| 6 | -0.139626000 | 3.840399000 | -0.016021000 |
| 6 | 5.420945000 | -0.486877000 | 0.025101000 |
| 6 | 6.247964000 | -1.651500000 | 0.046895000 |
| 6 | 7.659944000 | -1.504671000 | 0.062166000 |
| 6 | 8.250898000 | -0.208922000 | 0.055940000 |
| 6 | 7.412666000 | 0.943913000 | 0.034142000 |

| | | | |
|---|---|---|---|
| 6 | 5.998765000 | 0.818867000 | 0.018537000 |
| 1 | 3.621093000 | -1.619873000 | 0.013135000 |
| 1 | -3.668271000 | -0.155262000 | 1.970703000 |
| 1 | -6.152081000 | -0.384409000 | 2.035237000 |
| 1 | -7.371041000 | -1.559441000 | 0.167060000 |
| 1 | -6.069256000 | -2.511607000 | -1.770724000 |
| 1 | -3.583311000 | -2.299041000 | -1.844380000 |
| 1 | -2.798861000 | 1.627070000 | -0.233969000 |
| 1 | -4.079694000 | 3.785575000 | -0.276989000 |
| 1 | -2.849655000 | 5.984761000 | -0.154906000 |
| 1 | -0.334814000 | 6.005723000 | 0.010879000 |
| 1 | 0.947483000 | 3.833308000 | 0.052905000 |
| 1 | 5.796895000 | -2.648034000 | 0.051829000 |
| 1 | 8.291340000 | -2.396624000 | 0.078780000 |
| 1 | 9.337729000 | -0.099632000 | 0.067605000 |
| 1 | 7.858093000 | 1.942138000 | 0.028989000 |
| 1 | 5.348996000 | 1.692621000 | 0.001460000 |

**Table A3-3** Dithizonatomethylmercury(II) - orange (ADF)

| *Atom nr.* | *x* | *y* | *z* |
|---|---|---|---|
| 80 | 1.248138 | 1.893682 | 1.844764 |
| 16 | 1.185882 | -0.001023 | 3.558966 |
| 7 | 3.634237 | 1.255278 | 2.221826 |
| 7 | 3.931182 | 0.260106 | 2.972175 |
| 6 | 2.916991 | -0.372320 | 3.636956 |
| 7 | 3.385738 | -1.356688 | 4.405010 |
| 7 | 2.494527 | -2.025264 | 5.101827 |
| 1 | 1.506131 | -1.746512 | 5.006093 |
| 6 | 0.442581 | 3.434512 | 0.451110 |
| 6 | 4.724402 | 1.848238 | 1.548233 |
| 6 | 4.496248 | 3.087282 | 0.928995 |
| 6 | 5.525668 | 3.733895 | 0.250707 |
| 6 | 6.787548 | 3.142044 | 0.165944 |
| 6 | 7.013359 | 1.899122 | 0.769843 |
| 6 | 5.996049 | 1.252445 | 1.461137 |
| 6 | 2.834523 | -3.076846 | 5.952866 |
| 6 | 1.799090 | -3.726136 | 6.644774 |
| 6 | 2.094375 | -4.782195 | 7.504257 |
| 6 | 3.418836 | -5.197185 | 7.681280 |
| 6 | 4.444089 | -4.542243 | 6.987650 |
| 6 | 4.164632 | -3.486003 | 6.124803 |
| 1 | 0.797736 | 3.215205 | -0.561524 |
| 1 | -0.651159 | 3.423719 | 0.460629 |
| 1 | 0.794542 | 4.427822 | 0.748021 |
| 1 | 3.507911 | 3.542828 | 0.998094 |
| 1 | 5.342795 | 4.701883 | -0.213374 |
| 1 | 7.592521 | 3.642974 | -0.370578 |
| 1 | 7.994496 | 1.430809 | 0.695198 |
| 1 | 6.154606 | 0.287145 | 1.935934 |
| 1 | 4.951725 | -2.969597 | 5.580954 |
| 1 | 5.479789 | -4.860992 | 7.121208 |
| 1 | 3.651103 | -6.024801 | 8.353224 |
| 1 | 1.284581 | -5.283408 | 8.036937 |
| 1 | 0.765657 | -3.398906 | 6.503033 |

**Table A3-4** Dithizonatomethylmercury(II) - orange (G03)

| *Atom nr.* | *x* | *y* | *z* |
|---|---|---|---|
| 80 | -1.864524000 | -1.532834000 | -0.000243000 |
| 16 | 0.641118000 | -1.650261000 | 0.001076000 |
| 7 | -1.104632000 | 0.954143000 | 0.000466000 |
| 7 | 0.175754000 | 1.219899000 | 0.000338000 |
| 6 | 1.080672000 | 0.151721000 | 0.000495000 |
| 7 | 2.352717000 | 0.578008000 | 0.000248000 |
| 7 | 3.342796000 | -0.344555000 | 0.000320000 |
| 1 | 3.107600000 | -1.344272000 | 0.000484000 |
| 6 | -3.953885000 | -2.036695000 | -0.000958000 |
| 6 | -1.959248000 | 2.118108000 | 0.000282000 |
| 6 | -3.367201000 | 1.878396000 | 0.001156000 |
| 6 | -4.273185000 | 2.971740000 | 0.001022000 |
| 6 | -3.780209000 | 4.307057000 | -0.000010000 |
| 6 | -2.372449000 | 4.543728000 | -0.000889000 |
| 6 | -1.458035000 | 3.460516000 | -0.000749000 |
| 6 | 4.709979000 | 0.055435000 | 0.000064000 |
| 6 | 5.709048000 | -0.965745000 | 0.000104000 |
| 6 | 7.080941000 | -0.600378000 | -0.000131000 |
| 6 | 7.462121000 | 0.771817000 | -0.000401000 |

| | | | |
|---|---|---|---|
| 6 | 6.453912000 | 1.779633000 | -0.000436000 |
| 6 | 5.076731000 | 1.435510000 | -0.000207000 |
| 1 | -4.422651000 | -1.610027000 | -0.902449000 |
| 1 | -4.063315000 | -3.131676000 | -0.005271000 |
| 1 | -4.421464000 | -1.617251000 | 0.904526000 |
| 1 | -3.735948000 | 0.852001000 | 0.001992000 |
| 1 | -5.349274000 | 2.783052000 | 0.001717000 |
| 1 | -4.476900000 | 5.149027000 | -0.000129000 |
| 1 | -1.992077000 | 5.568318000 | -0.001682000 |
| 1 | -0.381276000 | 3.625585000 | -0.001404000 |
| 1 | 4.298345000 | 2.197142000 | -0.000228000 |
| 1 | 6.738117000 | 2.835184000 | -0.000640000 |
| 1 | 8.518602000 | 1.049617000 | -0.000583000 |
| 1 | 7.843987000 | -1.382863000 | -0.000099000 |
| 1 | 5.418720000 | -2.020422000 | 0.000316000 |

**Table A3-5** Dithizonatophenylmercury(II) - blue N(4)H (ADF)

| *Atom nr.* | *x* | *y* | *z* |
|---|---|---|---|
| 80 | 1.091852000 | 12.062574000 | 0.076343000 |
| 16 | 2.156412000 | 10.021000000 | 1.093251000 |
| 7 | -0.094913000 | 11.761433000 | 2.318706000 |
| 7 | 0.370386000 | 10.858651000 | 3.109380000 |
| 6 | 1.401469000 | 10.069828000 | 2.692676000 |
| 7 | 1.906324000 | 9.219923000 | 3.596613000 |
| 7 | 1.393690000 | 9.251646000 | 4.807891000 |
| 6 | 0.624640000 | 13.801126000 | -1.176313000 |
| 6 | -0.678916000 | 14.073123000 | -1.616555000 |
| 6 | -0.966601000 | 15.206627000 | -2.385185000 |
| 6 | 0.051378000 | 16.093252000 | -2.739204000 |
| 6 | 1.363621000 | 15.833103000 | -2.319488000 |
| 6 | 1.640678000 | 14.696635000 | -1.551803000 |
| 6 | -1.184379000 | 12.495155000 | 2.818626000 |
| 6 | -1.532715000 | 13.669031000 | 2.126732000 |
| 6 | -2.588792000 | 14.457465000 | 2.573388000 |
| 6 | -3.319002000 | 14.080474000 | 3.702804000 |
| 6 | -2.989480000 | 12.900700000 | 4.381933000 |
| 6 | -1.933789000 | 12.109595000 | 3.948357000 |
| 6 | 1.830376000 | 8.449771000 | 5.855510000 |
| 6 | 1.169065000 | 8.571206000 | 7.091817000 |
| 6 | 1.577562000 | 7.801689000 | 8.178817000 |
| 6 | 2.646169000 | 6.907694000 | 8.049456000 |
| 6 | 3.303706000 | 6.788150000 | 6.816567000 |
| 6 | 2.911064000 | 7.545193000 | 5.716144000 |
| 1 | 0.639272000 | 9.927184000 | 4.975828000 |
| 1 | -1.502800000 | 13.406419000 | -1.357437000 |
| 1 | -1.993008000 | 15.395182000 | -2.709970000 |
| 1 | -0.169661000 | 16.979988000 | -3.336934000 |
| 1 | 2.171931000 | 16.515613000 | -2.591954000 |
| 1 | 2.672214000 | 14.523770000 | -1.241483000 |
| 1 | -0.955163000 | 13.964729000 | 1.250476000 |
| 1 | -2.840512000 | 15.371622000 | 2.037190000 |
| 1 | -4.148099000 | 14.695853000 | 4.050275000 |
| 1 | -3.570053000 | 12.594416000 | 5.251752000 |
| 1 | -1.685263000 | 11.180892000 | 4.456656000 |
| 1 | 0.334595000 | 9.271206000 | 7.191660000 |
| 1 | 1.056272000 | 7.902160000 | 9.132107000 |
| 1 | 2.965127000 | 6.308164000 | 8.902751000 |
| 1 | 4.138712000 | 6.092647000 | 6.712600000 |
| 1 | 3.413738000 | 7.464810000 | 4.752663000 |

**Table A3-6** Dithizonatophenylmercury(II) - blue N(4)H (G03)

| *Atom nr.* | *x* | *y* | *z* |
|---|---|---|---|
| 80 | 1.560674000 | -1.174002000 | -0.019432000 |
| 16 | -0.700656000 | -2.167215000 | -0.051009000 |
| 7 | -0.067096000 | 0.944340000 | -0.008200000 |
| 7 | -1.350280000 | 0.676218000 | -0.007685000 |
| 6 | -1.768497000 | -0.658679000 | -0.021718000 |
| 7 | -3.089374000 | -0.899703000 | -0.015630000 |
| 7 | -3.961355000 | 0.138900000 | 0.005631000 |
| 6 | 3.639624000 | -0.730877000 | 0.006905000 |
| 6 | 4.338934000 | -0.427968000 | -1.204997000 |
| 6 | 5.732574000 | -0.130551000 | -1.185597000 |
| 6 | 6.446814000 | -0.132048000 | 0.045415000 |
| 6 | 5.763533000 | -0.432978000 | 1.257036000 |
| 6 | 4.370117000 | -0.731135000 | 1.238033000 |
| 6 | 0.280751000 | 2.339842000 | 0.004063000 |

| | | | |
|---|---|---|---|
| 6 | 1.680277000 | 2.635460000 | 0.017921000 |
| 6 | 2.118957000 | 3.985299000 | 0.030231000 |
| 6 | 1.169653000 | 5.046168000 | 0.027793000 |
| 6 | -0.227186000 | 4.750007000 | 0.013119000 |
| 6 | -0.677393000 | 3.406750000 | 0.001251000 |
| 6 | -5.365251000 | -0.085530000 | 0.013013000 |
| 6 | -6.228365000 | 1.053622000 | 0.037285000 |
| 6 | -7.635403000 | 0.864247000 | 0.045675000 |
| 6 | -8.187057000 | -0.448501000 | 0.030114000 |
| 6 | -7.313733000 | -1.575485000 | 0.005897000 |
| 6 | -5.904605000 | -1.408250000 | -0.002908000 |
| 1 | -3.590428000 | 1.094326000 | 0.017082000 |
| 1 | 3.811225000 | -0.425798000 | -2.162460000 |
| 1 | 6.251252000 | 0.095684000 | -2.121247000 |
| 1 | 7.516477000 | 0.094017000 | 0.059802000 |
| 1 | 6.305901000 | -0.439254000 | 2.206442000 |
| 1 | 3.866204000 | -0.963758000 | 2.179775000 |
| 1 | 2.400827000 | 1.817028000 | 0.020211000 |
| 1 | 3.188898000 | 4.203955000 | 0.041581000 |
| 1 | 1.507934000 | 6.085232000 | 0.036931000 |
| 1 | -0.956772000 | 5.563728000 | 0.010602000 |
| 1 | -1.741479000 | 3.174428000 | -0.010952000 |
| 1 | -5.808397000 | 2.063832000 | 0.049523000 |
| 1 | -8.293682000 | 1.736616000 | 0.064299000 |
| 1 | -9.270092000 | -0.590658000 | 0.036670000 |
| 1 | -7.728485000 | -2.586711000 | -0.006203000 |
| 1 | -5.228496000 | -2.261736000 | -0.021325000 |

**Table A3-7** Dithizonatophenylmercury(II) - blue N(2)H (ADF)

| *Atom nr.* | *x* | *y* | *z* |
|---|---|---|---|
| 80 | 1.098729000 | 12.072550000 | 0.095803000 |
| 16 | 2.188558000 | 10.001263000 | 1.120833000 |
| 7 | -0.099911000 | 11.829961000 | 2.262102000 |
| 7 | 0.431109000 | 10.870876000 | 3.015994000 |
| 6 | 1.424623000 | 10.044626000 | 2.673843000 |
| 7 | 1.891345000 | 9.173571000 | 3.644734000 |
| 7 | 1.303423000 | 9.289236000 | 4.782311000 |
| 6 | 0.643264000 | 13.778436000 | -1.198882000 |
| 6 | -0.669792000 | 14.037957000 | -1.618504000 |
| 6 | -0.973243000 | 15.153831000 | -2.402370000 |
| 6 | 0.035796000 | 16.035769000 | -2.792925000 |
| 6 | 1.353646000 | 15.785693000 | -2.395222000 |
| 6 | 1.650552000 | 14.665358000 | -1.611034000 |
| 6 | -1.178374000 | 12.511384000 | 2.817038000 |
| 6 | -1.577474000 | 13.700666000 | 2.168603000 |
| 6 | -2.631069000 | 14.457516000 | 2.663599000 |
| 6 | -3.319045000 | 14.054763000 | 3.813236000 |
| 6 | -2.944500000 | 12.869863000 | 4.451993000 |
| 6 | -1.894998000 | 12.096490000 | 3.963441000 |
| 6 | 1.779907000 | 8.458037000 | 5.800576000 |
| 6 | 1.092559000 | 8.529624000 | 7.027320000 |
| 6 | 1.508124000 | 7.765042000 | 8.115171000 |
| 6 | 2.619932000 | 6.924893000 | 7.994989000 |
| 6 | 3.314283000 | 6.850026000 | 6.776101000 |
| 6 | 2.907597000 | 7.602965000 | 5.681641000 |
| 1 | 0.152516000 | 10.736268000 | 4.003818000 |
| 1 | -1.486925000 | 13.376726000 | -1.326776000 |
| 1 | -2.006335000 | 15.334798000 | -2.708682000 |
| 1 | -0.199611000 | 16.911461000 | -3.401329000 |
| 1 | 2.155348000 | 16.465517000 | -2.694789000 |
| 1 | 2.687393000 | 14.502283000 | -1.315395000 |
| 1 | -1.032526000 | 14.028426000 | 1.283297000 |
| 1 | -2.913184000 | 15.376238000 | 2.150638000 |
| 1 | -4.142348000 | 14.651959000 | 4.202006000 |
| 1 | -3.485074000 | 12.533054000 | 5.336144000 |
| 1 | -1.666709000 | 11.154111000 | 4.462984000 |
| 1 | 0.232488000 | 9.198044000 | 7.100287000 |
| 1 | 0.967532000 | 7.827358000 | 9.061220000 |
| 1 | 2.951354000 | 6.331424000 | 8.848959000 |
| 1 | 4.185496000 | 6.197226000 | 6.688967000 |
| 1 | 3.437767000 | 7.562776000 | 4.729760000 |

**Table A3-8** Dithizonatophenylmercury(II) - blue N(2)H (G03)

| *Atom nr.* | *x* | *y* | *z* |
|---|---|---|---|
| 80 | 1.587562000 | -1.042421000 | -0.047806000 |
| 16 | -0.642655000 | -2.224227000 | -0.208699000 |
| 7 | -0.016645000 | 0.873873000 | 0.149630000 |
| 7 | -1.324657000 | 0.468001000 | 0.063955000 |
| 6 | -1.741355000 | -0.813732000 | -0.057297000 |
| 7 | -3.128798000 | -1.072393000 | -0.072168000 |
| 7 | -3.881527000 | -0.012769000 | 0.161249000 |
| 6 | 3.682673000 | -0.687661000 | -0.004995000 |
| 6 | 4.240621000 | 0.442969000 | -0.682389000 |
| 6 | 5.646111000 | 0.675616000 | -0.665347000 |
| 6 | 6.510591000 | -0.213976000 | 0.032109000 |
| 6 | 5.965852000 | -1.340629000 | 0.709649000 |
| 6 | 4.561203000 | -1.579000000 | 0.688948000 |
| 6 | 0.179414000 | 2.283004000 | 0.078081000 |
| 6 | 1.438617000 | 2.776987000 | 0.561603000 |
| 6 | 1.722627000 | 4.163663000 | 0.528161000 |
| 6 | 0.766577000 | 5.089719000 | 0.014037000 |
| 6 | -0.476331000 | 4.603510000 | -0.480722000 |
| 6 | -0.774483000 | 3.214539000 | -0.462124000 |
| 6 | -5.289550000 | -0.237564000 | 0.106217000 |
| 6 | -6.106079000 | 0.906496000 | 0.377059000 |
| 6 | -7.519896000 | 0.787618000 | 0.348620000 |
| 6 | -8.123157000 | -0.468368000 | 0.050801000 |
| 6 | -7.305835000 | -1.608993000 | -0.218774000 |
| 6 | -5.893360000 | -1.504524000 | -0.194252000 |
| 1 | -2.105259000 | 1.140124000 | 0.168532000 |
| 1 | 3.595164000 | 1.137420000 | -1.225471000 |
| 1 | 6.057389000 | 1.541558000 | -1.191376000 |
| 1 | 7.588925000 | -0.033815000 | 0.045475000 |
| 1 | 6.623795000 | -2.029769000 | 1.246161000 |
| 1 | 4.163567000 | -2.453435000 | 1.209572000 |
| 1 | 2.160045000 | 2.070619000 | 0.975169000 |
| 1 | 2.682399000 | 4.522279000 | 0.908518000 |
| 1 | 0.989002000 | 6.158910000 | -0.007571000 |
| 1 | -1.208525000 | 5.299905000 | -0.898151000 |
| 1 | -1.710935000 | 2.870387000 | -0.908877000 |
| 1 | -5.620057000 | 1.857023000 | 0.605334000 |
| 1 | -8.143814000 | 1.660319000 | 0.555978000 |
| 1 | -9.212025000 | -0.560379000 | 0.028708000 |
| 1 | -7.771732000 | -2.570935000 | -0.446372000 |
| 1 | -5.254516000 | -2.363953000 | -0.396927000 |

**Table A3-9** Dithizone (a) (ADF)

| *Atom nr.* | *x* | *y* | *z* |
|---|---|---|---|
| 6 | -0.000713000 | 0.010747000 | 0.000000000 |
| 7 | 1.105391000 | 0.807400000 | 0.000000000 |
| 7 | -1.108176000 | 0.805384000 | 0.000000000 |
| 7 | -2.221430000 | 0.135576000 | 0.000000000 |
| 7 | 2.219499000 | 0.138806000 | 0.000000000 |
| 1 | 2.111400000 | -0.902826000 | 0.000000000 |
| 1 | -2.112402000 | -0.905988000 | 0.000000000 |
| 6 | -3.471623000 | 0.753767000 | 0.000000000 |
| 6 | -4.617975000 | -0.055948000 | 0.000000000 |
| 6 | -3.586070000 | 2.152467000 | 0.000000000 |
| 1 | -4.514940000 | -1.141619000 | 0.000000000 |
| 1 | -2.680514000 | 2.753923000 | 0.000000000 |
| 6 | -5.876089000 | 0.538348000 | 0.000000000 |
| 6 | -4.850343000 | 2.728851000 | 0.000000000 |
| 1 | -6.765937000 | -0.089332000 | 0.000000000 |
| 1 | -4.941285000 | 3.814608000 | 0.000000000 |
| 6 | -5.999154000 | 1.930204000 | 0.000000000 |
| 1 | -6.985423000 | 2.392061000 | 0.000000000 |
| 6 | 3.469142000 | 0.757545000 | 0.000000000 |
| 6 | 4.619613000 | -0.060620000 | 0.000000000 |
| 6 | 3.583958000 | 2.154132000 | 0.000000000 |
| 1 | 4.513183000 | -1.146907000 | 0.000000000 |
| 1 | 2.679849000 | 2.757367000 | 0.000000000 |
| 6 | 5.875575000 | 0.534177000 | 0.000000000 |
| 6 | 4.854980000 | 2.732792000 | 0.000000000 |
| 1 | 6.767683000 | -0.092746000 | 0.000000000 |
| 1 | 4.946045000 | 3.819780000 | 0.000000000 |
| 6 | 6.001361000 | 1.931300000 | 0.000000000 |
| 1 | 6.990613000 | 2.390309000 | 0.000000000 |
| 16 | 0.000806000 | -1.709084000 | 0.000000000 |

**Table A3-10** Dithizone (b) (ADF)

| *Atom nr.* | *x* | *y* | *z* |
|---|---|---|---|
| 6 | -0.008110000 | -0.017207000 | -0.002858000 |
| 7 | 1.162571000 | 0.707859000 | -0.003307000 |
| 7 | -1.099065000 | 0.713681000 | -0.001366000 |
| 7 | -2.260542000 | 0.082599000 | 0.002290000 |
| 7 | 2.231957000 | 0.012485000 | -0.002279000 |
| 1 | -2.280402000 | -0.941450000 | 0.005084000 |
| 6 | -3.481699000 | 0.762042000 | 0.003097000 |
| 6 | -4.662661000 | 0.003205000 | 0.007173000 |
| 6 | -3.542730000 | 2.162961000 | -0.002710000 |
| 1 | -4.607305000 | -1.086773000 | 0.010857000 |
| 1 | -2.617257000 | 2.733645000 | -0.006409000 |
| 6 | -5.897266000 | 0.644965000 | 0.005417000 |
| 6 | -4.786458000 | 2.788281000 | -0.004484000 |
| 1 | -6.809191000 | 0.049542000 | 0.008139000 |
| 1 | -4.833095000 | 3.876906000 | -0.009380000 |
| 6 | -5.967785000 | 2.040291000 | -0.000482000 |
| 1 | -6.934952000 | 2.540765000 | -0.002386000 |
| 6 | 3.436130000 | 0.739262000 | -0.001425000 |
| 6 | 4.625154000 | -0.024185000 | 0.000632000 |
| 6 | 3.507824000 | 2.142638000 | -0.002693000 |
| 1 | 4.544866000 | -1.111594000 | 0.000954000 |
| 1 | 2.584532000 | 2.717285000 | -0.005897000 |
| 6 | 5.862007000 | 0.611666000 | 0.005403000 |
| 6 | 4.755699000 | 2.769738000 | 0.000371000 |
| 1 | 6.778091000 | 0.019685000 | 0.009615000 |
| 1 | 4.811483000 | 3.859726000 | -0.000740000 |
| 6 | 5.931420000 | 2.009830000 | 0.005374000 |
| 1 | 6.902287000 | 2.507866000 | 0.008811000 |
| 16 | 0.024767000 | -1.805140000 | -0.002741000 |
| 1 | 1.414478000 | -1.657728000 | -0.001326000 |

**Table A3-11** Dithizone (c) (ADF)

| *Atom nr.* | *x* | *y* | *z* |
|---|---|---|---|
| 6 | -0.044435000 | 0.106877000 | 0.001136000 |
| 7 | 1.175564000 | 0.697268000 | 0.002261000 |
| 7 | -1.124475000 | 0.967561000 | 0.001435000 |
| 7 | -2.248004000 | 0.297566000 | -0.000362000 |
| 7 | 1.235686000 | 2.000115000 | 0.004467000 |
| 1 | 0.352133000 | 2.526165000 | 0.005014000 |
| 1 | -2.069852000 | -0.760844000 | -0.001417000 |
| 6 | -3.509337000 | 0.864847000 | -0.000825000 |
| 6 | -4.614031000 | -0.009097000 | -0.001345000 |
| 6 | -3.711169000 | 2.256630000 | -0.000486000 |
| 1 | -4.443627000 | -1.085689000 | -0.001624000 |
| 1 | -2.848552000 | 2.918030000 | -0.000241000 |
| 6 | -5.902668000 | 0.507872000 | -0.001227000 |
| 6 | -5.007995000 | 2.756451000 | -0.000357000 |
| 1 | -6.753381000 | -0.172009000 | -0.001444000 |
| 1 | -5.166224000 | 3.834248000 | 0.000042000 |
| 6 | -6.108115000 | 1.891562000 | -0.000647000 |
| 1 | -7.120009000 | 2.294020000 | -0.000380000 |
| 6 | 2.443154000 | 2.700275000 | 0.002982000 |
| 6 | 2.389868000 | 4.104846000 | 0.002586000 |
| 6 | 3.674596000 | 2.030695000 | 0.000882000 |
| 1 | 1.422807000 | 4.610288000 | 0.004393000 |
| 1 | 3.688222000 | 0.943761000 | 0.001316000 |
| 6 | 3.568851000 | 4.839750000 | -0.000653000 |
| 6 | 4.855125000 | 2.782351000 | -0.004221000 |
| 1 | 3.526622000 | 5.927809000 | -0.000641000 |
| 1 | 5.815163000 | 2.264360000 | -0.006893000 |
| 6 | 4.813259000 | 4.181281000 | -0.004276000 |
| 1 | 5.737981000 | 4.759561000 | -0.007430000 |
| 16 | -0.190528000 | -1.604777000 | -0.000906000 |

**Table A3-12** Dithizone (d) (ADF)

| *Atom nr.* | *x* | *y* | *z* |
|---|---|---|---|
| 6 | -0.076124000 | -0.098533000 | 0.000943000 |
| 7 | -0.118417000 | -1.467972000 | -0.004353000 |
| 7 | -1.174435000 | 0.624749000 | 0.000704000 |
| 7 | -2.339025000 | -0.016672000 | -0.003181000 |
| 7 | 1.049897000 | -2.002813000 | -0.006198000 |
| 1 | -2.319433000 | -1.039037000 | -0.003325000 |

| | | | |
|---|---|---|---|
| 6 | -3.564406000 | 0.643903000 | -0.002761000 |
| 6 | -4.736430000 | -0.133211000 | 0.006683000 |
| 6 | -3.654849000 | 2.044882000 | -0.011160000 |
| 1 | -4.663749000 | -1.222218000 | 0.013886000 |
| 1 | -2.741783000 | 2.634959000 | -0.018504000 |
| 6 | -5.981907000 | 0.487183000 | 0.008194000 |
| 6 | -4.909229000 | 2.648332000 | -0.009709000 |
| 1 | -6.883378000 | -0.124381000 | 0.016312000 |
| 1 | -4.974337000 | 3.736197000 | -0.016215000 |
| 6 | -6.078548000 | 1.881169000 | 0.000037000 |
| 1 | -7.054385000 | 2.364728000 | 0.001489000 |
| 6 | 1.093468000 | -3.402787000 | -0.006314000 |
| 6 | 2.385857000 | -3.957417000 | -0.014537000 |
| 6 | -0.030575000 | -4.254157000 | 0.005170000 |
| 1 | 3.236238000 | -3.277322000 | -0.023383000 |
| 1 | -1.026414000 | -3.815643000 | 0.011480000 |
| 6 | 2.558030000 | -5.343935000 | -0.008608000 |
| 6 | 0.144441000 | -5.631848000 | 0.010222000 |
| 1 | 3.561954000 | -5.770335000 | -0.012941000 |
| 1 | -0.725197000 | -6.288871000 | 0.020482000 |
| 6 | 1.432606000 | -6.186694000 | 0.002966000 |
| 1 | 1.561935000 | -7.270291000 | 0.008702000 |
| 16 | 1.529244000 | 0.698948000 | 0.012453000 |
| 1 | 0.952839000 | 1.928773000 | 0.012712000 |

**Table A3-13** 16-Methyldithizonatophenylmercury(II) - isomer 1 (ADF)

| *Atom nr.* | *x* | *y* | *z* |
|---|---|---|---|
| 80 | 0.959134000 | 12.297715000 | 0.214907000 |
| 16 | 2.684741000 | 10.385001000 | 1.112317000 |
| 7 | 0.141847000 | 11.639173000 | 2.299104000 |
| 7 | 0.693878000 | 10.727565000 | 3.046935000 |
| 6 | 1.775560000 | 10.069130000 | 2.687110000 |
| 7 | 2.275347000 | 9.173346000 | 3.577357000 |
| 7 | 3.330684000 | 8.534366000 | 3.221115000 |
| 6 | 0.649065000 | 13.755578000 | -1.391456000 |
| 6 | -0.651631000 | 13.996272000 | -1.859412000 |
| 6 | -0.905304000 | 14.978868000 | -2.819306000 |
| 6 | 0.141385000 | 15.748280000 | -3.330906000 |
| 6 | 1.444900000 | 15.515545000 | -2.881351000 |
| 6 | 1.694586000 | 14.523884000 | -1.925361000 |
| 6 | -1.010608000 | 12.250831000 | 2.835803000 |
| 6 | -1.592384000 | 13.305206000 | 2.112078000 |
| 6 | -2.724237000 | 13.959560000 | 2.591361000 |
| 6 | -3.300076000 | 13.569509000 | 3.802143000 |
| 6 | -2.727241000 | 12.516499000 | 4.523725000 |
| 6 | -1.594835000 | 11.858860000 | 4.054698000 |
| 6 | 3.852134000 | 7.687115000 | 4.216073000 |
| 6 | 4.977300000 | 6.925396000 | 3.854084000 |
| 6 | 5.591362000 | 6.079985000 | 4.779288000 |
| 6 | 5.093564000 | 5.985083000 | 6.082364000 |
| 6 | 3.970357000 | 6.740414000 | 6.456561000 |
| 6 | 3.347767000 | 7.584189000 | 5.544373000 |
| 1 | -1.497007000 | 13.426298000 | -1.470744000 |
| 1 | -1.928285000 | 15.148827000 | -3.162850000 |
| 1 | -0.056495000 | 16.525016000 | -4.071725000 |
| 1 | 2.273293000 | 16.110775000 | -3.271498000 |
| 1 | 2.721694000 | 14.371030000 | -1.592943000 |
| 1 | -1.144694000 | 13.628897000 | 1.169460000 |
| 1 | -3.151392000 | 14.781016000 | 2.017644000 |
| 1 | -4.184397000 | 14.080879000 | 4.180955000 |
| 1 | -3.170416000 | 12.202893000 | 5.468638000 |
| 1 | -1.144063000 | 11.041925000 | 4.612938000 |
| 1 | 5.360674000 | 7.022671000 | 2.836188000 |
| 1 | 6.466908000 | 5.497920000 | 4.484948000 |
| 1 | 5.579106000 | 5.332103000 | 6.809402000 |
| 1 | 3.585687000 | 6.670492000 | 7.476421000 |
| 1 | 2.480633000 | 8.184616000 | 5.821767000 |
| 6 | 2.334320000 | 8.832455000 | 0.191210000 |
| 1 | 2.760284000 | 8.953408000 | -0.810394000 |
| 1 | 2.838620000 | 8.026857000 | 0.732163000 |
| 1 | 1.259802000 | 8.644620000 | 0.128402000 |

**Table A3-14** S-Methyldithizonatophenylmercury(II) - isomer 1 (G03)

| *Atom nr.* | *x* | *y* | *z* |
|---|---|---|---|
| 80 | -1.709843000 | -0.137095000 | -0.058833000 |
| 16 | 0.861720000 | -1.559678000 | -0.310620000 |
| 7 | -0.227312000 | 1.444862000 | -0.089462000 |
| 7 | 1.111957000 | 1.277275000 | -0.078617000 |
| 6 | 1.744304000 | 0.114319000 | -0.119560000 |
| 7 | 3.144961000 | 0.196454000 | -0.078313000 |
| 7 | 3.802914000 | -0.935293000 | -0.092057000 |
| 6 | -3.346153000 | -1.462082000 | -0.021859000 |
| 6 | -4.647617000 | -1.030171000 | 0.387988000 |
| 6 | -5.738188000 | -1.945796000 | 0.408528000 |
| 6 | -5.542494000 | -3.299979000 | 0.017239000 |
| 6 | -4.252921000 | -3.738373000 | -0.394492000 |
| 6 | -3.159641000 | -2.826045000 | -0.412543000 |
| 6 | -0.643816000 | 2.829695000 | -0.032507000 |
| 6 | -2.038879000 | 3.134942000 | -0.090176000 |
| 6 | -2.484283000 | 4.482395000 | -0.032131000 |
| 6 | -1.547057000 | 5.546138000 | 0.081454000 |
| 6 | -0.155913000 | 5.241058000 | 0.134156000 |
| 6 | 0.302225000 | 3.899256000 | 0.078205000 |
| 6 | 5.234905000 | -0.786382000 | -0.057361000 |
| 6 | 5.974171000 | -2.008536000 | -0.105979000 |
| 6 | 7.393824000 | -1.981290000 | -0.074632000 |
| 6 | 8.081065000 | -0.736323000 | 0.006472000 |
| 6 | 7.340583000 | 0.483691000 | 0.054151000 |
| 6 | 5.922951000 | 0.468315000 | 0.021764000 |
| 1 | -4.818867000 | 0.005639000 | 0.691184000 |
| 1 | -6.726974000 | -1.603395000 | 0.725059000 |
| 1 | -6.381124000 | -4.001103000 | 0.031640000 |
| 1 | -4.097220000 | -4.776579000 | -0.699229000 |
| 1 | -2.176562000 | -3.178230000 | -0.734482000 |
| 1 | -2.777843000 | 2.334226000 | -0.190244000 |
| 1 | -3.555379000 | 4.694411000 | -0.079677000 |
| 1 | -1.889107000 | 6.582736000 | 0.125240000 |
| 1 | 0.576779000 | 6.048196000 | 0.219171000 |
| 1 | 1.364266000 | 3.665012000 | 0.116125000 |
| 1 | 5.424271000 | -2.949330000 | -0.174381000 |
| 1 | 7.956992000 | -2.917252000 | -0.114364000 |
| 1 | 9.173721000 | -0.713950000 | 0.030839000 |
| 1 | 7.868510000 | 1.439033000 | 0.115472000 |
| 1 | 5.343783000 | 1.391241000 | 0.055410000 |
| 6 | 1.336172000 | -2.422508000 | 1.332710000 |
| 1 | 0.766920000 | -3.363028000 | 1.354608000 |
| 1 | 2.416080000 | -2.606033000 | 1.298620000 |
| 1 | 1.064592000 | -1.786137000 | 2.186171000 |

**Table A3-15** S-Methyldithizonatophenylmercury(II) - isomer 2 (ADF)

| *Atom nr.* | *x* | *y* | *z* |
|---|---|---|---|
| 80 | 0.932624000 | 12.334819000 | 0.292143000 |
| 16 | 2.491326000 | 10.322545000 | 1.400892000 |
| 7 | -0.015164000 | 11.837429000 | 2.342877000 |
| 7 | 0.438910000 | 10.931680000 | 3.162319000 |
| 6 | 1.490038000 | 10.192833000 | 2.919421000 |
| 7 | 2.001386000 | 9.253636000 | 3.786674000 |
| 7 | 1.362898000 | 9.100613000 | 4.889398000 |
| 6 | 0.802644000 | 13.636018000 | -1.465739000 |
| 6 | -0.476039000 | 13.901219000 | -1.984363000 |
| 6 | -0.658106000 | 14.795058000 | -3.042507000 |
| 6 | 0.439264000 | 15.448337000 | -3.607616000 |
| 6 | 1.720349000 | 15.188281000 | -3.112912000 |
| 6 | 1.899830000 | 14.282663000 | -2.051337000 |
| 6 | -1.173298000 | 12.518743000 | 2.772260000 |
| 6 | -1.682697000 | 13.541857000 | 1.955844000 |
| 6 | -2.815833000 | 14.256468000 | 2.335011000 |
| 6 | -3.463092000 | 13.960594000 | 3.536031000 |
| 6 | -2.960794000 | 12.939879000 | 4.350444000 |
| 6 | -1.829312000 | 12.220442000 | 3.981963000 |
| 6 | 1.932084000 | 8.163057000 | 5.767479000 |
| 6 | 1.231303000 | 7.969599000 | 6.972092000 |
| 6 | 1.706464000 | 7.083803000 | 7.939006000 |
| 6 | 2.891032000 | 6.376377000 | 7.717807000 |
| 6 | 3.599520000 | 6.558197000 | 6.518523000 |
| 6 | 3.135526000 | 7.438450000 | 5.546816000 |
| 1 | -1.359457000 | 13.422543000 | -1.558211000 |
| 1 | -1.664922000 | 14.986881000 | -3.421108000 |

| | | | |
|---|---|---|---|
| 1 | 0.297751000 | 16.156482000 | -4.426563000 |
| 1 | 2.588097000 | 15.691711000 | -3.543860000 |
| 1 | 2.911827000 | 14.106531000 | -1.683617000 |
| 1 | -1.178651000 | 13.792717000 | 1.019175000 |
| 1 | -3.188778000 | 15.051466000 | 1.690337000 |
| 1 | -4.347904000 | 14.520010000 | 3.836409000 |
| 1 | -3.458811000 | 12.701983000 | 5.289785000 |
| 1 | -1.429343000 | 11.428451000 | 4.610287000 |
| 1 | 0.313015000 | 8.539837000 | 7.122853000 |
| 1 | 1.153149000 | 6.949269000 | 8.870536000 |
| 1 | 3.268034000 | 5.686978000 | 8.475440000 |
| 1 | 4.527365000 | 6.006740000 | 6.350938000 |
| 1 | 3.681899000 | 7.599090000 | 4.616935000 |
| 6 | 2.020921000 | 8.757678000 | 0.558411000 |
| 1 | 2.580126000 | 8.717653000 | -0.382916000 |
| 1 | 2.323659000 | 7.934816000 | 1.212864000 |
| 1 | 0.945511000 | 8.716155000 | 0.366995000 |

**Table A3-16** S-Methyldithizonatophenylmercury(II) - isomer 2 (G03)

| *Atom nr.* | *x* | *y* | *z* |
|---|---|---|---|
| 80 | -1.783433000 | -0.045305000 | -0.067507000 |
| 16 | 0.466386000 | -1.977758000 | -0.420565000 |
| 7 | -0.014893000 | 1.189563000 | -0.162454000 |
| 7 | 1.263600000 | 0.740543000 | -0.155059000 |
| 6 | 1.643926000 | -0.514674000 | -0.215652000 |
| 7 | 2.993915000 | -0.937754000 | -0.187047000 |
| 7 | 3.905357000 | -0.021011000 | 0.034440000 |
| 6 | -3.640045000 | -1.031118000 | 0.039562000 |
| 6 | -4.831662000 | -0.328368000 | 0.406858000 |
| 6 | -6.079339000 | -1.011171000 | 0.477625000 |
| 6 | -6.151650000 | -2.400916000 | 0.180171000 |
| 6 | -4.972836000 | -3.108084000 | -0.187441000 |
| 6 | -3.723255000 | -2.428635000 | -0.256244000 |
| 6 | -0.130345000 | 2.628218000 | -0.083424000 |
| 6 | -1.426340000 | 3.224705000 | -0.171621000 |
| 6 | -1.576668000 | 4.634762000 | -0.090785000 |
| 6 | -0.438211000 | 5.471431000 | 0.073551000 |
| 6 | 0.854136000 | 4.875438000 | 0.154261000 |
| 6 | 1.018827000 | 3.468205000 | 0.077859000 |
| 6 | 5.254438000 | -0.523527000 | 0.023324000 |
| 6 | 6.254135000 | 0.436678000 | 0.373807000 |
| 6 | 7.623072000 | 0.059527000 | 0.397964000 |
| 6 | 8.001194000 | -1.272895000 | 0.065264000 |
| 6 | 7.002448000 | -2.228513000 | -0.294247000 |
| 6 | 5.632636000 | -1.863293000 | -0.318650000 |
| 1 | -4.797580000 | 0.738943000 | 0.638975000 |
| 1 | -6.981613000 | -0.462599000 | 0.760584000 |
| 1 | -7.110384000 | -2.923504000 | 0.233113000 |
| 1 | -5.022695000 | -4.175244000 | -0.419251000 |
| 1 | -2.828119000 | -2.986091000 | -0.542544000 |
| 1 | -2.314248000 | 2.601818000 | -0.317610000 |
| 1 | -2.575952000 | 5.071617000 | -0.162761000 |
| 1 | -0.552818000 | 6.556260000 | 0.133271000 |
| 1 | 1.738651000 | 5.506359000 | 0.277696000 |
| 1 | 2.004508000 | 3.010408000 | 0.137226000 |
| 1 | 5.935622000 | 1.451376000 | 0.619736000 |
| 1 | 8.385375000 | 0.794407000 | 0.669049000 |
| 1 | 9.055047000 | -1.563172000 | 0.079600000 |
| 1 | 7.294716000 | -3.248476000 | -0.557943000 |
| 1 | 4.859952000 | -2.578466000 | -0.601310000 |
| 6 | 0.990831000 | -3.028684000 | 1.087716000 |
| 1 | 0.487935000 | -3.999665000 | 0.974354000 |
| 1 | 2.081444000 | -3.142505000 | 1.037537000 |
| 1 | 0.685052000 | -2.536844000 | 2.021298000 |

**Table A3-17** PhHgHDz - Co Porphyrin adduct - orange (ADF)

| *Atom nr.* | *x* | *y* | *z* |
|---|---|---|---|
| 27 | -0.054627000 | -0.042620000 | 0.071680000 |
| 7 | -1.506330000 | 1.249944000 | -0.282851000 |
| 6 | -1.387621000 | 2.571894000 | -0.697819000 |
| 6 | -2.875886000 | 1.029516000 | -0.212381000 |
| 6 | -2.678779000 | 3.142736000 | -0.950731000 |
| 6 | -3.600354000 | 2.189599000 | -0.646669000 |
| 1 | -2.844765000 | 4.156847000 | -1.295998000 |
| 1 | -4.681121000 | 2.255261000 | -0.701650000 |
| 7 | 1.353703000 | -1.417767000 | -0.087790000 |

| | | | |
|---|---|---|---|
| 6 | 1.205172000 | -2.794474000 | -0.026809000 |
| 6 | 2.705696000 | -1.217375000 | -0.319175000 |
| 6 | 2.453428000 | -3.451154000 | -0.289918000 |
| 6 | 3.384979000 | -2.473853000 | -0.466766000 |
| 1 | 2.584280000 | -4.526650000 | -0.330899000 |
| 1 | 4.440089000 | -2.578013000 | -0.693999000 |
| 7 | -1.397837000 | -1.457607000 | 0.338178000 |
| 6 | -1.175728000 | -2.811789000 | 0.510881000 |
| 6 | -2.763686000 | -1.303230000 | 0.497285000 |
| 6 | -2.402707000 | -3.496267000 | 0.821126000 |
| 6 | -3.387115000 | -2.559277000 | 0.820012000 |
| 1 | -2.485559000 | -4.565582000 | 0.982588000 |
| 1 | -4.451577000 | -2.694567000 | 0.977692000 |
| 7 | 1.274433000 | 1.351918000 | -0.396014000 |
| 6 | 1.048118000 | 2.703288000 | -0.576505000 |
| 6 | 2.650962000 | 1.224035000 | -0.379040000 |
| 6 | 2.290263000 | 3.425526000 | -0.639598000 |
| 6 | 3.285421000 | 2.507463000 | -0.513327000 |
| 1 | 2.372580000 | 4.496355000 | -0.789552000 |
| 1 | 4.358594000 | 2.665109000 | -0.537584000 |
| 6 | -0.197555000 | 3.271151000 | -0.771980000 |
| 1 | -0.245813000 | 4.331359000 | -1.010998000 |
| 6 | 0.032935000 | -3.448381000 | 0.300731000 |
| 1 | 0.059088000 | -4.533154000 | 0.378883000 |
| 6 | 3.326038000 | 0.018970000 | -0.373669000 |
| 1 | 4.409643000 | 0.041658000 | -0.470997000 |
| 6 | -3.463004000 | -0.143100000 | 0.226003000 |
| 1 | -4.547819000 | -0.172205000 | 0.299580000 |
| 80 | -1.659165000 | 2.292692000 | 2.601281000 |
| 16 | 0.348467000 | 0.578294000 | 2.223175000 |
| 7 | -1.858838000 | 0.560117000 | 4.378061000 |
| 7 | -1.048535000 | -0.416769000 | 4.459462000 |
| 6 | -0.042387000 | -0.564208000 | 3.541655000 |
| 7 | 0.796668000 | -1.532458000 | 3.913527000 |
| 7 | 1.895343000 | -1.744070000 | 3.260022000 |
| 6 | -2.872900000 | 4.106981000 | 2.372977000 |
| 6 | -4.271326000 | 4.014430000 | 2.485065000 |
| 6 | -5.088023000 | 5.142399000 | 2.329992000 |
| 6 | -4.515836000 | 6.393317000 | 2.068728000 |
| 6 | -3.126262000 | 6.505004000 | 1.965602000 |
| 6 | -2.310064000 | 5.364080000 | 2.116082000 |
| 6 | -2.740528000 | 0.714253000 | 5.472763000 |
| 6 | -3.567601000 | 1.849215000 | 5.465180000 |
| 6 | -4.412168000 | 2.108897000 | 6.541601000 |
| 6 | -4.436402000 | 1.236408000 | 7.633829000 |
| 6 | -3.616134000 | 0.096857000 | 7.637906000 |
| 6 | -2.771080000 | -0.170264000 | 6.568305000 |
| 6 | 2.879660000 | -2.624099000 | 3.742771000 |
| 6 | 4.072893000 | -2.746419000 | 3.012487000 |
| 6 | 5.078859000 | -3.593834000 | 3.473763000 |
| 6 | 4.904877000 | -4.314301000 | 4.660006000 |
| 6 | 3.714072000 | -4.181908000 | 5.387906000 |
| 6 | 2.696466000 | -3.342516000 | 4.942502000 |
| 1 | 2.098756000 | -1.190224000 | 2.414264000 |
| 1 | -4.756813000 | 3.056294000 | 2.688606000 |
| 1 | -6.172647000 | 5.042232000 | 2.416125000 |
| 1 | -5.150124000 | 7.274570000 | 1.952228000 |
| 1 | -2.665377000 | 7.476486000 | 1.772151000 |
| 1 | -1.230210000 | 5.486480000 | 2.024566000 |
| 1 | -3.527851000 | 2.547178000 | 4.629321000 |
| 1 | -5.039744000 | 3.001632000 | 6.533133000 |
| 1 | -5.086609000 | 1.443442000 | 8.485407000 |
| 1 | -3.633545000 | -0.580022000 | 8.493420000 |
| 1 | -2.120682000 | -1.041803000 | 6.565296000 |
| 1 | 4.204315000 | -2.178695000 | 2.089583000 |
| 1 | 6.005313000 | -3.688099000 | 2.905578000 |
| 1 | 5.696453000 | -4.972178000 | 5.021821000 |
| 1 | 3.581217000 | -4.735492000 | 6.318683000 |
| 1 | 1.770068000 | -3.222020000 | 5.503095000 |

**Table A3-18** PhHgHDz - Co Porphyrin adduct - blue (ADF)

| *Atom nr.* | *x* | *y* | *z* |
|---|---|---|---|
| 27 | 1.488940000 | 2.542017000 | 3.321112000 |
| 7 | 0.175305000 | 3.785145000 | 2.510620000 |
| 6 | -0.453828000 | 4.871255000 | 3.108024000 |
| 6 | -0.311927000 | 3.775888000 | 1.208529000 |
| 6 | -1.284761000 | 5.561065000 | 2.164879000 |
| 6 | -1.201548000 | 4.879654000 | 0.990274000 |

| | | | |
|---|---|---|---|
| 1 | -1.870457000 | 6.444394000 | 2.393537000 |
| 1 | -1.695481000 | 5.095019000 | 0.049324000 |
| 7 | 3.082792000 | 1.607744000 | 4.012397000 |
| 6 | 3.899839000 | 0.720435000 | 3.338979000 |
| 6 | 3.569824000 | 1.623839000 | 5.306757000 |
| 6 | 4.941957000 | 0.231298000 | 4.199884000 |
| 6 | 4.730735000 | 0.783676000 | 5.424960000 |
| 1 | 5.729756000 | -0.444718000 | 3.885664000 |
| 1 | 5.310215000 | 0.662707000 | 6.333480000 |
| 7 | 1.761868000 | 1.706786000 | 1.556698000 |
| 6 | 2.691778000 | 0.742219000 | 1.216811000 |
| 6 | 0.992870000 | 1.870094000 | 0.417469000 |
| 6 | 2.490009000 | 0.289117000 | -0.132829000 |
| 6 | 1.428556000 | 0.981844000 | -0.625889000 |
| 1 | 3.108853000 | -0.448869000 | -0.631417000 |
| 1 | 0.990179000 | 0.936637000 | -1.616922000 |
| 7 | 1.351248000 | 3.543338000 | 5.028648000 |
| 6 | 0.460669000 | 4.552226000 | 5.350226000 |
| 6 | 1.985147000 | 3.240559000 | 6.218716000 |
| 6 | 0.535685000 | 4.872392000 | 6.750192000 |
| 6 | 1.477493000 | 4.053343000 | 7.290001000 |
| 1 | -0.055232000 | 5.639920000 | 7.238019000 |
| 1 | 1.827450000 | 4.006522000 | 8.315459000 |
| 6 | -0.354746000 | 5.204691000 | 4.446078000 |
| 1 | -0.959225000 | 6.033642000 | 4.808113000 |
| 6 | 3.714457000 | 0.301498000 | 2.035537000 |
| 1 | 4.414123000 | -0.426585000 | 1.630096000 |
| 6 | 3.029608000 | 2.346822000 | 6.352499000 |
| 1 | 3.482073000 | 2.236297000 | 7.335798000 |
| 6 | 0.023094000 | 2.839227000 | 0.247954000 |
| 1 | -0.463786000 | 2.909146000 | -0.722605000 |
| 80 | -2.220180000 | 2.082296000 | 3.325733000 |
| 16 | 0.038182000 | 1.086775000 | 4.234448000 |
| 7 | -2.110710000 | -0.336798000 | 2.497214000 |
| 7 | -1.067326000 | -1.034499000 | 2.743668000 |
| 6 | -0.026239000 | -0.508273000 | 3.450354000 |
| 7 | 1.004517000 | -1.316061000 | 3.737683000 |
| 7 | 0.974050000 | -2.521390000 | 3.240874000 |
| 6 | -3.961370000 | 3.364702000 | 2.953911000 |
| 6 | -4.517252000 | 3.442540000 | 1.665315000 |
| 6 | -5.606475000 | 4.280051000 | 1.395209000 |
| 6 | -6.165605000 | 5.056408000 | 2.417128000 |
| 6 | -5.630271000 | 4.984196000 | 3.707009000 |
| 6 | -4.537173000 | 4.142436000 | 3.969338000 |
| 6 | -3.178599000 | -1.005672000 | 1.874794000 |
| 6 | -4.342375000 | -0.248747000 | 1.652522000 |
| 6 | -5.462959000 | -0.834984000 | 1.072569000 |
| 6 | -5.436206000 | -2.185618000 | 0.713632000 |
| 6 | -4.277196000 | -2.947333000 | 0.937522000 |
| 6 | -3.154131000 | -2.368235000 | 1.511242000 |
| 6 | 1.913384000 | -3.512826000 | 3.524805000 |
| 6 | 1.723794000 | -4.772085000 | 2.927987000 |
| 6 | 2.615071000 | -5.808776000 | 3.198820000 |
| 6 | 3.697156000 | -5.599816000 | 4.059554000 |
| 6 | 3.889359000 | -4.342299000 | 4.651458000 |
| 6 | 3.014078000 | -3.290344000 | 4.399606000 |
| 1 | 0.164847000 | -2.767312000 | 2.657033000 |
| 1 | -4.104605000 | 2.857077000 | 0.840143000 |
| 1 | -6.017646000 | 4.326407000 | 0.384150000 |
| 1 | -7.013988000 | 5.710847000 | 2.208043000 |
| 1 | -6.061077000 | 5.580605000 | 4.514603000 |
| 1 | -4.141736000 | 4.114911000 | 4.985696000 |
| 1 | -4.372301000 | 0.796700000 | 1.956289000 |
| 1 | -6.362659000 | -0.238965000 | 0.911797000 |
| 1 | -6.315888000 | -2.652416000 | 0.267187000 |
| 1 | -4.262388000 | -4.003969000 | 0.664622000 |
| 1 | -2.259484000 | -2.957530000 | 1.694848000 |
| 1 | 0.873359000 | -4.936003000 | 2.260252000 |
| 1 | 2.459188000 | -6.785352000 | 2.738873000 |
| 1 | 4.388234000 | -6.415969000 | 4.275300000 |
| 1 | 4.731657000 | -4.185121000 | 5.327634000 |
| 1 | 3.141718000 | -2.310319000 | 4.860079000 |

**Table A3-19** PhHgHDz Molecular Orbitals (ADF)

| | PhHgHDz (orange) | PhHgHDz excited (orange) | PhHgHDz excited (blue) | PhHgHDz (blue) |
|---|---|---|---|---|
| LUMO+1 | 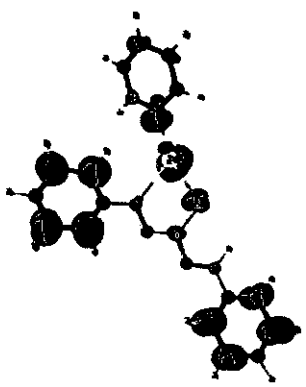 | 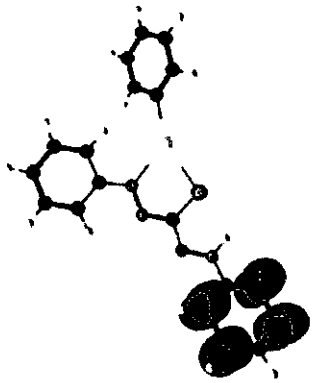 | 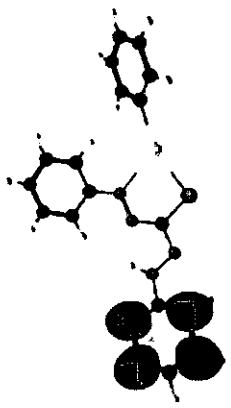 | 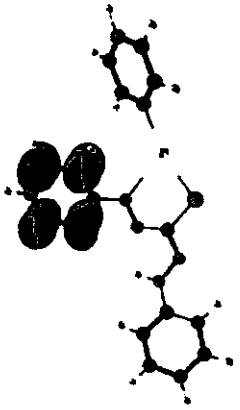 |
| LUMO | 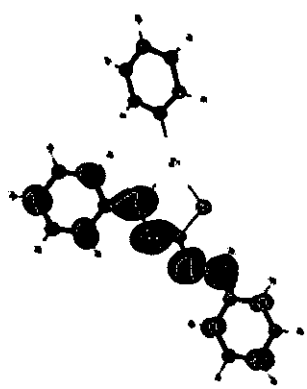 | 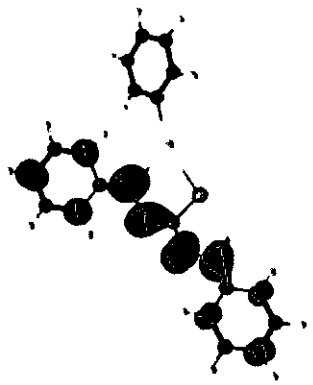 | 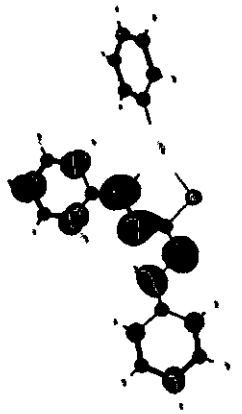 | 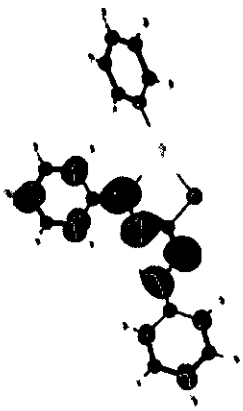 |
| HOMO | 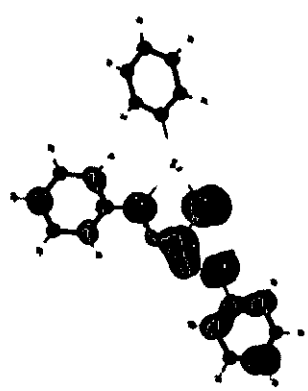 | 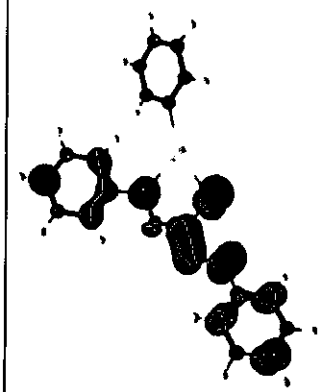 | 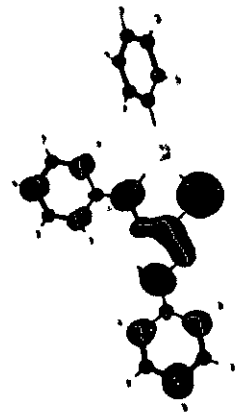 | 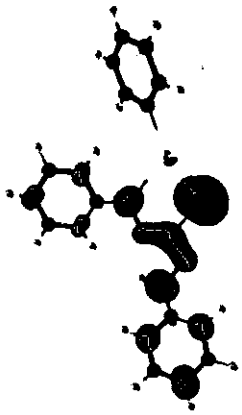 |

| | PhHgHDz (orange) | PhHgHDz excited (orange) | PhHgHDz excited (blue) | PhHgHDz (blue) |
|---|---|---|---|---|
| HOMO-1 |  |  |  |  |
| HOMO-2 |  |  |  |  |
| HOMO-3 |  |  |  |  |

| | PhHgHDz (orange) | PhHgHDz excited (orange) | PhHgHDz excited (blue) | PhHgHDz (blue) |
|---|---|---|---|---|
| HOMO-4 |  |  |  |  |
| HOMO-5 |  |  |  |  |
| HOMO-6 |  |  |  |  |